Universitat Autònoma de Barcelona

(BIO)ANALYTICAL MICROSYSTEMS BASED ON THE USE OF NANOPARTICLES

MICROREACTORS FOR THE SYNTHESIS OF NANOPARTICLES

SARA GÓMEZ DE PEDRO

DOCTORAL THESIS

PROGRAMA DE DOCTORAT DE QUÍMICA

DIRECTED BY: MARIA DEL MAR PUYOL BOSCH AND JULIÁN ALONSO CHAMARRO

DEPARTAMENT DE QUÍMICA
FACULTAT DE CIÈNCIES
2014

MEMÒRIA PRESENTADA PER ASPIRAR AL GRAU DE DOCTOR PER SARA GÓMEZ DE PEDRO:

SARA GÓMEZ DE PEDRO

VIST I PLAU:

MARIA DEL MAR PUYOL BOSCH	**JULIÁN ALONSO CHAMARRO**
Professor Lector (Ajudant Doctor)	Catedràtic de Química Analítica

BELLATERRA (CERDANYOLA DEL VALLÈS), 23 DE JULIOL DE 2014

The present dissertation has been carried out thanks to the following financial support:

Nanotecnologías en Biomedicina (CONSOLIDER INGENIO2010-CSD2006-12). Ministerio de Educación y Ciencia.

Construcción de Microanalizadores de Parámetros de Interés Medioambiental Mediante el Uso de Tecnologías IC y LTCC (CIT-310200-2007-29). Ministerio de Educación y Ciencia.

Nuevas plataformas de microfluidica para la miniaturizacion de sistemas (bio)analiticos integrados e intensificacion de procesos de produccion de nanomateriales (CTQ2009-12128). Ministerio de Educación y Ciencia.

Miniaturizacion, integracion y paralelizacion de ensayos quimicos y biologicos mediante nuevas plataformas de microfluídica (CTQ2012-36165). Ministerio de Educación y Ciencia co-funded by FEDER.

Grup de Sensors i Biosensors, Grupo de investigación consolidado (2009-SGR0323). Generalitat de Catalunya.

Grup de Sensors i Biosensors
Unitat de Química Analítica
Departament de Química
Universitat Autònoma de Barcelona
Edifici Cn 08193 Bellaterra, España
Telf. 0034 581 2533 Fax. 0034

GRUP DE SENSORS I BIOSENSORS

The described work result in the following publications:

Sara Gomez de Pedro, Mar Puyol, Julián Alonso, Continuous flow synthesis of nanoparticles using ceramic microfluidic devices, *Nanotechnology,* **2010,** 21, 41.

Sara Gomez-de Pedro, Mar Puyol, David Izquierdo, Iñigo Salinas, Jesús Martínez de la Fuente, Julián Alonso-Chamarro, A ceramic microreactor for the synthesis of water soluble CdS and CdS/ZnS nanocrystals with on-line optical characterization, *Nanoscale,* **2012,** 4(4), 1328-1335.

Sara Gómez-de Pedro, Cynthia S. Martínez-Cisneros, Mar Puyol and Julián Alonso-Chamarro, Microreactor with integrated temperature control for the synthesis of CdSe nano crystals, *Lab on a Chip,* **2012,** 12 (11), 1979-1986.

Cynthia S. Martínez-Cisneros, Sara Gómez-de Pedro, J. García-García, Mar Puyol and Julián Alonso-Chamarro, Design, fabrication and characterization of microreactors for high temperature syntheses, *Chemical Engineering Journal*, **2012,** 211-212, 432-441.

Sara Gómez-de Pedro, Daniela Lopes, Sergey Miltsov, David Izquierdo, Julian Alonso-Chamarro and Mar Puyol, Optical microfluidic system based on ionophore modified gold nanoparticles for the continuous monitoring of mercuric ion, *Sensors and Actuators B*, **2014**, 194, 19-26.

Sara Gómez, Alfonso Salinas-Castillo, Maria Ariza-Avidad, Ajejandro Lapresta, Cristina Sánchez-González, Cynthia Susana Martínez-Cisneros, Mar Puyol, Luis Fermin Capitan-Vallvey and Julián Alonso, Microsystem-assisted synthesis of carbon dots with fluorescent and colorimetric properties for pH detection, *Nanoscale*, **2014**, 6, 6018-6024.

Sara Gómez-de Pedro, Miguel Berenguel-Alonso, Pedro Couceiro, Julián Alonso-Chamarro, Mar Puyol, Automatic Microfluidic System to Perform a Multi-Step Magneto-Biochemical Assay. (Draft in progress).

Other publications related to this work and in collaboration with other studies are:

Sergey Miltsov, Vladimir Karavan, Vadim Boyarsky, Sara Gómez-de Pedro, Julian Alonso-Chamarro and Mar Puyol, New acyclic Pd-diaminocarbene catalyst for Suzuki arylation of meso-chlorosubstituted tricarboindocyanine dyes, *Tetrahedron Letters*, **2012**, 54(10), 1202-1204.

Pedro Couceiro, Sara Gómez-de Pedro and Julián Alonso-Chamarro, All-ceramic analytical microsystems with monolithically integrated optical detection microflow cells. *Microfluidics and Nanofluidics. Accepted manuscript.*

Sergey Miltsov, Vladimir Karavan, Mikhail Goikhman, Irina Podeshvo, Sara Gómez-de Pedro, Mar Puyol and Julian Alonso-Chamarro, Synthesis of bis-aminosubstituted indocyanine dyes for their use in polymeric compositions. *Dyes and Pigments*, **2014**, 109, 34-41.

Oriol Ymbern, Miguel Berenguel-Alonso, Antonio Calvo-López, Sara Gómez-de Pedro and Julián Alonso-Chamarro, Microfluidic cartridge reader for optical measurements in continuous flow and batch procedures. *Analytical Chemistry*. Submitted to the journal.

Sara Gómez-de Pedro, Sergey Miltsov, Julian Alonso-Chamarro and Mar Puyol, Spectroscopic characterization of new bis-acetylamino and bis-amino substituted cyanine dyes for their use in analytical applications. (Draft in progress).

Sergey Miltsov, Vladimir Karavan, Alexey Mindich, Mar Puyol, Sara Gomez, Julian Alonso, Synthesis and spectroscopic characterization of water-soluble ketocyanine dyes with cyclic fragments in the polymethine chain for their use in optical sensors. (Draft in progress).

TABLE OF CONTENTS

ACRONYMS

§	Section
A, Abs	Absorbance
A	Adenine
AA	Atomic Absorption
AES	Atomic Emission Spectroscopy
AFM	Atomic Force Microscopy
Ag NPs	Silver nanoparticles
AMD	Analytical microsystem
AOT	Dioctyl sulfosuccinate
Au NPs	Gold nanoparticles
b	Path length
BMD	Bioanalytical microsystem
c	Concentration
C	Cytosine
CAD	Computer-Aided Design
C-C	Carbon-Carbon
CCD	Charge-Coupled Device
C-dots/Cdots	Carbon dots
CE	Capillary Electrophoresis
CEC	Capillary Electrochromatography
CdO	Cadmium oxide
CLPL	Cold and Low Pressure Lamination
CNC	Computer Numerically Controlled
CNTs	Cabon Nanotubes
COC	Cyclic Olefin Copolymer
CTAB	Cetyltrimethylammonium bromide
DAQ	Data Acquisition Card
DDT	Dodecanethiol
DHLA	Dihygrolipid acid
DLS	Dynamic Light Scattering
DNA	DeoxyriboNucleic Acid
DWNTs	Double-Wall Nanotubes
ε	Molar Absorptivity
EA	Elemental Analysis
Escherichia coli	*E. coli*
EDS	Energy-Disperse X-Ray Spectroscopy
E-Field	Electromagnetic Field
ELISA	Enzyme-Linked ImmunoSorbent Assay
EPA	Environmental Protection Agency
FRET	Fluorescence Resonance Energy Transfer
FTIR	Fourier Transform Infrared Spectroscopy
FWHM	Full Width at Half Maximum
G	Guanine
ΔG	Gibbs free energy
GC	Gas Chromatography
GSB	Group of Sensors and Biosensors

GTF	Grupo de Tecnologías Fotónicas
HOMO	Highest Occupied Molecular Orbital
HRTEM	High Resolution Transmission Electron Microscopy
HTCC	High Temperature Co-fired Ceramics
I	Transmitted light intensity
I_0	Incident light intensity
ICP	Inductive Coupled Plasma
ICP-AES	Inductively Coupled Plasma Atomic Emission Spectrometry
ICP-MS	Inductive Coupled Plasma Mass Spectrometry
ICP-OES	Inductively Coupled Plasma Optical Emission Spectrometry
IR	Infrared
LC	Liquid Chromatography
LED	Light-emitting diode
LOC	Lab-on-a-chip
LTCC	Low Temperature Co-fired Ceramic
LUMO	Lowest Unoccupied Molecular Orbital
MAA	Mercaptoacetic acid
MB	Magnetic Bead
MCE	Microchip Electrophoresis
MEF	Metal Enhanced Fluorescence
MEMS	Micro Electro Mechanical Systems
MNPs	Metallic Nanoparticles
MOSFET	Metal Oxide Semiconductor Field Effect Transistor
MPA	Mercaptorpopionic acid
MR	Microreactor
MSA	Mercaptosuccinic acid
MUA	11-Mercaptoundecanoic acid
MUD	11-mercapto-1-undecanol
MWNTs	Multi-Wall Nanotubes
μ-TAS	micro Total Analysis System
MUA	Mercaptoundecanoic acid
NA POF	Low Numerical Aperture Polymer Optical Fiber
NMR	Nuclear Magnetic Resonance
NPs	Nanoparticles
NT	1,8-octanedithiol
NTC	Negative Temperature Coefficient
OA	Oleic acid
ODE	Octadecene
OLA	Oleylamine
ONP	Ortho-nitrophenol
ONPG	Ortho-nitrophenyl-β-galactoside
PCB	Printed Circuit Board
PCR	Polymerase Chain Reactions
PDMS	Polydimethylsiloxane
PEG	Poly(ethylene) glycol
PID	Proportional-Integral-Derivative

PMT	Photomultiplier Tube
PTC	Positive Temperature Coefficient
PTFE	Polytetrafluoroethylene
QDs	Quantum dots
QY, Φ_f	Quantum Yield
Rh	Rhodamine 6G
RTD	Resistance Temperature Detector
SAED	Selected Area Electron Diffraction
SEM	Scanning Electron Microscopy
SPP	bis-Sulphonated triphenylphosphine
SPR	Surface Plasmon Resonance
PSP	Pseudo-stationary Phase
SWCT	Single-Wall Nanotubes
TEM	Transmission Electron Microscopy
Tg	Glass-transition temperature
TOAB	Tetraoctylammonium bromide
TOP	Trioctylphosphine
TOPO	Trioctylphosphine oxide
TP	Tiopronin, N-(2-Mercaptopropionyl) glycine
TPP	Triphenylphosphine
RF	Radio Frequency
SAED	Selected Area Electron Diffration
SAXS	Small Angle X-ray Scattering
SCC	Signal Conditioning Circuit
SDS	Sodium dodecylsulfonate
SEM	Scanning Electron Microscopy
SERS	Surface Enhancement Raman Scattering
SIMS	Secondary Ion Mass Spectrsocopy
SPM	Scanning Probe Microscopy
SPR	Surface Plasmon Resonance
T	Thymine
TBP	Tributylphosphine
TEM	Transmission Electron Microscopy
Tg	Glass Transition Temperature
TOAB	Tetraoctylammonium bromide
TOP	Trioctylphosphine
TOPO	Trioctylphosphine oxide
TPP	Triphenylphosphine
PVP	Poly(vinylpyrrolidone)
UAB	Universitat Autònoma de Barcelona
UCPL	Up-Conversion Photoluminiscence
UV	Ultraviolet
Vis	Visible
WHO	World Health Organization
XRD	X-Ray Diffraction

SUMMARY

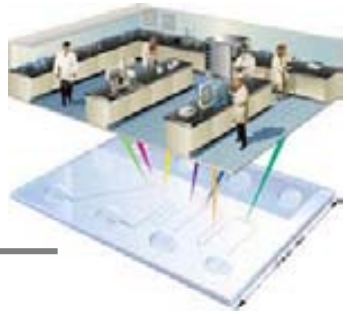

Image from Lab-on-a-chip.gene-quantification.info

Demand for new automated analytical procedures and instrumentation for the continuous monitoring of (bio)chemical parameters, such as those affecting water quality, gathers special importance due to the significant consequences that the use or the consumption of (bio)chemically contaminated water might have. μ- Total Analysis Systems or Lab-On-a-Chip devices are increasingly employed with this purpose owing to the high integration and automation of these devices that allow, through miniaturization, the possibility of performing *in situ* measurements. Besides, the use of nanoparticles with analytical purposes has demonstrated to improve the sensitivity and detection limits of optical methods. Within this general context, the present work is focused on the development of automated analytical microsystems to perform colorimetric or fluorimetric analyses, based on the use of nanoparticles as optical labels, for the rapid detection of water pollutants or organisms, such as heavy metals or bacteria.

However, the use of nanoparticles with identical physical characteristics is a must in order to obtain reliable and reproducible analytical measures. Therefore, the first part of this work is addressed to the development of microreactors for the synthesis of metallic, semiconductor and carbon nanoparticles. Seven different ceramic microreactors are developed, in which the influence of the design (dimensions and configuration of the channels) and the hydrodynamic (flow rates and dosage volumes) parameters have been studied. Moreover, a miniaturized optical detection system has been implemented for the in-line monitoring of the synthesis; and a thermal module has been also developed to reach and accurately control temperatures up to 300 ºC for when required. It is important to highlight that all prototypes operate automatically, which simplifies the syntheses and improves the reproducibility of the obtained nanoparticles.

The second part focuses on the development of analytical microsystems based on the use of the nanoparticles previously synthesized for water quality analysis. Two different prototypes have been constructed and tested. The first described allows the monitoring of mercuric ion in water. The system is based on the selective recognition of the analyte by an ionophore (a thiourea derivative), attached onto gold nanoparticles surface. The metal-ionophore interaction generates a change on the surface plasmon resonance band of the nanoparticles, resulting in a quantifiable optical signal, which is in-line registered by a miniaturized optical detection system integrated in the microfluidic platform. Once optimized, the device is capable to automatically detect up to 11 ppb of mercuric ion. Finally, and as a first approximation to the use of fluorescent nanoparticles within microsystems, a prototype for the determination of *Escherichia coli* in water has been developed, which uses the β-galactosidase enzyme as label. This change responds to the necessity of improving the miniaturized optical system (while maintaining its portability and

low cost) due to the low sensitivity observed when fluorescent nanoparticles were used as labels, which at the moment is not feasible. An oligonucleotide sandwich assay is performed in the microfluidic system based on the use of a specific oligonucleotide of the pathogen as target. On the other hand, magnetic beads are employed as substrate support of the assay, which allow simplifying and improving the different steps of the procedure, while the enzyme used as probe label generates a coloured product (o-nitrophenol) with the addition of the substrate, which is registered through the miniaturized optical system implemented. Once optimized, the device can detect up to 1 ppb of the target oligonucleotide in only 20 minutes.

The presented results demonstrate the great potential of automated analytical microsystems based on the use of nanoparticles for the monitoring of water quality. Similarly, the suitability of microreactors for the synthesis of nanoparticles has been well proved.

El desarrollo de nuevos procedimientos analíticos e instrumentación automáticos para la monitorización de parámetros (bio)químicos, tales como los que afectan a la calidad del agua, es de especial importancia debido a las graves consecuencias que puede tener el uso o consumo de un agua (bio)químicamente contaminada. Los microsistemas de análisis total o dispositivos *Lab-On-a-Chip* son cada vez más empleados con este propósito debido a la gran integración y automatización que ofrecen estos dispositivos, a través de la miniaturización, y a la posibilidad de realizar medidas *in situ*. Por otro lado, el uso de nanopartículas con fines analíticos ha demostrado mejorar la sensibilidad y límites de detección de métodos ópticos. Así, esta tesis se centra en el desarrollo de microsistemas analíticos automatizados que llevan a cabo análisis colorimétricos o fluorimétricos, basados en el uso de nanopartículas como marcadores ópticos, para la rápida detección de analitos o microorganismos de contaminación hídrica, tales como metales pesados o bacterias.

Sin embargo, es necesario utilizar nanopartículas con idénticas características físicas para obtener medidas analíticas fiables. Así, la primera parte de este trabajo abarca el desarrollo de microreactores para la síntesis controlada y reproducible de nanopartículas metálicas, semiconductoras y de carbono. Se muestran un total de siete microreactores, en los que se ha realizado un estudio de los parámetros de diseño e hidrodinámicos. Además, se ha implementado un sistema de detección óptica miniaturizado para la monitorización en línea de la síntesis; y se ha desarrollado un módulo térmico que permite alcanzar y controlar temperaturas de hasta 300 ºC para aquellas reacciones que lo requieran. Es de destacar que los microsistemas trabajan de forma automática y programable, lo cual simplifica el procedimiento de síntesis y mejora la reproducibilidad de las nanopartículas obtenidas.

La segunda parte del trabajo se centra en el desarrollo de microsistemas analíticos basados en la utilización de las nanopartículas sintetizadas para el análisis de algún parámetro de la calidad del agua. Se han construido y evaluado dos prototipos. El primero de ellos está diseñado para la monitorización de ión mercurio en agua. El sistema se basa en el reconocimiento selectivo del analito mediante un ionóforo (un derivado de la tiourea) unido a la superficie de nanopartículas de oro. La interacción metal-ionóforo provoca un cambio en la banda del plasmón superficial de las nanopartículas, generando una señal óptica cuantificable que se registra en línea mediante un sistema óptico integrado en la plataforma microfluídica. Una vez optimizado, el dispositivo es capaz de detectar hasta 11 ppb de mercurio(II). Finalmente, y como primera aproximación al uso de nanopartículas fluorescentes en microsistemas, se ha desarrollado un prototipo para la determinación de *Escherichia coli* en agua utilizando como marcador la enzima β-galactosidasa. Este cambio responde a la necesidad de mejorar el sistema óptico miniaturizado (manteniendo su portabilidad y bajo coste), debido a la baja sensibilidad observada cuando nanopartículas

fluorescentes fueron usadas como marcadores. El dispositivo desarrollado lleva a cabo un ensayo tipo sándwich de oligonucleótidos, dónde se emplea como sonda diana un oligonucleótido específico del patógeno. El uso de micropartículas magnéticas como sustrato soporte del ensayo permite simplificar y mejorar las distintas etapas del análisis, mientras que el enzima usado como marcador de la sonda de reconocimiento genera un producto coloreado al añadir el sustrato, registrado mediante el sistema óptico miniaturizado implementado. Tras su optimización, es posible detectar 1 ppb de la sonda diana en 20 minutos.

Los resultados presentados en este trabajo muestran el gran potencial de los microsistemas analíticos automatizados basados en el uso de nanopartículas para monitorizar la calidad del agua. Se ha demostrado también la idoneidad de los microreactores para la síntesis de nanopartículas.

INTRODUCTION

Contents

Image from Lab-on-a-chip journal

The constant demand to obtain real time information and the current strict regulations for environment, food and, generally, the quality control of products, make necessary the improvement of analytical instrumentation. Specifically, water quality determination gathers special importance due to the consequences that may have the use or consumption of contaminated water. For instance, the drinking of water which contain elevated concentrations of heavy metals can lead to the development of neurological, reproductive or cardiovascular diseases, among other disorders. On the other hand, the presence of viruses or pathogens can produce diarrhoea diseases, which can generate even to the death of the patient, when this water is used for its consumption or even only employed for recreational purposes. Therefore, the development of efficient and portable analysis systems for water quality determination is of special interest, since the classical methods employed are time-consuming and require qualified personnel, among other minor inconveniences. As a result, a great interest on this matter has arisen and huge efforts have been done in recent years to develop robust and efficient analytical instrumentation, capable to perform simple, rapid and reproducible analyses. [1]

For this purpose, the so called Total Analysis Systems (TAS) appeared with the aim of simplifying and automating the analytical process, namely sampling, sample transport, separation, reaction, transduction and signal acquisition. These systems endow connectivity and automation to the different steps of the analytical process, minimizing the operator intervention. In this way, both the costs and the analysis time of the whole process can be reduced as well as possible mistakes due to human manipulation are avoid. However, even these systems present some limitations, such as reduced portability and high reagents consumption. Miniaturization and integration seem to overcome these drawbacks, thus emerging the well-known *micro-Total Analysis Systems* (μ-TAS) or *Lab-on-a-Chip* (LOC).[2-3] Their reduced size and weight makes possible to minimize the energy consumption, making feasible to perform *in situ* measurements. Moreover, by volume miniaturization, the amount of required reagents and therefore also the generation of wastes are reduced, making these systems greener than the conventional ones. Furthermore, they can determine different components of a sample in the same analysis when multiplexing approaches are used. All this contributes to minimize the total cost of the analysis,

[1] Alegret, S.; in: *Integrated Analytical Systems*, Elsevier, Amsterdam, **2003,** 1-36.
[2] Manz, A.; Graber, N.; Widmer, H.M.*; Sens. Actuators, B*, **1990**, 1, 244.
[3] Van den Berg, A.; Bergveld, P.; *Lab Chip,* **2006,** 6, 1266.

allowing the development of customized systems for personal *in situ* diagnosis (point-of-care diagnosis) or the direct on-site monitoring of environmental parameters.

Besides miniaturization and automation, analytical instrumentation can also take advantage of the exceptional physicochemical properties of nanostructured materials in order to enhance the sensitivity, selectivity, specificity and rapidity of analytical methods by using simple strategies. [4] Nanomaterials are characterized for their large surface area-to-volume ratio, which have demonstrated great potential in all analytical separation techniques, by improving the selectivity, stability and efficiency of the separation. In the same manner, this property is specially interesting when nanomaterials are used as a substrate support for sensing schemes, since multiple molecules can be attached to each nanostructure, which can simplify the assay design and increase sensitivity.[5] Nanomaterials offer the possibility of detecting or manipulating atoms and molecules, such as when used in Surface-Enhanced Raman Spectroscopy (SERS) applications, and have great potential in the development of miniaturized analytical systems, when they are intended to be used for detection purposes. In concrete, the use of as well the electrochemical as the optical properties of some nanoparticles is of special interest, since they have shown enhanced sensitivity and low detection limits compared with some conventional analytical methods.[6] Moreover, the use of metallic or fluorescent nanoparticles as optical detection labels can provides some advantages regarding the use of dyes or fluorophores, such as higher photostability and quantum yields.[7] These materials have also given rise to the development of new types of analytical tools, such as bioimaging, which is very interesting and useful in medical and biochemical applications. [8]

The present thesis is addressed to achieve improved analytical instrumentation taking advantage from miniaturization and automation of analysis systems and also from the use of nanomaterials as optical labels to perform colorimetric and fluorimetric determinations.

For this purpose, the use of nanomaterials with the same physicochemical properties is essential in order to obtain confident and reproducible results. As it is well known, properties of nanostructured materials, and more concretely nanoparticles, are directly related to their composition, size and morphology, which depend on the followed synthetic procedure, and some related variables, such as the temperature reaction and the molar relationship of reagents.[7] Conventional synthetic methods are the most employed procedures for

[4] Zhang, X., Guo, Q., Cui, D., 2009. Sensors 9, 1033-1053.
[5] Kumar, C.S.S.R., 2007. Nanomaterials for biosensors. Vch Verlagsgesellschaft Mbh.
[6] Valcárcel, M.; Simonet, B.M.; *Anal. Bioanal Chem.,* **2011**, 399, 1.
[7] Cao, G.; Wang, Y.; in: *Nanostructures and Nanomaterials. Synthesis, Properties, and Applications*; World Scientific Publishing Co. Pte. Ltd. 2on edition, **2011.**
[8] Wu, C.-S.; Liu, F.-K.; Ko, F.-H.; *Anal. Bioanal Chem.,* **2011**, 399, 103.

nanomaterials synthesis because a high quantity of product is obtained. However, they are usually time-consuming and limited in some aspects, including a poor control of the reagents concentration in the whole of the solution, and the difficulty of managing the local temperature. As a consequence, heterogeneous products are often obtained within a batch synthesis or even more worse between different batches.

Process intensification, which appeared as a strategy for reducing the size of chemical plants so as to reach a given production objective, can help in this issue. It is focused on the development of novel devices to improve a manufacturing process, decreasing the required equipment or their size, energy consumption, or waste production.[9] These strategies are directly related with miniaturization and microfluidics. The main idea in the field of synthesis is to take advantage of the large surface area-to-volume ratios within microchannel structures to accelerate heat and mass transport during a synthetic process. [10] For nanomaterials synthesis in concrete, the rapid changes that can be performed in reaction temperatures and concentrations enables obtaining more uniform products in terms of size and improved reaction yields. In this sense, part of the work presented in this thesis is focused on the development of microfluidic platforms to synthesize homogeneous nanoparticles, which are intended to be exploited in μ-TAS.

Figure 1.1 outlines the multidisciplinary nature of the research that has been carried out and the area in which the thesis is framed. Taking this into account, the introduction section of this manuscript is organized in three main parts. The first one is addressed to the miniaturization of analytical systems, including basic concepts about microfluidics and microfabrication techniques. Then, some types of nanomaterials for analytical purposes are described, together with their synthetic methods and the different possible characterization techniques. Finally, the state-of-the-art to μ-TAS based on nanomaterials and also to microreactors for their synthesis of nanomaterials is reported.

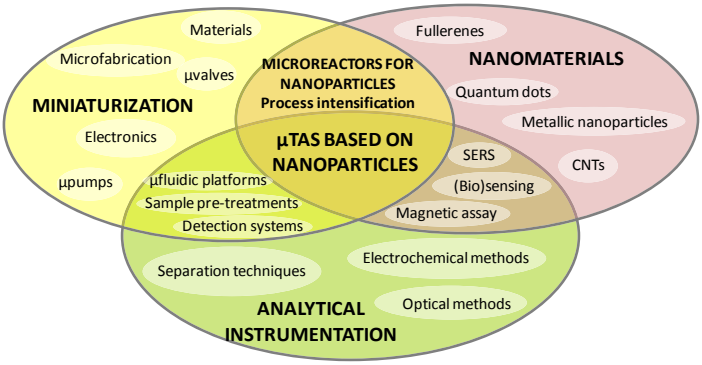

Figure 1.1: Scheme of the different related fields for the development of μ-TAS based on the use of nanomaterials.

[9] Ramshaw, C.; *Proceedings, 1st Intl. Conf. Proc. Intensif. for Chem. Ind.*, **1995**, *18*, 1.
[10] Stankiewicz, A. I.; Moulijn, J.A.; *Chem. Eng. Prog.*, **2000,** January, 22.

1.1 MINIATURIZATION OF ANALYTICAL SYSTEMS

Classical chemical analyses are usually performed in laboratories and involve sophisticated and expensive instruments, which require specialized personnel for their operation. Nowadays, an increasing demand of rapid, efficient and exact chemical information exists in order to control the quality of products, to monitor environmental contaminants or the results of a medical care. The development of miniaturized analytical systems becomes a key issue, since these devices are capable to provide *in situ* qualitative and quantitative information about the composition and nature of a sample in real time at a relative low cost.

Besides portability, integration and reduced energy consume, μ-TAS or LOC devices are characterized for their capability to process larger number of samples with limited errors and rapidness due to the lesser manual intervention than conventional instrumentation. Moreover, scaling down increases the surface area to volume ratio, which is very useful for a quick and efficient heat and mass transfer through the microfluidic system, resulting in systems of higher analysis throughput. In addition, miniaturized systems are usually fabricated by means of mass production techniques, which leads to decrease the manufacturing costs and encourage their marketing.

1.1.1 MICROFLUIDIC PLATFORMS

Microfluidic platforms are essential in the development of μ-TAS. They are structures that provide connectivity to the different operations of the chemical analysis such as reagents storage, pre-concentration steps or detection, and, on the other hand, that allow handling of fluids. Transport of fluids, mixing, separating and processing inside the microfluidic platform are performed by means of different fluidic structures by taking advantage of passive fluid control techniques like capillary forces,[11] or using external actuators such as centrifugal forces in rotary drives,[12] or by active (micro) components as (micro)pumps or (micro)valves.[13]

Rapid mixing is essential in chemical applications. However, this is difficult to achieve at laminar flows, where mass transport is mainly done by diffusion. Reynolds number, which quantifies the relative importance of the inertial and viscous forces, is the parameter normally used to characterize the different flow regimes, such as laminar or turbulent flows. The first is usually the dominant flow regime in microfluidics, which is characterized by a slow movement of the liquid

[11] Lynn, N. S.; Dandy, D.S.; *Lab Chip*, **2009,** 9(23), 3422.
[12] Ducrée, J.; Haeberle, S.; Lutz, S.; Pausch, S.; von Stetten, F.; Zengerle, R.; *J. Micromech. Microeng.*, **2007,** 17, S103.
[13] Gravesen, P.; Branebjerg, J.; Jensen, O.S.; *J. Micromech. Microeng.,* **1993**, 3, 168.

(low Reynolds numbers). The second is dominated by inertial forces and it is defined by flow instabilities as vortices (high Reynolds numbers).[14] The incorporation of passive or active mixers into the microfluidic platform plays major importance, since these structures enhance the grade of reagents mixture by generating turbulent regimes.[15]

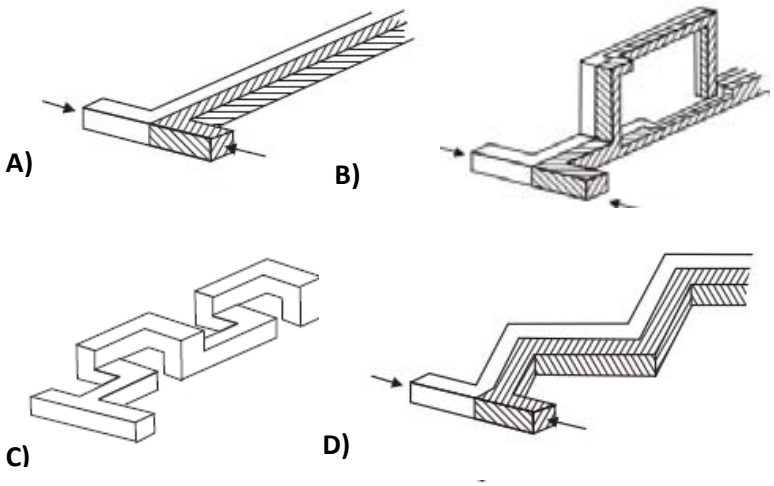

Figure 1.2: Most common passive micromixers. A) Basic T-shape mixer (parallel lamination). B) Join–split–join mixer (serial lamination). C) L-shape passive micromixer for mixing with chaotic advection. D) Zig-zag-shaped planar channel (chaotic advection).[15-16]

Active mixers take advantage of some kind of power source or mobile parts to induce a disturbance in the flow. Therefore, these mixers can be classified by the type of external disturber such as pressure or temperature, among others.[16] Active mixers are usually very efficient. Nevertheless, their use involves complex setups and external power sources, which difficult their implementation.

Conversely, passive mixers do not require any external power source, since they are based on the use of different geometries to achieve the mixture of reagents. On the one hand, they can increase the contact surface between the two phases or reagents to mix and decrease the diffusion path between them, which improves molecular diffusion, such as in case of parallel and serial lamination (Figure 1.2 A and B). On the other hand, passive micromixers can promote chaotic advection by manipulating the laminar flow in microchannels through special geometries, which short the diffusion path and thus improves mixing (Figure 1.2 C and D). Another alternative to reduce the mixing path is to form droplets of the mixed liquids, where the movement of the droplet causes an internal flow and achieves mixing inside the droplet.[17-18] Micromixers based on chaotic advection with three-dimensional structures are probably the more efficient passive mixers, stable in operation and easily integrated in complex systems. Therefore, they are often used for μ-TAS developments.

[14] Nguyen, N.-T.; Wu, Z.; *J. Micromech. Microeng.*, **2005**, 15, R1.
[15] Mansur, E.A.; Mingxing, Y.E.; Yundong, W.; Youyuan, D.; *Chinese J. Chem. Eng.,* **2008**, 16(4), 503.
[16] Petersson, F.; Nilsson, A.; Jonsson, H.; Laurell, T.*; Anal. Chem.,* **2005,** 77, 1216.
[17] Aref, H.; *Phys. Fluids*, **2002**, 14, 1315.
[18] Dertinger, S.K.W.; Chiu, D.T.; Jeon, N.L.; Whitesides, G.M.*; Anal. Chem.,* **2001,** 73, 1240.

A mixing technique related to parallel lamination is the so called hydrodynamic focusing. The most common configuration is a 3-inlet microchannels device, where the middle inlet is left for one flow (e.g. sample flow) while the side streams (solvent flow) work as sheath flows, reshaping the central one downstream (Figure 1.3). [19] In this way, the mixing path is reduced, since a very thin width central stream can be achieved. Moreover, the focused sheet can be deformed and moved out of the symmetry plane by changing flow rates of the side streams. This technique has been widely used in microfluidic applications to reduce mixing time.

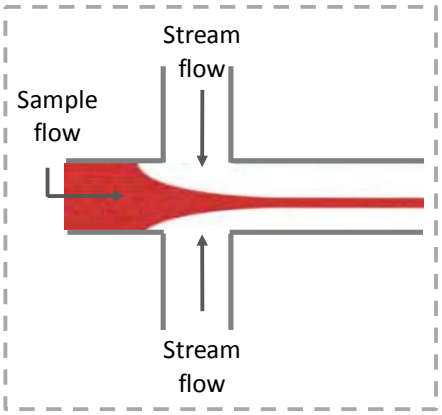

Figure 1.3: Schematic view of hydrodynamic focusing in a four-channel intersection.[20]

1.1.2 INTEGRATING OPERATIONS OF THE ANALYTICAL PROCESS IN MICROSYSTEMS

The development of μ-TAS entails the miniaturization and integration of sampling, transport, treatment, separation, reaction, detection and signal treatment and interpretation into a microfluidic platform.[20] Therefore, they should ideally incorporate microsensors, electronic components for the control and acquisition of signals, and microactuators for temperature or flow rate variations. Although the development of μ-TAS entails the miniaturization and integration of a complete analytical procedure and their required components, it is usual to find hybrid devices, since the miniaturization of some elements such as pumps or valves for the management of fluids, or some pre-treatment components and detection systems is still a challenge. [21]

Sample pre-treatment and detection systems are important operations to incorporate. The firsts include all the steps required for enabling the adaptation of the sample to the selected analytical method; while the seconds allows the determination of the desired analyte in the sample.

1.1.2.1 SAMPLE PRE-TREATMENT

Sample pre-treatment, namely derivatization, analyte separation and pre-concentration, have been integrated in microfluidic platforms.

---

[19] Dziubinski, M.; in: *Hydrodynamic Focusing in Microfluidic Devices, Advances in Microfluidics*; Dr. Ryan Kelly (Ed.), **2012**, ISBN: 978-953-51-0106-2, InTech.
[20] Martínez-Cisneros, C.S.; *Microsistemas analíticos basados en la tecnología LTCC*. Tesis Doctoral, UAB, Bellaterra, España**, 2010.**
[21] Suzuki, H.; Yoneyama, R.; *Sens. Actuators, B*, **2003**, 96, 38.

Derivatization operations such as labelling or complexation are performed by the use of auxiliary channels connecting the sample into specific areas, structures or mixers previous to analyte detection.[22]

On the other hand, the introduction of separation techniques in microfluidic systems has provide great advantages, since these approaches allow increasing sensitivity by pre-concentration of the sample or the selectivity by eliminating interferences from the matrix. With this aim, the introduction of adsorbent materials for solid phase extraction inside microfluidic structures has been used, despite the fact that the pre-concentration area/zone is often filled after the fabrication of the microfluidic platform.[23] Other approaches such as filtration, or precipitation can be also used to eliminate interferences of the sample.

Other sample pre-treatment procedures consist on heating or cooling. As well heating/cooling as temperature control has been integrated into microfluidic platforms. Some approaches are based on air or liquid cycles,[24] or integrated resistances fabricated by screen-printed techniques, which usually involve electronic instrumentation.[25] Regarding sensors for temperature control, examples of thermocouples or embedded thermistors can be also found in the literature.[26] In these fields, a monolithic integration of the thermoactuator and the microfluidic platform is usually preferred, because it confers better temperature control than modular approaches.

1.1.2.2 DETECTION SYSTEMS

Detection systems are responsible for identification and quantification of the analyte. The Group of Sensors and Biosensors (GSB) has a wealth of experience in the development of different microfluidic devices incorporating electrochemical (potentiometric[27] and voltammetric[28]) and optical (absorbance,[29] fluorescence[30] and chemioluminiscence[31]) detection systems. Electrochemical methods are easily integrated in microfluidic systems and provide high sensitivity. However,

---

[22] Chen , D.; Mauk, M.; Qiu, X.; Liu, C.; Kim, J.; Ramprasad, S.; Ongagna, S.; Abrams, W.R.; Malamud, D.; Corstjens, P.L.A.M.; Bau, H.H.; *Biomed. Microdevices*, **2010**, 12, 705.

[23] Fang, Z.L.; in: *Flow-Injection Separation and Preconcentration;* VCH, Weinheim, **1993**.

[24] Wittwer, C.T.; Garling, D.J.; *BioTechniques,* **1991**, 10, 76.

[25] Hsueh, Y. -T; Smith, R. L; Northrup, M. A; *Proc. 8th Int. Conf. Solid State Sensors Actuators (Transducers '95)*, **1995**, 768.

[26] Liu, J.; Lu, Y.; *J. Am. Chem. Soc.,* **2003,** 125, 6642.

[27] Martinez-Cisneros, C.S.; Ibañez-García, N.; Valdés, F.; Alonso, J.; *Anal. Chem.,* **2007**, 79(21), 8376.

[28] Martínez-Cisneros, S.C.; Da Rocha, Z.M.; Ferreira, M.; Valdés F.; Seabra, A.; Góngora-Rubio, M.; Alonso, J.; *Anal. Chem.,* **2009**, 81, 7448.

[29] Puyol, M.; Villuendas, F.; Domínguez, C.; Cadarso, V.; Llobera, A.; Salinas, I.; Garcés, I.; Alonso, J.; in: *Absorbance-based integrated optical sensors;* Springer Series on Chemical Sensors and Biosensors. Vol. 3 *Frontiers in Optical Sensing: Novel Principles and Techniques*, Ed. Springer-Verlag Berlin Heidelberg, **2005,** 1-44.

[30] Rivera, L.; Izquierdo, D.; Garcés, I.; Salinas, I.; Alonso, J.; Puyol, M.; *Sens. Actuators, B,* **2009**, 137, 2, 420.

[31] Ibanez-Garcia, N.; Puyol, M.; Azevedo, C. M.; Martinez-Cisneros, C. S.; Villuendas, F.; Gongora-Rubio, M. R.; Seabra, A. C.; Alonso, J.; *Anal. Chem*., **2008**, 80, 14, 5320.

bulky instruments must be connected to the integrated electrodes, which hinders the main idea of miniaturization, and usually present electrical interferences. Optical methods are usually simpler, easier to implement in microsystems and, especially fluorescence, highly sensitive. They are very common in classical chemical methods, and a large number of reference methods are based on optical measurements.

Indirect measurements based on the use of optical labels or indicators to detect and quantify the analyte are the preferred strategies and it is even possible to perform multiparameter analysis when different labels are used in the same analysis. Fluorescent labels are of special interest due to the high sensitivity of the technique and the possibility to improve selectivity, since one can discriminate between two wavelengths (excitation/emission). Moreover, few molecules show fluorescence, which considerably reduces any possible matrix interference.

The components of an optical system are basically a radiation source capable of emitting a beam of light at the wavelength where the analyte or even the label absorb (in case of polychromatic light sources, wavelength selectors are required), and a detector capable to detect the changes in the signal derived from the interaction of the analyte/label and radiation. In case of fluorescence, optical filters are also required in order to eliminate light from the excitation source and thus enhance fluorescence sensitivity. Due to the advances in optoelectronics, it is easy to find cheap commercial miniaturized optical components such as LEDs, laser diodes, photodiodes, filters or phototransistors, a fact that allowed the implementation of optical systems in μ-TAS. Although laser diodes offer the possibility of working in a range from the ultraviolet to far infrared, LEDs, which emit from the visible to the medium infrared spectrum, are more commonly used due to their lower price and robustness. Photodiodes are the usual detectors integrated in μ-TAS,[32-33] since they are simpler and cheaper than phototransistors, photoresistors or photomultipliers.

Despite all these features, certain limitations appear when miniaturizing optical systems. Sensitivity is compromised due to the reduction of the optical path lengths, which sometimes must be taken into account when designing optical cells in the microsystem, and more sensitive detectors as photomultipliers are required. Other limitations are related to sample matrix because turbidity can disturb the transmitted light. This issue can be overcome by coupling a simple turbidity measurement system with another light source employed as a signal reference.

---

[32] O'Toole, M.; Diamond, D.; *Sensors,* **2008**, 2453.
[33] Rocha, F.R.P.; Reis, B.F.; *Anal. Chim. Acta*, **2000,** 409(1-2), 227.

1.1.3 MATERIALS AND MICROFABRICATION METHODS

The proper selection of the microfluidic platform substrate is crucial in order to integrate all the required operations, and it is closely related to its final application. In this sense, some characteristics such us the possibility of integrating electronic components, the intrinsic properties of the materials (transparency, chemical stability, biocompatibility, flexibility or roughness), and prototyping simplicity must be taken into account. Besides, other considerations for their future market launch such as cost and mass production possibility are to be assessed.

An overview of the most commonly used materials and associated technologies is given in the future section.

1.1.3.1 SILICON TECHNOLOGY

As it can be observed for the number of publications, silicon is the most commonly used material for μ-TAS or Lab-on-a-Chip development. This responds to the well established associated technology and the extensive knowledge of its physical and chemical properties.[34-35] Silicon has also gained importance in the miniaturization field, since it is an economic and abundant material that can be obtained and processed in a controlled way. Moreover, it permits the integration of electronic components and imprinted patterns, and very complex small structures can be accurately fabricated in mass.

Silicon mechanization can be performed in surface or volume through different processes, such as photolithography, wet and dry etching. In surface mechanization elements are defined on layers deposited or grown on the substrate with the aid of sacrificial layers. In volume micromachining cavities are defined within the silicon wafer, sometimes crossing the entire wafer. In some cases it is necessary the sealing of the different mechanized silicon wafers, which can be performed by anodic bonding with glass, pressure[36] or adhesive layers.[37] Figure 1.4 shows an example of a microfluidic silicon/glass device constructed with the described technology.

Silicon technology requires the use of clean rooms and skilled professionals, and becomes a costly technique for prototyping purposes and therefore, it presents important limitations for research. However, silicon technology is widespread in the microelectronic field, since it is the material substrate for integrated electronic circuits and has been used in the development of passive electronic components,[38] microfluidic systems[39] or Micro Electro Mechanical Systems

[34] Bustillo, J.M.; Howe, R.T.; Muller, R.S.; *Proc. IEEE*, **1998,** 86, 1552.
[35] Kovacs, G.T.A.; Maluf, N.I.; Petersen, K.E.; *Proc IEEE,* **1998,** 86, 1536.
[36] Gong, S.C.; *Sens. Mater.,* **2004,** 16(3), 119.
[37] Kim, J.-M.; Oh, D.H.; Yoon, J.; Cho, S.; Kim, N.; Cho, J.; Kwon, Y.; Cheon, C.; Kim, Y.-K.; *J. Micromech. Microeng*., **2005,** 15(11), N11.
[38] Zhang, J.; Hon, W.C.; Leung, L.L.W.; Chen, K.J.*; J. Micromech. Microeng*., **2005,** 15, 328.

(MEMS).[40] Other silicon based devices are integrated optic systems, which are composed of all silicon-made refractive lenses, optical waveguides and diodes attached to polymeric or glass microfluidic platforms.[41]

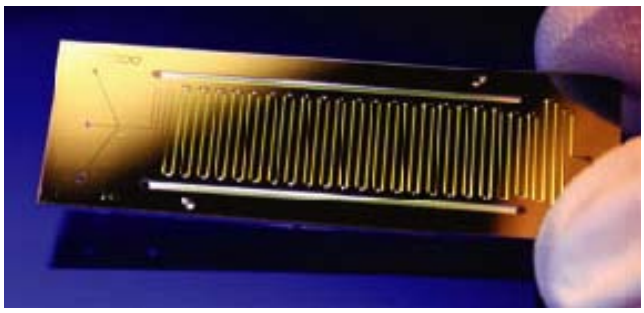

Figure 1.4: Glass-silicon chip, from *Micronit*.

1.1.3.2 POLYMERS TECHNOLOGY

The use of polymers has increased in recent years due to their low cost and their associated simple fabrication processes, which enable prototyping in shorter time than silicon. Polymers are macromolecular substances consisting of more than 1000 repeated structural units (monomers) synthesized through a process of polymerization, which is induced by initiators or an external physical parameter. In this process, the glass transition temperature (Tg) of the material plays an important role, since it enables its structuring by solidifying or becoming softer below or above this temperature. Polymers usually contain other compounds, such as filling elements (mica, talc, calcium carbonate), plasticizers, or temperature or UV radiation stabilizers. Thus, the derived diverse polymeric compounds, commonly called plastics, exhibit different optical, chemical and thermal properties.

One of the possible classifications of polymers depending on how they are linked (chemical bonds or intermolecular forces) and on the arrangement of the different chains that forms the polymer is themoplastics, elastomerics or duroplastics. [42] The firsts consist of chains of weakly attached molecules that can be modelled at temperatures above their Tg before they are cooled again. Elastomeric polymers are composed of weakly cross linked chains, and can be deformed using an external force and coming back to its initial state. Finally, duroplastic polymers are composed of strongly cross linked chains, which results in hard and fragile materials. The selection of the polymeric material to be employed for μ-TAS development will mainly depend on the chemical resistivity of the polymer, as well as its biocompatibility and transparency.

---

[39] Pal, P.; Sato, K.; *J. Micromech. Microeng*., **2009,** 19, 1.
[40] Wang, F.; Li, X.X.; Guo, N.X.; Wang, Y.L.; Feng, S.L.*; J. Micromech. Microeng.,* **2006,** 16(7), 1215.
[41] Cleary, A.; Glidle, A.; Laybourn, P.J.R.; *Appl. Phys. Lett*., **2007**, 91, 071123.
[42] Becker, H.; Gartner, C.; *Electrophoresis*, **2000,** 21(1), 12.

Polymeric platforms can be fabricated by diverse techniques, which include hot embossing,[43] injection molding,[44] laser photoablation[45] and soft lithography,[46] among others, for pattering the substrate. Once the substrate is mechanized, the different polymeric layers are linked by lamination,[47] thermo-compression,[48] laser welding,[49] plasma oxidation[50] or by means of adhesives.[51] Since the fabrication technology is based on a multilayer approach, one of the main advantages of these materials is the simple fabrication of complex structures, such as three-dimensional micromixers. Figure 1.5 shows an example of a microfluidic platform based on COC polymeric substrate. Nevertheless, delamination of the layers is still a handicap in order to avoid liquid leakage. Moreover, the difficult integration of electronic components limits the use of these materials in some applications such as the development of electrochemical devices.

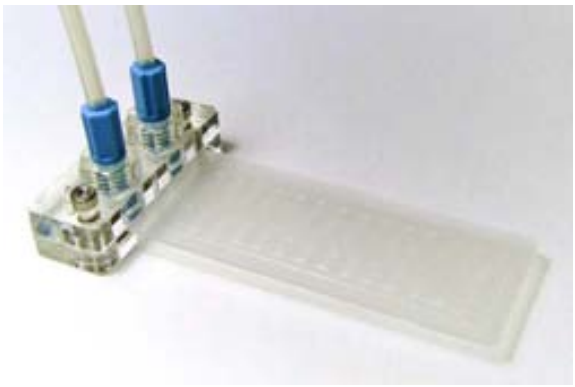

Figure 1.5: Plastic microfluidic chip, from *Microflexis*.

▪ CYCLIC OLEFIN COPOLYMER (COC)

Cyclic Olefin Copolymer (COC) consists of amorphous, transparent copolymers based on cyclic and linear olefins. It is a thermoplastic material that exhibits a unique combination of properties, which can be customized by the modification of the chemical structure of the copolymer. Performance benefits include low density, high transparency, variable heat deflection temperature up to 170 °C, excellent biocompatibility, good resistance to acid and alkali, good electrical insulating properties, good melt processability/flowability, and high rigidity,

[43] Soper, S.A.; Ford, S.M.; Qi, S.; McCarley, R.L.; Kelly, K.; Murphy, M.C.; *Anal. Chem.,* **2000,** 72, 624.
[44] Mekaru, H.; Yamada, T.; Yan, S.; Hattori, T.; *Microsyst. Technol.,* **2004,** 10, 682.
[45] Nayak, N.C.; Lam, Y.C.; Yue, C.Y.; Sinha, A.T.; *J. Micromech. Microeng.*, **2008**, 18, 1.
[46] McDonald, J.C.; Duffy, D.C.; Anderson, J.R.; Chiu, D.T.: Wu. H.; Schueller, O.J.; Whitesides, G.M.; *Electrophoresis*, **2000**, 21, 27.
[47] Soane, D.S.; Soane, Z.M.; Hooper, H.H.; Alonso-Amigo, M.G.; International Patent Application WO 98/45693.
[48] Paulus, A.; Williams, S.J.; Sassi, A.P.; Kao, P.H.; Tan, H.; Hooper, H.H.; *Proc. SPIE 3515*, Microfluidic Devices and Systems, **1998,** 94, 3515.
[49] Malek, C.G.K.; *Anal. Bioanal Chem.,* **2006**, 185, 1362.
[50] Duffy, D.C.; McDonald, J.C.; Schueller, O.J.A.; Whitesides, G.M.; *Anal. Chem.,* **1998**, 70, 4974.
[51] Chen, H.Y.; McClelland, A.A.; Chen, Z.; Lahann, J.; *Anal. Chem.,* **2008**, 80, 4119.

strength and hardness. All this enables the construction of microfluidic platforms for multiple possible applications.

The fact that one can find different COC polymerization degrees offers the possibility of working with materials/layers of different glass transition temperatures (Tg) according to the grade of the product, which simplifies the lamination process. One of the problems related to the construction of μ-TAS with polymers is the obstruction of the microfluidic structures during the sealing process. With COC, some layers of lower Tg can be used as sealing layers while others keep their structure during the lamination process. Therefore, no occlusion of deformation of the microstructures occur.

However, the monolithic integration of electronic components is still a limitation for this material, since this entails a considerable complex design, high cost and a long time fabrication process. Therefore, most of the presented works are based on modular or hybrid systems as an alternative, where the different necessary components are not integrated in a single device.[52-53]

1.1.3.3 LTCC TECHNOLOGY

The LTCC (*Low Temperature Co-fired Ceramics*) technology was originally developed by Hughes and DuPont with military purposes, and it was conceived as a hybrid sharing the advantages of thick film and *High Temperature Co-fired Ceramics* (HTCC) technologies. The term "*low temperature*" is related with the low temperatures required for the sintering process, which takes place at temperatures below 1000 °C; whereas "*co-fired*" refers to the possibility of sintering together screen-printing conductor pastes and the ceramic substrate, since both compounds are completely compatible. From here it follows that the technology enables the integration of other key elements, reducing significantly the total costs of the process.

The LTCC ceramics can be also called as green tapes, since the substrate is manipulated in its green state, when it is malleable and soft. Once sintered, the material turns hard. This is due to their chemical composition, which include a 45 % of alumina (Al_2O_3), a 40 % of silica (SiO_2) and a 15 % of organic components. These last organic compounds include plasticizers, which provides flexibility to the layers; an agglutinative agent or binder, which fix the ceramic particles; and solvents, which helps to solvate all the different organic additives, provides an adequate viscosity and aids to disperse the ceramic particles.[54]

The LTCC technology is compatible with screen-printing techniques (*thick-film* technology), allowing the deposition of conductive pastes, which makes feasible the integration of electronic components. However, the pastes must be

[52] Becker, H.; Locascio, L.E.*; Talanta,* **2002,** 56(2), 267.
[53] Pfohl, T.; Mugele, F.; Seemann, R.; Herminghaus, S.; *Chem. Phys. Chem.*, **2003,** 4(12), 1291.
[54] Luo, X.J.; Zhang, B.L.; Li1, W.L.; Zhuang, H.R.; *J. Mater. Sci.,* **2004**, 39, 4387.

compatible with the sintering process. The technology is simple, does not require the use of clean rooms or specific personnel, and the implementation of mass production at low costs is feasible.

Ceramic devices are fabricated by using a multilayer approach. During the procedure, the different LTCC layers are mechanized, conductive tracks are screen-printed into the necessary layers, and a lamination process is done before sintering the ceramic block. Is in this last step, where silica particles are melted and surrounds the alumina particles by capillarity, resulting in a rigid structure when the device is cooled to room temperature due to glass vitrification. In this process, the ceramic substrate suffers shrinkage. However, following the datasheets provided by the different suppliers this shrinkage is easily predictable and must be taken into account in the designing step.

Then, the technology and its associated materials appear as an alternative methodology for the construction of devices with chemical purposes, providing the possibility of integrating different steps of the analytical process, such as the sample preparation, detection systems (photometric, potentiometric or voltamperometric, among others), pretreatment steps (such as mixers, gas diffusers or preconcentration chambers) and microactuators for flow control (micropumps or microvalves).[55] In this sense, GSB is a pioneer in the development of microfluidic structures with this substrate, which has given rise to many different analytical microsystems.[27-28,31] Autonomous devices can be feasible obtained, which could detect different analytes as well as acquire and process the received signals. An example of a ceramic μ-TAS is presented in figure 1.6, where fluidics and electronics have been monolithically integrated in a single device.[27]

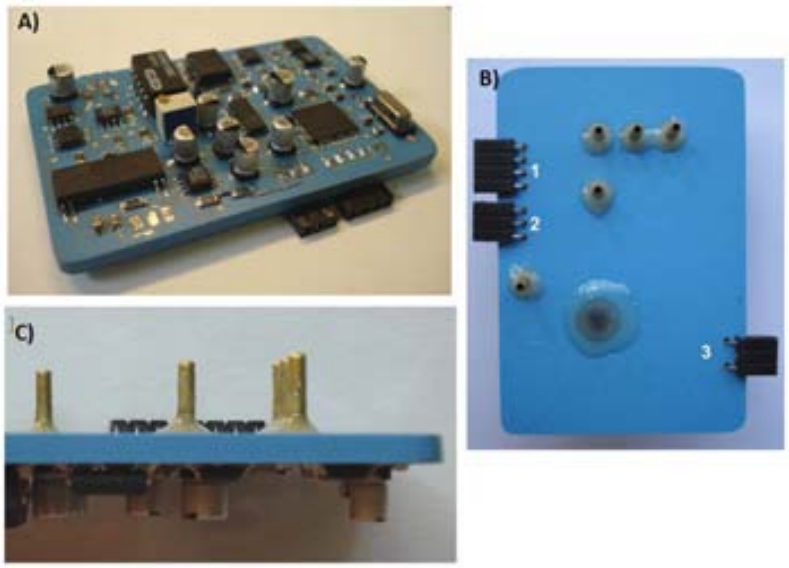

Figure 1.6: Ceramic microfluidic chip for potentiometric measurements, which integrates the fluidics and electronics in a single device. **A)** Bottom view of the monolithic with the electronics for data acquisition and digital signal processing. **B)** Top view of the microanalyzer. Fluidics and the detection system are integrated on this side. **C)** Lateral view of the device. [27]

[55] Gongora-Rubio, M.; Sola-Laguna, L.M.; Moffett, P.J.; Santiago Aviles, J.J.; *Sens. Actuators, A*, **1999,** 73, 215.

1.2 NANOTECHNOLGY AND ANALYTICAL CHEMISTRY

Nanotechnology has emerged in recent years as a key development technology in different fields, where it has decisive economic, ecological and social impact. Its most accepted definition is the understanding and development of matter at nanoscale. This involves not only the study, design, synthesis, manipulation and application of nanomaterials, apparatus and functional systems; but also taking advantage of the physicochemical properties of nanomaterials at the nanoscale.[7,56] The term nano refers to the size, and comes from the Greek word *nanos,* which means dwarf, and designates a billionth fraction of a unit. Nanosize generally deals from 1 to 100 nanometers (Figure 1.7). Therefore, nanotechnology studies materials, which are between atoms or molecules and bulk materials.

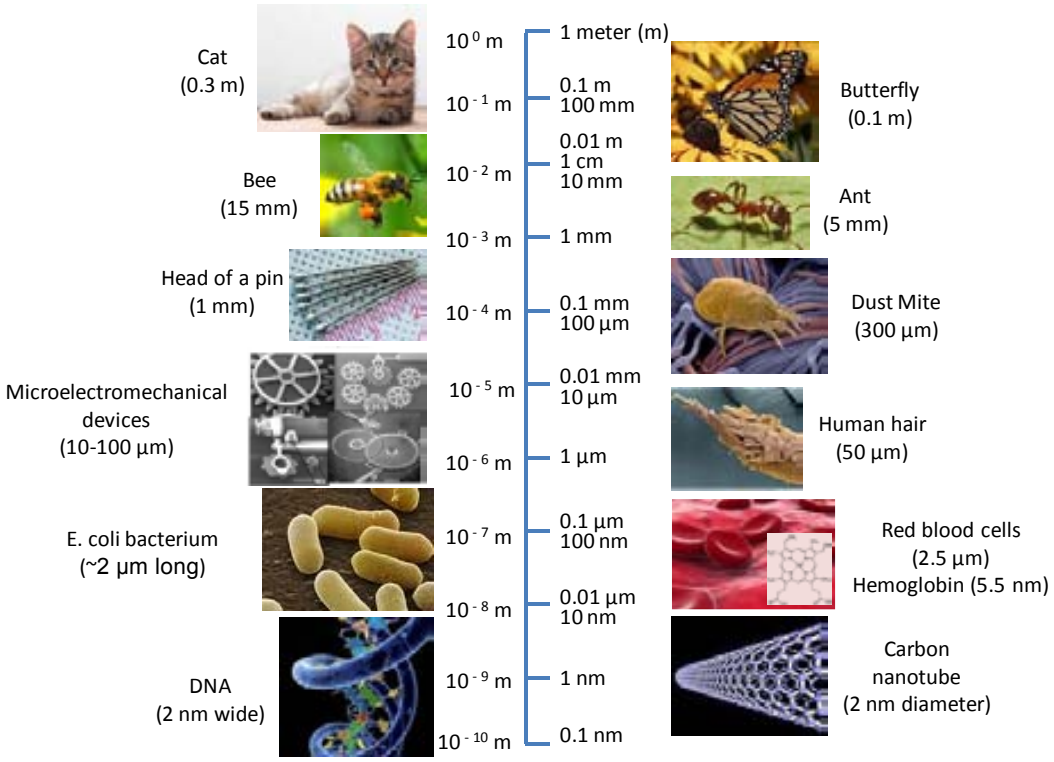

Figure 1.7: Comparing scale from meter to nanometer dimensions.

Althougth nanotechnology has begun to be a "well-known" technology at the end of the XX century, it has been widely used by ancient civilizations unconsciously to create beautiful and increadible materials. One of the first examples is the Lycurgus cup (Figure 1.8), from the 4th century before Christ, a Roman glass cage cup made of a dichroic glass, which makes use of small gold nanoparticles to create luminous green pigments when light comes from the front (reflected light),

[56] Ratner, M.; Ratner, D.; in: *Nanotechnology: A Gentle Introduction to the Next Big Idea;* Prentice Hall PTR 1st edition, **2003**.

whereas displays red when light comes from inside the cup (transmitted light).[57] Nanotechnology was also used by artisans in Mesopotamia (9th century) in order to generate a glittering effect on the surface of pots by the presence of cupper and silver nanoparticles on its surface.[58] In the medieval age, the artists changed the composition of the materials to create colors in the stained glass windows of churches. The study of this glasses revealed the existance of silver and gold nanoparticles.[59-60]

Figure 1.8: The Lycurgus Cup in reflected light (on the left) and in transmitted light (on the right). British Museum.[65]

As we have seen, the use of particles at nanosize was an usual methodology for the pigmentation of objects, but it was not until 1857 that the first scientific evaluation of nanoparticles took place, when Michael Faraday prepared the first pure sample of gold colloid (called "activated gold") and stated that the red colour was due to the small size of these particles.[61] Other more recent approaches involving technology at nanoscale are the development of powerful electron microscopes or in the industrial field the development of branching polymers and combinatorial chemistry. But it was not until the middle of the XX century, when all this works were included in the field of nanotechnology.

Ideas and concepts behind nanotechnology were firstly pointed out by the physicist Richard Feynman, which is today considered the father of the nanotechnology. On December 29th, 1959, Feynman gave a lecture in one of the American Physical Society meetings at the California Institute of Technology (CalTech), which he entiteled *"Why cannot we write the entire 24 volumes of the Encyclopaedia Brittanica on the head of a pin?".* [62] There, he exposed the possibility of manipulating and controlling individual atoms and molecules as a highly powerful tool for synthetic chemistry.[63] However, it was not until 22 years later, with the development of the scanning tunneling microscope, that individual atoms could be observed, ginving rise to the development of nanotechnology.

The importance of this technology arises in that, at nanoscale, the properties of matter show new physical or chemical effects, completely different from those

[57] Min'ko, N.I.; Nartsev, V.M.; *Glass Ceram*., **2008**, 65(5-6), 148.
[58] Padovani, S.; Sada, C.; Mazzoldi,P.; Brunetti, B.; Borgia, I.; A. Sgamellotti,A.; Giulivi, A.; D'Acapito, F.; Battaglin, G.; *J. Appl. Phys*., **2003**, 93, 10058.
[59] Vilarigues, M.; da Silva, R.C.; *Appl. Phys. A*, **2004**, 79(2), 373.
[60] Vilarigues, M.; Fernandes, P.; Alves, L.C.; da Silva, R.C.; *Nucl. Instrum Meth. B*, **2009**, 267(12-13), 2260.
[61] Faraday, M.; *Philos. Trans. R. Soc. London*, **1857**, 147, 145.
[62] Feynmann, R. P.; *Eng. Sci*., **1960**, 23, 22.
[63] Edwards, S.A.; in: *The Nanotech Pioneers. Where Are They Talking Us?*; WILEY-VCH Verlag GmbH & Co. KGaA, Weinheim, 1st edition, **2006**.

compared to atoms or molecules and their bulk material. As a consequence, many researchers are focusing their investigations on this “new” technology in order to develop novel materials with unique and unusual properties. However, it has to be highlighted that the fabrication of nanomaterials requires a multidisciplinary effort, since it is necessary to understand what is happening at this scale for developing useful materials.[64] In the last 20 years, huge advances have been done towards the understanding and control of matter at nanoscale. This has generated not only thousands of publications and patents in different fields, but also the development of companies with new or improved products, involving the use of nanomaterials. One can find lots of products in the market, including antibacterial socks, baseball bats with better flex and "kick", stiffer tennis rackets, wrinkle- and stain-resistant clothing, deep-penetrating therapeutic cosmetics, clear sunscreens, scratch-resistant glass coatings, faster-recharging batteries for cordless electric tools, and improved displays for televisions, cell phones, and digital cameras.[65]

A large amount of nanostructured compounds or materials in the nature exist, which researchers are beginning to locate, isolate, characterize and classify. The main characteristic of these materials is that they present no human modification or processing and show remarkable properties inherent to their nanostructures. An example can be the self-cleaning property of the lotus plant, which is the combination of the microstructure of the leaves and of the epidermal cells on its rough surface, which are covered with wax crystals (Figure 1.9).[66] Other example could be the large water-repellent force of water striders, which is produced by nanostructures on its leg. Besides the self-cleaning and water-repellent force properties, many other extraordinary characteristics such as high adhesion, high mechanical strength, biological self-assembly, antireflection, structural coloration or thermal insulation properties have been observed, which scientist are trying to mimic in the lab to develop new nanomaterials and nanodevices due to their commercial interests.[67]

Nanomaterials can be also manufactured and used at small scale, which normally include two main categories: fullerenes and nanoparticles.

Fullerenes are molecules completely composed of carbon sheets, similar in structure to graphite, rolled in the form of hollow sphere, ellipsoid, tube, etc. Different types of fullerenes exist depending on their structural variations, such as buckyball clusters (from C_{20} to C_{60} compounds), linked "ball-and-chain"

---

[64] Borisenko, V.E.; Ossicini, S.; in: *What is What in the Nanoworld A Handbook on Nanoscience and Nanotechnology;* WILEY-VCH Verlag GmbH & Co. KGaA, Weinheim, **2008**.
[65] http://nano.gov/timeline. [looked up on November 2013]
[66] Zhang, J.; Wang, J.; Zhao, Y.; Xu, L.; Gao, X.; Zheng, Y.; Jiang, L.; *Soft. Matter*., **2008**, 4, 2232.
[67] Bhushan, B.; *Phil. Trans. R. Soc. A,* **2009**, 367, 1445.

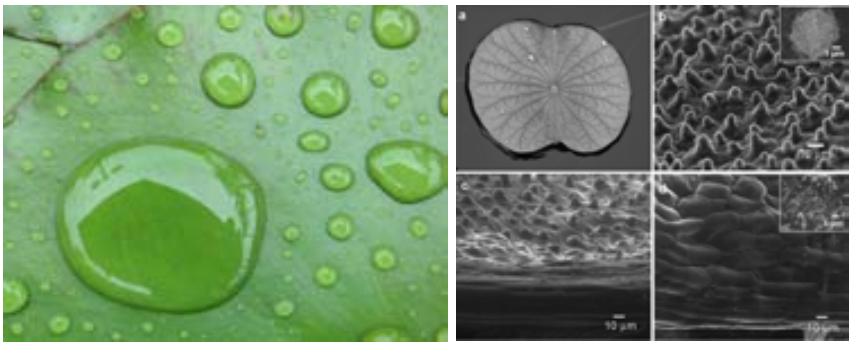

Figure 1.9: Photograph (left) and SEM images (right) from the lotus plant.[67]

dimmers or fullerene rings, among others.[68-69] However, ones of the most relevant types of fullerenes are carbon nanotubes (CNTs) due to their special properties. Whereas buckyball clusters are spherical in shape, nanotubes are cylindrical, with at least one end capped with a hemisphere of the buckyball structure. Although their length can be of several microns, their diameter is of few nanometers (from <1 nm up to 50 nm). [70-71] CNTs can have different structures depending on their thickness, length, type of helicity and number of layers, determining these parameters their final properties. Depending on the number of layers one can find single-wall nanotubes (SWNTs), multi-wall nanotubes (MWNTs) or double-wall nanotubes (DWNTs). The interest of CNTs resides in the combination of stiffness, strength, and tenacity observed by this material, since most of other commonly used compounds or materials present limitations in some of the presented properties. Moreover, this allotropic form of carbon presents comparable electrical and thermal conductivity to other conductive materials.[72] CNTs can be used for a wide range of applications such as in micro- and nano-electronics, technical textiles, conductive plastic, or in structural composite materials and chemical sensing, among others.

Of special interest is their use as analytical tools due to their unique properties.[73] CNTs have been satisfactory used as column packing material for gas chromatography,[74] and as pseudo-stationary phases in capillary electrophoresis for electrolyte separation.[75] On the other hand, this nanostructured material can be also used in analyte preconcentration steps or as sorbent packed materials. In this sense, CNTs have demonstrated their suitability for the elimination of hydrocarbons from petroleum[76] and also for pre-concentrate rare earth and trace

[68] Prato, M.; *J. Mater. Chem.,* **1997**, 7(7), 1097.
[69] Bosi, S.; Da Ros, T.; Spalluto, G.; Prato, M.; *Eur. J. Med. Chem.,* **2003,** 38, 913.
[70] Rao, C.N.R.; Satishkumar, B.C.; Govindaraj, A.; Nath, M.; *Chem. Phys. Chem.,* **2001,** 2, 78.
[71] Endo, M; Strano, M.; Ajayan, P.; in: *Carbon nanotubes;* Springer Berlin, Heildelberg, **2008**, 111, 13.
[72] Saito, R.; Dresselhaus, G.; Dresselhaus, M.S.; in: *Physical properties of carbon nanotubes;* Imperial College Press, London, **1998**.
[73] Valcárcel, M.; Simonet, B.M.; Cárdenas, S.; Suárez, B.; *Anal. Bioanal. Chem.,* **2005,** 382, 1783.
[74] Li, Q.L.; Yuan, D.X.; *J. Chromatogr. A,* **2003**, 1003, 203.
[75] Wang, Z.; Luo, G.; Chen, J.; Xiao, S.; Wang, Y.; *Electrophoresis,* **2003,** 24, 4181.
[76] Long, R.Q.; Yang, R.T.; *J. Am. Chem. Soc.,* **2001,** 123, 2058.

amounts of other metals.[77-78] On the other hand, CNTs have been widely used as substrates and transducer in sensors, and more concretely in electrochemical biosensors, since CNTs can promote electron-transfer reactions. The high conductivity of this nanostructured material and the possibility of modifying its surface allow their application in high sensitive and selective devices, [79] such as in the development of amperometric or voltamperometric sensors for DNA hybridization or uric acid detection.[80-81]

On the other hand, nanoparticles are another type of nanostructured material with exceptional properties. Their properties and applications are described next.

1.2.1 NANOPARTICLES AND ITS ROLE IN ANALYTICAL CHEMISTRY

Nanoparticles are commonly defined as particles which have one or more dimensions in the nanoscale order (between 1 and 100 nm), and what makes them so interesting is that these nanomaterials show different properties than the particles in the bulk size, even though they have the same chemical composition. Nanoparticles can be made of a wide range of materials, such as metals, metal oxides, silicates, non-oxide ceramics, polymers, organics, carbon and biomolecules; and can be found as spheres, cylinders, platelets, tubes, etc. As in Figure 1.10 can be observed, there exist a wide range of shapes and materials, but also different dispersion media, dispersion states and surface modifications.[82]

Nanoparticles exhibit some properties due to their size that makes them very interesting for their study and application.[83-84] Materials usually have the same physical and chemical properties independently of their size, while a size-dependent effect is observed at nanoscale due to quantum effects. Thus, properties like electrical conductivity, magnetic permeability, redox potential or fluorescence can be tuned depending on the size of the particle. For instance, cadmium selenide (CdSe) nanocrystals can emit fluorescence at different wavelengths depending on their size, being feasible to synthesize nanoparticles with optical properties in all the UV-Vis spectra for their use in optoelectronics as emitters or in (bio)chemical sensing as labels.[85] Moreover, these nanomaterials can act as nanoantennas, consuming very low energy.[86-87] Thus, nanoparticles with optical properties can be crucial in developing novel technologies for the

---

[77] Liang, P.; Liu, Y.; Guo, L.; *Spectrochim. Acta, Part B*, **2005**, 60, 125.
[78] Liang, P.; Liu, Y.; Guo, L.; Zeng, J.; Lu, H.; *J. Anal. At. Spectrom.* **2004,** 19, 1489.
[79] Zhang, M.G.; Smith, A.; Gorski, W.; *Anal. Chem,* **2004,** 76, 5045.
[80] Wang, Z.H.; Wang, Y.M.; Luo, G.A.; *Analyst,* **2002,** 127, 1353.
[81] Cai, H.; Jiang, X.N.; He, P.A.; Fang, Y.Z.; *Anal. Bioanal. Chem.,* **2003,** 375, 287.
[82] Nagarajan, R.; Hatton, T.A.; in: *Nanoparticles: synthesis, stabilization, Passivation and Functionalization*, American Chemical Society, 1st edition, **2008**.
[83] Plieth, W.J.; *J. Phys. Chem.,* **1982**, 86(16), 3166.
[84] Fendler J.H.; in: *Nanoparticles and Nanostructured Films*, Wiley-VCH, Weinheim, **1998**.
[85] Mansur, H.S.; *Wiley Interdiscip. Rev. Nanomed. Nanobiotechnol.,* **2010**, 2, 113.
[86] Hewageeganaa, P.; Stockman, M.I.; *Infrared Phys. Technol.,* **2007,** 50, 177.
[87] Pellegrini, G.; Mattei, G.; Mazzoldi, P.; *Nanotechol.,* **2009**, 20, 065201.

fast propagation along communication lines. For instance, photodetectors can be improved by incorporating nanomaterials, obtaining faster devices with lower consumption, by increasing their efficiency and reducing their size.[88]

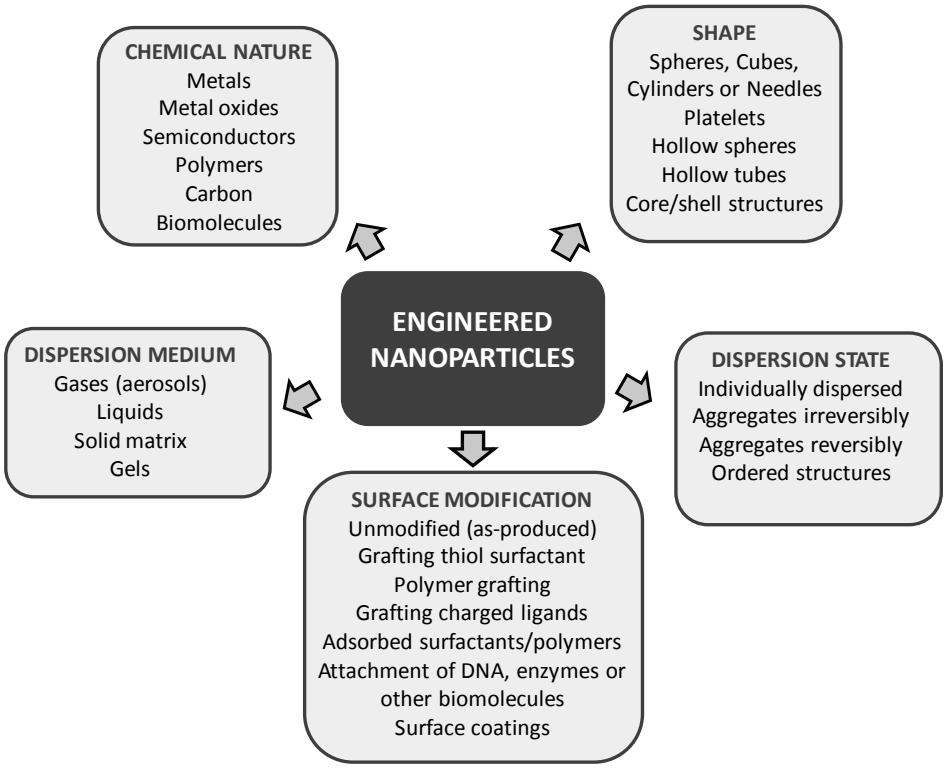

Figure 1.10: Diversity of engineered nanoparticles. [82]

Furthermore, nanoparticles display a higher surface area than similar materials at larger scale. Therefore, more surface is in contact with their outer surrounding. One of the greatest advantages of this property can be found in catalysis, which is enhanced by increasing surface area per unit volume, so more catalytic conversion is produced in the nano scale.[89] Many reports have described the catalytic activity of palladium nanoparticles in different C-C cross-coupling reactions.[90-91] Moreover, since nanoparticles can be dispersed in water, greener catalytic reactions can be carried out and it is also easier to separate the obtained products.[92] Platinum nanoparticles have also shown catalytical properties, [93] which are being used in efficient fuel cell electrocatalysis for many reactions (oxidation and reduction). [94-95] Ruthenium and copper metal nanoparticles show also promising catalytical properties.

[88] Schuller, J.A.; Barnard, E.S.; Cai, W.; Jun, Y.C.; White, J.S.; Brongersma, M.L.; *Nat. Mater.*, **2010**, 9, 193.
[89] Herves, P.; Perez-Lorenzo, M.; Liz-Marzan, L.M.; Dzubiella, J.; Lu, Y.; Ballauff, M.; *Chem. Soc. Rev.,* **2012**, 41 (17), 5577.
[90] Srimani, D.; Sawoo, S.; Sarkar, A.; *Org. Lett.,* **2007,** 9, 3639.
[91] Sawoo, S.; Srimani, D.; Dutta, P.; Lahiri, R.; Sarkar, A.; *Tetrahedron*, **2009**, 65, 4367.
[92] Astruc, D.; Lu, F.; Aranzaes, J. R.; *Angew. Chem. Int. Ed.,* **2005**, 44, 7852.
[93] Subhramannia, M.; Pillai, V.K.*; J. Mater. Chem*., **2008**, 18, 5858.
[94]Gasteiger, H.A.; Kocha, S.S.; Sompalli, B.; Wagner, F.T.; *Appl. Catal. B: Environ.,* **2005**, 56, 9.

On the other hand, the high surface-to-volume ratio of these nanostructures can be also advantageous in separation techniques, since in these applications it is really important to achieve a favorable mass transfer.[96] The large surface area of nanoparticles enables their use as chromatographic material achieving highly efficient separations. Thus, nanoparticles have been widely used in liquid chromatography (LC), gas chromatography (GC) or capillary electrophoresis (CE), among others.[96] The main drawback of using these nanostructured materials is their suspension stability, which it is still a challenge. Nevertheless, silica,[97] polymeric,[98] gold,[99] or titanium oxide[100] nanoparticles have been satisfactory used in this field. In extraction applications, cationic polystyrene nanoparticles have been used as binding affinity material for biocompounds, being successfully applied in extraction of oligonucleotides from human plasma.[101]

Nanoparticles can be also used for single-molecule detection via SERS (Surface-Enhanced Raman Scattering). Raman spectroscopy is a chemical analysis technique which provides information about the vibrational signature of a molecule, being sensitive to composition, bond strength, environment and structure. An enhanced signal of Raman spectra can be observed when molecules are adsorbed in the surface of nanoparticles.[102-103] Thus, SERS can be used as a low level detection and analysis technique.[104-105]

On the other hand, the exceptional optical properties of nanoparticles have promoted their use in other applications, such as in imaging, [106] where one can find its principal use in the fields of medicine, biology or bioanalytical chemistry, such as contrast agents along time derived to their long stability.[107] Nanosized materials are often on the biological size, comparable to bacteria, viruses, cells, antibodies and DNA. They can also incorporate different components to achieve multifunctional capabilities with high biocompatibility, specially in the case of metal nanoparticles. For example, gold nanoparticles can incorporate antibodies for selective imaging and killing cancerous cells with normal visible light (and leaving normal cells

---

[95] Peng, Z.; Yang, H.; *Nano Today*, **2009**, 4, 143.
[96] Nilsson, C.; Birnbaum, S.; Nilsson, S.; *J. Chromatogr. A,* **2007**, 1168, 212.
[97] Bächmann, K.; Göttlicher, B.; Haag, I.; Han, K.Y.; Hensel, W.; Mainka, A.; *J. Chromatogr. A,* **1994,** 688, 283.
[98] Wallingford, R.A.; Ewing, A.G.; *Adv. Chromatogr.,* **1989**, 29, 1.
[99] Huang, M.F.; Huang, C.C.; Chang, H.T.; *Electrophoresis,* **2003,** 24, 2896.
[100] Hsieh, Y.L.; Chen, T.H.; Liu, C.P.; Liu, C.Y.; *Electrophoresis,* **2005,** 26, 4089.
[101] Lu, J.; *Carbon*, **2007**, 45, 1599.
[102] Hanarp, P.; Kall, M.; Sutherland, D. S.; *J. Phys. Chem. B,* **2003**, 107, 5768.
[103] Gluodenis, M.; Foss, C.A., Jr.; *J. Phys. Chem. B,* **2002**, 106, 9484.
[104] Kneipp, K.; Wang, Y.; Kneipp, H.; Perelman, L.T.; Itzkan, I.; Dasari, R.R.; Feld, M.S.; *Phys. Rev. Lett.*, **1997**, 78, 1667.
[105] Nie, S.; Emory, S.R.; *Science*, **1997**, 275, 1102.
[106] Eghtedari, M.; Oraevsky, A.; Copland, J.A.; Kotov, N.A.; Conjusteau, A.; Motamedi, M.; *Nano Lett.,* **2007**, 7, 1914.
[107] Chen, J.; Saeki, F.; Wiley, B.J.; Cang, H.; Cobb, M. J.; Li, Z.Y.; Au, L.; Zhang, H.; Kimmey, M.B.; Li, X. D.; Xia, Y.; *Nano Lett.*, **2005**, 5, 473.

unharmed);[108-109] whereas silver nanoparticles, due to its bioactive properties, are being applied for developing new biosystems with antibacterial activity.[110] Other biomedical applications of nanoparticles involve DNA sequencing, cell labelling, [111] hyperthermia, [112] drug delivery, [113] gene therapy or pharmacokinetic studies.

Chemical sensing is another common application field of nanoparticles. Chemical sensors are those devices which are able to transform chemical information into a useful analytical signal.[114] They are usually composed of a recognition element, which interacts selectively with the analyte and generates the primary signal (mass, optical, electrical, thermal, etc). Then, this signal is transformed by the transducer into a secondary signal, normally on the electric domain, which is simpler of processing and amplifying, and gives the analytical information about the sample (Figure 1.11). Depending on the physical property measured by the transducer, sensors can be classified into mass[115], electrochemical[116] (e.g. amperometric, potentiometric, conductiometric or impedimetric), or optical sensors[117] (e.g. absorbance, luminescence or reflectance), among others. On the other hand, when the recognition element is of biologic nature, these devices can be called biosensors.[118] Sensors are characterized for their reduced size, robustness, simple use and continuous operation, being feasible to obtain information in real time.

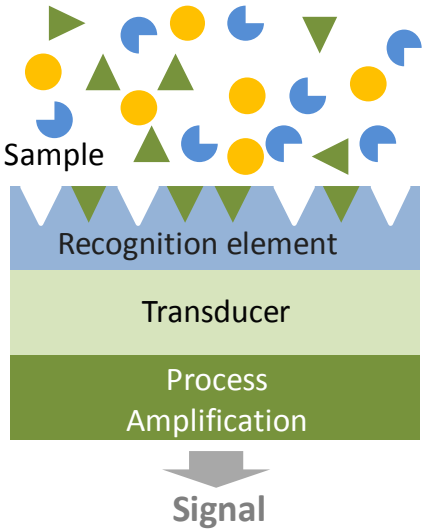

Figure 1.11: General scheme of a chemical sensor.

In chemical sensing, the use of nanomaterials as the transducing element, and more concretely nanoparticles, has shown major benefits, such as the enhanced sensitivity and reproducibility. Moreover, techniques involving surface modification offer the possibility of changing the surrounding molecules of the nanoparticles, making feasible the

[108] O'Neal, D.P.; Hirsch, L.R.; Halas, N.J.; Payne, J.D.; West, J.L.; *Cancer Lett.*, **2004**, 209 (2), 171.
[109] Zharov, V.P.; Galitovskaya, E.N.; Johnson, C.; Kelly, T.; *Lasers Surg. Med.*, **2005**, 37 (3) 219.
[110] Darouiche, R.O.; Raad, I.I.; Heard, S.O.; Thornby, J.I.;Wenker, O.C.; Gabrielli, A.; *New Engl. J. Med.*, **1999**, 340, 1.
[111] El-Sayed, I.H; Huang, X.; El-Sayed, M.A.; *Nano Lett.* **2005**, 5, 829.
[112] Tong, L.; Zhao ,Y.; Huff, T.B.; Hansen, M.N.; Wei, A.; Cheng, J.X.; *Adv. Mater.*, **2007**, 19, 3136.
[113] Podsiadlo, P.; Sinani, V.A.; Bahng, J.H.; Kam, N.W.S.; Lee, J.; Kotov, N.A.; *Langmuir*,**2008**, 24, 568.
[114] Catterall R.W.; in: *Chemical Sensors;* Oxford, U.K.: Oxford University Press, **1997**.
[115] Marco, M.P.; Gee, S.; Hammock, B.D.M.; *TrAC, Trends Anal. Chem.*, **1995**, 9, 373.
[116] Thébenot, D.R.; Toth, K.; Durst, R.A.; Wilson, G.S.; *Biosens. Bioelectron.*, **2001**, 16, 121.
[117] Byfield, M.P.; Abuknesha, R.A.; *Biosens. Bioelectron.*, **1994**, 9, 373.
[118] Tombelli, S.; Mascini, M.; Sacco, C.; Turner, A.P.F.; *Anal. Chim. Acta*, **2000**, 418, 1.

simple introduction of recognition elements, which leads to highly sensitive and cost-efficient detection systems. [119]

In this sense, numerous works can be found concerning electrochemical sensing due to their simplicity, where the voltammetric and potentiometric techniques are the most widely used.[120-121] Potentiometric sensing of diverse cations and anions using nanoparticles is extended. In this sense, some works relative to the high sensitive determination of proteins by using gold nanoparticles can be found.[122] Other methods, where the redox properties of quantum dots are used, have been also presented for the analysis of biomolecules.[123] On the other hand, direct and indirect methods based on the voltammetry are also a common approach, since they enable the simultaneous and rapid determination of several compounds. [124-125] Thus, the determination of numerous microorganisms as well as heavy metals has been presented by using this detection method. Stripping voltammetry by using modified electrodes is usually employed, since it allows an enhancement of the sensitivity and selectivity of the technique.[126-127] Other approaches use metal nanoparticles, such as bismuth or antimony colloids, for modified electrodes because this has shown to decrease detection limits by increasing the signal to noise ratio.[128] In the same manner, many works concerning nanomaterials combined with synthetic or biologic receptor modified electrodes have been presented.[129-130] However, electrochemical approach lack sometimes of robustness and reproducibility, which makes difficult in-field measurements.

On the other hand, the combination of optical sensing and nanoparticles has demonstrated to be simpler, obtaining better results in terms of detection limits, analysis time and reproducibility. Most of the papers thereon are based on the use of quantum dots (for fluorimetric assays) or gold nanoparticles (for colorimetric assays).[131] As the present work is based also in optical detection, a section devoted to this type of approaches is given.

Besides, other kind of sensors can be found in the literature including those

---

[119] Wang, L.; Ma, W.; Xu, L.; Chen, W.; Zhu, Y.; Xu, C.; Kotov, N. A.; *Mater. Sci. Eng., R,* **2010**, 70, 265.
[120] Pérez-López, B.; Merkoçi, A.; *Anal. Bioanal Chem.,* **2011**, 399, 1577.
[121] Denuault, G.; *Ocean Sci. Discuss*, **2009**, 6, 1857.
[122] Chumbimuni-Torres, K.Y.; Dai, Z.; Rubinova, N.;Xiang, Y.; Pretsch, E.; Wang, J.; Bakker, E.; *J. Am. Chem. Soc.,* **2006,** 128, 13676.
[123] Thuürer, R.; Vigassy, T.; Hirayama ,M.; Wang, J.; Bakker, E.; Pretsch, E.; *Anal. Chem.,* **2008**, 80(3), 707.
[124] Bakker, E.; Qin, Y.; *Anal. Chem*., **2006,** 78, 3965.
[125] Privett, B.J.; Shin, J.H.; Schoenfisch, M.H.; *Anal. Chem.,* **2008,** 80, 4499.
[126] Xiao, Y.; Rowe, A. A.; Plaxco, K. W.; *J. Am. Chem. Soc.,* **2007,** 129, 262.
[127] Liu, S.; Nie, H.; Jiang, J.; Shen, G.; Yu, R.; *Anal. Chem.,* **2009,** 81, 5724.
[128] Granado, M. A.; Olivares-Marín, M.; Pinilla, E.; *Talanta*, **2009**, 80, 631.
[129] Pan, D.; Wang, Y.; Chen, Z.; Lou, T.; Qin, W.; *Anal. Chem*., **2009,** 81, 5088.
[130] Miao, P.; Liu, L.; Li, Y.; Li, G.; *Electrochem. Commun.,* **2009,** 11, 1904.
[131] Wang, X.; Liu, M.; Cheng, X.; Lin, J.; *TrAC, Trends Anal. Chem.*, **2009**, 28, 75.

for the detection of explosives,[132] biowarfare agents,[133] biological molecules,[134] proteins[135] and nucleotides[136] based on SERS technique.

1.2.2 NANOPARTICLES FOR COLORIMETRIC ASSAYS

Nanoparticles, and especially metallic nanoparticles, can offer some increadible optical properties, making them ideal for their use in chemical sensing.

Most of the metallic nanoparticles are colored, being yellowish for silver and burgundy for gold spheric particles; and can exhibit strong absorption bands in the visible region of the spectrum.[137-138]

This optical absorption is due to the response of the conduction electron cloud, which moves away from its equilibrium position when an external electrical field of the electromagnetic radiation of light perturbs them (Figure 1.12), generating induced surface polarization charges that act as a resorting force for the electron cloud.[139] This produces an oscillator movement of the surface electrons, which is reflected in a band (for spherical nanoparticles) placed in the visible and near-infrared region of the spectrum, called surface plasmon resonance (SPR) band.[140-141]

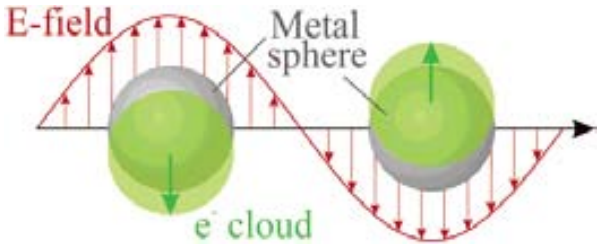

Figure 1.12: Scheme of Plasmon oscillation for a sphere, showing the displacement of the conduction electron charge cloud relative to the nuclei.[139]

This band is tunable as a function of the nanoparticle dimension, contour, aggregation state, and local environment.[142-143] Therefore, any change of color or absorption in the visible spectra can be achieved by changing the shape or structure of the nanoparticle. Nanorods,[144] nanocubes,[145] nanowires,

---

[132] Tao, A.; Kim, F.; Hess, C. ; Goldberger, J.; He, R.; Sun, Y.; Xia, Y.; Yang, P;. *Nano Lett.*, **2003**, 3, 1229.
[133] Haynes, C.L.; Yonzon, C.R.; Zhang, X.; Duyne, R.P.V.; *J. Raman Spectrosc.*, **2005**, 36, 471.
[134] Shafer-Peltier, K.E.; Haynes, C.L.; Glucksberg, M.R.; Duyne, R.P.V.; *J. Am. Chem. Soc.,* **2002**, 125, 588.
[135] Drachev, V.P.; Thoreson, M.D.; Khaliullin, E.N.; Davisson, V.J.; Shalaev, V.M.; *J. Phys. Chem. B,* **2004**, 108, 18 046.
[136] Tuan Vo-Dinh, L.R.A.D.L.S.; *J. Raman Spectrosc.*, **2002**, 33, 511.
[137] Henglein, A.; *Chem. Rev.*, **1989**, 89, 1861.
[138] Heilmann, A.; Kreibig, U.; *Eur. Phys. J. Appl. Phys.*, **2000**, 10, 193.
[139] Kelly, K.L.; Coronado, E.; Zhao, L.L.; and Schatz, G.C.; *J. Phys. Chem. B,* **2003**, 107, 668.
[140] Myroshnychenko, V.; Rodríguez-Fernández, J.; Pastoriza-Santos, I.; Funston, A.M.; Novo,C.; Mulvaney, P.; Liz-Marzán, L.M.; García de Abajo, F.J.; *Chem. Soc. Rev.*, **2008**, 37, 1792.
[141] Garcia, M.A.; *J. Phys. D: Appl. Phys.*, **2011**, 44, 283001.
[142] El-Sayed, M.A.; *Acc. Chem. Res.*, **2001**, *34*, 257-264.
[143] Daniel, M.-C.; Astruc, D.; *Chem. Rev.,* **2004**, *104*, 293-346.
[144] Yu, Y.Y.; Chang, S.S.; Lee, C.L.; Wang, C.R.C.*; J. Phys. Chem. B*, **1997**, 101, 6661.
[145] Sun, Y.; Xia, Y.; *Science*, **2002**, 298, 2176.

nanocages, nanoprisms[146] and nanoplates show diverse absorption bands, which are the result of multiple resonances. Thus, structures such as nanoprisms, nanocages and aggregates exhibit broad overall absorption bands;[147] while highly symmetric materials show well defined bands. For instance, spheric nanoparticles display a single scattering peak, while nanorods shows two due to highly localized charge polarizations at corners and edges (the longitudinal plasmon band, corresponding to light absorption and scattering along the long axis of the particle, and the transverse plasmon band, corresponding to light absorption and scattering along the short axis of the particle) [148-149] (Figure 1.13).[150]

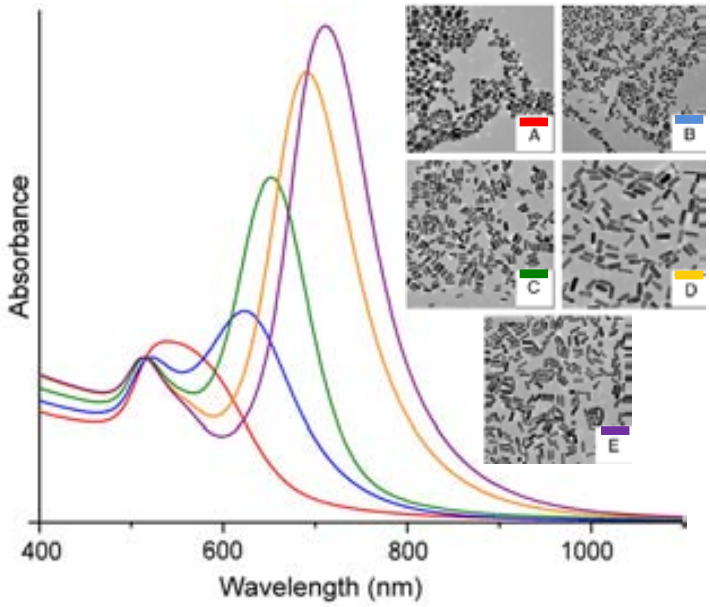

Figure 1.13: Example of UV–vis spectra and transmission electron micrographs of different size gold nanorods, increasing its size in one direction from A to E TEM images.[150]

For spherical particles, the linear optical properties can be explained theoretically by Mie's theory. [151] This theory can predict the position and shape of the plasmon absoption through a mathematical expression.[152-153]
Some direct aplications to this effect are, as cited, in imaging due to the absence of photobleaching. In the case of Raman spectroscopy, when molecules are absorbed in the surface of the metal nanoparticles (SERS) the plasmon band is coupled to the electronic states of the molecule, giving an enhanced signal. [154-155]

---

[146] Jin, R.; Cao, Y;. Mirkin, C.A;. Kelly, K.L.; Schatz, G.C.; Zheng, J. G.; *Science*, **2001**, 294, 1901.
[147] Zhang, J.Z.; Noguez, C.; *Plasmonics*, **2008,** 3, 127.
[148] Tao, A.R.; Habas, S.; Yang, P.; *Small*, **2008,** 4, 310.
[149] Murphy,C.J.; Sau, T.K.; Gole, A.M.; Orendorff, C.J.; Gao, J.; Gou,L.; Hunyadi, S.E.; Li, T.; *J. Phys. Chem. B,* **2005,** 109, 13857.
[150] Murphy, C.J.; Thompson, L.B.; Chernak, D.J.; Yang, J.A.; Sivapalan, S.T.; Boulos, S.P.; Huang, J.; Alkilany, A.M.; Sisco, P.N.; *Curr. Opin. Colloid Interface Sci.*, **2011,** 16, 128.
[151] Mie, G.; *Ann. Phys.,* **1908,** 25, 329.
[152] Schwartzberg, A.M.; Zhang, J.Z*; J. Phys. Chem. C*, **2008**, 112 (28), 10323.
[153] Link, S.; El-Sayed¸M.A.; *Annu. Rev. Phys. Chem*. **2003,** 54, 331.
[154] Garrell, R.; *Anal. Chem*., **1989**, 61, 401A.

1.2.2.1 SILVER NANOPARTICLES

It is well known the antibacterial, antifungal and antiviral activity of silver, since this metal is toxic for lots of microorganisms. Although the use of silver was diminished over the second World-War, the metal has been used in different forms to prevent infections in wounds for years.[156] The mechanism for their antimicrobial activity is based on its capability of interaction with thiol groups.[108157] When bacteria cells interact with silver, the metal binds to the membrane of the cell inhibiting their respiration. Since nanoparticles have higher surface area, enhanced interactions with microorganisms can be achieved, improving thus its action.[158] Furthermore, they have low toxicity to human cells, high thermal stability and low volatility.[109] An example in this regard could be wound dressings or coatings for medical devices, which are impregnate of silver nanoparticles inside and outside the material, improving its activity and avoiding infection.[156]

Many applications have been developed for silver nanoparticles (Ag NPs), including their use in burn treatment,[159] dental materials, [160] coating stainless steel materials, water treatment,[161-162] sunscreen lotions,[163-164] etc.

Probably, one can find their biggest application on SERS due to its incident light wavelength and its surface roughness.[165] Many works can be found concerning this field, such as the determination of herapin,[166] 2,4,6-trinitrotoluene,[167] or benzophenone and 4-methylbenzophenone.[168]

In the same way, silver nanoparticles are being used to enhance the fluorescence emission intensity of fluorescent molecules. When silver nanoparticles are located near fluorophore molecules, an increase in their quantum yield (QY), excitation rate and photostability has been observed.[157] Thus, research is focused to achieve the highest possible enhancement to make feasible the use of weak fluorophores in chemical sensing.

Silver nanoparticles show optical properties in the UV-Vis spectra, exhibiting a band located over 400 nm. Thus, one of their most interesting applications is in

---

[155] Campion, A.; Kambhampati, P.; *Chem. Soc. Rev.*, **1998**, 27, 241.
[156] Klasen, H.J.; *Burns,* **2000,** 26, 131.
[157] Aslan, K.;Holle y, P.; Geddes, C.D.; *J. Mater. Chem.,* **2006**, 16, 2846.
[158] Rai, M.; Yadav, A.; Gade, A.; *Biotechnol. Adv.*, **2009**, 27, 76.
[159] Fox, C.L.; Modak, S.M.*; Antimicrob. Agents Chemother.,* **1974**, 5(6), 582.
[160] García-Contreras, R.; Argueta-Figueroa, L.; Mejía-Rubalcava, C.; Jiménez-Martínez, R.; Cuevas-Guajardo, S.; Sánchez-Reyna, P.A.; Mendieta-Zeron, H.; *Int. Dent. J.;* **2011**, 61, 297.
[161] Gong, P.; Li, H.; He, X.; Wang, K.; Hu, J.; Tan, W.; *Nanotechnology*, **2007,** 18, 604.
[162] Jain, P.; Pradeep, T.; *Biotechnol. Bioeng.*, **2005**, 90(1), 59.
[163] Leaper, D.L.; *Int. Wound J.,* **2006,** 3(4), 282.
[164] Tian, J.; Wong, K.K.Y.; Ho, C.M.; Lok, C.N.; Yu, W.Y.; Che, C.M.; Chiu, J.F.; Tam, P.K.H.; *ChemMedChem*, **2007,** 2(1), 129.
[165] Nie, S.; Emory, S.R.; *Science,* **1997**, 275, 1102.
[166] Wang, X.; Chen, L.; Fu, X.; Chen, L.; Ding, Y.; *ACS Appl. Mater. Interfaces,* **2013**, 5 (21), 11059.
[167] Liu, M.M.; Chen, W.; *Biosens. Biolectron.,* **2013,** 46, 68.
[168] Droghetti, E.; Nicoletti1, F.P.; Guandalini, L.; Bartolucci, G.; Smulevich, G.; *J. Raman Spectrosc.* **2013**, 44, 1428.

colorimetric chemical sensing. Silver nanoparticles have been used for the determination of diverse metals, including some hazardous heavy metals such mercury, cadmium, chrome or lead. For instance, the determination of Cr (VI) by the aggregation of Ag NPs (and the subsequent displacement of its absorption band) due to the interaction of the reduced metal (Cr (III)) and the silver colloid has been presented.[169] Many examples can be found concerning the detection and quantification of mercury, such as its spectral and colorimetric determination using silver nanoparticles immobilized onto the surface of SiO_2 particles.[170] Another example of metal determination could be the highly sensitive and selective detection of cobalt ions by using glutathione-modified silver nanoparticles.[171] This work takes advantage of the use of different morphologies of Ag NPs (spherical particles, plates, and rods) to detect different metal ions (Ni^{2+}, Co^{2+}, Cd^{2+}, Pb^{2+}, and As^{3+}), and in particular rod-type Ag NPs allows the trace determination of Co^{2+} (Figure 1.14). Other colorimetric applications of silver nanoparticles involve the determination of small molecules, such as the naked-eye detection of triethylamine through the change of colour (yellow-orange-gray) of sucralose-capped Ag NPs.[172]

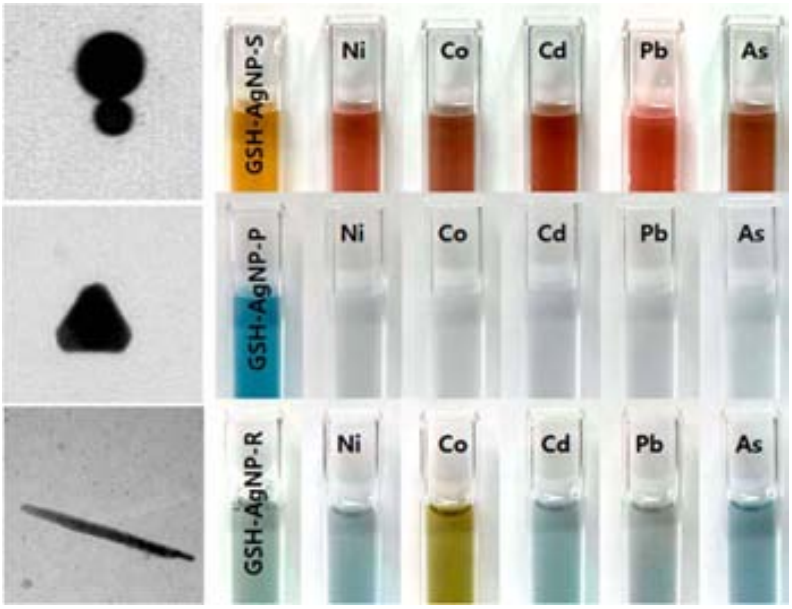

Figure 1.14: Metal detection using different shapes (spherical, plate and rod) of silver nanoparticles. As can be observed, the use of rods permitted the visual sensitive and selective determination of cobalt ion.[171]

1.2.2.2 GOLD NANOPARTICLES

As well as silver nanoparticles, gold suspensions (Au NPs) have a surface plasmon resonance band located over 520 nm in the UV-Vis spectrum, which can be displaced to lower energies when the size of the particle is increased.

[169] Ravindran, A.; Elavarasi, M.; Prathna, T.C.; Raichur, A.M.; Chandrasekaran, N.; Mukherjee, A.; *Sens. Actuators, B*, **2012**, 166-167, 365.
[170] Rameshkumar, P.; Manivannan, S.; Ramaraj, R.; *J. Nanopart. Res.,* **2013,** 15, 1639.
[171] Sung, H.K.; Oh, S.Y.; Park, C.; Kim, Y.*; Langmuir*, **2013**, 29, 8978.
[172] Filippo, E.;, Manno, D.; Buccolieri, A.; Serra, A.; *Sens. Actuators, B,* **2013**, 178, 1.

Thus, a red-shift and broadening of the SPR band is produced when Au NPs aggregates, obtaining purple solutions.[173-174] On the other hand, as metallic nanoparticles, gold nanoparticles allow direct electron transfer between redox species and bulk electrode materials, which enables electrochemical measurements without the requirement of a transfer mediator.[175]

As earlier argued, gold suspensions can be used in a wide range of applications. The nanoparticles surface can be modified for being used in molecular recognition, chemical sensing or even in imaging. Probably, the most interesting application is their use in bioanlytical sensing because gold nanoparticles can provide stable immobilization of biomolecules while mantaining their properties. Thus, many type of assays can be performed by immobilizing enzymes, antibodies or oligonucleotides, among others, over their surface for their use in pathogens detection or disease diagnosis.[64]

On the other hand, many works can be found related to colorimetric sensors using gold suspensions for detecting and quantifying ions. These analytical methods take advantage of the dependence not only of the size, shape and distribution of the gold nanoparticles, but also of their surrounding media and stabilizing molecules.[176-177] Thus, the absorption wavelength of a gold colloid can change from red to blue when a capping ligand immobilized onto the surface of the particles interacts with an analyte, since it produces their complexation and therefore the particle aggregation (Figure 1.15).[178-179] Much literature for the detection of mercury,[180] lead,[181-182] cooper[183] and cadmium[184] can be found using this methodology. An example could be the use of pyridine and gold nanoparticles for the determination of Hg^{2+}, which inhibits the aggregation of the colloid;[185] or the detection of Pb^{2+} by the interaction of the metals with the ligand shell of thiosulfate ($S_2O_3^{2-}$)-passivated Au NPs. [186] Recently, the used of oligoucleotides or DNAzymes with Au NPs has shown high sensitivity in the determination of copper, lead and mercury ions. [187]

---

[173] Brus L.; *Acc. Chem. Res.*, **2008,** 41(12), 1742.
[174] Tran, T.-H.; Nguyen, T.-D.; *Colloids Surf., B*, **2011**, 88, 1.
[175] Liu, S.; Leech, D.; Ju, H.; *Anal. Lett,*. **2003,** 36, 1.
[176] Xue, X.; Wang, F.; Liu, X.; *J. Am. Chem. Soc.,* **2008**, 130(11), 3244–3245.
[177] Tanaka, Y.; Shuji, O.; Yamaguchi, H.; Kondo, Y.; Kojima, C.; Ono, A.; *J. Am. Chem. Soc*., **2007,** 129(2), 244.
[178] Lin, C.Y.; Yu, C.J.; Lin, Y.H.; Tseng, W.L.; *Anal. Chem*., **2010,** 82, 6830.
[179] Chen, X.J.; Zu, Y.B.; Xie, H.; Kemas, A.M.; Gao, Z.Q.; *Analyst,* **2011,** 136, 1690.
[180] He, S.; Li, D.; Zhu, C.; Song, S.; Wang, L.; Long, Y.; *Chem. Commun.,* **2008**, 4885.
[181] Liu, J.; Lu, Y.; *J. Am. Chem. Soc.,* **2003,** 125, 6642.
[182] Wang, Z.; Lee, J. H.; Lu, Y.; *Adv. Mater.,* **2008**, 20, 3263.
[183] Liu, J.; Lu, Y.; *Chem. Commun.*, **2007,** 4872.
[184] Slocik, J. M.; Zabinski, J. S.; Phillips, D. M.; Naik, R. R.; *Small*, **2008**, 5, 548.
[185] Yang, X.R.; Lui, H.X.; Xu, J.; Tang, X.M.; Huang, H.; Tian, D.B.; *Nanotechnology,* **2011**, 22 (27), 275503.
[186] Hung, Y.-L.; Hsiung, T.-M.; Chen, Y.-Y.; Huang, C.-C.; *Talanta,* **2010,** 82, 516.
[187] Wang, C.; Yu, C.; *Rev. Anal. Chem.,* **2013,** 32(1), 1.

On the other hand, small compounds or molecules can be also detected by using Au NPs and their optical properties. For instance, the determination of H_2O_2 has been successfully carried out by employing cysteine-stimulated aggregation of Au nanoparticles. [188] Another examples could be the detection of 2,4,6-trinitrotoluene by cysteine functionalized Au NPs, which reacts with the organic molecule generating the aggregation of particles;[189] or the determination of organophosphate compounds by the blue-shift of the SPR band of the particles due to the adsorption of the analyte onto their surface.[190] The detection and quantification of sub-ppm levels of inorganic pollutants, such as nitrite ions, has been possible by means of its interaction with gold colloid.[191]

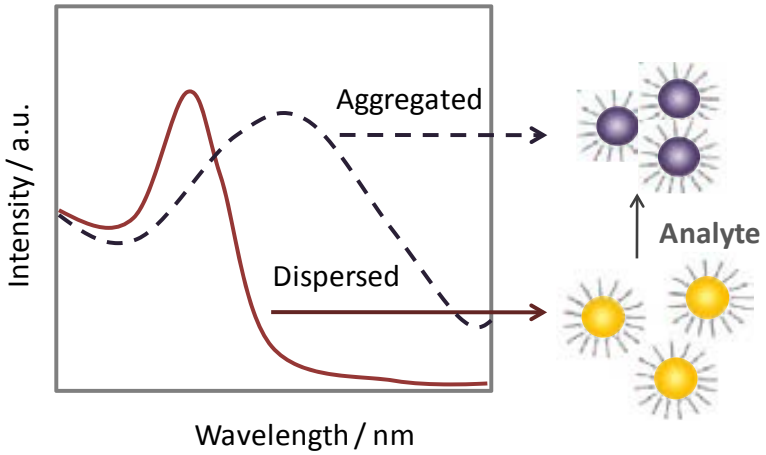

Figure 1.15: Example of heavy metal detection using gold nanoparticles as a immobilizing and transducing agent. The colloid remains dispersed in solution until the presence of analyte (heavy metal); then, the aggregation of the particles is produced for the interaction of the metal with the specific receptor attached to the particles.

1.2.3 NANOPARTICLES FOR FLUORIMETRIC ASSAYS

Fluorecence methods are well known to be highly sensitive and selective due to the scarce fluorescent species that exists. Thus, many analytical applications have been based in these methods, especially (bio)analytical sensors. However, it normally involves the use of fluorophors, which usually are organic substances characterized for their high fluorescence but also for their poor photostability.

Advances in nanotechnology has permitted the substitution of the previous dyes for fluorescent nanoparticles. As it will be discussed in the following sections, the use of these particles enables sensitive and reproducible chemical determinations, since they exibit an intense fluorescence for a long time.

[188] Wang, F.; Liu, X.; Lu, C.-H.; Willner, I.; *ACS Nano*, **2013**, 7 (8), 7278.
[189] Dasary, S.S R.; Singh, A.K.; Senapati, D.; Yu, H.; Ray, P.C.; *J. Am. Chem. Soc.,* **2009**, 131, 13806 .
[190] Newman, J.D.S.; Roberts, J.M.; Blanchard, G.J.; *Anal. Chem*., **2007**, 79, 3448.
[191] Daniel, W.L.; Han, M.S.; Lee, J.S.; Mirkin, C.A.; *J. Am. Chem. Soc.,* **2009**, 131, 6362.

1.2.3.1 QUANTUM DOTS

Inorganic semiconductor nanoparticles or quantum dots (QDs) are a type of fluorophor nanoparticles which are composed by elements from the periodic groups II-VI, III-V or IV-VI, and present sizes between 1 and 12 nm.[192]

QDs, as all semiconductors, are characterized for presenting a band gap between their conduction and valence band. When the material is excited with a photon with enough energy to overcome its band gap, the energy is absorbed by the material and the electrons are excited from its valence to its conduction band. Then, the electron will be relaxed by coming back to the valence band. In the case of quantum dots, this relaxation generates the emission of a photon with equal energy as its band gap.[193] When the scale of a material is reduced, quantum size effects plays a crucial role, since their physical dimensions are smaller than the exciton Bohr radius.[194] This value is the limit size where a material maintains its continuous band structure. Thus, when one of its dimensions is reduced below this limit, the densities of electronic states are no longer continuous, and their band gaps can be tuned by controlling their size and shape. This entails that the electronic and optical properties of the nanocrystals can be altered as desired, which makes this material of special interest.[195-196] As the size of the nanocrystal is decreased, its band gap increases, entailing higher energies for being excited and thus, shorter emission wavelengths (Figure 1.16).[197-198]

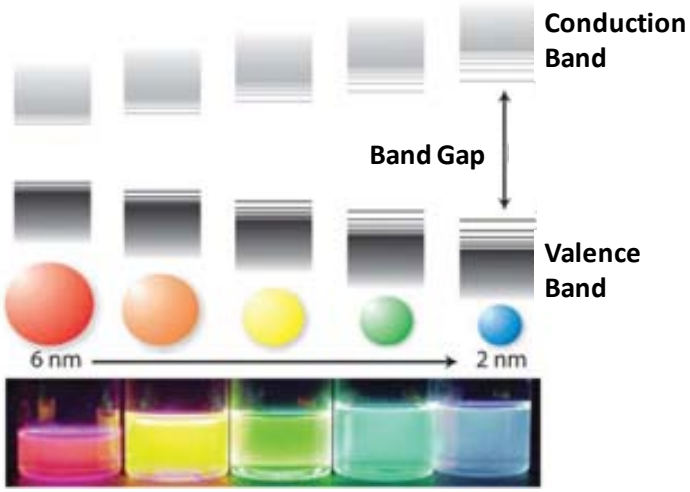

Figure 1.16: Scheme of the conduction and valence bands of different size semiconductor CdSe nanocrystals. CdSe colloids under UV light.[198]

[192] Niemeyer, C.M.; *Angew. Chem. Int. Ed.*, **2001**, 40, 4128.
[193] Weller, H.; *Angew. Chem. Int. Ed.,* **1993**, 32, 41.
[194] Alivisatos, A.P.; *Science*, **1996**, 271, 933.
[195] Murray, C. B.; Kagan, C. R.; Bawendi, M. G.; *Annu. Rev. Mater. Sci.,* **2000**, 30, 545.
[196] Yin, Y.; Alivisatos, A.P.; *Nature*, **2005,** 437, 664.
[197] Zhuang, Z.; Qing Peng, Q.; Li, Y.; *Chem. Soc. Rev.,* **2011**, 40, 5492.
[198] de Mello Donega C.; *Chem. Soc. Rev*., **2011**, 40, 1512.

However, each material presents physical and chemical limitations, and depending on its composition it will emit on a concrete range of energies, from ultraviolet (UV) to infrared (IR). For example, CdSe QDs can emit in the 450 - 700 nm range[199], while different sizes of PbS QDs can operate between 700 and 1800 nm (figure 1.17).[200-201]

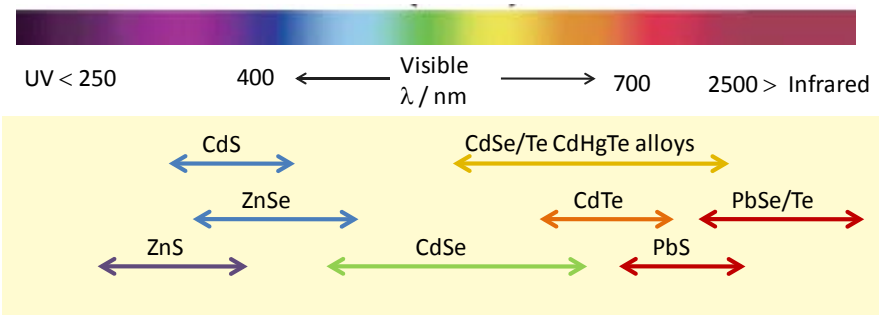

Figure 1.17: Emission wavelength of diverse QDs with different core materials.[201]

Another important characteristic of nanocrystals is their narrow emission band in contrast to their wide absorption band, specially compared to dyes (figure 1.18).[202-203] Moreover, QDs present large Stokes shifts (the difference in wavelength between the position of the absorption and emission bands of the same electronic transition), which means that the wavelength where they emit are larger from their absorption peaks. That makes easier their use in optical applications like in microscopy, as it simplifyes the requierements for these applications, such as the necessity of using high quality spectral filters to remove the excitation light with dyes.

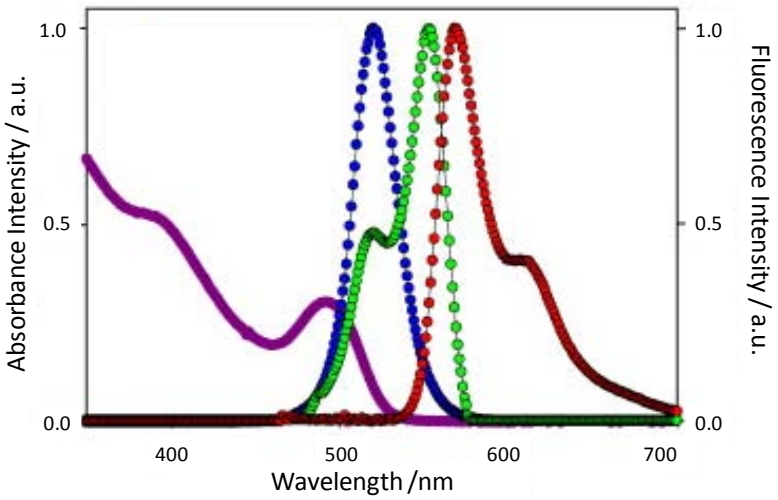

Figure 1.18: Normalized absorption and emission profiles of the 530 nm QDs and Cy3 dye. In purple, QDs absorption; blue, QDs emission; green, Cy3 absorption; red, Cy3 emission.[203]

[199] Murray, C.B.; Norris, D.J.; Bawendi, M.G.; *J. Am. Chem. Soc.,* **1993**, 115, 8706.
[200] Costa-Fernández, J.M.; Pereiro, R.; Sanz-Medel, A.*; TrAC, Trends Anal. Chem.*, **2006**, 25 (3), 207.
[201] Medintz, I.L.; Uyeda, H.T.; Goldman, E.R.; Mattoussi, H. *Nat. Mater.*, **2005,** 4, 435.
[202] Chan, W.C.W.; Maxwell, D.J.; Gao, X.H.; Bailey, R.E.; Han, M.Y.;, Nie, S.M.; *Curr. Opin. Biotechnol.,* **2002**, 13, 40.
[203] Sapsford, K.E.; Farrell, D.; Sun, S.; Rasoolya, A.; Mattoussi, H.; Medintze, I.L.; *Sens. Actuators, B,* **2009**, 139 (1), 13.

Furthermore, QDs exhibit the same emission peak and full width at half maximum (FWHM) independently of the excitation wavelength. Thus, contrary to common dyes, which requiere a specific excitation wavelength, the emission of different nanocrystals is achieved by exciting with a unique source, which results highly useful in many applications such as multiplexed sensing or imaging.[204]

It also has to be remarked the photostability of QDs, which usually is a critical parameter in organic dyes. Nanocrystals have shown to maintain their intensity of fluorescence during hours (at least 14 hours), while dyes, including Alexa 488, which is supposed to be one of the most stable organic colorants,[205] can not (figure 1.19).[206-207] Thus, QDs can be applied in those experiments requiering long-term interactions of multiple labeled molecules, such in monitoring.

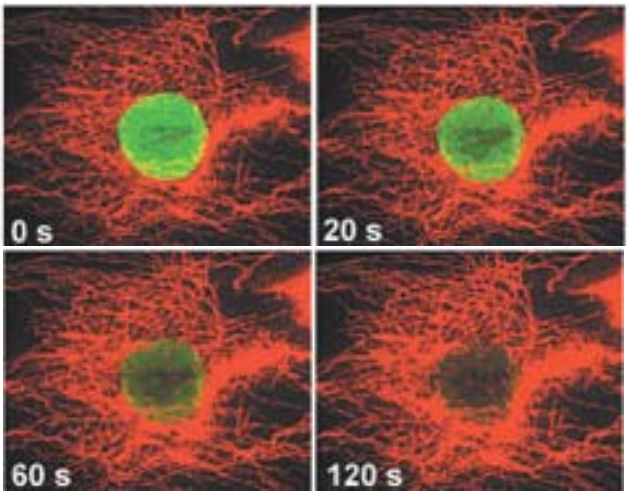

Figure 1.19: Comparison of dye Alexa 488 and QDs photostability in cell labeling. In the images, the nucleus of cells is marked with the dye in green, and fibers are stained with QDs in red. [207]

Furthermore, this type of nanoparticles present higher quantum efficiencies (quantum yields) than the common fluorophores. Moreover, when nanocrystals are capped with a shell of an inorganic wide-band semiconductor, it results in higher quantum efficiencies, the so called core-shell QDs. For instance, it has been estimated that single ZnS-capped CdSe QDs are 20 times brighter than single Rhodamine 6G molecule.[206]

Therefore, QDs are of increasingly interest due to all the described advantages these nanomaterial conffer. One of their most common applications in the field of optics involves the development of lifetime and robust light-emitting diodes (LEDs), tuning the color of light produced by changing the band gap of

[204] Yu, W.W.; Chang, E.; Drezek, R.; Colvin, V.L.; *Biochem. Biophys. Res. Commun*., **2006,** 348, 781.
[205] Panchuk-Voloshina, N.; Haugland, R.P.; Bishop-Stewart, J.; Bhalgat, M.K.; Millard, P.J.; Mao, F.; Leung, W.Y.; Haugland, R.P.; *J. Histochem. Cytochem*., **1999**, 47, 1179.
[206] Chan, W.C.W.; Nie, S.M.; *Science*, **1998**, 281, 2016.
[207] Wu, X.Y.; Liu, H.; Liu, J.; Haley, K.N.; Treadway, J.A.; Larson, J.P.; Ge, N.; Peale, F.; Bruchez, M.P.; *Nat. Biotechnol*., **2003**, 21, 41.

the material.[208] Solar cells can also incorporate QDs, which allow increasing its efficiency from the 30 % to the 42 % of sun's energy into energy for human use.[209] Moreover, nanocrystals have also application in computing, since their use permits compleating more computations in a second than silicon could ever do.

Besides, QDs can be used for the detection of specific analytes or to visualize some concreate areas of cells.[210-211] In this sense, *in vivo* imaging with near IR QDs is of increasing interest, due to the possibility of obtaining relevant information by following biologic mechanisms and their kinetics in real time.[212] However, all these biological applications are limitted by their cytotoxicity, which vary depending on the nanocrystal surface coating.[213] Several *in vitro* studies have observed the toxicity of the nanocrystals, affecting cell growth and their viability.[214-215] The ideal particle for biologic applications should be smaller than 5 nm, since it has been proved that are quickly eliminated by the urine system, emitting between 700 and 1000 nm, since the required energy for its excitation is low, and should be highly stable or be made of non-toxic compounds.[216]

Moreover, semiconductor nanoparticles can be employed for measuring protein conformational changes,[217] monitoring protein interactions [218] or even for enzyme activity determinations[219] by fluorescence resonance energy transfer (FRET) processes. When the distance between two particles or molecules are shorter than the critical Förster radius,[220] a transference of fluorescence energy is possible from the donor to the acceptor, which generates an increase in the emission intensity of the acceptor and a decrease in the donor´s emission and its excited lifetime. This process is known as FRET and it is very usefull for measuring distances between molecules and its changes.[221]

Sensing systems based on fluorescent nanoparticles have shown to provide high sensitivity. Nanocrystals can be conjugated with a wide range of molecules to

---

[208] Smydera, J.A.; Kraussa, T.D.; *Mater. Today*, **2011**, 14, 382.
[209] Shockley, W.; Queisser, H. J.*; J. Appl. Phys.*, **1961,** 32, 510.
[210] Chan, W. C.; *Science*, **1998,** 281, 2016.
[211] Gao, X.; Cui, Y.; Levenson, R.M.; Chung, L.W.K.; Nie, S.; *Nat. Biotechnol.*, **2004,** 22, 969.
[212] Dubertret, B.; *Science*, **2002,** 298, 1759.
[213] Lewinski, N.; Colvin, V.; Drezek, R.; *Small,* **2008**, 4, 26.
[214] Lovric, J.; Bazzi, H.S.; Cuie, Y.; Fortin, G.R.A.; Winnik, F.M.; Maysinger, D;. *J. Mol. Med.,* **2005**, 83, 377.
[215] Chen, F.Q.; Gerion, D.; *Nano Lett.,* **2004,** 4, 1827.
[216] Soo Choi, H.; Liu, W.; Misra, P.; Tanaka, E.; Zimmer, J.P.; Ipe, B.I.; Bawendi, M.G.; Frangioni, J.V.; *Nat. Biotechnol.*, **2007,** 25, 1.
[217] Heyduk, T.; *Curr. Opin. Biotechnol.*, **2002,** 13, 292.
[218] Day, R.N.; Periasamy, A.; Schaufele, F.; *Methods*, **2001**, 25, 4.
[219] Li, J.J.; Bugg, T.D.H.; *Chem. Commun.*, **2004**, 182.
[220] Riegler, J.; Nann, T.; *Anal. Bioanal. Chem.*, **2004**, 379, 913.
[221] Selvin, P.R.; *Nat. Struct. Biol.***, 2000**, 7, 730.

perform (bio)analytical assays. For instance, they can be modified with common antibodies for selectively detecting different antigens of bacteria, viruses or parasites. These sensors seem to be very attractive, since they show very low detection limits in a simple way.[222] On the other hand, nanocrystals can be also used for heavy metals detection by using fluorescence quenching, which means that the interaction of the quantum dot with the metal induces the lost of fluorescence of the particle.[223] An example could be the detection of mercury and silver using an electron-transfer-quenching path,[224] where modified QDs with thymine or cytosine interacts with the metals causing the lost of transfer energy from the nanocrystals. However, more complex inverse mechanisms can be also used, such as the interaction of a negatively charged stabilizer of gold nanoparticles with a heavy metal, which liberates the interaction of the gold colloid with nanocrystals, making feasible the emission of fluorescence by the nanocrystals (Figure 1.20). [225] Therefore, well defined synthetic procedures are required in order to exploit all the potential of nanocrystals.

Nevertheless, their optical properties strongly depend on their synthesis. For instance, their FWHM depen on the size distribution of the colloid. As with metallic nanoparticles, homogeneus and well defined nanocrystals will lead to narrow band spectra.[226] Moreover, the surface of the particles directly affects their quantum efficiency, since it leads to non-radiative electron-hole recombination, which competes with the intrinsic radiative recombination.[227]

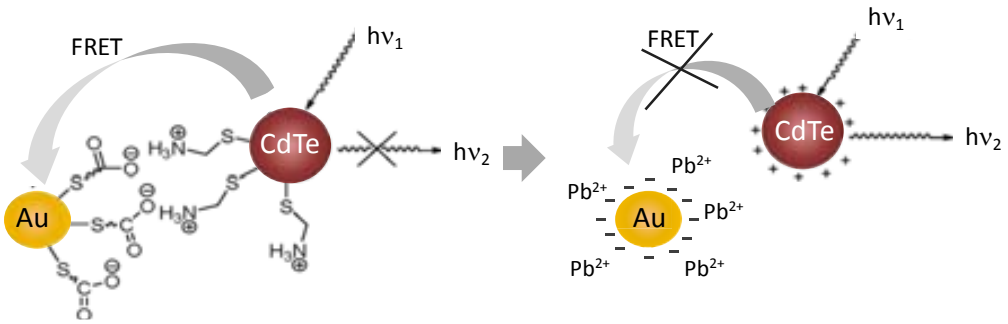

Figure 1.20: Schematic representation of the inhibition assay method for Pb^{2+} determination using QDs and FERT. [225]

1.2.3.2 CARBON DOTS

Carbon dots (C-dots) are small carbon nanoparticles with various levels of surface passivation and sizes usually below 10 nm. C-dots were obtained for the first time in 2004 during the purification of single-walled carbon

[222] Lodeiro, C.; Capelo, J. L.; Mejuto, J. C.; Oliveira, E.; Santos, H. M.; Pedras, B.; Nuñez, C.; *Chem. Soc. Rev.,* **2010**, 39, 1.
[223] Xie, J.; Zheng, Y.; Ying, J.Y.*; J. Am. Chem. Soc.*, **2009**, 131, 888.
[224] Freeman, R.; Finder, T.L.; Willner, L.; *Angew. Chem. Int. Ed.,* **2009,** 48, 7818.
[225] Wang X.; Guo, X.; *Analyst*, **2009**, 134, 1348.
[226] Peng, Z.A.; Peng, X.*; J. Am. Chem. Soc.,* **2001**, 123, 183.
[227] Yu, W.W.; *Expert Opin. Biol. Ther.*, **2008**, 8(10), 1571.

nanotubes through preparative electrophoresis.[228] Surprisingly, the new nanomaterial showed an intense fluorescence, on the contrary to other carbon materials, which promoted the interest of many scientists.[229] Nuclear magnetic resonance (NMR) C-dots characterization showed up a nanocrystalline core featuring graphitic sp^2 carbon atoms (d = 10 - 180 ppm range) with no saturated sp^3 carbon atoms (d = 8 - 80 ppm), which indicates that C-dots are conjugated systems (Figure 1.21 A).[230-231] Actually, three types of carbon signals were found: external and internal C=C bonds and C=O bonds. Moreover, fourier transform infrared spectroscopy (FTIR) measurements also confirmed the presence of C=C aromatic ring stretches. Therefore, C-dots typically contain many carboxylic/carbonyl moieties at their surface (Figure 1.21 B).[232] C-dots are thus water soluble but they can also be functionalized with various organic, inorganic or biological species, conferring non-aqueous solvent solubility as well. In fact, the dependence of fluorescence on the surface passivation/functionalization has been observed. Surface passivation steps with for instance amino-terminated reagents usually enhances the fluorescence brightness. These carbon colloids are therefore called as graphene quantum dots, carbon quantum dots, fluorescent carbon, carbon nanodots or simply carbon dots.

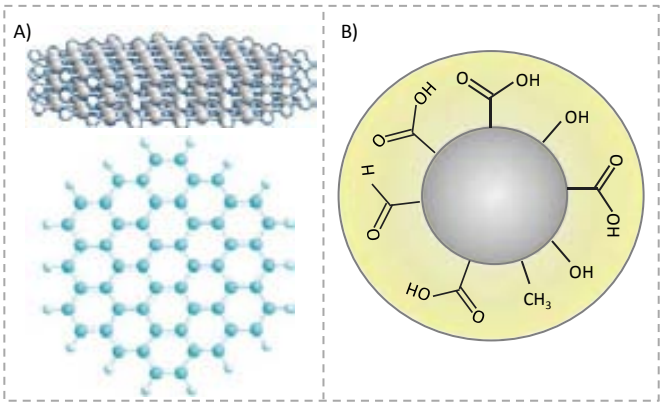

Figure 1.21:
A) Depiction of the nanocrystalline core structure of C-dots with graphitic sp^2 carbon atoms.
B) General functionalized C-dots with peripheral carboxylic/carbonyl moieties at their surface. [230-232]

Optical properties of C-dots are still in study and require further clarification. Nevertheless, some aspects are well determined, such as the strong absorption band found in the UV region, which normally is extended in the visible range after surface passivation of the nanoparticles. The fluorescence spectra of C-dots are normally broad, with the dependence of the emission location and intensity on the excitation wavelength (Figure 1.22).[233]

---

[228] Xu, X.Y; Ray, R; Gu, Y.L; Ploehn, H.;. Gearheart, L; Raker K;. Scrivens, W.A.; *J. Am. Chem. Soc.,* **2004**, 126, 12736.
[229] Esteves da Silva J.C.G.; Goncalves, H. M. R.; *TrAC, Trends Anal. Chem.,* **2011**, 30, 1327.
[230] Liu, H.P.; Ye T.; Mao, C.D. *Angew. Chem., Int. Ed.,* **2007**, 46, 6473.
[231] Wang, X.H.; Qu, K.G.; Xu, B.L.; Ren J.S.; Qu, X.G. *Nano Res.*, **2011**, 4, 908.
[232] Shen, J.; Zhu, Y.; Yang, X.; Li, C.; *Chem. Commun.*, **2012**, 48, 3686.
[233] Shen, J.; Zhu, Y.; Chen, C.; Yang X.; Li, C.; *Chem. Commun.,* **2011**, 47, 2580.

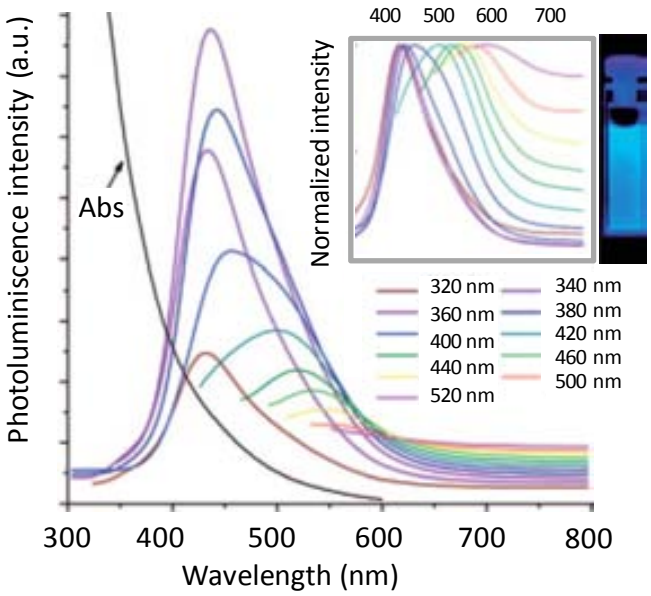

Figure 1.22: UV-Vis absorption and photoluminiscence spectra of C-dots at different excitation wavelengths. Inset: photograph of a C-dots solution in water under UV light. [233]

The luminescence properties of C-dots can be explained by a surface-defect-based luminescent mechanism, where the presence of defect states introduced by the passivation/functionalization of particles is responsible of the fluorescence. [234-235] In fact, the carbon-oxygen bonds present in the particles seem to be necessary.[236] However, other mechanisms should be also considered, such as HOMO–LUMO transitions.[233] Figure 1.23 shows the two possible processes. The transition from the lowest unoccupied molecular orbital (LUMO) to the highest occupied molecular orbital (HOMO) from carbene can be also the responsible from the luminescent properties of C-dots, where the energy of the HOMO–LUMO gap depends on the size of the graphene fragments.[237] Therefore, as the size of C-dots increase, the band gap decreases, emitting at higher wavelengths. Nevertheless, the relation of surface passivation and fluorescence properties is still poorly understood, and it is considered to be related to the synthetic method performed to obtain the C-dot colloidal suspension.[238]

In the same manner, the quantum yield (QY) of C-dots varies depending on the synthesizing method used and the passivating agent employed. Low values of QYs are usually obtained in one-step thermal decomposition methods (circa 3 %),[239] while by laser ablation QY up to 10 % can be

[234] Hu, S.L.; Niu, K.Y.; Sun, J.; Yang, J.; Zhao, N.Q.; Du, X.W.; *J. Mater. Chem.*, **2009,** 19, 484.
[235] Li, X.Y.; Wang, H.Q.; Shimizu, Y.; Pyatenko, A.; Kawaguchi, K.; Koshizaki, N.; *Chem. Commun.,* **2011,** 47, 932.
[236] Esteves da Silva, J.C.G.; Gonçalves, H.M.R.; *Trends in Analytical Chemistry*, **2011**, 30(8), 1327.
[237] Eda, G.; Lin, Y.-Y.; Mattevi, C.; Yamaguchi, H.; Chen, H.-A.; Chen, I.-S.; Chen C.-W.; Chhowalla, M.; *Adv. Mater.,* **2010,** 22, 505.
[238] Li, H.; Kang, Z.; Liu Y.; Lee, S.-T.; *J. Mater. Chem.,* **2012**, 22, 24230.
[239] Sun, Y.P.; Zhou, B.; Lin, Y.; Wang, W.; Fernando, K.A.S.; Pathak, P.; Meziani, M.J.; Harruff, B.A.; Wang, X.; Wang, H.F.; Luo, P.J.G.; Yang, H.; Kose, M.E.; Chen, B.L.; Veca, L.M.; Xie, S.Y.*; J. Am. Chem. Soc.,* **2006,** 128, 7756.

reached. [240] In general, the QYs of those C-dots, which emit photoluminescence with carboxylic moieties at their surface can be increased by further surface passivation with for instance organic polymers and diamine compounds, achieving QYs of 20 % and even of 60 % upon purification.

The pH has been also found to be a photoluminescence intensity tunable factor. When pH-dependant molecules are introduced in the C-dot surface, such as carboxylic acid groups, they vary its intensity depending on this parameter, even sometimes totally quenching the fluorescence. Thus, the maximum fluorescence intensity is achieved at a concrete pH value. The complete reversibility of this interaction has been demonstrated even at repeated switches from 1 to 13 pH values.[241]

Besides photoluminescence emission under UV light, C-dots are able to strongly emit in the visible region when they are excited in the NIR region (600 - 800 nm), the so called upconversion photoluminescence (UCPL).[242] As in case of fluorescence, the emission peak is located at a wavelength depending on the excitation wavelength. Some authors assign this property to a multi-photon active process.[243] When multiple low-energy photons excite a C-dot particle, they induce the excitation of an electron that would be excited by a higher energy photon, thus relaxing with higher energy than a excited single photon.[234] However, other authors consider that it is related to an anti-Stokes photoluminescence process, since some experiments performed showed the almost constant energy difference between the upconverted emission and the excitation light. Figure 1.23 shows both possible processes. As represented in the scheme, σ and π orbitals are from carbene ground-state multiplicity. Thus, when π-orbital electrons are excited at low energies to the LUMO state, the electrons come back to a low-energy state, the σ orbital. However, σ orbital electrons, although they can be excited, only emit normal fluorescence. This process also explains the constant dependence from the excited and emitted energy. [233]

Photostability of C-dots has been also proved. Many experiments have been done in which the nanoparticles are continuously exposed to excitation sources for several hours. C-dots have shown neither blinking nor meaningful reduction in photoluminescence (PL) intensity. For instance, the fluorescence intensity of C-dots was only decreased in a 4.5 % even after 4 h irradiation,[235] whereas other fluorescent materials, such as polystyrene nanospheres, would photo-bleach within 0.5 h with the same source. In the same manner, other

[240] Bourlinos, A.B.; Stassinopoulos, A.; Anglos, D.; Zboril, R.; Karakassides, M.; Giannelis, E.P.; *Small,* **2008**, 4, 455.
[241] Pan, D.; Zhang, J.; Li Z.; Wu, M.; *Adv. Mater.*, **2010,** 22, 734.
[242] Cao, L.; Wang, X.; Meziani, M. J.; Lu, F.; Wang, H.; Luo, P. G.; Lin, Y.; Harruff, B. A.; Veca, L. M.; Murray, D.; Xie; S.-Y.; Sun, Y.-P.; *J. Am. Chem. Soc.,* **2007,** 129, 11318.
[243] Peng, H.; Travas-Sejdic, J.; *Chem. Mater*. **2009,** 21, 5563.

studies demonstrated a 17 % of intense decrease after 19 h of continuous excitation at 360 nm.[235]

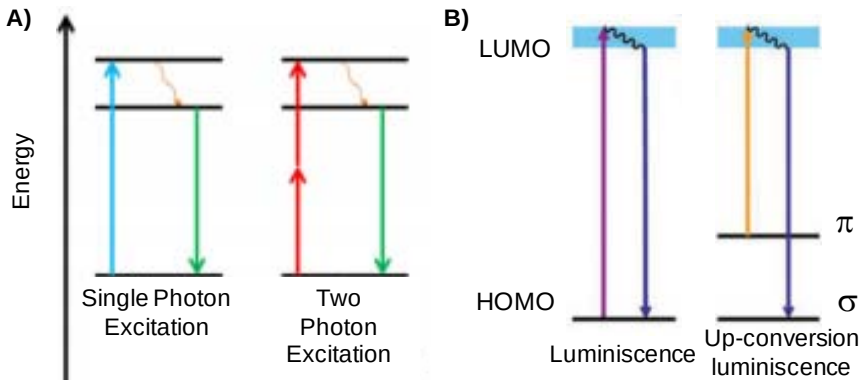

Figure 1.23: Scheme of the different possible mechanisms responsible for the luminescent properties of C-dots. A) Single-photon excitation for PL, and multi-photon active process for UCPL. B) PL and UCPL by a HOMO-LUMO energy mechanism. [233-234]

Moreover, C-dots have demonstrated its low cytotoxicity through the slight reduction of cell viability only for extremely high concentrations of C-dots.[244] However, more studies should be done, such as median lethal dose (LD_{50}) measurements. Nevertheless, C-dots are better in terms of chemical inertness, low cytotoxicity and excellent biocompatibility compared with other nanomaterials. Moreover, recent studies show that C-dots can emit fluorescence in the NIR region being also excited as well in the NIR, which makes them more interesting for bionanotechnology applications[245] because it is predicted that their biocompatibility can be similar to the common approved dyes, such as indocyanine green.

On the other hand, C-dots are either excellent electron donors or acceptors, since they can be efficiently quenched by both kinds of molecules in solution. Thus, C-dots could be employed in light energy conversion applications. Other applications of C-dots are in the development of photovoltaic devices and related applications[246] or in catalysis for the oxygen reduction reaction.[247]

Recent studies have demonstrated the advantages of using C-dots with SERS sensors, since when combined with other materials, such as Au NPs, they exhibit 8 to 11 times stronger SERS than the gold colloid SERS substrate alone for the sensitive detection of target molecules.[248]

Other sensing applications of C-dots have been also developed for nitrite,[249] phosphate[250] or metal ions[251] determination; or biosensors for DNA[252] or α-

[244] Ray, S. C.; Saha, A.; Jana, N. R.; Sarkar, R.*; J. Phys. Chem. C,* **2009**, 113, 18546.
[245] Li, H. T.; He, X. D.; Liu, Y.; Huang, H.; Lian, S. Y.; Lee, S. T.; Kang, Z. H.; *Carbon*, **2011**, 49, 605.
[246] Li, Y. ; Hu, Y.; Zhao, Y.; Shi, G.; Deng, L.; Hou Y.; Qu, L.; *Adv. Mater.,* **2011**, 23, 776.
[247] Li, Y.; Zhao, Y.; Cheng, H.; Hu, Y.; Shi, G.; Dai L.; Qu, L.; *J. Am. Chem. Soc.,* **2012,** 134, 15.
[248] Fan, Y. Q.; Cheng, H. H.; Zhou, C.; Xie, X. J.; Liu, Y.; Dai, L. M.; Zhang, J.; Qu, L. T.; *Nanoscale,* **2012**, 4, 1776.
[249] Lin, Z.; Xue, W.; Chen H.; Lin, J. M.; *Anal. Chem.,* **2011**, 83, 8245.
[250] Zhao, H. X.; Liu, L. Q.; Liu, Z. D.; Wang, Y.; Zhao, X. J.; Huang, C. Z.; *Chem. Commun.,* **2011**, 47, 2604.
[251] Zhou, L.; Lin, Y. H.; Huang, Z. Z.; Ren J. S.; Qu, X. G.; *Chem. Commun*., **2012**, 48, 1147.

fetoprotein[253] detection, among others. These applications can use the photoluminescence or up-converting fluorescence properties of the particles by their direct detection or by FRET processes. On the other hand, pH is an important parameter in many chemical and biological systems, which can be well determined by the use of C-dots. Diverse works can be found in the literature, which describe the sensitivity of C-dots to pH depending on their external composition (carbonyls, amines, hydroxyls, esters, etc). For instance, colorimetric and fluorimetric sensing of pH changes have been reported by using acidic moieties present in the particles, when C-dots are synthesized from ascorbic acid pyrolisis.[254]

1.2.4 THE CASE OF BIOSENSORS (GENOSENSORS)

As earlier explained, when the recognition element of a sensor is a bioreceptor, it is generally called biosensor. Thus, the biological element (such as enzymes, antibodies, microorganisms or cells) of biosensors must be capable of selectively interact with the analyte and generate a primary signal, which is transformed into an electric one by the transductor.[255] Usually, the biologic material is immobilized on a substrate surface, which can also be the transducer, by means of adsorption or cross-linking techniques. This step is crucial, because the immobilization has to assure the correct activity of the biologic material and the sensitivity of the transducer must not be damaged.

Biosensors can be classified according to the bioreceptor (antibodies/antigen, enzyme, nucleic acids/DNA, cell, etc) used. Enzymatic biosensors measures the selective inhibition or the catalysis of enzymes generated from a specific target. However, the employment of enzymes as labels in biosensors, such as in enzyme-labelled antigens and antibodies, is more frequent, since their use allow to amplify the signal by the continuous generation of the enzymatic product. [256] Antibodies as bioreceptors are very common. Antibodies specifically recognize a unique part of a foreign target, called antigen, in a similar lock-and-key fit. Different strategies can be employed for the development of an immunosensor. However, the most usual one is the Enzyme-Linked ImmunoSorbent Assay (ELISA), where the antigen interacts with two different antibodies, one immobilized onto a surface, and another tagged with an enzyme to perform a colorimetric enzymatic reaction. On the other hand, the use of nucleic acids (oligonucleotides)

---

[252] Zhao, J.; Chen, G.; Zhu L.; Li, G.; *Electrochem. Commun*., **2011**, 13, 31.
[253] Dai, H.; Yang, C. P.; Tong, Y. J.; Xu, G. F.; Ma, X. L.; Lin Y. Y.; Chen, G. N.; *Chem. Commun.,* **2012**, 48, 3055.
[254] Jia, X.; Li, J.; Wang, E.; *Nanoscale*, **2012**, 4, 5572.
[255] Eggins, B. R.; in: *Chemical Sensors and Biosensors. Analytical Techniques in the Sciences;* Ed. D. J. Ando., Northern Ireland, UK: John Wiley & Sons, **2002.**
[256] Velusamy, V.; Arshak, K.; Korostynska, O.; Oliwa, K.; Adley, C.; *Biotechnol. Adv.*, **2010**, 28, 232.

as bioreceptors has received more attention in recent years, evolving in the well known DNA biosensors. This responds not only to the highly specific identification of the target analyte, which is achieved by matching the complementary base pairs of the target organism (hybridization), [257] but also to their higher stability and simpler manipulation when compared with enzymes or antibodies. Moreover, oligonucleotides can be synthesized in the laboratory, which reduces their cost and therefore the price of the whole assay. Oligonucleotides are linear chains of nucleotides, each of them composed of a base, adenine (A), cytosine (C), guanine (G) or thymine (T), and a sugar backbone.[258] The specificity of DNA biosensors arises in two properties: every oligonucleotide is characterized for a concrete sequence of bases, unique for each organism; and when an oligonucleotide binds another one to form a double helix; A can only bind T, and C only G. One of the advantages of using DNA instead of other molecules such as antibodies for immunoassays, is the resistivity of DNA to solvents and changes to ionic force. Therefore, the developed devices show a long life-span compared to other approaches, e.g. immunosensors. Other advantages of these sensors are the easy manipulation of the DNA sequences, and their simple functionalization or labelling.[259] Regeneration is also possible as dehybridization of DNA take place at 95 ºC, where oligonucleotides are still stable.

The typical DNA biosensor measures the hybridization of ssDNA of a sample to its complementary strand, which most of times is immobilized onto a solid surface, such as polystyrene plates.[260] The employment of magnetic beads (MBs), which have been started to use in recent years, offer more advantages as substrate surface. These beads consist of superparamagnetic particles of iron oxide (maghemite Fe_2O_3 or magnetite Fe_2O_4) [261] of a few micrometers embedded in a polymeric matrix. Due to their magnetic properties, MBs can be retained or moved in the presence of a magnetic field, but in its absence, they do no present any residual memory. Thus, they can be easily retained by the action of a magnet and dispersed again when it is removed. This fact can help to perform certain necessary steps of DNA assays such as washing or pre-concentration. [262-263] Furthermore, their large surface-to-volume ratio increases the sensitivity of the assays, since they allow the immobilization of more bioreceptor with access to the target. The MBs polymer shell is easily functionalized with different

[257] Yang, M.; McGovern, M.E.; Thompson, M.; *Anal. Chim. Acta*, **1997**, 346, 259.
[258] Stryer, L.: in: *Biochemistry;* Freeman, New York, 4th edition, **1995**.
[259] Kricka, L.J.; in: *Nonisotopic DNA Probe Techniques;* Academic Press, Inc.: San Diego, **1992**.
[260] Stepaniak, L.; Sorhaug, T.; Jedrychowski, L.; in: *Immunochemical. Ancyclopedia of Dairy Sciences; Elservier, Oxford,* **2004**.
[261] Sivagnanam V., Ph. D. Thesis, École Polytechnique Fédérale de Lausanne, **2010**.
[262] Solé, S.; Merkoçi, A.; Alegret, S.; *TrAC, Trends Anal. Chem.*, **2001**, 20, 102.
[263] Gijs, M.*; Microfluid. Nanofluid.*, **2004**, 1, 22.

functional groups (e.g. acid, amino or tosyl groups) or even with biologic material (e.g. proteins, enzymes, oligonucleotides, antibodies) (Figure 1.24).[264]

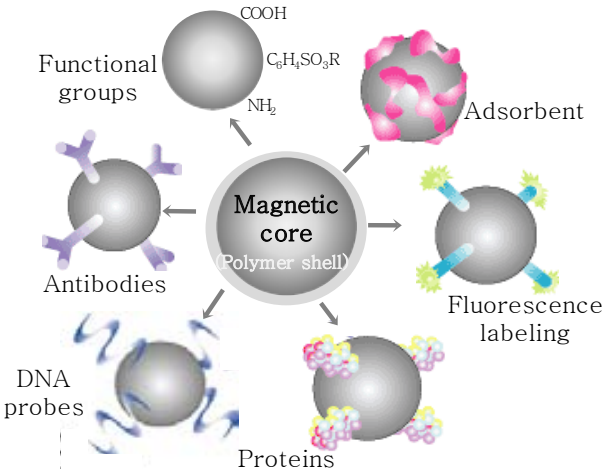

Figure 1.24: Schematic representation of Magnetic Beads with some different functional modifications.[264]

Assays based on hybridization require thus knowing the sequence of the analyte oligonucleotide (target), since the recognition is performed by its complementary oligonucleotide (probe), which is often labelled for the hybridization phenomenon detection. Different possibilities for the detection of DNA can be performed. Some of them consist on the direct union of a label to the probe. Other more versatile approaches, require a secondary recognition after the hybridization, which could involve other biomolecules, such as proteins, or a second hybridization step (Figure 1.25).[258]

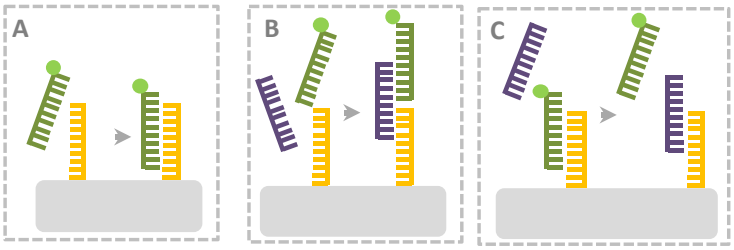

Figure 1.25: Different approaches for DNA detection. **A)** Direct assay. Direct union of a label to the probe. **B)** Sandwich assay. The analyte is recognized by two different biomolecules, one normally attached to a surface, and the other labeled for the detection. **C)** Competitive assay. The unlabeled analyte in a sample competes with labeled analyte to bind the biomolecule. [258]

A wide range of labels for bioanalytical detection can be used. Enzymes are one of the preferred ones, since they can highly amplify the signal. The most employed enzymes are alkaline phosphatase, glucose oxidase or peroxidase. However, fluorescence or chemiluminiscent compounds, e.g. fluorescein, Texas Red or luminal, are gaining interest as markers due to the sensitivity of luminescent techniques. In this sense, nanoparticles can provide some advantages when they are used in DNA biosensors, such as an enhancement of the detection limit and sensitivity. Oligonucleotides can be attached by thiol-gold bonds to gold nanoparticles surface,[265- 266] any other covalent bonding,[206,267] or

[264] Pamme, N.; *Lab Chip*, **2006**, 6, 24.
[265] Alivisatos, A.P.; Johnsson, K.P.; Peng, X:; Wilson, T.E.; Loweth, C.J., Bruchez, M.P.; Schultz, P.G.; *Nature,* **1996**, 382, 609.

by biotin-avidin linkage, where avidin is absorbed on the nanoparticle surface.[268] Thus, a huge number of works can be found in the literature using nanoparticles as markers in DNA sensing. Some of them are based on gold nanoparticles, which can be detected optically or electrochemically. [269] Most of the optical approaches take advantage of the change of colour of the colloid from red to blue when the particles aggregate due to the interaction of the analyte with the biomolecules immobilized onto the surface of the NP.[270] In this way, methods capable of detecting trace amounts of oligonucleotides has been described.[143] Others methods based on dynamic light scattering (DLS) measurements, which is a technique that determines the size distribution of small particles in suspension, are extremely easy and do and not require separation and amplification steps (Figure 1.26).[271] Electrochemical based approaches for DNA sensing takes a large part of the literature. Many strategies based on Au NPs can be performed, such as the total dissolution of Au NPs to Au(III) ions for its detection, or the coating of the nanoparticle with another metal for its subsequent determination.[272]

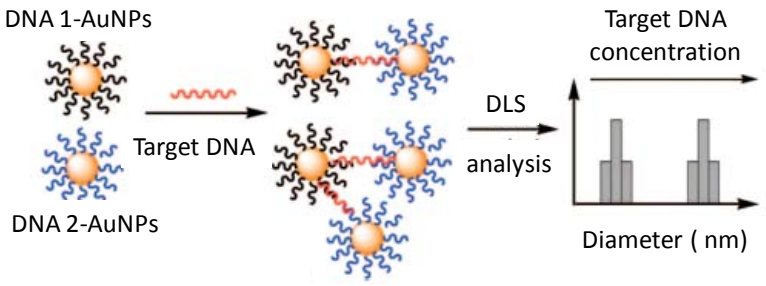

Figure 1.26: Scheme of DNA detection using Au NPs probes and DLS.[271]

On the other hand, quantum dots are also gaining interest in biosensing. Although some works based on their electrochemical properties have been presented,[273] their most common use as marker is as a fluorescent.[274] Multiplexing can be easily performed by the use of different emitting QDs and using a unique excitation source.[275] Moreover, a great number of FRET based approaches can be also found in the literature, where QDs acts as FRET energy donors (Figure 1.27).[276] Molecular beacons, usually composed of an oligonucleotide, a 5´ end fluorophore, and a 3´ end quencher, are another strategy for FRET assays, existing a wide range of possibilities for performing

[266] Zanchet, D.; Micheel, C. M.; Parak, W. J.; Gerion, D.; Alivisatos, A. P.; *Nano Lett.,* **2001**, 1, 32.
[267] Bruchez, M.J.; Moronne, M.; Gin, P.; Weiss, S.; Alivisatos, A.P.; *Science,* **2002,** 281, 2013.
[268] Florin, E.L.; Moy, V.T., Gaub, H.E.; *Science*, **1994**, 264, 415.
[269] Elghanian, R.; Storhoff, J.J.; Mucic, R.C.; Letsinger, R.L.; Mirkin, C.A.; *Science,* **1997,** 277, 1078.
[270] Storhoff, J.J.; Elghanian, R.; Mucic, R.C.; Mirkin, C.A.; Letsinger, R.L.*; J. Am. Chem. Soc.*; **1998,** 120, 1959.
[271] Dai, Q.; Liu, X.;. Coutts, J.; Austin, L.; Huo, Q.; *J. Am. Chem. Soc.*, **2008,** 130, 8138.
[272] Castañeda, M.T.; Alegret, S.; Merkoçi, A.; *Electroanal.*, **2007,** 19, 743.
[273] De la Escosura-Muñiz, A.; Paroloa, C.; Merkoçi, A.; *Mater. Today,* **2010**, 13, 24.
[274] Alivisatos, A.P.; *Sci. Am.*, **2007,** 23, 73.
[275] Mingyong, H.; Gao, X.; Su, J.Z.; Nie, S.; N*at. Biotechnol.,* **2001**, 19, 631.
[276] Zhang, C.-Y.; Yeh, H.-C.; Kuroki, M.T.; Wang, T.-W.; *Nat. Mater.*, **2005**, 4, 826.

these assays.[277-278] In order to attach oligonucleotides to QDs surface, parallel strategies to those presented for gold nanoparticles can be used, which means adsoption,[279] linkage via mercapto groups,[280] electrostatic interaction[281] and covalent bonding.[282] Again, covalent bonding is preferable for stability reasons. Many different crosslinker molecules are commercially available, which are reactive towards groups such as –COOH (carboxyl), $–NH_2$ (amine), or –SH (thiol, mercapto).

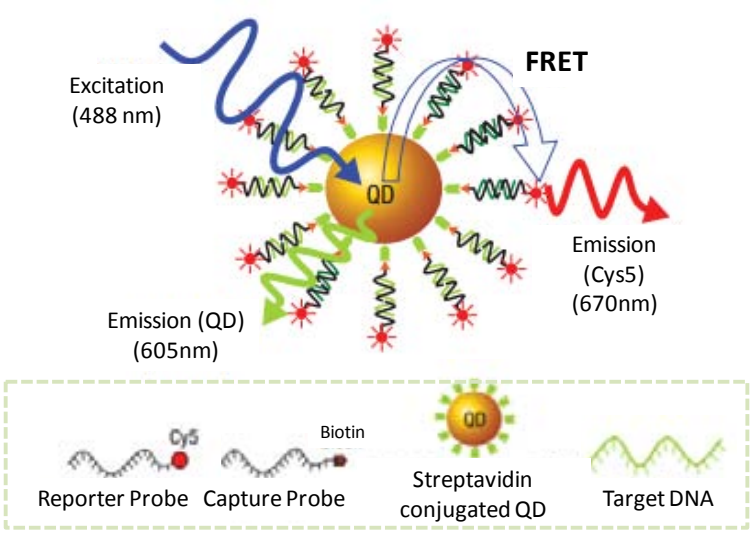

Figure 1.27: Scheme of single-QD-based DNA nanosensor. Fluorescence emission from labeled target with Cys5 on illumination on QD caused by FRET between Cys5 acceptors and a QD donor when hybridization takes place.[276]

In general, first applications of DNA biosensors involved clinical diagnosis for the detection of hereditary diseases, cancer, and viral or bacterial infections by the detection of human, virus or bacteria gene sequences. Nowadays, their application goes beyond that, being possible to find applications in the environmental monitoring field, being feasible the real-time pathogen detection in a precise and simple way.

[277] Kim, J.H.; Morikis, D.; Ozkan, M.; *Sens. Actuators, B*, **2004**, 102, 315.
[278] Ezzati, J.; Dolatabadi, N.; Mashinchian, O.; Ayoubi, B.; Jamali, A.A.; Mobed, A.; Losic, D.; Omidi, Y.; de la Guardia, M.; *TrAC, Trends Anal. Chem.,* **2011**, 30, 459.
[279] Lakowicz, J. R.; Gryczynski, I.; Gryczynski, Z.; Nowaczyk, K.; Murphy C. J.; *Anal. Biochem.*, **2000**, 280, 128.
[280] Mitchell, G. P.; Mirkin, C. A.; Letsinger, R. L.; *J. Am. Chem. Soc.*, **1999**, 121, 8122.
[281] Mattoussi, H.; Mauro, J. M.; Goldman, E. R.; Anderson, G. P.; Sundar, V. C.; Mikulec, F. V.; Bawendi, M.G.*; J. Am. Chem. Soc.*, **2000**, 122, 12142.
[282] Mamedova, N. N.; Kotov, N. A.; Rogach, A. L.; Studer, J.; *Nano Lett.,* **2001**, 1, 281.

1.3 SYNTHESIS AND CHARACTERIZATION OF NANOPARTICLES

Nanoparticles have a wide range of applications due to its special characteristics. However, it is very important to achieve homogeneous and reproducible materials of well-defined characteristics. This, strictly depends on the nanoparticle size, shape and composition, and therefore, are very affected by their synthesis.

There are two main synthetic procedures for nanomaterials and nanostructures: the top-down and the bottom-up approaches (Figure 1.28). Top-down methods consist on breaking down large entities to create smaller features. It normally uses micro-fabrication methods to cut, mill and shape materials to obtain the desired nanostructure. The main problem of these approaches is the imperfection on the surfaces achieved and the contaminations formed in the nanostructures, since techniques such as lithography can cause crystallographic damages when pattering materials.[283-284] These imperfections introduced on the materials are difficult to control, what produces a significant impact on their physical and chemical properties. However, these procedures are usually employed to obtain nanocomposites and nanograined materials with a post sintering process that diminishes the defects on the surface, and on applications where impurities are not of significant importance.

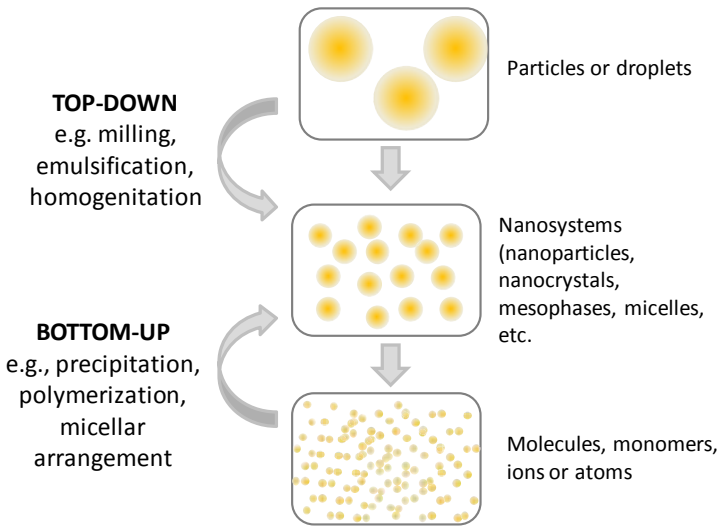

Figure 1.28: Scheme of top-down and bottom-up approaches.

Bottom-up approaches consist on creating materials by self-assembling atom-by-atom, molecule-by-molecule, or cluster-by-cluster on a larger scale. These methods usually generate more uniform structures with fewer defects. Moreover, bottom-up methods are cheaper than the top-down, since no special equipments are required. Therefore, they are the common employed approach for developing

[283] Temperley, H.N.V.; *Proc. Cambridge Phil. Soc.*, **1952**, 48, 683.
[284] Burton, W.K.; *Trans. Electron Dev.,* **1976,** ED-23, 621.

nanomaterials. However, between the different syntheses and processes appreciable differences in chemical composition, crystallinity, and microstructure of the materials exist, which is reflected on the chemical and physical properties.[7] This issue has been addresses in the present thesis.

1.3.1 SYNTHESIS OF NANOPARTICLES

Many synthetic methods to obtain uniform and stable nanoparticles by using bottom-up approaches exist, which can be included in two main categories, the kinetic (or heterogeneous nucleation) and the thermodynamic (or homogeneous nucleation) approaches.

Kinetic approaches are those in which the growth of particles takes place by limiting the amount of precursors or the available space. In general, special confinements can be divided in four groups: liquid droplets in gas phase (aerosol synthesis[285-286] and spray pyrolysis[287-288]), liquid droplets in liquid (micelle microemulsions synthesis[289-290] including reverse micelles[291-292]), template-based synthesis[293-294] and self-termination synthesis.[295-296]

Thermodynamic approaches are those in which the synthetic process consists on the generation of supersaturated solutions to make feasible the *nucleation* (first step), and the subsequent *growth* of the seeds formed (second step). Figure 1.29 shows a scheme of the process of nanoparticles formation.[297] There are several examples of homogeneous nucleation, such as the synthesis of semiconductor nanoparticles by pyrolysis of organometallic compounds[298-299] or the synthesis of metal colloidal dispersions by the reduction of metal complexes in dilute solutions.[300-301]

The base of the homogeneous nucleation step is the solubility equilibrium present in a solution.[7] For instance, a solution with supersaturated concentration of a solute has large values of Gibbs free energy (ΔG), so in order to diminish this value and maintain the equilibrium concentration in the sine of the solution, this

---

[285] Ingebrethsen, B.J.; Matijevic, E.; *J. Aerosol Sci*., **1980**, 11, 271.
[286] Nakamura, K.; Partch, R.E.; Matijevic, E.; *J. Colloid Interface Sci.*, **1984**, 99, 118.
[287] Kieda, N.; Messing, G.L.; *J. Mater. Res*., **1998**, 13, 1660.
[288] Osakada, K.; Yamamoto, T.; *Chem. Commun*., **1987**, 1117.
[289] Boutonnet, M.; Kizling, J.; Stenius, P.; Maire, G.*; Colloids Surf*., A, **1982**, 5, 209.
[290] Petit, C.; Lixon, P.; Pileni, M.P.*; J. Phys. Chem*., **1990**, 94, 1598.
[291] Capek, I; *Adv. Colloid Interface Sci*., **2004**, 110, 49.
[292] Ganguli, A.K.; Ahmad, T.; Nanosci, J.; *Nanotechnology*, **2007**, 7, 2029.
[293] Wang, Y.; Herron, N; *J. Phys. Chem*., **1987**, 91, 257.
[294] Bawendi, M.G.; Steigerwald, M.L.; Brus, L.E.; *Annu. Rev. Phys. Chem*., **1990**, 41, 477.
[295] Selvan, S.T.; Bullen, C.; Ashokkumar, M.; Mulvaney, P.; *Adv. Mater*., **2001**, 13, 985.
[296] Dabbousi, B.O.; Rodriguez-Viejo, J.; Mikulec, F.V.; Heine, J.R.; Mattoussi, H; Ober, R.; Jensen, K.F.; Bawendi, M.G.*; J. Phys. Chem.,* **1997**, B101, 9463.
[297] Haruta, M.; Delmon, B.*; J. Chim. Phys. Phys.,* **1986**, 83, 859.
[298] Wang, Y.; *Acc. Chem. Res*., **1991**, 24, 133.
[299] Murray, C.B.; Kagan, C.R.; Bawendi, M.G.; *Ann. Rev. Mater. Sci*., **2000**, 30, 545.
[300] Henglein, A.; *Chem. Rev*., **1989,** 89, 1861.
[301] Schmid, G.; *Chem. Rev*., **1992**, 92, 1709.

segregates its excess of solute by forming a solid phase (monomers or seeds) until ΔG reaches its highest value. Then, the concentration of solute decreases, diminishing ΔG value, and no more nuclei will be formed. The growth of the seed formed is carried out by the rest of solute present in the solution. Although nucleation and growth are inseparable processes, their kinetic is completely different, since nucleation has quick kinetics whereas growth is a slower process.

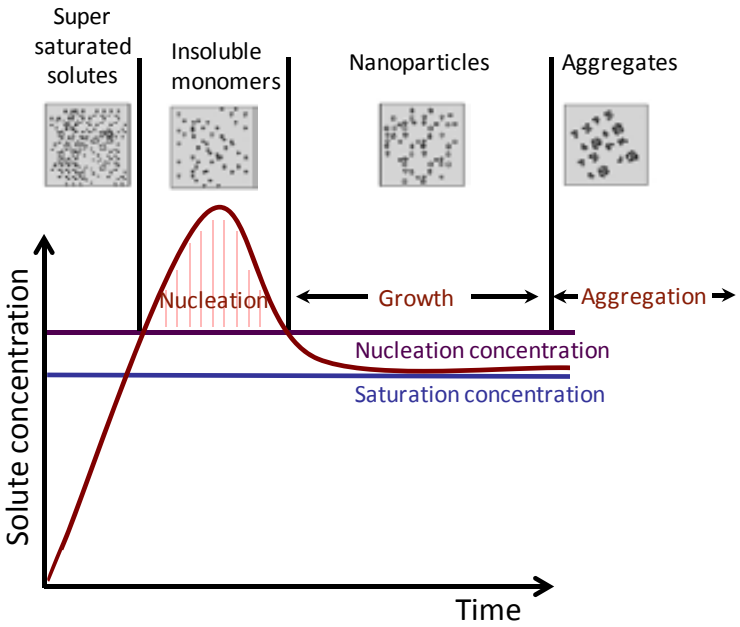

Figure 1.29: Process of nanoparticles formation for homogeneous nucleation. [287]

On the other hand, three different processes can be involved in the growth of seeds. First, the mononuclear growth, which consists of sequentially growing layer after layer only when the layer that is being formed is complete. This mechanism is not the preferred one for nanoparticles formation, since it does not generate homogeneous suspensions.[302] Another process is the polynuclear growth, which occurs when the surface concentration of the seed is very high. In this case, the growth of layers is performed in an uncontrolled way, as a second layer can be formed when the first one is still not finished. Finally, the third mechanism is based on diffusion, which consists on supplying the grow species to the grow surface. When the solute concentration decreases until the minimal concentration due to seeds formation, nucleation stops; and then only growth takes place. If growth is controlled by diffusion, the formation of nanoparticles will be uniform. However, some authors state that nanoparticles growth involve all three mechanisms and that small nuclei prefer monolayer growth, while larger nuclei are related to polynuclear mechanisms. In general, diffusion based approaches are preferred to synthesize large particles.[303]

[302] Nielsen, A.E.; in: *Kinetic of Precipitation;* MacMillan, New York, **1964**.
[303] Williams, R; Yocom, P.M.; Stofko, F.S.; *J. Colloid Interface Sci*., **1985**, 106, 388.

Ostwald ripening phenomenon can also happen. When two particles with different size are in the same solvent, each particle develops equilibrium with its surroundings. Owing to the higher solubility of the smaller particles, a net diffusion of solute from the surface of the small particle to the proximity of the large one will occur. This solute will be deposited into the surface of the larger particle, increasing as a result its size, while the small one become smaller (Figure 1.30). This phenomenon is enhanced when increasing the temperature of the solution due to solubility increases.[7] Ostwald ripening can have either positive or negative effects on the size distribution of colloids, depending on the conditions of the process.

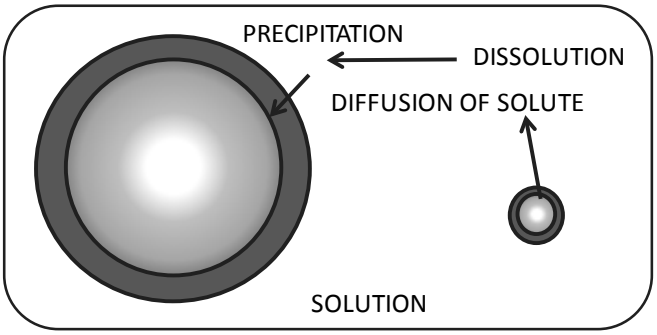

Figure 1.30: Scheme of Ostwald ripening.[7]

Finally, a surface modification of the nanoparticles is usually necessary for different purposes, such as for the passivation of reactive sites on the nanocrystals, for the stabilization of nanoparticles suspension in a medium, for surface functionalization to give chemical reactivity or to assemble nanoparticles.
Surface modification to stabilize nanoparticles against aggregation can be done in different ways. The simplest stabilization is achieved by electrostatic repulsions (electrostatic stabilization), which is generally obtained with the medium of synthesis. However, better and more durable results are achieved when ligands are attached to the particles surface (steric stabilization), usually performed by adding the ligand during the synthesis reaction. For this purpose, the employed ligands must have chemical functional groups with affinity for the nanoparticle, such as thiol groups for stabilizing gold nanoparticles. Obviously, the selection of the ligand and its nature will depend on the medium where nanoparticles are being suspended. For instance, ligands with thiol groups can be used in aqueous solutions; while other ligands such as trioctylphosphine oxide (TOPO) can be used when nanoparticles are suspended in organic mediums (Figure 1.31, top).[304] In aqueous solutions, molecules with strong charged groups (Figure 1.31, bottom), like carboxylic or sulphonic acids, have shown the best results for nanoparticles stabilization. However, they are affected by the salt concentration or the pH of

[304] Sperling, R.A.; Parak, W.J.; *Phil. Trans. R. Soc. A*, **2010**, 368, 1333.

the solution. Therefore, these parameters must be taken into account to assure the stabilization.[305]

Electron-donating groups like thiols, [306-307] amines or phosphines [308] can easily bind the surface of the nanoparticle, but can be also removed in the presence of other ligands. [309- 310] This reactivity based on ligand exchange is commonly used to provide new properties or functionality to the nanoparticles. For example, nanoparticles stabilized with phosphines can be replaced for thiol-modified ligands containing deoxyribonucleic acid (DNA) for sensing applications.

The different synthetic strategies and the stabilization of nanoparticles is being further explained, classifying them according to the type of nanoparticle.

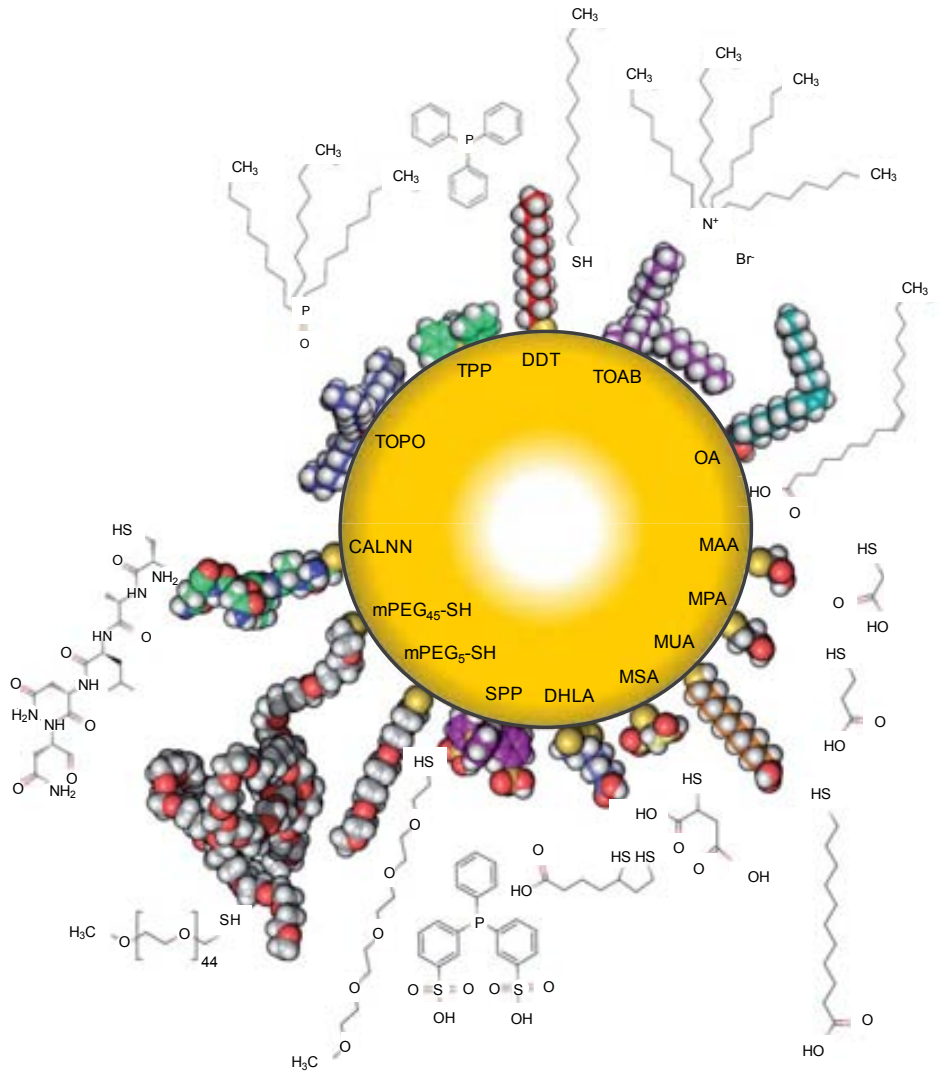

Figure 1.31: **Top:** Hydrophobic ligands usually used for nanoparticles stabilizing with their spatial conformation (not in scale). From left to right, trioctylphosphine oxide (TOPO), triphenylphosphine (TPP), dodecanethiol (DDT), tetraoctylammonium bromide (TOAB) and oleic acid (OA). **Bottom:** Hydrophilic ligands usually used for nanoparticles stabilizing with their spatial conformation (not in scale). From right to left, mercaptoacetic acid (MAA), mercaptopropionic acid (MPA), mercaptoundecanoic acid (MUA), mercaptosuccinic acid (MSA), dihygrolipid acid (DHLA), bis-sulphonated triphenylphosphine (SPP), $mPEG_5$-SH, $mPEG_{45}$-SH (2000 g mol^{-1}) and a short peptide of CALNN. [304]

[305] Laaksonen, T.; Ahonen, P.; Johans, C.; Kontturi, K.; *ChemPhysChem,* **2006**, 7, 2143.
[306] Weisbecker, C.S.; Merritt, M.V.; Whitesides, G.M.; *Langmuir*, **1996**, 12, 3763.
[307] Lin, S.Y.; Tsai, Y.T.; Chen, C.C.; Lin, C.M.; Chen, C.H.; *J. Phys. Chem. B,* **2004,** 108, 2134.
[308] Leff, D.V.; Brandt, L.; Heath, J.R.; *Langmuir,* **1996,** 12, 4723.
[309] Döllefeld, H.; Hoppe, K.; Kolny, J.; Schilling, K.; Weller, H.; Eychmüller, A.; *Phys. Chem. Chem. Phys.,* **2002**, 4, 4747.
[310] Ji, X.; Copenhaver, D.; Sichmeller, C.; Peng, X.; *J. Am. Chem. Soc.,* **2008**, 130, 5726.

1.3.1.1 METALLIC NANOPARTICLES

Metallic nanoparticles (MNPs) have been widely studied due to their easy synthesis and their unique properties originated from its quantum scale dimensions, which make them very interesting candidates for nanotechnological applications in catalysis, sensors, photochemistry or optoelectronics among others. Silver and gold nanoparticles exhibit tuneable optical properties depending on their size and shape. In the same manner, the chemical reactivity of nanoparticles strongly depends not only on their composition but also on their dimensions and aspect. The surface area-to-volume ratio, the bounding facets or the number of step edges are characteristics which determine the chemistry on the surface of the nanoparticles.[311-312] Thus, it is very important to study and control the synthetic procedure of the nanoparticles in order to obtain resproducible particles with well-known properties for their subsequent use.

- **SILVER NANOPARTICLES**

The synthesis of silver nanoparticles usually involves the reduction of metal salts by a reducing agent such as hydrazine, citrate, borohydride, ascorbate or ethylene oxide.[313] This method usually produces spherical nanoparticles, while more specific procedures, which employ different reductant or/and ligands, can give nanorods, nanowires or nanoprisms.

The selection of the reducing agent will depend on the desired size of nanoparticles. For instance, the use of citrate as a reductant generate nanoparticles of around 40 nm, while the employment of borohydride produces smaller particles. With polyols, particles between 40 and 70 nm are obtained.[314]

The temperature of synthesis is also an important parameter to control, since higher temperatures increase the reaction velocity and can affect to the capacity of the reducing reagent.[315]

On the other hand, it is very important to introduce electrostatic or steric stabilization during the reaction in order to achieve long-time stable suspensions and isolable nanoparticles from the solution. The stabilizing agent can also determine the size, morphology, size distribution and chemistry of the silver nanoparticles obtained.

The stabilization can be performed by many different ways, and sometimes the same reducing agent act as the stabilizer, as it is in the case of citrate of borohydride. Other examples of stabilization are micelles, dendrimer structures, polymer assemblies, surfactants, thiols, etc.[316]

---

[311] Tao, A.R.; Habas, S.; Yang, P.; *Small,* **2008**, 4 (3), 310.
[312] Ahmadi,T.S.; Wang, Z.L.; Green, T.C.; Henglein, A.; El-Sayed, M.A.; *Science,* **1996**, 272, 1924.
[313] Chou, K.; Ren, C.; *Mater. Chem. Phys.,* **2000,** 64, 241.
[314] Kurihara, L.K.;Cho w, G.M.; Schoen, P.E.; *Nanostruct. Mater.,* **1995**, 5, 607.
[315] Pastoriza-Santos, I.; Liz-Marzan, L.M.; *Pure Appl. Chem.,* **2000**, 72, 83.
[316] El-Nour, K.M.M.A.; Eftaiha, A.; Al-Warthan, A.; Ammar, R.A.A.; *Arabian J. Chem* ., **2010**, 3(3), 135.

▪ GOLD NANOPARTICLES

For the past few years, many methodologies [317 - 318] to synthesize monodispersed nanoparticles in a wide range of sizeshave been proposed. [319] As for silver nanoparticles, chemical reduction is the most employed methodology, since colloidal suspensions of different sizes and shapes can be obtained by the control of the reaction parameters. These are the selection of the precursors, surfactants, reducing agents, solvents and additives, the reaction time and temperature of the synthesis.

The so called Turkevich method is the most employed procedure for the gold nanoparticles synthesis. It consists in the reduction of tetrachloroauric acid with small amounts of sodium citrate in aqueous media.[320] In general, spherical particles of 10-20 nm can be obtained.[321] In fact, depending on the relationship of reagents and the temperature, the method can generate spherical particles between 10 and 150 nm, [322] since increasing the ratio reducing agent/gold salt produces smaller crystals.[323-324] In this procedure, the citrate acts both as reducing agent and as a stabilizer for the generated nanoparticles, by getting adsorbed on their surface. Thus, when high amounts of citrate are used, the nanoparticles are quickly stabilized leading to smaller particles.[325] Nevertheless, many other syntheses based on different reducing agents have been proposed, such as the use of hydroquinones for obtaining nanoparticles between 50 and 200 nm.[326]

For smaller particles, the Brust–Schiffrin methodology is usually employed. The method consists in reducing the metal salt with sodium borohydride in organic medium, such as toluene, hexane or chloroform, using tetraoctylammonium bromide (TOAB) as a phase-transfer reagent, and employing alkanethiols as stabilizer. This approach generates smaller nanoparticles than the other methods (2 - 5 nm).[327] Up to date, many modified procedures of this approach have been presented, mostly based on the use of bifunctional thiol ligands for their further application in sensing.[328]

---

[317] Zhou, J.; Ralston, J.; Sedev, R.; Beattie, D.; *J. Colloid Interface Sci.,* **2009**, 331 (2), 251.
[318] Sakamoto, M.; Fujistuka, M.; Majima, T.; *J. Photochem. Photobiol. C: Photochem. Rev.,* **2009**, 10, 33.
[319] Ackerson, C.J.; Jadzinsky, P.D.; Sexton, J.Z.; Bushnell, D.A.; Kornberg, R.D.; *Bioconjugate Chem.,* **2010,** 21 214.
[320] Turkevich, J.; Stevenson, P. C.; Hillier, J.; *Faraday Discuss.,* **1951**, 11, 55.
[321] Frens, G.; *Kolloid-Z. Z. Polym.,* **1972,** 250(7), 736.
[322] Frens, G.; *Nat. Phys.*, **1973**, 241, 20.
[323] Ji, X.; Song, X.; Li, J.; Bai, Y.; Yang, W.; Peng, X.; *J. Am. Chem. Soc*., **2007**, 129, 13939.
[324] Kumar, S.; Gandhi, K.S.; Kumar, R.; *Ind. Eng. Chem. Res.,* **2007**, 46, 3128.
[325] Kimling, J.; Maier, M.; Okenve, B.; Kotaidis, V.; Ballot, H.; Plech, A.*; J. Phys. Chem. B,* **2006,** 110, 15700.
[326] Perrault, S.D, Chan, W.C.W.; *J. Am. Chem. Soc.*, **2009**, 131(47), 17042.
[327] Brust, M.; Walker, M.; Bethell, D.; Schiffrin, D.J.; Whyman, R.; *J. Chem. Soc., Chem. Commun.,* **1994,** 7, 801.
[328] Porter, L.A.; Ji, D.; Westcott, S.L.; Graupe, M.; Czernuszewicz, R.S.; Halas, N.J.; Lee, T.R.; *Langmuir*, **1998,** 14(26), 7378.

On the other hand, non spherical particles can be obtained by means of an anisotropic growth of gold nuclei with the adding of specific stabilizing agents such as cetyltrimethylammonium bromide (CTAB), sodium dodecylsulfonate (SDS) or poly(vinylpyrrolidone) (PVP).[329-330]

1.3.1.2 QUANTUM DOTS

In recent years, many synthetic methods have been developed for the synthesis of nanocrystals of different nature. Some of them are based on chemical precipitation or thermal decomposition, which will be commented in more detail. Others, are based on solvothermal or hydrothermal methods, which require of high temperatures and high vapor pressures for obtaining nanoparticles, and are normally done in an apparatus consisting of a steel pressure vessel called an autoclaves. In any case, a proper selection of the precursors is crucial to obtain well defined nanoparticles, since they will determine the rate of monomers generation, which is directly related to the nucleation and growth steps. The reaction conditions like the temperature, pH or chemical concentrations have also a critical influence in the stability of nanocrytals. Moreover, and as in all nanoparticle synthesis, an accurate selection of ligands is also decisive, since they can adjust the surface energy of QDs.[331]

- **CHEMICAL PRECIPITATION (AQUEOUS MEDIA APPROACHES)**

Aqueous approaches for the synthesis of QDs are based on chemical precipitation of precursors in the presence of stabilizers, where metal cations directly react with an inorganic chalcogenide source. An example of it is the one purposed by Henglein and co-workers for the synthesis of strong luminiscent cadmium sulfide (CdS) nanocrystals by the reaction of a soluble cadmium source and hydrogen sulfide (H_2S) under a strict control of pH, and with the presence of stabilizing molecules to prevent the precipitation of the formed QDs.[332] The initial pH value of the starting reaction is found to be relevant, since it determines the size of the obtained QDs. As the pH increases, the synthesized nanocrystals are smaller (Figure 1.32).

Other synthesis of nanocrystals in water are based on the use of sodium hydrogen telluride (NaHTe) or sodium hydrogen selenide (NaHSe) reagents, which are unstable and must to be formed *in situ* by the reaction of selenium or tellurium precursors and sulfuric acid (H_2SO_4) under an inert atmosphere.

---

[329] Hu, J.; Zhang, Y.; Liu, B.; Liu, J.; Zhou, H.; Xu, Y.; Jiang, Y.; Yang, J.; Tian, Z.-Q.; *J. Am. Chem. Soc.*, **2004,** 126, 9470.
[330] Kuo, C.-H.; Huang, M.H.; *Langmuir*, **2005**, 21, 2012.
[331] Zhuang, Z., Peng, Q.; Li, Y.; *Chem. Soc. Rev*., **2011**, 40, 5492.
[332] Spanhel, L.; Haase, M.; Wellerm H.; Henglein, A.; *J. Am. Chem. Soc*., **1987,** 109, 5649.

In this case, gases are formed and refluxes are required in order to obtain adequate photoluminescent emissions. [333-334]

Obviously, all these synthetic methods requiere of stabilizing molecules, such as mercapto-acids (e.g. thioglycolic acid or thiolactic acid) or mercapto-alcohols (e.g. 2-mercaptoethanol or 1-thioglicerol) , which form thiol-capped QDs.[335] Thiol groups allow to control the kinetics of the nanocrystals synthesis, passivate the surface, and provide stability, solubility and surface functionality to the nanoparticles.

The use of inverse micelles is also a typical synthetic method for controlling the size of quantum dots. Micelles are nanometer size water droplets where the precipitation process of QDs takes place. Their grouth is controlled by this confination and the product is also stabilized. CdS quantum dots have been obtained with this methodology by limiting the reaction of cadmium perchlorate ($Cd(ClO_4)_2$) and sodium sulfide (Na_2S) in water droplets of the micelles formed by dioctyl sulfosuccinate (AOT).[336]

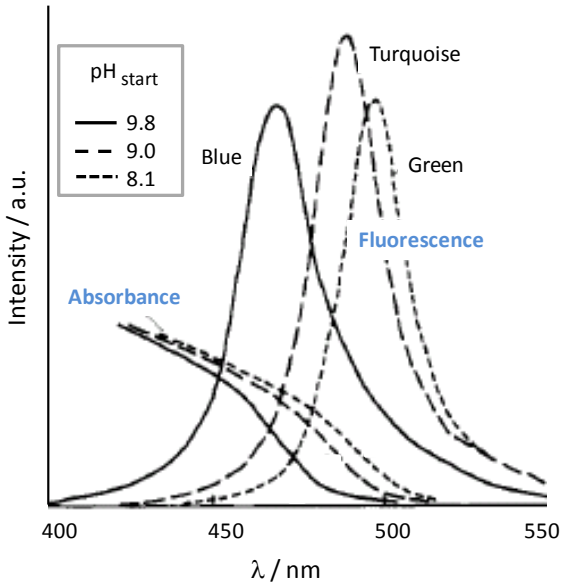

Figure 1.32: Absorption and emission spectra of three different sizes of CdS QDs for different values of the starting pH solution.[332]

▪ THERMAL DECOMPOSITION (ORGANIC MEDIA APPROACHES)

Although the sythesis of QDs in aqueous medium by chemical precipitation is simple and does not require further reagents for their solubilization when they are intended to be applied in water based system, the procedures involve fast kinetics which are usually difficult to control. As a result, non homogeneous QDs (in terms of sizes and shapes) are obtained, which limits their applications.

[333] Qi, L.; Colfen, H.; Antonietti, M.; *Nano Lett.,* **2001,** 1(2), 61.
[334] Peng, H.; Zhang, L.; Soeller, C.; Travas-Sejdic, J.; *J. Lumin.,* **2007,** 127, 721.
[335] Rogach, A.L.; Kornowski, A.; Gao, M.; Eychmüller, A.; Weller, H.; *J. Phys. Chem. B,* **1999**, 103, 3065.
[336] Colvin, V. L.; Goldstein, A. N.; Alivisatos, A. P.; *J. Am. Chem. Soc.,* **1992**, 114, 5221.

Synthetic methodologies based on thermal decomposition of (organo)metallic compounds are nowadays the most employed ones for growing semiconductor nanoparticles. Early syntheses based on this method were performed by Bawendi and co-workers in 1993,[337 - 338] where dimethyl cadmium ($Cd(CH_3)_2$) was used as the cadmium source, solved in trioctylphosphine oxide (TOPO); and trioctylphosphine (TOP) or tributylphosphine (TBP) was used to dissolve selenium pellets. The cadmium precursor is placed in a flask and heated to a high temperature (up to 360 ºC) under inert gas. Then, the selenium precursor precursor is quickly injected into the hot solution (figure 1.33). The mixture of TOP and TOPO were found to be good solvents for the high temperature growth and anneling of CdSe nanocrystals. The coordination solvent plays a crucial role in controlling the growth process, stabilizing the resulting colloidal suspension and passivating the surface of QDs. Moreover, high temperatures entail better solubility, and thus, Ostwald ripening can occur, obtaining as a result narrow size distributions with high photoluminiscent properties. The key point of this procedure is the rapid injection of selenium precursor, since it confers a short and fast nucleation, which is basic for the formation of well defined nanocrystals.

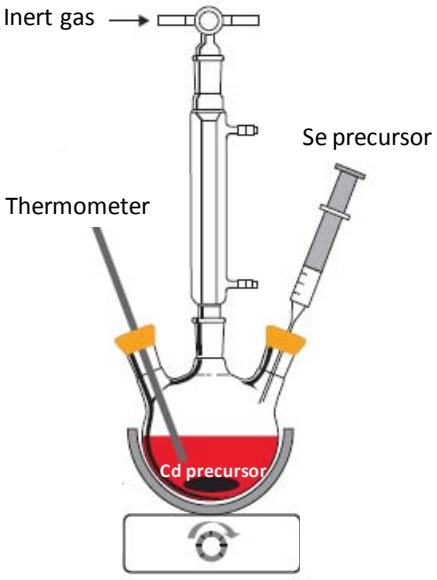

Figure 1.33: Experimental set-up for the synthesis of QDs by thermal decomposition. Cadmium precursor is placed in the flask and is heated to a certain temperature; Se stock solution is injected into the hot solution to start the reaction.[193]

More recetly, Peng and co-workers replaced the toxic dimethyl cadmium for cadmium oxide (CdO) and other inorganic cadmium salts, which also generate more reproducible syntheses; and introduced octadecene (ODE) as a non-toxic, low cost and non-coordinating organic solvent, which minimizes the use of the expensive and toxic TOPO.[339]

Until the date, this method has been applied to the synthesis of diverse QDs, such as cadmium sulfide (CdS),[339] cadmium telluride (CdTe),[339] zinc selenide

[337] Murray, C.B.; Norris, D.J.; Bawendi, M.G.; *J. Am. Chem. Soc.,* **1993,** 115, 8706.
[338] Steigerwald, M.L.; Alivisatos, A.P.; Gibson, J.M.; Harris, T.D.; Kortan, R.; Muller, A.J.; Thayer, A.M.; Duncan, T.M.; Douglas, D.C.; Brus, L.E.; .; *J. Am. Chem. Soc.*, **1988**, 110, 3046.
[339] Peng, Z.A.; Peng, X.*; J. Am. Chem. Soc.*, **2001**, 123, 183.

(ZnSe),[340] zinc sulfide (ZnS), lead (II) sulfide (PbS),[341] lead selenide (PbSe),[342] lead telluride (PbTe),[343] indium arsenide (InAs)[344] or indium phosphide (InP).[345] Another possible reaction is the decomposition of a single precursor containing both the metal and the chalcogenide sources. O'Brien and co-workers obtained CdSe QDs by the decomposition of $[CH_3CdSe_2CN(C_2H_5)_2]_2$ precursor in hot TOPO.[346] However, these special compounds are difficult to synthesize.

■ NANOCRYSTAL SOLUBILIZATION

The obtained QDs by thermal decomposition are highly luminiscent and stable, but only soluble in non-polar organic solvents, which limits their application in most of fields. Therefore, further solubilization steps are required in order to extend their use. Moreover, the exchange of the ligand coating the QD permits to give functionality to the particle by incorporating chemical groups , which can be subsequently attached to biochemical recognition elements, such as antibodies or fluorescent species. Current solubilization methods are mostly based on the exchange of the original hydrophobic capping surface with an hydrophilic one (Figure 1.34),[211] which present one end for being attached to the QD surface (e.g., -SH), and another one to provide water-solubility and chemical reactivity (e.g., $-NH_2$, -COOH). Some example found in the literature include mercaptocarbonic acids,[346] phosphines,[347] peptides,[348] thiolated poly(ethylene

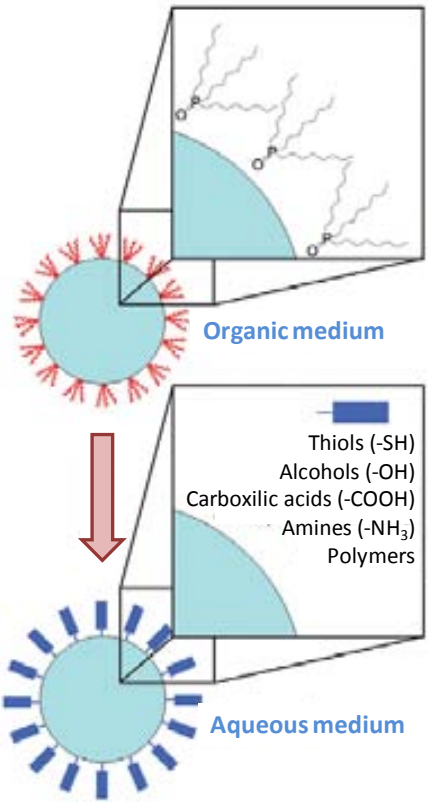

Figure 1.34: Ligand exchange of QDs. Hydrophobic surface capping ligands (TOP) (top); and different possibilities of hydrophilic ligands exchange (bottom).[211]

[340] Hines, M.A.; Guyot-Sionnest, P.; *J. Phys. Chem. B,* **1998,** 102, 3655.
[341] Lin, S.L.; Pradhan, N.; Wang, Y.J.; Peng, X.G.; *Nano Lett.*, **2004**, 4, 2261.
[342] Lipovskii, A.; Kolobkova, E.; Petrikov, V.; Kang, I.; Olkhovets, A.; Krauss, T.; Thomas, M.; Silcox, J.; Wise, F.; Shen, Q.; Kycia, S.; *Appl. Phys. Lett.*, **1997**, 71, 3406.
[343] Lu, W.G.; Fang, J.Y.; Stokes, K.L.; Lin, J.; *J. Am. Chem. Soc.*, **2004**, 126, 11798.
[344] Battaglia, D.; Peng, X.G.; *Nano Lett.*, **2002**, 2, 1027.
[345] Trindade, T.; Obrien, P.; *Adv. Mater.*, **1996**, 8, 161.
[346] Aldana, J.; Wang, Y.A.; Peng, X.; *J. Am. Chem. Soc.,* **2001**, 123, 8844.
[347] Kim, S.; Bawendi, M.G.; *J. Am. Chem. Soc.*, **2003**, 125, 14652.
[348] Pinaud, F.; King, D.; Moore, H.-P.; Weiss, S.; *J. Am. Chem. Soc.,* **2004**, 126, 6115.

glycol)[349], ciclodextrins[350] and dendrons.[351]

It is also also feasible to cover the QDs with amphiphilic polymers, since their hydrophilic part provide the water solubility and the hydrophobic one interacts with the ligand coating of the nanocrystals.

However, most of the times this step of solubilization worsens the luminiscent properties of the nanocrystals or even results in toxic effects, such as some ligands as MUA or cysteamine, which damage DNA.[352]

- **CORE SHELL QUANTUM DOTS**

Nanocrystals are often covered with an outer layer of few atoms thick of another semiconductor material, what it is known as core-shell QDs. The purpose of this shell is to passivates the core surface defects of the core QD surface.[353] Moreover, when using covering materials, the optical properties of the QDs improve, [354] increases considerably their quantum yield up to values of ~ 80 %, althougth typical values are in the range of 20-50 %, and they show better photostability as well.[355] On the other hand, the emission peaks of these core-shell nanocrystals suffer a shift to larger wavelengths, compared with their original core emission band. The fluorescence intensity rises by increasing the number of shell layers, until no improvement is observed. In fact, it has been demostrated that too many layers covering the core of the nanocrystal involve a decrease of the quantum yield.[296]

1.3.1.3 CARBON DOTS

Synthetic approaches for C-dots are also divided into bottom-up and top-down strategies. The later refer to the cutting of graphene into carbon nanoparticles, where C-dots are formed or ''broken off'' from larger graphene sheets. Bottom-up methods involve the synthesis of graphene moieties with certain number of conjugated carbon atoms, such as the cage-opening of fullerene or other reactions in solution from molecular precursors. Both procedures are performed by chemical and physical methods. Physical ones include arc discharge,[356] laser ablation/passivation[242] and oxigen plasma

---

[349] Susumu, K.; Uyeda, H.T.; Medintz, I.L.; Pons, T.; Delehanty, J.B.; Mattoussi, H.; *J. Am. Chem. Soc*., **2007**, 129, 13987.

[350] Palaniappan, K.; Xue, C.; Arumugam, G.; Hackney, S.A.; Liu, J.*; Chem. Mater.*, **2006**, 18(5), 1275.

[351] Guo, W.; Li, J.J.; Wang, Y.A.; Peng, X.; *Chem. Mater*., **2003,** 15, 3125.

[352] Hoshino, A.; Fujioka, K.; Oku, T.; Suga, M.; Sasaki, Y.F.; Ohta, T.; Yasuhara, M.; Suzuki, K.; Yamamoto, K.*; Nano Lett.,* **2004,** 4, 2163.

[353] Kortan, A.R.; Hull, H.; Opila, R.L.; Bawendi, M.G.; Steigerwald, M.L.; Caroll, P.J.; Brus, L.E.; *J. Am. Chem. Soc*., **1990,** 112, 1327.

[354] Eychmüller, A.; Mews, A.; Weller, H.; *Chem. Phys. Lett.*, **1993**, 59.

[355] Peng, X.; Schlamp, M.C.; Kadavanich, A.V.; Alivisatos, A.P.; *J. Am. Chem. Soc.,* **1997**, 119, 7019.

[356] Xu, X. Y.; Ray, R.; Gu, Y. L.; Ploehn, H. J.; Gearheart, L.; Raker, K.; Scrivens, W. A.; *J. Am. Chem. Soc*., **2004**, 126, 12736.

treatment,[357] among others, and are characterized for producing more irregular nanoparticle surfaces, generating nonhomogeneity in their optical properties.

On the other hand, chemical methods include electrochemical oxidation,[358] supported synthetic procedures,[359] thermal/hydrothermal methods,[230] microwave/ultrasonic syntheses[360] or other chemical methods. Among all, the two latter are the most usual ones. Hydrothermal methods obtain C-dots by placing a solution of carbon source in a autoclave equipment, where high temperature and pressure are applied.[230] On the other hand, a typical example of microwave synthesis is the one, where polyethylene glycol 200 (PEG200) and a saccharide are mixed in distilled water and heated in a 500 W microwave oven for several minutes. This procedure has evolved in the synthesis of C-dots by any carbohydrate (glycerol, glycol, glucose, sucrose, etc.) and an amount of an inorganic ion, being completed in just a few minutes without the requirement of any passivation reagent.[361] Other chemical dots synthesis, based on reverse micelles as nanoreactors can be also used.[362] In these methods, there is a first carbonization of the carbon source followed by an *in situ* surface passivation.

As stated before, the size of the resulting C-dots strongly depens on the synthetic approach. For instance, microware pyrolysis based methods produce C-dots of about 3 nm, while by graphene ablation C-dots of a mean size of 10 nm are obtained. In any case, more research must be performed in order to obtain homogeneous C-dots with improved QYs for the real application of the colloid.

1.3.2 CHARACTERIZATION OF NANOPARTICLES

The technological advances of recent years have been crucial for the development of new nanomaterials. The chemical, physical and structural characterization of nanoparticles is critical in order to know and foresee their the properties of each nanomaterial in different purposes.

There are many techniques for the structural characterization of nanoparticles, such as X-ray diffraction (XRD), small angle X-ray scattering (SAXS), scanning electron microscopy (SEM), transmission electron microscopy (TEM) or scanning probe microscopy (SPM), among others. For chemical

---

[357] Gokus, T.; Nalr, R. R.; Bonettl, A.; Bohmler, M.; Lombardo, A.; Novoselov, K. S.; Gelm, A. K.; Ferrarl A. C.; Hartschuh, A.; *ACS Nano*, **2009**, 3, 3963.

[358] Zhou, J. G.; Booker, C.; Li, R. Y.; Zhou, X. T.; Sham, T. K.; Sun X. L.; Ding, Z. F.; *J. Am. Chem. Soc.*, **2007,** 129, 744.

[359] Liu, R. L.; Wu, D. Q.; Liu, S. H.; Koynov, K.; Knoll, W. ; Li, Q.; *Angew. Chem., Int. Ed.,* **2009**, 48, 4598.

[360] Wang, X. H;. Qu, K. G.; Xu, B. L.; Ren J. S.; Qu, X. G.; *J. Mater. Chem.*, **2011**, 21, 2445.

[361] Tang, L. B. ; Ji, R. B.; Cao, X. K.; Lin, J. Y.; Jiang, H. X.; Li, X. M.; Teng, K. S.; Luk, C. M.; Zeng, S. J.; Hao, J. H.; Lau, S. P.; *ACS Nano*, **2012**, 6, 5102.

[362] Wang, J.; Xin X.; Lin, Z.; *Nanoscale*, **2011**, 3, 3040.

characterization, one can employ absorption spectroscopy, photoluminescence, electron spectroscopy, ion spectroscopy or secondary ion mass spectroscopy (SIMS). For physical characterization, melting points and lattices constants are usually measured. The combination of these techniques is necessary to have information of the material features. Some of these techniques are being briefly described next.

1.3.2.1 MICROSCOPIC TECHNIQUES

Characterization and manipulation of individual nanoparticles requires extreme sensitivity and accuracy at atomic level resolution. Therefore, microscopic techniques play an important role.

Microscopic techniques may be divided in three main branches: optical, electron and scanning probe microscopy. Optical (optical or confocal) and electron (for instance transmission or scanning) microscopies involve the diffraction, reflection, or refraction of electromagnetic radiation/electron beams interacting with the sample, and the subsequent collection of this scattered radiation or another signal in order to create an image. Otherwise, scanning probe microscopy, such as atomic force microscopy, involves the interaction of a scanning probe tip with the surface of the sample.

- **TRANSMISSION ELECTRON MICROSCOPY (TEM)**

In transmission electron microscopy a beam of electrons, with an energy between 80 and 200 KeV in a vacuum of aproximately 10^{-6} mmHg, is transmitted through the sample, creating an image produced from the elastic and inelastic dispersion of the crossed electrons of the sample. This image is amplified by a system of magnetic lenses and displayed in a screen.

The major advantage of this technique is its capability of high amplification, since it is posible to magnify from 50 to 10^6 any signal. Elastic scattering of electrons involves no energy loss and provides the diffraction pattern; while inelastic scattering due to dislocations, defects or density variations of the sample, leads to spacial variation in the intensity of the transmission electrons.

The sample preparation for nanoparticles for TEM analysis involves the use of copper or brass grids, where a drop of sample is placed and dried before being introduced in the TEM equipment. Successful imaging of nanoparticles using TEM strongly depends on the contrast of the sample relative to the background.

TEM is the preferred method to directly measure nanoparticle size, grain size, size distribution, and morphology. Effective treatment of TEM images can lead to obtain histograms, where the distribution of nanoparticles is easily observed. For this purpose, it is necessary the recount of a minimal number of

nanoparticles and, by adjusting the graphic obtained from the total recount in function of their frequency, a 3-parameter Gaussian curve is obtained.

▪ ATOMIC FORCE MICROSCOPY (AFM)

Atomic force microscopy is one of the most employed techniques for imaging and manipulating the surface of nanosized samples. It consists of a cantilever (fabricated with piezoresistive elements) with a sharp tip, which scans the surface of the sample (dried on a mettal support) providing structural information. When the tip is near the surface, a deflection of the cantilever is produced due to forces created by the tip and the surface sample. The deflection is measured using a laser spot reflected from the cantilever in a photodiode array, and with this signal the images are generated.

Depending on the sample and the AFM operating mode used, different forces can be measured. For instance, ionic repulsions can be determined in contact mode (where distances between the cantilever and the sample are lower than 1 nm), and magnetic, electrostatic or van der Waals forces can be mesuared in non-contact mode.

The main advantage of this technique is that it provides a three-dimensional surface profile without the requirement of high vacuum, and do no require any special sample treatment. However, its limitation is the single scan size and the scanning speed, since AFM only can make an image of a maximum height of 10 - 20 μm an a maximum scanning area of 150 x 150 μm.

As well as TEM, AFM can furnish structural information of nanomaterials as individual particles and groups of particles can be visualized and, unlike other microscopy techniques, in three dimensions.

▪ CONFOCAL LASER SCANNING MICROSCOPY (CLSM)

Confocal laser scanning microscopy is a high resolution imaging technique which allows obtaining optical images of a sample at different depths and therefore, with depth resolution. By the reconstruction of different scanned sections, a three-dimensional (3D) image is obtained.

CLSM combines the laser scanning process with the 3D detection using fluorescent markers, scanning point by point the surface of the material with a focused laser beam and creating the image similarly to scanning electron microscopes.

A confocal microscope uses point illumination and a pinhole in a conjugate optical plane in front of the detector to eliminate the information from the out of focus plane, detecting only the light that is within this plane, and obtaining, as a result, sharper images than those from conventional fluorescence microscopes. Since it only illuminates a concrete point of the sample, a horizontal scanning is necessary to be performed to obtain the

whole image of the sample from the detected fluorescent light. The information of focal planes can be collected and assembled to create a 3D image of the sample.

CLSM is a noninvasive technique, therefore it has been widely used in biological science and clinical diagnosis to provide optical information of thick living specimens with a minimal sample. In recent years, it is also being applied in nanomaterials science for characterization and analysis purposes.

1.3.2.2 SPECTROSCOPIC TECHNIQUES

Spectroscopic techniques are based on the principle that, under certain conditions, materials absorb, emit or scatters light. Therefore, they supply very useful information about the sample. Spectroscopic techniques operate over different limited frequency ranges within the electromagnetic spectrum, depending on the processes and magnitudes of the energy changes. Spectroscopic methods can be classified depending on these frequency regions in X-rays, ultraviolet, visible, infrared, microwave and radio frequency. However, they can be also classified according to the interaction of the analyte and the electromagnetic radiation (absorption, emission or scattering techniques).

- **UV-VIS ABSORPTION SPECTROSCOPY**

When a beam of UV-Vis electromagnetic radiation passes through a sample, some photons can be absorbed by molecules, which undergoes a transition from its lower energy level to a higher one, decreasing the total number of photons that crosses though the sample (Figure 1.35). The measurement of this decrease in photons, called absorbance, is a very useful analytical signal. Absorption only happens when the photon's energy matches the difference in energy between the two energy levels of the molecule.

Transition metal ions, highly conjugated organic compounds, and biological macromolecules, are common analytes determined by this technique. For organic compounds, absorption is due to energy transitions from $\sigma \rightarrow \sigma^*$, $n \rightarrow \sigma^*$, $n \rightarrow \pi^*$ or $\pi \rightarrow \pi^*$, since antibonding orbitals ($\sigma^*$and π^*) are higher in energy than bonding orbitals (σ, n and π). On the other hand, transition metal ion absorptions are due to valence electrons of *d*-orbitals, which display different energy when the metal is complexing a ligand or in the presence of a solvent molecule. *d–d* transitions for transition metal ions are relatively weak. [363]

Samples for UV-Vis spectrophotometry are normally liquids. Absorbance measurements are usually done placing the sample solution in a transparent cuvette, which is located in the UV-Vis spectrophotometer. The instrument measures the difference of intensity of light (*I*) before and after passing though

[363] Ríos, A.; Moreno-Bondi, Maria C.; Simonet Suau, B.M.; in: *Técnicas espectroscópicas en química analítica*, Vol.1, Editorial Síntesis S.A., Madrid, **2012**.

the sample and compares them. Absorbance spectrums are plotted by representing absorbance as a function of the photon's energy. Beer-Lambert law can relate the concentration of an analyte with its transmitted light or absorbance: $A = log_{10}(I_0 / I) = \varepsilon \cdot b \cdot c$, where A is the measured absorbance, I_0 is the incident light intensity, I the transmitted light intensity, ε a constant known as the molar absorptivity (cm^{-1} M^{-1}), b the path length measure in cm, and c the concentration of the sample given in molarity.

As some of the metallic and semiconductor nanoparticles have optical properties that are sensitive to size, shape, concentration, agglomeration state, and refractive index near the nanoparticle surface, UV-Vis spectroscopy is a helpful technique for identifying, characterizing, and studying these nanomaterials. Moreover, the optical properties of nanoparticles have been followed when used as labels for the detection and quantification of analytes such as heavy metals, explosives, or bacteria among others.

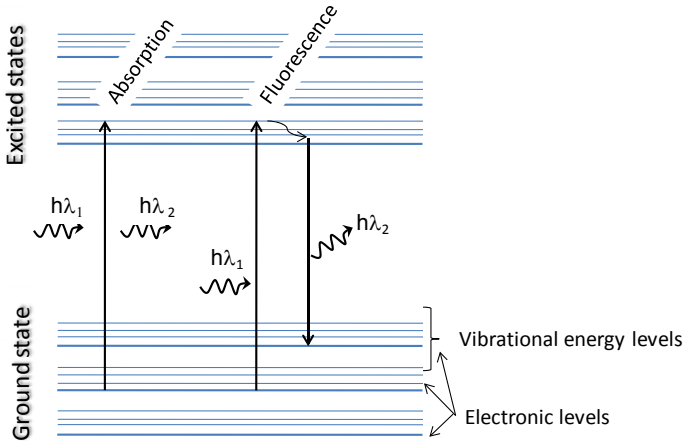

Figure 1.35: Energy diagram showing the absorption and emission of a photon by a molecule.[363]

▪ FLUORESCENCE SPECTROSCOPY

Fluorescence spectroscopy is based on the light emission of molecules, usually in the visible spectrum, that have been excited to higher energetic levels by the absorption of electromagnetic radiation. When a compound is irradiated with light and absorbs a photon, it is excited from its ground electronic state to one of its vibrational states in the exited electronic state. Due to collisions with other molecules, the system undergoes a nonradiative internal relaxation, and the excited electron relaxes to the lowest vibrational state of the excited electronic state. The subsequent relaxation that suffers the molecule from this position to the fundamental state is what produces a photon of energy, triggering the fluorescence emission (Figure 1.35).

Fluorescence normally involve $\pi \rightarrow \pi^*$ transition of molecules, although $n \rightarrow \sigma^*$ can also show weak fluorescence. Since the change in energy for fluorescent emission is generally less than for absorption, a molecule's fluorescence spectrum is shifted to higher wavelengths than its absorption spectrum.

In the case of fluorescent nanoparticles or quantum dots, the excitation process is generated by an electron from the valence band, which is excited to the conduction band (electron-hole creation) by means of electromagnetic radiation. The nonradiative internal relaxation involves the movement of the excited electron to a more stable excited level, such as the bottom state of the conduction band. The radiative process, where a photon is emitted from the quantum dot, is due to the total relaxation of the electron to the valence band.

A quantitative expression of fluorescence efficiency is the fluorescent quantum yield, Φf (QY), which is the fraction of excited state molecules returning to the ground state by fluorescence. Its maximum value is 1.0, or expressed in percentage, 100 %, which means that all the absorbed photons have been emitted. The QY value of a compound usually is calculated by comparison with a standard such as rhodamine, quinine or fluorescein. The selection of the standard depends on the nature of the analyte to quantify and its solubility.

Fluorescence measurements are also done by placing the sample solution in a transparent cuvette, which is located in the spectrofluorometer. Similarly to absorbance measurements, fluorescence spectrums are plotted by representing fluorescence intensity as a function of the photon's energy.

In diluted solutions, usually in the range of μg mL^{-1} (when absorbance is lower than 0.01), fluorescence intensity is proportional to the concentration of the sample, following the expression: $I_f = 2.303 \cdot \varepsilon \cdot b \cdot c \cdot K \cdot \Phi f \cdot I_0 = k' I_0$, where I_f is the intensity of fluorescent emission, ε the molar absorptivity, b the path length, c the concentration of the sample, K a constant accounting for the efficiency of collecting and detecting the fluorescent emission, Φf the quantum yield, I_0 the incident light, and k' a collection of constants. The intensity of fluorescent emission increases thus with an increase of quantum efficiency, the source's incident light, and the molar absorptivity and the concentration of the analyte.

Fluorescence spectroscopy is a highly sensitive technique, since the fluorescence signal has theoretically zero background; and because there are few luminescent molecules which can interfere in the analyte signal.

▪ ATOMIC EMISSION SPECTROSCOPY (AES)

Atomic emission spectroscopy (AES) is a method that uses the intensity of emitted light to determine and quantify an element in a sample. Atomic emission occurs when a valence electron in a higher energy atomic orbital returns to a lower energy atomic orbital. The emitted electromagnetic radiation, which is displayed as atomic spectral lines instead of the common bands in molecular emission, is characteristic of each element.

Atomic emission requires a source of thermal energy to convert the liquid analyte, which is aspirated to the equipment, into gaseous atoms or ions, which usually also serves as the excitation source. The most common methods are flames and

plasmas. When a plasma source, which is a hot partially ionized gas that contains an abundant concentration of cations and electrons, is used, the technique is called inductively coupled plasma atomic emission spectroscopy (ICP-AES) or inductively coupled plasma optical emission spectrometry (ICP-OES). Atomization of samples by means of a plasma have some advantages, such as lower interferences and combustion times.

Atomic emission spectroscopy is ideal for multielemental analysis because all analytes in a sample are excited simultaneously. The intensity of an atomic emission line (I_e) is proportional to the number of atoms (N^*) in the excited state: $I_e = k \cdot N^*$, where k is a constant accounting for the efficiency of the transition. Therefore, the technique allows to perform elemental analysis of most of the elements of the periodic table.

▪ ENERGY-DISPERSE X-RAY SPECTROSCOPY (EDS, EDX, XEDS)

In energy-dispersive X-ray spectroscopy (or energy dispersive X-ray microanalysis), a high energy beam of charged particles, such as electrons, protons or a beam of X-rays, interacts with the sample and stimulates the emission of the X-rays from the specimen under study.

When the energy beam interacts with the sample, electrons of the inner shell of atoms are released to the exterior, creating an electron hole which is immediately filled with an outer electron from a higher energy shell. The difference of energy between the lower and the higher energy shell is released as X-rays.

The X-ray energy is characteristic of each element of the periodic table, since this energy difference between shells is distinctive for every atomic structure; and its intensity is proportional to the concentration of the element. Thus, an EDS analysis is an analytical technique, which can qualitative and semi-quantitative determine the elements present in a sample.[364]

A detector converts the x-ray energy into voltage signals, which pass into an analyzer and displays the data as a spectrum, in which the x-axis represents X-ray energy and the y-axis the number of counts per channel (figure 1.36). The combination of TEM technique with EDS is commonly found. In this case, it is possible to establish the distribution of an element in a sample and also its purity. However, EDS spectrum is affected by some factors. Many elements show overlapping peaks and the lightest elements of the periodic table (such as H, B, N or O) are difficult to be analyzed, because they have few electrons. In any case, heavy elements are easily determined, resulting in a powerful tool for the characterization of metallic and semiconductor nanoparticles.

[364] Skoog, D. A.; Holler, J. H.; Nieman, T. A.; in: *Principios de Análisis Instrumental;* Mc Graw Hill: Madrid, **2001**.

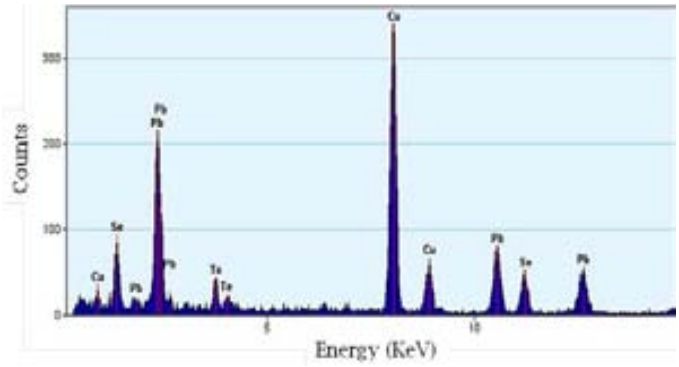

Figure 1.36: Example of EDS spectra of PbSe and PbTe nanoparticles present on carbon support film Cu grid. (*NREL).*

▪ SELECTED AREA ELECTRON DIFFRACTION (SAED)

Selected area electron diffraction is a crystallographic experimental technique similar to X-ray diffraction (XRD), since it is used to determine the atomic and molecular structure of crystals and detect their defects. In the case of SAED, the examined area is of a hundred of nanometers, while in XRD it is of centimetres. They are both based on the unique and characteristic X-ray powder pattern of each crystalline solid as a "fingerprint" for its identification.

Diffraction techniques have been widely used in all the issues related to solid state chemistry and materials science, i.e. the determination of the crystal structure of solids, including lattice constants and geometry, identification of unknown materials, orientation of single crystals, defects, stresses, etc.

SAED technique can be performed inside a transmission electron microscopy, where the lenses are defocused to produce a parallel illumination of the sample and a selected area aperture limits the diffraction volume. As a result, the TEM image is a series of spots arranged as ring of reflections, which corresponds to a concrete diffraction condition of the crystalline structure of the specimen.

Therefore, with SAED patterns it is possible to determined the Bravais lattices and lattice parameters of crystalline materials by the same procedure as XRD. SAED patterns of nanoparticles displays ring patterns similar to those obtained by XRD powder. Data is very useful to determine if the material is crystalline or amorphous, and what elements are in the sample by using pattern matching/ auto indexing.

▪ DYNAMIC LIGHT SCATTERING (DLS)

Dynamic light scattering is a non-invasive physical technique that measures the size distribution profile of small particles in suspension, providing the hydrodynamic diameter of the sample, which refers to how a particle scatters light within a fluid (Figure 1.37). When particles in solution are irradiated with a beam of monochromatic light like a laser, the light is scattered by the particles and fluctuates over time depending on the particle size present in the sample. Thus, this intensity fluctuations contains information about the time scale of

movements of the particles and thus, its diffusion. Since the velocity of the Brownian motion (random motion of particles suspended in a liquid resulting from their collision) can be determined by the intensity fluctuations, the particle size can be obtained by using the diffusion coefficients and the Stokes-Einstein equation ($D= \mu k_B T$, where D is the diffusion constant, μ the mobility, k_B the Boltzmann's constant and T the temperature). The larger the particle size, the slower it will diffuse. DLS measure, which is performed by placing a transparent cuvette in the DLS equipment, provides a plot from the particle distribution in a sample. If the sample is monodisperse, a unique population will be obtained, whereas polydisperse samples will generate multiple populations.

DLS measurement depends not only on the size of the particle core, but also on the surface structure, the particle concentration and the medium. By periodically measuring DLS, stability studies of a sample can also be performed.

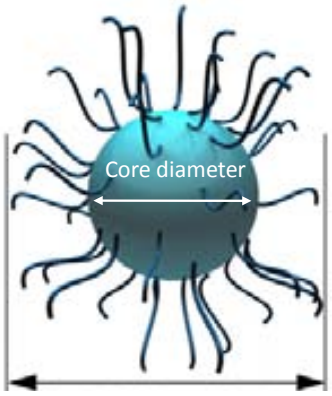

Figure 1.37: Representation of the hydrodynamic diameter of a nanoparticle, measured in DLS, compared to core diameter, obtained by TEM technique. (Image from *Malvern* website*).*

1.3.2.3 OTHER TECHNIQUES

- **GRAVIMETRIC ANALYSIS**

Gravimetric analysis involves measuring the mass of a product to calculate the amount of analyte in a sample. Thus, the sample is analyzed for its elemental composition, since the method provides the mass fractions of carbon, hydrogen and nitrogen of a sample (CHNX analysis), obtaining thus its qualitative and quantitative composition.

From the different methods that can be used, combustion analysis is one of the most usual. The technique consists in the quantitative combustion of the sample, which is placed in a tin capsule, at high temperature (1000 ºC) in an excess of oxygen. The combustion gases formed are then transformed to carbon dioxide (CO_2), water (H_2O), nitrogen (N_2) and sulfur dioxide (SO_2) by means of a tungsten trioxide (WO_3) and copper based-catalyst reactor. The gas mixture is separated by gas chromatography and each component is measured by a thermal conductivity detector. A gas chromatographic register is obtained, where the peak area is proportional to the mass of each product. From this information, it is possible to calculate the composition of the sample by determining the ratio of elements within the sample.

ZETA POTENTIAL (ζ POTENTIAL)

ζ potential is a physical property characteristic of particles in suspension. When particles are dispersed in solution, surface charges are generated by the ionization of surface functional groups or adsorption of the charged species. These charges generate an electrical double layer around the particles, which depends on the solution nature. The double layer surrounding the particle has two main zones: the Stern layer, which is located in the inner region and where the ions are strongly bound to the particle; and the diffuse layer, which is outer and where the ions have higher mobility. A stable entity called slipping plane can be defined, where ions move with particles as a part of a whole, whereas the rest of ions outside this region will move independently (Figure 1.39). The ζ potential is the electric potential difference between the interfacial double layer at the slipping plane and any other point of the bulk fluid.

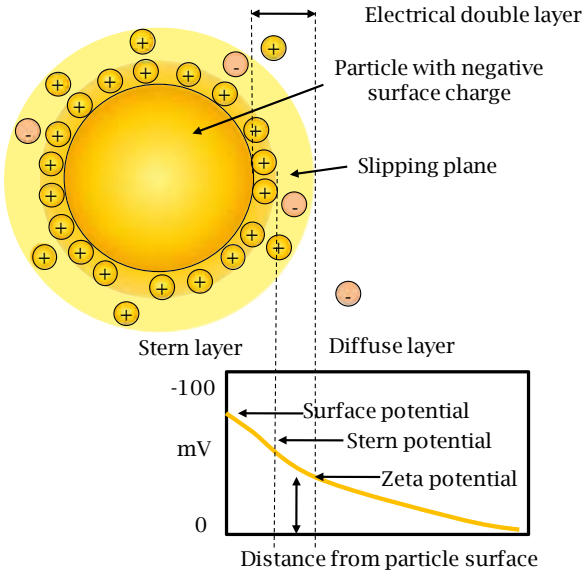

Figure 1.38: Schematic representation of ζ potential as a function of distance from the particle surface. (Image from *Malvern* website*).*

The value of ζ potential is related to the stability of nanoparticles in suspension, since it indicates the repulsion between particles similarly charged. When ζ potential values are lower than 30 mV in absolute value (>-30 mV and < +30 mV), the attraction between the particles is higher than the repulsions, and the colloid is no stable enough and aggregates. On the other hand, when its value is higher than 30, the solution is electrically stabilized and do not flocculate. Thus, the measurement of the ζ potential is very useful to determine and predict the stability of nanoparticles.

Samples for ζ potential measurements are prepared by placing a representative solution of the sample in a cuvette, which includes the electrodes assembly to the electrodes of the equipment. ζ potential measures provides a plot from the sample potential as a function of its number of counts.

1. 4 MICROSYSTEMS AND NANOTECHNOLOGY

Microfluidic systems are optimal structures for the integration and simplification of analytical procedures based on nanomaterials. Trends in microsystems are currently focused on obtaining devices with a higher grade of miniaturization, which implies the use of very small volumes, but with more restrictions regarding high sensitivity (low detection limits), selectivity and reproducibility. The chemical, physical and electronic properties of nanomaterials have demonstrated its benefits in this sense, which make them specially suitable for their use in detection purposes as for building blocks to perform a (bio)assay. However, the use of nanomaterials in analytical applications is still in an incipient stage due to reproducibility problems on the signal when different commercial batches are employed.

For any analytical application, nanomaterials must be thoroughly purified and characterized once synthesized, and functionalized for their subsequent use. Therefore, it is very important to control the core material of nanoparticles as well as their surface chemistry.

Microreaction technology takes advantage of the large surface area-to-volume ratios within microchannel structures to accelerate heat and mass transport, and of their easy automation. This leads to a more uniform and controlled heating and mixing, which in the case of most synthesis is a crucial factor. Therefore, the use of microsystems for nanoparticles synthesis opens up the opportunity for new synthetic routes and process methodologies. Since the GSB has a huge experience in the development of microfluidic systems with microfabrication materials, the design and fabrication of microsystems for the synthesis of nanoparticles for analytical applications a challenge.

1. 4.1 MICROSYSTEMS BASED ON NANOPARTICLES

Microfluidic systems can greatly take advantage from the use of nanoparticles. Their main application areas are mostly the improvement of analytical processes, the development of transducing elements and their use as labels.

Nanoparticles can be used as stationary or pseudostationary phases, or as modifiers of packing materials to improve analyte separation or sample pre-treatment in microchip-based capillary electrochromatographs.[365] Some of the most employed nanoparticles for the modification of packing materials are gold or silica nanoparticles. [366] Moreover, gold nanoparticles have been also incorporated onto the surface of microfluidic channels of electrophoretic polydimethylsiloxane (PDMS) microsystems, as Wang et al. proposed for the

[365] Pumera, M.; *Talanta,* **2005,** 66, 1048.
[366] Lin, Y.W.; Huang M.J.; Chang, H.T.; *J. Chromatogr. A*, **2003,** 1014, 47.

separation of dopamine and pinephrine. The obtained results demonstrated the effectiveness of nanoparticles for the control of the electro-osmotic flow, which made feasible the separation of both compounds (Figure 1.39).[367]

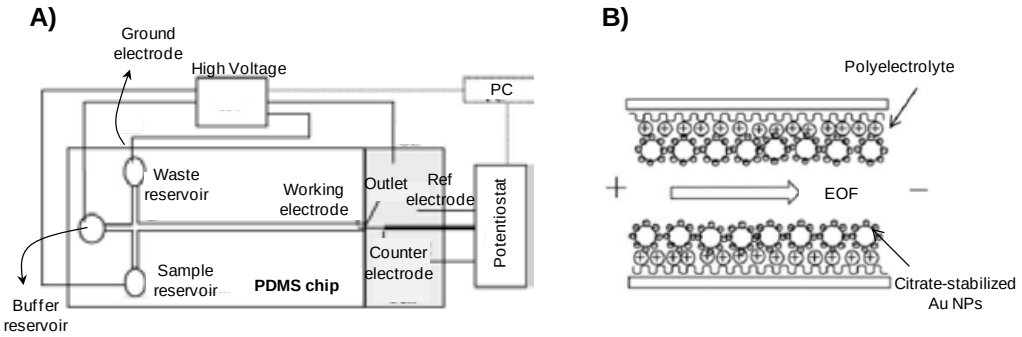

Figure 1.39: **A)** Schematic representation of the PDMS electrophoretic microsystem for the separation of dopamine and pinephrine. **B)** PDMS–PDMS modification using gold nanoparticles.[371]

Nanoparticles have been employed in the development of sensors using both their electrical and optical properties. Their electrical properties can be used in the modification of transducers to enhance the signal response in amperometric, impedimetric or potentiometric measurements, since they normally allow a high-surface area interface that enables the sensitive/catalytic detection of a specific analyte.[368] Moreover, the use of nanoparticles allows the use of larger currents and provides higher stability.[369] Thus, some reports can be found demonstrating the higher sensitivity achieved employing nanoparticles, when compared with conventional electrodes for the detection of bioanalytes, explosives or environmental pollutants.[370] For instance, copper or nickel nanoparticle-based electrodes have been fabricated in microfluidic devices and employed for the detection of carbohydrates or amino acids.[31] Indium oxide and silica nanoparticles modified electrodes have been also applied to the highly sensitive glucose detection by conductimetry (Figure 1.40A). [371]

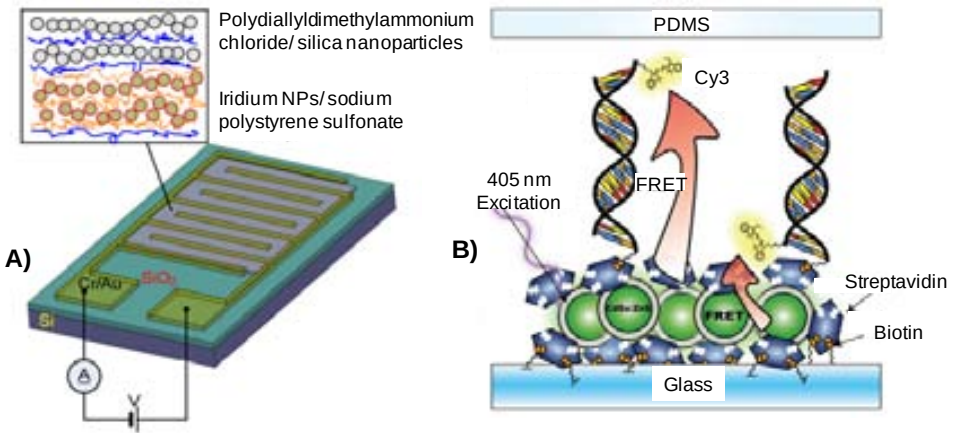

Figure 1.40: **A)** Schematic representation of a microsystem based on indium oxide and silica nanoparticles modified electrodes for glucose detection.[371] **B)** Cross-section of a microfluidic channel for the transduction of hybridization using FRET and CdSe/ZnS QDs. Hybridization with Cy3 labeled target provides the necessary distance for energy transfer and yields FRET sensitized Cy3 emission upon excitation by a 405 nm laser.[372]

[367] Wang, A.J.; Xu, J.J.; Zhang, Q.; Chen, H.Y.; *Talanta*, **2006**, 69(1), 210.
[368] Medina-Sánchez, M.; Miserere, S.; Merkoçi, A.; *Lab Chip*, **2012**, 12, 1932.
[369] Pumera, M.; *Chem. Eur. J.,* **2009**, 15, 4970.
[370] Pumera, M.; *Chem. Commun.,* **2011**, 47, 5671-5680.
[371] Lee, D.; Ondrake, J.; Cui, T.; *Sensors,* **2011**, 11(10), 9300.

The improvement of optical transducers has been also addressed. For instance, Krull et al. immobilized QDs onto a microfluidic platform surface, where hybridization of nucleic acids was performed. The nanoparticles acted as energy donors of a dye, labeled to the complementary nucleic acid, and a FRET mechanism was employed for the quantitative determination of nucleic acids(Figure 1.40B).[372]

SERS detection with nanoparticles has been also employed in microsystems, such as the proposed by Choo et al, [373] who developed a SERS device for mercury determination. The microsystem uses gold nanoparticles modified with Rhodamine B, which can be replaced by mercuric ion due to the stronger affinity of gold and mercury. Consequently, SERS signal from the fluorophore changes as a function of the mercuric ion concentration (Figure 1.41A). Another interesting strategy is using magnetic Fe_3O_4-Au core-shell nanoparticles for the fast concentration, detection and differentiation of bacterial cells by using external magnetic fields and also the SERS technique (Figure 1.41B).[374]

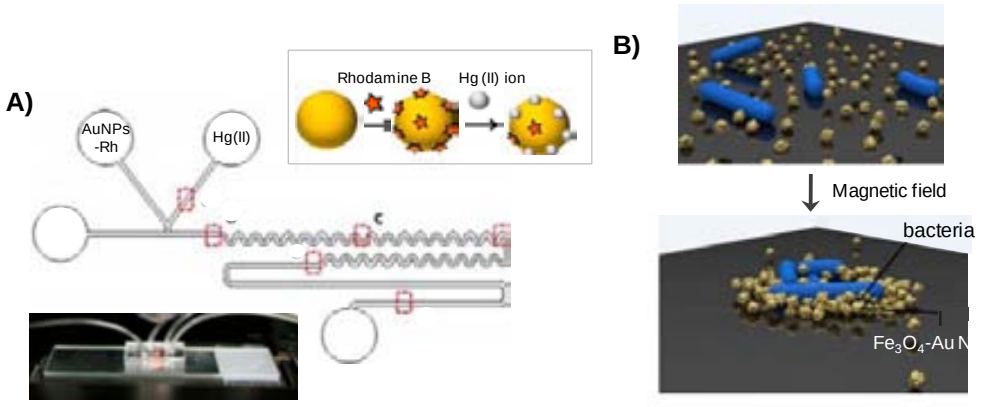

Figure 1.41:
A) Illustration and image of a microsystem for Hg^{2+} ions detection. Scheme of the Hg^{2+} sensing principle based on the replacement of Rhodamine B with Hg^{2+} ions on the surface of Au NPs. [373] **B)** Schematic representation of the condensation of bacteria using Fe_3O_4-Au core-shell nanoparticles in a microfluidic system with SERS detection for waterborne pathogen isolation and detection.[374]

The use of nanoparticles as labels is probably the most interesting analytical application. In this sense, the employment of nanoparticles as electrochemical labels has been reported. For example, QDs can be modified with antibodies for the selective determination of aprotein tumor marker, such as the carcinoembryonic antigen, by voltammetry. The use of the nanostructured material allowed improving the sensitivity and selectivity of the system (Figure 1.42A).[375] However, it is even more interesting to take advantage of the optical properties of nanoparticles. For instance, QDs offer the possibility of a highly sensitive detection of analytes in microfluidic systems by using them as markers. Some of these advantages are related to the possibility of selecting their emitted light by a proper choice of the nature and size of the quantum dot used, or to

[372] Tavares, A.J.; Noor, M.O.; Vannoy, C.H.; Algar, W.R.; Krull, U.J.; *Anal. Chem.,* **2012**, 84, 312.
[373] Wang, G.; Lim, C.; Chen, L.; Chon, H.; Choo, J.; Hong, J.; de Mello, A. J.; *Anal. Bioanal. Chem.*, **2009**, 394, 1827.
[374] Zhang, L.; Xu, J.; Mi, L.; Gong, H.; Jiang, S.; Yu, Q.; *Biosens. Bioelectron.,* **2012**, 31, 130.
[375] Wang, S.; Mamedova, N.; Kotov, N.A.; Chen, W.; Studer, J.; *Nano Lett.*, **2002,** 2, 817.

their lower photobleaching and high stability. For instance, Remcho et al. performed an on-chip aptamer-based fluorescence assay for thrombin detection and quantification based on sandwich ELISA principles and employing MBs and QDs (Figure 1.42B). Aptamer-functionalized MBs were used to capture the target analyte, while a second aptamer functionalized with QDs was employed for on-chip detection. The detection of the analyte was performed by means of a fluorescence microscope.[376] Some other examples can be found in the literature involving the use of nanocrystals for protein[377] or virus[378] detection on microfluidic devices.

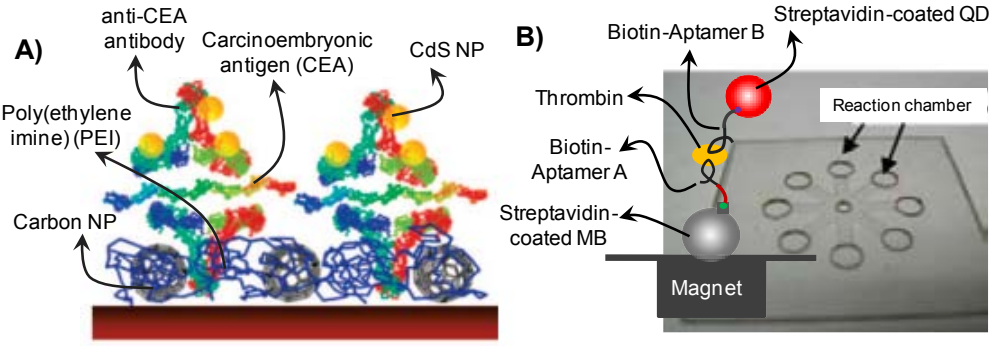

Figure 1.42:
A) Representation of the assay used for carcinoembryonic antigen detection by voltammetry using QDs as electrochemical label.[375]
B) Photograph of the microchip used for magnetic bead-based aptamer assays. Reaction scheme for an aptamer-based sandwich assay. [376]

Metallic nanoparticles can be also used as labels. Liu et al. presented a microsystem for the detection of prostate specific antigen based on a surface immobilized biobarcode assay. It employs micro channel walls functionalized with antibodies that bind with the target, which is subsequently tagged with co-functionalized nanoparticles containing polyclonal antibodies and barcode DNA oligonucleotides. The barcode DNA is then released from the nanoparticles and transferred to the detection area, where the complementary sequence is patterned and a scanometric detection (visualization in the Visible spectrum) is performed. The antigen was detected at very low concentrations (Figure 1.43A).[379] Other colorimetric microsystems based on metallic nanoparticles have been also proposed. For instance, copper ion has been determined in a microfluidic device by employing alkyne and azide terminated thiol functionalized gold nanoparticles.[380] The change of color of the solution, when it interacts with the analyte can be readout by naked eye (Figure 1.43B).

[376] Tennico, Y.H.M.; Hutanu, D.; Koesdjojo, M.T.; Bartel, C.M.; Remcho, V.T.M.; *Anal.Chem.,* **2010**, 82(13), 5591.
[377] Hu, M.; He, Y.; Song, S.; Yan, J.; Lu, H.-T.; Weng, L.-X.; Wang L.-H.; Fan, C.; *Chem. Commun.,* **2010,** 46, 6126.
[378] Zhang, H.; Xu, T.; Li C.-W.; Yang, M.; *Biosens. Bioelectron.,* **2010,** 25, 2402.
[379] Goluch, E.D.; Stoeva, S.I.; Lee, J-S.; Shaikh, K.A.; Mirkin, C.A.; Liu, C.; *Biosens. Bioelectron.,* **2009**, 24(8), 2397.
[380] Yingyi, L.; Jie, Y.; Wenwen, C.; Dingbin, L.; Zhuo, W.; Xingyu, J.; *Chin. J. Chem.*, **2012**, 30, 2047.

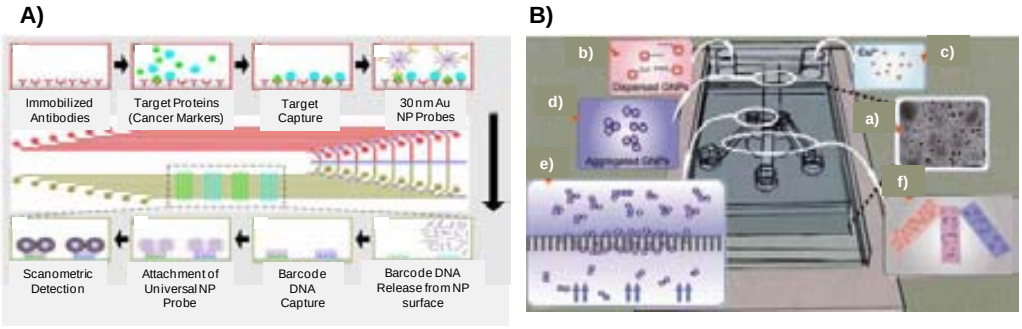

Figure 1.43:
A) Schematic diagram of the surface immobilized biobarcode assay protocol.[379]
B) Colorimetric microsystem for Cu^{2+} detection based on Au NPs: a) SEM image of a filter membrane. b) Detection reagents. c) Cu^{2+} solution.d) Aggregated Au NPs. e) Concentration of Au NPs f) Colorimetric strips.[380]

On the other hand, lateral-flow devices or paper-based microfluidics have been widely used in the last decades for medical diagnostics either for home testing, point of care testing, or laboratory use due to the rapidness of the diagnostics, the reduced size, portability and facile results interpretation. Gold nanoparticles are commonly used as markers due to their simple visualization, such as in the well known pregnancy test, which measures the peptide hormone associated with pregnancy (Figure 1.44). Fluorescent or magnetic labeled particles can also be used, being in this case necessary the use of an electronic reader. However, these devices usually lack of analyte quantification.

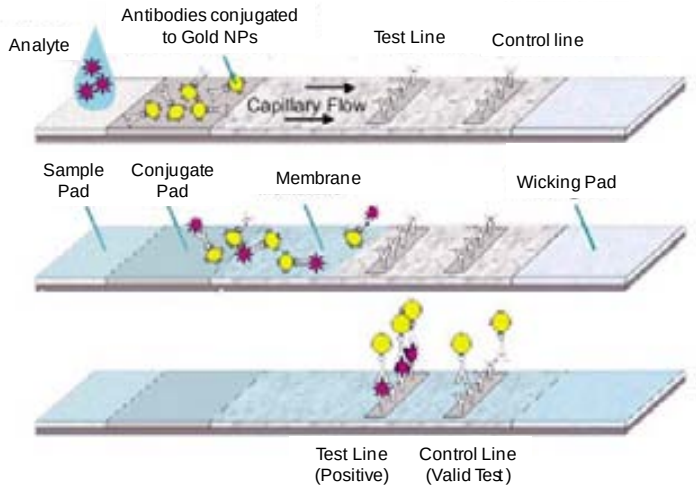

Figure 1.44:
General scheme of a lateral flow test based on gold nanoparticles. *Cytodiagnostics.*

Finally, the use of nanomotors or nanobots, which are mobile self-propelled active nano- or micromaterials,[381-382] opens a large number of applications for microsystems and nanotechnology. Catalytic nanomotors can be directed through a microfluidic system using an external magnetic field, which enables moving the particle into the desired microfluidic channel or carrying cargo through it (Figure 1.45). Recent advances in this field have shown how these materials can move and transport different entities, such as living organisms.[383]

[381] Paxton, W.; Sundararajan, S.; Mallouk, T.; Sen, A.; *Angew. Chem. Int. Ed.,* **2006**, 45, 5420.
[382] Sanchez, S.; Pumera, M.; *Chem. Asian J.,* **2009,** 4, 1402.
[383] Sanchez, S. ; Solovev, A. A. ; Harazim S. M.; Schmidt, O. G.; *J. Am. Chem. Soc.,* **2011,** 133, 701.

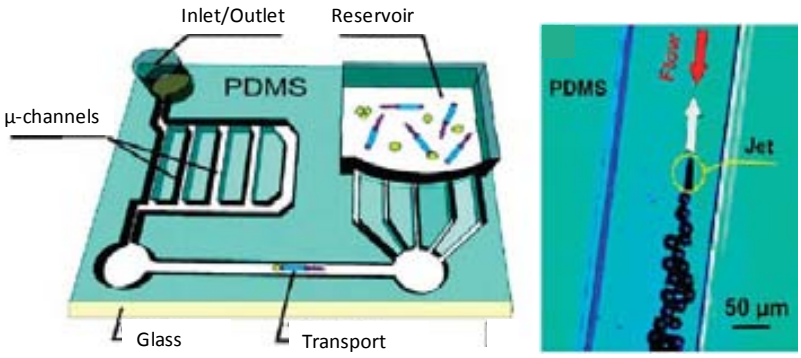

Figure 1.45:
On the left, schematic representation of a PDMS microchip used for the transport of microparticles. On the right, microrobots swimming against a continuous induced flow of fuel into the microchannels.[383]

As a result of all the advantages and possible strategies that the combination of microfluidics and nanoparticles can offer, several companies are developing miniaturized analytical devices for the rapid and *in-situ* determination of pathogens or the development of point-of-care devices, such as Philips, Cytodiagnostics, Future Diagnostics or iMICROQ.

1. 4.2 MICROREACTORS FOR THE SYNTHESIS OF NANOPARTICLES

As stated before, nanoparticles are mainly obtained using bottom-up approaches by batch chemical syntheses. However, it is known that these techniques are sometimes time-consuming and it is often difficult to control product homogeneity. Some of the drawbacks of batch nanoparticles synthesis include little control of reagents concentration and difficult management of the local stirring and temperature, which leads to variations in the size and therefore properties of nanoparticles in the diverse synthetic batches.

Microreactors offer a better control over many reaction conditions such as mixing rates or reaction temperatures. This is the consequence of the small reaction volumes employed, which allows reducing diffusion times and leads also to accelerate heat and mass transfer, mixing times are also reduced.[384] All this permits a strict control of the different stages of the synthesis of nanoparticles, producing homogeneous particles in size and shape with higher yields than the typical ones obtained in batch syntheses. Moreover, the ability to work at elevated temperatures and pressures, while confining toxic and high reactive reagents provides a safer environment for the synthesis.

As previously discussed, the synthesis of nanoparticles can be thought in two well defined stages, the nucleation and the growth of particles. By ensuring a rapid nucleation stage and avoiding the formation of new nuclei during the growth of nanoparticles, the reaction can be perfectly controlled. It is also important to provide an identical chemical environment, since variations in physical conditions across the reaction leads to non-uniform particles.

[384] Park, J.I.; Saffari, A.; Kumar, S.; Günther, A.; Kumacheva, E.; *Annu. Rev. Mater. Res.* **2010**, 40, 415.

One of the great benefits of using microreactors for the synthesis of nanoparticles is that they enable an automatic and a fine control and manipulation of fluids. Mixing is achieved by simple diffusion in linear or patterned channels. But playing with the channel geometry and the microfluidic platform design one can define the mixing profile required for each synthesis. Some examples are the introduction of hydrodynamic focusing,[385] flow lamination,[386] fluid folding[387] or chaotic mixing.[388]

Moreover, by means of microreactors some parameters such as the flow rate can be perfectly selected, which plays an important role in the synthesis of nanomaterials. For instance, some studies have demonstrated that the use of large flow rates in the synthesis of silver nanoparticles results in a broader particle size distribution.[389] However, these effects cannot be generalized, being necessary a optimization of each microfluidic parameter for each reaction. The proper control of the reaction time is another advantage of using microreactors, which entails the control of the kinetics.[390]

Furthermore, microreactors offer the possibility of continuously varying the composition of a reaction mixture by simply modifying the reagents dosing rates. In this sense, if detection systems, such as miniaturized spectrometers, are integrated in the course of the synthetic process, not only the synthetic procedure can be followed but also any possible problem can be detected and in-line corrected.

On the other hand, sequential reactions can be easily integrated as a result of the feasible control of reaction times and the successive addition of other reagents. This approach has been demonstrated for instance for the synthesis of core-shell nanoparticles.[391]

Microreactors for continuous-flow nanoparticles synthesis can be developed in single-phase or multi-phase solution. Single-phase or homogeneous syntheses are those which take place in a single liquid or a mixture of miscible liquids. Normally, a mixing step is performed at the beginning, namely in the first section of the microreactor, to ensure a good mixture of reagents. Then, reaction can take place by simple diffusion of reagents under a laminar flow, or by additional mixers to promote convective mixing. Finally, the obtained particles are collated via an outlet of the microreactor (Figure 1.46 B).[384]

---

[385] Knight, J.B.; . Knight, J. B.; Vishwanath, A.; Brody, J.P.; Austin, R. H.; *Phys. Rev. Lett.*, **1998**, 80(17), 3863.
[386] Bessoth, F.G.; deMello, A.J.; Manz, A.; *Anal. Commun.*, **1999,** 36(6), 213.
[387] Johnson, T.J.; Ross, D.; Locascio, L.E.; *Anal. Chem.*, **2002,** 74(1), 45.
[388] Stroock, A.D.; Dertinger, S.K.W.; Ajdari, A.; Mezić, I.; Stone, H.A.; Whitesides, G.M.; *Science*, **2002**, 295(5555), 647.
[389] Lin, X.Z.; Terepka, A.D.; Yang, H.; *Nano Lett.,* **2004,** 4, 2227.
[390] Sounart, T. L.; Safier, P. A.; Voigt, J. A.; Hoyt, J.; Tallant, D. R.; Matzke, C. M.; Michalske, T. A.; *Lab Chip*, **2007,** 7, 908.
[391] Dendukuri, D.; Pregibon, D.C.; Collins, J.; Hatton, T.A.; Doyle, P.S.; *Nat. Mater.,* **2006,** 5, 365.

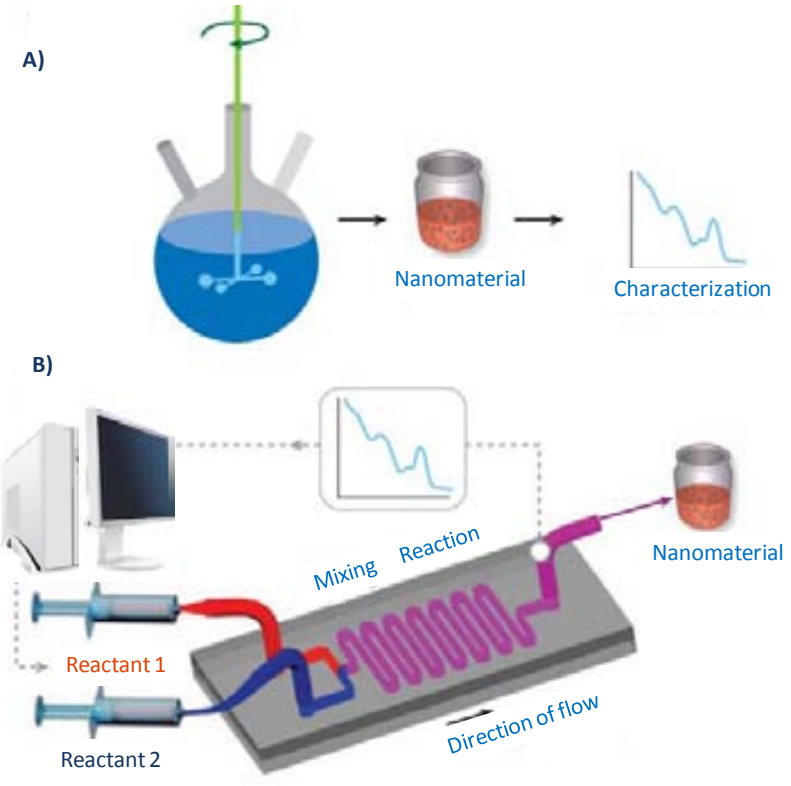

Figure 1.46: Schematic comparison of the synthesis and inspection of nanomaterials in conventional flask methods (**A**) and in microfluidic reactors (**B**).[377]

On the other hand, multi-phase solutions or droplet based processes are those which introduce a second immiscible phase, a gas or liquid, in the system. Reagents in a solvent, usually water, are brought to the system separately by means of different inlets before contacting in the microreactor with an organic phase. In this way, aqueous droplets are formed, such as in a segmented flow (Figure 1.47).[392] This approach allows a convective mixing inside each droplet and confine the reaction in a well defined volume, since the oil prevents contact between growing particles inside the droplets. With these approaches very narrow size distributions for the synthesis of a wide range of nanoparticles have been achieved.[393-394] However, it is difficult to find a suitable reagent-carrying couple, since both phases should be non-miscible in all the range of the experimental conditions, and it is necessary a further separation step.[395]

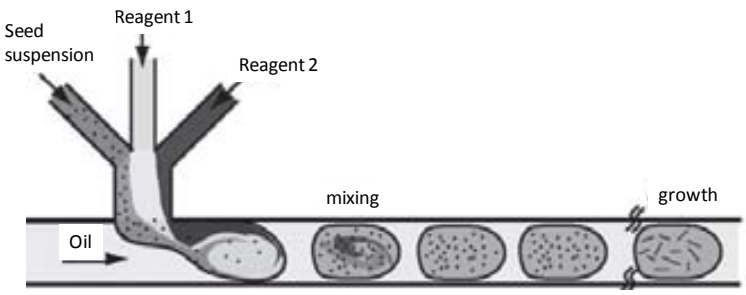

Figure 1.47: General strategy for the multiphase or droplet-based synthesis of nanoparticles. [392]

[392] Duraiswamy S.; Khan, S.A.; *Small,* **2009,** 5, 2828.
[393] Wagner, J.; Tshikhudo T. R.; Koehler, J. M.; *Chem. Eng. J.,* **2008**, 135, S104.
[394] Marre, S.; Jensen, K.F.; *Chem. Soc. Rev.,* **2010,** 39, 1183.
[395] Sahoo, H.R.; Kralj J.G.; Jensen, K.F.; *Angew. Chem. Int. Ed.*, **2007,** 46, 5704.

The first synthesis of nanoparticles in a microfluidic system was performed in 2002 by Edel and co-workers for the synthesis of cadmium sulfide (CdS) quantum dots.[396] The reaction consists on mixing of cadmium nitrate ($CdNO_3$) and sodium sulfide (Na_2S) in aqueous solution in the presence of a sodium polyphosphate stabilizer to form CdS nanocrystals (Figure 1.48). Lately, Chan et al. studied the formation of cadmium selenide (CdSe) nanocrystals in a microreactor, changing different variables such as the flow rate, the concentration of reagents or the synthesis temperature.[397] The study demonstrated that microreactors enable the optimization of nanoparticles synthesis and that the variation of certain parameters can tune the properties of the obtained colloid.
Since then, multiple approaches for the synthesis of different kind of nanoparticles have been presented (semiconductor,[398] metal,[399] silica,[400] and hybrid nanoparticles[401]) in microreactors constructed in glass, silicon or polymers. The first synthesis of gold nanoparticles in microreactors demonstrated to obtain spherical particles from 5 to 50 nm by mixing a gold salt and ascorbic acid.[402] Nowadays, spherical, spheroid, rod-like, and extended sharp-edge shapes of different sizes, even smaller than 5 nm, can be prepared by tuning the concentration of reactants in microfluidic reactors.[403]

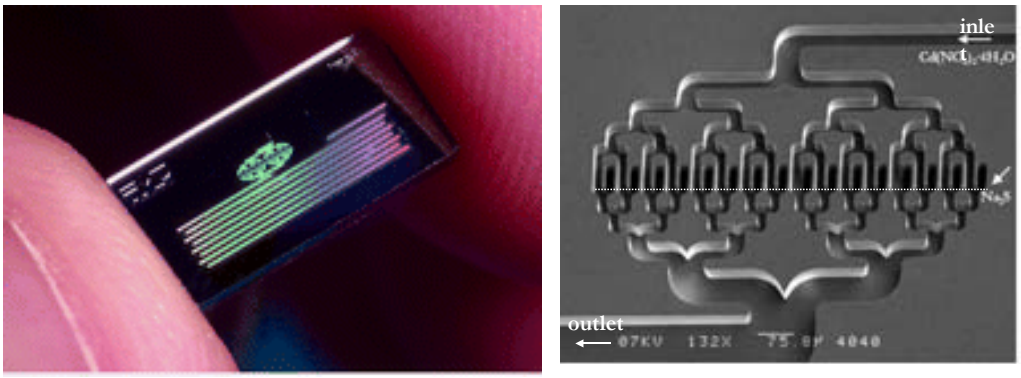

Figure 1.48: Image from the first microreactor for the synthesis of CdS nanoparticles. After mixing the channels, where sodium sulfide and cadmium nitrate are supplied, particles are formed in another microfluidic channel.[396]

Microfluidic devices for nanoparticles synthesis can be also classified in two broad types, especially those for high temperature syntheses. The first type includes simple capillaries of typical inner diameter 100 - 1000 μm, into which precursor solutions are injected usually by means of syringe pumps. The capillaries are usually made of glass and polytetrafluoroethylene (PTFE), since these materials are chemically inert; although stainless steel, silica and other

[396] Edel, J.B.; Fortt, R.; deMello, J.C.; deMello, A.J.; *Chem. Commun.,* **2002,** 10, 1136.
[397] Chan, E.M.; Mathies, R.A.; Alivisatos, A.P.; *Nano Lett.*, **2003**, 3(2), 199.
[398] Wang, H.Z.; Nakamura, H.; Uehara, M.; Yamaguchi, Y.; Miyazaki M.; Maeda, H.; *Adv. Funct. Mater.,* **2005,** 15(4), 603.
[399] Shalom, D.; Wootton, R.C.R.; Winkle, R.F.; Cottam, B.F.; Vilar, R.; deMello A.J.; Wilde, C.P.; *Mater. Lett.,* **2007**, 61(4–5), 1146.
[400] Khan, S.A.; Gunther, A.; Schmidt, M.A.; Jensen, K.F.; *Langmuir,* **2004**, 20(20), 8604.
[401] Abou-Hassan, A.; Bazzi, R.; Cabuil, V.; *Angew. Chem. Int. Ed.,* **2009**, 48(39), 7180.
[402] Wagner, J.; Köhler, J.M.; *Nano Lett.,* **2005**, 5, 685.
[403] Duraiswamy, S.; Khan, S.A.; *Small,* **2009,** 5, 2828.

polymers have been also used. In most cases, capillaries are raised to high temperatures (up to 300 ºC) by immersing the capillary into heated oil-baths, such as in the synthesis of nanocrystals. [404-405]

The second type of microfluidic reactors are based on microfluidic platforms, where different structures can be mechanized to ensure the mixture of reagents. Actuating and monitoring components can be also easily integrated in such microreactors. They are constructed using several materials, such as glass, silicon and polymers, where heating is commonly achieved by placing the entire microfluidic platforms over a hot-plate. [406] An example of both types of microreactors is shown in figure 1.49.

It has been well demonstrated that an efficient mixing in microfluidic systems produces particles with improved monodispersity. [407 - 408] In fact, it is also established that with only downsizing the reaction vessel from bulk to microliter volumes is enough to improve monodispersity of nanomaterials.

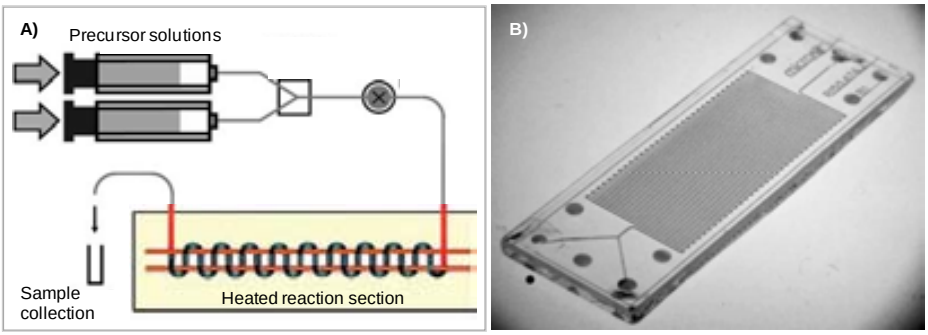

Figure 1.49: Examples of the two types of microreactors for the QDs synthesis. **A)** A scheme of a typical capillary reactor, where reagents are previously mixed before the PTFE capillary is submerged in a heated section.[406] **B)** An example of a glass microfluidic platform based on a serpentine channel, which is later placed on a hot plate to achieve high temperature.[408]

Examples of sequential synthesis involve the use of segmented or single flow, such as the scheme shown in figure 1.50, where sequential reactions in separate microreactors take place.[409]

However, some drawbacks derived from miniaturization can be expected. For instance, the obstruction of the microfluidic channels caused by nanoparticle agglomeration or by a side-reaction with channel surfaces.[410] In this sense, the direct transfer of a batch synthetic route into a microfluidic reactor process is not an easy task, being necessary a detailed study and optimization of the system for each particular synthesis, evaluating not only the different possible configurations of the reactor but also the nature of reagents employed and the reaction conditions.

---

[404] Luan, W.L.; Yang, H.W.; Tu, S.-T.; Wang, Z.M.; *Nanotechnology,* **2007,** 18(17), 175603.
[405] Yang, H.W.; Fan, N.N.; Luan W.L.; Tu, S.T.; *Nanoscale Res. Lett,* **2009**, 4(4), 344.
[406] Nightingale, A.M.; de Mello, J.C.*; J. Mater. Chem.,* **2010**, 20, 8454.
[407] Song, Y.; Hormes, J.; Kumar, C.S.S.R.; *Small,* **2008**, 4 (6), 698.
[408] Song, Y.; Kumar, C.S.S.R.; Hormes, J.; *J. Nanosci. Nanotechnology,* **2004,** 4, 788.
[409] Wang, H. Z.; Li, X. Y.; Uehara, M.; Yamaguchi, Y. ; Nakamura, H.; Miyazaki, M. P.; Shimizu, H.; Maeda, H.; *Chem. Commun*., **2004,** 48.
[410] Xia, Y. N.; Whitesides, G. M.; *Annu. Rev. Mater. Sci.,* **1998,** 28, 153.

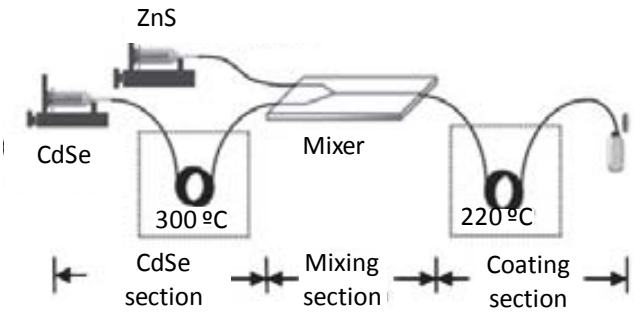

Figure 1.50: Scheme of sequential microreactor for the synthesis of core-shell CdSe/ZnS quantum dots.[409]

Nevertheless, an important application of microreactors for the synthesis of nanoparticles is in the area of high throughput screening. These systems permit carrying out multiple experiments in a short time, accumulating large experimental databanks more easily obtained and reliably than in conventional bulk-scale syntheses.

The application of these methods depend on the ability to increase their productivity. In this sense, process intensification to synthesize at large scale nanoparticles is a promising application of microreactors. Since the volume of products obtained in microsystems are reduced, performing simultaneously identical reactions in parallel reactors, appears as an alternative, being feasible to obtain comparable amounts of product to those by batch processes. In this sense, implementing this approach in multiple-phase reactors is a difficult task, since the integration of multiple droplet generators may lead to a complex fluid behaviour. In any case, there are still few reports that have successfully implemented this methodologies to microsystems.

OBJECTIVES

The Group of Sensors and Biosensors has an extensive experience in the development of microfluidic systems for the determination of water quality parameters and also for quality control of some industrial processes, among other applications. It is generally difficult to develop ideal microsystems, which fulfil all the expected characteristics. Usually, dedicated devices are developed for concrete applications, outside of which would not have much utility.

Being committed to the idea of obtaining new miniaturized systems to perform real-time and *in situ* optical measurements of parameters of water pollution, the main objective of the present work is to demonstrate the advantages of combining nanotechnology with microfluidics in order to provide new reagents and analytical instrumentation of better operational and analytical features.

An important condition for achieving this overall objective is to have a starting nanomaterial perfectly characterized and of well known optical properties. Therefore, the following partial purposes have been established:

1.- Development of microreactors for the synthesis of nanoparticles (silver, gold, quantum dots and carbon dots), which must integrate pre-treatment operations as heating and temperature control systems, as well as adapted detection systems.

2.- Development of a microsystem for heavy metals monitoring based on the use of the previously synthesized gold nanoparticles, modified with a selective ionophore, and applied to mercuric ion determination.

3.- Development of a microsystem for *E-coli* determination, taking advantage of performing an hybridization assay onto magnetic beads and based on the use of quantum or carbon dots as fluorescent labels.

FABRICATION PROCEDURES

Contents

Image from Du Pont website

As previously discussed in the introduction part, the LTCC (*Low Temperature Cofired Ceramics*) technology has been widely employed in the development of electronic circuits because of their electrical and mechanical properties, compatibility with screen printing techniques and the possibility of a multilayer integration. In recent years, the Group of Sensors and Biosensors has promoted its use for analytical purposes leading to multiple microfluidic systems. Due to the high chemical resistivity presented by these platforms (since a wide range of reagents could be used with no degradation of the device) and its simple and rapid prototyping, this material was been chosen for the development of the microreactors for the synthesis of nanomaterials in the present thesis.

On the other hand, Cyclic Olefin Copolymer (COC) technology enables also the construction of microfluidic structures in a simple way and it is highly compatible with a wide range of reagents. Moreover, optical detection is more feasible to be implemented due to its transparency and this permits the visualization of any liquid inside the microfluidic platform meanwhile the analysis is taking place. Although the monolithic integration of electronic components presents a limitation, it is compatible with other materials, such as photocurable resins. Thus, the integration of other parts/components can be simply performed. This material has been used in the present work for the development of the analytical systems.

The fabrication procedure of both materials for the construction of synthetic and analytic devices is detailed next.

3.1 LOW T EMPERATURE CO FIRED CERAM ICS FABRICATION PROCEDURE

The general fabrication procedure of the LTCC microfluidic platforms is depicted in Figure 3.1. As it can be observed, the procedure starts with the design of the device split into different layers, which are individually machined later. In case of integrating electrical or electronic components, the next step is the deposition of tracks by screen-printing pastes (conductive, dielectric and/or resistive). Then the whole layers are aligned and laminated by a thermo-compression process and finally sintered.

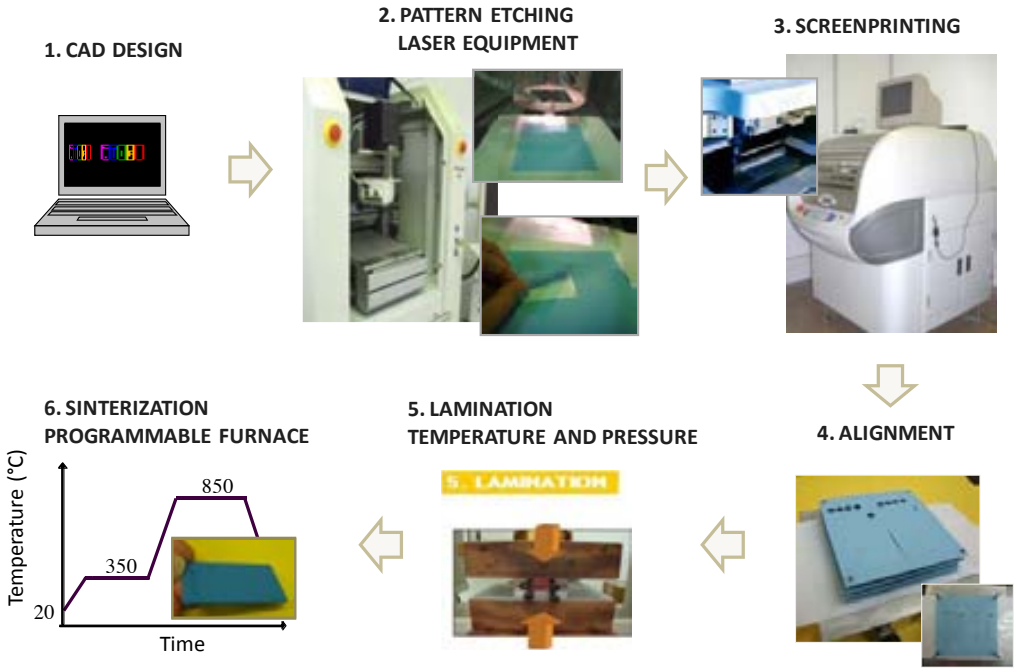

Figure 3.1: Scheme of the general fabrication procedure of the LTCC devices.

3.1.1 DESIGN

The fabrication of ceramic microfluidic platforms is based on a multilayer approach. Thus, the design is based on the superposition of structures into layers, giving rise to the desired internal structure by their posterior overlapping. In other words, different layers will be designed by means of CAD (*Computer-Aided Design*) software and mechanized with different patterns, which once overlapped in an appropriate order will give the desired three-dimensional structure.

Consider, as an example, the fabrication of a microfluidic system consisting in two inlets, a three-dimensional passive micromixer and an outlet, such as represented in figure 3.2. As it can be seen, five different layers are at least required. From top to bottom, the first layer contains the drilled inlets and outlet of the device. The next three layers will define the three-dimensional channel, based in "L" shape and finally, the last layer acts as a cover to seal the system. Thus, when liquids are delivered into the system thought the two inlets, they are displaced from one plane to another with movements of 90 °, which promotes turbulence in the system and improves their mixture. Depending on the number of layers used in the construction, the depth of the microfluidic structure will vary. Moreover, the different thickness of the substrate material used will also determine the dimensions of the final system. Theoretically, the number of layers and their thickness can be modified as desired. However, the fabrication of very thick microfluidic platforms requires longer lamination times, which increase the risk of structures deformation.

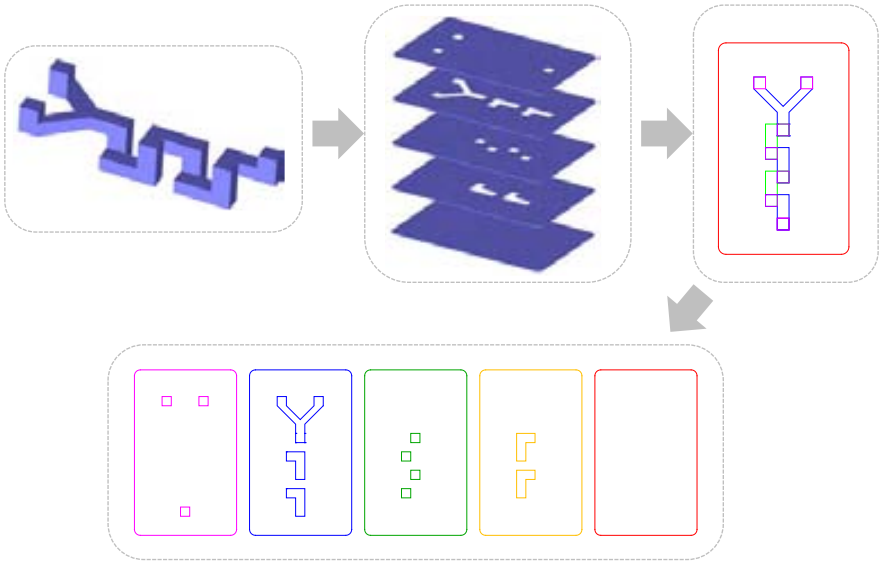

Figure 3.2:
Scheme of the general fabrication procedure of the LTCC devices.

The size of the microfluidic platform is limited by different factors, such as the thickness of the green tapes, the operational area of the metallic plates used in the lamination process and the grade of shrinkage during the sintering step. In the present thesis, only ceramic layers provided by DuPont with a thickness of 254 ± 13 µm (Dupont 951 AX) are used, which presents shrinkage in the xy axis of 12.7 ± 0.3 % and of 15 ± 0.5 % in the z axis.[1]

The diverse CAD designed layers are then transferred to independent files to CircuitCAM program (DXF extension) and lately to Circuit Master, which is related to the laser machining equipment.

3.1.2 LAYERS MACHINING

The micromachining process consists on transferring the computer designed patterns to the different ceramic layers by removing or etching portions of the material. In the present work, a LPKF ProtolLaser 200® (LPKF Laser & Electronics AG, Garbsen, Germany) laser machine has been used for this purpose.
The Protolaser 200 is a Nd: YAG type, and works in the infrared region at 1064 nm. This machine is one of the most common laser equipments, using a light source based on diodes. It has a highly developed system, which produces fine structures with high speed and accuracy. Its micromachining capacity is limited by the diameter of the laser beam, which correspond to 25 µm. The working area is defined by the work-table (30.5 x 22.9 cm), which is automatically moved by its associated software (Circuit Master). This software of control enables modifying some operating parameters, such as the beam intensity, the frequency of operation, the feed rate on the substrate, or the location in the z axis of the

[1] Dupont 951 datasheet.

substrate. Thus, these parameters must be optimized for each different substrates used.

Depending on the operating parameters introduced, it is possible to perform cutting or low relief micromachining (figure 3.3). The low relief micromachining, which is related to the use of high frequencies of operation, do not completely cut the ceramic substrate, but removes a portion of it generating grooves. This approach reduces the fragility of the layer and allows fabricating more complex designs, such as structures with very small dimensions. On the other hand, the complete cut of the substrate is limited by the thickness of the layers supplied by the ceramic manufacturer, making necessary to adjust the desired structure to the available substrate. However, this approach generates structures with less surface roughness. That is, the wall roughness is limited on the *z* axis, while in low relief micromachining, surface irregularities are present in all the substrate walls, since also the *xy* axis is mechanized. Nevertheless, in both cases final dimensions are given by the ceramic shrinkage during the sintering process.

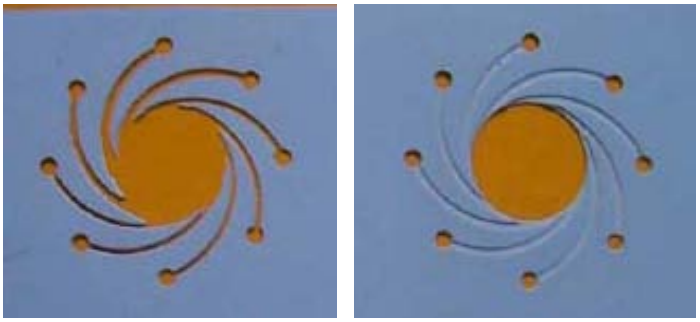

Figure 3.3: Examples of a ceramic substrate, where cutting (left) or low relief (right) micromachining is performed with the laser machine.

In some applications, where roughness is highly important such as in bioanalytics, where unspecific adsorption of biological materials increases with the roughness of the material, the use of a different pattering technique, such as hot-embossing is preferable approaches to minimize surface irregularities.

3.1.3 SCREEN-PRITING OF CONDUCTIVE PASTES

Once mechanized the substrate material and before superimposing the different layers to perform the lamination process, serigraphy of conductive tracks can be necessary for different purposes; which means the deposition of conductive, dielectric and/or resistive pastes, and their required vias to establish the electrical connexion between them and the electronic components.

Figure 3.4 shows a scheme of the complete process, which starts with the fabrication of the screen with the corresponding patterns and the further printing.

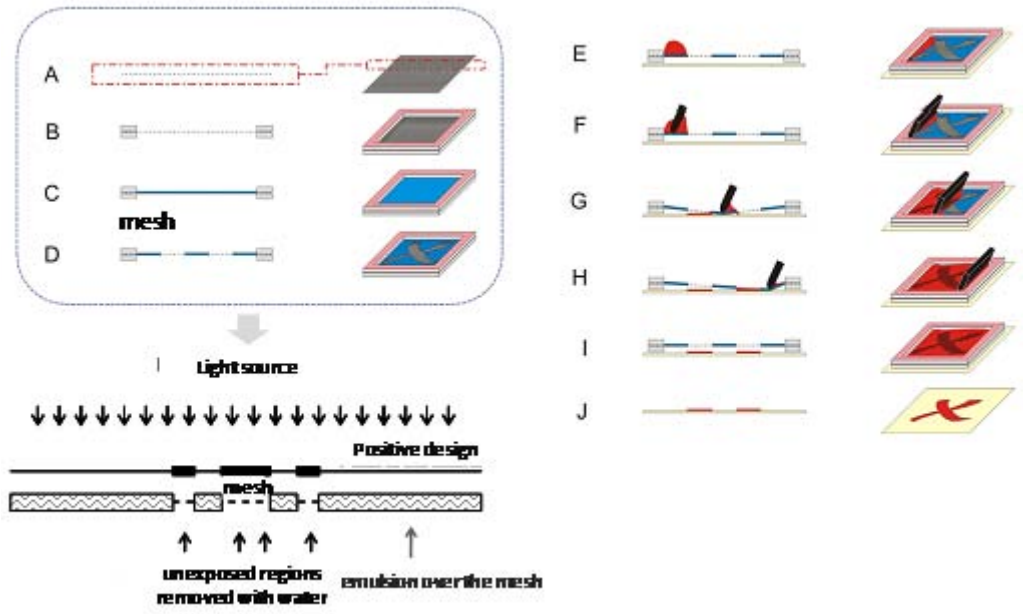

Figure 3.4: Scheme of the complete screen-printing process. **A-D:** Screen fabrication. **E-J:** Printing process.

The screen consists of a metal frame, where a mesh is tensed, that support a stencil with open areas that transfer the pastes when they are pressed through the mesh onto the substrate. The design is defined by photolithography. The most common materials employed to fabricate screens are stainless steel, nylon and polyester. The firsts are those mainly used when thicker tracks are required, since they provide high tensile strength and low compressibility. However, nylon and polyester screens are cheaper. Photolithographic open areas are produced by an emulsion in the mesh. The positive (or negative) of the design is then placed over the emulsion, which is exposed to ultraviolet light. When the mesh is cleaned with water, the negative (or positive) design is obtained (see figure 3.4 A-D).

Once the screen has been fabricated, the desired paste is deposited over it, placing under the screen the ceramic substrate (Figure 3.4 E). Then, the pattern is printed in the green tape by means of a squeegee (a flexible polyurethane or neoprene sheet coupled to a metallic or wooden made support), which forces the paste to pass thought the mesh (Figure 3.4 F-J). Some factors such as the applied pressure, the geometry and hardness of the squeegee, the application angle or the distance between the mesh and the ceramic substrate are relevant for obtaining well defined patterns.

Automatic screen-printing process are often used for finished developments, and the GSB has a DEX 248 (Asflex Internacional, ALgete, Spain) to do so. However, manual screen-printing is preferred for prototyping. In the present work, nylon screens have been used, trying to apply the same pressure in the different screen-printed layers. Two screen-printed pastes have been used, an internal

silver conductive paste (DuPont 6141, with fired resistivity < 3 mΩ/sq)[2] and a gold cofireable conductor paste (DuPont 5742 with fired resistivity < 5 mΩ/sq),[3] selected on the basis of its suitability to provide high conductive paths. Both conductive pastes are perfectly compatible with the whole LTCC fabrication process.

3.1.4 LAMINATION

The lamination process is a key step in the construction process of ceramic devices. A correct lamination process of a microfluidic platform avoids the deformation of its inner structures, which could cause liquid leakage or obstructions in the system, or shorts or open lines in electronic circuits.

In order to avoid the described problems, layers alignment is very important and an efficient way to do it is to drill four holes at the end corners of each layers, called fiducials, which are previously defined in the CAD design and machined during the micromachining process. All layers are easily placed in their correct order in a metallic sandwich plates, which contains four pivots fitting exactly into the defined holes (figure 3.5).

This aluminium plates determine the maximum working area. Our research group have different size plates available (65x65, 92x92, 100x100, 150x150 and 165x165 mm).

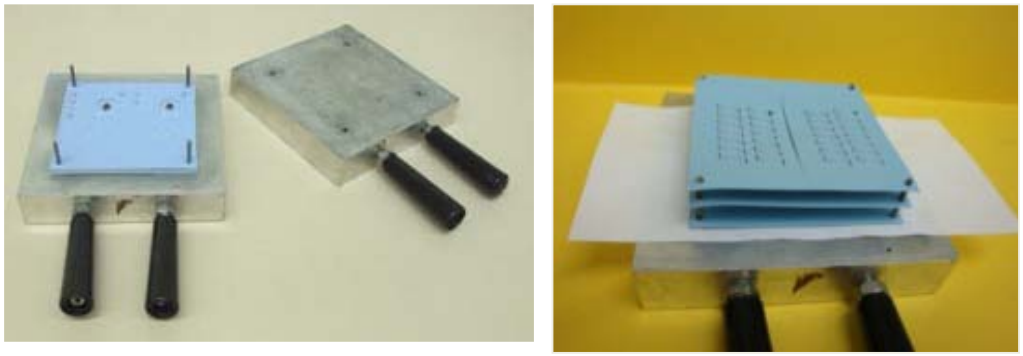

Figure 3.5: Images from the metallic sandwich plates containing pivots for the correct alignment of the ceramic layers (left), and an example of the overlapped layers (right).

Once all layers are aligned, the whole block is placed in a laminating machine, such as in figure 3.1. It consists of a hydraulic press with two hot plates of 25x15 cm (Talleres Francisco Camps SA, Granollers, Spain)., which includes a control system based on thermocouples that maintain the temperature of the plates at the desired value. The equipment bears a maximum pressure of 420 kg/cm^2 for an area of 77x77 cm, and includes automatic and manual modes, where one can define operating time or the user can manually stop it.

Lamination conditions are usually specified in the substrate datasheet. In the case of Dupont ceramic layers, a pressure of 3000 psi at 70 ºC during 10 min is

[2] Dupont 6141 Ag Cofireable Via Fill datasheet.
[3] Dupont 5742 Au Cofireable Paste datasheet.

recommended. However, if the device presents complex fluidic structures, such as wide channels or big cavities, the process is delicate and must be carefully performed in order to avoid the obstruction or deformation of such structures. When an unfinished lamination is obtained, this leads to a lack of layers contact, what results in liquid leakage. An example of well laminated devices is shown in Figure 3.6.

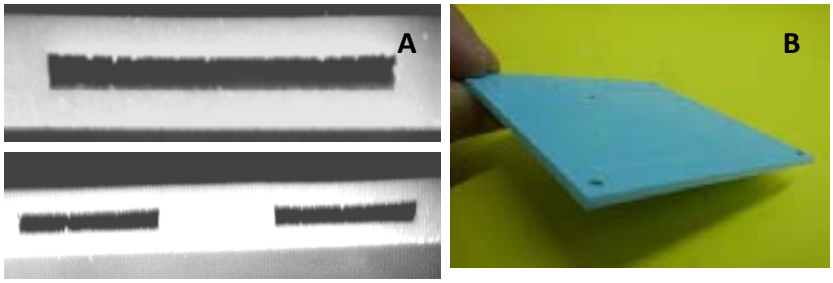

Figure 3.6:
A) Picture of three channels obtained by lamination. Profiles of well laminated channels. **B)** Image of the overall look of a laminated device.

Moreover, the use of a plastic (Mylar®), which is usually supplied with the ceramic tapes, is required for the laminating process, because it avoids adhesion of the ceramic layers to the steel plate.
After lamination, the different microsystems are removed by cutting the excess of laminated substrate. This can be performed by a Computer Numerically Controlled (CNC) machine or by the laser equipment.

3.1.5 SINTERING PROCESS

The last step in the construction of ceramic devices is the sintering process, which consist on applying a temperature profile to the laminated layers, finally obtaining a rigid block, where the different component layers cannot be distinguished. With this purpose, a programmable furnace (CarboliteCBCWF11/2316, Afora S.A., Barcelona, Spain), which can reach temperatures up to 1100 ºC is used. Moreover, it can work under inert atmosphere and enables 16 different programmable temperature profiles.

The protocol used for the fabrication of the microsystem present in this manuscript is the one recommended by the substrate supplier, and it consists of applying two temperature profiles, both at a rate of 10º C/min, and 30 min of stabilization between them. In the first ramp the temperature is raised until 350 ºC, producing the volatilization of the organic components. At approximately 850 °C, the glass transition of most glasses occurs, taking place the interpenetration of alumina particles between the layers. Assuming a random distribution of alumina particles, presumably spherical, the process can be schematized as in figure 3.7 A, where the solid glass granules become viscous and can move around alumina granules, which maintain their solid state. Finally, cooling is performed to 25º C at approximately 5º C/min, where vitrification of the glass material is achieved and the density of the material is increased and

layer cannot be distinguished. The whole profile for the sintering process is depicted in Figure 3.7 B.

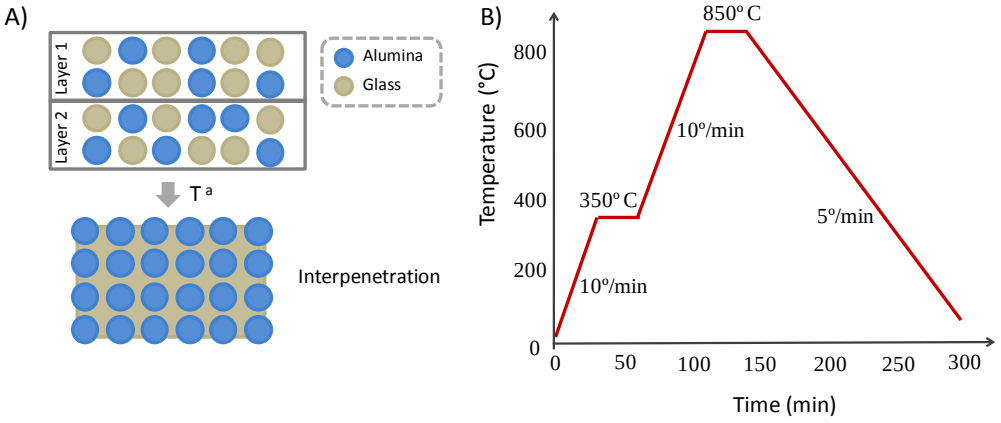

Figure 3.7:
A) Sintering process. Interpenetration of alumina particles between the layers. **B)** Temperature profile of the ceramic tapes sintering process.

3.1.6 INSPECTION OF THE FABRICATION PROCESS

Inspection of all layers, laminated block, and final microfluidic platforms is performed during the different stages of the fabrication process to ensure the adequate construction of the microsystem. In this sense, magnifying glasses, microscopes or special inspection tools are commonly used for this purpose. The different component layers are examined individually before they are laminated, in order to find possible ceramic breaks or the absence of some fluidic structures, or shorts in the screen-printed tracks.

Once the system is sintered, the conductivity of electronic components must be also tested by means of multimeters to verify their voltage and proper connection, since the shrinkage can alter these values or generate open lines due to cracks in the tracks. Involving fluidic structures, the most accurate inspection is by inserting liquid in the ceramic device to ensure the absence of liquid leakage or obstructions.

3.2 CYCLIC OLEFIN COPOLYMER FABRICATION PROCEDURE

The whole process for the fabrication of COC microfluidic platforms is drawn in Figure 3.8. Since it is a multilayer approach, the procedure begins with the CAD design of the whole system split into different layers, which are to be individually machined in a micromilling CNC machine. Then, all layers are aligned and overlapped, and as a final step, a lamination process is performed, where a thin COC substrate is used as a sealing layer. The different fabrication stages are detailed next.

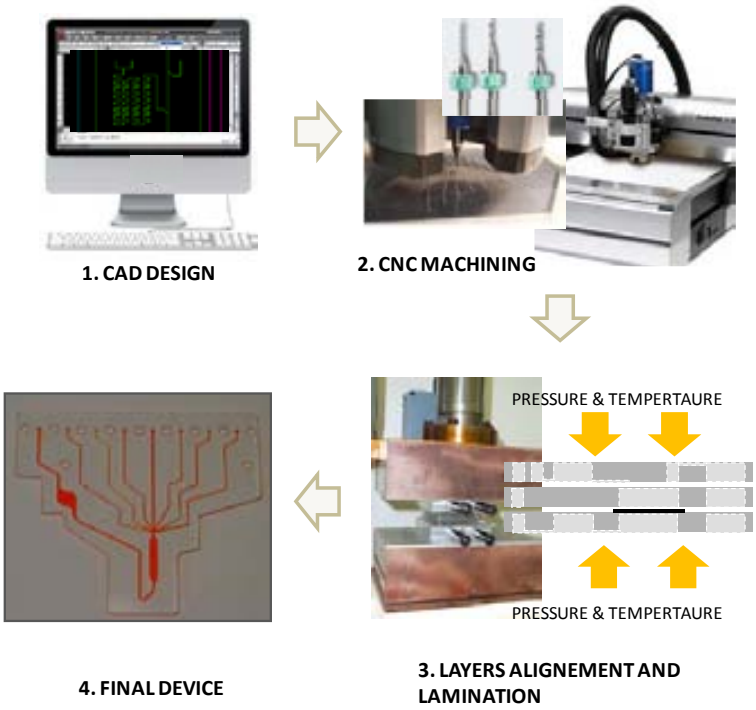

Figure 3.8: Scheme of the general fabrication procedure for COC microfluidic systems.

3.2.1 DESIGN

The fabrication of a COC microfluidic platform begins with the design in a CAD software, where its desired final 3-D structure has to be split into different layers (equivalent procedure to LTCC technology).

The COC substrate is provided by Topas, (Topas Advanced Polymers Inc., Florence, KY), and it is available in rigid plates of 15 x 15 cm or A4 sheets, with a variable thickness of 400 - 2000 µm. This company can also provide foils or sheets between 25 to 200 µm of thickness.

Although the fabrication of COC devices does not entail shrinkage at any stage, the available tools to process the substrate define the width of the fluidic structures. Therefore, the minimum size of the patterns are determined by the minimum diameter of the drill bit used.

CAD design of the different layers is transferred to different CircuitCAM files, and subsequently to Circuit Master.

3.2.2 LAYERS MACHINING

CAD design is transferred to a micromilling CNC machine for the polymeric substrate machining.

The micromilling machine used in this work is a ProtoMat® C100/HF LPKF (LPKF Laser & Electronics AG, Garbsen, Germany). This instrument is specially designed for the development of PCB (Printed Circuit Board) circuits applied to radio frequency (RF) or microwave. The rotational speed of the engine is of 100,000

rpm, and it is possible to use of a broad set of tools (including drill bits of diameters up to 0.15 mm). This enables fabricating a large variety of designs with highly precision and suitable for diverse applications.

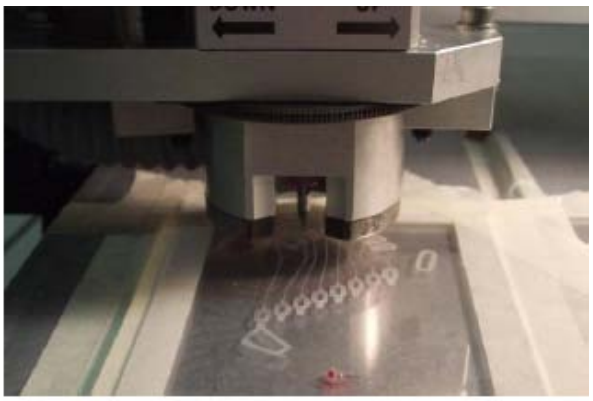

Figure 3.9: Image of the CNC machine during a COC substrate micromachining.

The CNC integrates a high precision micrometer, which enables defining the depth in the course of the micromachining. In order to protect the steel base of the equipment, a sacrificial timber is placed over the working area, fixing the substrate material by means of two metal pins located along the axis of the base. Polymeric layers are located over the sacrificial timber.

Tools ranging from 0.15 to 3.0 mm diameter are used. Some of them are specified in table 3.1.

Table 3.1: Most common tools in CNC micromilliing. Shape and function.

TOOLS	SHAPE	FUNCTION
Universal Cutter		• Cut and remove the designed patterns of the polymeric substrate. • Make higher diameter holes than 0.2 mm.
Contour Router		• Perform fiducial holes. • Perform low-relief channels.
Spiral Drill		• Perform low-relief channels. • Trim the final device.
End Mill		• Make smaller diameter holes than 0.2 mm.

In the present thesis, only End Mill Tools are used to generate a flat cutting profile for microchannels pattering; and penetrating tools (Spiral Drill Tools) are used to cut the final device.

3.2.3 LAMINATION

After the diverse polymeric substrates are machined, the lamination of the different layers is performed by thermo compression bonding. As for ceramic tapes, this is a crucial step in the fabrication of COC microfluidic systems, since this process ensures the proper alignment of the layers, which define the internal 3-D structure of the whole.

The same aluminium sandwich plates are used for lamination (§ 3.1.4). However, in the case of COC substrate, plastic blocks are used instead of Mylar®, to prevent the adherence of the polymeric substrate in the aluminium plate and to provide a uniform pressure in the polymeric layers, in order to avoid its cracking. The equipment used for lamination the diverse layers is the same hydraulic press as for ceramic tapes (Talleres Francisco Camps SA, Granollers, Spain).

The thermo-compression process consists on the application of a temperature profile at 4 - 6 bar pressure, where a first ramp from room temperature to 108 ºC is performed, followed by a stabilizing step at 108 ºC during 10-15 min. Then, the system is left for cooling to room temperature.

The main disadvantage of performing this process to polymeric substrates is the possible occlusion of the microfluidic structure due to the substrate melting. However, as discussed in the introduction part, in the case of COC with which it is possible to work with substrates with different grade of polymerization, specific thermo-compression conditions can be applied in order to melt only those layers with lower glass transition temperature for using them as sealing layers.

Consider as an example a polymeric device consisting of just one inlet and one outlet, connected by a simple channel (figure 3.10).[4] In this case, three rigid layers of 15 x 15 cm with variable thickness of 150 µm and 2 mm are required (TOPAS 6013). The thinner layers will act as top and cover, and the thicker one will provide the fluidic structure. In this case, two polymeric foils of 25 µm of thickness are also required (TOPAS 8007), since will act as adhesive between the before layers.

This lamination/sealing process generates a hermetic sealing of the microfluidic system without distort or deform the microfluidic structures, since the structural layers never exceed its Tg temperature. Once the lamination process is finished, a rigid device is obtained, where it is impossible to differentiate the original layers.

[4] Steigert, J.; Haeberle, S.; Brenner, T.; Müller, C.; Steinert, C.P.; Koltay, P.; Gottschlich, N.; Reinecke, H.; Rühe, J.; Zengerle, R.; Ducrée, J.; *J. Micromech. Microeng.*, **2007**, 17(2), 333.

The constructed microfluidic platforms must be separated from the spare material, which is usually done with the CNC machine.

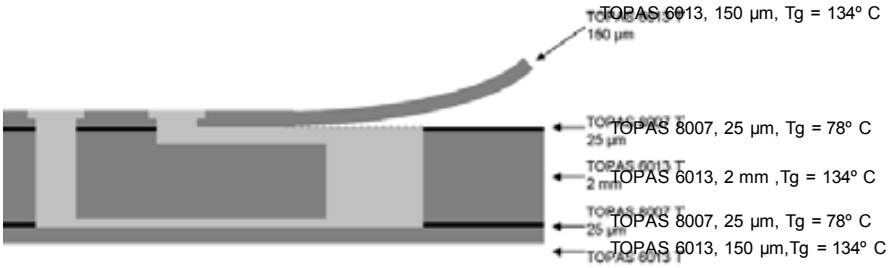

Figure 3.10: Scheme of a multilayered COC device with the structural and sealing layers.[4]

3.2.4 INSPECTION OF THE FABRICATION PROCESS

It is necessary to check the correct machining of the diverse microfluidic structures before performing the laminating process by means of magnifying glasses and microscopes. On the other hand, fluidic structures must be tested in order to check any possible obstruction of liquid leakage in the system.

3.3 CONSTRUCTED MICROFLUIDIC PLATFORMS AND INTEGRATION OF OTHER COMPONENTS

Nine different prototypes have been constructed, some of them intended for microreactors and the others for microanalyzers. Other components as detection systems and thermal conditioning systems have been also integrated. All prototypes are classified in table 3.2 with the corresponding acronym (MR for microreactor, AMS for analytical microsystem and BMS for bioanalytical microsystem), their main characteristics and other integrated components.

Table 3.2: Summary of the diverse constructed microfluidic systems. **MR:** microreactor; **AMD:** Analytical microsystem; **BMD:** Bioanalytical microsystem.

MICROSYSTEM	MATERIAL	CHARACTERISTICS	OTHER COMPONENTS
MR1 Ag NPs	Ceramic	• Two-dimensional micromixer • Discontinuous dispensing of reagents	• None
MR2 Au NPs	Ceramic	• Three-dimensional micromixer • Discontinuous dispensing of reagents	• None
MR3 Au NPs with Alkanethiols	Ceramic	• Three-dimensional micromixer • Discontinuous dispensing of reagents • Sequential reactions	• Absorbance optical system
MR4 CdS QDs	Ceramic	• Three-dimensional micromixer • Water media	• None
MR5 CdS/ZnS QDs	Ceramic	• Three-dimensional micromixer • Water media • Sequential reactions	• Absorbance and fluorescence optical system

MICROSYSTEM	MATERIAL	CHARACTERISTICS	OTHER COMPONENTS
MR6 CdSe QDs	Ceramic	• Two-dimensional micromixer • Organic media • Monolithic and modular approaches	• Thermal conditioning system
MR7 C-dots	Ceramic	• Two-dimensional micromixer	• Thermal conditioning system
AMD	COC	• Two-dimensional micromixer • Gold NPs labels	• Absorbance optical system
BMD	COC	• Reaction and detection chambers • MB-based bioassay	• Absorbance optical system • Magnetic actuator

A description concerning the design, construction, optimization and evaluation of all microfluidic systems is presented in the next chapters. In addition, the characterization of the synthesized nanoparticles is included. On the other hand, analytical features of the developed (bio)analytical systems are also presented and discussed.

MICROREACTORS FOR THE SYNTHESIS OF METALLIC NANOPARTICLES

Contents

Image from Imperial College of London website

The use of metallic nanoparticles can be very advantageous in the development of analytical devices due to their extraordinary optical properties. Thus, the development of microreactors for the reproducible synthesis of these nanomaterials is the first purpose of this work.

The design and construction of different devices for the synthesis of silver and gold nanoparticles will be presented throughout the following chapter, along with the discussion of the results obtained for other failed microfluidic platforms. These devices are based on the LTCC technology and their substrate material, since ceramic tapes enable to work with the required synthetic reagents while allowing a rapid prototyping. Moreover, all the microreactors developed include the automation of the whole process, which reduces many variables of the process.

The first microreactor presented takes on the synthesis of silver nanoparticles (**MR1**). Its fluidic design is based on a hydrodynamic focusing of reagents and a bi-dimensional serpentine micromixer, which allow a high and rapid degree of mixing.

Once verified the potential of ceramic tapes for the construction of microreactors, we proceeded with the development of a microfluidic platform for the synthesis of gold nanoparticles (**MR2**), due to this nanomaterial presents some advantages such as its chemical inertness and simple surface modification for further development of optical sensors. Its design was based on the **MR1**, so it includes the same conformation for the entrance of reagents, but a three-dimensional serpentine micromixer instead of the bi-dimensional.

The evolution of this second microreactor led to the **MR3**, where an extra channel for the addition of stabilizers/modifiers is incorporated. Furthermore, a miniaturized optical system is adapted to the microreactor in order to make feasible the reaction monitoring.

4.1 MICROREACTOR FOR THE SYNTHESIS OF SILVER NANOPARTICLES (MR1)

The below described microreactors for the synthesis of Ag NPs pretends to evaluate the possibility of constructing microfluidic devices by using the LTCC

technology as well as studying the different design and chemical parameters involved in the development of these devices. For this purpose, a procedure consisting on the chemical reduction of a silver salt by a reducing agent was preferred, since these chemical methods usually generate more uniform nanoparticles. In concrete, Ag NPs have been synthesized by a simple one-phase reaction in which silver nitrate is reduced by sodium borohydride in aqueous medium. [1] Therefore, the chemical compatibility of ceramics with these type of synthetic reagents could be also tested.

As there was no previous experience in the research group in developing synthetic devices, it has been necessary to start from scratch. Thus, it has been required not only an optimization of the chemical and hydrodynamic parameters (as in all microsystems), but also of all design parameters, which means the manifold configuration, channel characteristics and the construction of micromixers when necessary. Although the optimization of all parameters is an iterative process which involves all the variables at the time, they have been differentiated in order to simplify some conclusions.

4.1.1 MATERIALS, REAGENTS AND METHODS

The synthesis of silver nanoparticles in the ceramic microfluidic platform requires the equipment and materials listed in table 4.1, which are related with dispensing the reagents to the microsystem and to the characterization of the nanoparticles.

Table 4.1: General list of equipments used in the synthesis of silver NPs.

EQUIPMENT	PROVIDER
• 2 or 3 syringes pumps, 540060 TSE systems	TSE systems, Bad Homburg, Germany
• 1 syringe of 1mL, GASTIGHT 1000 TLL series	Hamilton, Bonaduz, GR, Switzerland
• 1 or 2 syringes of 10 mL, GASTIGHT 1000 TLL series	Hamilton, Bonaduz, GR, Switzerland
• Tygon tube (i.d. 1.2 mm)	Ismatec, Zurich, Switzerland
• PTFE tubes (i.d. 0.8 mm)	Techny Fluor, Barcelona, Spain
• UV-310PC UV-Vis-NIR double-beam scanning spectrophotometer	Shimadzu, Kyoto, Japan
• High Resolution Transmission Electron Microscopy (HRTEM) JEOL 2011	JEOL, Tokyo, Japan
• Transmission Electron Microscopy (TEM) JEOL 1400	JEOL, Tokyo, Japan
• Atomic Force Microscopy (AFM)	JEOL, Tokyo, Japan

[1] Douglas, F.; Yañez, R.; Ros, J.; Marín, S.; de la Escosura, A.; Alegret, S.; Merkoçi, A. *J.; Nanopart. Res.,* **2008,** 10, 97–106.

The double-beam scanning spectrophotometer is used to record spectra between 800 and 200 nm to verify the formation of particles. On the other hand, the shape and dimensions of the particles core are measured by a High Resolution Transmission Electron Microscopy, Transmission Electron Microscopy and Atomic Force Microscopy.

On the other hand, the reagents used for this purpose are presented in table 4.2. All solutions are prepared in double distilled water.

Table 4.2: Reagents used for the synthesis of silver NPs.

REAGENT	PROVIDER
• Silver nitrate	ACS grade, Fluka, 99 %
• Sodium borohydride	PS grade, Panreac, 96 %
• Sodium citrate	PA ACS, Panreac

4.1.2 EXPERIMENTAL SET-UP

The experimental set-up used for the synthesis of silver nanoparticles is shown in figure 4.1. Different syringes (1-10 mL) are connected to the ceramic microfluidic system by means of PTFE tubes and tygon tubes glued to the device. The syringes are placed in syringe pumps, which are computer controlled, for the propulsion of reagent solutions.

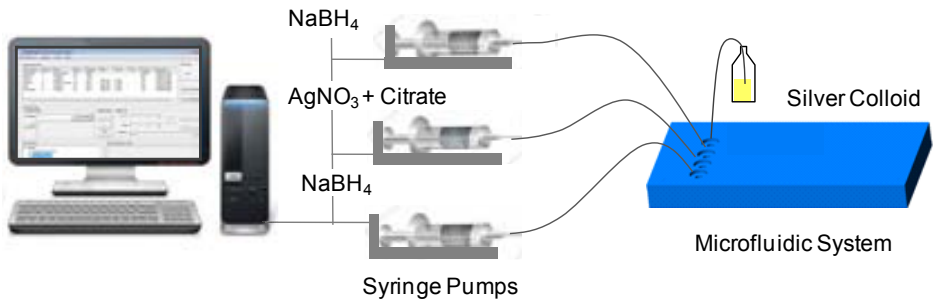

Figure 4.1: Microsystem set-up for the synthesis of silver nanoparticles

The use of such syringe pumps provides certain advantages over the conventional peristaltic pumps. They allow a quiet operation with high accuracy and virtually pulseless flow, and permits working at very slow flow rates, providing microlitre per second flow rates (flow rates from 0.001 µl h^{-1} up to 147 ml min^{-1} can be displayed). Thus, they confer a simple and controlled dispensing of reagents, which is a key point if well-defined particles are desired to obtain. As explained before, the pumps are computer controlled by simple software (WinPump Control), which provides a user interface for the control of one or more programmable syringe pumps configured as a network. Some of the advantages of using these pumps are:

- Possibility of working modes of infusing or withdraw.
- Synchronize multi-pump operations.
- Easily configure and control multi-pump protocols.
- Start and stop pumps individually (you select the pump from a list of connected pumps) or as a group (all connected pumps told to start and stop as a group).
- Upload pump programs to each pump.
- Different pumping programs to each connected pump.
- Each pump can have its own rates and flows.
- Pump response history – pump commands and responses are logged on the screen.
- Send commands manually to connected pumps - just type your command and click enter.
- PPL file functionality – upload a program to the pump from a text file.
- Assign labels to each pump to help with identification.

The diverse syringe pumps are connected by a USB-RS232 device to the computer. Once installed the controlling program, certain variables must be introduced, concerning the syringe size to be used, the dispense volume and the required flow rate.

540060 TSE systems syringe pumps are used in this work for the synthesis of all nanomaterials. Figure 4.2 shows an image of three syringes connected in series and the WinPump Control software. Moreover, some of their characteristics are presented in table 4.3, such as their minimum and maximum speed or the motor steps per revolution, among others.

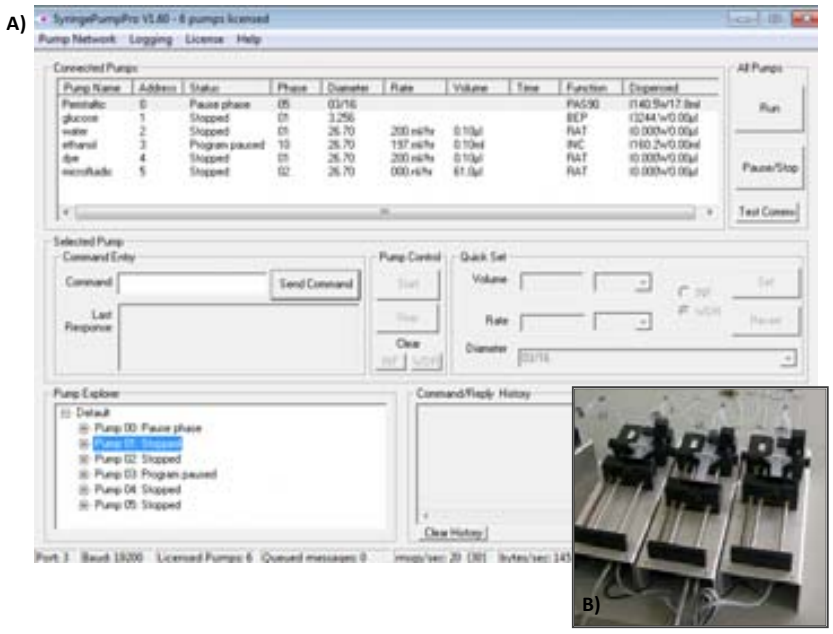

Figure 4.2:
A) Image from the WinPump Control software. **B**) Image from three different syringes connected in series.

SPECIFICATION	VALUE
Model	540060
Operation mode	Infusion/ Withdrawal
Syringe sizes	0.5 µL up to 60 mL
Max. syringe number	1
Maximum flow rate	6120 mL h^{-1} with a 60 mL syringe
Minimum flow rate	0.001 µL h^{-1} with a 0.5 µL syringe
Selectable rate units	µL h^{-1}, µL min^{-1}, mL h^{-1}, mL min^{-1}
Syringe inside diameter range	0.100 to 50.00 mm
Motor type	Step motor
Motor steps per revolution	400
Motor to drive screw ratio	15/28
Maximum speed	5.10 cm min^{-1}
Minimum speed	0.004205 cm h^{-1}
Maximum force to all syringes	15.9 Kg at minimum speed, 8.2 Kg at maximum speed
RS-232 pump network	100 pumps maximum
RS-232 select able baud rates	300, 1200, 2400, 9600, 19200
Programmable phases	41
Interface	RS-232 Interface Bi-Directional TTL Logic Control Interface
Accuracy	+/ - < 1 %
Reproducibility	+/ - < 0.1 %
Dimensions	23 cm x 15 cm x 11 cm
Weight	1.63 Kg

Table 4.3: General characteristics of 540060 TSE systems syringe pumps.

4.1.3 OPTIMIZATION OF THE MICROFLUIDIC PLATFORM

It is important to have in mind the formation process of metallic nanoparticles when the optimization of the different design parameters of the ceramic microreactor is intended. As stated in the introduction section, in order to produce highly uniform nanoparticles it is necessary to have a supersaturated concentration of reagents in a short time at the beginning of the synthesis. In this way, seeds of particles are quickly formed and the subsequent growth is carried out in longer times due to a diffusion stage.[2] Thus, a high concentration of the reagent solutions and an efficient mixing are necessary for seeds formation.

Figure 4.3 shows the diverse microfluidic structures designed, fabricated and tested for the synthesis of these NPs, while Table 4.4 sums up their different parameters. As it can be observed, different configurations for the entrance of reagents were studied as well as diverse lengths and structures for the following reaction channel. The initial meeting of reagents should be related to the first formation stage of the nanoparticles, whereas the growth of the particles is concerned to the following channel until the outlet.

[2] Lamer, V.K.; Dinegar, R. *J. Am. Chem. Soc.*, **1950**, *11*, 4847.

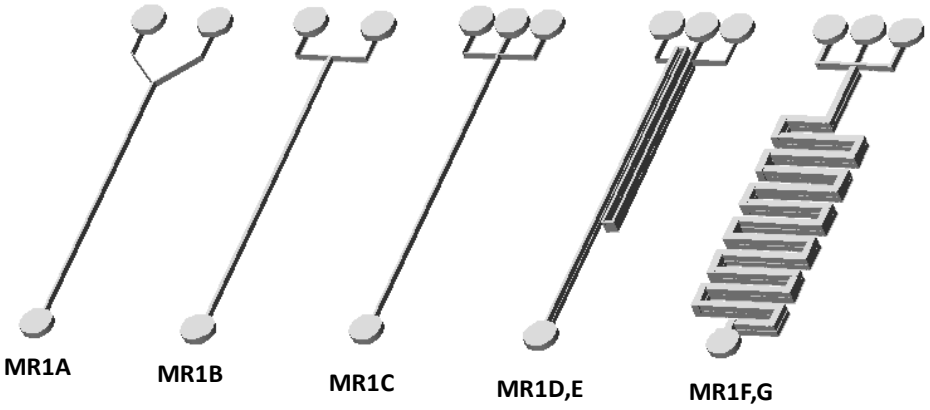

Figure 4.3: Scheme form the diverse microfluidic platforms designed, constructed and tested for the synthesis of silver NPs microreactors.

Table 4.4: Summary of the different parameters of the microfluidic platforms studied for the synthesis of silver NPs.

IDENTIFICATION NUMBER	FLOW SYSTEM CHARACTERISTICS	DESIGN			
		N inlets	Injection configuration	Mixer configuration	Volume (µL)
MR1A	Simple Injection	2 inlets	Y	-	3
MR1B			T	-	4
MR1C		3 inlets	T	-	7
MR1D	Simple Injection + Residence Zone	3 inlets	T	-	18
MR1E					27
MR1F	Passive Mixers	3 inlets	T	2D	70
MR1G					124

First prototypes were based on a simple short channel, where reagents were pumped into the device by two inlets (one for the metal and another for the reducing agent) with a Y or T shape as converging point (microfluidic platforms **MR1A** and **MR1B**). It was observed that these microreactors, where two laminar streams prevail along the whole microfluidic platform, produced unstable nanoparticles due to a poor mixture of reagents. Therefore, aggregation of NPs outside the microfluidic platform was observed using these simple designs.

Next prototypes were designed in order to avoid the existence of these two main streams of reagents in the microfluidic channel and to generate a higher mixture degree. A hydrodynamic focusing configuration, which permits an effective and controllable lamination of the flow, thus reducing the mixing path, was preferred for this purpose. The typical design for this parallel lamination micromixer consists of three inlets and a long channel. Therefore, the central stream strongly depends on the flow rate of the side channels. In the designed microreactor, the configuration of the confluence point of the inlets and flows acquires a trident shape where the middle inlet is for the silver salt and the other two inlets are for the borohydride, working as the sheath flows (**MR1C**). With this conformation, the metal is surrounded by the reducing agent, and thus, a more efficient mixture is generated. A yellow coloured solution confirmed the formation of silver nanoparticles, which absorbed over 400 nm. TEM measurements revealed the

presence of the colloid. However, as it can be observed in figure 4.4, the particles presented an irregular shape and were not uniform.

Then, diverse microfluidic systems were designed and constructed in order to improve the homogeneity and stabilization of the silver suspension. Microreactors **MR1D** to **MR1G**, which incorporate stabilization zones or passive mixers, were tested. No significant improvement was observed by the enlargement of the microfluidic channel (**MR1D - MR1E**). However, the construction of a bi-dimensional micromixer generated well defined nanoparticles (**MR1F**). This is probably due to the chaotic advection that causes these mixers, improving the mixture of reagents. On the other hand, by using deeper micromixers no improvement was observed (**MR1G**).

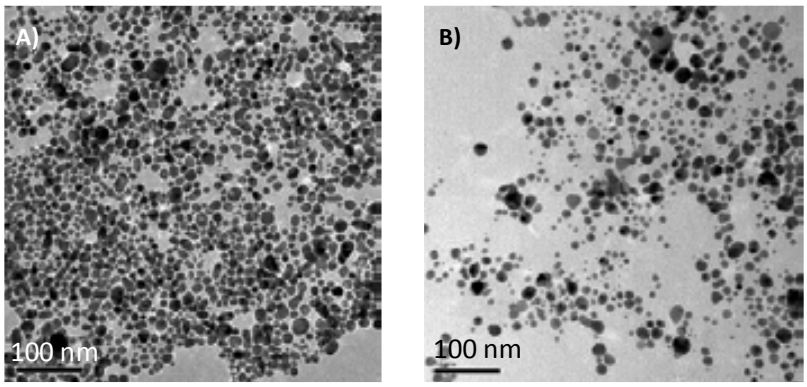

Figure 4.4: TEM images from silver NPs synthesized with **MR1C** ceramic microfluidic systems. The hydrodynamic and chemical parameters consisted on: **A)** 5mM $NaBH_4$ solution pumped at 2 µL s^{-1} syringe flow rate, and 3 mM $AgNO_3$ at 1µL s^{-1}. **B)** 5 mM $NaBH_4$ solution pumped at 2 µL s^{-1} syringe flow rate, and 1 mM $AgNO_3$ at 1µL s^{-1}.

Therefore, the microreactor used for the synthesis of silver nanoparticles, which showed the tighter particle distribution, is composed of three inlets for reagents, which converge in a trident shape point, followed by a bi-dimensional micromixer (**MR1F**). The total reaction volume is 70 µL. Figure 4.5 shows an image from this ceramic device. The absorption band and TEM images of the obtained silver nanoparticles using the optimized chemical and hydrodynamic parameters are shown in figure 4.8.

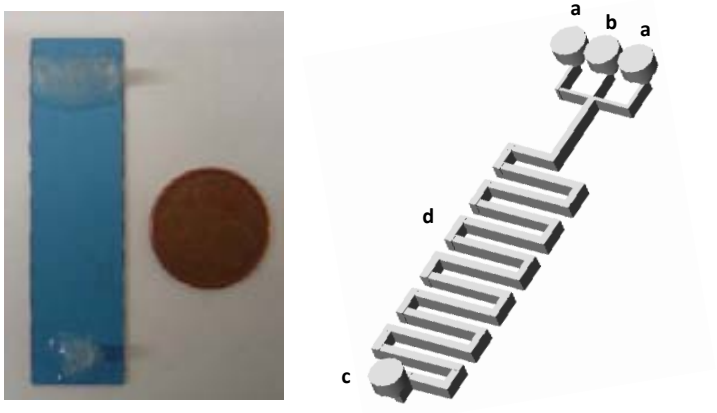

Figure 4.5: **A**) Image from the optimized microfluidic platform for the synthesis of silver nanoparticles (**MR1F**). **B**) Intern design of the **MR1F** microfluidic platform, where a: reducing agent inlets, b: silver salt inlet, c: outlet, bi-dimensional micromixer.

On the other hand, an important consideration when fabricating synthetic devices is the materials used in the whole microreactor and set-up. First

prototypes employed for the synthesis of silver nanoparticles made use of metallic flanges glued to the ceramic devices for the insertion of reagents into the microreactor, as normally done in the research group. However, X-ray energy dispersion spectroscopy (EDS, EDX, EDAS) analysis performed in TEM measurements revealed the presence of silver but also of cooper and zinc, since these connection pieces are made of brass (alloy of copper and zinc). This experiment made clear the impossibility of using any metallic component for the synthesis of metallic particles, since the reducing agents used interacts with these components. Thus, the brass pieces were changed for a little fragment of tygon tubes, which were directly glued to the ceramic device (Figure 4.5). Similarly, all the other materials used should be metal-free, such as the syringes employed, which have the end of their plunger and their luer lock connections made of PTFE (GASTIGHT 1000 TLL series).

4.1.4 OPTIMIZATION OF THE CHEMICAL AND HYDRODYNAMIC PARAMETERS

The optimization of the chemical and hydrodynamic parameters is of crucial importance in all analytical microsystems, and also in synthetic devices. Thus, different variables were tested in order to obtain the most uniform particles in a reproducible way.

Concentrations of diverse order of magnitude were tested in the first microfluidic platforms, which involved solutions of between 0.01 M and 0.01 mM for silver nitrate, and between 0.01 M and 0.9 mM for reducing agent. Continuous flow rates of 1 µL s^{-1} in infusing operation mode were only used to evaluate the unique influence of concentration. In these first testes the extreme importance of the concentration of reagents was observed. High concentrations of metal generated precipitated particles, since a black solid suspension in the outlet channel was observed. The registered UV-Vis spectrum confirmed the no formation of nanoparticles in the solution. Moreover, the use of such concentrations generated most of times the obstruction of the microfluidic platforms, being necessary the construction of a new device. On the other hand, no formation of colloidal was observed at low concentrations of one of the reagents, since the obtained solution was completely transparent and no band appeared in the UV-Vis spectrum.

The use of intermediate concentrations in the milimolar range resulted in the formation of yellowish solutions, matching with the correspondent colour of silver NPs. The formation of the colloid was confirmed by spectroscopic methods, since its absorption spectrum generated a band located over 420 nm.

Once the concentrations of reagents were roughly optimized, the influence of the hydrodynamic parameters was studied. Actually, varying these parameters entail

changes in the molar relationship of reagents, and thus, in their concentrations. These changes can be better controlled by the use of syringe pumps, since it can be automatically done.

In this sense, first testes were based on continuously varying the flow rate of silver or borohydride by infusion. Continuous flow rates from 0.5 until 2.5 µL s^{-1} were evaluated for each reagent, considering passive mixing with an equivalent flow of reagents, but also active due to the different flows dispensed. High values of flow rates generated uncontrolled and big nanoparticles, which precipitated in few time as previously seen in the optimization of the concentration of reagents. However, better results were obtained for intermediate or low flow rate values, although homogeneity could not even be well controlled (Figure 4.6).

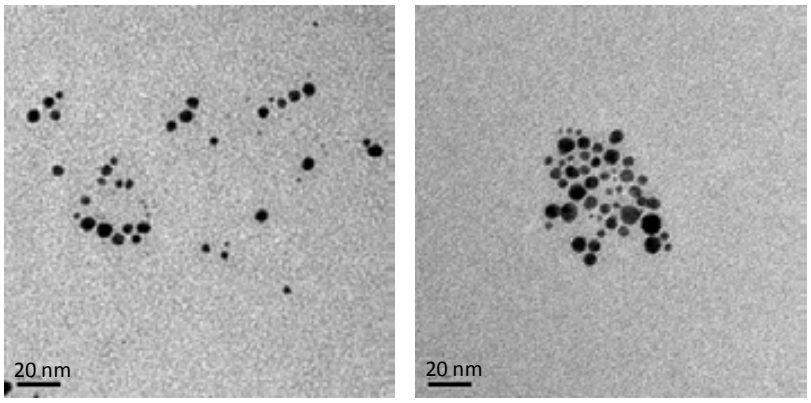

Figure 4.6: TEM images from silver NPs synthesized with **MR1F** ceramic microfluidic system. The hydrodynamic and chemical parameters consisted on 5 mM $NaBH_4$ solution continuously pumped at 1µL s^{-1} syringe flow rate, and 1 mM $AgNO_3$ at 1µL s^{-1}.

Since the use of continuous flow rates did not generate homogeneous particles, the next step in the optimization of the hydrodynamic parameters was testing discontinuous flow rates. The injection of controlled dosage volumes of the metal agent while the reducing agent flowed continuously in the system was tried. In this way, the environment of silver nitrate is well defined, simplifying the control of the reaction. Thus, two extra parameters, the time spent between dosages and the volume of dosage, are introduced in the system. The creation of pumping programs, which must be uploaded to the different pumps from a text file (PPL), is necessary to perform these kind of operations, while so far have been working by simply sending the different commands manually to the diverse pumps. However, these programs are really simple to do.

Then, the volume of dosage, the time spent between dosages (pas), and the flow rates used should be studied for the metal reagent, which was used in a 1 mM concentration. The conditions of reducing agent were fixed to 5 mM at 2 µL s^{-1}.

The advantages of using this dispensing protocol were immediately noticed. First, pas was fixed to 2 seconds and the flow rate to 150 µL s^{-1}, since these parameters allows a well defined and quickly deliver of the reagent into the microsystem. Then, the dosage volume was tested between 0.1 and 1.1 µL. High dosage values generated bigger and less uniform particles, probably due to the poor control of the reaction zone achieved. However, a compromise situation exists for low

dosage volumes, since the lower the dosage volume is, the less particle concentration (and amount) is obtained, generating almost invisible SPR bands for smaller values than 0.3 µL. Thus, 0.7 µL was chosen as the optimal dosage volume.

Then, the influence of the time spent between dosages was investigated. No significant variations were observed from the diverse values tested (from 1 to 4 seconds). Thus, an intermediate value of 2 seconds was preferred, as it confers the required limitation of reagents with a desired final concentration of nanoparticles.

Finally, the silver reagent flow rate was studied, testing values between 0.8 and 4.1 µL s^{-1}. The more uniform particles were obtained for the highest values used. However, 2.5 µL s^{-1} was preferred for the synthesis, since it provided the same grade of particles dispersion by diminishing the pressure in the system, which can cause the obstruction of the microfluidic system.

Tests performed in the optimized microreactor (**MR1F**) with the previous dispensing protocol, consisting in a solution of 5 mM $NaBH_4$ continuously pumped at 1µL s^{-1} syringe flow rate, and 0.7 µL of a 1 mM $AgNO_3$ solution sequentially injected every 2s at a 2.5 µL s^{-1} syringe flow rate, provided uniform particles. The molar relationship of the $AgNO_3$ and $NaBH_4$ solutions is 1:16, and the total residence time of the silver colloid inside the microfluidic device is estimated at approximately 30 s.

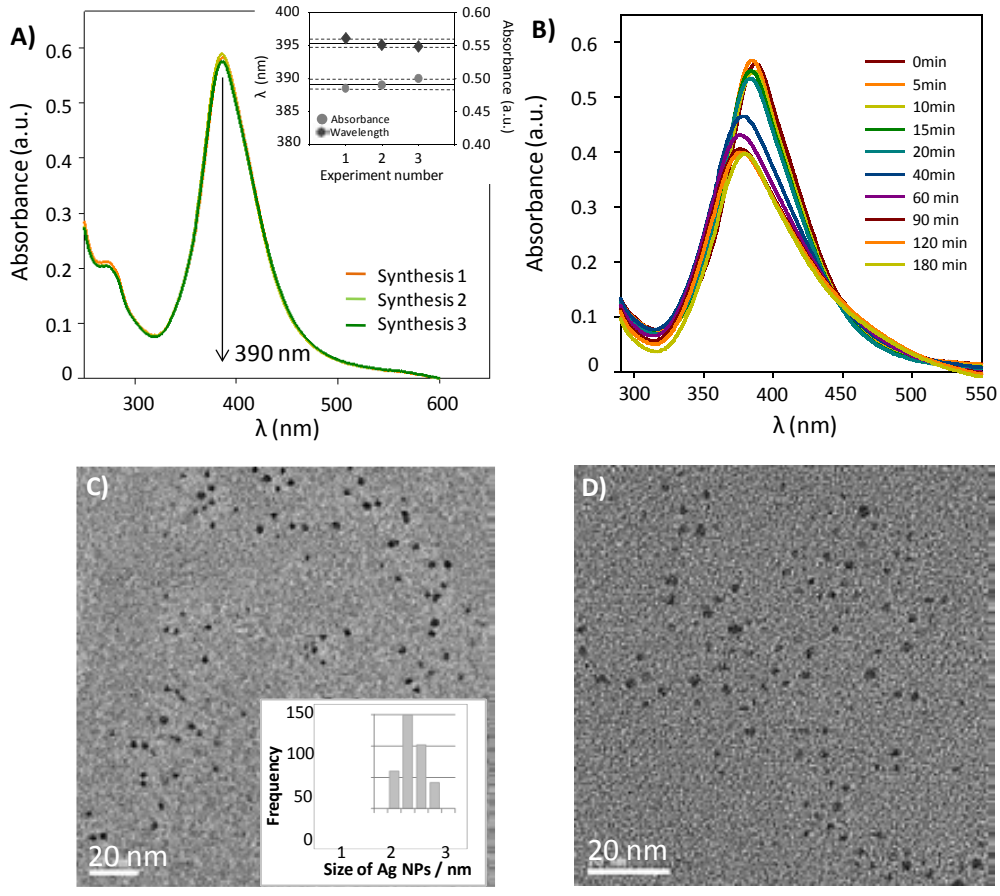

Figure 4.7:
A) UV-Vis spectra of silver nanoparticles from 3 different syntheses with their correspondent standard deviations. **B**) Diverse UV-Vis spectra from one of the Ag NPs synthesis recorded with time. The displacement observed in the band indicates the instability of the particles. **C**) and **D**) Correspondent TEM images from the Ag NPs synthesized in the **MR1F** microreactor.

As it can be observed in figure 4.7A, absorption measurements revealed an SPR centred at 390 nm. Moreover, TEM images (Figure 4.7C and D) showed well defined and uniform nanoparticles, with a medium core size of 2.0 ± 0.7 nm.
The repeatability of the method was studied by the synthesis of 3 different batches of the nanomaterial. As it can be observed in figure 4.7A, almost no variations were found in the three different syntheses, being its absorption wavelength of 390.0 ± 0.7 nm and its absorbance intensity of 0.55 ± 0.01a.u.
Although the synthesis of silver nanoparticles was finally controlled, and uniform and reproducible nanoparticles could be obtained, deviations in its SPR band recorded with time revealed their instability (Figure 4.7B).

4.1.4.1 STABILIZING AGENT

As it has been shown, silver nanoparticles have been homogeneously synthesized in a reproducible way in a ceramic microreactor by using a discontinuous dispensing protocol of reagents. However, its stability with time could not be achieved by the modification of the hydrodynamic and chemical parameters. Moreover, the construction of new devices generated no improvement in this sense.
Thus, it was clear that the colloidal required, as most of particles, the addition of a stabilizing agent. As discussed in the introduction part, some examples of stabilization are encapsulation in microemulsions, micelles, vesicles, dendritic structures, polymer assemblies, surfactants, thiols, etc. Some of the more usual stabilizing agents for silver nanoparticles are sodium citrate, ethylene glycol with PVC, ascorbic acid in a basic solution of CTAB, or oleic acid with H_3PO_4. In this work, the preferred to use as stabilizer sodium citrate.
Thus, different concentrations of citrate were prepared and tested. In order to simplify the fluidic structure and avoid the construction of another device, the stabilizer solution was prepared jointly with the metal solution.
Diverse syntheses were performed to validate the use of the stabilizer. Low concentrations of citrate did not prevent the following aggregation of the particles. However, the use of a 3-fold concentration of citrate than the metal (3 mM) finally generated stable particles.
Therefore, the most uniform, stable and reproducible silver nanoparticles can be synthesized with the **MR1F** microfluidic system with the optimized dispensing protocol consisting in a 5 mM $NaBH_4$ solution continuously pumped at 1µL s^{-1} syringe flow rate, and 0.7 µL of a 1 mM $AgNO_3$ and 3 mM sodium citrate solution sequentially injected every 2 s at a 2.5 µL s^{-1} syringe flow rate (Figure 4.8A).
As it can be observed in figure 4.8B, the SPR band recorded with time showed no deviation in almost 180 min, and the homogeneity of the particles was

demonstrated not only by TEM measurements (size core of Ag NPs of 3 ± 0.5 nm) (Figure 4.8C), but also by AFM images (Figure 4.8D).

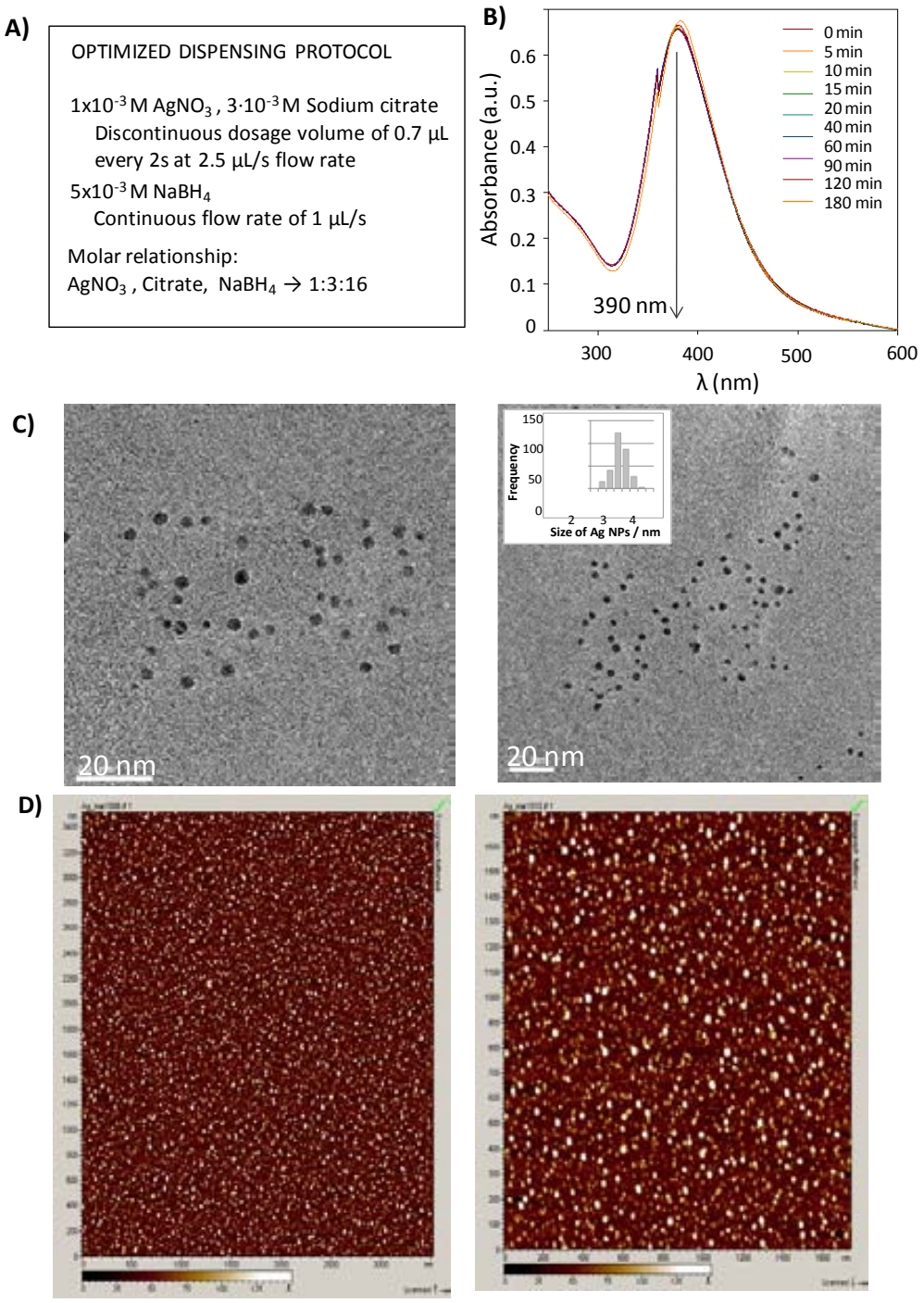

Image 4.8:
A) Optimized dispensing protocol conditions. **B)** UV-Vis spectra of silver nanoparticles recorded with time. No displacement of the SPR was observed in 180 min, indicating the stability of particles. **C)** Correspondent TEM images and (**D)** AFM images from the Ag NPs synthesized in the ceramic microreactor.

4.1.5 CONCLUSIONS

The potential use of ceramic tapes and the LTCC technology for the development of microreactors to carry out the synthesis of nanoparticles has been well proved in this chapter. The chemical resistivity of the substrate material enables its perfect working in harsh conditions, such as the use of reducing agents, since no

interaction between the substrate and the chemical reagents has been observed during the synthesis of silver nanoparticles.

The design and construction of a trident shape configuration for the entrance and meet of reagents allow the use of a hydrodynamic focusing, which enables a better control of the diffusion of reagents. Moreover, the use of little volumes of metal dosed in certain time while the rest of channels are pumped in a continuous way has shown its advantages, since it provides the more homogeneous colloids. Besides, the construction of a bi-dimensional micromixer improves the mixture of reagents as well as increases the residence time of reagents in the microfluidic platform. As result, uniform and reproducible Ag NPs are obtained. On the other hand, the automation of the whole process allows a proper control of the different parameters involved in the synthesis, which is of extreme importance to prepare reproducible nanomaterials.

The present approach appears, thus, as an excellent alternative for the synthesis of nanoparticles, taking advantage of the substrate material and its simple, cheap and quickly fabrication procedure.

4.2 MICROFLUIDIC PLATFORMS FOR THE SYNTHESIS OF GOLD NANOPARTICLES (MR2, MR3)

Each microfluidic platform presented in the following section has its precedent in the Ag NPs microreactor (**MR1**). In fact, some of the previous microsystems and hydrodynamic parameters employed in the development of the **MR1** have been tested again to investigate if same considerations can be applied for the development of this microreactor. However, the design and construction of new others have been necessary to achieve the optimized microfluidic platform, which could perform the gold colloid synthesis.

The reduction of tetrachloroauric (III) acid with sodium borohydride in water has been preferred for the synthesis of gold nanoparticles, which are stabilized by the electrostatic repulsions generated by the remaining reducing agent (**MR2**).[1] Later, different alkanethiols have been used in order to provide of chemistry to the nanoparticle surface and improve their stability (**MR3**). These stabilizers have been selected in function of their functional groups, since their moieties can be very useful in the future. Thus, one could choose the required colloid according to the final application.

On the other hand, a miniaturized optical system for absorbance measurements based on commercial optical components has been developed and adapted to the microreactor. This system, which has been developed in collaboration with the "*Grupo de Tecnologías Fotónicas*" (GTF) of the University of Zaragoza, aims to

evaluate the possibility of monitoring the synthesis of nanoparticles. Thus, any possible variation of the synthetic procedure owing to, for instance, channel obstruction or incorrect dispensing of reagents, can be immediately detected and one can take appropriate actions to solve the problem in the shortest time. Moreover, the system can be very useful in the optimization process of a synthetic procedure, since changes in the optical properties of the nanomaterial due to variations of the hydrodynamic parameters can be simply followed.

4.2.1 MATERIALS, REAGENTS AND METHODS

As for the synthesis of silver nanoparticles, the required equipments for the production, manipulation and characterization of gold colloidal in **MR2** and **MR3** are listed in table 5.1.

Table 4.5: General list of equipments used in the synthesis of gold NPs.

EQUIPMENT	PROVIDER
• 3 (**MR2**) or 4 (**MR3**) syringes pumps, 540060 TSE systems	TSE systems, Bad Homburg, Germany
• 1 syringe of 1 mL, GASTIGHT 1000 TLL series	Hamilton, Bonaduz, GR, Switzerland
• 2 syringes of 10 mL, GASTIGHT 1000 TLL series	Hamilton, Bonaduz, GR, Switzerland
• 1 syringe of 2.5 mL, GASTIGHT 1000 TLL series (**MR3**)	Hamilton, Bonaduz, GR, Switzerland
• 4 Three-way solenoid isolation valves	NResearch incorporates®, Bern, Switzerland
• User-friendly connection system	GSB
• Conical PTFE connectors (Cones 1.6 mm)	Omnifit, Cambridge, UK
• Tygon tube (i.d. 1.2 mm)	Ismatec, Zurich, Switzerland
• PTFE tubes (i.d. 0.8 mm)	Techny Fluor, Barcelona, Spain
• 4 mL centrifugal tubes, CENTRIPLUS YM30, MICROCON, MWCO 30000	Millipore™, Centriplus™ Centrifugal Concentrators, Billerica, USA
• Angular centrifuge Cencom II	J. P. Selecta, S.A., Abrera, Spain
• pH meter GL22	Crison, Alella, Spain
• LyoQuest freeze dryer	Telstar, Terrassa, Spain
• UV-310PC UV-Vis-NIR double-beam scanning spectrophotometer	Shimadzu, Kyoto, Japan
• High Resolution Transmission Electron Microscopy (HRTEM) JEOL 2011	JEOL, Tokyo, Japan
• Transmission Electron Microscopy (TEM) JEOL 1400	JEOL, Tokyo, Japan
• Zeta sizer nano ZS	Malvern, Worcestershire, UK
• Flash EA 2000 CHNS	Thermo Fisher Scientific, Cambridge, UK

The spectrophotometer is useful for the rapid identification of the SPR band of the colloid; meanwhile the shape and dimensions of the particles core are measured by TEM or HRTEM. Zeta sizer nano ZS is employed to characterize the stability of the synthesized nanoparticles as well as to obtain DLS measurements. On the other hand, CHNS elemental analysis is used to determine the number of chains onto the nanoparticles surface.
In all cases, and prior to characterization, the purification of the colloid is performed by centrifugal filtration with water in 4 mL centrifugal filter devices at 3000 rpm for 30 min by triplicate. The pH of the final solution is adjusted to 9-10. Freeze-drying of gold nanoparticles is done in order to long-term store the colloid.

The required reagents for obtaining the gold colloid are presented in table 4.2. Again, all solutions were prepared in double distilled water.

Table 4.6: Reagents used for the synthesis of gold NPs.

REAGENT	PROVIDER
• Gold (III) chloride hydrate	PA ACS, Fluka, ≥ 49 % Au
• Sodium borohydride	PA ACS, Panreac, 96%
• 11-Mercaptoundecanoic acid (MUA)	Aldrich, 98 %
• 3-mercaptopropanoic acid (MPA)	Aldrich, 99 %
• 11-mercapto-1-undecanol (MUD)	Aldrich, 99 %
• N-(2-Mercaptopropionyl) glycine (TP)	Aldrich, 99 %
• 1,8-octanedithiol (NT)	Nanothinks ^{TM}THIO8, Sigma, 5 mM (97 %) in 99.9 % v EtOH solution
• Gold suspension, 5 nm ~ 0.01 % $HAuCl_4$	Sigma

4.2.2 EXPERIMENTAL SET-UP

The synthesis of gold nanoparticles (**MR3**) is carried out by the set-up schematized in figure 4.9 A. The automated and continuous flow system consists of four syringe pumps with their correspondent 1-10 mL syringes connected to the microreactor with PTFE tubes. Again, the pumps are controlled by a computer and allow dispensing of reagents in a rapid, simple and controlled way. In this approach, the automatic filling of syringes is feasible with computer-controlled three-way valves, connected between the syringes and the microreactor. This allows the continuous loading of reagents. In this case, PTFE tubes are connected to the ceramic device by means of a home-made user-friendly connection piece (figure 4.9 B) with conical PTFE connectors. This avoids the possibility of collateral reactions with metals due to the use of reducing agents by providing a simple connection of tubes. Finally, o-rings are used to seal the connection system.

A simplification of this diagram is used when preparing gold suspensions only stabilized by electrostatic interactions (**MR2**), since no syringe, pump and valve for a stabilizer are required.

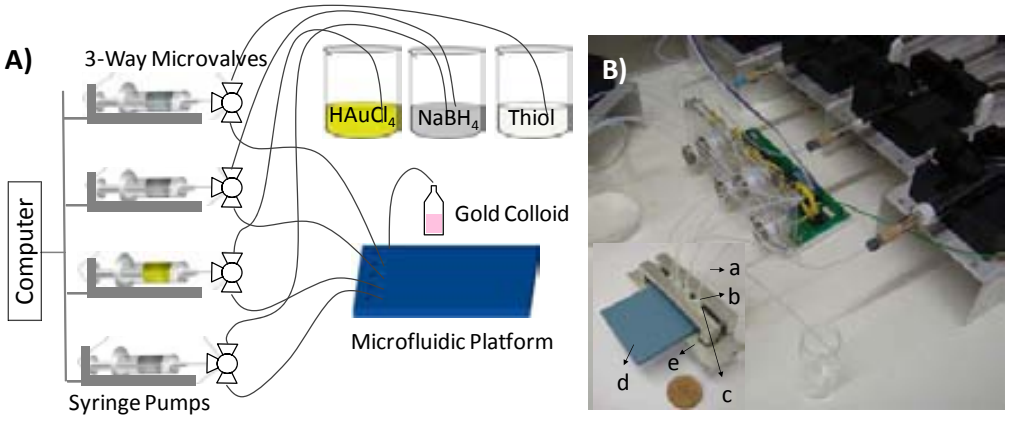

Figure 4.9:
A) Diagram of the entire flow microsystem setup for the synthesis of gold nanoparticles. B) Image from the whole set-up, where it can be observed the simple user-friendly connection system, designed to attach the microfluidic device with the PTFE tubes. a: PTFE tubes, b: PTFE cones, c: o-rings, d: ceramic microreactor, e: connection piece.

4.2.3 OPTIMIZATION OF THE MICROFLUIDIC PLATFORM

As for the synthesis of silver nanoparticles, the formation process of gold colloid and its chemical reaction should to be taken into account when designing the microfluidic platform. Since the procedure used for obtaining gold nanoparticles is also based in a chemical reduction, the first prototypes tested were those previously constructed for the optimization of the silver colloid microreactor, essentially based on simple channels with different configurations for the entrance of reagents (**MR2A-C**) (Figure 4.10, Table 4.7). Same results as for silver nanoparticles were observed, due to in most of cases aggregation was obtained outside the microreactor. However, the use of hydrodynamic focusing by the construction of microreactors with three inlet channels (one for the metal and two for the reducing agent) considerably improved the synthetic procedure, making feasible obtaining the first gold colloids. Nevertheless, the particles were extremely poor in homogeneity and stability.

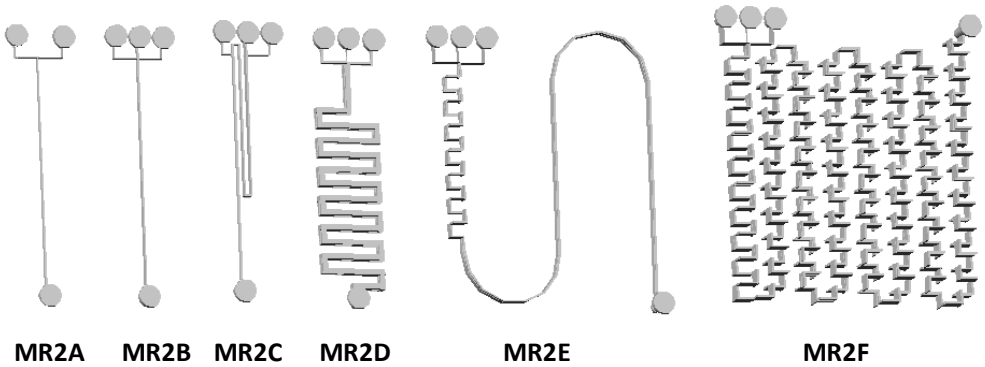

Figure 4.10:
Scheme of some of the different microfluidic platforms designed, constructed and tested for the synthesis of gold NPs.

IDENTIFICATION NUMBER	FLOW SYSTEM CHARACTERISTICS	DESIGN			
		N inlets	Injection configuration	Mixer configuration	Volume (µL)
MR2A	Simple Injection	2 inlets	T	-	3
MR2B		3 inlets		-	7
MR2C	Simple Injection + Residence Zone			-	18
MR2D	Passive Mixer			2D	70
MR2E	Passive Mixer + Residence Zone			3D	28
MR2F	Enlarged Passive Mixer				96
MR2G	Passive Mixer				24

Table 4.7: Summary of the different parameters of the microfluidic platforms studied for the synthesis of gold NPs.

On the other hand, the use of bi-dimensional micromixers (**MR2D**) did not confer any relevant betterment to the system, since more stable particles were obtained but with a wide size distribution.

However, these previous experiments let us to check the faster kinetic of the gold nanoparticle synthesis when compared to the silver one. Thus, it probably was necessary incrementing the grade of mixture inside the microfluidic channels. This can be achieved by the introduction of passive three-dimensional micromixers, which can provide chaotic advection.[3-4] Therefore, a microfluidic platform consisting of three inlets for the entrance of reagents followed by a three-dimensional serpentine mixer and a simple channel for the stabilization of the particles was design and constructed to test its feasibility in the synthesis of Au NPs (**MR2E**). Nevertheless, unstable particles with no homogeneity were synthesized with this microsystem, as it can be observed in Figure 4.11.

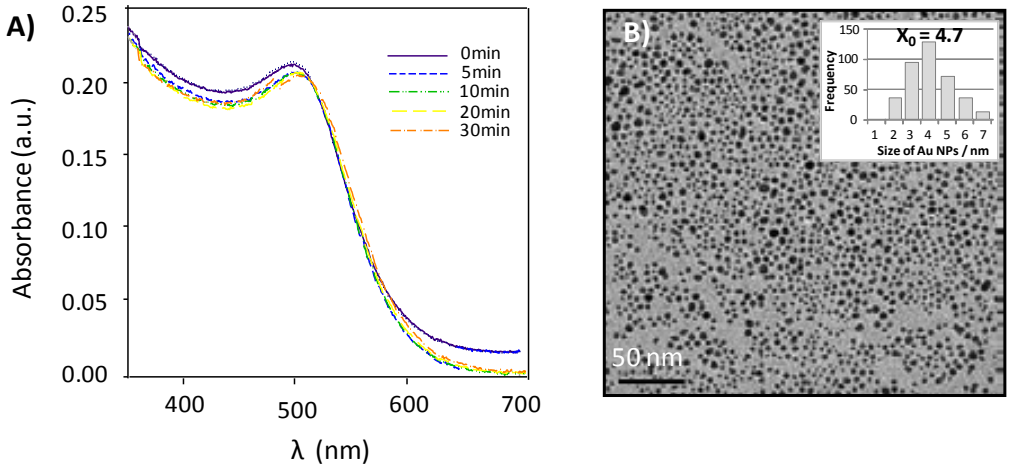

Figure 4.11: UV-Vis spectra and TEM images from Au NPs synthesized with **MR1D** ceramic microfluidic systems. The hydrodynamic and chemical parameters consisted on 3 mM $NaBH_4$ solution pumped at 2 µL s^{-1} syringe flow rate, and 2.5 mM $HAuCl_4$ at 1µL s^{-1}.

[3] Liu, R. H.; Stremler, M.A.; Sharp, K.V.; Olsen, M.G.; Santiago, J.G.; Adrian, R J.; Aref, H.; Beebe, D. J.; *J. Microelectromech. Syst.,* **2000**, *9* ,190.

[4] Vijayendran, R.A.; Motsegood, K.M.; Beebe, D.J.; Leckband, D.E.; *Langmuir*, **2003**, *19,* 1824.

In order to increment the time that reagents spend inside the microsystem, an enlarged microfluidic platform was fabricated, composed basically of a three-dimensional micromixer (**MR2F**). The obstruction of the microchannels was observed most of times when performing the synthesis. However, the synthesis that did no generate the clogging of the fluidic structures produced much more uniform and stable particles. Therefore, a shorter microsystem based on the before was constructed (**MR2G**). Its use could finally provide a uniform and stable gold colloid, due to this device allows the enough grade of mixture while also the time to totally react reagents. A scheme of the device is shown in figure 4.12, where the different components of the platform have been depicted. The total volume of the device is of 24 µL. Gold nanoparticles obtained with this optimized microreactor using the optimized chemical and hydrodynamic parameters are shown in figure 4. 13.

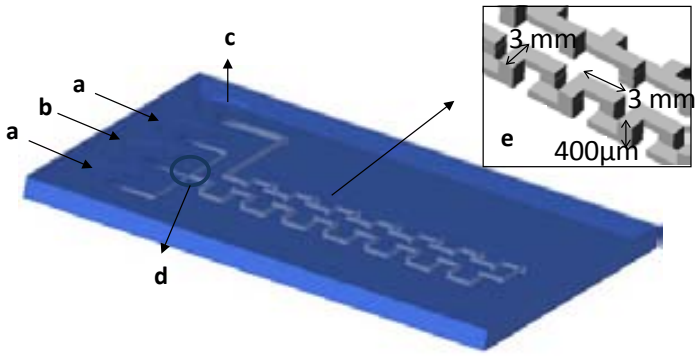

Figure 4.12: Scheme of the **MR2G** microfluidic platform for gold nanoparticles synthesis, where a: reducing agent inlets, b: gold precursor inlet, c: outlet, d: confluence point (hydrodynamic focusing), e: three-dimensional micromixer consisting of a series of L-shaped segments in perpendicular planes.

4.2.4 OP TIMIZATION OF TH E CHEMICAL A ND HYDRODYNAMIC PARAMETERS

The chemical and hydrodynamic parameters are also important factors which determine the quantity and quality (stability and size distribution) of the obtained NPs. As in the case of silver nanoparticles, different solutions of sodium borohydride and gold (III) chloride hydrate were tested in the microfluidic platforms, covering a wide concentrations range (0.05 M and 0.01 mM). As before, the use of the more concentrate solutions produced precipitated particles or the clogging of the microchannels, while no formation of colloid was observed when employing the more diluted. The use of milimolar concentrations for both, the reducing agent and the metal precursor, made possible obtaining pale red solutions, which is related to the SPR band of gold nanoparticles.

Concerning the hydrodynamic parameters, although some continuous flow rates were tested, the use of a dosage protocol was preferred due to the good results observed for the synthesis of silver nanoparticles. The dosage of small volumes of gold (III) solution in certain time intervals, while borohydride was continuously flowing, favours the formation of gold seeds due to the creation of

supersaturated zones in each dosed volume and makes feasible a stricter control of the concentration fluctuations. Moreover, an additional mixing is generated by the use of different flow rates for the borohydride solution channels in relation with the gold (III) solution channel, which improves the reaction solution mixture. The dispensing protocol which generated the more uniform, stable and reproducible particles consists of the continuous pumping of a 1.5 mM $NaBH_4$ solution at a 1 µl s^{-1} flow rate, and a dosage of 0.5 µl of a 1 mM $HAuCl_4$ solution sequentially dispensed every 2 s at a 2.5 µl s^{-1} flow rate. The molar relationship of the $HAuCl_4$ and $NaBH_4$ solutions is 1:10, the pH of the final solution is 9.8, and the total residence time of the gold colloid inside the microfluidic device is of approximately 9 s.

Figure 4.13 A shows the complete characterization of the colloid. The SPR band was centred at 512 nm and no shifts were observed over time, demonstrating the stability of the synthesized particles. However, the band is located at lower wavelengths than expected (520 nm). This effect can be explained for the high electron density of the colloid probably due to the excess of borohydride of the colloid, since the surface plasmon modes on small metal particles are sensitive to various perturbations, including electron charging.[5]

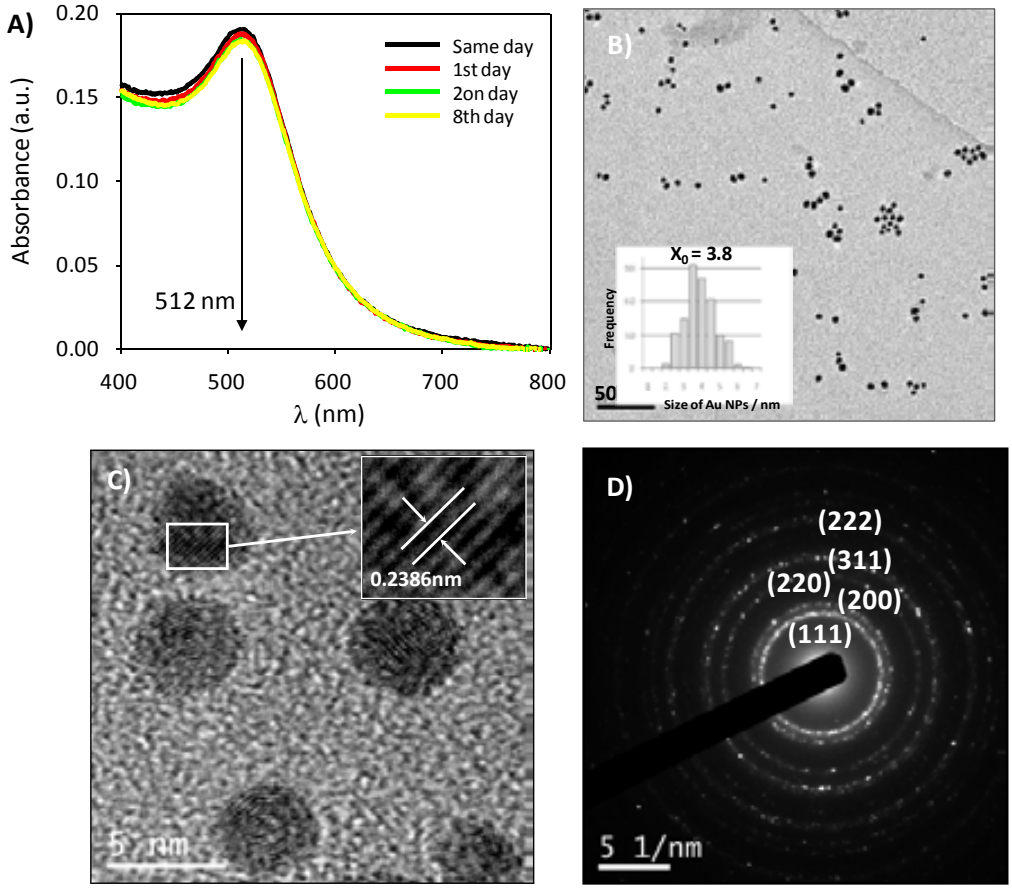

Figure 4.13: Characterization of the Au NPs synthesized in the **MR2G** ceramic microreactor at the optimized conditions. **A)** UV-Vis spectra recorded with time. **B)** TEM image and its correspondent histogram. **C)** HRTEM image with its lattice fringes. **D)** Electron diffraction (SAED) pattern of the selected area. **E)** DLS spectrum. **F)** ζ potential measure.

[5] Mulvaney, P.; Perez-Juste, J.; Giersig, M.; Liz-Marzan, L.M.; Pecharroman, C.; *Plasmonics*, **2006**, *1*, 61.

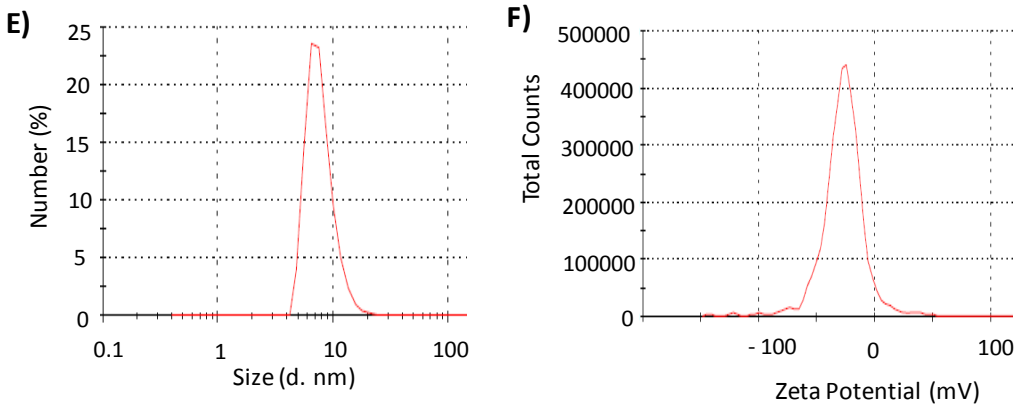

The shape and dimensions of the core of the particles measured by TEM are also shown (Figure 4.13 B), where it can be observed spherical particles of 3.8 ± 0.6 nm. HRTEM images displayed 0.239 nm lattice fringes, which reveals a preferential fcc growth of Au NPs on the (111) plane in agreement with the 0.2355 nm d-spacing of bulk Au (JCPDS card No: 04-0784) (Figure 4.13 C). The electron diffraction (SAED) pattern of the selected area showes single crystalline particles, the patterns of which index according to (111), (200), (220), (311) and (222) reflections of the fcc structure of Au (Figure 4.13 D). TEM images from commercial nanoparticles are also shown in figure 4.14 for comparative purposes. Besides, DLS and ζ potential measurements show the hydrodynamic diameter and stability of the colloid, revealing particles of 7.8 ± 2.2 nm and -30.1 ± 14.4 mV (Figure 4.13 E-F).

The concentration of the solution was calculated by two different ways, one experimental and other theoretical. Firstly, by the interpolation of the colloid absorbance in a calibration curve done with commercial gold colloid of a 5 nm mean size (Aldrich).[6] Secondly, by following the next expression: $C = N_T/(N \cdot V \cdot N_A)$, where C is the final concentration of the colloid, N_T is the number of gold atoms from $HAuCl_4$, N the mean number of gold atoms in a nanoparticle (calculated as $N = 4\Pi(d/2)3/V$, where d is the nanoparticle diameter and V the volume of a gold atom), V the total volume of solution obtained, and N_A the Avogadro constant.[7] Both expressions provided a colloid concentration of 7.9×10^{-8} M (4×10^{-3} % $HAuCl_4$) and an extinction coefficient of 2.3×10^6 M^{-1} cm^{-1}.

[6] Liu, X.; Atwater, M.; Wang, J.; Huo, Q.; *Colloids Surf. B*, **2007,** *58.* 3.
[7] Maye, M.M. Han, L.; Kariuki, N.N.; Ly, N.K.; Chan, W.B.; Luo, J.; Zhong, C. J.; *Anal. Chim. Acta*, **2003,** *469*, 17.

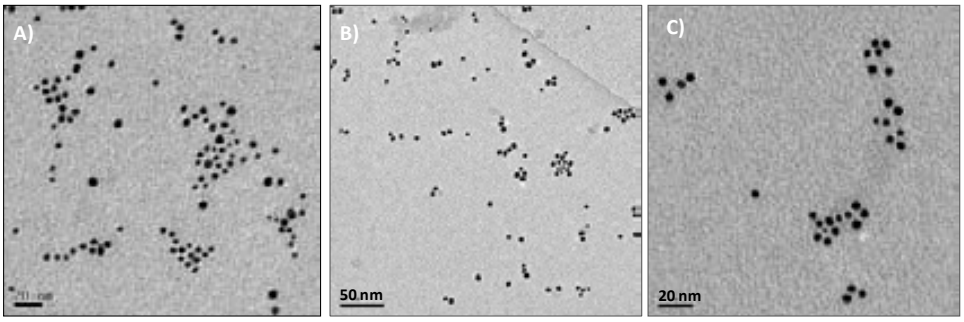

Figure 4.14: TEM images from the synthesized nanoparticles (**A** and **B**) and from the commercial (**C**).

4.2.5 STABILIZING AGENTS (MR3)

The use of stabilizing or modifying agents usually lengthens the lifetime of colloids as well as they extend their range of applications, since most of these stabilizers incorporate functional groups.[8] In this way, some essential active groups such as -OH, -COOH or -SH can also be attached to NPs for analytical, biological and biotechnological applications. Alkanethiols are commonly used for this purpose, which usually forms a monolayer coating the nanoparticle, such as in the two-phase Brust-Schiffrin method.[9-10] In fact, most of the synthetic approaches for the synthesis of gold nanoparticles with alkanethiols as stabilizer take as reference this methodology. It consists on the first mixture of hydrogen tetrachloroaurate in water with tetraoctylammonium bromide in toluene, followed by the addition of dodecanethiol to form an Au-thiol complex. Then, an aqueous solution of sodium borohydride is added to the mixture to obtain the gold colloid. Thus, first constructed devices to carry out this synthesis were based on this approach. These devices incorporated two initial inlets, where tetrachloroauric acid and alkanethiol were added, followed by a micromixer to achieve their mixture; then, two other inlet channels for sodium borohydride met the before mix, which generated the reduction of the gold precursor. Again, different chemical and hydrodynamic parameters of the microsystems were tested. However, the characterization of the diverse gold colloids obtained with these devices revealed agglomerated particles or with a really wide size distribution. In these devices, although the configuration of the microfluidic platform permitted the use of hydrodynamic focusing, since two inlets for the reducing agent were incorporated at both sides of the main channel, the employment of dosage volumes was not feasible due to gold precursor was already flowing in the microchannel. As a result, unstable particles were formed in all the syntheses performed.

[8] López-Cartes, C.; Rojas, T.C.; Litrán, R.; Martínez-Martínez, D.; de la Fuente, J.M.; Penedés, S.; Fernández, A.; *J. Phys. Chem. B*, **2005**, *109,* 8761.
[9] Brust, M.; Walker, M.; Bethell, D.; Schiffrin, D.J.; Whyman, R.J.; *Chem. Soc. Chem. Commun.,* **1994**, *801.*
[10] Liz-Marzán, L.M.; *Chem. Commun.,* **2013,** *49*, 16--18

Therefore, an inverse procedure was tried, where the synthesis of the colloid is firstly carried out and its stabilization is obtained in a second step. For this purpose, the previous microfluidic platform design for the synthesis of the colloid (**MR2G**) was modified by introducing an auxiliary channel for the addition of the alkanethiol, and by increasing the length of the microreactor to favor the mixture between the nanoparticles and the stabilizer, obtaining the **MR3** (Figure 4.15). This microreactor has total reaction volume of 45 µL, 21 µL for the Au NPs synthesis and 24 µL for the alkanethiol mixing.

As for the previous procedures, it is necessary to optimize the chemical and hydrodynamic parameters of the synthesis, mainly those related to the stabilizer. Different alkanethiols were employed in order to test their stability and to have a set of Au NPs with different surface modification. In this way, one could select the alkanethiol with its optimized chemical and hydrodynamic parameters depending on the final application.

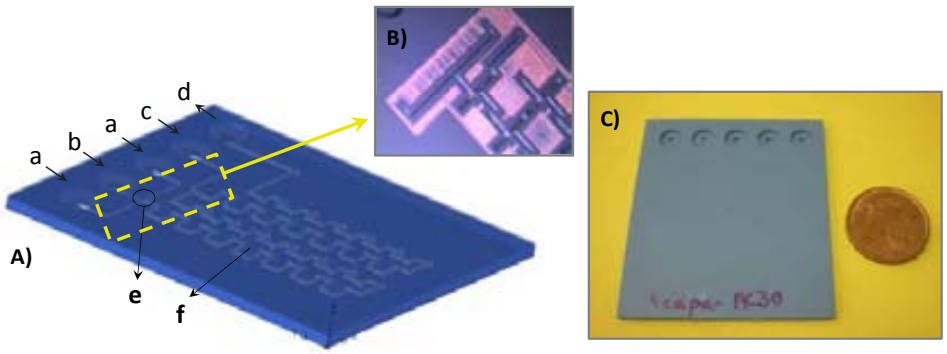

Figure 4.15: Microfluidic platform for Au NPs synthesis with alkanethiols (**MR3**). **A)** Schematic representation, where a: reducing agent inlets, b: gold precursor inlet, c: alkanethiol inlet, d: outlet, e: confluence point (hydrodynamic focusing), f: three-dimensional micromixer. **B)** Magnification image of the channel inlets and the L-shaped segments of the mixer. **C)** Image of the microreactor.

The first stabilizer used was 11-mercaptoundecanoic acid (MUA). It can offer great possibilities derived of attaching its carboxylic group to, for instance, biological material, and it confers a great stability to the particles due to its ionizable group. Thus, its chemical and hydrodynamic variables were optimized. As Figure 4.16A shows, as the MUA flow rate is increased, the Au SPR band is displaced to larger wavelengths. This effect can be explained by the number of molecules which surrounds the particle. As the amount of MUA in the reaction mixture is increased, more molecules of modifier are attached to the NPs giving larger SPR bands. A continuous pumping of a 1.5 mM $NaBH_4$ solution at a 1 µl s^{-1} flow rate, a dosage of 0.7 µL of a 1 mM $HAuCl_4$ solution sequentially dispensed every 2 s at a 2.5 µl s^{-1} flow rate, and a 1 mM solution of alkanethiol flowing at 1 µl s^{-1} were the optimal conditions for the synthesis of MUA stabilized Au NPs, which entail a residence time of approximately 13 s.

The characterization of the synthesized nanoparticles revealed an invariable SPR band located at 518 nm (figure 4.16B), which entails a 6 nm-shift when compared with the colloid only stabilized by electrostatic repulsions. The analysis of the TEM images showed well-defined nanoparticles with a mean size of 2.7 ± 0.5 nm,

while HRTEM results made feasible the visualization of their lattice fringes, which were again in concordance with the d-spacing bulk Au (Figure 4.16C and D). On the other hand, ζ potential and DLS analyses confirmed the presence of stable particles (-44.2 ± 7.61 mV) with a hydrodynamic diameter of 10.23 ± 2.80 nm (Figure 4.16E and F).

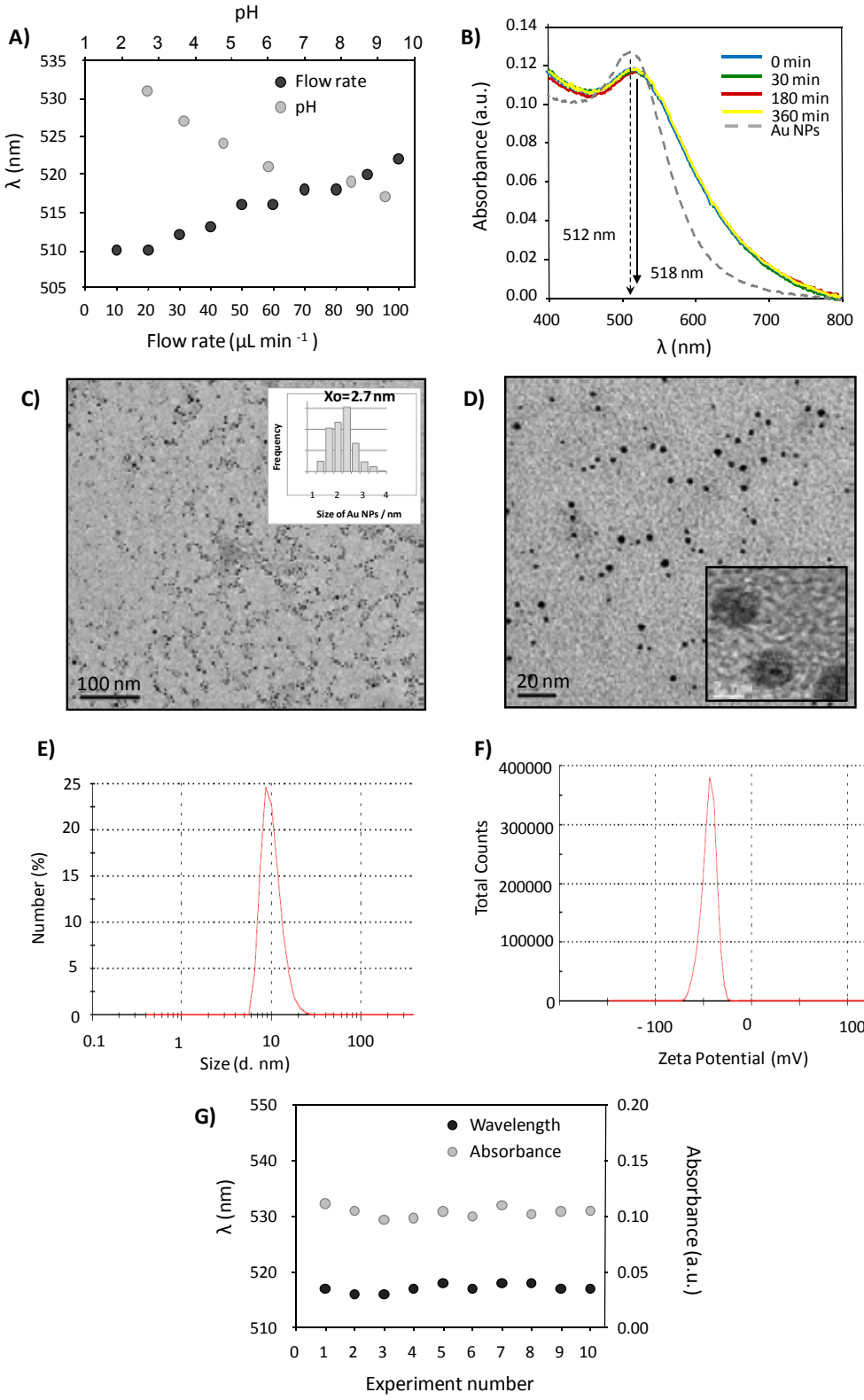

Figure 4.16: Results from the MUA stabilized Au NPs, obtained in the **MR3** microreactor. **A)** Study of the effect of MUA flow rate and pH on the SPR band position. **B)** UV-Vis spectra recorded with time and its comparison with Au NPs. **C)** and **D)** TEM images and its correspondent histogram. **E)** DLS spectrum. **F)** ζ potential measure. **G)** Characterization of the synthesis repeatability following the position and the intensity of the SPR band.

The colloid was also characterized by elemental analysis, since this technique provides quantitative information about the composition of the sample, being feasible to calculate the number of alkanethiolate chains in a nanoparticle. Thus, one can have quantitative information of the specific molecules present in the colloid when they have been bind to the nanoparticles by coupling reactions through the modifier, which is extremely important in analytical applications. The relationship between elemental analysis and core size of the MUA stabilized gold colloid gave a 20.86 % (12.64 % C and 4.47 % H from CHNS data) of organic material, which means that the nanoparticle surface has 145 alkanethiolate chains. This result is in concordance with other related in the literature.[11]

The repeatability of the synthesis was also studied by using the SPR band intensity and shift as indicator parameters, since obtaining nanoparticles with the same properties from the different synthesis performed is one of the purposes of this work. Thus, ten different synthesis were carried out at the same conditions showing a band located at 517 ± 0.7 nm and an absorbance of 0.104 ± 0.005 a.u., which demonstrates the robustness of the proposed flow system (figure 4.16G).

Once tested the feasibility of the microreactor to obtain Au NPs stabilized with MUA; the chemical and hydrodynamic parameters of other alkanethiols were studied. In concrete, 3-mercaptopropanoic acid (MPA), 11-mercapto-1-undecanol (MUD), N-(2-Mercaptopropionyl) glycine (TP) and 1,8-octanedithiol (NT) were used for this purpose, since these molecules incorporates different moieties which can be useful in the future. Since similar behaviour was observed for all of them, only the optimized conditions for their synthesis and the characterization of each colloid (done at pH values of approximately 9.5) are shown in the following figures.

Figure 4.17 shows the results obtained for Au NPs stabilized with MPA. A stable SPR band located at 515 nm and nanoparticles with a mean size of 3.0 ± 0.9 nm (figure 4.17B-D) can be observed from the UV-Vis spectra recorded and the TEM measurements performed at the conditions described the figure 4.17A. Besides, DLS and ζ potential confirm the formation of a stable colloid (-36.1 ± 9.6 mV) with a hydrodynamic diameter of 8.15 ± 1.71 nm (figure 4.17E-F). The analysis of the elemental analysis results gave a 10.27 % of organic material (3.51 % C and 5.23 % H from CHNS data), which corresponds to 177 alkanethiolate chains. The colloid concentration and the extinction coefficient attained for this colloid are of 9.9×10^{-8} M and an of 1.5×10^{6} M^{-1} cm^{-1}, respectively.

[11] Hostetler, M.J.; Wingate, J.E.; Zhong, C.-J.; Harris, J.E.; Vachet, R.W.; Clark, M.R.; Londono, J.D.; Green, S.J.; Stokes, J.J.; Wignall, G.D.; Glish, G.L.; Porter, M.D.; Evans, N.D.; Murray, R.W.; *Langmuir*, **1998**, *14*, 17.

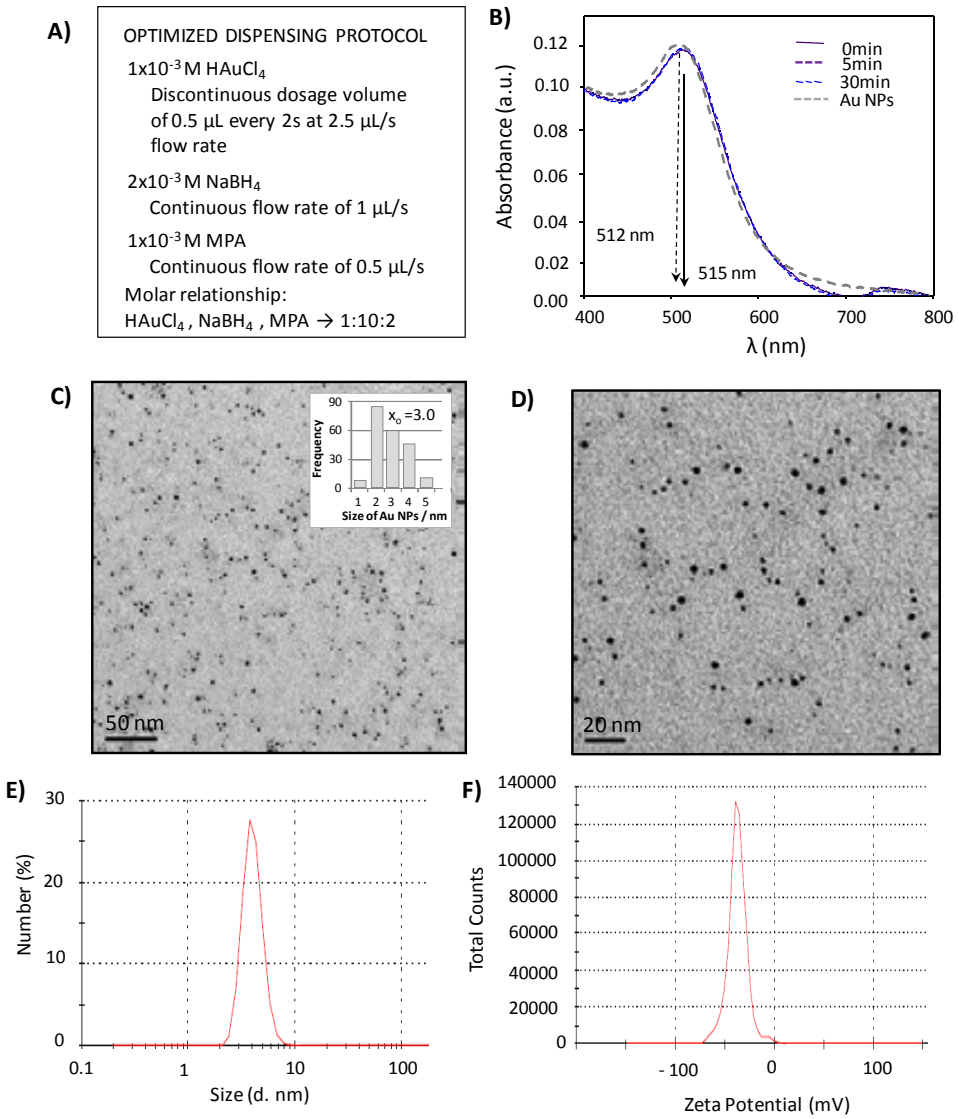

Figure 4.17: Results from the MPA stabilized Au NPs, obtained in the **MR3** microreactor. **A)** Optimized chemical and hydrodynamic parameters**.** **B)** UV-Vis spectra recorded with time and its comparison with Au NPs. **C)** and **D)** TEM images and its correspondent histogram. **E)** DLS spectrum. **F)** ζ potential measure.

Results concerning MUD alkanethiol are shown in figure 4.18, which has a concentration of 4.1×10^{-8} M and an extinction coefficient of 2.9×10^{6} M^{-1} cm^{-1}. The colloid shows uniform and stable particles with an absorption band centred at 529 nm, an average core size of 3.8 ±0.8nm, a hydrodynamic diameter of 15.82 ± 5.10 nm and a ζ potential of -36.4 ± 10.1 mV at the optimized conditions shown.

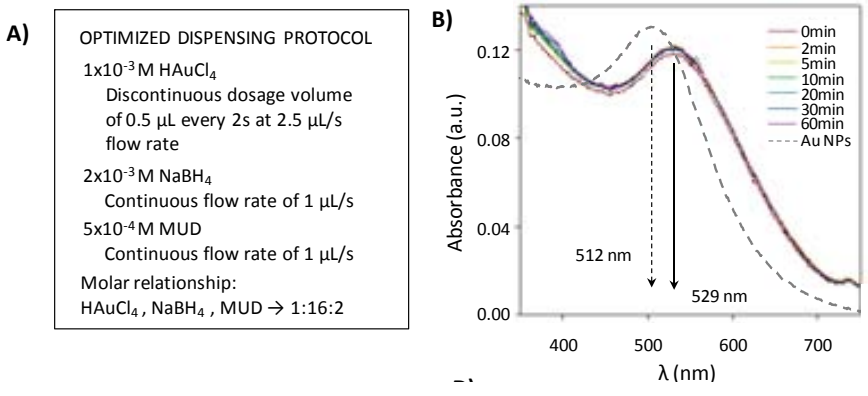

Figure 4.18: Results from the MUD stabilized Au NPs, obtained in the **MR3** microreactor. **A)** Optimized chemical and hydrodynamic parameters**.** **B)** UV-Vis spectra recorded with time and its comparison with Au NPs.

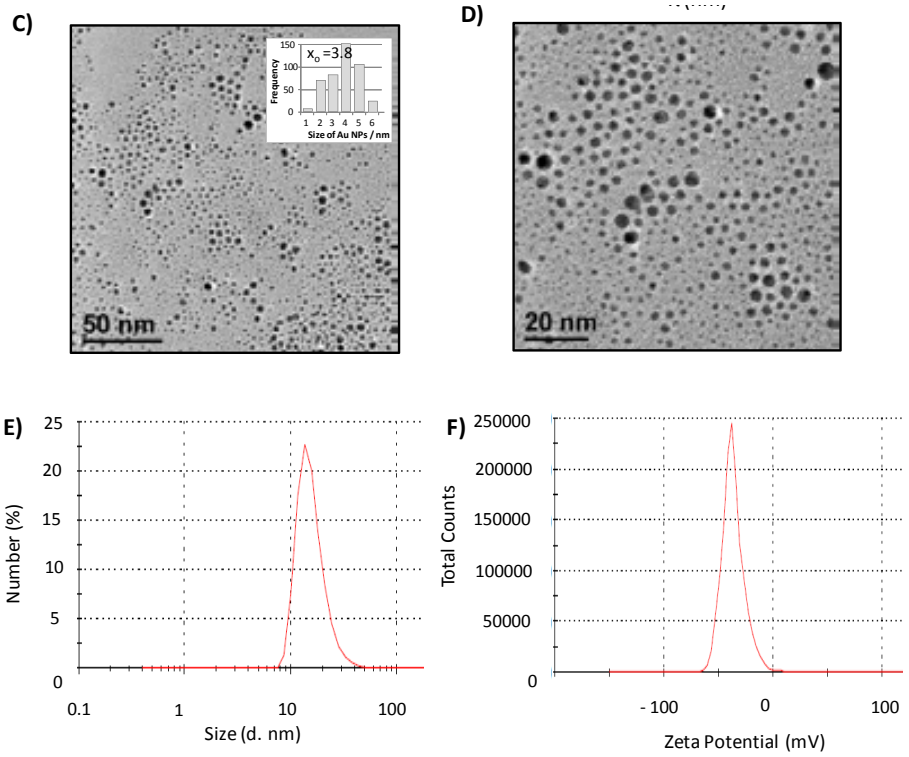

Figure 4.18: Results from the MUD stabilized Au NPs, obtained in the **MR3** microreactor. **C)** and **D)** TEM images and its correspondent histogram. **E)** DLS spectrum. **F)** ζ potential measure.

Figure 4.19 shows the characterization of Au NPs stabilized with TP. This time, the SPR band remained stable at 518 nm, a mean value of 3.4 ± 0.4 nm were attained for the diameter core of the particles by TEM measurements while a 10.1 ± 3.09 nm of hydrodynamic diameter was obtained from DLS measurements. The ζ potential showed nanoparticles of -36.1 ± 11.9 mV. A colloid concentration of 9.0 × 10^{-8} M and an extinction coefficient of 2.8 × 10^{6} M^{-1} cm^{-1} were attained.

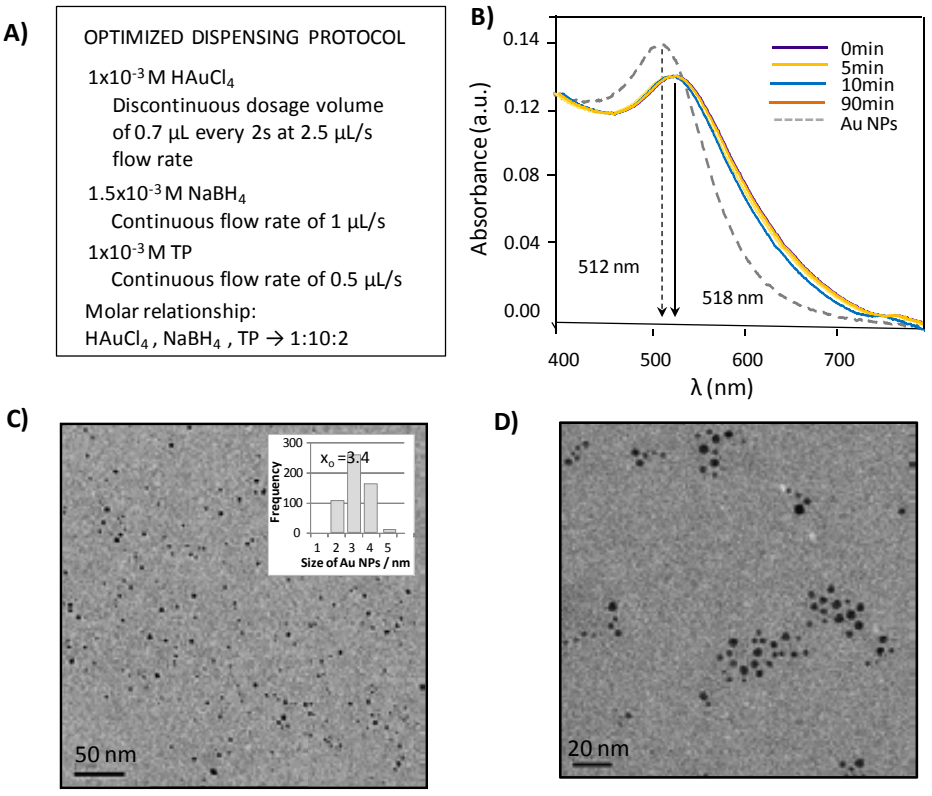

Figure 4.19: Results from the TP stabilized Au NPs, obtained in the **MR3** microreactor. **A)** Optimized chemical and hydrodynamic parameters**.** **B)** UV-Vis spectra recorded with time and its comparison with Au NPs. **C)** and **D)** TEM images and its correspondent histogram. **E)** DLS spectrum. **F)** ζ potential measure.

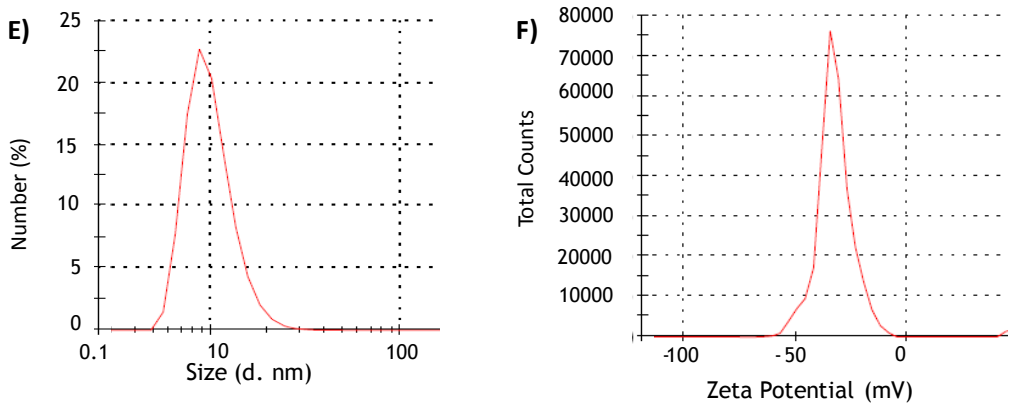

On the other hand, results obtained by the use of the NT stabilizer are summed up in figure 4.20. The use of this dithiol could be very useful for (bio)analytical applications, since it can be attached, for instance, to other modified gold nanoparticles. As it can be observed, the colloid shows stable particles with an absorption band located at 522 nm. The concentration of this colloid is 3.4×10^{-8} M and its extinction coefficient is 3.3×10^{6} M^{-1} cm^{-1}. Besides, TEM characterization revealed nanoparticles of 3.7 ± 0.6 nm, which in most of cases formed some type of net, as figures 4.20C-D show. In fact, the shape and size of the net changed depending on the hydrodynamic parameters or the concentration of NT used. This is probably due to the attachment of the thiol groups to two different gold nanoparticles. An hydrodynamic diameter of 12.80 ± 3.86 nm and a ζ potential of -43.3 ± 8.2 mV were obtained from the characterization done by the zeta sizer nano ZS.

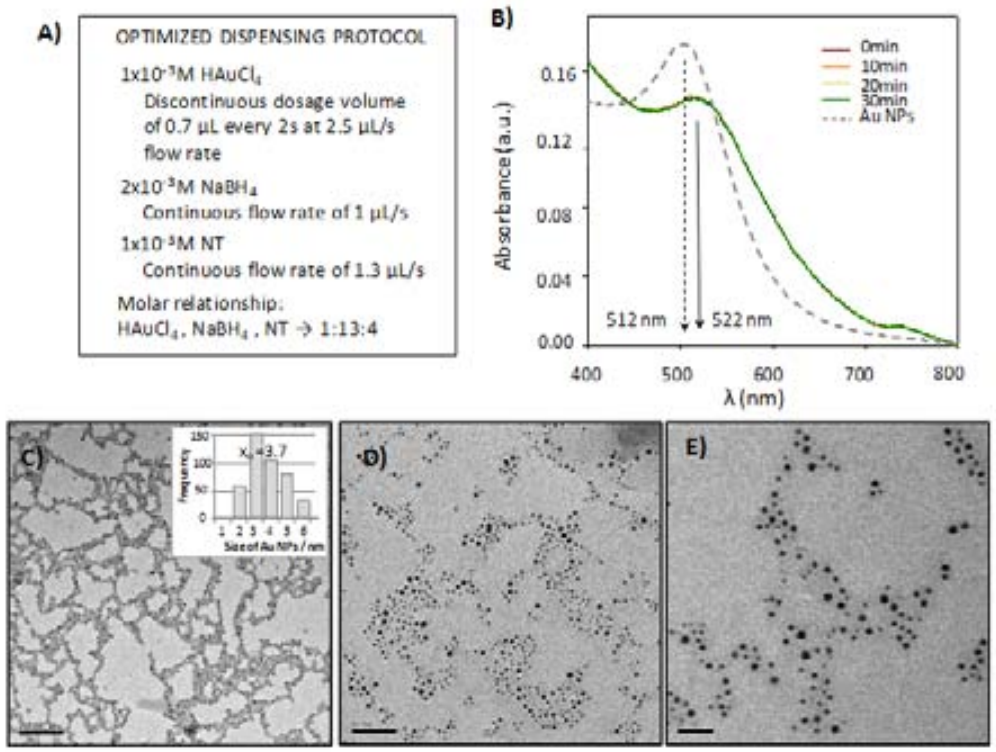

Figure 4.20: Results from the NT stabilized Au NPs, obtained in the **MR3** microreactor. **A)** Optimized chemical and hydrodynamic parameters**.** **B)** UV-Vis spectra recorded with time and its comparison with Au NPs. **C)**, **D)** and **E)** TEM images and its correspondent histogram. **F)** DLS spectrum. **G)** ζ potential measure.

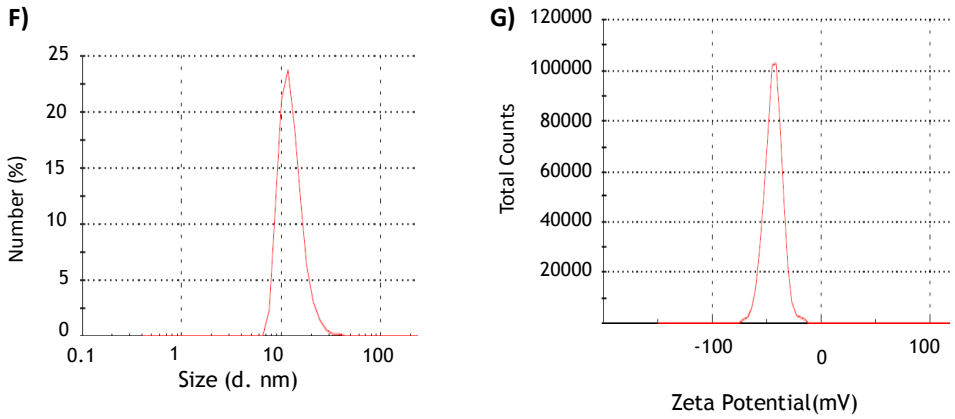

4.2.6 MONITORIZATION

The last challenge in order to achieve an automated and controlled system for the synthesis of reproducible and stable gold nanoparticles is the integration of an optical monitoring system. In this way, any possible variation of the synthetic procedure owing to, for instance, channel obstruction or incorrect dosage of the reagents can be immediately detected and solved.

The miniaturized optical system has been developed by the "*Grupo de Tecnologías Fotónicas*" (GTF) of the University of Zaragoza, and it is based on cheap optical and electronic components, which minimizes the cost of the system. It consists on a PCB Printed Circuit Board), where it has been mounted a Light Emitting Diode (LED) and a photodetector (PIN Hamamatsu S1337-66BR large active area photodiode), soldered in front of the LED. The PCB has two grooves to simplify the alignment of the optical system with the ceramic microreactor. The LED (B5B-433-B505 Roithner, Vienna, Austria) has its emission peak at 505 nm, which matches with the SPR band of the particles. The emission source is modulated by a Data Acquisition Card (DAQ, NI USB-6211 from National Instruments), which generates the modulating signal for the LED and captures the detected signal to transfer it to a control PC, where it is processed using a lock-in amplification to increase the signal to noise ratio and the dynamic range of the measurement. This amplification also allows the use of the detection system in ambient light without interferences. The whole system, DAQ and board, are powered by the computer through an USB connector, simplifying the system. An image of the system is shown in figure 4.21.

It was necessary to modify the microreactor (**MR3**) to incorporate an optical window, embedded at the end of the three-dimensional channel. Thus, the channel carrying the synthesized nanoparticles was enlarged and brought to the surface of the microfluidic platform, where a 2 mm-diameter round hollow was drilled in all the layers to define an optical flow cell. Two transparent glass layers were attached in the top and bottom of the ceramic layers by means of epoxy, ensuring the sealing of the detection chamber. An image of the optical window is

also shown in figure 4.21. The device was aligned with the LED and photodetector of the PCB.

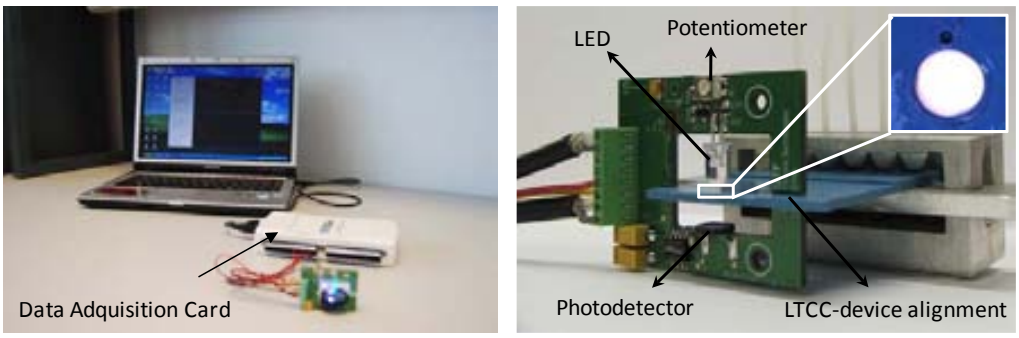

Figure 4.21: Images of the miniaturized optical system for monitoring the synthesis of gold nanoparticles. An image of the optical window is shown in the inner box of the right image.

In order to test the feasibility of the miniaturized optical system for absorbance measurements of nanoparticles, the absorption intensity of the SPR band from different concentrations of gold nanoparticles was registered. The experiment consisted on making flow Au NPs and water through two inlet channels, which were joined in a T shape confluence point. The following three-dimensional micromixer enabled the mixture of both liquids, and the diluted colloid advanced inside the microfluidic platform to the optical chamber, where its absorbance intensity was registered. Seven concentration of the colloid were used, which were obtained by employing different flow rates of water (30 - 150 µL min $^{-1}$) while the gold nanoparticles were pumped at a fixed one (120 µL min $^{-1}$). Figure 4.22A shows the signal recording from the different gold colloid dilutions. Its maximum absorption corresponds to the non-diluted gold nanoparticles, while lower values of absorbance intensity were obtained when increasing the flow rate of water, since a higher dilution of the colloid is obtained. As it can be observed, sharp and well-defined peaks were obtained. A linear response was attained from the representation of the absorbance intensity *versus* the dilution of the colloid (Figure 4.22B), which indicates the perfect function of the system.

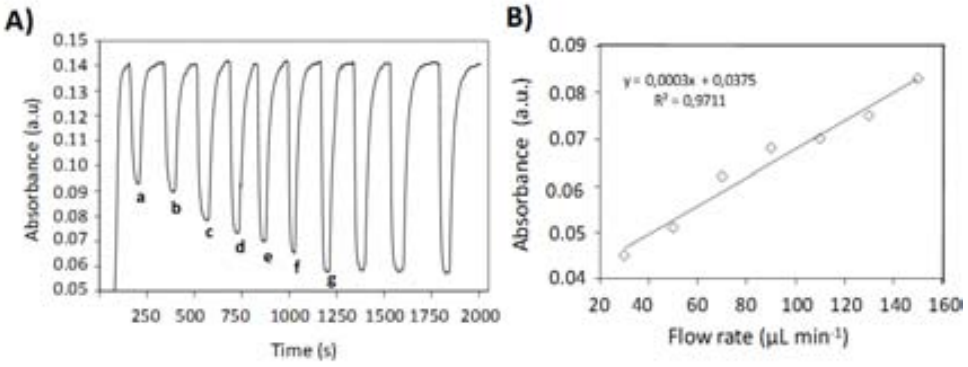

Figure 4.22: Signal recording (**A**) and obtained calibration curve (**B**) for the dilution of gold nanoparticles at different flow rates of water; a: 30 µL min $^{-1}$ b: 50 µL min $^{-1}$, c: 70 µL min $^{-1}$, d: 90 µL min $^{-1}$, e: 110 µL min $^{-1}$,f:130 µL min $^{-1}$, g: 150 µL min $^{-1}$.

Then, the absorption of gold nanoparticles was registered while taking place their synthesis, where the dosage volume of gold was intentionally modified on-line. As shown in figure 4.23, the four different employed volumes, corresponding to

0.7, 0.5, 0.3 and 0.1 µL, can be perfectly distinguished. The maximum absorption value corresponds to the higher dispensed volume, and the minimal value with the lower dosage.

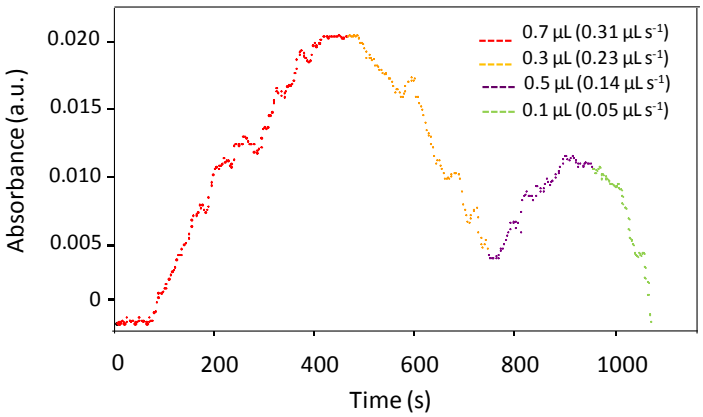

Figure 4.23: Signal recording of a gold nanoparticles synthesis, where different dosages have been employed. Experimental conditions: 1.5 mM $NaBH_4$, 1 µL s^{-1} syringe flow rate; 1mM MUA, 1µL s^{-1} syringe flow rate. 1mM $HAuCl_4$, at variable syringe flow rates.

Therefore, a change in the optical system while carrying out a synthesis of gold colloid implies the malfunction of the synthetic procedure, making it feasible to take appropriate actions to solve any problem in the shortest time.

4.2.7 CONCLUSIONS

Gold nanoparticles can be successfully synthesized using ceramic microreactors. Firstly, a ceramic microfluidic platform, which integrates a three-dimensional micromixer and that makes use of hydrodynamic focusing, enables synthesizing uniform and monodispersed nanoparticles stabilized by the electrostatic repulsions by employing a well-defined dispensing protocol. Since the whole process is automated, a proper control of the different synthetic variables is achieved, obtaining reproducible colloids in the diverse syntheses performed.

Secondly, the addition of an auxiliary channel for alkanethiols (MUA, MPA, MUD, TP or NT) and the enlargement of the main micromixer of the microfluidic platform allows, once the gold colloid is synthesized in the microreactor, obtaining stable and uniform modified nanoparticles in all cases using the optimized chemical and hydrodynamic parameters. These gold colloids can be employed for a wide range of analytical applications due to the different moieties that these molecules incorporate. Therefore, one can select the required colloid according to its final application.

Besides, the use of the miniaturized optical system has shown its potential use for monitoring the synthesis of nanoparticles, since it is able to distinguish the absorption of different colloids. The system can be very useful to detect any malfunction of the system, making feasible taking appropriate actions in the shortest time.

MICROREACTORS FOR THE SYNTHESIS OF FLUORESCENT NANOPARTICLES

Contents

Image from Fraunhofer IAP website

Fluorescent nanoparticles are one of the most interesting nanomaterials due to their different emission colours caused by their size-dependent properties. Their unusual properties make them very interesting for their use as luminescent labels in the development of miniaturized analytical systems, since nanocrystals are not limited by the usual photobleaching problems of organic dyes. Thus, the development of microreactors for the reproducible and controlled synthesis of fluorescent nanoparticles is the next challenge of the thesis.

The design and construction of diverse devices for the synthesis of different inorganic nanocrystals and carbon dots will be presented throughout the following chapter, along with the characterization of the obtained colloids. Due to the good performance of ceramic microreactors in the synthesis of metallic nanoparticles, the following devices are also based on the LTCC technology. Moreover, most of the necessary reaction conditions for the preparation of these fluorescent particles are harsher than the before used, which can be borne by this ceramic material.

First microreactors presented are addressed to the synthesis of water soluble CdS (**MR4**) and CdS/ZnS nanocrystals (**MR5**). The aqueous procedure employed can provide lots of advantages, such as the possibility of directly using the nanocrystals synthesized in analytical microsystems, avoiding the frequently required solubilization procedures when using organic synthetic approaches. **MR4** design was based on the previous microreactors employed for the synthesis of metallic NPs. Therefore, it uses a hydrodynamic focusing of reagents and incorporates a passive micromixer for an efficient mixture of reagents. Then, the microreactor was slightly modified by incorporating an auxiliary channel and a simple microchannel, leading to **MR5**. This microreactor takes on the synthesis of core-shell nanocrystals, which usually provides higher quantum yields. Furthermore, the microsystem integrates the reaction monitoring by the adaption of the previous developed miniaturized optical system to the microreactor, where both the absorbance and fluorescence intensities of the nanocrystals formed can be recorded.

The design and construction of microreactors for high temperature synthesis of nanomaterials has also been an objective of this work. Quantum dots obtained with these procedures, which involve the use of organic solvents, usually generates more homogeneous nanocrystals and with higher quantum yields.

Thus, **MR6** is focused on the synthesis of CdSe quantum dots, and integrates both the microfluidics and a thermally controlled platform. The fluidic platform includes the necessary inlets for reagents and a bi-dimensional micromixer, which allows an improved mass transference between reagents. Besides, the thermal platform enables the heating of reagents with a strict temperature control, which is of extreme importance in such syntheses. An exhaustive study of the heating platform is also presented, which ensures the proper working of the system to obtain well-defined nanoparticles in the different synthesis performed.

Then, a simple modification in the microfluidic platform of **MR6** leads to obtain a microreactor for the synthesis of homogeneous carbon dots (**MR7**). Since the formation of this nanostructured material only requires of one reagent, only one inlet and a large microchannel is necessary to generate the carbon colloid. Although these nanoparticles normally show lower quantum yields than the previous, their biocompatibility and low cost synthesis results very attractive for bioanalytical applications.

5.1 MICRORECTOR FOR THE SYNTHESIS OF WATER SOLUBLE CdS AND CdS/ZnS NANOCRYSTALS (MR4, MR5)

The design and construction of the following microreactors are addressed to the synthesis of reproducible, uniform and stable water soluble quantum dots. For this purpose, a simple and direct aqueous synthetic approach consisting on the reaction of cadmium nitrate with sodium sulfide, using tiopronin (TP) as stabilizing agent at room temperature, has been employed (**MR4**).[1-2] Therefore, the procedure does not require the *in situ* formation of some precursor reagents (which can generate gases), such in the synthetic routes that involve the use of NaHTe or NaHSe reagents, formed by the reaction of aluminum or tellurium precursors and H_2SO_4 under an inert atmosphere.[3] The use of tipropinin as stabilizing agent provides stability to the nanocrystals as well as active groups for their subsequent modification, such as when the nanocrystals are used as labels in analysis systems.

Later, an auxiliary channel has been added to the microreactor and its main microchannel has been enlarged in order to synthesize controlled core-shell CdS/ZnS nanocrystals. The coverage of nanoparticles with ZnS allows increasing the quantum yield of the nanocrystals, obtaining comparable or even higher

[1] Spanhel, L.; Haase, M.; Weller, H.; Henglein, A.; *J. Am. Chem. Soc*., **1987**, *109*, 5649.

[2] de la Fuente, J.M.; Fandel, M.; Berry, C.C.; Riehle, M.; Cronin, L.; Aitchison, G.; Curtis, A.S.G.; *ChemBioChem,* **2005,** *6*, 989.

[3] Qi, L.; Colfen, H.; Antonietti, M.; *Nano Lett.,* **2001**, *1(2),* 61.

values than the commonly dyes used. Moreover, it would be possible to directly attach the microreactor to other analytical systems, since both microfluidic platforms (microreactor and analytical device) are related to aqueous medium.
The miniaturized optical detection system previously employed for monitoring the gold nanoparticles synthesis has been improved and adapted to the microreactor to monitor not only the absorbance but also the fluorescence of the colloid. The final objective is therefore obtaining a ceramic microreactor for the easy, controlled and automated synthesis of water soluble CdS/ZnS quantum dots with *in situ* optical characterization.

5.1.1 MATERIALS, REAGENTS AND METHODS

The instruments and equipments listed in table 5.1 are required for the synthesis and characterization of CdS and CdS/ZnS nanocrystals.

Table 5.1: General list of equipments used in the synthesis of CdS and CdS/ZnS nanocrystals.

EQUIPMENT	PROVIDER
• 3 (**MR4**) or 4 (**MR5**) syringes pumps, 540060 TSE systems	TSE systems, Bad Homburg, Germany
• 1 syringe of 1 mL, GASTIGHT 1000 TLL series	Hamilton, Bonaduz, GR, Switzerland
• 1 syringes of 2.5 mL, GASTIGHT 1000 TLL series (only for **MR5**)	Hamilton, Bonaduz, GR, Switzerland
• 2 syringes of 10 mL, GASTIGHT 1000 TLL series	Hamilton, Bonaduz, GR, Switzerland
• Three-way solenoid isolation valves	NResearch incorporates®, Bern, Switzerland
• User-friendly connection system	GSB
• Conical PTFE connectors (Cones 1.6 mm)	Omnifit, Cambridge, UK
• Tygon tube (i.d. 1.2 mm)	Ismatec, Zurich, Switzerland
• PTFE tubes (i.d. 0.8 mm)	Techny Fluor, Barcelona, Spain
• 4 mL centrifugal tubes, CENTRIPLUS YM30, MICROCON, MWCO 30000	Millipore™, Centriplus™ Centrifugal Concentrators, Billerica, USA
• Angular centrifuge Cencom II	J. P. Selecta, S.A., Abrera, Spain
• pH meter GL22	Crison, Alella, Spain
• UV-310PC UV-Vis-NIR double-beam scanning spectrophotometer	Shimadzu, Kyoto, Japan
• High Resolution Transmission Electron Microscopy (HRTEM) JEOL 2011	JEOL, Tokyo, Japan
• Transmission Electron Microscopy (TEM) JEOL 1400	JEOL, Tokyo, Japan
• Zeta sizer nano ZS	Malvern, Worcestershire, UK

The pH meter is used to adjust the pH of the precursor solutions. The purification of the colloids is carried out prior to characterization by centrifugal filtration in centrifugal filter devices at 3000 rpm for 30 min.

The spectrophotometer is used to record spectra between 800 and 200 nm. The shape and dimensions of the core of the particles are measured by transmission electron microscope, preparing the samples in a copper grid coated with a thin carbon film.

Reagents used for these syntheses are shown in table 5.2. All solutions are prepared in double distilled water.

Table 5.2: Reagents used for the synthesis of CdS and CdS/ZnS NPs.

REAGENT	PROVIDER
• Cadmium nitrate tetrahydrate	Purum p.a≥99.0 %, Sigma - Aldrich
• Sodium sulfide	Aldrich, 99 %
• N-(2-mercaptopropionyl glycine (tiopronin)	Aldrich, 99 %
• Zinc nitrate hexahydrate (for MR5)	Purum p.a., ≥99.0 %, Sigma- for
• Rhodamine 6G	For fluorescence, Sigma

Rhodamine 6G in water (Φ_f = 0.95, λ_{exc} = 488 nm) is used to determine the fluorescence quantum yield (Φ_f or QY) of the nanocrystals as $\Phi_f = \Phi_{f,\,st}\,(F/F_{st})(A_{st}/A)$;[4] where $\Phi_{f,\,st}$ is the fluorescence quantum yield of the standard, *F* the integrated area under the fluorescence emission profile (quanta units) and *A* the absorbance intensity (always lower values than 0.05). In the expression, the subscript *st* is referred to the standard compound, and where nothing is specified is referred to the nanocrystals under study.

5.1.2 EXPERIMENTAL SET-UP

The synthesis of CdS/ZnS core-shell QDs stabilized with tiopronin (**MR5**) is performed using the experimental set-up schematized in figure 5.1, which is based on the one used for the synthesis of Au NPs stabilized with alkanethiols. Briefly, the automated and continuous flow system consists of four syringe pumps with their correspondent syringes connected to the microreactor with PTFE tubes by means of conical PTFE connectors and the home-made user-friendly connection piece showed in the previous chapter. Again, o-rings are used to seal the system and three-way valves make feasible the automatic refilling of syringes. A simplification of this set-up is used for the synthesis of single CdS nanocrystals (**MR4**), where the syringe, pump and valve for zinc precursor are not employed.

[4] Drushel, H.V.; Sommers, A.L.; Cox, R.C.; *Anal. Chem.,* **1963,** *35*, 2166.

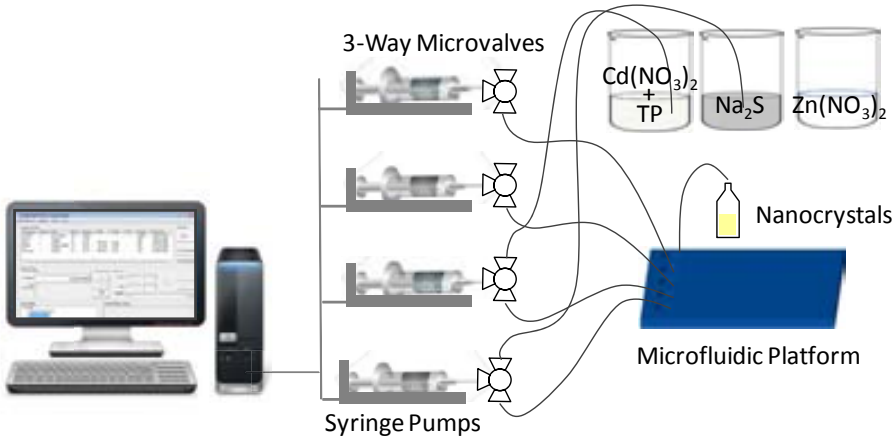

Figure 5.1: Microsystem set-up for the synthesis of CdS/ZnS core-shell nanocrystals.

5.1.3 CdS NANOCRYSTALS SYNTHESIS

A thoroughly optimization of the design parameters of the microreactor was done in order to obtain the microreactor which synthesized the best nanocrystals in terms of stability, fluorescence bandwidth, and quantum yield, taking in consideration parameters such as the channel dimensions of the microfluidic platform or the use of simple channels or micromixers. In the same manner, the concentration of reagents and the hydrodynamic parameters of the reaction were also optimized following the same criteria, as the molar relationship of reagents strongly affects the properties of the obtained nanoparticles.

Finally, a mixed solution of 5 mM $Cd(NO_3)_2$ and 10 mM of TP, previously adjusted to pH 10.0 with NaOH, and a 10 mM solution of Na_2S were employed. The microsystem used to perform the synthesis was basically the same as the used for the synthesis of gold nanoparticles stabilized with electrostatic repulsion (**MR2G**). Therefore, the microreactor consists in 3 inlet channels joined in a unique point to employ a hydrodynamic focusing of reagents followed by a three-dimensional micromixer to generate an efficient mixture. The mixture of cadmium nitrate and tiopronin solution is inserted in the central inlet channel, while at both sides sodium sulfide is flowed in. In this case, the total volume of the microreactor is of 31 µL (**MR4**).

On the other hand, a continuous flow rate of 0.5 µL s^{-1} for both reagents provided the more uniform nanocrystals with the higher quantum yield and narrower bandwidth. In these conditions, the molar relationship of the Cd^{2+}, TP and S^{2-} is 1 : 2 : 4, and the total residence time of reagents inside the microsystem is of approximately 20 s.

The use of the described microreactor in the detailed conditions generates yellowish water soluble CdS quantum dots, which under UV radiation emit in the green. Figure 5.2 shows the complete characterization of the colloid. The absorption band was centred at 368 nm, while the emission of the particles when excited at this wavelength gave a band located at 583 nm with a full width at half-maximum (FWHM) of 180 nm. A quantum yield lower than 5 % was obtained.

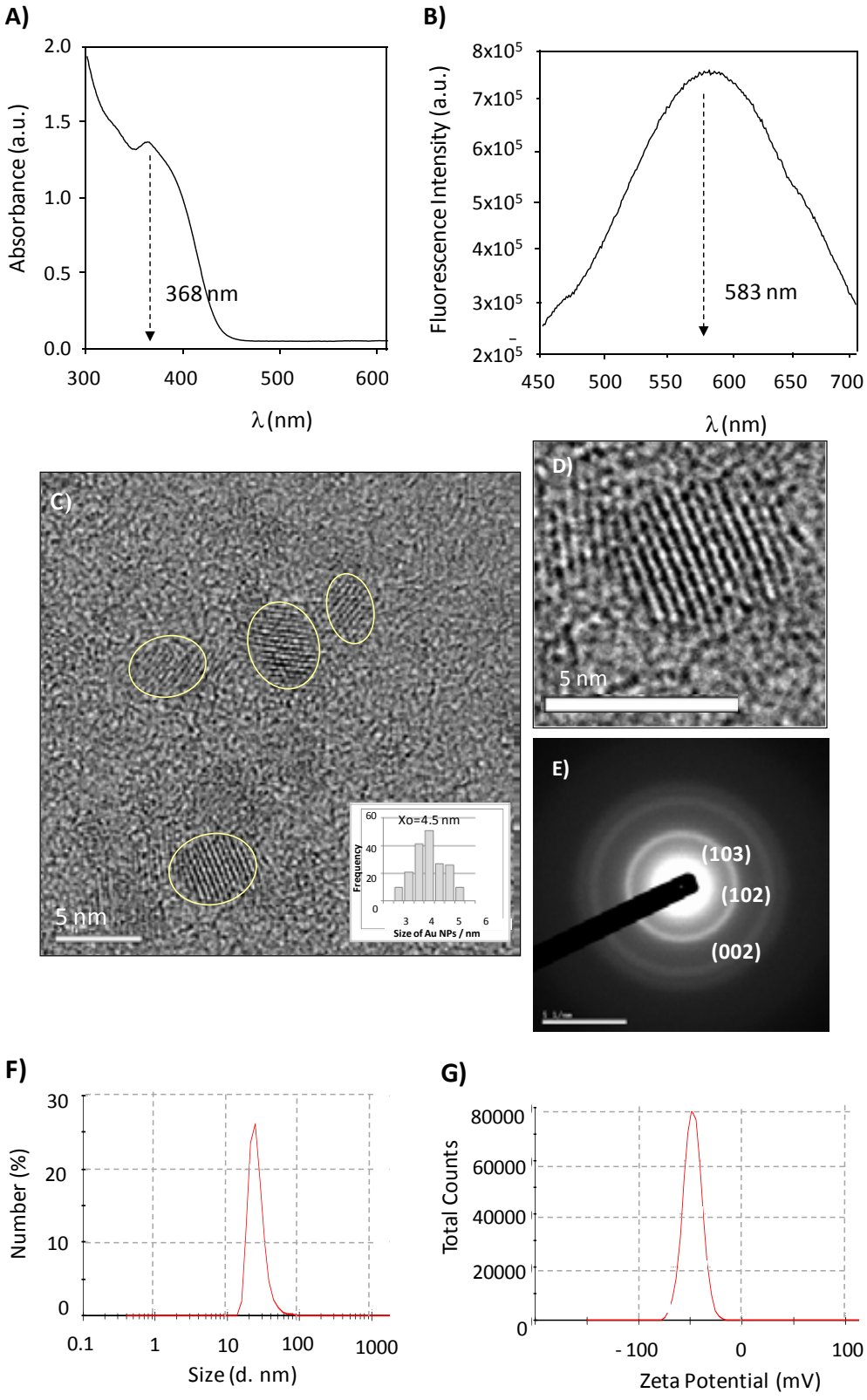

Figure 5.2: Characterization of the CdS nanocrystals synthesized in **MR4** at the optimized conditions. **A)** UV-Vis spectrum. **B)** Emission fluorescence spectrum. **C)** TEM image and its correspondent histogram. **D)** HRTEM image. **E)** Electron diffraction (SAED) pattern of the selected area. **F)** DLS spectrum. **G)** ζ potential measure.

The shape and dimensions of the core of the particles measured by HRTEM are also shown (Figure 5.2 C and D), where it can be observed almost spherical particles of 4.5 ± 0.9 nm. The electron diffraction (SAED) pattern of a selected area showed bright rings at distances of 0.340, 0.251 and 0.193, which

corresponds to (002), (102) and (103) lattice planes of the hexagonal (wurtzite) crystal structure of CdS (Figure 5.2 E).

Besides, DLS and ζ potential confirmed the presence of stable particles (-47.7 ± 8.87 mV) with a hydrodynamic diameter of 26.09 ± 8.37 nm (Figure 5.2 F and G).

5.1.4 CORE-SHELL CdS/ZnS NANOCRYSTALS SYNTHESIS

Although the previous fluorescent nanocrystals synthesized with **MR4** are well dispersed and stable, the use of fluorescent labels with higher quantum yields than the obtained is always preferred when developing analytical microsystems. It is well known that QY of nanoparticles can be increased by covering the nanoparticle with an outer layer of few atoms of thick of another semiconductor material with higher band-gaps, obtaining core-shell quantum dots.

With this aim, the configuration of the microreactor was modified to incorporate an additional auxiliary channel for the addition of a zinc nitrate solution, and the main channel was elongated to ensure the coverage of the previously synthesized CdS nanocrystals with ZnS. However, a simple microchannel was preferred for this second reaction step, since in this case the use of three-dimensional micromixers can produce the formation of ZnS particles, obtaining a mixture of CdS, ZnS and CdS/ZnS colloid. Thus, a slow mass transference of zinc nitrate, sodium sulphide and CdS nanoparticles is achieved due to diffusion is the only transport phenomena present when using these simple channels (laminar flow). A schematic representation of the microreactor designed and constructed is shown in figure 5.3 (**MR5**). The microreactor has a total volume of 40 µL.

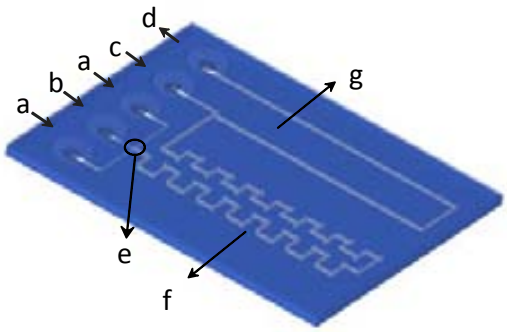

Figure 5.3: Schematic representation of the microfluidic platform for the synthesis of core-shell CdS/ZnS nanocrystals (**MR5**), where a: Na_2S, b: $Cd(NO_3)_2$, c: $Zn(NO_3)_2$, d: outlet, e: confluence point (hydrodynamic focusing), f: three-dimensional micromixer for CdS NPs formation, g: simple microchannel for CdS/ZnS NPs synthesis.

As for all microreactors, the concentration of reagents and the hydrodynamic parameters of the system must be optimized. The use of a 5 mM cadmium nitrate and 10 mM tiopronin solution (adjusted at pH 10.0), a 10 mM sodium sulfide solution and a 5 mM zinc nitrate solution generated the better nanocrystals in terms of stability, uniformity, QY and FWHM. In this case, the use of dosage volumes for the cadmium nitrate solution offered the better results taking into account the same quality values. Some of the results obtained for the hydrodynamic parameters optimization of the CdS/ZnS quantum dots synthesis are sum up in the graphics presented in figure 5.4.

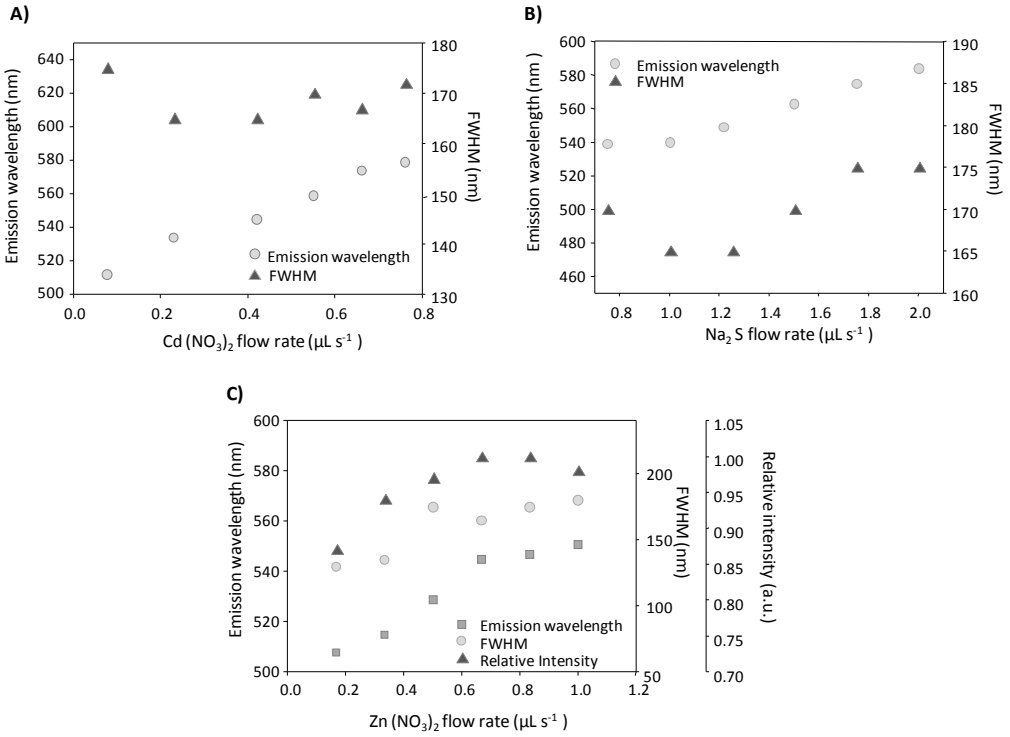

Figure 5.4: Optimization of the hydrodynamic parameters. Reagent concentrations and flow rates were of 0.5 µL of a 5 mM $Cd(NO_3)_2$ and 10 mM TP (pH 10.0) solution every 1 s at 2.5 µL s^{-1} flow rate, 10 mM of Na_2S solution at 1.25 µL s^{-1}, and a 5 mM $Zn(NO_3)_2$ solution at 0.67 µL s^{-1}; except for the reagent of study in each case. **A)** Influence of $Cd(NO_3)_2$ dosages (tested volumes: 0.08, 0.25, 0.50, 0.70, 0.90 and 1.10 µL). **B)** Influence of the Na_2S flow rate. **C)** Influence of $Zn(NO_3)_2$ flow rate.

As shown in figure 5.4A and B, increasing the flow rate of cadmium nitrate (related to its dosage volume) or sodium sulfide produces a bathochromic effect in the emission wavelength of the particles, since the higher amount of reagents in the medium generates bigger particles. Nevertheless, wider bands (FWHM) are achieved in all cases by incrementing flow rates, since the colloid have not enough time to grow inside the microreactor obtaining, as a result, an uncontrolled growth of the nanocrystals. Therefore, a 0.5 µL of cadmium nitrate dosage volume every 1 s at 2.5 µL s^{-1} and a continuous flow rate of 1.25 µL s^{-1} for Na_2S solution provided the minimal FWHM, which means a more uniform colloidal suspension.

Besides, the flow rate of the zinc nitrate solution was also studied, since this parameter is associated with the thickness of the covering layer of the nanocrystals, determining the final quantum yield of the colloid. As it can be observed in figure 5.4C, increasing the flow rate of this reagent generates a displacement of the emission wavelength to higher values and an intensity enhance, until no relevant betterment in its intensity is observed.[56] In fact, the deposition of too many layers of ZnS over a CdS particle can decrease its QY. Therefore, a flow rate of 0.67 µL s^{-1} was chosen as the optimized, since it conferred the highest fluorescence intensity with a moderate band width. At the optimized conditions, the molar relationship of Cd^{2+}, TP, Zn^{2+} and S^{2-} is 1 : 2 : 1.6 : 10, and the total residence time is of ~ 12 s.

[5] Dabbousi, B.O.; Rodriguez-Viejo, J.; Mikulec, F.V.; Heine, J.R.; Mattoussi, H.; Ober, R.; Jensen, K.F.; Bawendi, M.G.; *J. Phys. Chem. B*, **1997**, *101*, 9463.
[6] Talapin, D.V.; Rogach, A.L.; Kornowski, A.; Haase, M.; Weller, H.; *Nano Lett.*, **2001**, *1*, 207–211.

The colloid characterization revealed stable particles with a maximum absorption band centred at 363 nm, while its maximum emission was located at 545 nm with a FWHM of 165 nm (Figure 5.5A and B). Comparing both synthesized colloidal (CdS and CdS/ZnS) one can notice the lower emission wavelength of core-shell nanoparticles, which is probably due to the slightly different mean size of the nanocrystals, confirmed by microscopy measurements. In this sense, TEM characterization showed crystalline core-shell nanoparticles of 4.2 ± 0.6 nm (Figure 5.5C-E). Besides, 33.90 ± 12.10 nm nanocrystals of hydrodynamic diameter were obtained from DLS measurements. The ζ potential showed nanoparticles of -60.6 ± 9.14 mV (Figure 5.5F and G). The quantum yield attained for the colloid was of 27 %, which is considerably higher than the obtained for CdS nanocrystals.

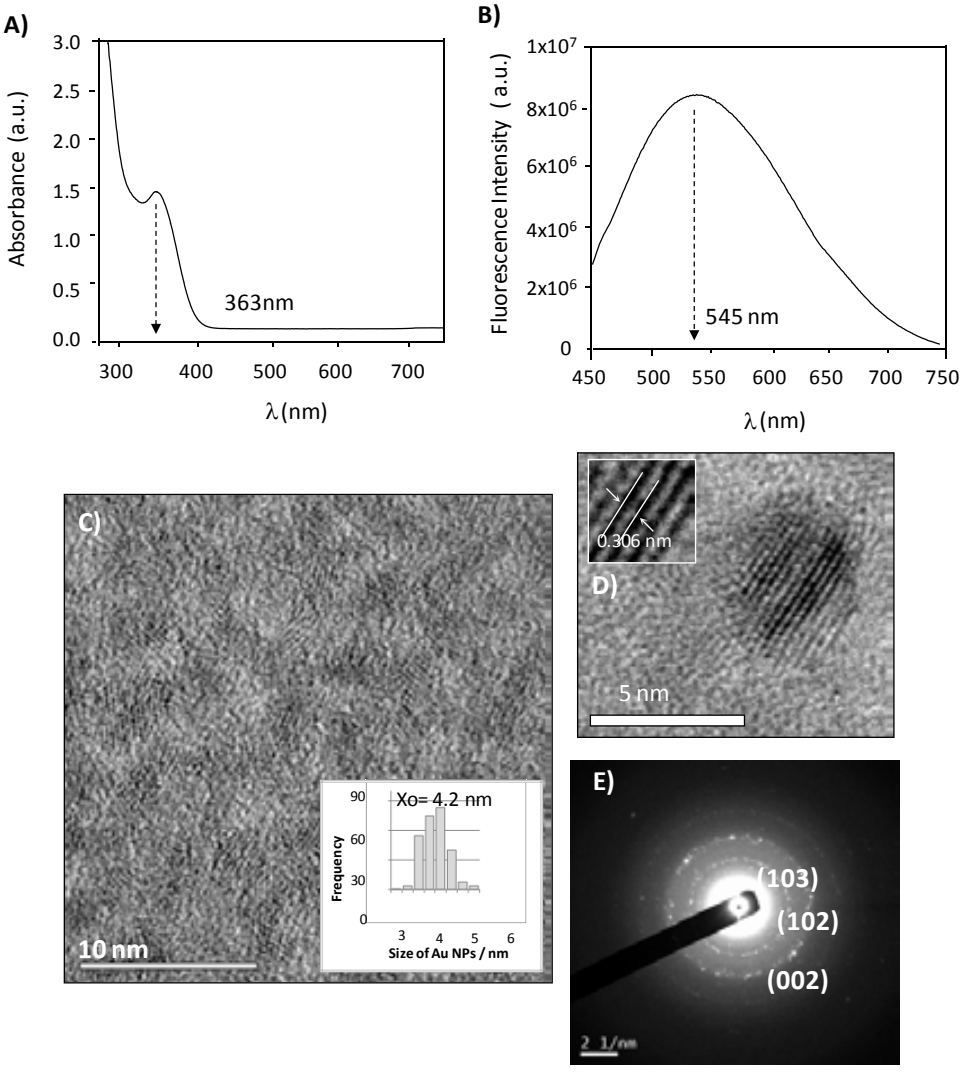

Figure 5.5: Characterization of the CdS/ZnS nanocrystals synthesized in **MR5** at the optimized conditions. **A)** UV-Vis spectrum. **B)** Emission fluorescence spectrum. **C)** TEM image and its correspondent histogram. **D)** HRTEM image. **E)** Electron diffraction (SAED) pattern of the selected area.

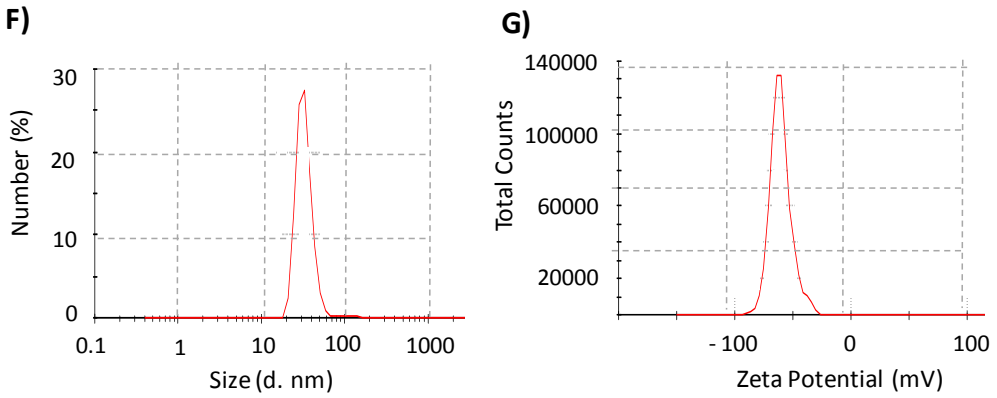

Figure 5.5: Characterization of the CdS/ZnS nanocrystals synthesized in **MR5** at the optimized conditions. **F)** DLS spectrum. **G)** ζ potential measure.

The repeatability of the synthesis was also evaluated by comparing the maximum emission fluorescence wavelength and FWHM from ten identical syntheses (Figure 5.6). A medium emission wavelength of 540 ± 8 nm and a FWHM of 170 ± 10 nm are achieved.

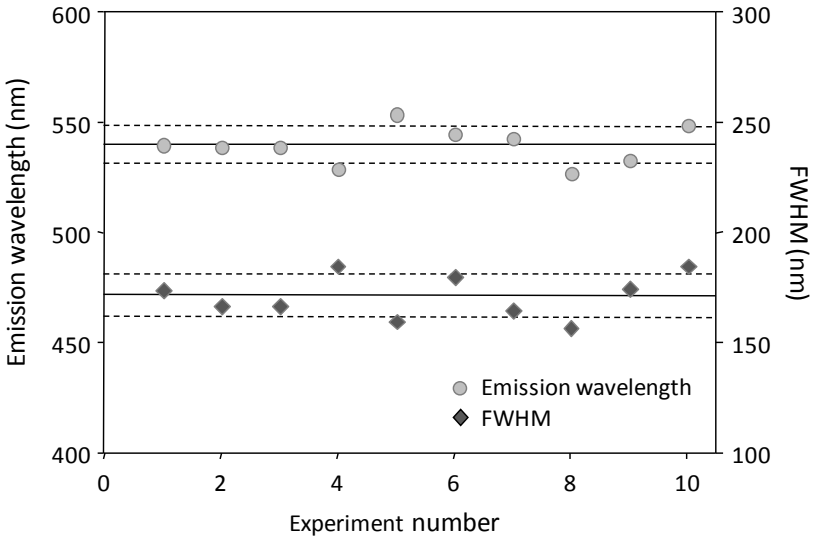

Figure 5.6: Characterization of the synthesis repeatability following the position and the FWHM of the emission band of the core-shell nanocrystals.

5.1.5 ABSORBANCE AND FLUORESCENCE MONITORING

In order to achieve an automated and controlled microreactor for the synthesis of CdS/ZnS nanocrystals, it is necessary the integration of a detection system. Thus, the previously miniaturized optical system employed in the monitoring of Au NPs synthesis was improved to make feasible not only the absorbance but also the fluorescence register of the colloid.

Normally, fluorescence measures require of a filter in order to avoid the excitation light and only register the emission light of the sample. Due to the absorbance and excitation wavelengths of nanocrystals are the same, two different PCBs are necessary for the simultaneous absorbance and fluorescence measurements. Thus, two LEDs (one for absorbance and another for fluorescence) with a maximum emission peak located at 365 nm are employed (Roithner

Lasertechnik XSL-365-5E, Vienna, Austria), which matches with the absorption and excitation bands of the particles. The excitation LED has been tilted 45 degrees from the normal to the microreactor surface to reduce interferences of the light source to the detector, and the rest is avoided by using a high pass optical filter with a cut-off wavelength at 500 nm (FEL500 from Thorlabs). Besides, the absorbance LED is mounted in front of the photodetector, as in Au NPs monitoring. Figure 5.7A shows the components and configuration of the PCBs, where both systems are drown together but they are actually separated in two modules. Moreover, the LEDs can be easily changed if necessary, since in this case they have been connected to the PCB by an intermediate piece, instead of their direct solder. Both absorbance and fluorescence boards are connected to the same DAQ, as it is shown in figure 5.7B, which simplifies the whole optical set-up. As previously, the emission sources are modulated by the DAQ, which in this case generates two sine waves at different frequency (f1 and f2) and sends them to the PCBs. The sampling frequency used to generate these waves inside the DAQ is dynamically adjusted to 128 times the highest modulation frequency to avoid problems in the synchronization of the signals inside the DAQ. Again, the detected signals are amplified by a lock-in amplification, which increases the signal to noise ratio and allows the use of both optical systems in ambient light.

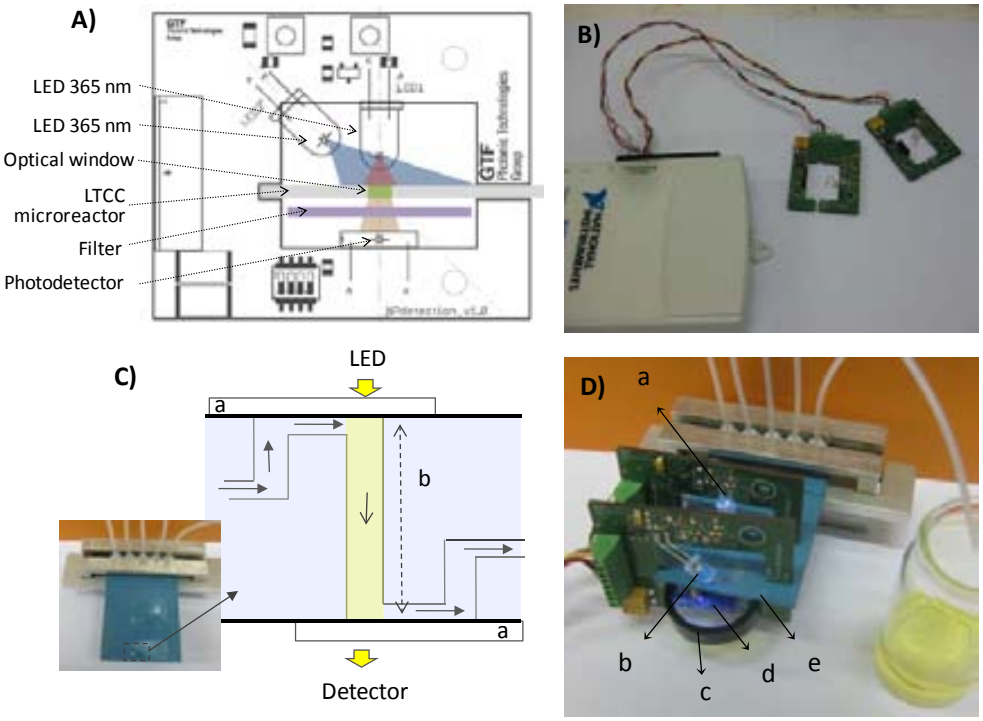

Figure 5.7: **A)** Scheme of the different components of the absorbance and fluorescence PCBs. **B)** Image of the PCBs connected to the DAQ. **C)** Image of the optical microreactor and schematic representation of the inner structure of the microreactor in the optical cell zone. **D)** Optical system and microreactor coupling. a: Absorbance LED, b: fluorescence LED, c: high pass filter, d: PIN photodetector, e: ceramic microreactor.

On the other hand, the microreactor was modified in a similar way as done for the microreactor to monitor gold nanoparticles synthesis, but incorporating two optical windows instead of only one. Thus, the main channel of the microreactor was enlarged, widened and brought to the surface, where a round hollow defines

the diameter of the optical window and the optical path length, since it is machined in all layers (Figure 5.7C). The diameters of these holes were of 1.7 mm for absorbance and 2.5 mm for fluorescence, which corresponds to a volume of 3.6 and 8.0 µL, respectively. Glass layers were attached in the top and bottom of the round holes using polydimethylsiloxane (PDMS). Then, the alignment of the optical windows of the microreactor with the absorbance and fluorescence optical systems is achieved by the grooves of the PCBs. The high pass optical filter was placed behind the window for fluorescence measurements, just before the photodetector, as it can be observed in figure 5.7D.

The performance of the optical system was evaluated by recording the absorbance and fluorescence of nanocrystals during a synthesis, where the dosage of cadmium nitrate was intentionally modified. As it can be observed in figure 5.8, the recorded measurements have the same tendency, as a decrease in absorbance intensity entails a reduction in its fluorescence. The three different dosage volumes used (0.5, 0.25 and 0.08 µL) can be perfectly distinguished following both, absorbance or fluorescence, signals. The higher dosage volume used, which corresponds to the optimized one, generates the more intense absorbance and fluorescence signals; while the lower dosage volume proportionate the less intense ones. Likewise, the intensity values are constant when using the same dosages, demonstrating the repeatability of the synthesis. Therefore, if any change in the absorption or fluorescence intensities is observed, correct actions can be done, since it should entail the malfunction of the synthetic procedure.

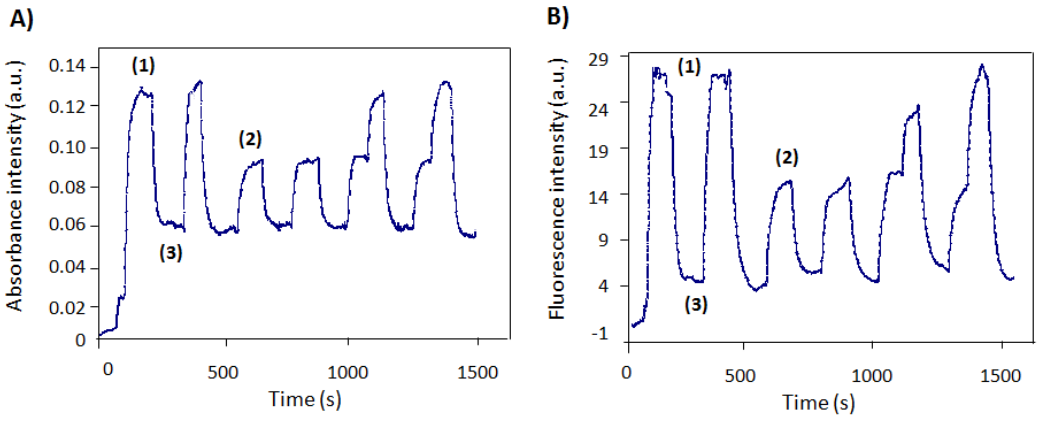

Figure 5.8: Absorbance **(A)** and fluorescence emission **(B)** graphics recorded using the miniaturized optical system at different cadmium dosage volumes, where 1: 0.5 µL, 2: 0. 25 µL and 3: 0.08 µL.

5.1.6 CONCLUSIONS

This chapter has shown the possibility of synthesizing water soluble nanocrystals using ceramic microreactors. Reproducible, uniform and stable CdS quantum dots can be obtained by a simple and direct aqueous synthetic approach using a

microreactor based on a hydrodynamic focusing of reagents and a three-dimensional micromixer.

Similarly, monodispersed CdS/ZnS nanocrystals can be synthesized by using **MR5**, which incorporates an auxiliary channel for the addition of the zinc reagent and elongates the fluidic system by a simple microchannel. The use of this microreactor at the optimized conditions enables synthesizing core-shell quantum dots with reproducible optical properties in terms of fluorescence emission wavelengths, bandwidth, and high quantum yield, which is of special relevance in analytical applications.

Besides, the use of the miniaturized optical system makes feasible the monitoring of the reaction by following the absorbance and fluorescence intensities of the nanocrystals synthesized. Thus, the microreactor could be directly integrated in subsequent microfluidic platforms to develop Lab-on-a-Chip with on-line synthesis of the labels.

5.2 MICROREACTORS FOR THE SYNTHESIS OF CdSe QUANTUM DOTS (MR6)

The main objective of this chapter is the development of a microreactor for the synthesis of nanoparticles at high temperatures, specifically for the synthesis of CdSe nanocrystals, since these chemical approaches usually generate more stable nanocrystals with higher quantum yields. Moreover, temperature is a relevant synthetic parameter, which can determine the optical properties of the nanocrystals obtained. Therefore, a strict temperature control is a must in these syntheses. Thus, it has been firstly necessary to design, construct and evaluate a thermal module (**TM**) consisting of a temperature actuator and a sensor for its control. In this sense, it has been taken advantage from the compatibility of the LTCC technology with screen printing techniques to construct a compact device. Initially, the thermal actuator and the sensor have been based on resistor/thermistor couples, which have been constructed and validated using different configurations for the resistor. Nevertheless, better results in terms of temperature stability, reproducibility and robustness have been obtained by means of a circular screen-printed gold resistor and a commercial platinum sensor. Additionally, the necessary electronics has been also designed and implemented in the research group to attain a highly stable temperature profile. The characterization of the thermal module demonstrated its perfect function.

Secondly, a microfluidic platform has been design and constructed, which consists of two inlet channels for the entrance of reagents and a bi-dimensional

micromixer. The mixing efficiency of the microfluidic platform has been also evaluated by employing two different dyes in a qualitative visual characterization. Finally, the synthesis of different sizes of CdSe nanocrystals has been performed by using both ceramic modules (thermal and microfluidic) that compose the microreactor (**MR6**). The reaction used to synthesize these tunable size-dependent nanocrystals has been a modification of the Peng's procedure, which is based on cadmium oxide, selenium powder and the triple ligand of TOPO, OA and OLA.[7-8] The reliability and performance of a modular and a monolithic approach have been evaluated.

5.2.1 MATERIALS, REAGENTS AND METHODS

In table 5.3 are listed the instruments and equipments employed for the synthesis and characterization of CdSe quantum dots.

Table 5.3: General list of equipments and instruments used in the synthesis of CdSe quantum dots.

EQUIPMENT	PROVIDER
• 2 syringes pumps, 540060 TSE systems	TSE systems, Bad Homburg, Germany
• 2 syringes of 10 mL, GASTIGHT 1000 TLL series	Hamilton, Bonaduz, GR, Switzerland
• 2 three-way solenoid isolation valves (161T031)	NResearch, NJ, USA
• User-friendly connection system	GSB
• Conical PTFE connectors (Cones 1.6 mm)	Omnifit, Cambridge, UK
• Tygon tube (i.d. 1.2 mm)	Ismatec, Zurich, Switzerland
• PTFE tubes (i.d. 0.8 mm)	Techny Fluor, Barcelona, Spain
• EMC Scanner with an integrated IR Probe (RS321EH)	Detectus AB, Malung, Sweden
• PIC18F4431 microcontroller	Microchip Inc., USA
• Stereo microscope Leica S6D equipped with a DFC290 digital camera	Leica, Microsystems S.L.U., Spain
• Class A PT100 sensor	Innovative Sensor Technology, Switzerland
• 2 Power supplies	Blausonic, Hospitalet, Spain
• Multimeter	Fluke 179 Multimeter, Everett, USA
• UV-310PC UV-Vis-NIR double-beam scanning spectrophotometer	Shimadzu, Kyoto, Japan
• Fluorolog® Modular Spectrofluorometer	Horiba, Jobin Yvon, Kyoto, Japan
• High Resolution Transmission Electron Microscopy (HRTEM) JEOL 2011	JEOL, Tokyo, Japan

[7] Yang, H.; Luan, W.; Tu, S.; Wang, Z.M.; *Cryst. Growth Des.*, **2009**, *9*, 1569.
[8] Luan, W.; Yang, H.; Tu, S.; Wang, Z.; *Nanotechnology,* **2007**, *18*, 175603.

The EMC Scanner with an integrated IR Probe is used to perform the thermal characterization of the microreactor. The stereo microscope is employed to evaluate the mixing efficiency of the microfluidic platform by means of a qualitative visual characterization. The PIC18F4431 microcontroller is used to implement a digital PID (proportional-integral-derivative) control system to maintain temperature at the desired value. All the electronic components used to implement the digital PID control are carefully selected to improve the system response and reduce noise effects in the signal. The spectrophotometer is employed to record the absorption bands of the synthesized nanocrystals. The excitation and emission spectra of quantum dots are recorded using the spectrofluorometer. Emission spectra were obtained from the excitation of quantum dots using the first absorption peak, being checked by the excitation spectrum of the nanocrystals. HRTEM is used for the core characterization of the nanoparticles.

Reagents used for these syntheses are shown in table 5.4.

Table 5.4: Reagents used for the synthesis of CdSe NPs.

REAGENT	PROVIDER
• Cadmium oxide (CdO)	99.99 %, Aldrich
• Selenium powder (Se)	99.5 %, Aldrich
• Trioctylphosphine (TOP)	90 %, Aldrich
• Tryoctylphosphine oxide (TOPO)	99 %, Aldrich
• Oleic acid (OA)	Ph Eur, Fluka
• Oleylamine (OLA)	70 %, Aldrich
• 1-Octadecene (ODE)	90 %, Aldrich
• Chloroform	Analytical grade, Aldrich
• Methanol	Analytical grade, Aldrich
• Rhodamine 6G	For fluorescence, Sigma

In order to obtain a set of nanocrystals with different optical properties, it is necessary to prepare three different stock solutions of a cadmium precursor and one of a selenium precursor, involving thus 1:10, 1:1 and 1:2 molar ratios of Cd:Se reagents. The first Cd stock solution consists of 32.1 mg of CdO (0.25 mmol), 317 mL of OA (1 mmol), 2.5 g of TOPO (6.45 mmol) and 5 mL of OLA (15.2 mmol). The mixture is warmed up in a round bottom flask at 190 ºC until a pale yellow solution is observed (around 40 min). The mixture obtained is diluted with 7.5 mL of ODE. The other two Cd precursors are similarly prepared. The 1:1 molar ratio consists of 321.25 mg of CdO (2.5 mmol), 4 mL of OA (12.6 mmol), 3 g of TOPO (7.8 mmol), 5 mL of OLA (15.2 mmol) and 3 mL of ODE. The 2:1 molar ratio

employs 802.5 mg of CdO (6.25 mmol), 10 mL of OA (32 mmol), 3.3 g of TOPO (8.5 mmol) and 5 mL of OLA (15.2 mmol). Besides, the selenium precursor is prepared mixing 197.4 g (2.5 mmol) of selenium powder with 5 mL of TOP (10.1 mmol) and 10 mL of OLA (21.25 mmol) in another round-bottom flask at room temperature. Stock solutions are newly prepared for each synthesis.
A reversible flocculation is done by means of anhydrous methanol prior to characterization to clean the quantum dots synthesized. The obtained flocculate is separated from the supernatant by centrifugation and re-dispersed again in chloroform. Rhodamine 6G in chloroform is used to determine the fluorescence quantum yield (Φf or QY) of the nanocrystals as described in the 5.1.1 section.

Different conductive pastes are used to fabricate the temperature module (resistor/thermistor couple). Their use and properties are described in the next table. Epoxy (EPO-TEK® H20E) is used to glue the 100 PT sensor over the surface the ceramic device.

Table 5.5: Conductive pastes used for the fabrication of the temperature actuator for the synthesis of CdSe QDs.

CONDUCTIVE PASTE	PROPERTIES	USE
• DuPont 5742	Fired resistivity < 5 mΩ/sq. Au paste	Resistor
• DuPont 6141	Fired resistivity < 3 mΩ/sq Ag paste	Conductor Via Fill
• DuPont 6142D	Fired resistivity 3 mΩ/sq Ag paste	Conductor Internal
• DuPont 6146	Fired resistivity 60 mΩ/sq Pd/Ag paste	Conductor Solderable
• Heraeus R131	Fired resistivity 1000 Ω/sq Rh paste	NTC Thermistor

5.2.2 EXPERIMENTAL SET-UP

The complete set-up used for the synthesis of CdSe quantum dots is shown in Figure 5.9. The fluidic set-up is composed of two syringe pumps with their correspondent syringes connected to the ceramic fluidic platform with PTFE tubes by means of conical PTFE connectors and the home-made connection piece. O-rings are used to seal the system and three-way valves make feasible the automatic refilling of syringes. Besides, the heating module required two power supplies connected to the electronic circuit and the ceramic thermal module, and a multimeter to ensure the sensor intensity and to close the whole circuit. Crocodile or alligator clips were employed to connect the electrical circuit with the screen printed paths of the thermal platform.

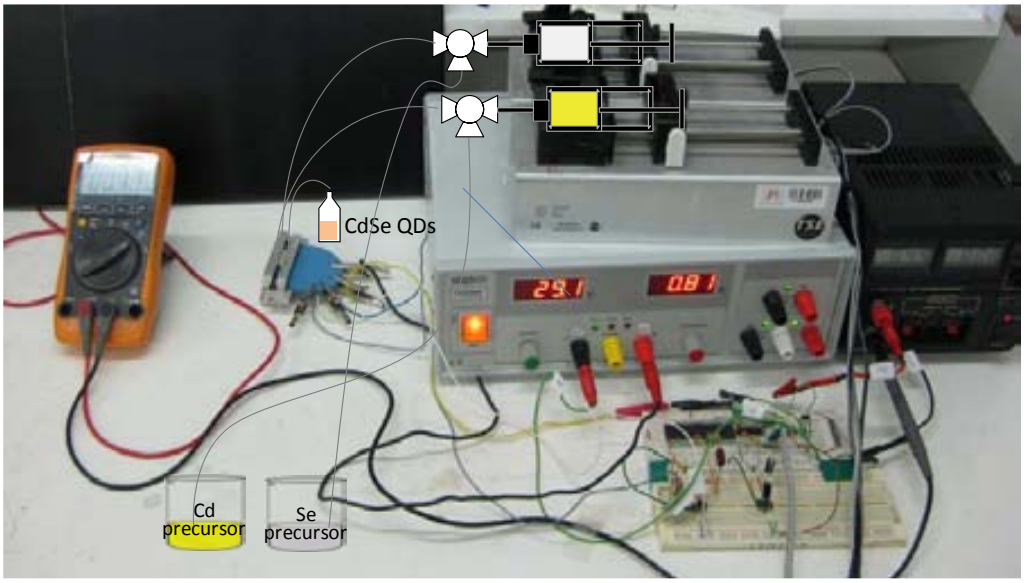

Figure 5.9: Microsystem set-up for the synthesis of CdSe quantum dots.

5.2.3 DEVELOPMENT OF THE THERMAL PLATFORM

The implementation of a temperature control module requires of a sensor capable to determine with accuracy the desired temperature, a heating element able to generate a uniform heat in the area of interest, and a control system for regulating the operation of both sensor and heater. There exist different mechanisms to heat and cold, including devices based on the Peltier effect or heaters integrated in a device by means of screen printing techniques. On the other hand, thermocouple or integrated thermistors are the most usual temperature sensors. In this case, it was preferred the development of a temperature actuator based on resistor/thermistor couples, since the multilayer approach of the LTCC technology and its compatibility with screen printing techniques allows embedding flat elements capable to fulfil these functions, obtaining as a results compact devices.[9-10]

The use of resistors as heating elements is based on the Joule effect, which is the irreversible phenomenon whereby part of the energy is converted to heat when electric current circulates in a conductor material, raising the temperature thereof. Therefore, it is preferred the use of a material, which can provide the higher temperature by applying the minimal power. In all cases, the constructed resistances presented below are based on a gold conductive paste (DuPont 5742) screen printed in ceramic substrates, following the procedure described in the 3.1.3 section. This paste was selected on the basis of its suitability to provide high conductive paths where high power dissipation is a must. Since the resistance is

[9] Martínez-Cisneros, C.S.; in: *Microsistemas analíticos basados en la tecnología LTCC.* PhD Thesis. UAB, Bellaterra, Spain, **2010**.
[10] Ymbern, O.; in: *Construcció i avaluació de dispositius per al control de la temperatura en microsistemes de PCR basats en la tecnologia LTCC.* Master Thesis. UAB, Bellaterra, Spain, **2007**.

confined inside the ceramic platform, conductive *vias* (DuPont 6141) are required to allow its connection with the surface of the platform, where paths are screen-printed (DuPont 6146) in order to solder wires. The characterization of a resistor is normally done by measuring the temperature at different points of the material surface, where the resistor is placed, using a thermocouple when a voltage is applied.

On the other hand, the operation of thermistors is also based on the variation of the semiconductor resistance with temperature. In this case, an optimal thermistor should have a good linearity in the working temperature range. Two main classes of thermistors can be found NTC (Negative Temperature Coefficient) or PTC (Positive Temperature Coefficient), which depend on whether the resistance decreases or increases when temperature is raised, respectively. Ideally, thermistors should be located in direct contact with the sample or in the proximity of the heating element. The fabrication of the following screen printed thermistors is based on the deposition of two different conductive pastes, one for the thermistor (rhodium paste) and other for its terminal connections (internal paste). The deposition of the first is done by a stainless steel screen, since a thick structure is desired (50 µm-thick), while the other tracks are screen printed using nylon meshes. The resistance of a thermistor basically depends on its geometry, obtaining the higher resistive values with flat structures. In this case, 5 mm x 3 mm rectangles of thermistor paste were deposited once the terminal connections were screen printed. This design allows a higher dissipation of the temperature, avoiding errors in the measure that their heating could generate.[9-10] The characterization of a thermistor is carried out by varying the temperature of the device (using a programmable oven), checking the temperature with a thermocouple, and measuring in an electronic circuit the potential difference obtained as a result of the thermistor resistance changes. Although the response of the thermistors is very accurate, it is necessary its linearization ($T= 1/(A_0+A_1(\ln R_T)+A_3(\ln R_T^3))$).[11]

The first resistor/thermistor couple constructed (**TM1**) was based on the idea of using a microfluidic platform which integrated a three-dimensional micromixer, such as microreactors developed for the synthesis of metallic nanoparticles. Initially, only the thermal platform was constructed in order to simplify its evaluation. Previous studies performed in the research group revealed a short reach and a high temperature dissipation of screen printed heaters in the ceramic material. Therefore, relatively large resistors are necessary to heat a complete fluidic structure, which provide a better distribution of temperature and lower oscillations. The use of the gold conductive paste, with small resistivity, enables the construction of large heaters without greatly increasing its resistance,

[11] Lepkowski, J.;: *Microchip Application Notes AN685*, Microchip Technology Inc., **1999.**

allowing the use of low/moderate voltages to reach the desired temperature. Thus, a gold screen printed resistor based on a zigzag configuration was designed and constructed, which had a resistance of 6.7 Ω. As it can be observed in figure 5.10A, three thermistors were also constructed to evaluate the temperature at different points of the platform. The characterization of the resistor using a thermometer based on a thermocouple (Fluke 179 Multimeter) as above described, revealed a radial distribution of the temperature, in concordance with previous works of the group, showing a highly elevated heat point in the centre of the platform. Then, the characterization of the three thermistors was done in a programmable oven (Carbolite CBC2F11/23P16, Afora, Spain) using the thermocouple. First tests performed made clear the impossibility of using soldered wires in the ceramic platform, since at the high temperatures employed (250-300 ºC) the wires got de-soldered. Thus, the electrical connections were done by means of crocodile clips, as shown in figure 5.10B. Nevertheless, during the repeated cycles of temperature necessary to characterize the thermistors, the heating platform was broken, probably due to the stress generated by the high density of conductive tracks of the ceramic platform.

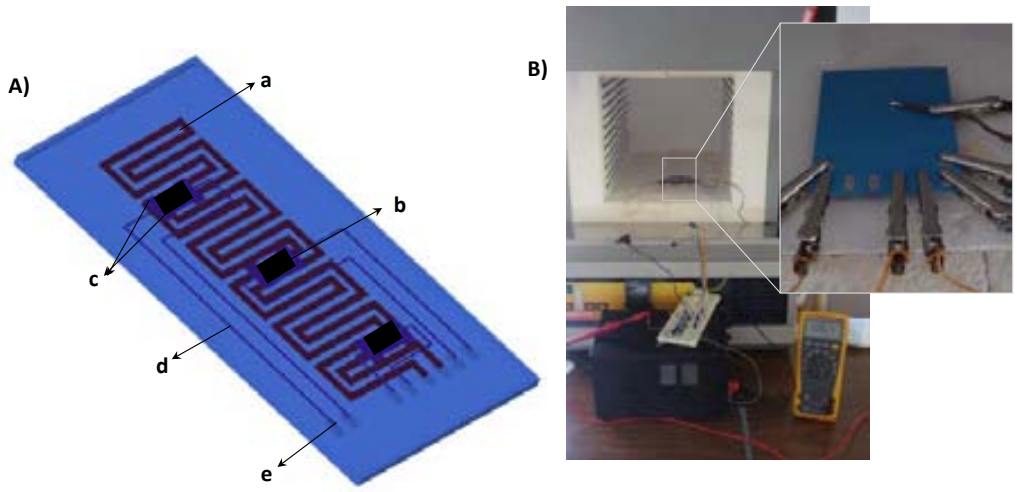

Figure 5.10:
A) Scheme of the inner structure of the first thermal module (**TM1**) developed for the synthesis of CdSe QDs. a: Resistor, b: thermistor, c: thermistor connections, d: *vias*, e: paths. **B)** Image of the experimental set-up and the thermal platform during the characterization of the thermistors using alligator clips.

Then, a new heater design was developed on the basis of a radial and uniform distribution of temperature and trying to avoid a highly elevated heat point in the center of the platform. By defining seven laps in a radial configuration of a gold-based screen printed conductor (0.7 mm width, 8 µm height), a 17 Ω heater was obtained. Three thermistors were also constructed, distributing them in different points of the heater to minimize the stress of the ceramic platform but also to ensure a homogeneous temperature along the whole platform.

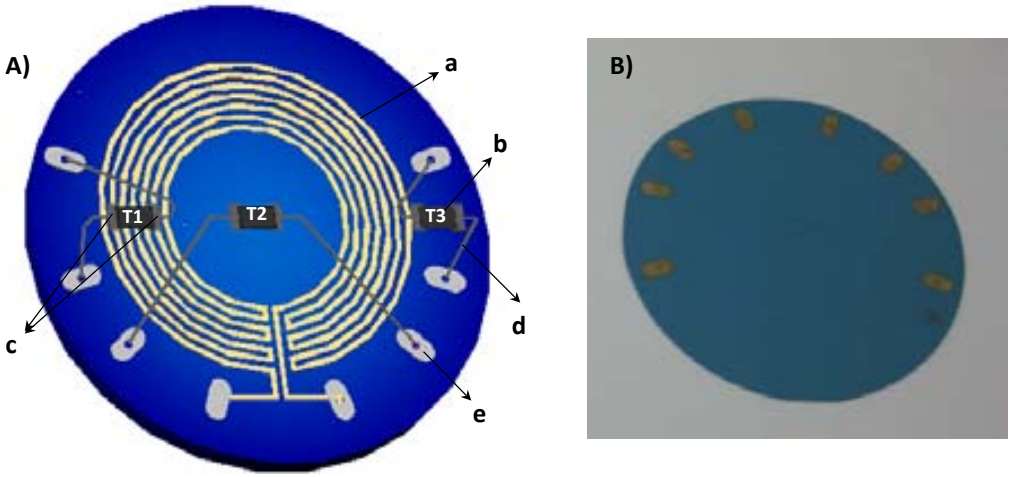

Figure 5.11:
A) Scheme of the inner structure of the **TM2** constructed based on a radial configuration of the resistor. a: Resistor, b: thermistor, c: thermistor connections, d: *vias*, e: paths. **B)** Image of the electronic connections side of the thermal platform.

The characterization of the circular resistor by means of the thermocouple showed a radial and more uniform distribution of the temperature when a certain and constant voltage is applied. A more accurate characterization was also done, which involved the measure of the temperature in a concrete point of the heater when increasing the voltage. As it can be observed in figure 5.12, a linear response was obtained in all cases.

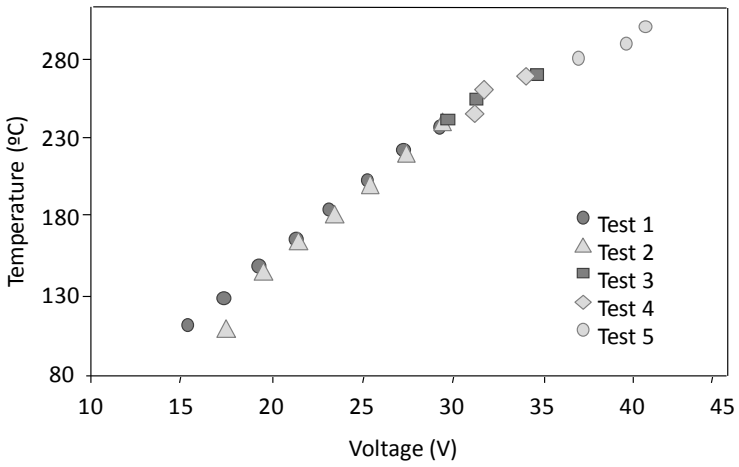

Figure 5.12:
Characterization of the circular gold screen printed resistor. The different calibration curves represent the variation of the temperature when different voltages are applied.

Besides, the constructed thermistors showed resistance values of 1.245, 16.80 and 1.055 kΩ for T1, T2 and T3 (Figure 5.11A), respectively, measured at room temperature. The different values between them are probably due to the lack of reproducibility in the deposition process of the conductive pastes. However, this can be settled by a well characterization of these components. The calibration curves obtained for the three thermistors are shown in figure 5.13. Since they are NTC elements, a negative slope is obtained for all of them.

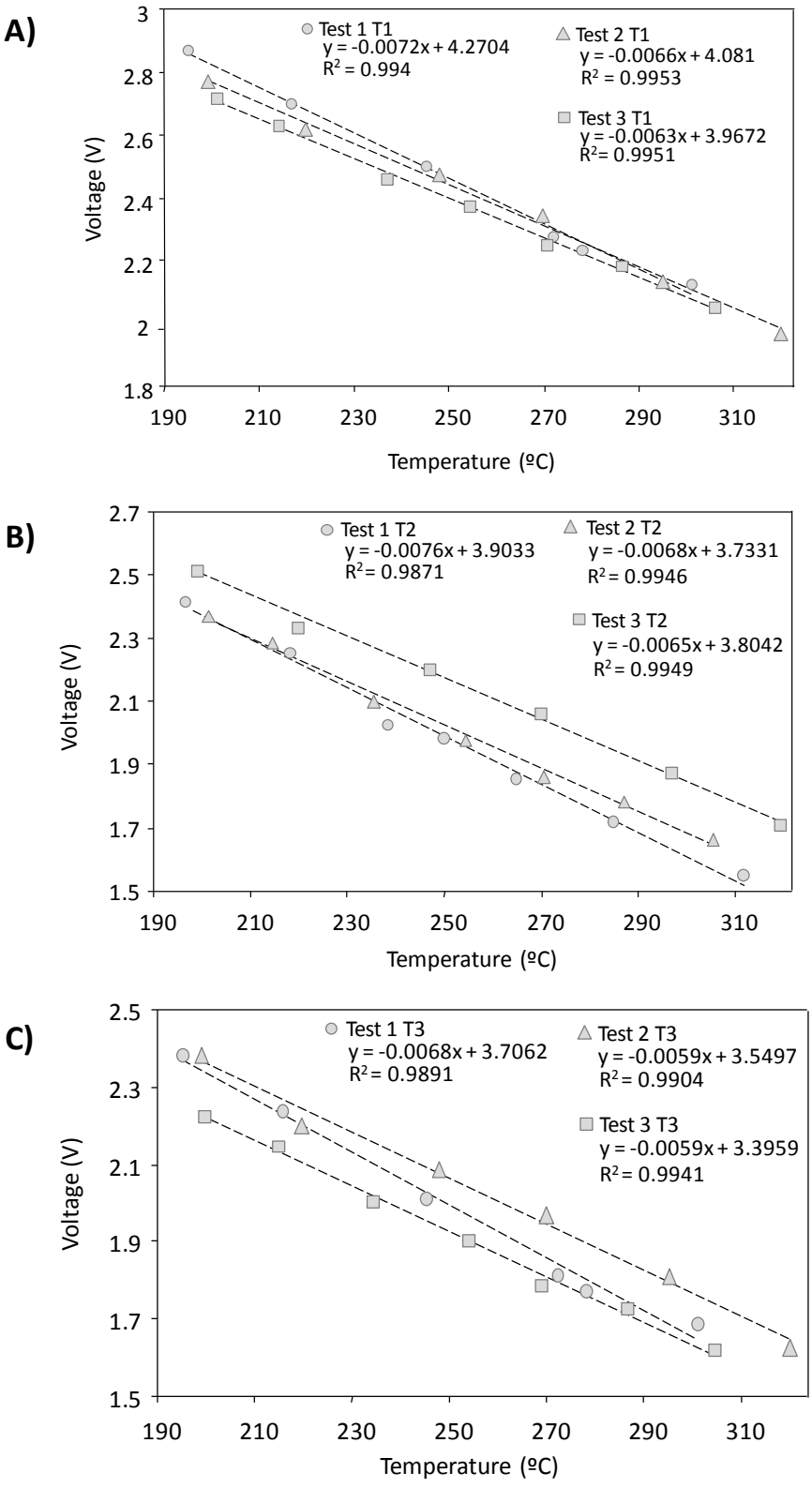

Figure 5.13: Characterization of thermistors. The different calibration curves (by triplicate) represent the variation of the voltage in the electronic circuit with the temperature. **A)** Thermistor 1. **B)** Thermistor 2. **C)** Thermistor 3.

Although a linear behavior is attained in all cases and the response do not differ significantly between thermistors (slopes of the lines), considerable differences can be observed between the diverse replicates done for the same thermistor, which entails a poor accuracy in the temperature determination. Taking as an

example the best, which corresponds to T1, a register of 2.4 V can entail a temperature of 260, 254 or 248 ºC depending on the calibration curve used. Same results were obtained when calibrating the diverse thermistors with a previous conditioning step, consisting of 20 temperature cycles (from room temperature to 250 ºC).

As stated in the introduction part, a strict control of the temperature is necessary when synthesizing size-dependent quantum dots by using thermal decomposition approaches, being desirable a precision of at least ± 1 ºC. Therefore, the use of these thermistors is not appropriate, since they do not confer the accuracy and reproducibility necessary for the intended application. On the other hand, resistance temperature detector (RTD) sensing elements constructed of platinum, copper or nickel have a repeatable resistance versus temperature relationship. Specially, platinum RTD has the most linear, stable and repeatable resistance-temperature relationship over the largest temperature range. Although platinum RTDs have slower response time when compared to thermistors, they have a higher temperature range and accuracy, and can maintain their stability for many years. Thus, a thin film class A PT100 commercial sensor, which means the sensor has a resistance of 100 Ω at 0ºC, was preferred as temperature sensor, since it can work in a wide range of temperature (-200 – 600 ºC) while providing accuracy and stability. It is based on a very thin layer (usually 1 to 10 nanometers-thick) of platinum on a ceramic substrate coated with epoxy to protect the deposited film (Figure 5.14C).

Therefore, the final thermal module (**TM3**) consisted on the gold-based heater and a PT100 sensor. Specifically, the thermal platform was composed of a nine-layer ceramic block with a screen-printed gold-based heater embedded in the middle of the block (fifth layer) to promote a more uniform heat distribution through the z-axis. External paths were defined on the top layer of the thermal platform to connect the embedded heater to an external electronic control set-up, since the high working temperatures associated to the microreactor avoids the surface integration of the involved electronics for the control system. The nine layers that constitute the thermal platform provide it robustness. For temperature sensing and establishing a control feedback, the PT100 sensor was glued by means of epoxy over the thermal platform, trying to obtain the optimum xy-alignment with the heating zone. An image and a schematic representation of the thermal platform are shown in figure 5.14.

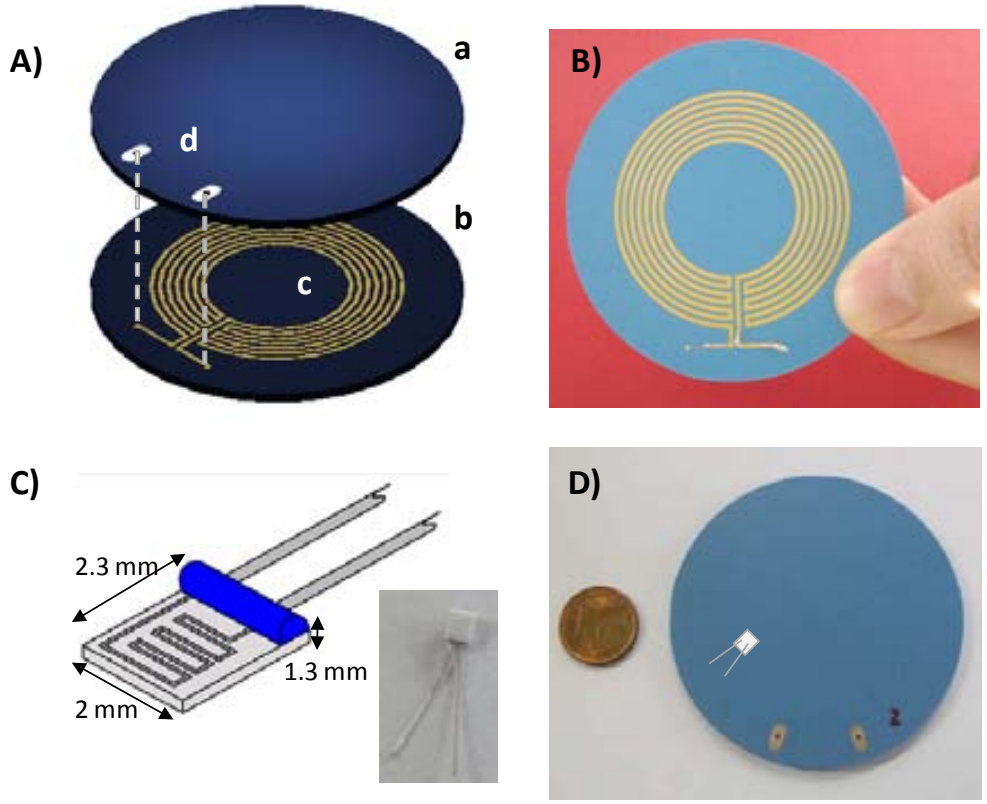

Figure 5.14:
A) Scheme of the thermal platform; a: cover of the heater, b: base where heater was screen-printed, c: embedded gold-based heater, d: paths for external electronic control. **B)** Image of the screen printed resistor. **C)** Schematic representation and image from the PT100 sensor. **D)** Image of the final thermal platform (**TM3**).

5.2.3.1 ELECTRONICS FOR TEMPERATURE CONTROL

Since temperature level and distribution are crucial parameters to be considered for a proper synthesis of nanoparticles, a dedicated temperature controller with a digital proportional-integral-derivative (PID) topology was designed in the research group, which was implemeted on a PIC18F4431 microcontroller. A personal computer was applied as a user interface for monitoring purposes. A PCB for temperature control was separately fabricated to avoid any damage due to the high temperatures at which the thermal module operates. A block diagram of the electronics involving the digital PID control is shown in figure 5.15. Temperature is measured with the PT100 sensor, whose signal is conditioned through a signal conditioning circuit (SCC), which kepts current at a constant value in accordance to the PT100 datasheet. In this way, interference with temperature measurements due to self-heating can be avoided. The SCC provides a potential directly related to the resistive changes produced in the PT100 as a consequence of temperature. The signal provided by the SCC is applied to the analog to digital converter integrated in the PIC microcontroller as a feedback to the digital PID control system. This signal is traduced to temperature according to the equation corresponding to class A PT100 sensors, which is included in the microcontroller software: $t \geq 0°C$, $R(t) = R0 \cdot (1 + A \cdot t + B \cdot t^2)$, where: A = $3.9083 \cdot 10^{-3}$ ºC^{-1}, B = $-5.775 \cdot 10^{-7}$ ºC^{-1}, R_0 = 100 Ω. The feedback signal is used

to estimate the error and to correct it using the differential equations programmed in the digital PID control. The control signal produced by the PID is amplified and applied to the gold-based resistor through a MOSFET (metal oxide semiconductor field effect transistor). The thermal platform was configured to work at different temperature levels, from 180 to 300 ºC.

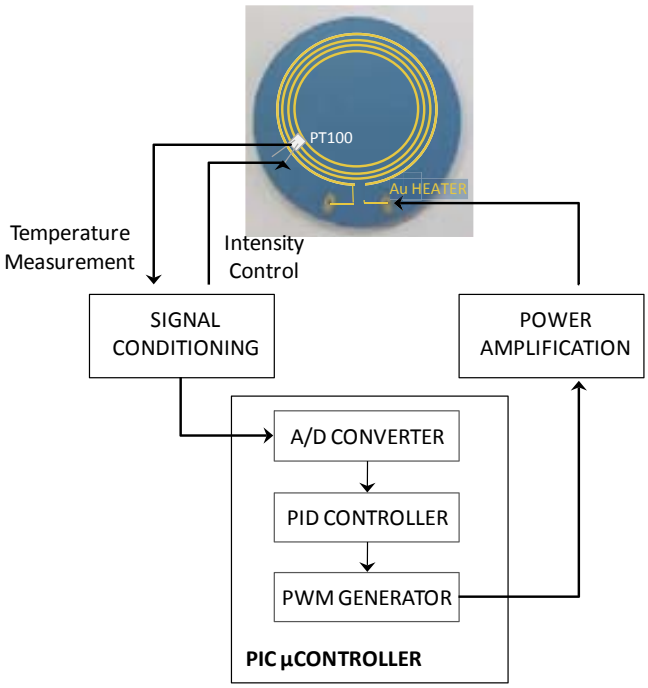

Figure 5.15: Block diagram of the electronics developed for a precise digital PID temperature control.

In figure 5.16 is shown an example of the temperature response. As it can be observed, a highly stable temperature profile is always obtained, with small variations in the order of ± 0.5 ºC. The system takes about ten minutes to stabilize before reaching a steady state at the desired temperature. Slow temperature transitions during stabilization were preferred in order to avoid abrupt thermal changes.

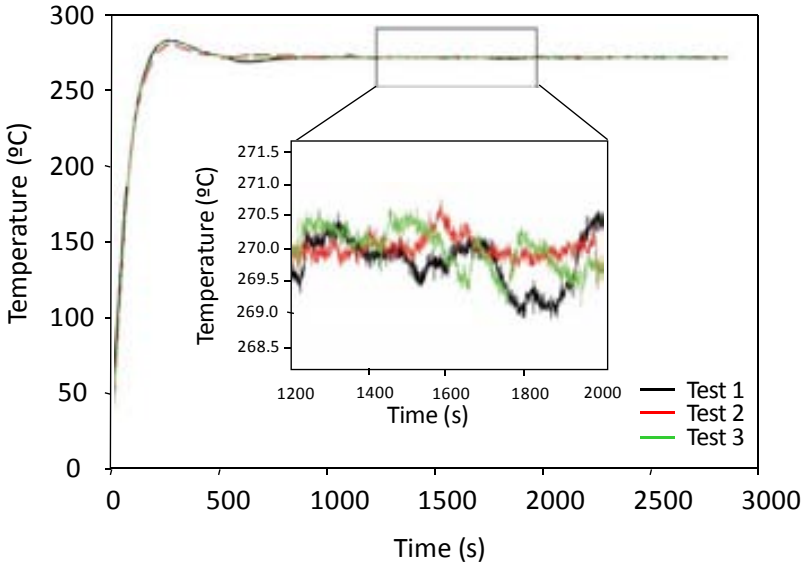

Figure 5.16: System responses obtained during three experiments performed at a set-point of 270 ºC, once the PID parameters were optimized.

5.2.4 DEVELOPMENT OF THE MICROFLUIDIC PLATFORM

Due to the final configuration of the gold screen printed resistor, the initial idea of integrating a linear three-dimensional micromixer similar to the previous constructed was neglicted. Actually, the use of micromixers that involve the flown of the liquid at different levels in the z-axis can produce thermal fluctuations on the liquid. Therefore, a bi-dimensional one was preferred for this approach, since it introduces the chaotic mixing profile required while ensuring a more homogeneous temperature profile.

The complete microfluidic platform consisted of eight stacked layers, where the micromixer is embedded (figure 5.17). Its structure includes two inlets for reagents and one outlet through which the synthesized quantum dots are collected. Once reagents are inside the microfluidic platform, they flow around the microreactor through two simple channels before they meet each other downstream. This structure acts as a pre-treatment step for pre-heating reagents before mixing. Then, channels converge in a Y-shape point downstream before getting into a Z-shape bi-dimensional micromixer. A circular configuration for the micromixer was used, making it coincide with the screen printed resistor of the thermal platform, in accordance to the expected radial thermal distribution. Both the pre-treatment channels and the micromixer are located as closer as possible in the z-axis of the heater (seventh layer of the platform) in order to achieve an effective heat transference. The total volume of the platform was of 55 µL.

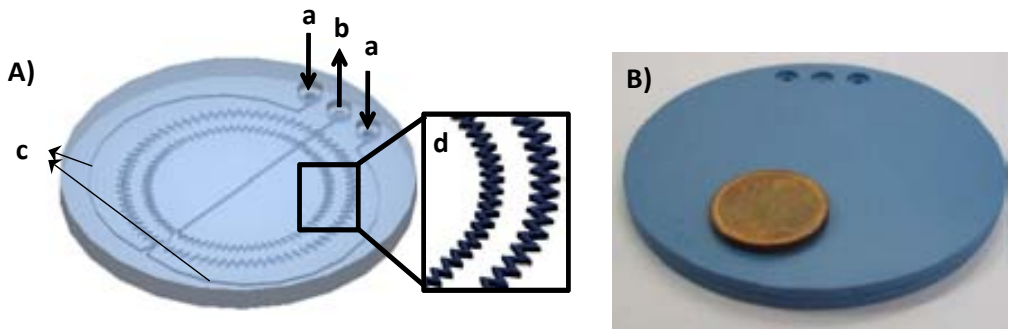

Figure 5.17: Schematic representation (**A**) and photograph (**B**) of the microfluidic platform; a: inlets, b: outlet, c: conditioner channels, d: amplification of a bi-dimensional micromixer.

5.2.5 CHARACTERIZATION OF THE THERMAL AND FLUIDIC PLATFORMS OF THE MICROREACTOR

The complete microreactor for the high temperature synthesis of quantum dots is composed of both the thermal and the microfluidic platforms previously described. Two different approaches has been taken into account: the monolithic and the modular configuration of the microreactor. The first one consist on the contruction of both platforms in a sigle device, which normally conffers more confident results. The second offers the possibility of replacing one of the modules without rebuilding the complete device if

different reaction conditions are required or in case of malfunction of one of the platforms. In the case of the modular configuration, a proper alignment between both platforms is mandatory to achieve a more uniform heat distribution on the xy plane of the microchannel. Therefore, their mechanical attachment must be carefully done.

In order to characterize the hydrodynamic and thermal performance of both approaches, four devices were designed and fabricated: a modular thermal platform, a modular microfluidic platform, a modular microfluidic platform with exposed channels and a monolithic system with both platforms integrated in the same unit.

5.2.5.1 THERMAL CHARACTERIZATION OF THE MICROREACTOR

With the aim of evaluating the thermal distribution of the monolithic and the modular configurations, and studying the possible diffences between them, a EMC scanner with an IR Probe was used, which allows obtaining the corresponding isothermal maps of each ceramic device. All the evaluation procedures were performed at 270 ºC.

- **MODULAR CONFIGURATION**

An isothermal map from both sides of the single modular thermal platform was initially done. As expected, both maps were highly similar, since the heat transfer is equal above and below the module due to the resistor is located in its central ceramic layer. Figure 5.18 shows one of the isothermal maps obtained, coupled to a picture of the experimental set-up used during this experiment, where a radial and uniform heat distribution in the xy plane is obtained over the thermal platform.

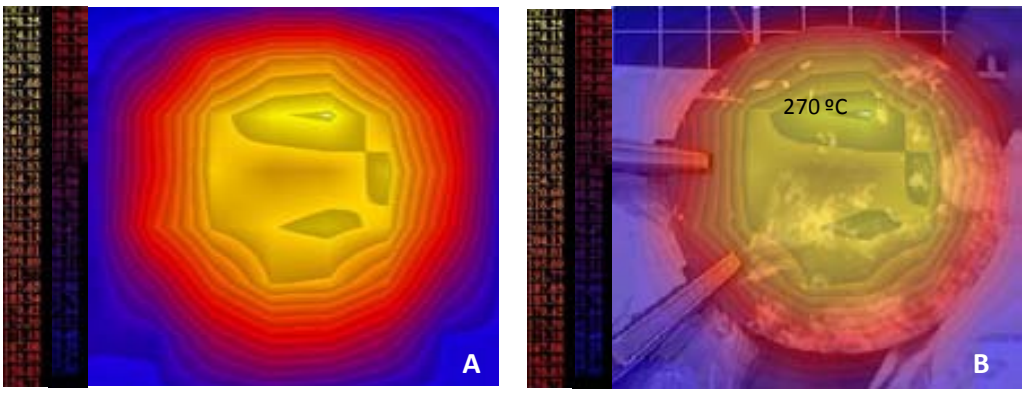

Figure 5.18: **A)** Isothermal map obtained on the surface of the modular thermal platform. **B)** Isothermal map of the modular thermal platform overlapped to a picture of the experimental set-up. A punctual temperature measurement in the zone of the sensor is indicated.

Besides, punctual measurements at the top and the bottom of the device were carried out at the zone where the temperature sensor was placed in order to study the z-axis thermal distribution. Both measurements corresponded to the

predefined set point: 270 ºC. Therefore, an efficient thermal distribution over the z-axis can be assumed.

Then, the modular microfluidic platform was mechanically coupled, taking care on obtaining the highest surface contact to achieve an optimum heat transfer between them. A radial distribution over the region corresponding to the placement of the microchannels (orange dashed lines in figure 5.19A) inside the microfluidic platform was obtained, assuring a xy uniform thermal distribution.

The thermal gradient in the z-axis was determined by punctual measurements performed on both sides of the microsystem, achieving 270 ºC and 255 ºC on the thermal and microfluidic platforms, respectively. This difference can be related not only to the thermal dissipation of heat along the different layers, but also to the presence of an air gap at the coupling region, which can be minimized using a thermal conductive paste among the surface in contact. The diagram presented in figure 5.19B allows estimating the temperature inside the embedded microfluidic channel. A temperature gradient of about 1.8 ºC per layer can be calculated. Therefore, a temperature of 268.2 ºC is assumed inside the microfluidic channel, pretty close to the desired temperature predefined as set point (270 ºC).

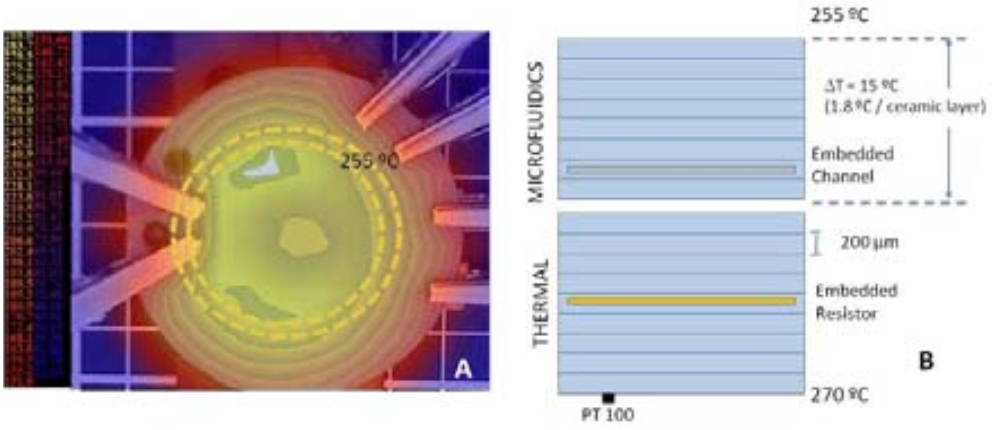

Figure 5.19: **A)** Isothermal map obtained on the surface of the modular microfluidic platform coupled to the thermal one. A punctual temperature measurement in the zone of the sensor is indicated. **B)** Schematic diagram of the temperature analysis developed to estimate temperature inside the microfluidic channel.

▪ MONOLITHIC CONFIGURATION

The thermal characterization of the monolithic configuration was performed similarly to the previous modular. Isothermal maps obtained from both sides of the microreactor using the IR probe revealed an equivalent radial and uniform heat distribution in the xy plane, as it can be observed in figure 5.20. Again, punctual measurements in the top and bottom of the microreactor in the regions corresponding to the sensor position were performed. Temperatures of 260 ºC and 270 ºC were obtained for the microfluidic and heating systems (top and bottom), respectively. A temperature gradient of 1.2 ºC / layer for the z-axis can be obtained taking into account the same diagram used in the modular approach. Therefore, a temperature of 268.8 ºC is estimated inside the microchannel. The smaller temperature gradient obtained in this case is probably due to the

elimination of the air gap between platforms, which favors the heat transfer since no additional interface is introduced.

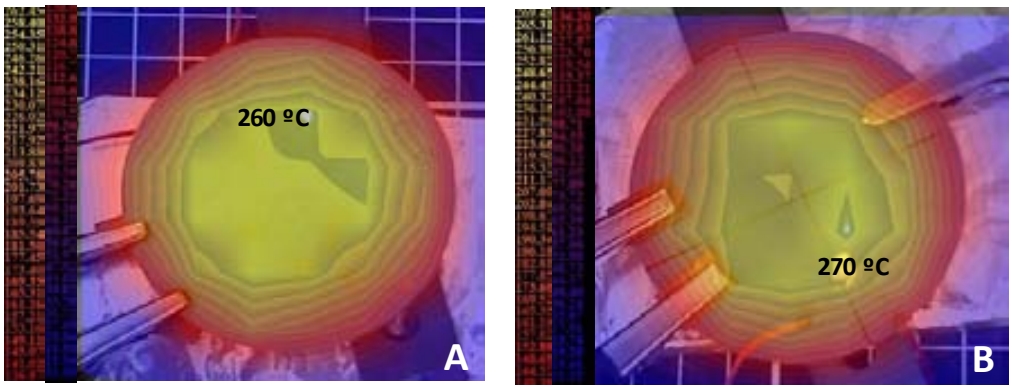

Figure 5.20: Isothermal maps obtained on the top (**A**) and the bottom (**B**) of the monolithic microsystem. Punctual temperature measurements in the sensor zone are indicated.

Nevertheless, form the obtained results it can be concluded that, using either of both configurations, reagents are exposed to specific, uniform and controlled temperature levels provided by the thermal platform during their flow through.

5.2.5.2 FLUIDIC CHARACTERIZATION OF THE MICROREACTOR

In order to perform a qualitative visual characterization of the fluidics/hydrodynamics of the microreactor, a new modular microfluidic platform, identical to that previously presented, was constructed, but leaving half of its structure open to air. Once sinterized, the open area was covered with a polymeric foil, ensuring its hermetic sealing but permitting its inner visualization. An image of the microfluidic platform constructed is shown in figure 5.21A.

The qualitative visual characterization of the mixing efficiency of the microfluidic structure embedded in the microreactor was performed by means of a stereo microscope. The experiment consisted on mixing two different dyes (phenol red and methylene blue, both 1 mM and propelled by syringe pumps at 60 µL min^{-1}) along the bi-dimensional micromixer. Different zones of the micromixer were selected to evaluate the mixing efficiency, marked in figure 5.21 A and B. Low and high magnification pictures were taken at the indicated regions, shown in figure 5.21C, which allows visualizing the mixing process through the microreactor. As it can be observed, at the beginning of the micromixer both dyes are clearly differentiated. As reagents advances, the laminar flow profile disappears, showing an almost homogeneous coloration at the zone enclosed by frame 5 (first turn of the micromixer). At the sixth box, a complete homogeneous mixture can be observed, which makes clear the efficiency provided by the micromixer embedded into the LTCC microreactor.

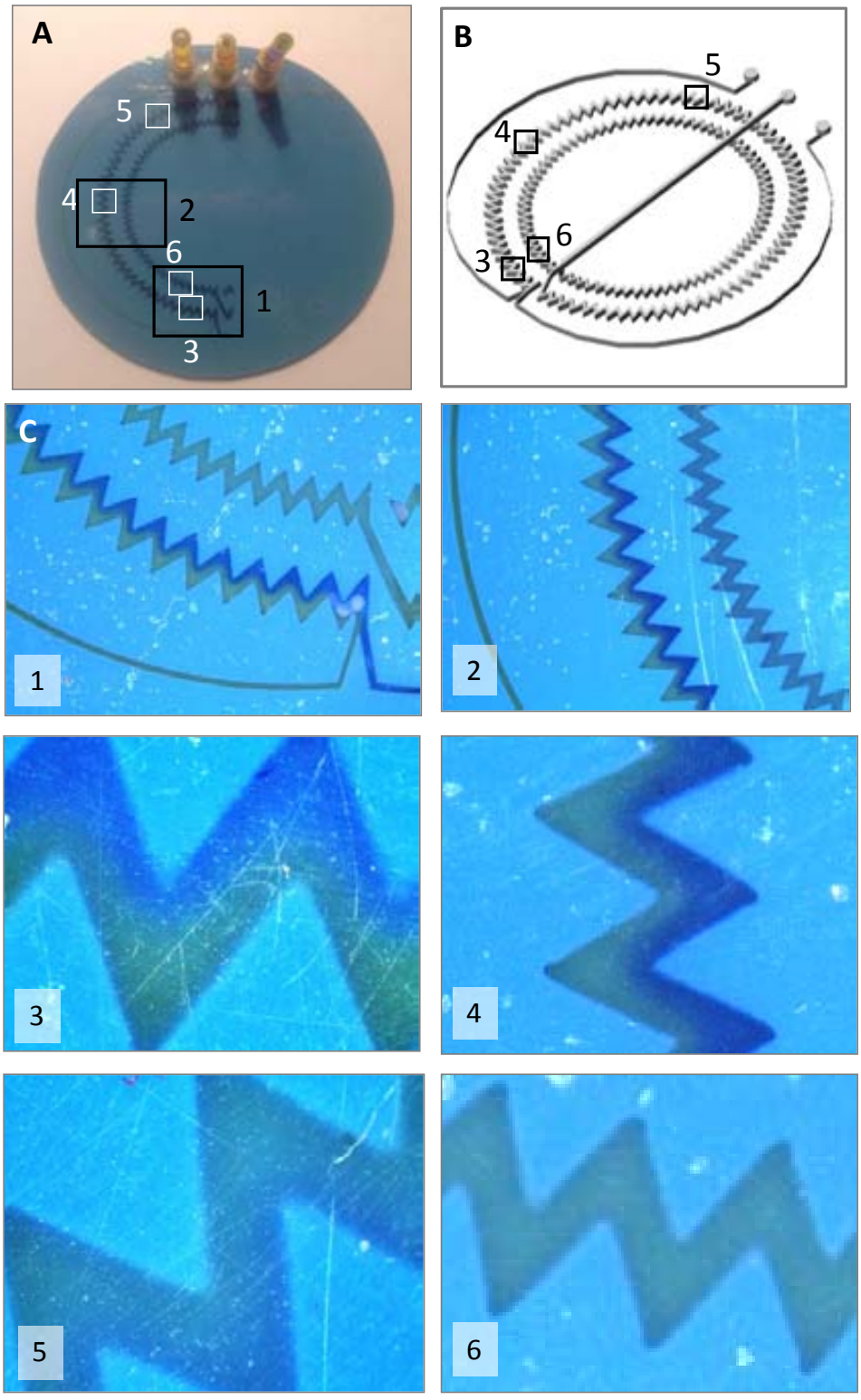

Figure 5.21: Fluidic/hydrodynamic qualitative visual characterization of the microfluidic system. **A)** Picture of the open to air microfluidic platform covered with a polymeric foil. **B)** Three-dimensional inner view of the microfluidic platform. **C)** Photographs corresponding to frames at different points of the micromixer.

5.2.6 SYNTHESIS OF NANOCRYSTALS

Once tested the performance of the thermal and fluidic platforms, the modular microreactor was employed for the synthesis of CdSe quantum dots. As previously stated, the chosen reaction was a modification of the Peng's

procedure based on cadmium oxide, selenium powder and the triple ligand of TOPO, OA and OLA. Therefore, the procedure uses the trioctylphosphine-selenium (TOPSe) / trioctylphosphine oxide-cadmium (TOPOCd) system.[12-13] The use of this modified procedure provides some advantages, since it employs stable and less hazardous reagents and does not require an inert environment. Specifically, TOPO is capable to reduce the reaction time of the synthesis by maintaining a good reproducibility.[14-15] By using TOPO and OA it is possible to passivate the more reactant sites of the nanocrystals, obtaining as a result more homogeneous QDs with higher QYs. [16-17] Besides, the employment of OLA has show to reduce the temperature necessary for synthesizing bigger nanocrystals.[18-19] The employment of octadecene (ODE) as non-coordinating solvent was preferred due to its high boiling point (320 ºC), low toxicity and low reactivity with precursors. The molar relationship of all these reagents is one of the factors that determine the final size of nanocrystals. Thus, different molar ratios has been tested at different temperatures, including 1:10, 1:1 and 1:2 molar ratios of Cd:Se, in order to obtain a set of nanocrystals with different optical properties. For instance, the use of the first molar ratio should provide the smallest nanoparticles (lower absorption and emission wavelengths), since cadmium precursor is rapidly consumed by the excess of selenium of the medium.[20]

As in all microfluidic systems, it is necessary an optimization of the hydrodynamic parameters. However, some conclusions from related works were taken into account, [21-22] and therefore, only a basic study regarding flow rates and residence time, which are closely related, was performed. As a matter of fact, the use of large residence times entails an uncontrolled growth of nanocrystals, producing a wider size distribution of quantum dots, while short times normally generates the uncompleted formation of the colloid.[22] A flow rate of 60 µL min^{-1} with a microreactor volume of 55 µL were finally selected to carry out the following syntheses. Therefore, the residence time of reagents inside the microreactor is of approximately 28 s.

---

[12] Nakamura, H.; Yamaguchi, Y.; Mikazaki, M.; Maeda, H.; Uehara, M.; Mulvaney, P.; *Chem. Commun*, **2002**, *23*, 2844.
[13] Chan, E.M.; Alivisatos, A.P.; Mathies, R.A.; *J. Am. Chem. Soc.,* **2005**, *127*, 13854.
[14] Dai, Q.; Li, D.; Chen, H.; Kan, S.; Li, H.; Gao, S.; Hou, Y.; Liu, B.;Zou, G.; *J. Phys. Chem. B*, **2006**, *110*, 16508.
[15] Yang, H.; Luan, W.; Tu, S.; Wang, Z.M.; *Cryst. Growth Des.,* **2009**, *9*, 1569.
[16] Wu, D.;. Kordesch, M.E.; Patten, P.G.V.; *Chem. Mater.,* **2005,** *17*, 6436.
[17] Luan, W.; Yang, H.; Tu, S.; Wang, Z.; *Nanotechnolology,* **2007**, *18*, 175603.
[18] Zhong, X.; Feng, Y.; Zhang, Y.; *J. Phys. Chem. C,* **2007**, *111*, 526.
[19] Landes, C.; Braun, M.; Burda, C.; El-Sayed, M.A.; *Nano Lett.,* **2001**, *1*, 667.
[20] Yen, B.K.H.; Stott, N.E.; Jensen, K.F.; Bawendi, M.G.; *Adv. Mat.,* **2003**, *15(21),* 1858.
[21] Nakamura, H.; Tashiro, A.; Yamaguchi, Y.; Miyazaki, M.; Watari, T.; Shimizu, H.; Maeda, H.; *Lab Chip,* **2004**, *4(3),* 237.
[22] de Mello, A.J.; *Chem. Phys. Chem*., **2009**, *10*, 2612.

The study of the temperature synthesis in the microreactor was the central focus of this work, since this parameter can also determine the size of nanocrystals. The use of low temperatures cannot allow exceeding the energy barrier for the formation of monomers, while the employment of high temperatures can produce an uncontrolled growth of the seeds. Thus, temperature was varied in the range from 180 ºC to 280 ºC.[23-24] Figure 5.22 shows the recorded spectra and images from the different nanocrystals synthesized with a 1:10 molar ratio of Cd:Se at the described temperature range. A displacement of 48 nm in the fluorescence emission peak was attained between the lower and higher temperature of synthesis of the nanocrystals. In all cases, sharp emission bands with a ~ 50 nm FWHM were obtained, indicating the narrow size distribution of the synthesized QDs.

Nevertheless, an optimum temperature of synthesis can be found, since it is intrinsic on each reaction.[21,23] In this case, it was at 270 ºC, as this value provides the narrowest absorption and emission bands as well as the highest emission intensity. At this temperature, the FWHM was minimal, of *ca.* 40 nm. The complete characterization of this colloid is shown in figure 5.23.

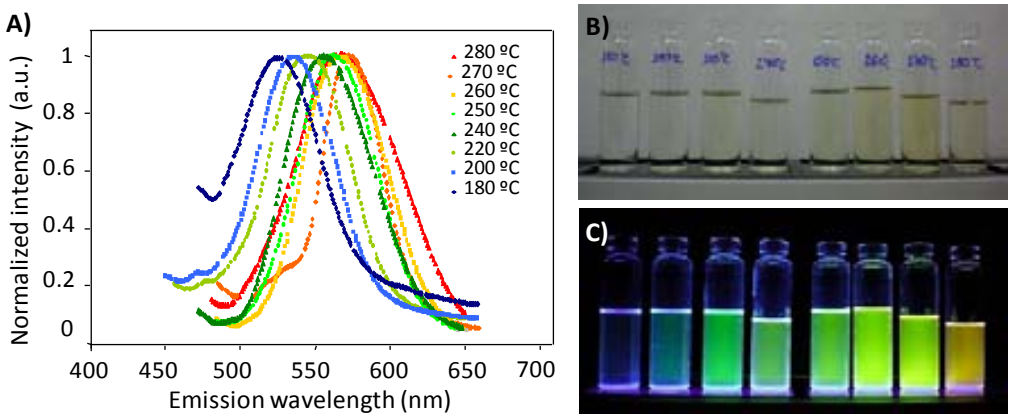

Figure 5.22: **A)** Fluorescence emission spectra of the nanocrystals synthesized in the microreactor from 180 to 280 ºC with a molar ratio of Cd : Se 1 : 10. Images of the obtained QDs colloidal solutions, highly diluted with chloroform (1:50), from the different tested range of temperatures under room (**B**) and UV (**C**) light.

As it can be seen in HRTEM images, homogeneous and well dispersed nanoparticles were synthesized, with an average size of 3.3 ± 0.4 nm. The crystalline structure of the nanoparticles was confirmed by the lattice fringe distance found at 0.215 nm, which reveals the preferential hexagonal growth of CdSe nanocrystals on the (110) plane. Besides, a ring structure on the SAED pattern was observed. Its bright rings can be attributed to (101), (102), (110), (103) (112) and (203) lattice planes of the hexagonal (wurtzite) crystal structure of CdSe.

[23] Yin, Y.; Alivisatos, A.P.; *Nature,* **2005**, *437,* 664.
[24] de Mello C.D.; Liljeroth, P.; Vanmaekelbergh, D.; ***Small,*** 2005, *1,* 1152.

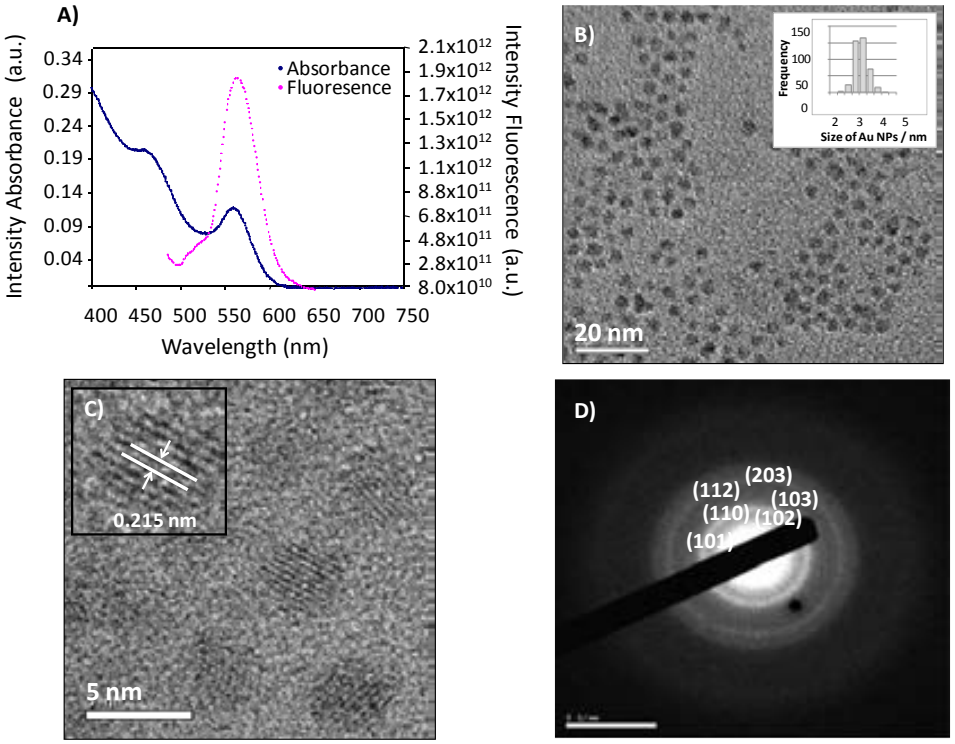

Figure 5.23: Characterization of CdSe nanocrystals synthesized in **MR6** at 270 ºC. **A)** UV-Vis absorption band (blue, 463 nm) and emission fluorescence (pink, 562 nm) spectra. **B)** TEM image and its correspondent histogram. **C)** HRTEM image. **D)** SAED pattern image.

A dependance of fluorescence emission and excitation wavelength, and therefore also of the absorption band, with temperature was observed in all cases for the 1:10 molar ratio of Cd:Se, as it shows figure 5.24A. The value of these parameters increase as raising the temperature of synthesis. As well the maximum fluorescence peaks as the excitation wavelengths followed a positive straight line as increasing temperature. Excitation peaks (absorption maxima) were correlated with the emission maxima obtained for nanocrystals, in agreement with other works.[15,25] On the other hand, large Stokes shifts were obtained (figure 5.24B) for all the synthesis, since almost negligible variation for this parameter were observed (mean value of 103 ± 3.2 nm). Moreover, the determined QYs provided values from 25 to 55 %,[26] making clear the feasibility of the synthesized QDs for analytical applications.

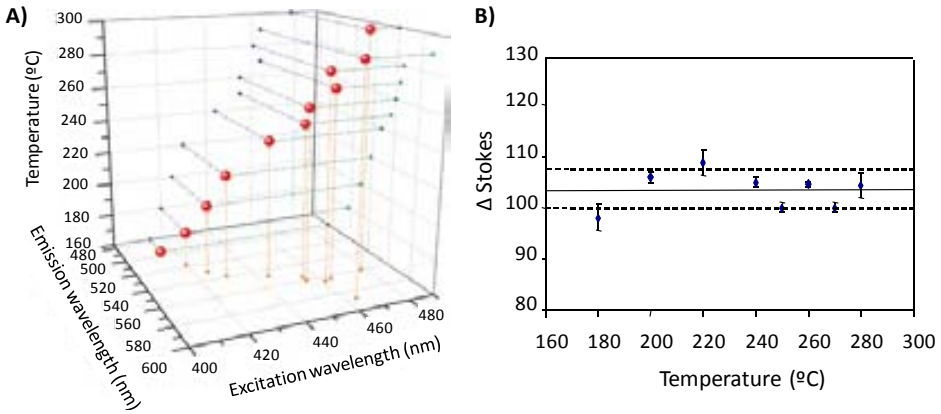

Figure 5.24: Results obtained for the synthesis of QDs in **MR6** with a 1:10 molar ratio of Cd:Se. **A)** Correlation between fluorescence emission peaks, excitation wavelengths and the different temperatures tested. **B)** Stokes shifts with the mean value and the standard deviation represented.

[25] Toyota, A.; Nakamura, H.; Ozoco, H.; Yamashita, K.; Uehara, U.; Maeda, H.; J. *Phys. Chem. C,* **2010**, *114*, 7527.
[26] Drushel, H.V.; Sommers A.L.; Cox, R. C.; *Anal. Chem.,* **1963,** *35*, 2166.

The synthesis of QDs with 1:1 and 2:1 molar ratios of Cd:Se were performed almost at the same range of temperatures. On the one hand, the syntheses carried out with the 1:1 molar ratio showed equivalent behavior as the previous observed for 1:10 molar relationship. Thus, as raising the temperature of synthesis, the absorption and emission peaks increased maintaining constant Stokes shifts. However, above 240 ºC both bands remained constant although temperature was raised (Figure 5.25A and B). This is probably due to that selenium reagent hinders the formation of higher nanocrystals for its low amounts present in the medium. Nevertheless, FWHM of ~ 50 nm were calculated, which demonstrates the narrow size distribution of nanocrystals obtained. An example of the nanocrystals obtained in these syntheses (above 240 ºC) is shown in figure 5.25C and D.

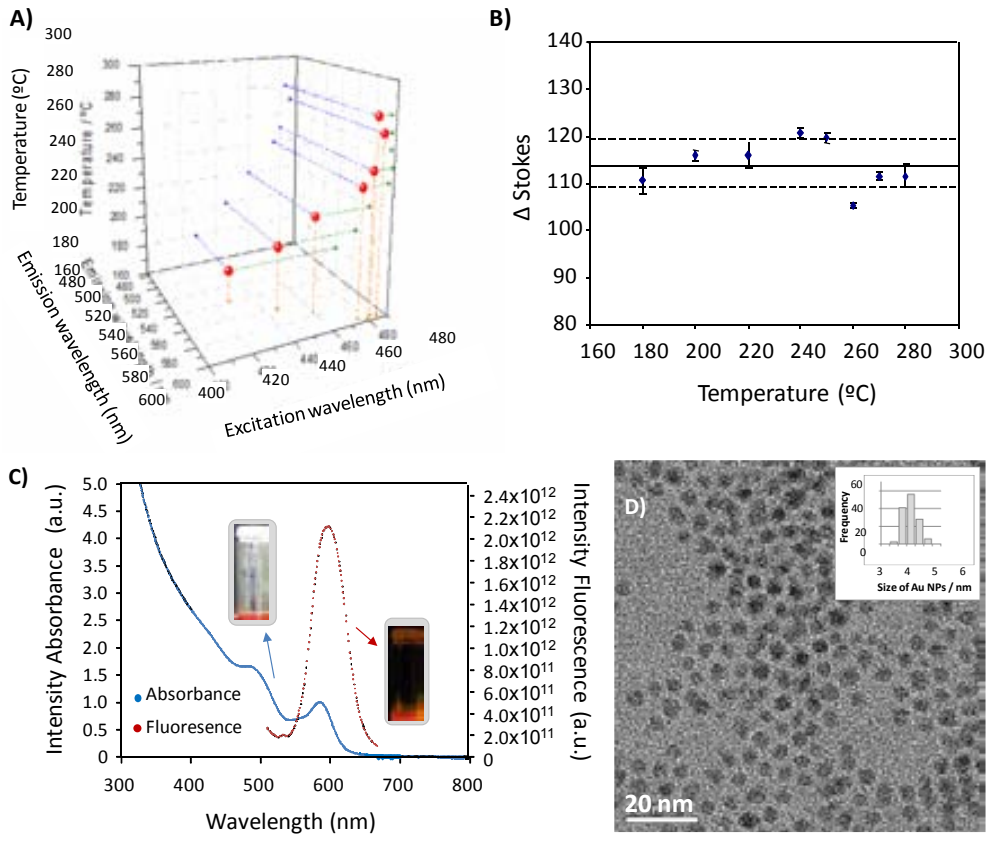

Figure 5.25: Results obtained for the synthesis of QDs in **MR6** with a 1:1 molar ratio of Cd:Se. **A)** Correlation between fluorescence emission peaks, excitation wavelengths and the different temperatures tested. **B)** Stokes shifts. Mean value of 114 ± 4.3 nm. **C** and **D)** UV-Vis absorption band (blue, 485 nm), emission fluorescence (red, 596 nm) spectra and TEM image with its correspondent histogram of 4.4 ± 0.6 nm QDs synthesized at 270ºC.

On the other hand, the use of a 2:1 molar ratio generated almost the same QDs, since the absorption and emission peaks, Stokes shifts and quantum yields obtained were practically the same in all synthesis performed from 200 to 270 ^{o}C (Figure 5.26). Actually, the synthesis of CdSe nanocrystals at 200 ºC with 2:1 molar ratio generated larger nanoparticles than the obtained with the 1:10 molar relationship. From these results, it can be concluded that there exist a temperature threshold for each molar ratio, from which no larger particles can be formed, although raising the temperature, because there is a

lack of selenium. Besides, increasing the molar ratio of Cd:Se, larger nanocrystals can be obtained at the same temperature. A comparative graphic of the three molar ratios of Cd:Se tested is shown in figure 5. 27.

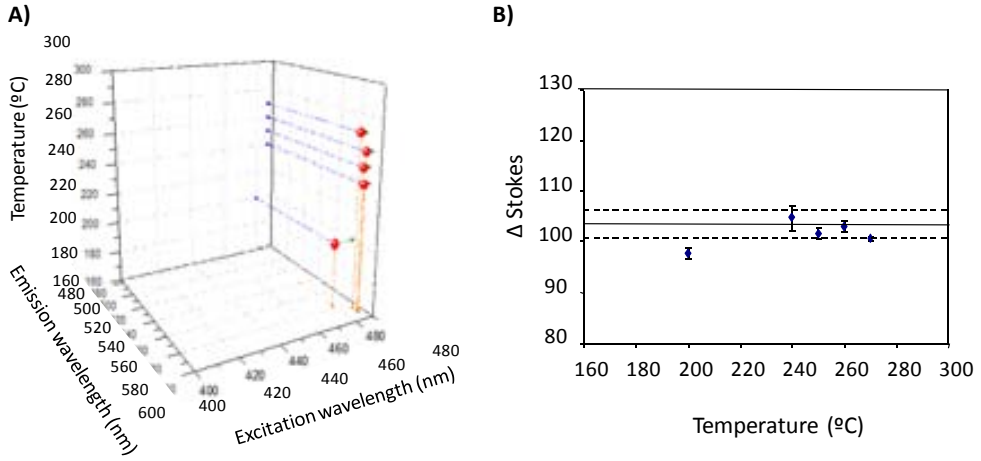

Figure 5.26: Correlation between fluorescence emission peaks, excitation wavelengths and temperatures for QDs synthesis (**A**) and Stokes shifts (mean value of 103 ± 2.5 nm) (**B**) for a 2:1 molar ratio of Cd:Se.

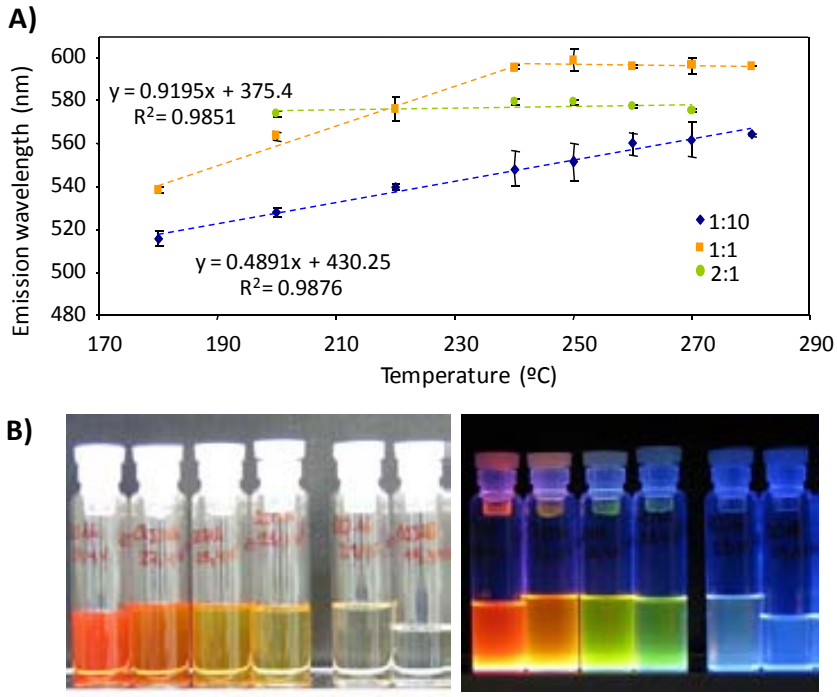

Figure 5.27: **A)** Maximum intensity of fluorescence emission peaks obtained for the three different tested Cd:Se molar ratios 1:10, 1:1 and 2:1 with the error bars. **B)** Images under room (left) and UV (right) light of the wide range of QDs synthesized with the different molar ratios and temperatures tested.

5.2.7 CONCLUSIONS

This section has described the development of a microreactor, which integrates both the microfluidics and a thermally controlled platform, for the high temperature synthesis CdSe quantum dots (**MR6**). The thermal platform has been based on a screen-printed gold-based heater, since it has been taking advantage from the compatibility of the LTCC technology with screen printing techniques, and a commercial platinum sensor. An external electronic control set-up for the strict managing of the temperature has been also implemented, which allow the

working of the platform from 180 to 300 ºC. The microfluidic platform has been based on a bi-dimensional micromixer disposed in a circular configuration, making it coincide with the gold resistor of the thermal platform in order to achieve an effective and uniform heat transfer.

The performance of the monolithic and the modular configurations have been tested. In both cases, the characterization of the thermal device has shown a radial thermal distribution of the temperature with a highly stable temperature profile (± 0.5 ºC), with minimal differences regarding the z-axis temperature transfer. Besides, the micromixer has shown its performance for reagents mixture during its characterization while ensuring a homogeneous temperature profile.

The synthesis of tunable size-dependent quantum dots has been successfully carried out by means of the designed and constructed modular microreactor. Reproducible, uniform and stable CdSe nanocrystals have been obtained in all cases. Moreover, the narrow size distribution of the synthesized QDs confirms the uniform temperature profile applied for each synthesis process.

The use of the monolithic approach confers more confident results and a higher integration level, while the modular increases the system reliability, offering the possibility of replacing one of the modules without rebuilding the complete device. Nevertheless, it can be stated from the obtained results that negligible differences can be observed using either of them, since in both cases reagents are exposed to specific, uniform and controlled temperature levels provided by the thermal platform during their flow through the microfluidic channels.

5.3 MICROREACTOR FOR THE SYNTHESIS OF CARBON DOTS (MR7)

This section is focused on the development of a microreactor for the synthesis of uniform and reproducible carbon dots (Cdots), since these nanoparticles present excellent luminescent properties and elevated biocompatibility, which is of special interest for bioanalytical applications. From the different synthetic procedures for obtaining Cdots, the chemical thermal decomposition of molecular precursors is the most usual due to their simplicity and low cost.[27] Thus, this approach has been preferred. As in the case of CdSe nanocrystals synthesis, a strict control of the temperature is critical for obtaining well dispersed and uniform nanoparticles due to it is one of the parameters which determine their final optical properties.

[27] Salinas-Castillo, A.; Ariza-Avidad, M.; Pritz, C.; Camprubí-Robles, M.; Fernández, B.; Ruedas-Rama, M.J.; Megía-Fernández, A.; Lapresta-Fernández, A.; Santoyo-Gonzalez, F.; Schrott-Fischer, A.; Capitan-Vallvey, L.F.*; Chem. Commun.*, **2013**, *49*, 1103.

The development of this microreactor has been based on the ceramic device **MR6**, since the synthetic procedure used for QDs synthesis has similar requirements to the one for Cdots. In this case, only a modular approach has been designed, constructed and tested (**MR7**) due to it confers versatility while also generating well-controlled and reproducible nanoparticles, as previously seen. Actually, the heating platform has been basically the same, consisting on a screen printed gold resistor and a platinum sensor. The microfluidic platform only has consisted of an inlet channel and a bi-dimensional micromixer to ensure a confident and homogeneous temperature profile, since only one reagent solution is used.

5.3.1 MATERIALS, REAGENTS AND METHODS

Table 5.6 shows the instruments and equipments used for the synthesis and characterization of Cdots.

Table 5.6: General list of equipments and instruments used in the synthesis of Cdots.

EQUIPMENT	PROVIDER
• 1 syringes pumps, 540060 TSE systems	TSE systems, Bad Homburg, Germany
• 1 syringes of 10 mL, GASTIGHT 1000 TLL series	Hamilton, Bonaduz, GR, Switzerland
• User-friendly connection system	GSB
• Conical PTFE connectors (Cones 1.6 mm)	Omnifit, Cambridge, UK
• Tygon tube (i.d. 1.2 mm)	Ismatec, Zurich, Switzerland
• PTFE tubes (i.d. 0.8 mm)	Techny Fluor, Barcelona, Spain
• PIC18F 4431 microcontroller	Microchip Inc., USA
• DuPont 5742 Au co-fireable conductive paste	Dupont™, Germany
• DuPont 6141 Ag co-fireable conductive paste	Dupont™, Germany
• Class A PT100 sensor	Innovative Sensor Technology, Switzerland
• Power supply	Blausonic, Hospitalet, Spain
• Multimeter	Fluke 179 Multimeter, Everett, USA
• Varian Cary Eclipse Spectrofluorometer	Varian Ibérica, Madrid, Spain
• Fluorolog® Modular Spectrofluorometer	Horiba, Jobin Yvon, Kyoto, Japan
• High Resolution Transmission Electron Microscopy (HRTEM) JEOL 2011	JEOL, Tokyo, Japan
• ThermoNicolet IR200FTIR	Thermo Fisher Scientific Inc.,Madrid, Spain
• Zetasizer Nano ZS90	Malvern, Worcestershire, U.K
• Crison pH meter, model Basic 20	Crison Instruments, Barcelona, Spain

The co-fireable gold conductive paste is used to screen printing the resistor and the silver one for *vias* filling, while the PT100 sensor is used for the temperature measurements. Epoxy (EPO-TEK® H20E) is used to glue the 100 PT sensor over the surface ceramic device. The PIC18F4431 microcontroller is used to implement

the digital PID control system. Optical properties of the nanoparticles are obtained using the spectrofluorometers. ζ potential and DLS measurements are carried out on the Zetasizer Nano ZS90. XRD are performed at the Centre of Scientific Instrumentation (University of Granada, Spain) on a Fisons-Carlo Erba analyzer model EA 1108. The FTIR spectra on powdered samples are recorded with a IR200FTIR by using KBr pellets. The shape and dimensions of the core of the particles are measured by a HRTEM. The pH meter is used for pH measurements.

For the synthesis of Cdots, ascorbic acid is chosen as a simple and low cost source of carbon, and DMSO is preferred as solvent due to the high temperatures that this compound can bear (table 5.7).

REAGENT	PROVIDER
• Ascorbic acid	99 %, Panreac
• Dimethyl sulfoxide (DMSO)	Baker Chemical, 0.3 % water
• Quinine sulphate	Reference Standard, Fluka

Table 5.7: Reagents used for the synthesis of Cdots.

Previous to characterization, the synthesized Cdots are dialyzed against Milli-Q water using spectra/pro dialysis membrane with cut-off of 1 KDa for their purification. Quinine sulphate in water is used to determine the fluorescence quantum yield (Φf or QY) of the nanocrystals as described in the 5.1.1 section.

5.3.2 EXPERIMENTAL SET-UP

The synthesis of carbon dots (**MR7**) is carried out using the experimental set-up schematized in figure 5.28. Again, the set-up that involves the fluidic components is composed of a syringe placed in a syringe pump for dispensing the reagent solution, PTFE tubes for connecting the microfluidic platform and the syringe, o-rings to seal the system and the home-made piece to simplify the connection of the microfluidic platform and the tubes. The heating and temperature control set-up requires of a power supply connected to the developed electronic circuit and to the ceramic thermal module, placed just below the microfluidic platform. A multimeter is used to ensure the sensor intensity and to close the circuit. As for the synthesis of quantum dots, alligator clips are used to connect the electrical circuit with the screen printed paths of the thermal platform. All the system is computer controlled.

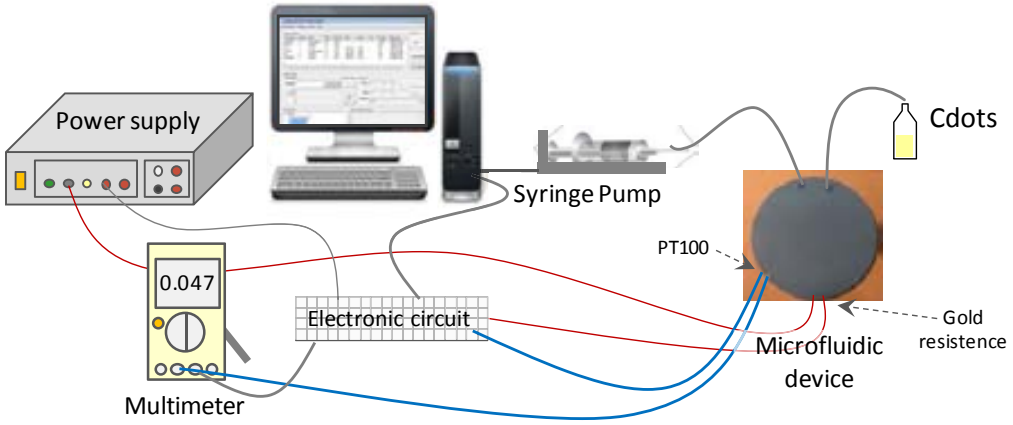

Figure 5.28: Schematic representation of the experimental set-up used for the synthesis of carbon dots using **MR7**.

5.3.3 DEVELOPMENT OF THE MICROREACTOR

The microreactor used for the synthesis of Cdots was based in two separate ceramic modules, one for the microfluidics and another for the heating and temperature control. On the one hand, the thermal platform used was basically the same as the described for the synthesis of CdSe quantum dots. Therefore, the module was a ceramic platform where seven laps in radial configuration of a gold-based screen printed conductor were embedded, acting as the resistor. This time, only 7 LTCC layers of the substrate material were required, since it confers the necessary robustness for the temperatures used in the synthesis of carbon dots. As before, the resistor was constructed in the central layer of the platform to achieve a uniform and equal heat transfer at both sides of the thermal module. External paths were also screen printed on the top layer of the platform to connect the heater to the electronic control set-up. A class A PT100 temperature sensor was employed for the control of the temperature, which was also glue in the bottom of the heating module by means of epoxy, making it coincide with the heater zone. The necessary electronics for controlling the system was adequate to the conditions required for this synthesis. Thus, the thermal platform was configured to work from 140 to 240 ºC. On the other hand, the fluidic platform was composed of one inlet for the entrance of reagents, a Z-shape channel to increase the residence time of reagents inside the microreactor and allow their thermal conditioning, and an outlet for Cdots evacuation (total volume of 48 µL). Again, the Z-shape channel was constructed in one layer of the ceramic substrate and in a circular shape, making it coincide with the resistance of the heating module, to achieve a uniform thermal distribution. Both modules were mechanically attached taking care of obtaining the best contact between them. A schematic representation and an image of the complete microreactor are shown in figure 5.29.

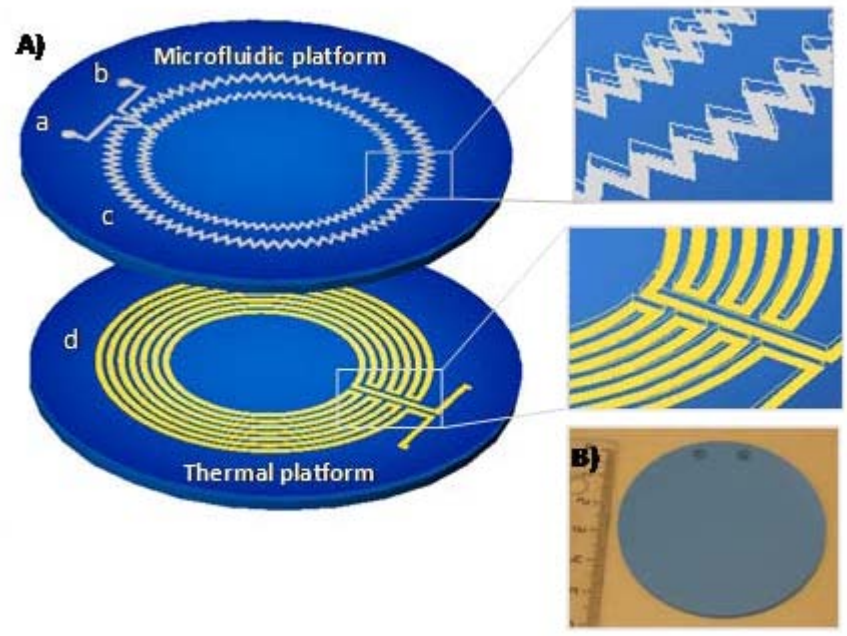

Figure 5.29: **A)** Scheme and of the microreactor **MR7**. Both thermal and the microfluidic platforms are indicated. a: inlet, b: outlet, c: bi-dimensional micromixer, d: embedded screen printed gold-based heater. The side boxes show an amplification of the micromixer and resistor. **B)** Photograph of the microreactor.

5.3.4 SYNTHESIS OF CARBON DOTS

Ascorbic acid was chosen as a simple and low cost carbon source for synthesizing Cdots by thermal decomposition in the described microreactor, while DMSO was preferred as solvent due to the high temperatures that this compound can bear. An optimization of certain reaction parameters of the microsystem was required, since no system addressed to the synthesis of Cdots had been developed until that date. The optimized values were determined as a function of the maximum fluorescence intensity recorded with a spectrofluorometer. The first parameter studied was the reaction temperature due to the importance of this factor in thermal decomposition approaches. Thus, the use of 180, 190, 195, 200, 210 and 240 ºC were evaluated, since ascorbic acid has a melting point of 188 ºC. A weak fluorescence was observed when synthesizing Cdots at 180 ºC, indicating the poor formation of the nanoparticles under the ascorbic acid melting point. Nevertheless, syntheses performed from 190 to 240 ºC showed strong fluorescence intensities at 420 nm, remaining practically constant for all the temperature range, as it can be noticed in figure 5.30. The small differences observed were probably due to generation of gaseous species such as SO_2 from DMSO decomposition (boiling point of 189 ºC).[28] Thus, 190 ºC was selected as optimized temperature value. Then, four different concentrations of ascorbic acid, corresponding to 0.1, 0.2, 0.3 and 0.4 mg mL^{-1}, were tested at the optimized temperature reaction. A middle concentration of 0.2 mg mL^{-1} generated the more intense emission fluorescence, being selected for the subsequent syntheses.

Finally, diverse flow rates were evaluated (5, 10, 20, 40, 60 and 80 µL min^{-1}). The higher fluorescence intensity was attained by using the slowest flow rate, since it

[28] Thyrion, F.C.; Debecker, G.; *Int. J. Chem. Kinet.,* **1973**, *5,* 583.

confers the higher reaction time. However, 10 µL min^{-1} was preferred as optimized flow rate due to this value provides almost the same intensity fluorescence while generating more amounts of Cdots. Therefore, the residence time of the reagent inside the microreactor is of approximately 5 min. A graphic concerning the whole optimization is shown in figure 5.30.

The carbon colloid synthesized in the ceramic microreactor at the optimized conditions was dialyzed against water and characterized using different techniques (figure 5.31). On the one hand, the colloid exhibited an intense blue luminescence under a common UV lamp (λ_{exc} = 365 nm), with an emission peak centered at 420 nm when excited at 325 nm. Interestingly, the nanoparticles also showed good upconversion emission fluorescence under NIR excitation sources, concretely a band located at 505 nm when excited at 850 nm. The quantum yield calculated was of 2.6 %, which is in comparable to other works.

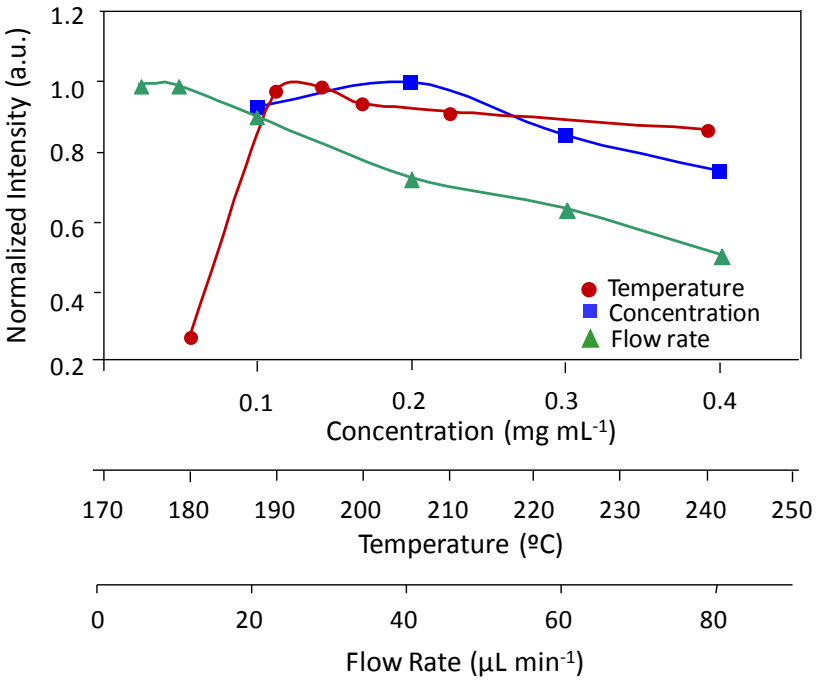

Figure 5.30: Optimization of the chemical and hydrodynamic parameters for the synthesis of Cdots in the ceramic microfluidic system (λ_{exc}= 325 nm, λ_{em}= 420 nm). Temperature optimization was done with a 0.1 mg mL^{-1} of ascorbic acid solution pumped at 20 µL min^{-1}; concentration tests were performed at 190 ºC at a 20 µL min^{-1} flow rate; and the flow rate study was carried out at 190 ºC with a 0.2 mg mL^{-1} of ascorbic acid solution.

On the other hand, the use of microscopic techniques revealed monodisperse and spherical nanoparticles with an average size of 3.3 ± 0.3 nm. Images obtained by HRTEM confirmed the crystallinity of the Cdots synthesized, which was also probed by the clear rings of the SAED pattern, attributed to the (100) and (102) lattice planes of graphite. The 0.18 nm spacing found in HRTEM images was also consistent with the (102) diffraction plane of sp^2 graphitic carbon. X-ray diffraction (XRD) pattern displayed a broad diffraction peak at 2Φ = 20.5 º. Besides, fourier transform infrared spectroscopy (FTIR) spectrum of nanoparticles exhibited bands located at 3400, 1780 and 1622 cm^{-1}, typical from stretching vibrations of O-H, ester groups and C=O, respectively. The presence of carboxyl groups on the surface of the nanoparticles was also confirmed by the different

values obtained of ζ potential when carrying out the characterization at acid (8 mV) and basic (-14 mV) pH values.

The intense fluorescence and upconversion properties of the uniform and stable Cdots synthesized in **MR7** suggest that these particles can be used in biological applications as well as in the development of sensors for environmental applications. As a matter of fact, these optical properties are directly related to their surface passivation level (carboxylic/carbonyl moieties at their surface). Thus, the presence of pH-dependant molecules, including carboxylic groups, may vary the fluorescence intensity of the colloid, such as in Cdots herein synthesized. Results concerning these experiments are not shown in the present manuscript due to this work was developed by the department of analytical chemistry of the University of Granada. Nevertheless, it has to be remarked that the obtained Cdots have been used for pH detection using both fluorescence and upconversion properties of the particles. Moreover, the naked eye or photograph digital camera have been implemented as detection systems, showing in both cases a linear pH range. The cytotoxicity and permeability of the Cdots were also evaluated on human embryonic kidney cells, revealing their adsorption on cells without causing any impact on the cellular morphology, demonstrating that these non-toxic nanoparticles can act as suitable biosensors. More information concerning both topics can be found in one of the attached works (Appendix I.6).

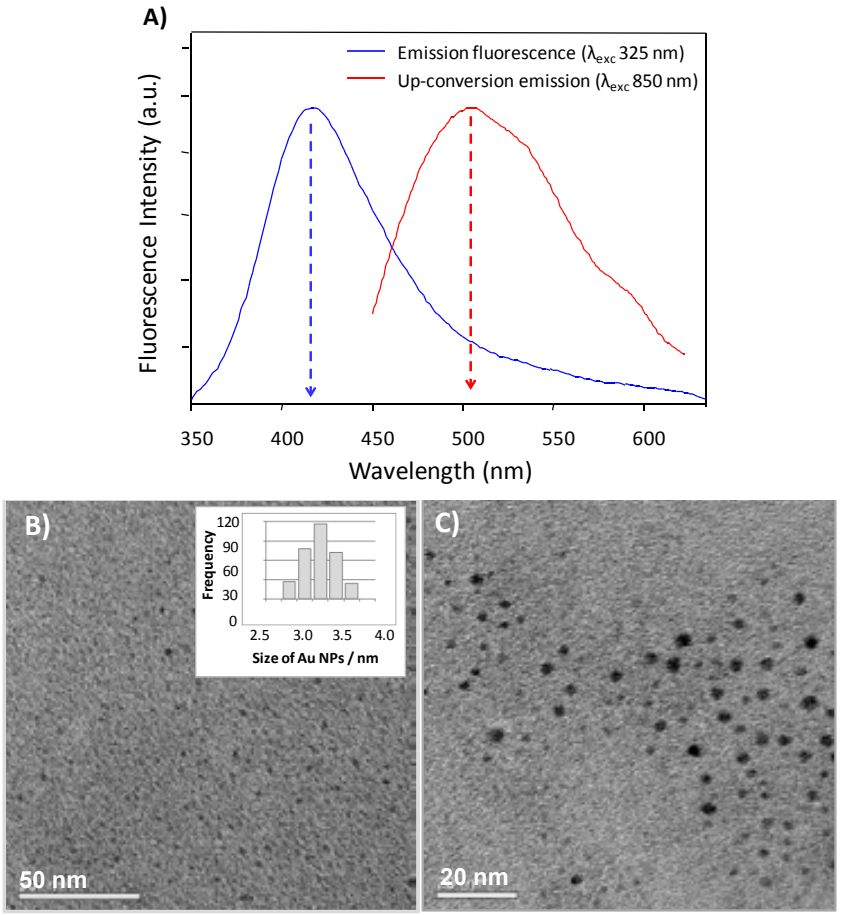

Figure 5.31: Characterization of the Cdots synthesized in **MR7**. **A)** Fluorescence emission spectra by UV (blue) and NIR (red) excitation. **B** and **C)** TEM images with the size-histogram and the calculated average size. **D)** HRTEM image and an amplification with the lattice fringes highlighted. **E)** SAED pattern of the nanoparticles.

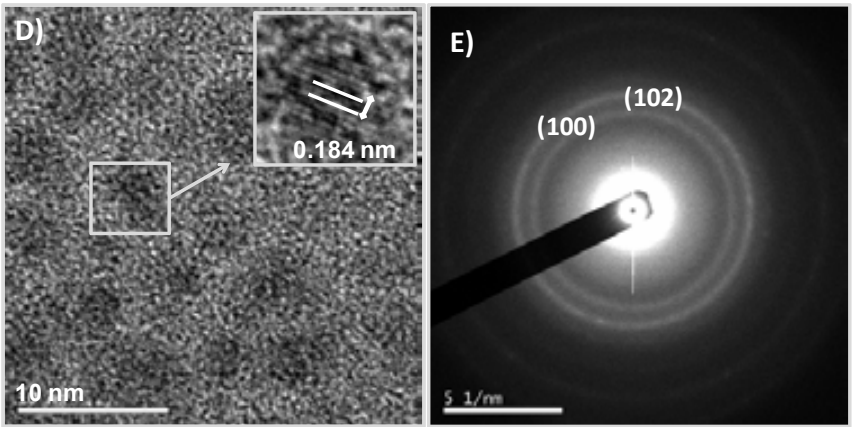

5.3.5 CONCLUSIONS

A microreactor for the controlled synthesis of carbon dots has been presented in this chapter. The synthesis has been based on the thermal decomposition of a carbon source, thus it has been necessary a strict control of the temperature. Therefore, the design of the microreactor has been based on the previously developed microsystem for quantum dots synthesis. The constructed fluidic platform has been based on a simple circular Z-shape microchannel for the conditioning and decomposition of the carbon source solution, and the thermal platform on a screen-printed gold-based heater and a commercial platinum sensor. The carbon dots obtained in the developed microreactor (**MR7**) have a spherical morphology and well dispersion, as well as an intense fluorescence using both UV and NIR exciting sources. Moreover, the pH-dependant properties of the present moieties of Cdots have allowed the development of a pH sensor. The uniform size distribution of the colloid makes clear the perfect function of the microreactor, achieving an effective and homogeneous heat and mass transfers. Thus, these experiments demonstrate the versatility and robustness of the designed and constructed thermal and microfluidic platforms, which can be employed to carry out the synthesis of diverse nanoparticles by slightly changes in their design.

ANALYTICAL MICROSYSTEMS BASED ON THE USE OF NANOPARTICLES

Contents

Image from Lab Chip Journal

This last chapter of experimental results is finally addressed to the development of automated and miniaturized analytical systems for the monitoring of environmental parameters in water samples. The following microsystems have been intended to be based on the use of the previously synthesized nanoparticles to improve their analytical features in order to obtain sensitive and selective devices capable to perform the *in situ* determination of a specific analyte. Therefore, an optical detection system has been implemented in the microfluidic platforms for the detection and quantification of analytes. COC has been preferred for the construction of these analytical devices due to the biocompatibility and transparency of this polymeric material.

The first analytical device (**AMS**) presented takes over the determination of mercuric ion, which gathers special interest due to its bioaccumulation and the severe damage that this heavy metal can cause in organisms. The system has been based on the specific recognition of Hg (II) by a new synthesized ionophore, which is attached to the previously obtained gold nanoparticles, generating a change on the gold SPR band. Initially, the analytical features of the selective recognition optical element have tested in batch conditions. Then, a polymeric microfluidic platform has been constructed, where it has been possible to exploit the rapid signal change observed during the interaction of the metal and the modified gold nanoparticles. A miniaturized optical system has been also implemented in the microfluidic platform to perform the on-line optical measurements. As it will be shown, the use of the microsystem improves the analytical features (sensitivity, detection limit and analysis time) of the method.

The second microsystem developed is addressed to the determination of pathogens in water, and more specifically to the detection and quantification of *Escherichia coli* (*E. coli*). This pathogen has been selected on the basis that it is normally employed as indicator of water quality in routine analysis in order to monitor whether it is contaminated or not.[1] Thus, a simple and automatic microfluidic system for the specific determination of this bacterium has been developed, which takes over a multistep magnetic bead-based enzyme-linked oligonucleotide sandwich assay. The bioanalytical device (**BMS**) has taken advantage of using magnetic beads in the oligonucleotide incubations stages as well as in the cleaning steps of the assay by employing a magnetic actuator

[1] World Health Organization; in: *Guideline for drinking-water quality*; Fourth edition, **2011**.

developed in the research group.[2] The detection of the target oligonucleotide sequence has been *in situ* determined through an enzymatic reaction, which generates a coloured product. Although the initial objective of this work was employing fluorescent nanoparticles as labels for the detection of the pathogen, it has not been possible due to the completion of this dissertation. Nevertheless, the proposed microsystem has a good repeatability, high robustness and re-usability, and relatively high sensitivity with short analysis times.

6.1 MICROSYSTEM FOR MONITORING MERCURIC ION (AMS)

It is well known the necessity of certain metals in the right concentrations for ecosystems and living specimens, such as in the case of cobalt, copper, iron, manganese and zinc, among others. However, the same metals in excess, or other metals, can be very dangerous and poisonous. The most concerning of these compounds are, without any doubt, heavy metals, because these species cannot be degraded by nature as other organic compounds.[3] Thus, they are accumulated in the environment and organisms causing severe damage.[4] For instance, lead can cause neurological, reproductive, cardiovascular and developmental disorders; [5] while high exposure levels of cadmium are also associated with increased risks of cardiovascular diseases, damage to liver and kidneys, and cancer mortality.[6] Besides both previous, mercury is well known as one of the most toxic metals. It can cause strong damage to the central nervous system, and its accumulation can lead to various cognitive and motor disorders and Minamata disease.[7-8]

In recent years, the growth of industrialization, urbanization and human population have increased pollution problems. Industrial wastes, even in very small concentrations, are often extremely toxic. For instance, mercury is generated by gold production, coal plants, thermometers, barometers, caustic soda, or mercury lamps.[9] The transport and accumulation of heavy metals by air, water or soil have led to an increase of concern on the population, which have promote national and international regulations such as the European Union's

---

[2] Berenguel-Alonso, M.; Granados, X.; Faraudo, J.; Alonso-Chamarro, J.; Puyol, M.; *Anal. Bioanal. Chem.,* **2014**, under revision.

[3] Wang L.K., Chen J.P., Hung Y.-T., Shammas N.K.; in: *Heavy metals in the environment;* CRC Press, **2009**.

[4] Kim, H.N.; Ren, Kim, W.X.; J.S.;Yoon, J.; *Chem. Soc. Rev.*, **2012,** 41, 3210–3244.

[5] Meyer, P.A.; Pivetz, T.; Dignam, T.A.; Homa, D.M.; Schoonover, J.; Brody, D.; *MMWR Morb. Mortal. Wkly. Rep.,* **2003,** 52(SS-10), 1-21.

[6] McFarland, C. .; Bendell-Young, L.I.; Guglielmo C.; Williams, T.D.*; J. Environ. Monit.*, **2002,** 4, 791.

[7] Carvalho, C. M. L.; Chew, E.-H.; Hashemy, S. I.; Lu J.;Holmgren, A.; *J. Biol. Chem*., **2008**, 283, 11913.

[8] Clarkson, T. W.; Magos L.; Myers, G. J.; *New Engl. J. Med.,* **2003**, 349, 1731.

[9] Di Natale,F.; Lancia, A.; Molino, A.; Di Natale, M.; Karatza, D.; Musmarra, D.; *J. Hazard. Mater.,* **2006**, 132, 220.

Dangerous Substances Directive, the U.S. Environmental Protection Agency (EPA) for water, the E.U. Air Quality Framework Directive and the World Health Organization (WHO) for air. [10-11]

Current analytical methods for mercury determination in environmental samples are based on electrochemical methods,[12] inductively coupled plasma mass spectrometry,[13] cold vapor atomic absorbance[14] or fluorescence[15] spectrometry and high performance liquid chromatography [16], which require qualified personnel and lengthy sample preparations. Therefore, it is important to develop new methods for the rapid, precise and low cost determination of mercury. In this sense, the employment of simple devices such as optical sensors has provided many advantages. Moreover, the use of nanomaterials, and more specifically of gold nanoparticles, as signal transduction elements has shown an enhancement of sensitivity and detection limits of many analytical methods as pointed out in the general introduction section. Although there are several proposed optical sensors based on this nanostructured material, which demonstrates the simplicity and the good performance of its use, these devices have still not been designed for the *in situ* monitoring. Thus, the purpose of this chapter has been the development of a microsystem based on gold nanoparticles for the monitoring of mercuric ion. With this aim, the previously synthesized gold nanoparticles have been modified with a new ionophore (a thiourea derivative), obtaining a recognition optical element selective to mercury. Then, it has been designed and constructed a polymeric microfluidic platform to carry out the determination of mercuric ion by the selective recognition element. The platform consists on the necessary inlets/outlet for the entrance and evacuation of reagents and waste, respectively, a bi-dimensional micromixer for reagents mixture, and an optical chamber to perform the optical measures. An optical system has been implemented in the microfluidic device, which makes feasible the monitoring of the heavy metal in a simple way.

6.1.1 MATERIALS, REAGENTS AND METHODS

All equipment and components necessary for the construction and evaluation of the microsystem for monitoring mercuric ion are listed in table 6.1.

---

[10] World Health Organization; in: *Guidelines for drinking-water quality;* vol. 1, 188, 3rd edition, **2004**.
[11] Wang, L.K.; Chen, J.P.; Hung, Y.-T.; Shammas, N.K.; in: *Heavy metals in the environment;* CRC Press, **2009**.
[12] Khani , H.; Rofouei, M.K.; Arab, P.; Gupta, V.K.; Vafaei, Z.; *J. Hazard. Mater.*, **2010**, 183, 402.
[13] Rashed, M.N.; J. *Hazard. Mater.*; **2010**, 178, 739.
[14] Ferrúa, N.; Ceruttia, S.; Salonia, J.A.; Olsina, R.A.; Martinez, L.D.; *J. Hazard. Mater.*; **2007**, 141 (3), 693.
[15] Yu, L.P.; Yan, X.P.; *Atom. Spectrosc.*, **2004**, 25(3), 145.
[16] Krishna, M.V.B.; Castro, J.; Brewer, T.M.; Marcus, R.K.; *J. Anal. Atom. Spectrom.*, **2007**, 22, 283.

Table 6.1: General list of equipment and components used in the development of the microsystem for monitoring mercuric ion.

EQUIPMENT	PROVIDER
• Peristaltic pump Miniplus 3	Gilson, Middleton, USA
• 6-way injection valve	Hamilton MVP, Bonaduz, GR, Switzerland
• Tygon tube (i.d. 1.2 mm)	Ismatec, Zurich, Switzerland
• PTFE tubes (i.d. 0.8 mm)	Techny Fluor, Barcelona, Spain
• 525 nm LED	Roithner Lasertechnik B5B-433-B525, Vienna, Austria
• H6780-03 Photomultiplier	Hamamatsu, Japan
• DAQ	National Instruments NI USB-6211, Austin, USA
• Low Numerical Aperture Polymer Optical Fiber (NA POF) (light injection)	Toray PMU-CD 1002–22-E, Tokyo, Japan
• High NA POF (light collection)	Mitsubishi ESKA Premier GH4001, Tempe, USA
• NOA61 UV-Curing Norland Optical Adhesive	Cranbury, NJ, USA
• 4 mL centrifugal tubes, CENTRIPLUS YM30, MICROCON, MWCO 30000	Millipore™, Centriplus™ Centrifugal Concentrators, Billerica, USA
• Angular centrifuge Cencom II	J. P. Selecta, S.A., Abrera, Spain
• Shimadzu UV-310PC UV-Vis-NIR double-beam scanning spectrophotometer	Kyoto, Japan
• High Resolution Transmission Electron Microscopy (HRTEM) JEOL 2011	Tokyo, Japan
• Transmission Electron Microscopy (TEM) JEOL 1400	Tokyo, Japan
• Zeta sizer nano ZS	Malvern, Worcestershire, UK
• Optima 4300DV, Inductively Coupled Plasma Optical Emission Spectrometry (ICP-OES)	Perkin-Elmer, Massachusetts, USA
• pH meter GL22	Crison, Alella, Spain

The centrifugal tubes and the angular centrifuge are used at 3000 rpm for 30 min for the purification of the selective recognition optical element. Its characterization is performed by means of the UV-visible spectrophotometer, the TEM and HRTEM, ζ sizer nano ZS and the ICP-OES equipments. pH meter is used to adjust pH of reagents. The spectrophotometer is also employed for the initial analytical evaluation of the selective recognition optical element.

Reagents used with this purpose are presented in table 6.2. Mercuric ion stock solution is prepared with mercury (II) nitrate monohydrate and sodium acetate and acetic acid in double distilled water. Different dilutions are done in 0.01 M acetic acid/sodium acetate buffer adjusted to pH 5.5 to a cover a wide range of Hg(II) concentrations.

REAGENT	PROVIDER
• Mercury (II) nitrate monohydrate	puriss. p.a., ACS reagent, ≥98.5 %, Sigma-Aldrich
• Sodium acetate	ACS reagent, ≥99.0 % , Sigma-Aldrich
• Acetic acid	ACS reagent, ≥99.7 %, Sigma-Aldrich

Table 6.2: Reagents employed for the evaluation of the microsystem developed using the selective recognition optical element.

On the other hand, the following reagents are also necessary for the synthesis of the ionophore, purchased from Sigma-Aldrich: p-hydroxyacetanilide; potassium carbonate; 1,4-dibromobutane; carbon tetrachloride; thiourea; n-butanol; ethanol; NaOH; HCl; CH_2Cl_2; Na_2SO_4; sulfanilic acid; thiophosgene; THF and ether. Boron trifluoride dimethanol complex 50 % is supplied from Acros. A Bruker 250 MHz equipment (Karlsruhe, Germany) is used for RMN measurements.

6.1.2 EXPERIMENTAL SET-UP

A scheme of the complete experimental set-up used for the *in situ* determination of mercuric ion is shown in figure 6.1. A continuous flow injection system is used, which incorporates a peristaltic pump to propel reagents to the microfluidic platform or to a 6-way injection valve. The use of the valve allows injecting a certain volume of the sample (mercuric ion) into a carrier solution of 0.01 M acetic/acetate buffer at pH=5.5, which is continuously pumped to one of the device inlets. Gold nanoparticles modified with the ionophore are also continuously pumped into the other inlet of the microfluidic platform.

The detection set-up implemented to register the optical signals consists of a 525 nm LED mounted in a PCB, which matches the absorption maximum of the Au NPs SPR band; a photomultiplier to ensure a high intensity signal; and a DAQ connected to a PC that controls the system, modulates the LED signal to make feasible the working of the system in ambient light, and amplifies the detected signal by a lock-in amplification. A low NA POF is used for light injection and a high NA POF for light collection from the optical window of the microfluidic platform. These fibers are directly glued using a UV-Curing adhesive to the platform. The miniaturized optical system is continuously recording the signal during the whole measures. The blank signal is taken when the gold nanoparticles modified with the ionophore reach the detection area of the microfluidic platform. A transitory signal (peak) is therefore obtained when injecting the sample.

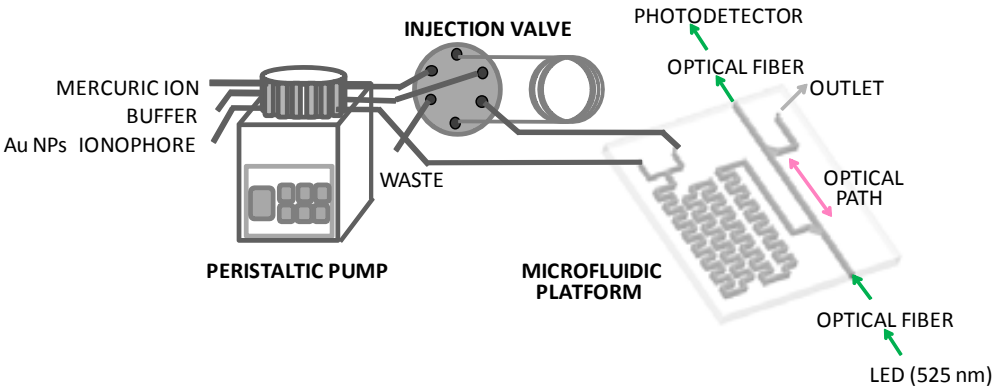

Figure 6.1: Experimental set-up for the monitoring of Hg (II) in the microsystem (**AD**).

6.1.3 DEVELOPMENT OF TH E SELECTIVE R ECOGNITION OP TICAL ELEMENT

For the development of a selective recognition optical element it is necessary a specific receptor, which selectively interacts with the analyte and generates a primary signal, and a transducer, which transforms this signal to an electrical. From the different transducing elements or platforms that can be used, gold nanoparticles can provide selectivity, sensitivity and reproducibility to the system. Moreover, their simple surface modification techniques make feasible the easy introduction of recognition elements. The interaction of the capping receptor with the analyte is capable to produce a change on the SPR band of the colloid, normally generating a shift of its absorption band, leading to obtain highly sensitive and cost-efficient heavy metal detection systems.[17] On the other hand, diverse receptor molecules can be used for detecting mercury within gold nanoparticles. The specific interaction of the receptor and the analyte normally involves non-covalent bonding, such as hydrogen bonding, van der Waals forces, metal coordination, hydrophobic forces, π-π interactions, and electrostatic and/or electromagnetic effects.[18] Nevertheless, the capping recognition molecule should fulfil the necessities for stabilizing the colloid and for selectively detect the analyte. On the one hand, biological receptors or bioreceptors, such as proteins, nucleic acids or antibodies, are of increasing interest due to the high sensitivity that these elements can achieve.[19] For instance, the use of oligonucleotides in mercury detection, which is based on the high specific interaction of hybridization and the formation of DNA-Hg^{2+} complexes by T-T mismatches,[20] have achieved very low detection limits.[21-22] Similarly, the use of proteins such as antibodies seems to present high affinity to heavy metals too due to their amino

[17] Wang, L.; Ma, W.; Xu, L.; Chen, W.; Zhu, Y.; Xu, C.; Kotov, N. A.; *Mater. Sci. Eng., R* **2010**, 70, 265.
[18] Aragay, G.; Pons, J.; Merkoçi, A.; *Chem. Rev.,* **2011**, 111, 3433–3458.
[19] Verma, N.; Singh, M.; *BioMetals.,* **2005,** 18, 121.
[20] Yamane, T.; Davidson, N.; *J. Am. Chem. Soc.*, **1961,** 83, 2599.
[21] Lee, J.-S.; Han, M.S.; Mirkin, C.A.; *Angew. Chem. Int. Ed.,* **2007,** 46 (22), 4093–4096.
[22] Xue, X.; Wang, F.; Liu, X.; *J. Am. Chem. Soc.,* **2008,** 130(11), 3244–3245.

acid side chains.[23-24] However, all these biologic materials increase considerably the cost of the whole methodology. On the other hand, compounds known as ionophores, which are synthetic or natural molecules also used as receptors, seems to be a better alternative for heavy metals detection, since these compounds not only present high selectivity as bioreceptors, but also are extremely cheaper compared with the former. Macrocyclic compounds and caged molecules such as podands, crown ethers,[25-26] cryptands, spherands, cyclodextrins[27-28] or calixarenes[29] can accept heavy metal ions in their cavities with high selectivity and in a reversible way.[30] Besides this macrocycles, small molecules can also act as ionophores for heavy metals by non-covalent binding in a simple way. These chelating ligands, which usually have more than one donor atom, selectively bind heavy metals by the high affinity that present towards oxygen, nitrogen, and sulfur donor atoms. Taking into account Pearson acid base concept (which describes that soft acid better reacts with soft bases, and the equivalent for hard compounds),[31-32] Cr^{3+} and Al^{3+}, classified as hard acids, will prefer the coordination with ligands containing oxygen as donor atom, whereas chelates through sulphur ligands will be favoured with soft acids such as Cd^{2+}, Hg^{2+} and Ag^{+} metals. Nitrogen donor atoms of receptors should prefer Co^{2+}, Ni^{2+}, Cu^{2+}, Pb^{2+} or Zn^{2+}.[210] The geometric shape of the ion, its charge density and its size have to be taken into account, since these factors plays also an important role in the selectivity of the ionophore. The use of these small molecules as ionophores has been preferred in this work, since they are cheaper and simpler to manipulate than bioreceptors while conferring high selectivity.

Therefore, it was necessary to design and synthesize a new ionophore selective to mercury capable to be attached onto the surface of Au NPs and allow their stabilization. Thus, the whole compound (nanoparticles and ionophore) will act as the recognition and transducing element.

6.1.3.1 DESIGN AND SYNTHESIS OF THE IONOPHORE

The first step in the development of the selective recognition optical element was the synthesis of a new ionophore in order to make selective the response of the

[23] Wylie, D. E.; Lu, D.; Carlson, R.; Babacan, K. F.; Schuster, S. M.; Wagner, F. E.; *Proc. Natl. Acad. Sci. U. S. A.,* **1992,** 89, 4104.
[24] Blake, D. A.; Chakrabarti, P.; Khosraviani, M.; Hatcher, F. M.; Westhoff, C. M.; Goebel, P.; Wylie, D. E.; Blake, R. C.; *J. Biol. Chem.,* **1996**, 271, 27677.
[25] Kwon, O. S.; Kim, H. S.; *Supramolecular Chem*., **2007**, 19, 277.
[26] Srivastava, S. K.; Gupta, U. K.; Jain, S.; *Analyst,* **1995**, 120, 495.
[27] Norkus, E.; *J. Incl. Phenom. Macrocycl. Chem*., **2009,** 65, 237.
[28] Fragoso, A.; Ortiz, M.; Sanroma, B.; O'Sullivan C. K.; *J. Incl. Phenom. Macrocycl. Chem.,* **2011,** 69 (3-4), 355- 360.
[29] Othman, A. B.; Lee, J. W.; Wu, J.; Kim, J. S.; Abidi, R.; Thuéry, P.; Strub, J. M.; Dorsselaer, A. V.; Vicens, J.; *J. Org. Chem.,* **2007,** 72, 7634.
[30] Lehn, J. M.; *Pure Appl. Chem.,* **1978,** 50, 871.
[31] Parr, R. G.; Pearson, R. G.; *J. Am. Chem. Soc.,* **1983,** 105, 7512.
[32] Pearson, R. G.; *J. Chem. Sci*., **2005,** 117, 369.

system to mercuric ion. A thiourea derivative was preferred, which could also be easily attached to the gold surface, due to these compounds usually present chelating capability towards heavy metals.

From the different possible strategies for the surface modification of nanoparticles, a covalent coupling was selected, since a higher stability is normally achieved when compared to hydrophobic or electrostatic interactions. Thus, the N-(4-sulfonatophenyl)-N'-[4-(4-mercaptobutoxy)-phenyl]thiourea was designed and synthesized through the synthetic route depicted in figure 6.2. As it can be observed, the structure of the ionophore has a C_4 hydrocarbon chain with a -SH terminal group (a mercaptobutoxy group) to be linked to the gold surface. A sulfonate group has been also introduced to assure its solubility in water.

Experimental details of its synthesis are not shown in the present manuscript due to this work was developed by the department of chemistry of the St. Petersburg State University. Nevertheless, the synthesis consisted on five simple reactions, with a total yield of 9.3 %. More information concerning the synthesis and characterization (^{1}H RMN and mass spectroscopy data) of the ionophore can be found in the related attached work (Appendix I.5).

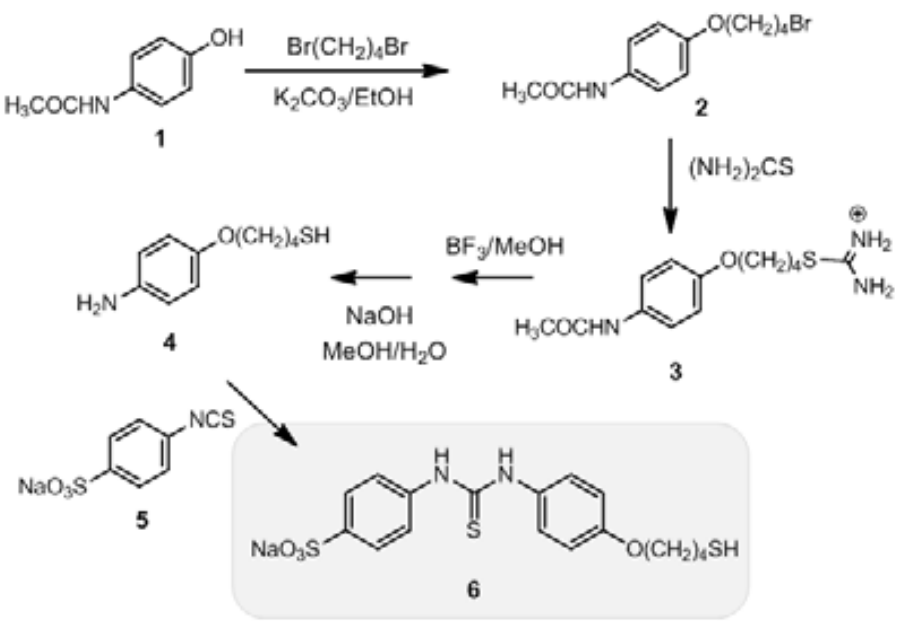

Figure 6.2: Synthetic route of the ionophore. 1: p-hydroxyacetanilide; 2: 4-(4-Bromobutoxy)-acetanilide; 3: 4-(4-acetamidophenoxy)-butylisothiuronium bromide; 4: 4-(4-Aminophenoxy)-butanethiol; 5: 4-Isothiacyanatobenzoic acid sodium salt; 6: N-(4-sulfonatophenyl)-N'-[4-(4-mercaptobutoxy)-phenyl]thiourea sodium salt.

6.1.3.2 PREPARATION O F T HE G OLD N ANOPARTICLES M ODIFIED W ITH T HE IONOPHORE

The preparation of the selective recognition optical element was performed through ligand exchange on the surface of gold nanoparticles. Au NPs stabilized with tiopronin were used with this purpose, since the simple ligand exchange of this stabilizer has been well reported.[33] The synthesis of these nanoparticles has

[33] Templeton, A.C.; Cliffel, D.E.; Murray, R.W.; *J. Am. Chem. Soc.*, **1999**, 121, 7081.

been well described in section 4.2.5 of this manuscript. This ligand exchange reaction consisted on mixing a solution of Au NPs stabilized with TP with an aqueous solution of the ionophore during 12 hours. The ionophore solution was added in excess (1 : 10 of Au NPs : Ionophore) to ensure the ligand exchange.

The presence of the thiourea derivative onto gold nanoparticles surface was verified by UV-Vis spectroscopy once the colloid was purified by repeated filtration using the centrifugal equipment. The recorded spectrum showed the characteristic SPR band of Au NPs at ~ 525 nm and a new absorption peak located at 260 nm, corresponding to the ionophore (figure 6.3A). The selective recognition optical element was also characterized by different techniques. As it can be seen in figure 6.3, TEM images revealed well dispersed nanoparticles with a mean size of 3.7 nm. A hydrodynamic diameter of 17.8 ± 4.9 nm and a ζ potential of -31.4 ± 7.7 mV were obtained from the analyses performed with zeta sizer nano ZS, demonstrating the stability of the colloid. The ligand exchanged was also ensured by results obtained from ICP-OES, where the calculated ratio of S : Au before and after the ligand exchange were 0.1 and 0.3, respectively.

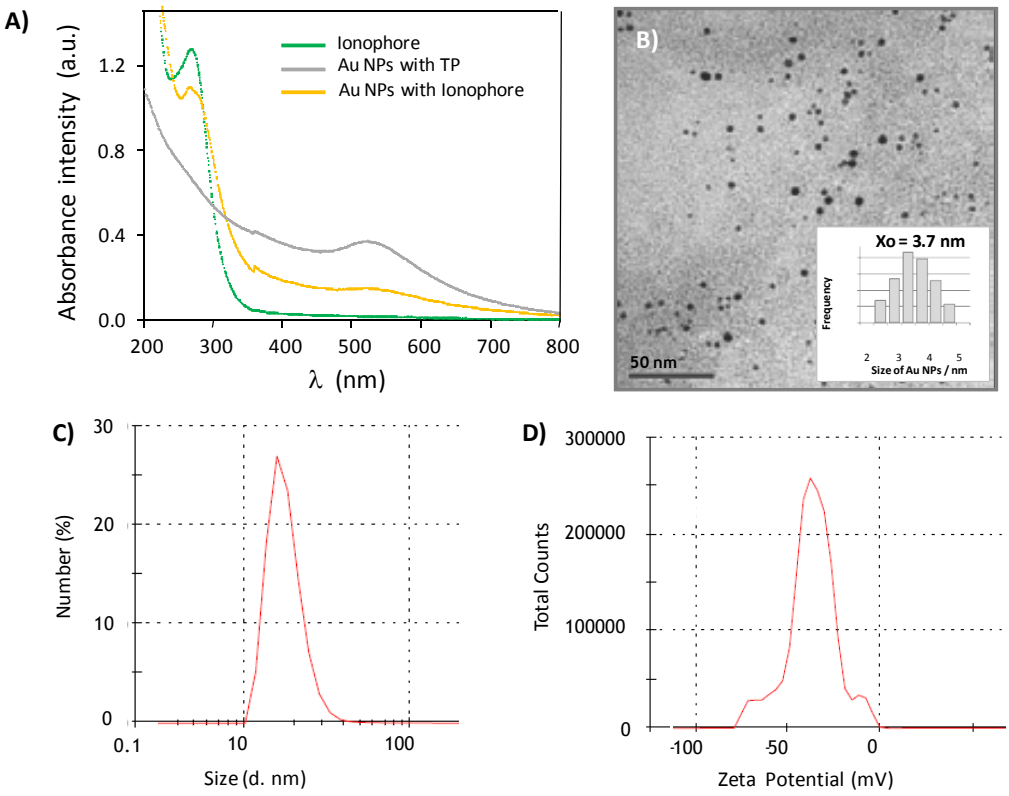

Figure 6.3:
A) UV-Vis spectra of the ionophore, the gold nanoparticles stabilized with tiopronin and with the ionophore in solution. **B)** TEM image with its correspondent histogram, **C)** DLS spectrum and **D)** ζ potential measure of Au NPs modified with the ionophore. **E)** ICP-OES results and calculated ratio of S : Au for both colloidal.

E)

Sample	Au (mg/L)	S (mg/L)	S:Au
Au NPs with TP	29.2	2.1	0.1
Au NPs with Ionophore	26.4	7.1	0.3

6.1.4 EVALUATION OF TH E SELECTIVE R ECOGNITION O PTICAL ELEMENT

The selective recognition optical element was initially evaluated in batch in order to test its feasibility for the mercuric ion determination. The experiments consisted on mixing different aliquots of the gold nanoparticles modified with the ionophore with increasing concentrations of mercuric ion. Changes on the SPR band of the gold colloid generated from the interaction with the heavy metal were recorded by means of a spectrophotometer.

Different concentrations of gold colloid were tested in order to achieve the maximum sensitivity and detection limit of the method. Thus, solutions of approximately 1.5×10^{-3} % $HAuCl_4$ (4.7×10^{-8} M), 2.3×10^{-3} % (7.5×10^{-8} M) and 3.0×10^{-3} % (9.6×10^{-8} M), calculated by a calibration curve using a commercial gold colloid of a 5 nm mean size ($\varepsilon = 2.3 \times 10^{6}$ M^{-1} cm^{-1}) and obtained by dilution, were evaluated. Although it was expected to notice a change on the SPR band location when adding the diverse mercuric ion solutions owing to nanoparticles aggregation, the observed response was surprisingly an intensity change of the SPR band. Nevertheless, this response has been also previously reported, being related to a change in the refractive index on the surface of the Au NPs generated from the interaction metal-ionophore.[34-35] The employment of the intermediate concentration generated the biggest spectral changes in the colloidal, being thus selected for further experiments.

Then, two different concentration ranges of mercuric ion were tested to assure the interaction of the metal with the ionophore. Thus, 20, 40, 60, 80 and 100 ppm solutions of Hg^{2+} were employed to perform three different calibration curves, obtaining a linear response in all cases as it can be observed in figure 6.4. Linear least squares fitting of the calibration curves gave a mean sensitivity of 4.03 x 10^{-4} a.u. ppm^{-1} Hg^{2+}.

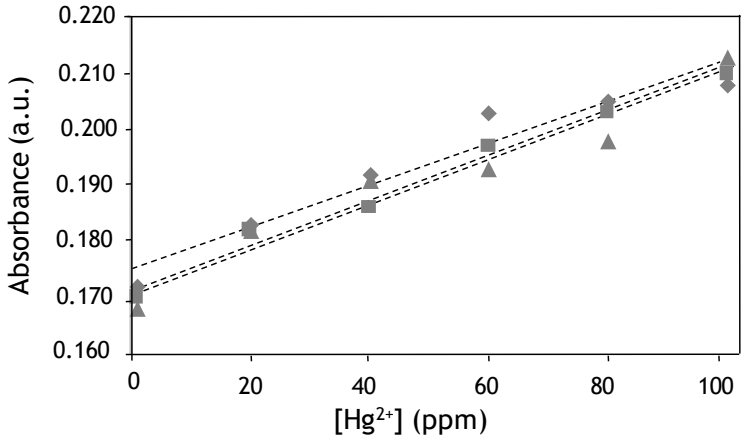

Figure 6.4: Response of the Au NPs modified with the ionophore at a high concentration range (20-100 ppm) of mercuric ion.

[34] Aragay, G.; Pons, J.; Ros, J.; Merkoçi, *A.*; *Langmuir*, **2010**, 26(12), 10165.
[35] Dang, Y.; Li, H.W.; Wang, B.; Wu, Y.; *ACS Appl. Mater. Interfaces*, **2009**, 1, 1533.

Testes carried out with a lower concentration range of mercuric ion (20, 40, 60, 80, and 100 ppb) revealed an equivalent behaviour, achieving a sensitivity of 6.3 x 10^{-5} a.u. ppb^{-1} Hg^{2+} (Figure 6.5).[36] From these results, a detection limit of 67 was obtained, calculated as three times the standard deviation of the blank signal (Au NPs modified with the ionophore).

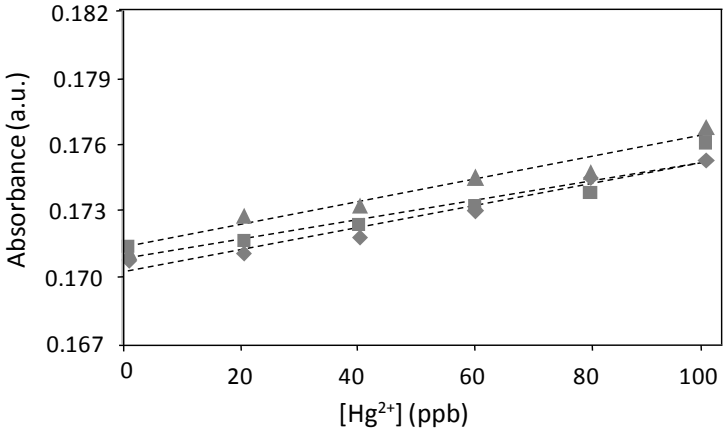

Figure 6.5: Response of the Au NPs modified with the ionophore at a low concentration range (20-100 ppb) of mercuric ion.

The necessary reaction time to observe the interaction between the selective recognition optical element and mercuric ion was also evaluated by recording the absorption spectrum of the mixed solutions with time. However, no changes were observed when comparing the spectra recorded within few seconds with the registers from 60 minutes later. Therefore, it can be concluded that the complete reaction takes place in few seconds. This incredibly rapid interaction time of the metal-ionophore to achieve a stationary signal should be remarked, since it makes feasible the development of a simple microsystem for monitoring mercuric ion.

On the other hand, the selectivity of the method was also evaluated. The response of the selective recognition optical element to mercury was compared with the observed to other potential interfering ions. Specifically, Ni^{2+}, Pb^{2+}, Cd^{2+}, Fe^{2+}, Mg^{2+}, Na^{+}, K^{+}, Ba^{2+}, Cu^{2+} and Al^{3+} were tested in a concentration of 100 ppm. The graphic depicted in figure 6.6 shows the results obtained, where only mercuric ion gave a significant change on the absorption signal of the SPR band.

[36] Slocik, J.M.; Zabinski, J.S.; Phillips, D.M.; Naik, R.R.; *Small*, **2008**, 5, 548.

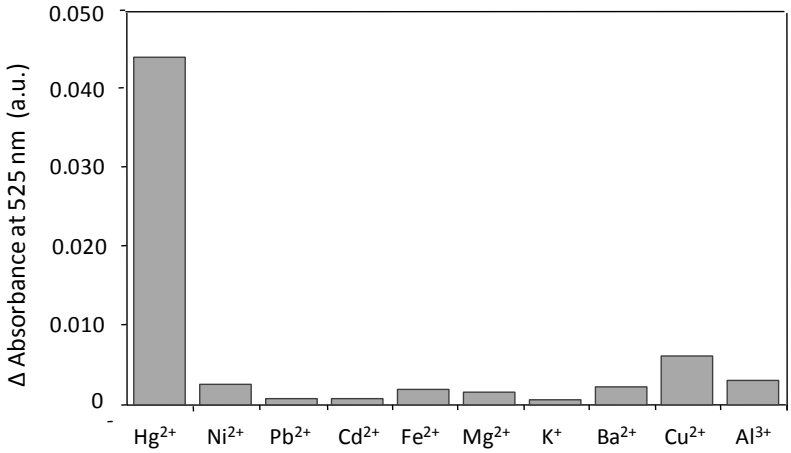

Figure 6.6: Absorbance signals at 525 nm from the Au NPs modified with the ionophore in the presence of different ions. **A)** Absorbance signal variation at 100 ppm concentration level of all the metals

In order to evaluate the selectivity of the method in a closer situation to the analytical measurement, a simplification of the Fixed Interference Method (FIM) was also carried out. These experiments consisted on comparing the signal obtained from a solution of Au NPs modified with the ionophore containing 1 ppm of Hg^{2+} with the registered when also having an interfering ion as a background. In this case, only Pb^{2+} (1 ppm), Ni^{2+} (10 ppm), Cu^{2+} (10 ppm) and Cd^{2+} (1 ppm) were tested due to these ions are the most common interfering in such measures. As figure 6.7 shows, no significant variation on the intensity signal was observed.

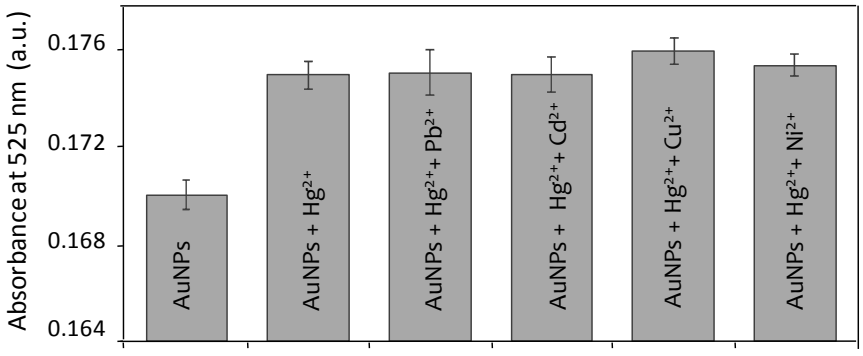

Figure 6.7: Absorbance signals at 525 nm from the Au NPs modified with the ionophore in the presence of different ions. Signal from blank and 1 ppm Hg^{2+} solutions containing 1 ppm Pb^{2+}, 10 ppm Ni^{2+},10 ppm Cu^{2+}, 1 ppm Cd^{2+}.

6.1.5 MICROFLUIDIC PLATFORM DESIGN

Once verified the feasibility of the selective recognition optical element for the mercuric ion determination in batch, the next dare was the construction of a simple and portable microsystem, which allows the *in situ* monitoring of this ion. As previously detailed, the microsystem is composed of a flow set-up for the fluids management, a miniaturized optical set-up to register the generated signals, and a microfluidic platform where takes places the metal-ionophore interaction.

In this case, COC was preferred for constructing the microfluidic platform, since the proposed method takes place in aqueous medium and it does not require of aggressive reagents. Moreover, this material enables the easy integration of other components, such as optical fibres, by means of UV curing adhesives. The final microfluidic platform was constructed using three different polymeric layers (two 500 µm-thick layers and one 1000 µm-thick layer). Its design consisted of two inlet channels for the entrance of reagents, which converges in a T-shape confluence point to assure an efficient first mixture of solutions; a bi-dimensional micromixer for the total mixture of the solutions (400 µm-wide channel); a 2 cm x 1 mm x 1 mm optical detection chamber, where the absorbance signal of the SPR band is continuously recorded; and a collection channel to the outlet. The total volume of the microfluidic platform is of 130 µL (95 and 20 µL for the micromixer and detection chamber, respectively). Once the microfluidic platform was constructed, two plastic optical fibres (1 mm-diameter) were connected to both sides of the optical chamber, defining the optical path length. Images from the platform are shown in figure 6.8.

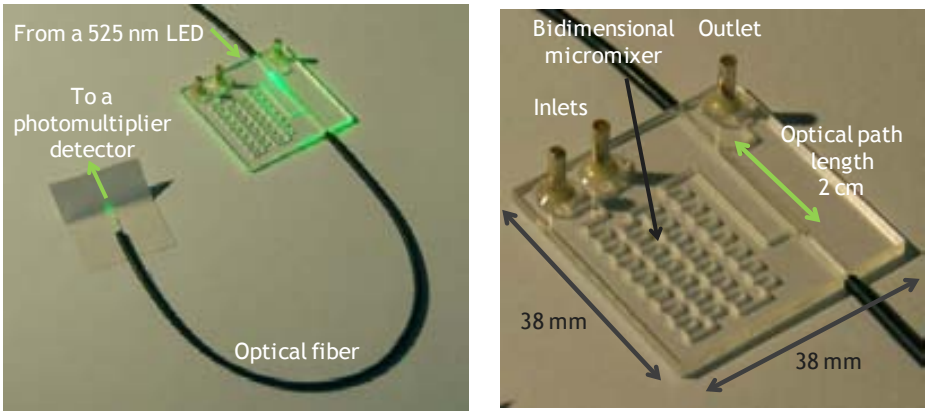

Figure 6.8: Images of the microfluidic platform constructed for the continuous monitoring of mercuric ion.

6.1.6 EVALUATION OF THE MICROSYSTEM FOR THE MERCURIC ION MONITORING

As in any other microsystem, it is necessary to optimize the hydrodynamic parameters prior to its use, since its analytical features, such as sensitivity or detection limit, are highly affected by kinetics. In this way, it can be get the most of the microsystem.

An concentration of 100 ppb of mercuric ion was employed to optimize both the injection volume and the flow rate. On the one hand, a flow rate of 0.8 mL min^{-1} was used for testing injection volumes of 100, 300 and 500 µL of sample. As figure 6.9 shows, there were a significant signal increase when using the middle or the bigger volume when compared to the smallest. Although the employment of 500 µL of injection loop generated the more intense transitory signal, 300 µL were preferred as optimized volume, since it conferred almost the same signal

while minimizing the waste of reagents. On the other hand, 0.8, 1.6 and 3.2 mL min^{-1} flow rates were evaluated using 300 µL of injection volume. Figure 6.9 demonstrates that the use of 1.6 mL min^{-1} generated the higher intensity signal, being thus preferred for further experiments.

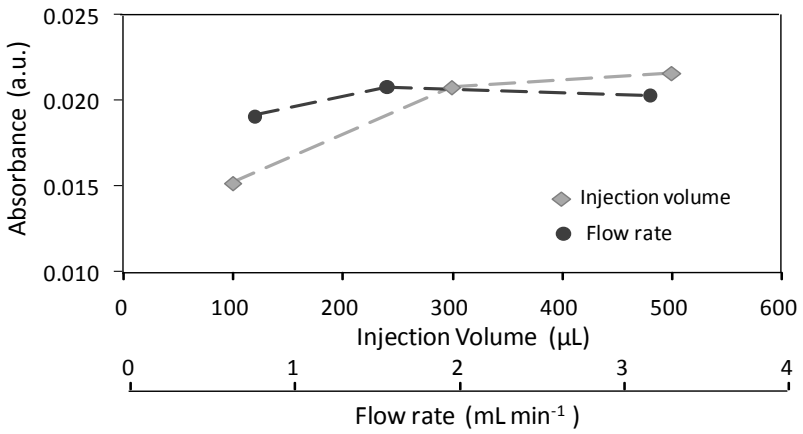

Figure 6.9: Optimization of the hydrodynamic parameters of the microsystem using 100 ppb of mercuric ion. In light grey: Optimization of the injection volume (flow rate: of 1.6 mL min^{-1}). In dark grey: Optimization of the total flow rate used (measured at the outlet) (injection volume: 300 µL).

Once optimized the hydrodynamic parameters, the sensitivity and detection limit of the method using the microsystem were evaluated. Thus, mercuric ion solutions at the low concentration range (20 - 100 ppb) were injected in the microfluidic platform. As figure 6.10 shows, clear transitory signals, with a very high signal to noise ratio, were obtained in the whole register. Moreover, the baseline was totally recovered in all peaks, which indicates the complete renewal of the volumes on the detection chamber.

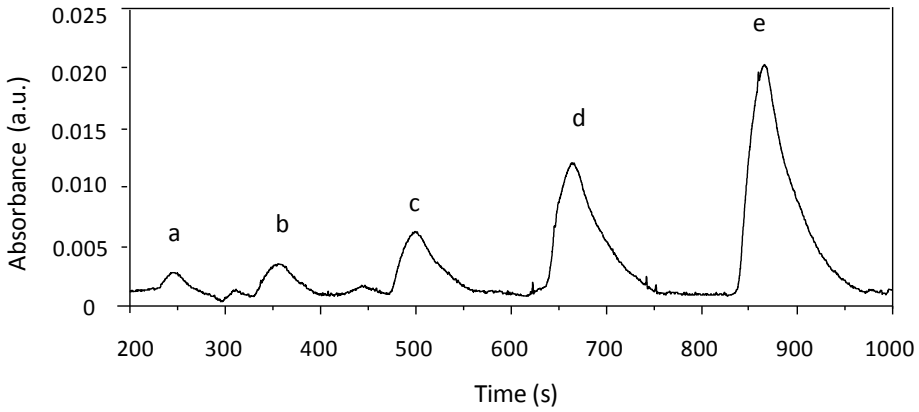

Figure 6.10: Example of the register obtained from a Hg^{2+} calibration. From ***a*** to ***e***: 20, 40, 60, 80 and 100 ppb mercuric ion solutions.

Figure 6.11 represents three different calibration curves obtained with the microsystem (in light grey). From these results it is possible to calculate a sensitivity of 2.07 x 10^{-4} a.u. ppb^{-1} Hg^{2+} (mean slope) and a detection limit of 11.0, calculated as three times the standard deviation of the blank signal. The graphic also shows the results previously obtained in bath conditions for comparative purposes. As it can be noticed, a clear sensitivity improvement in terms of slope and detection limit is achieved using the optimized microsystem. Moreover, it has

to be pointed out that the analytical features obtained could be probably improved to reach the regulations from the World Health Organization (WHO) (1 ppb)[10] or the Environmental Protection Agency (EPA) (2 ppb)[37] by for example elongating the optical path length of the microfluidic platform.

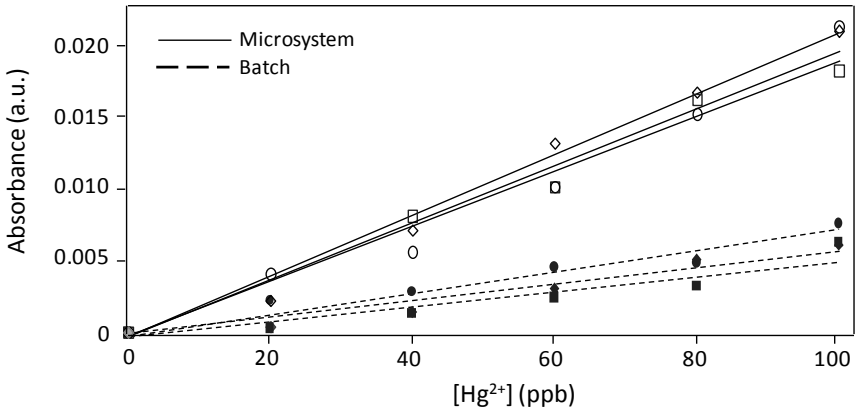

Figure 6.11: Calibration curves obtained with the polymeric microfluidic platform and its comparison with the previously obtained in batch.

Nevertheless, the approach enables the determination of mercuric ion in a simple, rapid and cheap way due to the rapid interaction metal-ionophore, and the use of low cost reagents and materials. Actually, a sample throughput of 18 samples h^{-1} has been calculated.

6.1.7 CONCLUSIONS

This chapter has shown the great advantages of using nanomaterials, and more specifically nanoparticles, within microsystems for the development of μ-TAS. In this case, it has been designed and constructed a microfluidic platform for the monitoring of mercuric ion in water samples. The device integrates an optical detection set-up based on optical fibers, which enables the continuous register of the optical signals generated in the platform. A new ionophore (thiourea derivative) has been synthesized, which has allowed developing of a highly sensitive and selective optical recognition element for mercuric ion based on the gold nanoparticles synthesized in microreactors. Once optimized, the analytical microsystem has been capable to determine up to 11 ppb of mercuric ion through the changes generated on the gold SPR band due to the metal-ionophore interaction. As it has been proved, the use of the microsystem has improved the analytical features of the method, leading to a simple, rapid and low cost device capable to monitor the analyte. Moreover, the low standard deviations attained, which means the method is highly repeatable, makes clear the advantage of using uniform and well defined nanoparticles.

[37] EPA, U. S.; **2001**; EPA-823-F-01-01.

6.2 MICROSYSTEM TO PERFORM MU LTI-STEP M AGNETO-BIOCHEMICAL ASSAYS (BMS)

Over the last years, the concern about pathogen contamination has been of increased interest due to the many studies which demonstrates the risk to human health of microbial pollutants such as bacteria. Disease outbreaks from bacteria are mostly related to food contamination owing to an improper storage, undercooking or cross- contamination; or to waterborne pathogens. Bacteria present in water can lead to serious illnesses or diseases, such as gastroenteritis or salmonellosis, causing diarrhoea, cramps, nausea, headaches or other symptoms. Moreover, they may have a major health risk for infants, young children and people with severely compromised immune systems, occasioning in many cases death.[38] According to the WHO, the mortality of water associated diseases exceeds 5 million people per year.

In general terms, the greatest microbial risks associated with water are due to its contamination with human or animal feces.[39] The infection can be generated owing to its ingestion, but also can result during bathing, washing, in the preparation of food, or the consumption of food thus infected. Bacteria causing waterborne diseases normally come from human, animal or agricultural wastes, including waste water treatment plants, livestock or poultry manure, sanitary landfills, septic systems, sewage sludge, pets and wildlife. Thus, most of waterborne disease outbreaks results from untreated ground water that has become contaminated.

In recent years, the annual number of drinking water-borne disease outbreaks has been doubled, and the associated with recreational water use has more than tripled. Actually, microorganisms causes 75 % of all waterborne illnesses associated with drinking water. These data can be clearly reflected in developing countries, where many people do not have access to clean and safe drinking water and many die of waterborne bacterial infections. Indeed, diarrhoea diseases in these countries cause about 1.8 million human deaths annually.[40] In addition, waterborne diseases are also a concern in developed countries. An example could be the rural areas, where it is rarely to found treated water. In other cases, inadequate treatment or breakdowns in treatment plants have been evolved in large-scale disease outbreaks. Furthermore, globalization of commerce has promoted changes in food supply production. For instance, fruits or vegetables often come from other countries, where the food may have been processed with inadequately treated irrigation water. On the other hand,

[38] Fenwick, A.; Waterborne Diseases-Could they be Consigned to History?; *Science,* **2006**, 313, 1077.
[39] Grabow WOK; in: *Waterborne Diseases: Update on Water Quality Assessment and Control,* Water SA., **1996**, 22, 193.
[40] *Burden of disease and cost-effectiveness estimates,* WHO, **2014**.

waterborne diseases from pathogenic microorganisms also cause a large economic loss, since their medical diagnosis and treatment, especially in chronic diseases, can entail lots of money. Control of waterborne disease is therefore an important element of public health, being extremely important to rapidly determine if a water body is contaminated or not.

To assess the risk of exposure to pathogens in water, either for its consumption or for its recreational use, public agencies rely on indicator bacteria, since the variety and often low concentrations of the different pathogens in environmental water makes them difficult to test for individually. Indicator organisms are more abundant bacteria, such as non-specific coliforms, *E. coli* and *Pseudomonas aeruginosa*. These bacteria are commonly found in the human or animal gut and if detected, may suggest the presence of sewage. Actually, an infected organism excretes many millions times more of indicator organisms than of pathogens. It is therefore reasonable to surmise that if indicator organism levels are low, then pathogen levels will be very much lower or absent. These indicator bacteria are easy and inexpensive to detect, thus they are usually selected for determining water quality.[41] Current approved analytical methods for drinking water quality are based on membrane filtration and its culture on selective media (MI medium).[42-43] When more than a 5 % of water samples in month give positive for these pathogens, the water is considered biologically contaminated. When the indicator organism level exceeds this pre-set trigger, specific analysis for pathogens may be undertaken, using specific culture methods or molecular biology.

Other methods of detection are based on the use of chromogenic substances, immunological methods using monoclonal antibodies, immune magnetic separation and culture, gene sequence-based methods and other rapid culture-based methods. The use of hybridization methods has demonstrated many advantages, since they depend on the recognition of exclusive gene sequences of specific strains of organisms. Compared to immunological methods, they are faster and show higher specificity, sensitivity and lower cross-reactivity. Polymerase chain reaction (PCR) and microarray-based DNA chips are gene sequence-based methods currently used to detect specific strains of indicator bacteria.[44] The former presents many advantages, such us their sensitivity and speed over the culture traditional detection methods. However, they still involve expensive and complicated protocols, which must be done by skilled personnel.[45]

---

[41] LeChevallier, M.W.; Au, K.-K.; in: *Water treatment and pathogen control: Process efficiency in achieving safe drinking water*, WHO, **2004**. ISBN 92 4 156255 2.

[42] EPA Method 1604.

[43] *Guidelines for Drinking-water Quality*, 4th Edtition, WHO, **2011**, p. 294. ISBN 978 92 4 154815 1.

[44] Nicholas J. Ashbolt, Willie O.K. Grabow and Mario Snozzi Indicators of microbial water quality. WHO, 2001, IWA Publishing, London, UK. ISBN: 1 900222 28 0

[45] Velusamy, V.; Arshak, K.; Korostynska, O.; Oliwa, K.; Adley, C.; *Biotechnol. Adv.,* **2010**, 28, 232.

The later has demonstrated high-throughput and DNA multiplexing analysis,[46] but they are limited by their high cost and chip variations.[47] Moreover, these methods normally require of several hours to perform the analysis because the hybridization process is limited by diffusion.[48] Thus, the biggest challenges of these analysis methods remain mostly in the analysis time, costs and the elaborated protocols required.

Therefore, the purpose of this chapter has been the development of a simple and automatic microsystem for the rapid detection and quantification of *E. coli* for water quality analysis. Specifically, the device has taken over a magnetic bead-based oligonucleotide sandwich assay. The magnetic properties of MBs, where the capture probe has been covalently immobilized, has been taken into advantage not only to simplify the cleaning steps but also to enhance the reagents mixture inside the microsystem by implementing a magnetic actuator.[2] Indeed, the incubation steps have taken place in a very short time. On the other hand, quantum dots were initially conceived as labels of the probe oligonucleotide for the optical detection of the target molecule. As seen, these fluorescent nanoparticles can provide highly sensible signals at low cost, conferring greater sensitivity and shorter response times than other labels. However, this is a very challenging goal, and thus, the feasibility of the microsystem has been firstly tested by using an enzyme as marker, since these compounds can highly amplify the signal by continuously generating the enzymatic product. Thus, *E. coli* has been optically determined through the enzymatic reaction of β-galactosidase (attached to the oligonucleaotide probe) with ortho-nitrophenyl-β-galactoside (ONPG), which generates o-nitrophenol (ONP) that absorbs at 420 nm.

The microsystem is composed of a microfluidic platform, where takes place the magnetic bead-based enzyme-linked oligonucleotide sandwich assay; the magnetic actuator, responsible of moving MBs along the reaction chamber of the platform;[2] a flow set-up for propelling reagents to the device; and a miniaturized detection system to register the optical signals. The cost of the whole microsystem is considerably small, since the employed magnetic actuator and optical detection system are based on cheap components. The microfluidic platform has been constructed with COC substrate material due to its biocompatibility and transparency, and is composed of the necessary inlet / outlet channels for the entrance and evacuation of reagents, and the reaction and detection chambers. The reaction and detection stages have been carried out in separate chambers to avoid the interference of MBs in the optical signal.

---

[46] Kim, H.J.; Park, S.H.; Lee, T.H.; Nahm, B.H.; Kim, Y.R.; Kim, H.Y.; *Biosens. Bioelectron.,* **2008**, 24, 238.
[47] Hsiao, C.R.; Chen, C.H.; *Anal. Biochem.,* **2009**, 389, 118.
[48] Rampal, J.B.; in: *Microarrays: Volume 2 Applications and Data Analysis (Methods in Molecular Biology)*, 2nd ed. Humana Press, **2007**.

As the following results will demonstrate, the microsystem is capable to determine the target *E. coli* oligonucleotide in a rapid and reproducible way due to the automation of the different stages.

6.2.1 MATERIALS, REAGENTS AND METHODS

The materials and equipments required to perform the multi-step magneto-biochemical assay in the microsystem for the determination of *E. coli* are listed in table 6.3.

Table 6.3: General list of equipments used for the determination of *E. coli* in **BMS**.

EQUIPMENT	PROVIDER
• 7 syringes pumps, 540060 TSE systems	TSE systems, Bad Homburg, Germany
• 3 syringe of 1 mL, 2 syringe of 2.5 mL and 2 syringes of 10 mL, GASTIGHT 1000 TLL series	Hamilton, Bonaduz, GR, Switzerland
• Tygon tube (i.d. 1.2 mm)	Ismatec, Zurich, Switzerland
• PTFE tubes (i.d. 0.8 mm)	Techny Fluor, Barcelona, Spain
• 420 nm LED	Roithner Lasertechnik LED420-33, Vienna, Austria
• PIN photodetector	PIN Hamamatsu S1337-66BR, Japan
• DAQ	National Instruments NI USB-6211, Austin, USA
• Polymeric Fibers (NA POF)	Mitsubishi ESKA Premier GH4001, Tempe, USA
• Neodymium iron boron block magnets, grade N50	Chen Yang Technologies GmbH, Finsing, Germany
• D.C. geared motor from Crouzet	Farnell, Barcelona, Spain
• PMMA support	GSB
• Thermomixer	Eppendorf, Hamburg, Germany

Chemicals and ssDNA oligonucleotides used with this purpose are presented in table 6.4. Milli-Q water (18.2 MΩ cm) was used in all solutions.

Table 6.4: Reagents used to perform the multi-step magneto-biochemical assay for the determination of *E. coli* in **BMS**.

REAGENT	PROVIDER
• Carboxylic acid modified MBs, Dynabeads® M-270 Carboxylic Acid	Invitrogen Dynal AS, Oslo, Norway
• ssDNA oligonucleotides, deprotected and desalted	HPLC purification, Sigma-Aldrich, Madrid, Spain
• Streptavidin- β-galactosidase conjugate, lyophilized powder	Sigma-Aldrich, Madrid, Spain
• O-nitrophenyl β-D-galactopyranoside (ONPG)	≥ 98 % (enzymatic), Sigma
• Saline-sodium citrate (SSC) buffer 20x	For molecular biology, Sigma
• Potassium chloride	≥ 99 %, Sigma-Aldrich
• Magnesium sulfate	≥ 97 %, Sigma-Aldrich

• Sodium hydrogenphosphate	ACS reagent, ≥ 99.0 %, Sigma-Aldrich
• Sodium dihydrogen phosphate	ACS reagent, ≥ 99.0 %, Sigma-Aldrich

Carboxylic acid modified MBs (2.8 µm diameter-size), ssDNA oligonucleotides, streptavidin- β-galactosidase conjugate and ONPG are the main reagents of the assay. Three different ssDNA sequences are acquired:

- Capture *E. coli*: 5´-CCGCAGCAGGGAGGCAAACA-$(CH_2)_7$-NH_2-3´
- Target *E. coli*: 5´-
  TGTTTGCCTCCCTGCTGCGGTTTTTCACCGAAGTTCATGCCAGTCCAGCGTTTTTGCAG
  CAGAAAAGCCGCCGACTTCGGTTTGCGGTCGCGGGTGAAGATCCCCTTCTTGTTACCG
  CCAACGCGCAATATGCCTTGCGAGGTCGCAAAATCGGCGAAATTCCATA- 3´
- Probe *E. coli*: 5´-biotin-TATGGAATTTCGCCGATTTT-3´

Capture and probe sequences are complementary to the beginning and end of the target sequence, respectively (both complementary regions are underlined). Capture oligonucleotide is provided with an aliphatic chain as spacer, bearing a final primary amine in order to form an amide with the carboxylic acid of MBs. Probe is provided functionalized with biotin to bind the enzyme, which bears a streptavidin protein, by means of the well-known and strong non-covalent interaction of both compounds.

The different lyophilized oligonucleotides are re-suspended in sterile water and frozen at - 20 ºC in 100 µL aliquots of 100 µM concentration until further use. Once needed, the required target and probe oligonucleotide solutions are obtained by dilution using 5x SSC buffer. In case of probe, a final concentration of 200 nM is prepared; meanwhile 10, 20, 30, 40 and 50 nM solutions are done for target oligonucleotide. Capture sequence is used in the same concentration as stored in the freezer. A 1.5 µg μL^{-1} streptavidin-β-galactosidase conjugate solution is prepared in z-buffer by directly weighting the solid. A 30 mM substrate solution (ONPG) is also prepared in water.

5x SSC buffer solution (hybridization buffer) is done by further dilution of its 20x concentrate, obtaining a 750 mM NaCl and 75 mM sodium citrate solution at pH 7. A solution containing 100 mM PO_4^{3-}, 20 mM KCl and 1 mM $MgSO_4$ at pH 7.0 is used as Z-buffer (amplification buffer). Both SSC buffer and Z-buffer are used in the hybridization and amplification reactions.

On the other hand, a 25 mM 2-(N-morpholino)ethanesulfonic acid (MES) buffer solution adjusted to 5.0, a 50 mM tris(hydroxymethyl)aminomethane (Tris) buffer solution at pH to 7.4, and a 0.01 M phosphate buffered saline (PBS) solution with 0.05 % Tween®20 and 2 % of bovine serum albumin (BSA) at pH 7.4 are also prepared for the functionalization of MBs. Casein blocking buffer 10x is used for the microfluidic platform conditioning. N-hydroxysulfosuccinimide (Sulfo-NHS) and 1-ethyl-3-[3-dimethylaminopropyl]carbodiimide (EDC) are also employed for

MBs functionalization. All reagents are purchased from Sigma-Aldrich. A pH meter is employed to adjust the pH of solutions.

6.2.2 EXPERIMENTAL SET-UP

The whole microsystem to perform the multi-step magneto-biochemical assay for the determination of *E. coli* is composed of a microfluidic platform, a flow set-up, a magnetic actuator and a miniaturized optical system (figure 6.12A). The flow set-up for the dispensing of reagents consists of a set of seven syringe pumps coupled to syringes and connected to the microfluidic platform with PTFE tubes. Syringe pumps are used to independently control the input flow rates of each reagent or buffer solution (MBs-capture, target, probe, enzyme, substrate and buffers). Additionally, a three-way valve and a T-shape connector are also used to simplify the change of buffer when required. A home-made adaptor enables the connection of the PTFE tubes to the microfluidic platform, where o-rings are employed to secure the sealing of the system. The use of this flow set-up allows a continuous or stopped flow working, since it is computer controlled.

The magnetic actuator has been developed in the GSB. However, details of the system are not given in this manuscript due to this work is a fundamental part of another doctoral dissertation, which is currently under development. For further information about it, please refer to the related article.[2] A short description of the system is however detailed below to understand its operation. It consists of a rotating unit where a set of neodymium iron boron block magnets are placed eccentrically to the rotation axis. The rotational movement is provided by a D. C. geared motor. When the microfluidic platform is mounted on top of the actuator (fixed to a support), the reaction chamber of the device is positioned on top of the magnets, under the influence of their magnetic field. The position of the inner and outermost magnets coincides with the extremes of the reaction chamber, so that when the magnetic actuator rotates, the MBs are dragged back and forth (figure 6.12B), allowing the mixture of reagents. On the other hand, when the actuator is stopped, the beads of the reaction chamber are retained due to the magnetic field of a stopped magnet, which is useful to perform the cleaning steps of the assay.

Finally, the miniaturized optical system used for absorbance measurements is based on the one described in previous chapters. In this case, a 420 nm LED, which matches the absorption maximum of ONP, and a photodetector are mounted and integrated in the PCB. A DAQ is employed to modulate the LED and to process the detected signal. Two polymeric fibers (1 mm of diameter) are also used in order to bring light from the emitting source to the microfluidic platform, and to collect the transmitted to the detector. Both fibers are fixed on the top and bottom of the optical detection chamber of the microfluidic system by means of a homemade connection adaptor.

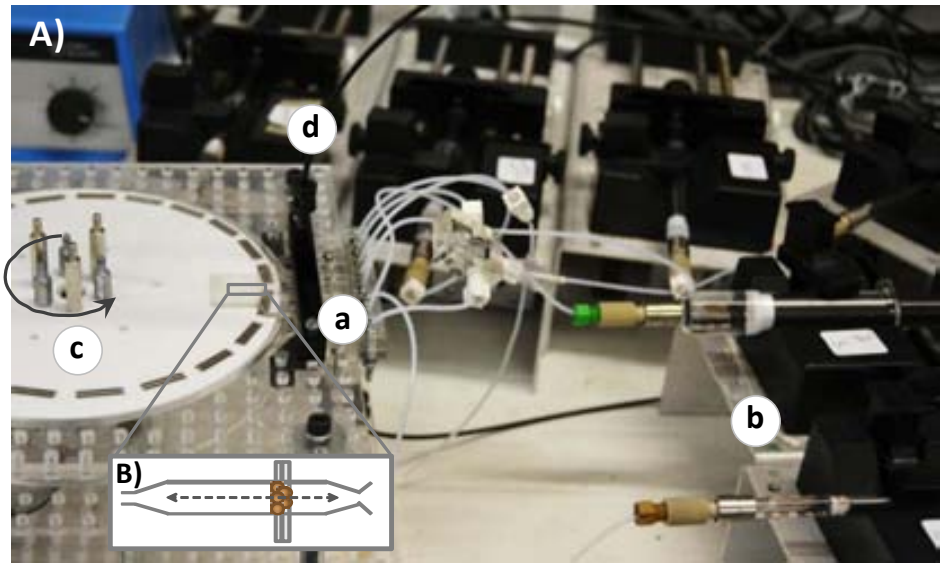

Figure 6.12:
A) Image from the experimental set-up used to perform the multi-step magneto-biochemical assay for the determination of *E. coli*, where the microfluidic platform (a), flow set-up (b), magnetic actuator (c) and optical fibers (d) are depicted. **B**) Amplification of the reaction chamber of the microfluidic platform. The image schematizes the movement of MBs along the chamber due to the magnets movement.

6.2.3 FUNCTIONALIZATION OF MAGNETIC BEADS

Prior to the assay, it is necessary to functionalize the surface of the magnetic microparticles with the capture strand. This conjugation was done following a procedure recommended by Invitrogen Dynal, which consisted on the initial activation of the carboxylic acid-beads with a carbodiimide followed by covalently coupling the amine of the capture oligonucleotide, resulting in a stable amide bond between the bead and the capture. Thus, 100 µL (3 mg) of carboxylic acid-MBs solutions were firstly placed in a 1.5 mL eppendorf tube. The supernatant was pipetted off from the eppendorf by trapping the beads with a magnet, and 100 µL of a 25 mM MES buffer solution at pH 5.0 were added to the eppendorf. The re-suspended particles were placed in a Thermomixer and rocked for 5 min at 850 rpm. This washing process was carried out by triplicate. Later, 21 µL of a 100 µM (2.1 nmols) capture oligonucleotide solution were added to the cleaned and dried MBs of the eppendorf and brought to a final volume of 100 µL with MES solution. The mixture was incubated in the Thermomixer during 30 min under the same rocking conditions as before to immobilize the DNA probe on the surface of the paramagnetic beads by electrostatic interactions. Then, 3 mg of EDC recently weighted and 9 mg of sulfo-NHS were added to the incubated solution and placed again in the rocking machine during 12 h to ensure the complete formation of the amide. The supernatant was removed again, and 100 µL of 50 mM Tris solution at pH 7.4 were added to the eppendorf. The solution was rocked for 10 min in order to block the remaining carboxylic acid groups of MBs. Once discarded the excess of Tris, a PBS solution (0.01 M of PBS with Tween® 20 solution and 2 % BSA) was used as blocking buffer to clean the conjugated MBs (by triplicate). Finally, the capture functionalized beads were re-suspended in SSC buffer and washed again by triplicate. All procedure was carried

out at room temperature. The obtained capture probe functionalized MBs (MBs-capture) were stored at 4 ºC until their use.

6.2.4 DEVELOPMENT OF THE MICROFLUIDIC PLATFORM

First microfluidic devices to perform the multi-step magneto-biochemical assay were developed using ceramic material. Their designs were based on mixing strategies,[49-50] where microfluidic meanders were introduced to achieve the mixture and incubation of reagents while flowing inside the microsystem. A magnet was placed at the end of the micromixers to simplify cleaning steps. However, occlusion of the fluidic structures was observed in all experiments performed. Due to the opacity of the material, which did not allow the inner visualization of the solution, it was very difficult to know what was happening inside the microsystem. Nevertheless, the occlusion was probably due to the accumulation of MBs on the corners of the micromixers for the small dimensions of the constructed microchannels, which pretended to minimize incubation times. On the other hand, the use of a continuous flow of bioreagents presented a huge waste of these expensive compounds. Therefore, the strategy was completely changed, and the idea of using ceramic material was dismissed.

As an alternative, the use of a transparent substrate material for the construction of the microfluidic platform was clear. Thus, COC was preferred, since it confers a high transparency in the UV-Vis region and it is highly compatibility with bioreagents. The new approach was based on using the magnetic properties of MBs not only as substrate support of the bioassay to simplify the cleaning steps but also as the tool for the mixture of the bioreagents making use of a magnetic actuator. Therefore, the design was conceived based on a reagent chamber to perform the incubation steps, and another chamber to carry out the detection stage. The device was constructed using three different polymeric layers (two 500 µm-thick layers and one 1000 µm-thick layer). Its final design consisted of seven different inlets, which converged in a reaction chamber. Five of the inlets allow the entrance of the different necessary reagents: MBs-capture, target, probe, enzyme and substrate. The MBs-capture are entered in the system through a simple straight channel to avoid the possible deposition of beads in corners or irregularities of the microchannel. The two other inlets are used for buffer solution, and are located one opposite to the other to ensure a correct cleaning of the reaction chamber in the different incubations performed. A T-shaped junction was used to branch off the buffer solution coming from the syringe to both buffer inlets. The reaction chamber of 25 µL (2 mm wide, 12 mm long and 1

[49] Sochol, R.D.; Casavant, B.P.; Dueck, M.E.; Lee, L.P.; Lin, L.; *J. Micromech. Microeng.*; **2011**, 21, 054019.
[50] Chen, L.; Lee, S.; Lee, M.; Lim, C.; Choo, J.; Park, J.Y.; Lee, S.; Joo, S.-W.; Lee, K.-H.; Choi, Y.-W.; *Biosens. Bioelectron.*, **2008**, 23, 1878.

mm high) enables the incubation, cleaning and amplification steps. Since the microfluidic platform was located on the top of the magnetic actuator, MBs can be moved along the reaction chamber and retained depending on whether the magnets are moving or stopped.[2] A simple channel connects the reaction chamber with an optical detection chamber (25 µL), which perfectly matches with the optical fibers, located on top and bottom of the device, to register the optical signal of the coloured compound. Finally, a collection channel to the outlet enables the evacuation of liquids. An image of the microfluidic platform is shown in figure 6.13.

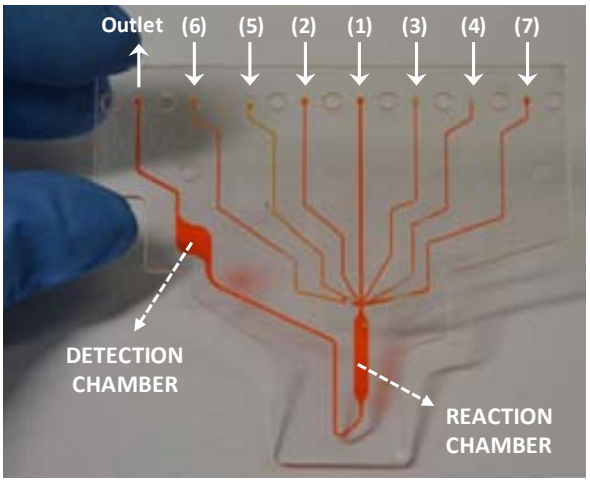

Figure 6.13: Image from the microfluidic platform, where the seven different inlets, the reaction chamber, the optical detection chamber and the outlet are marked. 1: MBs-capture, 2: target oligonucleotide, 3: probe oligonucleotide, 4: enzyme, 5: substrate, 6 and 7: SSC buffer or Z-buffer inlets.

6.2.5 MULTI-STEP MAGNETO-BIOCHEMICAL ASSAY

As previously stated, the determination of *E. coli* was done by a magnetic bead-based enzyme-linked oligonucleotide sandwich assay. A 166-bp structural fragment of the *uid A* gene was used as target, which has been reported to be unique and well conserved in general *E. Coli*.[51 - 52] Complementary fragments of 20-bp were employed to ensure a selectively identification of the beginning and end of the gene fragment.

A sequential approach was preferred to simplify the whole system. Thus, three different steps were required, as many as incubations, two for the hybridization of the oligonucleotides (MBs-capture with the target, and the last one with the probe) and another to perform the labelling of the probe oligonucleotide with the enzyme; each one with its corresponding washing step. A final amplification stage was also required, where ONPG was hydrolyzed to galactose and ONP, which could be monitored at 420 nm.[53] Thus, the presence of ONP at the end of the assay entailed the formation of the whole complex. An scheme of the assay is depicted in figure 6.14A. The

[51] Iqbal, S.; Robinson, J.; Deere, D.; Saunders, J.R.; Edwards, C.; Porter, J.; *Lett. Appl. Microbiol.*, **1997**, 24, 498.
[52] Sun, H.; Choy, T.S.; Zhu, D.R.; Yam, W.C.; Fung, Y.S.; *Biosens. Bioelectron.*, **2009**, 24, 1405.
[53] Baeza, M.; López, C.; Alonso, J.; López-Santín, J.; Álvaro, G.; *Anal. Chem.,* **2010**, 82, 1006.

procedure used as well as the optimization and the analytical features of the microsystem are described below.

6.2.5.1 DESCRIPTION OF THE ASSAY PROCEDURE

The procedure to perform the entire assay in the microsystem was the following described. As pointed out, a set of syringe pumps, a magnetic actuator and a miniaturized optical system were employed. Due to the computer controlled operation of the syringe pumps and the optical system it is feasible to automate the whole assay. Figure 6.14B and C shows an schematic representation of the experimental set-up and a diagram of the different status of the syringes and the magnetic actuator during an assay. One should be referred to them to understand the whole procedure. It should be noticed that syringe pumps and magnetic actuator operate alternately.

Prior to the assay, the whole microfluidic platform was flushed with casein blocking buffer solution for 10-15 min to remove air as well as to minimize unspecific adsorptions of reagents and sticking of particles to the walls of the polymeric platform. This was followed by flushing hybridization buffer (SSC buffer).

MBs-capture (**a**) were firstly pumped to the microfluidic platform at 80 µL min^{-1} through inlet **1** in a concentration of 0.09 µg $µL^{-1}$ of MBs with approximately 65 nM of immobilized capture oligonucleotide. To ensure the total retention of beads in the reaction chamber, the magnetic actuator was maintained stopped, so beads were retained in a particular point of the chamber, where a magnet was located. Thereafter, 50 µL of target oligonucleotide solution (**b**) were pumped through inlet **2** at 30 µL min^{-1} in a concentration covering the range of 10 - 50 nM. This volume ensures the presence of reagent in the whole reaction chamber (25 µL). Then, the magnetic actuator was switched on, so the magnets began to move during certain time (1 - 20 min), enabling the mixture of target and capture through the movement of MBs along the whole chamber. Its cleaning was performed by flowing SSC buffer (**f**) across the microfluidic platform by inlets **6** and **7** at 50 µL min^{-1} for 1 min. This process was carried out, as in all the following necessary washing steps, while the magnetic actuator was stopped, since in this way all MBs were retained in a specific point. Moreover, the simultaneous operation of both (syringe pumps and magnetic actuator) could cause the outflow of some beads. Once streamed the hybridization buffer, probe-biotin oligonucleotide (**c**) was pumped to the microfluidic platform through inlet **3** (50 µL of 200 nM solution at 30 µL min^{-1}). The operation of the magnetic actuator was again activated to promote the second hybridization of oligonucleotides.

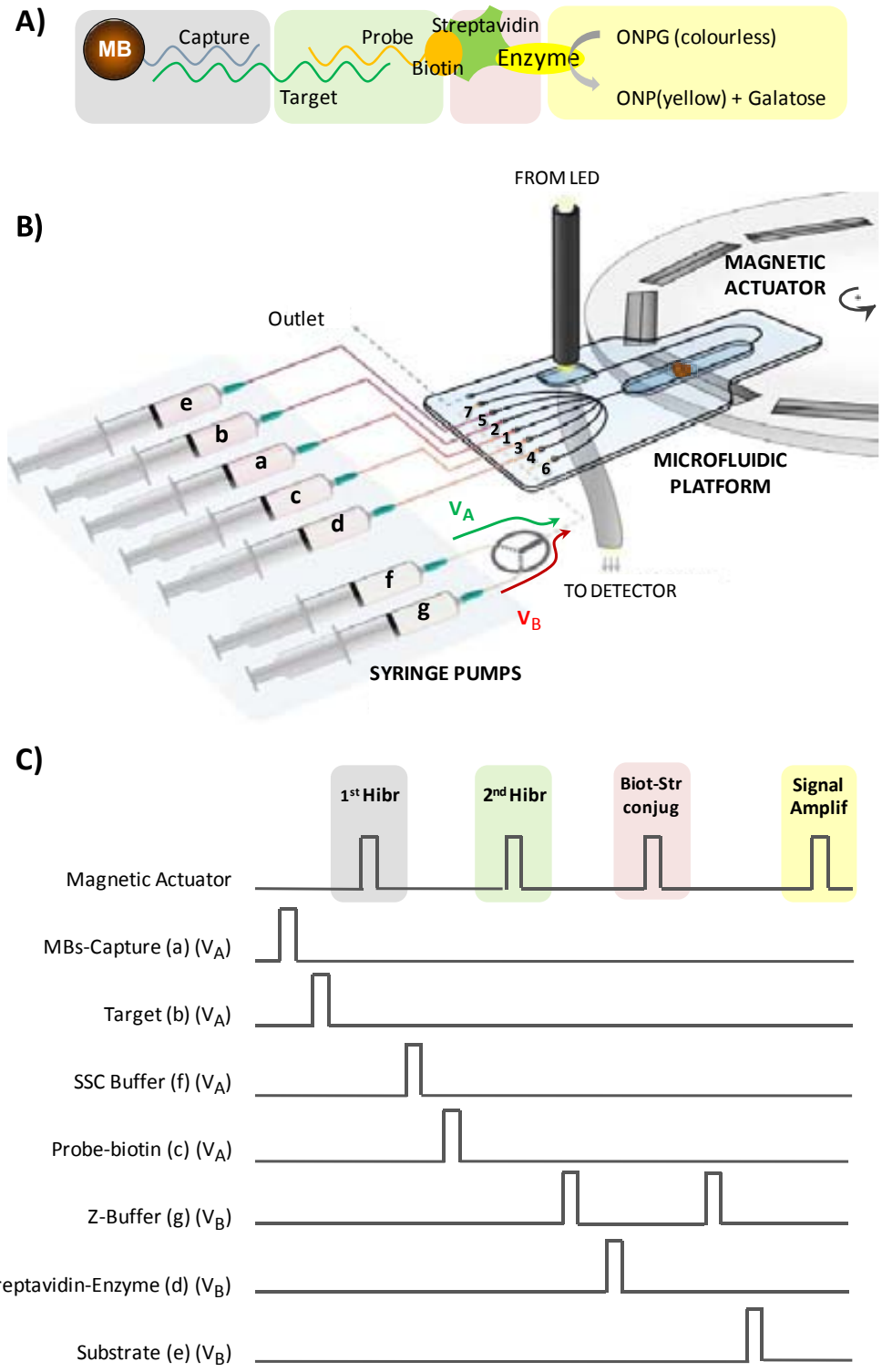

Figure 6.14: **A**) Schematic representation of the complete assay. **B**) Scheme of the experimental set-up, where the microfluidic platform, magnetic actuator, optical components and flow components are depicted. Syringe reagents: a: MBs-Capture; b: Target; c: Probe-biotin; d: Streptavidin-Enzyme; e: ONPG; f: SSC buffer; g: z-buffer. Inlet channels: 1: MBs-Capture; 2: Target; 3: Probe-biotin; 4: Streptavidin-Enzyme; 5: ONPG; 6 and 7: buffers. **C**) Diagram of the different status of the syringes and the magnetic actuator during the assay. Each change of state in the signal involves the on/ off of the different components (high level: on/working; low level: off/stopped). V_A and V_B refers to the position of the valve for the buffer selection.

The reaction chamber was conditioned thereafter with z-buffer (**g**) (amplification buffer), since the manipulation of β-galactosidase is preferred in those conditions.[53] It was pumped through the same inlets as the previous buffer (**6** and **7**) by means of a three-way valve, which permitted the entrance of hybridization or z buffers. Once z-buffer was flushed in the whole microfluidic platform, 50 µL of streptavidin- β-galactosidase conjugate solution (1.5 µg μL^{-1}) (**d**) were pumped

at 30 µL min^{-1} through inlet **4** to the reaction chamber, and the magnetic actuator took over the last incubation reaction, where probe oligonucleotide was linked to the enzyme through the streptavidin-biotin complex.

Once the excess of the enzyme was removed from the reaction chamber with z-buffer, its filling with substrate solution was accomplished by pumping 100 µL of a 30 mM ONPG solution (**e**) at 100 µL min^{-1} through inlet **5**. The MBs-oligonucleotides-enzyme conjugate was mixed with the substrate by means of the magnetic actuator until obtaining a reliable signal of product (ONP) (from 1 to 15 min). The read out of ONP was carried out in a separate chamber (detection chamber) to minimize noise from the colloid. Once performed the amplification reaction, the substrate solution was continuously pumped to the microfluidic platform, so the generated product moved from the reaction to the detection chamber. Since the optical system was continuously working, a transitory signal was attained, where its maximum intensity corresponded to the absorbance value of the sample analyzed. At the time, the continuous flow of substrate generated the renovation of the solution in the reaction chamber, so a new amplification reaction could be performed in order to obtain a replicate of the measure. Three measures were done for each assay, where ONPG absorbance intensity was used as baseline and blank signal.

6.2.5.2 OPTIMIZATION OF THE MICROSYSTEM FOR THE MULTISTEP DNA ASSAY

The optimization of certain parameters is necessary in order to minimize the total analysis time while obtaining a maximum sensitivity in the assay. Thus, the concentration of MBs, amplification time, rotation speed and incubation time were studied. All assays were performed by triplicate at room temperature using a 20 nM target solution. Assays in absence of target oligonucleotide were also done (n=3), which were used as blanks.

Two different concentrations of MBs were tested for its optimization. As described in the assay procedure, a diluted solution from the stock prepared in the functionalization of beads (0.09 µg $µL^{-1}$ MBs) was used. A total amount of 1000 or 1500 µL of this solution was pumped into the microfluidic system. Since beads are retained in the reaction chamber by means of magnets, a final concentration of 3.6 µg $µL^{-1}$ or 5.0 µg $µL^{-1}$ of MBs were respectively achieved. The minimal rotation speed at which the magnetic actuator can work was employed (3.3 mm s^{-1}) to ensure the higher magnetic field from magnets. The insertion of 1000 µL did not enable the complete trigger of the beads from one side to the other of the chamber. On the other hand, a block movement of the particles was observed when using 1500 µL of MBs. Thus, this volume was selected as the optimized one and is used hereafter.

Then, the influence of the amplification time of the enzymatic reaction was studied. The complete assays were performed by using the magnetic actuator at 3.3 mm s^{-1}. A reaction time of 20 min was preferred for all three incubations to ensure the complete hybridization of all oligonucleotides and the formation of the avidin-streptavidin complex. From the three different amplification times tested (2, 10 and 15 min), the larger provided the higher absorbance signal while offering the lower relative standard deviations (RSD) as well (figure 6.15A). Thus, 15 min were preferred for further experiments.

Then, the rotation speed of the magnetic actuator was studied. This is a critical parameter, since it is related to the efficient mixing of reagents and also to the effective surface area of MBs. Thus, a correct movement of beads inside the reaction chamber permits MBs to reach all reagents. Therefore, the process is no longer controlled only by diffusion. Furthermore, when the particles are moved as a loose cloud, its effective surface area is increased, which improves the accessibility of reagents to the reactive site of beads. All this contributes to enhance the sensitivity and detection limit of the assay.[2] So, the working of the magnetic actuator at 3.3, 5.0 and 6.7 mm s^{-1} was tested while employing 20 min of incubation time. A clear improvement of the signal, with a minimum RSD, was observed at 3.3 mm s^{-1} (figure 6.15B) because at higher rotation speeds the beads cannot follow the movement of the magnets along the chamber. No lower values of rotation speed were possible to test due to limitations of the spindle motor used. Nevertheless, previous works developed in the research group showed the existence of an optimized rotation speed over the same value, since at lower rotation speeds the particle cloud becomes more compact, diminishing the effective surface area of beads.[2] Therefore, a rotation speed of 3.3 mm s^{-1} was used hereafter.

In the proposed microsystem, three different incubations are required. The optimization of their duration is therefore of major interest, since the reduction of incubation times can extremely decrease the total analysis time. Four different incubation times were tested (1, 5, 10 and 20 min), which showed equivalent absorbance signals as shown in figure 6.15C. Therefore, 1 min was chosen as optimized value. The entire procedure required of approximately 20 minutes, being the amplification stage the larger one.

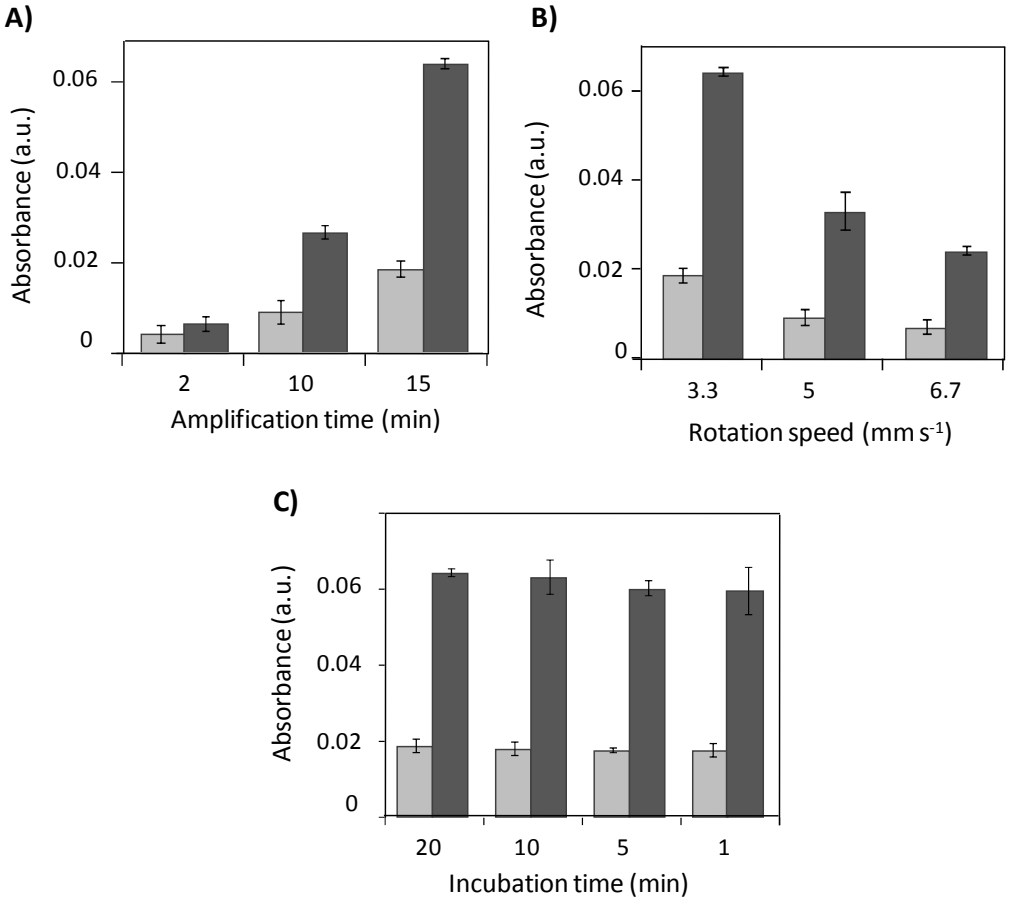

Figure 6.15: Signals obtained from the different experiments performed during the optimization of the microsystem (n=3). (**A**) Amplification time, (**B**) rotation speed and (**C**) incubation time of the assay. Dark bars show the absorbance signal for a 20 nM *E. coli* target. Light bars are blank signals.

6.2.5.3 ANALYTICAL FEATURES OF THE MICROSYSTEM FOR THE DETERMIANTION OF *E. COLI*

Once optimized the different studied parameters of the microsystem, its sensitivity and detection limit were evaluated from calibration curves, since a proportional relation between the concentration of the target oligonucleotide and the absorption intensity registered exists. Thus, 10, 20, 30, 40 and 50 nM target solutions were tested at room temperature in the microfluidic platform using the optimized parameters. Figure 6.16A shows the linear response observed (R^2 = 0.991), where a sensitivity of 0.0026 a.u. nM^{-1} was attained. The limit of detection of the method, calculated as three times the standard deviation of the blank signal, was of 1.1 nM. The reproducibility of the method was also evaluated, obtaining a relative standard deviation of 4.1 % (n=3) (figure 6.17B).

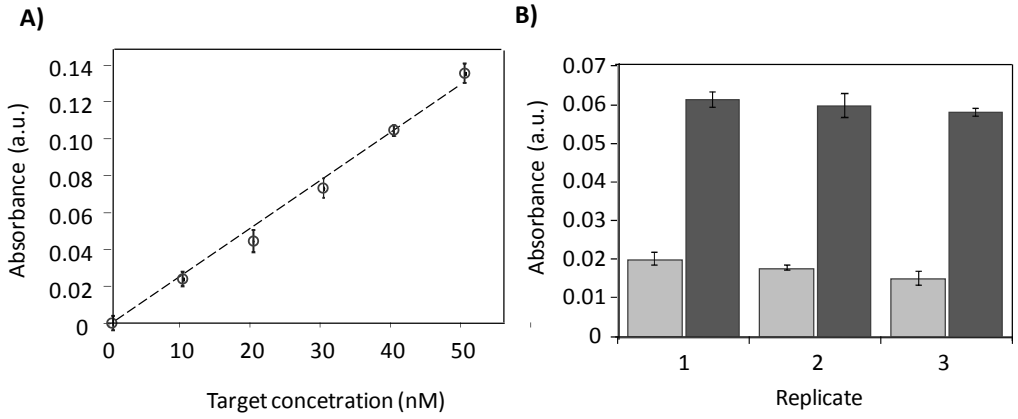

Figure 6.16:
A) Calibration curve for *E. coli* using **BMS**. **B**) Reproducibility of the method for three different assays for a 20 nM *E. coli* solution. Dark bars are the absorbance signal for *E. coli* target, and light bars are blank signals.

6.2.6 CONCLUSIONS

In this chapter, it has been designed, constructed and evaluated an automatic microsystem for the determination of *E. coli* in water through a magnetic bead-based enzyme-linked oligonucleotide sandwich assay. As seen, the use of MBs in the microfluidic platform as both the bioassay support and the active agent for mixing reagents, by means of a magnetic actuator, allows, on the one hand, to simplify the cleaning steps of the assay and, on the other hand, to achieve an efficient mixing of reagents. After the optimization of the concentration of the MBs used, the amplification time of the enzymatic reaction, the rotation speed of the magnetic actuator, and the incubation time of the oligonucleotide hybridizations and the labelling reaction, the detection limit of the microsystem has been in the nanomolar range with a total analysis time of approximately 20 minutes. The speed of the assay is partly due to the use of microfluidics, which minimizes the diffusion distances of reactants, partly due to the employment of the magnetic actuator, which generates an effective mixture, helping both to reduce incubation times to only one minute.

Due to the automation of the different stages of the assay, the microfluidic system presents an easy operation and no significant variations between assays have been obtained. Although the system has been developed for the determination of *E. coli*, it can be simple adapted to perform any multi-step magneto-biochemical assay by only changing the sequence of the oligonucleotides. Moreover, the system could be capable to perform multiplexing by using different microfluidic platforms in a parallel configuration or, more interestingly, by carrying out different assays in the same platform by using different absorbing or emitting compounds. Therefore, the microsystem is a useful alternative to perform automatic hybridization analyses in a rapid, simple and reproducible way.

It has not been possible to perform the evaluation of the microsystem based on the use of fluorescent particles during the course of this dissertation due to the

completion of this thesis. Nevertheless, this challenge is left as future perspectives to the research group. The use of these fluorescent nanoparticles within the microsystem will probably provide better analytical features.

CONCLUDING REMARKS AND FUTURE PERSPECTIVES

Results obtained along the diverse steps of the present work thesis have demonstrated the advantages of using nanomaterials in conjunction with microfluidics. Thus, efficient miniaturized equipments/instrumentation have been developed in terms of sensitivity, selectivity and easy operation, which can perform *in situ* measurements. Good repeatability and reproducibility is also achieved with the use of the developed analytical systems thanks to the automation of all the analytical procedure and, on the other hand, to the homogeneous and well defined nanoparticles employed as labels or as selective recognition elements. In this sense, the development of microreactors for the synthesis of these nanostructured materials has been crucial. The constructed devices have allowed to obtain uniform, well dispersed and stable particles in a very reproducible way.

Specific conclusions on each proposed microsystem have been presented at the end of the different section of the manuscript. In general, we here achieved to integrate and combine the necessary microfluidics for each purpose, miniaturized optical detection systems (both absorbance and fluorescence), the required pre-treatment steps (mixing, heating and temperature control and electronics), and other actuators such as magnetic platforms, the development of which is part of another thesis project in the research group. Other external components such as bulky syringe pumps for microfluidics control and dosing is still a challenge in our research group. However, strategies such as multicommutation and aspiration would lead to at least reduce the number of employed syringe pumps.

Finally, it is important to mention that the present work has opened a new research line in the research group, focused on process intensification based on the use of miniaturized instrumentation and microfluidics. In fact, a challenging long term goal in the field of microsystems and nanotechnology is the integration of diverse modular devices, which include all the required steps for a μ-TAS, involving devices for the synthesis of nanomaterials and their purification, and platforms for the selective recognition of different types of analytes, based on the previous nanomaterials synthesized.

Another issue for further investigation is the development of compatible miniaturized optical systems in order to achieve the detection of a bioassay in the fabricated microsystems by using fluorescent nanoparticles as labels at low

concentration. On the other hand, electrochemical miniaturized analytical systems based on nanomaterials could also be developed.

ANNEX A: CAD DESIGNS

Contents

The design of the different layers which constitute the final ceramic or polymeric devices are presented below.

A.1 CAD DESIGN OF MR1

In this case, three different prototypes are designed in the same ceramic layer. The designs correspond, from left to right, to the microreactors **MR1B**, **MR1C**, **MR1F**, employed in the synthesis of silver nanoparticles . In all cases the main channel is of 1.1 mm.

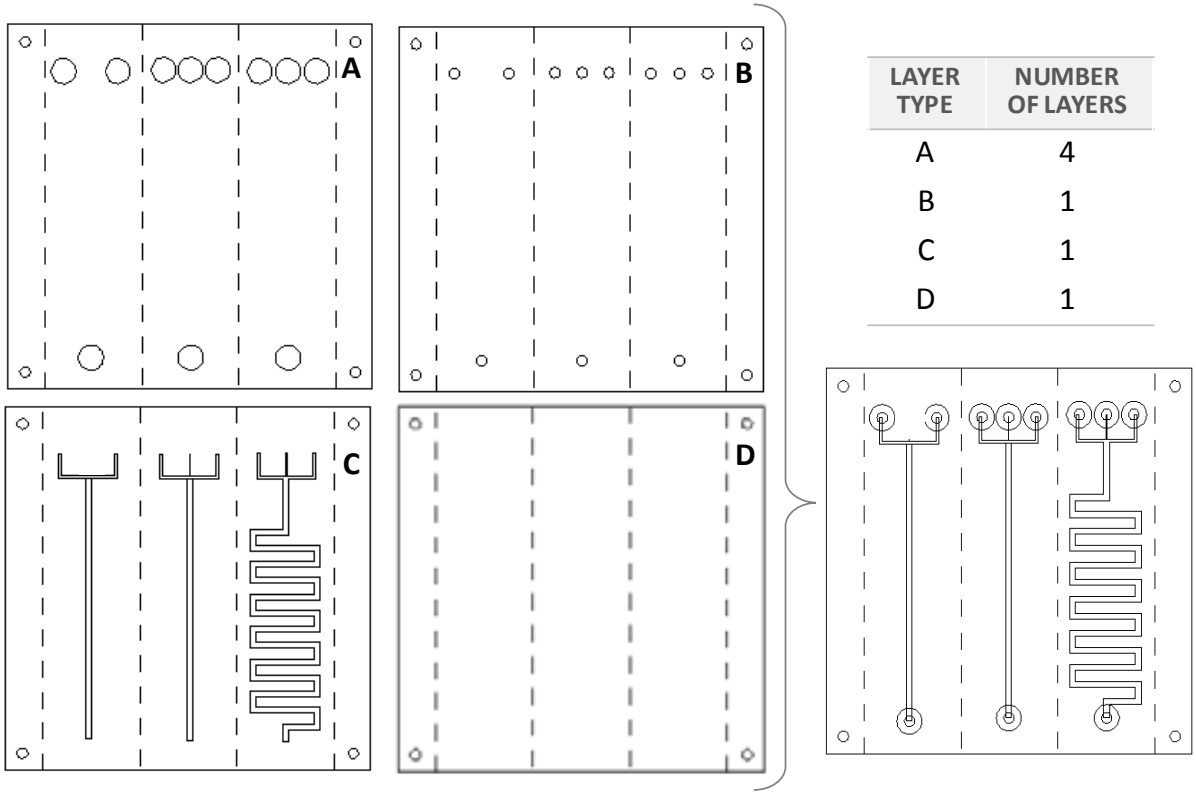

LAYER TYPE	NUMBER OF LAYERS
A	4
B	1
C	1
D	1

A.2 CAD DESIGN OF MR2

The ceramic layers depicted bellow correspond to the design of two identical microreactors for the synthesis of gold nanoparticles (**MR2**). The dimensions of the three-dimensional micromixer are shown in the amplification box.

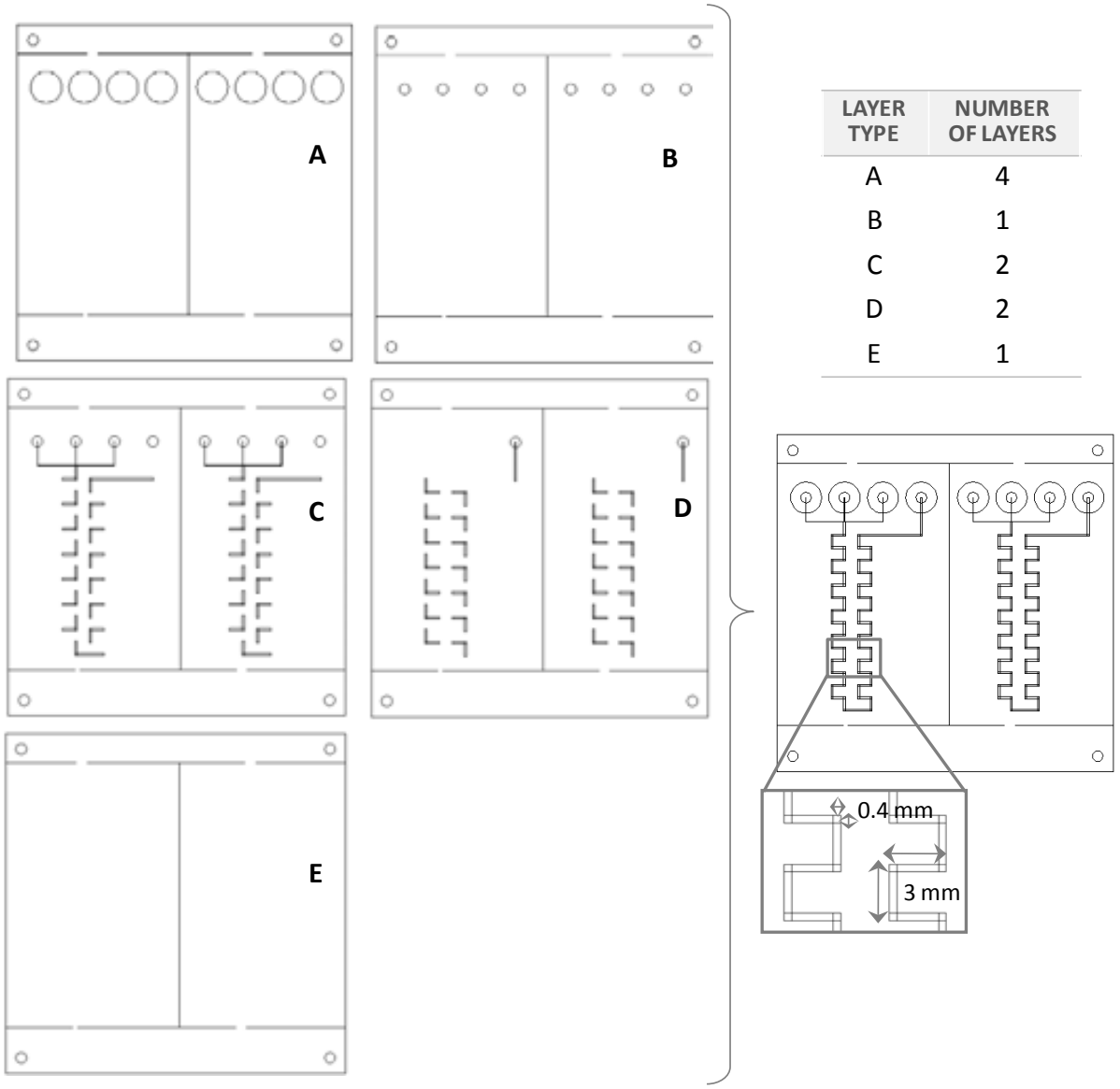

LAYER TYPE	NUMBER OF LAYERS
A	4
B	1
C	2
D	2
E	1

A.3 CAD DESIGN OF MR3

The following layers compose the microreactor used in the synthesis of gold nanoparticles stabilized with alkanethiols (**MR3**). The dimensions of the three dimensional micromixer are the same as for **MR2**.

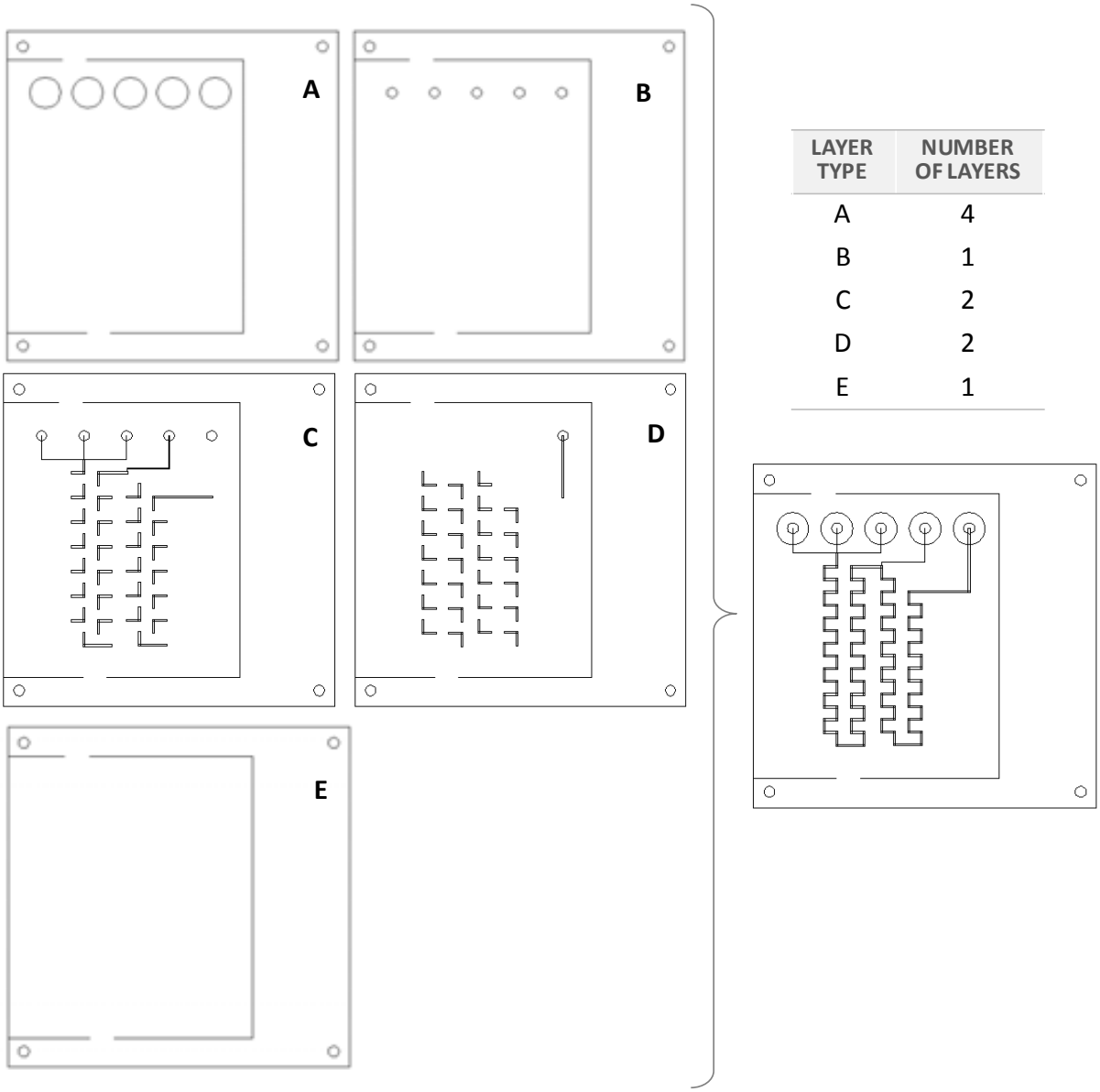

LAYER TYPE	NUMBER OF LAYERS
A	4
B	1
C	2
D	2
E	1

A.4 CAD DESIGN OF MR3 WITH INTEGRATED OPTICAL DETECTION

Ten layers compose this microreactor. The design of the device is the same as for **MR3**, but including an optical window for the optical monitoring of the reaction. *A* and *A'* designs are mechanized in a unique ceramic substrate. *A* design is drilled from one side to the other of the ceramic substrate , while *A'* is mechanized by means of low relief. The same goes with *F* and *F'* designs. However, they are reverse designed, since they must be mechanized in the opposite face of the ceramic substrate.

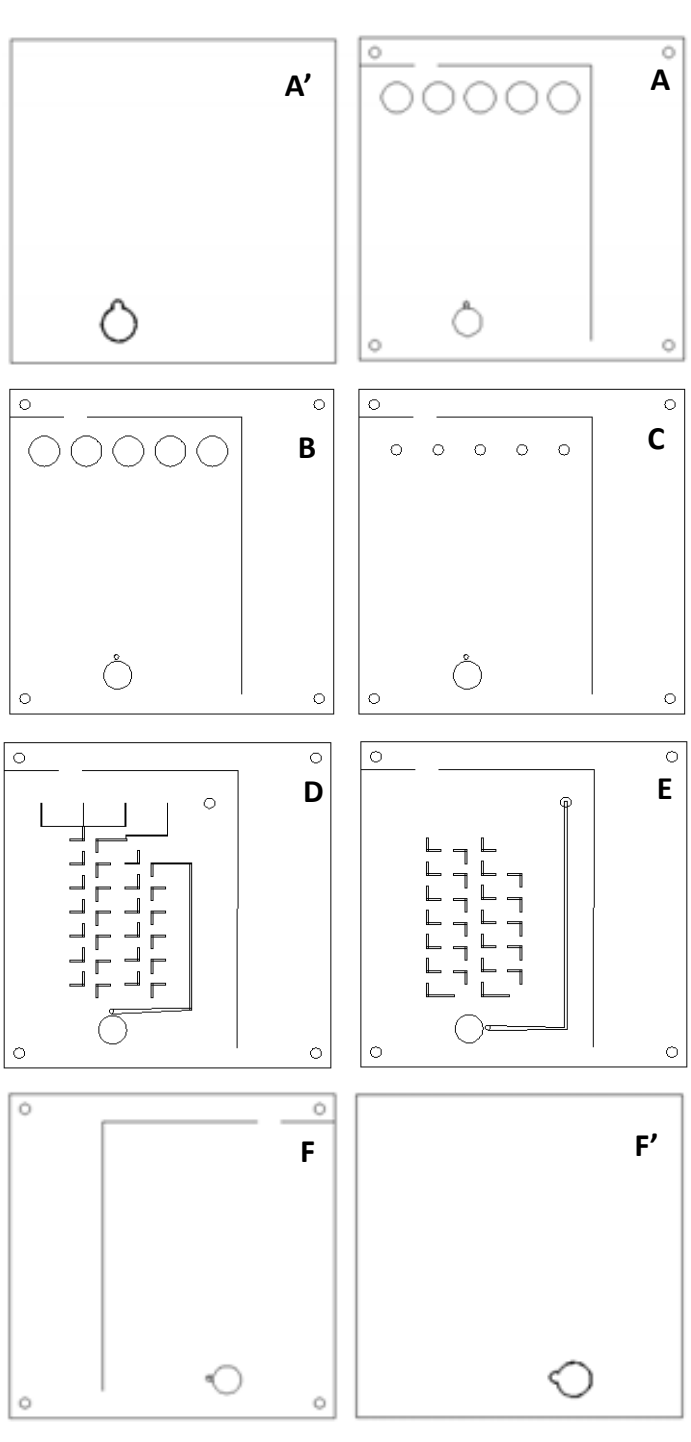

LAYER TYPE	NUMBER OF LAYERS
A+A'	1
B	3
C	1
D	2
E	2
F+F'	1

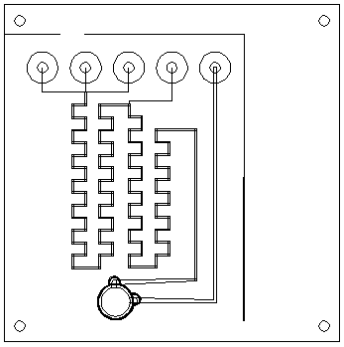

A.5 CAD DESIGN OF THE MR4

The following design corresponds to two identical microreactors for the synthesis of CdS nanoparticles. The dimensions of the three dimensional micromixer are the same as for **MR2**.

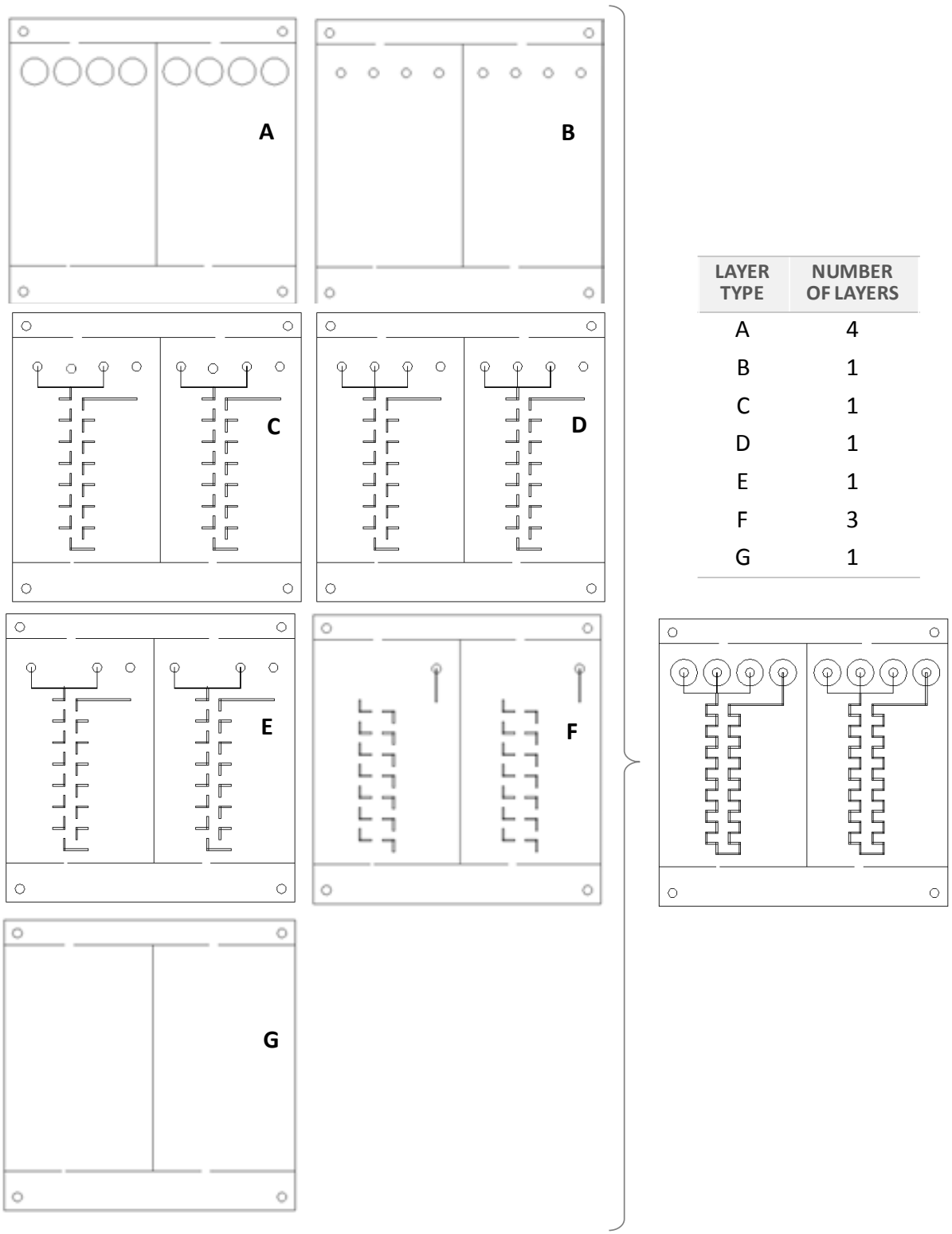

LAYER TYPE	NUMBER OF LAYERS
A	4
B	1
C	1
D	1
E	1
F	3
G	1

A.6 CAD DESIGN OF MR5

Ten layers compose the microreactor for the synthesis of CdS/ZnS core-shell quantum dots in aqueous medium, which are depicted below. Again, the three dimensional micromixer is the same as for **MR2**.

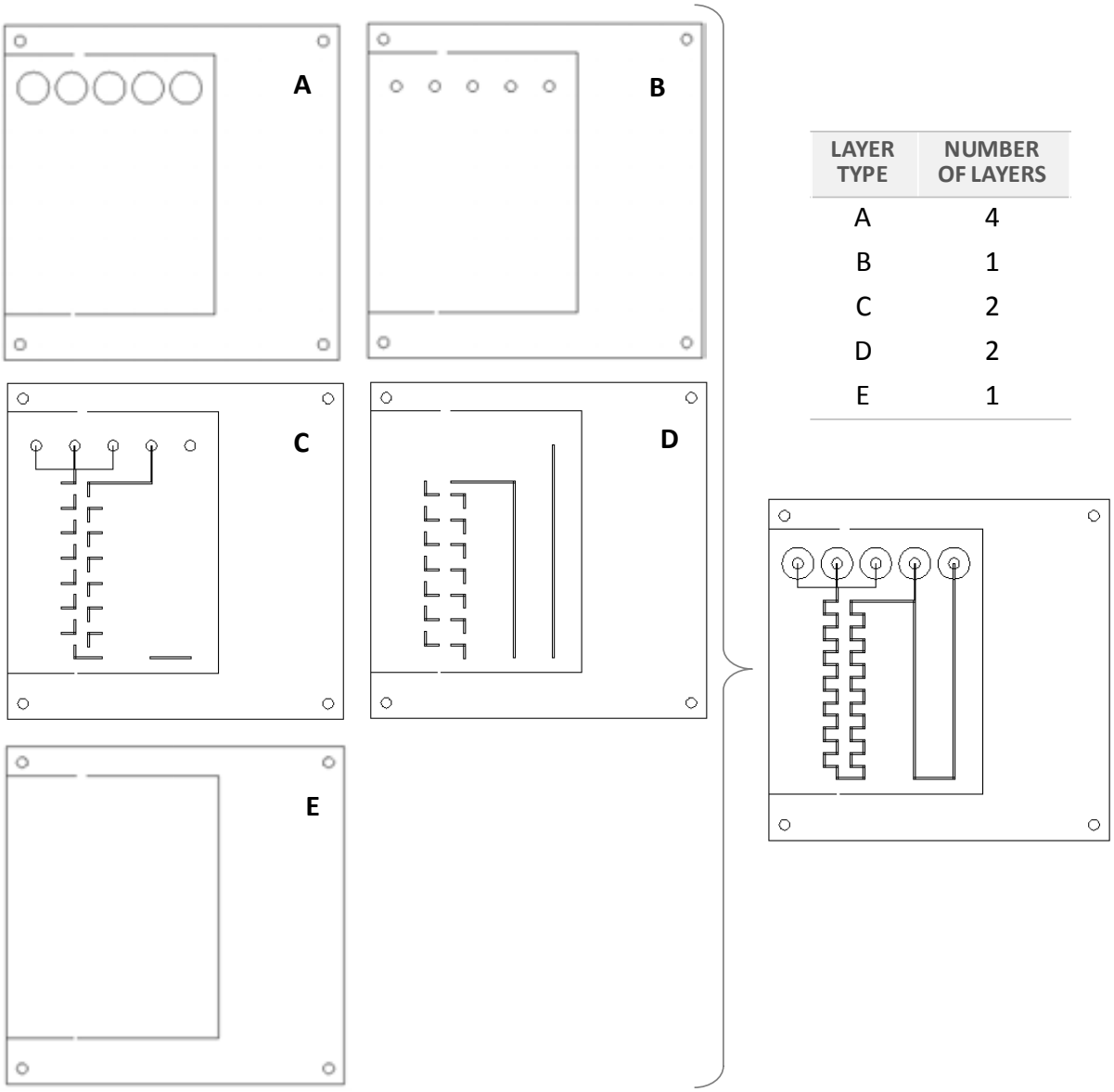

LAYER TYPE	NUMBER OF LAYERS
A	4
B	1
C	2
D	2
E	1

A.7 CAD DESIGN OF MR5 WITH INTEGRATED OPTICAL DETECTION

The following ceramic layers correspond to the design of the microreactor for the synthesis of CdS/ZnS core-shell quantum dots with an optical window for the absorbance and fluorescence monitoring of the reaction. Again, the three-dimensional micromixer is identical to **MR2**. The layers corresponding to the upper and lower sides of the optical window (*B, B'* and *G, G'*) are mechanized as **MR3** with optical window (A.4).

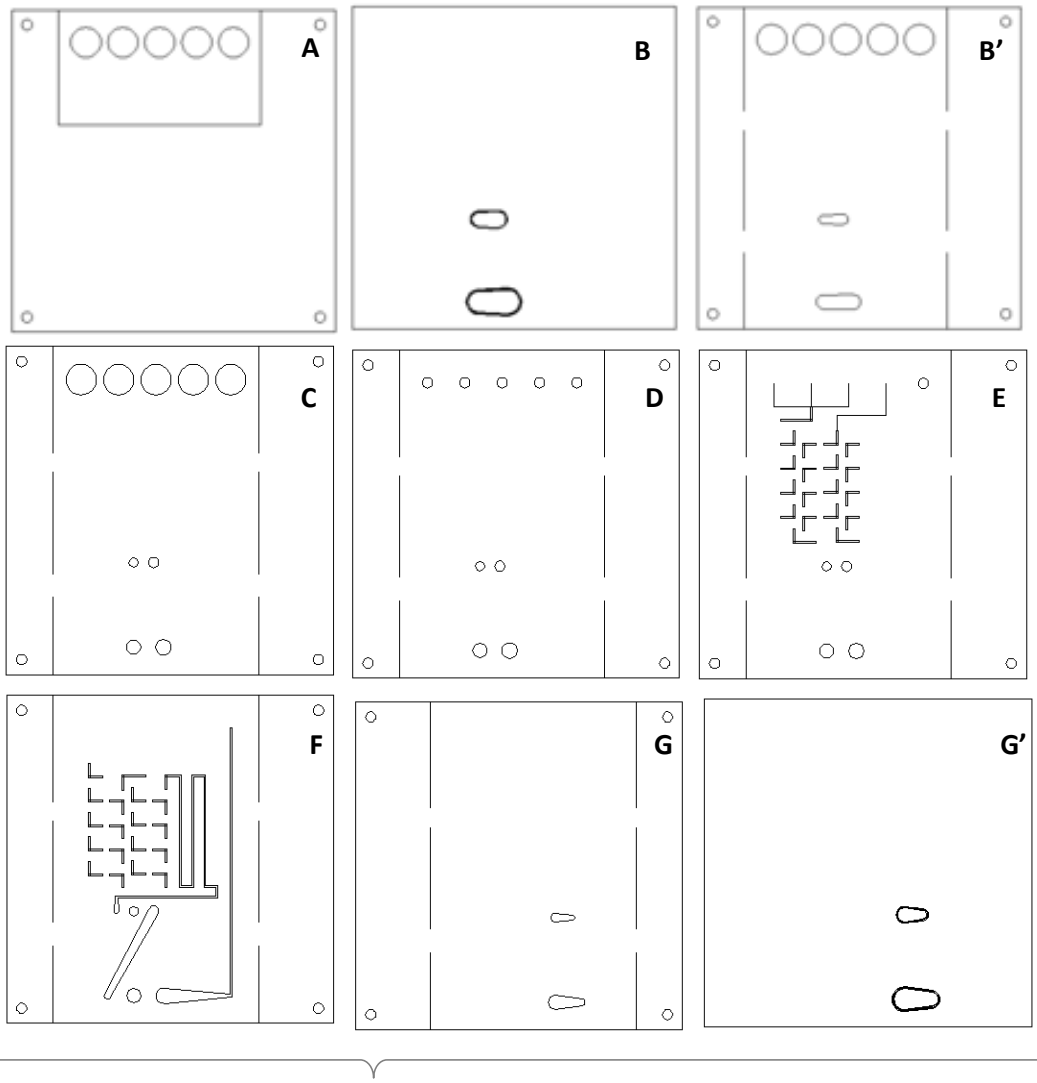

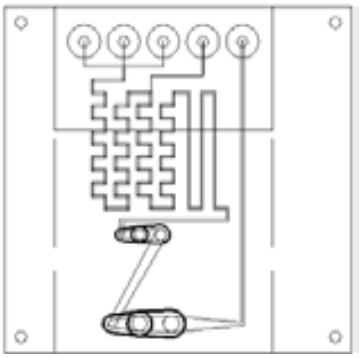

LAYER TYPE	NUMBER OF LAYERS
A	2
B+B'	1
C	1
D	1
E	2
F	2
G+G'	1

A.8 CAD DESIGN OF MR6 MICROREACTOR

The design of **MR6** for the synthesis of nanocrystals at high temperatures are presented below. The dimensions of the bi-dimensional micromixer are also shown in the amplification box. The overlapped layers of the heater is represented with the screen printing of the necessary pastes to make simpler its understanding.

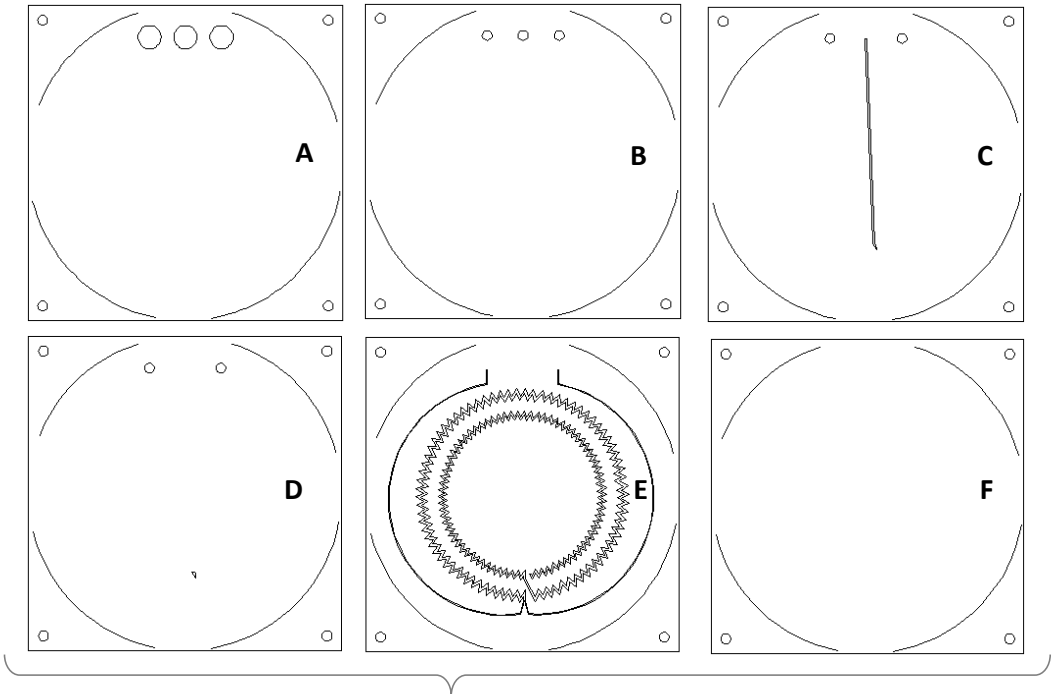

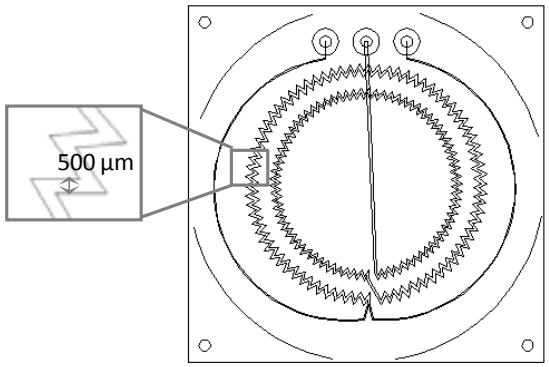

LAYER TYPE	NUMBER OF LAYERS
A	3
B	1
C	1
D	1
E	1
F	1
G	4
H	5

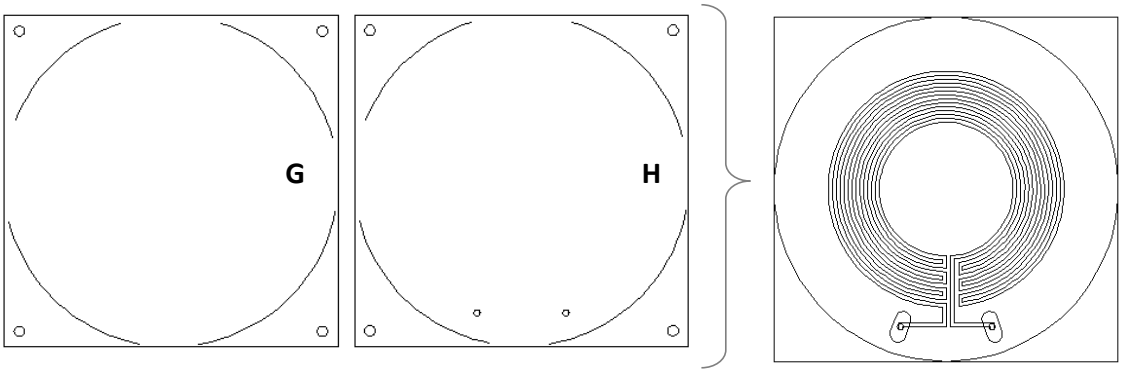

A.9 CAD DESIGN OF THE MR7 MICROREACTOR

Eight layers compose the microfluidic platform for the synthesis of Cdots and seven layers are required for the construction of its necessary heater. The micromixer designed is the same as in **MR6.** Again, the screen printed pastes are depicted in the overlapped layers of the heater.

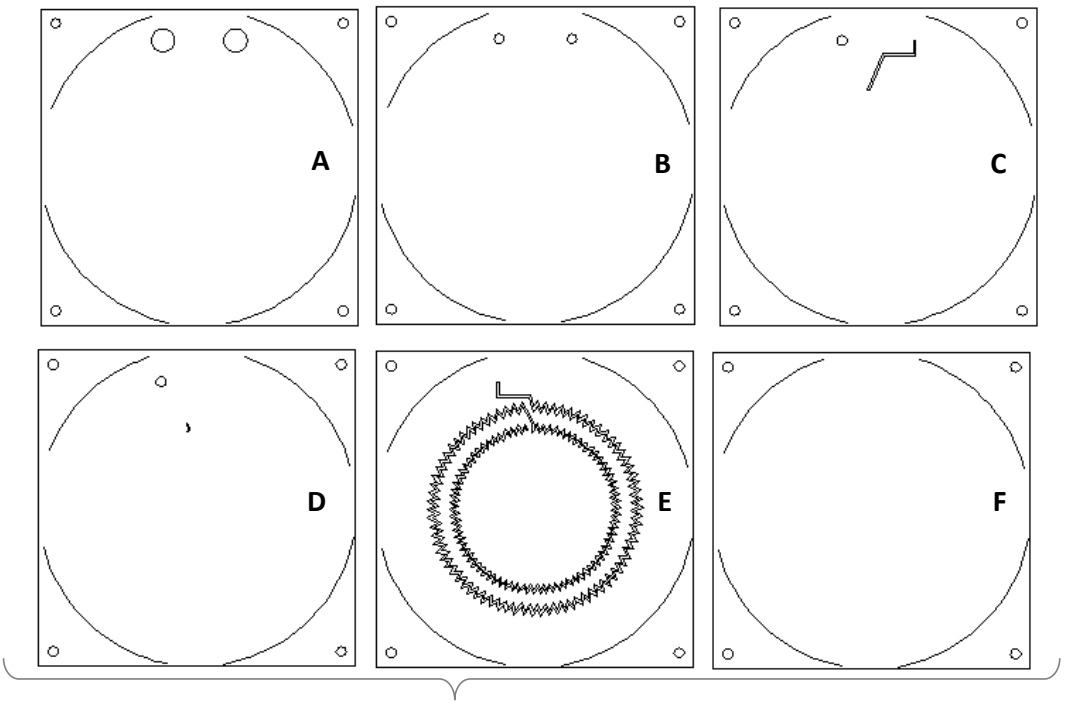

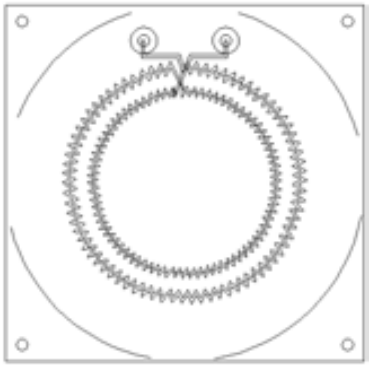

LAYER TYPE	NUMBER OF LAYERS
A	3
B	1
C	1
D	1
E	1
F	1
G	3
H	4

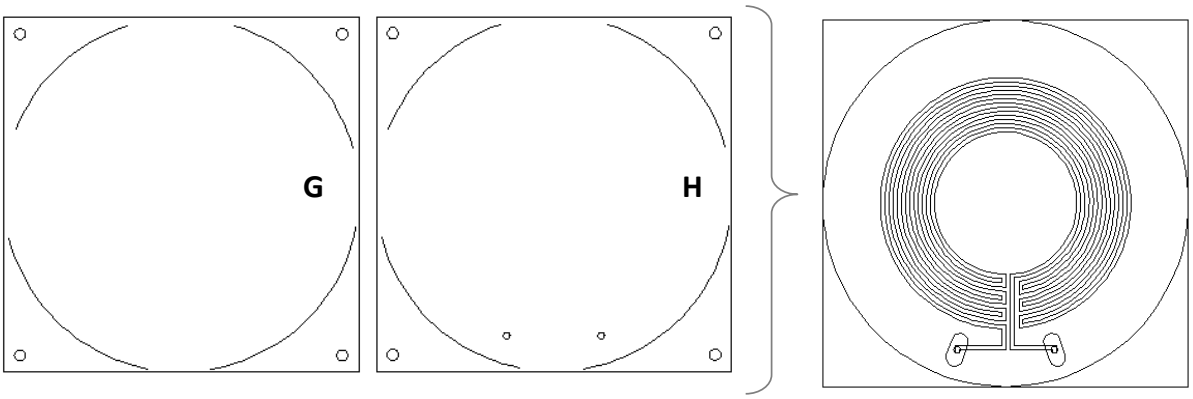

A.10 CAD DESIGN OF AD FOR MERCURIC ION MONITORING

The design of the device for the optical monitoring of mercuric ion is depicted below. Since it is constructed on COC polymeric substrate, the dimensions of the channels depend on the drill bits employed. Thus, *A1, A2* and *B2* are mechanized with a 400 µm-diameter, *B1* with a 200 µm-diameter, and *B3* with a 1000 µm-diameter drill bits. Besides *A1*, which is low relief mechanized, all designs are completely drilled. *C* layer is used as base of the device, as structural layer. Nevertheless, its design is also employed for cutting of the whole device.

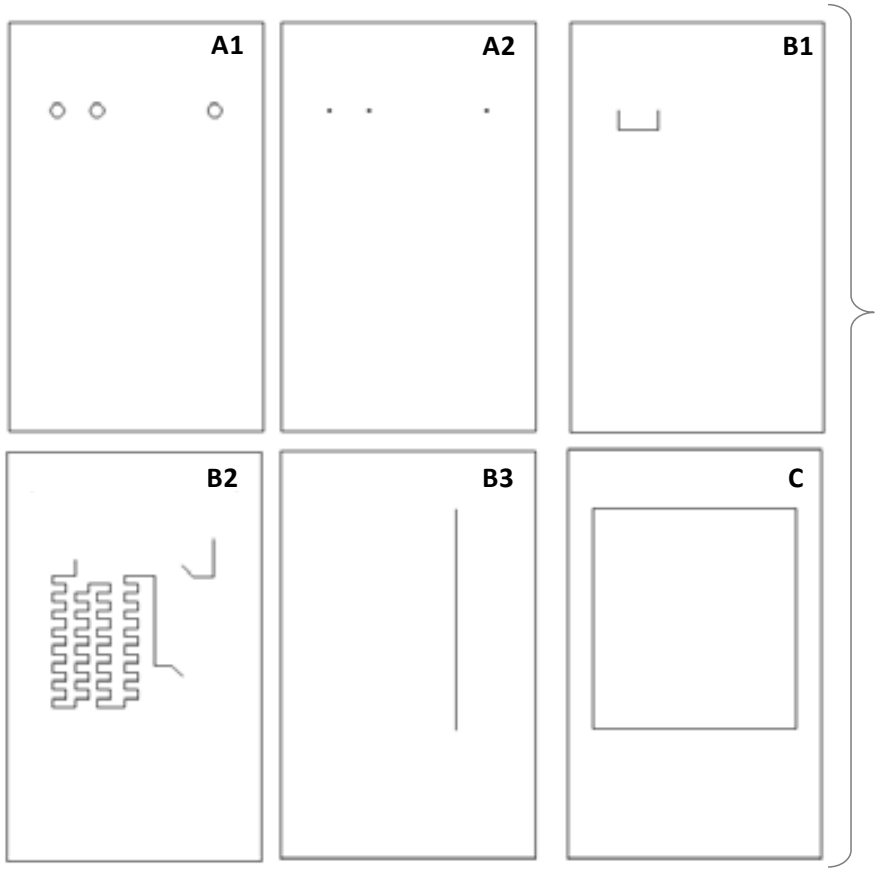

LAYER TYPE	NUMBER OF LAYERS
A	1 (400 µm)
B	1 (1000 µm)
C	1 (400 µm)

A.11 CAD DESIGN OF BD FOR E. COLI DETECTION

The following design is used for the construction of the polymeric bioanalytical device. Two identical devices are designed in the same substrate to use its complete area. Thus, *A*, *B1* and *B4* were mechanized with 400 µm-diameter drill bits, while *B2* and *B3* are mechanized with 800 and 250 µm-diameter drill bits, respectively. Only *B4* layer is low relief drilled. Again, *C* layer, drilled with a 2 mm-diameter drill bit, is used as base of the device, and its design is employed for the cut of the whole device.

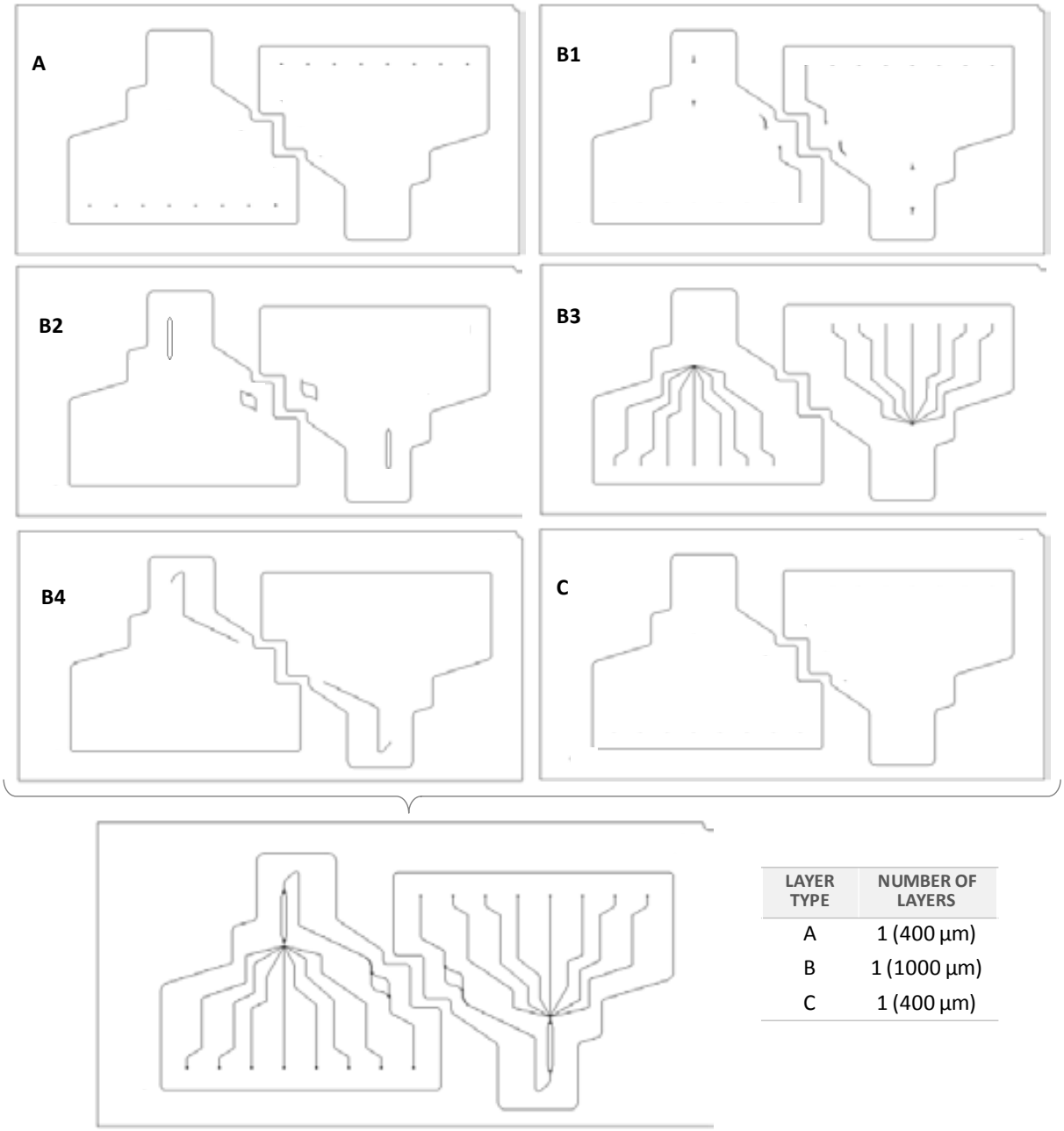

LAYER TYPE	NUMBER OF LAYERS
A	1 (400 µm)
B	1 (1000 µm)
C	1 (400 µm)

ANNEX B: PUBLICATIONS

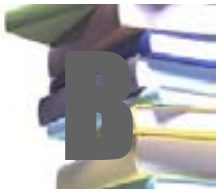

Contents

The work presented has given rise to six peer-reviewed journal publications. An additional publication concerning this dissertation is prepared to send.

B.1 Continuous flow synthesis of nanoparticles using ceramic microfluidic devices. Sara Gómez de Pedro, Mar Puyol and Julián Alonso. Nanotechnology, 21, 41 (2010).

B.2 A ceramic microreactor for the synthesis of water soluble CdS and CdS/ZnS nanocrystals with on-line optical characterization. Sara Gómez de Pedro, Mar Puyol, David Izquierdo, Íñigo Salinas, Jesús Martínez de la Fuente and Julián Alonso Chamarro. Nanoscale, 4(4), 1328-1335 (2012).

B.3 Microreactor with integrated temperature control for the synthesis of CdSe nanocrystals. Sara Gómez de Pedro, Cynthia S. Martínez Cisneros, Mar Puyol and Julián Alonso Chamarro. Lab on a Chip, 12 (11), 1979-1986 (2012).

B.4 Design, fabrication and characterization of microreactors for high temperature syntheses. Cynthia S. Martínez Cisneros, Sara Gómez de Pedro, Joan García García, Mar Puyol and Julián Alonso Chamarro. Chemical Engineering Journal, 211-212, 432-441 (2012).

B.5 Optical microfluidic system based on ionophore modified gold nanoparticles for the continuous monitoring of mercuric ion. Sara Gómez de Pedro, Daniela Lopes, Sergey Miltsov, David Izquierdo, Julián Alonso Chamarro and Mar Puyol. Sensors and Actuators B, 194, 19-26 (2014).

B.6 Microsystem-assisted synthesis of carbon dots with fluorescent and colorimetric properties for pH detection. Sara Gómez de Pedro, Alfonso Salinas Castillo, María Ariza Avidad, Alejandro Lapresta, Cristina Sánchez-González, Cynthia S. Martínez-Cisneros, Mar Puyol, Luis Fermín Capitán Vallvey and Julián Alonso. Nanoscale, 6, 6018-6024 (2014).

B.1 Continuous flow synthesis of nanoparticles using ceramic microfluidic devices.

Sara Gómez de Pedro, Mar Puyol and Julián Alonso. Nanotechnology, 21, 41 (2010).

Continuous flow synthesis of nanoparticles using ceramic microfluidic devices

2010 Nanotechnology 21 415603

(http://iopscience.iop.org/0957-4484/21/41/415603)

Nanotechnology **21** (2010) 415603 (6pp) doi:10.1088/0957-4484/21/41/415603

Continuous flow synthesis of nanoparticles using ceramic microfluidic devices

S Gómez-de Pedro, M Puyol and J Alonso-Chamarro

Grup de Sensors i Biosensors, Departament de Química, Facultat de Ciències, Edifici Cn, Universitat Autònoma de Barcelona, Bellaterra 08193, Spain

E-mail: julian.alonso@uab.es

Received 17 June 2010, in final form 23 August 2010
Published 16 September 2010
Online at stacks.iop.org/Nano/21/415603

Abstract

A microfluidic system based on the low-temperature co-fired ceramics technology (LTCC) is proposed to reproducibly carry out a simple one-phase synthesis and functionalization of monodispersed gold nanoparticles. It takes advantage of the LTCC technology, offering a fast prototyping without the need to use sophisticated facilities, reducing significantly the cost and production time of microfluidic systems. Some other interesting advantages of the ceramic materials compared to glass, silicon or polymers are their versatility and chemical resistivity. The technology enables the construction of multilayered systems, which can integrate other mechanical, electronic and fluidic components in a single substrate. This approach allows rapid, easy, low cost and automated synthesis of the gold colloidal, thus it becomes a useful approach in the progression from laboratory scale to pilot-line scale processes, which is currently demanded.

(Some figures in this article are in colour only in the electronic version)

1. Introduction

In recent years, the research on nanoscale science has been growing considerably due to the potential applications of nanomaterials in electronics, materials science and physical, chemical, biological and biomedical fields.

However, transference of this promising technology into new industrial technologies still represents a bottleneck. The most recent research efforts have been focused on the scale-up of innovative nanotechnology based and laboratory scale processes to pilot-line scale for industrial applications. The goal on this research should be thus to facilitate the transfer from laboratory scale activities to larger scale processes that would open the way for industrial production lines.

It is well known that materials can be modulated to exhibit improved or novel properties using nanotechnology because at nanoscale, their properties differ from both those of individual atoms and molecules and from the bulk matter [1].

Particular interest has been taken in metallic nanoparticles (MNPs). A colloidal dispersion of nanoparticles (NPs) shows unique catalytical [2, 3], optical [4–6] and electronic properties originating from its quantum scale dimensions [7, 8]. These properties depend strongly on their size [9] and shape [10] distributions, so a careful control of their synthesis is extremely important [11, 12].

NPs are usually prepared by means of batch methods, where some steps, such us the addition of reagents, rate of stirring, local temperature and concentration fluctuations, are difficult to control, obtaining, as a result, disparity from the different batches in terms of size distribution. Moreover, these colloidal suspensions are required in high quantities for their later application in a number of areas, so it is a great disadvantage to synthesize them in different batches.

Automated and miniaturized continuous flow methods have been proposed as an alternative to overcome these limitations. These methodologies allow variation in a rapid, controlled and precise way of most of the required experimental variables. Moreover, microfluidics reduces the consumption of reagents and, with automated chain microsystems, it is possible to obtain nanoparticles on demand [13–16].

Materials such as glass, silicon and polymers have been used in the fabrication of microfluidic devices [17–21]. However, most of the employed manufacturing methods not only require a post-fabrication sealing of the microchannels (which produces leaks at the joins) but also exhibit slow

prototyping procedures and poor chemical and thermal inertness [22].

In this paper, we report an automated LTCC-based microfluidic device for the one-phase continuous flow synthesis of stabilized and monodispersed gold nanoparticles (Au NPs). The microreactor takes advantage of the substrate material (ceramic tapes) and its associated microfabrication technology. For instance, it allows a multilayer approach, making feasible the design and fabrication of 3D structures, where mechanical, electronic and fluidic components (such as static or dynamic mixers and resistors/thermistors couples) can be integrated in a single device [23–26]. Moreover, post-fabrication steps are avoided and the technology does not require the use of special facilities such as clean rooms. This permits a rapid prototyping, reducing significantly the costs and the production time [27, 28]. Therefore it becomes a great alternative in the progression from laboratory scale to pilot-line scale processes.

2. Materials and methods

2.1. Construction of the ceramic devices

The construction of the microreactor begins with the microfluidic platform design using a CAD program. Each ceramic layer must be designed taking into account an approximate 15% of shrinkage at each axis due to the sintering process [29]. Then, the pattern is etched on the ceramic layers (low-temperature co-fired ceramic 951 AX tapes with a thickness of 254 μm supplied by DuPont) with a laser micromachining tool (Protolaser 200). The different layers are overlapped before performing a lamination step, consisting of a thermo-compression process by the application of approximately 3000 psi for 30 s at 100 °C. Finally, the laminated block is sintered in air atmosphere in a programmable box furnace (Carbolite CBCWF11/23P16, Afora, Spain) by applying a temperature profile. An initial increasing temperature ramp of 2 °C min^{-1} is applied until 350 °C, and after 30 min of temperature stabilization, a second increasing ramp at the same rate is applied until 850 °C. This temperature is maintained for 30 min and then cooling to 25 °C is performed.

2.2. Microsystem setup

Other components that constitute the automated and continuous flow system are syringe pumps (540060 TSE systems) and 1–10 ml syringes (Hamilton series GASTIGHT 1000 TLL) connected to the microreactor with PTFE tubes (i.d. 0.9 mm). These pumps are controlled by a computer and allow the reagents to be dispensed, providing microliter per second flow rates, in a rapid, simple and controlled way. The automatic filling of syringes is feasible with three-way solenoid isolation valves (NResearch incorporates®), connected between the syringes and the microreactor. This allows the continuous loading of reagents. On the other hand, PTFE tubes are connected to the ceramic device by means of a connection aluminum piece (figure 1(a)) with conical PTFE connectors (Cones 1.6 mm Omnifit). This avoids the possibility of collateral reactions with metals due to the use of reducing agents. Finally, o-rings are used to seal the connection system. A diagram of the entire setup is depicted in figure 1(b).

2.3. Chemicals and apparatus

All solutions were prepared in double distilled water. Hydrogen tetrachloroaurate (III) hydrate was provided by Fluka (p.a. ACS, $\geqslant$49% Au); sodium borohydride by Panreac with 98% purity and 11-mercaptoundecanoic acid (MUA) was obtained from Sigma-Aldrich, with 99% purity.

A Shimadzu UV-310PC UV–vis–NIR double-beam scanning spectrophotometer (Kyoto, Japan) was used to record spectra between 800 and 400 nm.

The shape and dimensions of the core of the particles were measured by a transmission electron microscope (TEM), JEOL 1400, and a high resolution electron microscope (HRTEM), JEOL 2011 (Tokyo, Japan). The samples were prepared by dipping a copper grid, which was coated with a thin carbon film, in the gold nanoparticles suspension.

The purification of the colloidal obtained was performed by centrifugal filtration in 4 ml centrifugal filter devices (CENTRIPLUS YM30, MICROCON, MWCO 30000) at 3000 rpm for 35 min, and lyofilization was carried out in a LyoQuest freeze dryer (Telstar).

3. Results and discussion

Different microsystems based on the LTCC technology have been developed to automate and miniaturize the continuous flow synthesis and surface modification of gold nanoparticles and thus overcome the limitations of some conventional batch methods. Moreover, the presented microfluidic devices, which are based on ceramic materials, show some advantages in comparison with previously reported devices made of glass, silicon or polymers.

The main parameter that influences the design of a microreactor is the type of reaction to carry out. Colloidal dispersions of gold can be synthesized by many methods, such as photolysis, ultrasonic reductions, electrochemical deposition or radiolysis of metal salts [30, 31]. However, one of the most common procedures is chemical reduction [32–34]. Our choice was to obtain the colloidal crystal by a simple one-phase reaction in which gold (III) is reduced by sodium borohydride and the stabilization is due to the electrostatic repulsions generated by the remaining reducing agent [35].

As was stated by Lamer and Dinegar [36] in the theory of colloidal formation by chemical synthesis, it is necessary to have a supersaturated concentration of reagents in a short time at the beginning of the synthesis to produce highly uniform nanoparticles. In this way, seeds of particles are initially quickly formed and the subsequent growth is carried out in longer times due to a diffusion stage. Therefore, the first manifold configuration studies were focused on the step of the formation of the seeds. In this phase, a high concentration of the reagent solutions and an efficient mixing are necessary. A hydraulic focusing configuration, which permits an effective and controllable lamination of the flow, thus reducing the

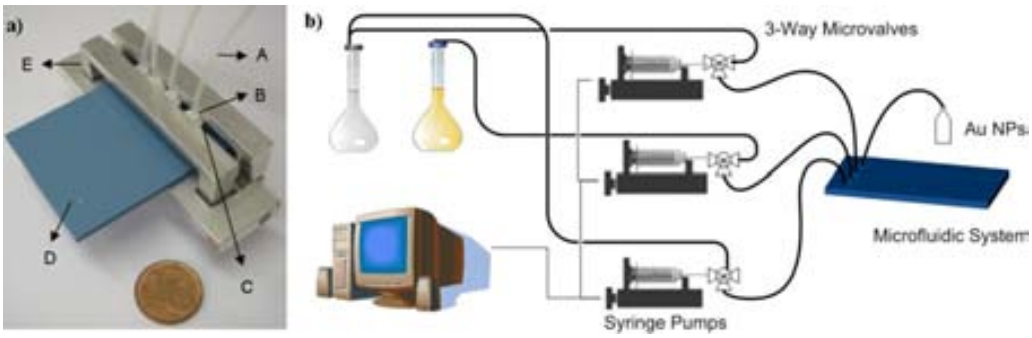

Figure 1. (a) Simple user-friendly connection system, designed to attach the microfluidic device with the PTFE tubes. A: PTFE tubes, B: PTFE cones, C: o-rings, D: LTCC microreactor, E: connection piece. (b) Diagram of the entire flow microsystem setup for the synthesis of Au NPs.

mixing path, was chosen for this purpose [37, 38]. The typical design for this parallel lamination micromixer consists of three inlets and a long channel. Thus, the central stream depends strongly on the flow rate of the side channels. In our proposal, the configuration of the confluence point of the inlets and flows acquired a trident shape where the middle inlet was the metal salt and the other two inlets were the reducing agent, working as the sheath flows. With this conformation, the metal is surrounded by the reductant, and thus, a more efficient mixture is generated.

Other manifold considerations were aimed at the growth of the generated seeds. It was observed that reactors based on short linear channels, where laminar flows prevail, produce unstable nanoparticles due to a poor mixture of reagents. Using these simple designs, aggregation of NPs outside the microfluidic platform was observed. The best results, in terms of stability, were obtained by forcing the diffusion of reagents with passive micromixers. Three-dimensional serpentine mixers cause a chaotic advection that improves the mixture [39, 40]. Incrementing also the length of the reaction channel favored the stability and homogeneity of the colloid until a certain value, where no improvement was observed.

Gold colloidal suspensions showing a tighter particle distribution were obtained using the microreactor depicted in figure 2. This microfluidic platform consists of three reagent inlets (120 μm × 150 μm middle channel and 120 μm × 300 μm side channels) and a three-dimensional micromixer as a reaction channel consisting of a series of L-shaped segments in perpendicular planes. The total reaction volume is 24 μl.

Other factors such as the chemical and hydrodynamic parameters also determine the quantity and quality (stability and size distribution) of the obtained NPs. Different solution concentrations of sodium borohydride and hydrogen tetrachloroaurate (III) hydrate were prepared in double distilled water and tested in the microfluidic platforms. It is well known that the molar relationship of reagents and concentration fluctuations in the bulk of the reaction solution are important points to take into account in the synthesis of nanocrystals. Dosage of small volumes of gold (III) solution in certain time intervals, while borohydride was continuously flowing, favored the formation of gold seeds due to the creation of supersaturated zones in each dosed volume and made feasible

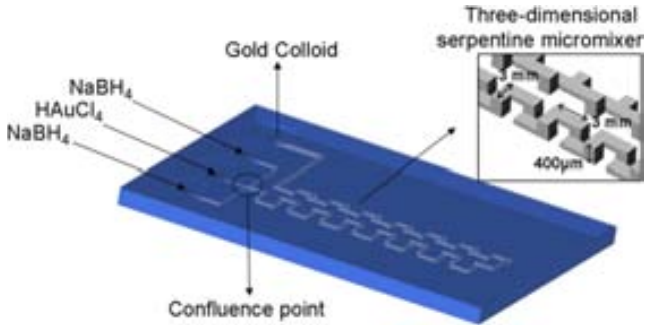

Figure 2. Microfluidic LTCC platform design for the synthesis of gold nanoparticles consisting of the concept of hydraulic focusing and a three-dimensional serpentine micromixer for the reagent mixture.

a stricter control of the concentration fluctuations. Moreover, an additional mixing was generated by means of the use of different flow rates for the borohydride solution channels in relation with the gold (III) solution channel to improve the reaction solution mixture. The optimized dispensing protocol consists of the continuous pumping of a 1.5 mM $NaBH_4$ solution at a 1 μl s^{-1} flow rate, and a dosage of 0.5 μl of a 1 mM $HAuCl_4$ solution sequentially dispensed every 2 s at a 2.5 μl s^{-1} flow rate. The molar relationship of the $HAuCl_4$ and $NaBH_4$ solutions is 1:10. The total residence time of the gold colloidal suspension inside the microfluidic device was estimated at approximately 9 s.

The characterization of the obtained nanocrystals was carried out by UV–vis absorption spectroscopy. The surface plasmon resonance (SPR) band of the absorption spectrum gives information about the size and morphology of the obtained NPs. Gold colloidal suspensions show a characteristic pale/strong red color depending on their concentration. When these particles begin to form aggregates a blue color is observed, obtaining at the end a colorless solution with a black solid suspended [41]. The obtained colloidal suspension with the optimized microfluidic system had a final concentration of about 4×10^{-3}% $HAuCl_4$ (7.9×10^{-8} M), calculated by a calibration curve using a commercial gold colloid of a 5 nm mean size (Aldrich), with an extinction coefficient of 2.3×10^6 M^{-1} cm^{-1} [42, 43]. The SPR band was centered at

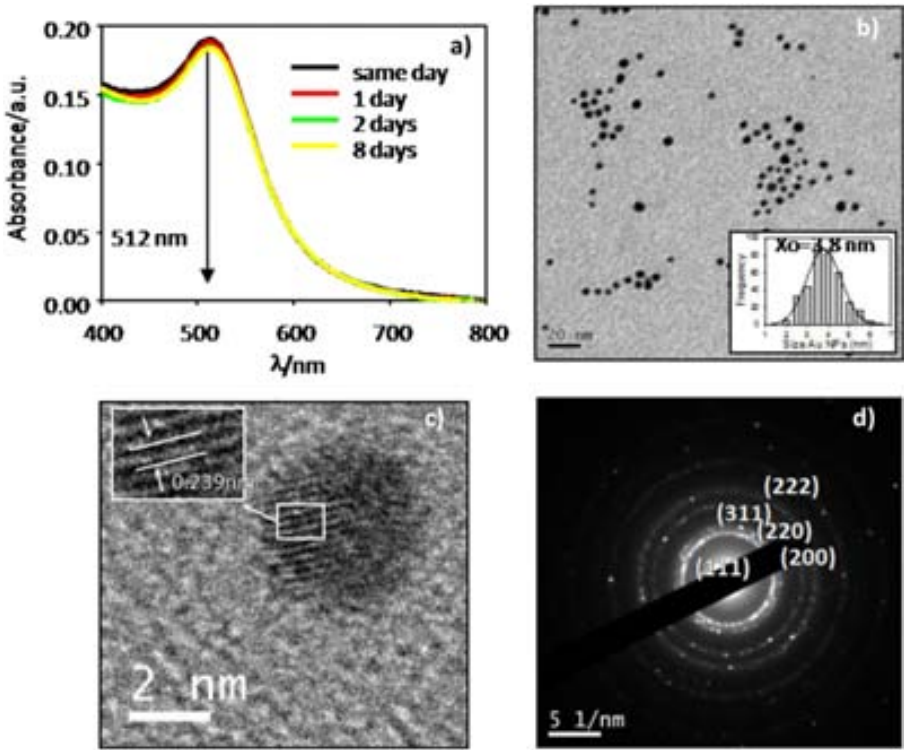

Figure 3. (a) UV–vis spectra showing the stability of the obtained gold colloid, (b) TEM image of one of the obtained gold colloids using the optimized system, (c) HRTEM image with the lattice fringes highlighted, and (d) SAED pattern of the obtained Au NPs.

512 nm and no shifts were observed over time, demonstrating the stability of the synthesized particles (figure 3(a)). However, the obtained band is displaced at shorter wavelength than expected (520 nm). This effect can be explained for the high electron density of the colloidal solution. As was stated by Pecharroman *et al* the surface plasmon modes on small metal particles are sensitive to various perturbations, including electron charging [44], which can be for instance due to the chemical reductants of the colloid. This effect is more stressed in rod-shaped particles than in spheres [45, 46], and results in higher oscillator strengths, leading to a blue-shift in the absorption spectrum.

The shape and dimensions of the core of the particles were measured by transmission electron microscopy (TEM). The represented histograms are the result of the measurement of more than 500 nanoparticles. The analysis by low magnification TEM images showed well-dispersed NPs of a medium size distribution of 3.8 nm and almost spherical shapes (figure 3(b)). The distance of the lattice fringes was determined to be 0.239 nm using HRTEM images (figure 3(c)), which reveals a preferential fcc growth of Au NPs on the (111) plane in agreement with the 0.2355 nm d-spacing of bulk Au (JCPDS card No: 04-0784). The electron diffraction (SAED) pattern of the selected area (figure 3(d)) shows single crystalline particles, the patterns of which index according to (111), (200), (220), (311) and (222) reflections of the fcc structure of Au.

With the purpose of extending the range of applications of the synthesized stable, homogeneous and well-dispersed gold colloids, other stabilizing strategies such as the incorporation of modifiers with functional groups were thought of [47]. The two-phase Brust–Schiffrin method is the most employed one in the synthesis of gold colloidal suspensions, where a monolayer of alkanethiols coating the nanoparticle is obtained [48, 49]. In this way, some essential active groups such as –OH, –COOH or –SH can also be attached to NPs for analytical, biological and biotechnological applications [50]. For that purpose, the previous design was easily modified by introducing an auxiliary channel for the addition of alkanethiols and by increasing the length of the microreactor to favor the mixture between the nanoparticles and the modifier. Then, a total reaction volume of 45 μl (21 μl for the Au NPs synthesis and 24 μl for the alkanethiol mixing) was obtained. 11-mercaptoundecanoic acid (MUA) was chosen as modifier agent due to the great possibilities derived of attaching a carboxylic group in the field of the immobilization of biological material and its stabilizing capability being an ionizable group.

The chemical and hydrodynamic parameters of the extended microreactor were again optimized. Figure 4(a) shows the effect of varying the flow rates of the MUA solution on the position of the SPR band. By increasing the MUA flow rate a displacement of the band towards larger wavelengths was observed. As the amount of MUA in the reaction mixture is increased, more molecules of modifier are attached to the NPs giving larger NPs. On the other hand, the study of the effect of pH of the gold colloidal was performed owing to the fact that the stability of NPs depends strongly on pH and hence, on the net charge of the functionalized colloid [51]. As the pH was increased, the SPR band decreased in intensity and shifted to shorter wavelengths (figure 4(a)). At basic pH values carboxylic groups are deprotonated giving an extra stability to

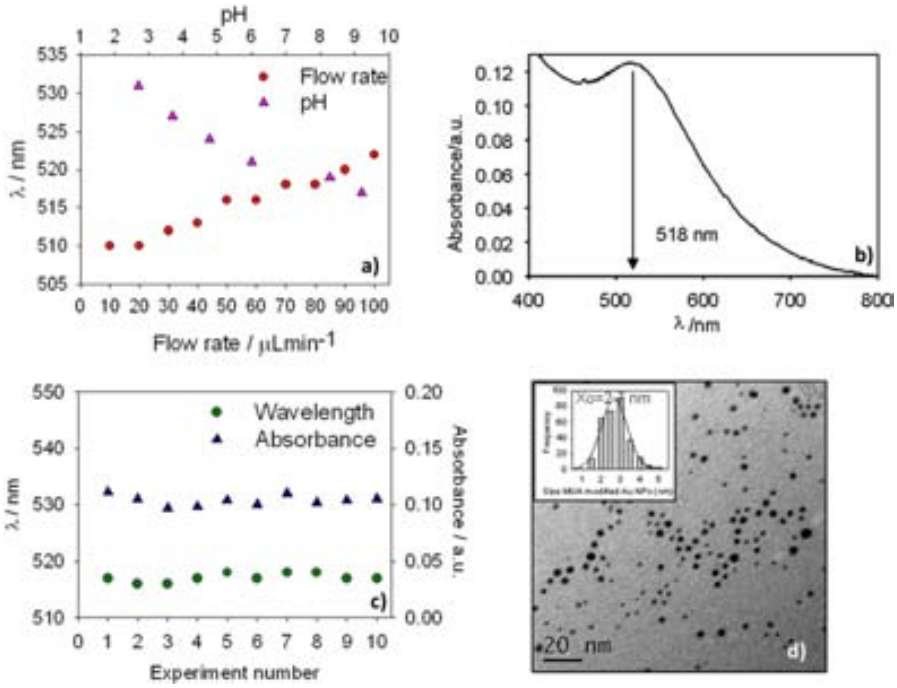

Figure 4. Results from the MUA Au NPs, obtained in the ceramic microreactor. (a) Study of the effect of pH and MUA flow rate on the SPR band position. (b) UV–vis spectra from the synthesized modified Au NPs using the optimized experimental conditions. (c) Characterization of the synthesis repeatability of the modified AuNPs following the position and the intensity of the SPR band. (d) TEM image from the obtained 2.7 nm NPs.

the NPs due to electrostatic repulsions; however the electronic density on the metal is incremented, resulting in the observed changes of the SPR spectrum. A continuous pumping of a 1.5 mM $NaBH_4$ solution at a 1 μl s^{-1} flow rate, and a dosage of 0.7 μl of a 1 mM $HAuCl_4$ solution sequentially dispensed every 2 s at a 2.5 μl s^{-1} flow rate, were the optimal conditions for the initial step of synthesis of gold nanoparticles. Then, modification of the surface was accomplished by continuously mixing the main channel, through a confluence point with a 1 mM solution of MUA flowing at 1 μl s^{-1} in the auxiliary channel. In these conditions, the pH of the final solution was 9.2 and the molar relationship of the reagents $HAuCl_4$, $NaBH_4$ and MUA is 1:10:3. The gold colloidal suspension obtained showed an invariable SPR band located at 518 nm (figure 4(b)). Hence, a shift of 6 nm is observed, comparing results with the colloidal suspensions synthesized with the first microsystem. This displacement is only caused by the modification with MUA and not due to the microreactor configuration. This was confirmed by performing the synthesis adding double distilled water instead of the modifier. In this case, the SPR band was located again at 512 nm.

After each synthesis, and prior to the NPs characterization, the water soluble gold colloidal suspensions were purified by centrifugal filtration. Then, the remaining solutions were washed with water and filtered three times more and, finally, the purified gold colloids were lyofilized, obtaining a solid, which can be easily stored and is suitable for many applications.

Additionally, synthesis repeatability was characterized using the SPR band intensity and shift as indicator parameters. Ten syntheses were carried out at the same conditions (same day, reagents, microfluidic device, etc) showing a band located at 517 $\pm$ 0.7 nm and an absorbance of 0.104 $\pm$ 0.005 au, demonstrating the robustness of the proposed flow system, which employs a ceramic microreactor (figure 4(c)). Moreover the TEM images revealed the procurement of well-defined and dispersed spherical particles of an average diameter of 2.7 nm (figure 4(d)).

4. Conclusion

To summarize, a novel and versatile microfluidic system based on the use of ceramic microreactors for the simple and reproducible production of stabilized gold nanoparticles is presented. Versatility is feasible due to the simple, fast and low cost prototyping of the LTCC technology, which allows adaptation of the design to each particular set of conditions of the synthesis. Moreover, by the integration of passive mixers and a well-defined dispensing protocol, the size distribution of gold colloidal suspensions can be controlled, obtaining stable, uniform and monodispersed NPs.

The present approach is an example of the potential of using ceramic tapes in this field. This technology allows us to work with a wide range of solvents and permits two-phase reactions to be performed. Similarly, temperature control systems based on resistor/thermistor couples components can be easily integrated, being feasible synthetic reactions that require a strict control of this parameter.

Thus, the presented procedure represents an improvement in the progression of laboratory scale processes to pilot-line

scale, in as much as it involves an easy, low cost, versatile and automated setup.

Acknowledgments

This work has been supported by the Spanish 'Comisión Interministerial de Ciencia y Tecnología' through projects CICYT-TEC2006-13907-C04/MIC and CTQ2009-12128 and the Consolider Ingenio 2010 project CSD2006-12. We thank Emma Rossinyol for performing the HRTEM measurements.

References

[1] Moriarty P 2001 *Rep. Prog. Phys.* **64** 297–381
[2] Narayanan R and El-Sayed M A 2003 *J. Am. Chem. Soc.* **125** 8340–7
[3] Lewis L N 1993 *Chem. Rev.* **93** 2693–730
[4] Alvarez M M, Khoury J T, Schaaff T G, Shafigullin M N, Vermar I and Whetten R L 1997 *J. Phys. Chem.* B **101** 3706–12
[5] Creighton J A and Eadon D G 1991 *J. Chem. Soc. Faraday Trans.* **87** 3881–91
[6] Dick L A, McFarland A D, Haynes C L and Van Duyne R P 2002 *J. Phys. Chem.* B **10** 853–60
[7] Brust M and Kiely C 2002 *J. Colloids Surf.* A **202** 175–86
[8] Murray C B, Kagan C R and Bawendi M G 2000 *Annu. Rev. Mater. Sci.* **30** 545–610
[9] Alivisatos A P 1996 *Science* **271** 933–93
[10] Puntes V F, Krishnan K M and Alivisatos A P 2001 *Science* **291** 2115–7
[11] Sun Y and Xia Y 2002 *Science* **296** 2176–8
[12] Xie Q, Dai Z, Huang W W, Liang J B, Jiang C L and Qian Y T 2005 *Nanotechnology* **16** 2958–62
[13] Reyes D R, Lossifidis D, Auroux P A and Manz A 2002 *Anal. Chem.* **74** 2623–36
[14] Wagner J, Kirner T, Mayer G, Albert J and Köhler J M 2004 *Chem. Eng. J.* **101** 251–60
[15] Lin X Z, Terepka A D and Yang H 2004 *Nano Lett.* **4** 2227–32
[16] DeMello J, Habgood M, Llewellyn N, Welton T and Wootton R C R 2004 *Lab Chip* **4** 417–9
[17] Chan E M, Mathies R A and Alivisatos A P 2003 *Nano Lett.* **3** 199–201
[18] Chan E M, Alivisatos A P and Mathies R A 2005 *J. Am. Chem. Soc.* **127** 13854–61
[19] Ho Y P, Chen H H, Leong K W and Wang T H 2009 *Nanotechnology* **20** 095103
[20] Bilitewski U, Genrich M, Kadow S and Mersal G 2003 *Anal. Bioanal. Chem.* **377** 556–69
[21] Becker H and Locascio L E 2002 *Talanta* **56** 267–287
[22] Leatzow D M, Dodson J M, Golden J P and Ligler F S 2002 *Biosens. Bioelectron.* **17** 105–10
[23] Teterycz H, Kita J, Bauer R, Golonka L J, Licznerski B W, Nitsch K and Wisniewski K 1998 *Sensors Actuators* B **47** 100–3
[24] Groß G A, Thelemann T, Schneider S, Boskovic D and Köhler J M 2008 *Chem. Eng. Sci.* **63** 2773–84
[25] Golonka L J, Roguszczak H, Zawada T, Radojewski J, Grabowska I, Chudy M, Dybko A, Brzozka Z and Stadnik D 2005 *Sensors Actuators* B **111** 396–402
[26] Li J and Ananthasuresh G K 2002 *J. Micromech. Microeng.* **12** 198–203
[27] Ibañez-García N, Martínez-Cisneros C S, Valdés F and Alonso J 2008 *Trends Anal. Chem.* **27** 24–33
[28] Gongora-Rubio M R, Espinoza-Vallejos P, Sola-Laguna L and Santiago-Aviles J 2001 *J. Sensors Actuators* A **89** 222–41
[29] Ibañez-García N, Puyol M, Azevedo C M, Martínez-Cisneros C S, Villuendas F, Góngora-Rubio M R, Seabra A C and Alonso J 2008 *Anal. Chem.* **80** 5320–4
[30] Perez-Juste J, Pastoriza-Santos I, Liz-Marzan L M and Mulvaney P 2005 *Coord. Chem. Rev.* **249** 1870–901
[31] Pillalamarri S K, Blum F D, Tokuhiro A T and Patino M F 2005 *Chem. Mater.* **17** 5941–4
[32] Schulz J, Roucoux A and Patin H 2002 *Chem. Rev.* **102** 3757–78
[33] Grzelczak M, Pérez-Juste J, Mulvaney P and Liz-Marzán L M 2008 *Chem. Soc. Rev.* **37** 1783–91
[34] Hostetler M J *et al* 1998 *Langmuir* **14** 17–30
[35] Douglas F, Yañez R, Ros J, Marín S, De la Escosura-Muñiz A, Alegret S and Merkoçi A 2008 *J. Nanopart. Res.* **10** 97–106
[36] LaMer V K and Dinegar R 1950 *J. Am. Chem. Soc.* **11** 4847–54
[37] Knight J B, Vishwanath A, Brody J P and Austin R H 1998 *Phys. Rev. Lett.* **80** 3863–6
[38] Walker G M, Ozers M S and Beebe D J 2004 *Sensors Actuators* B **98** 347–55
[39] Liu R H, Stremler M A, Sharp K V, Olsen M G, Santiago J G, Adrian R J, Aref H and Beebe D J 2000 *J. Microelectromech. Syst.* **9** 190–7
[40] Vijayendran R A, Motsegood K M, Beebe D J and Leckband D E 2003 *Langmuir* **19** 1824–8
[41] Shipway A N, Katz E and Willner I 2000 *Chem. Phys. Chem.* **1** 18–52
[42] Liu X, Atwater M, Wang J and Huo Q 2007 *Colloids Surf.* B **58** 3–7
[43] Maye M M, Han L, Kariuki N N, Ly N K, Chan W B, Luo J and Zhong C 2003 *J. Anal. Chim. Acta* **469** 17–27
[44] Mulvaney P, Perez-Juste J, Giersig M, Liz-Marzan L M and Pecharroman C 2006 *Plasmonics* **1** 61–6
[45] de Abajo F J G 2008 *J. Phys. Chem.* C **11** 17983–7
[46] Kreibig U 1977 *J. Phys.* **7** C2–91
[47] López-Cartes C, Rojas T C, Litrán R, Martínez-Martínez D, de la Fuente J M, Penedés S and Fernández A 2005 *J. Phys. Chem.* B **109** 8761–6
[48] Brust M, Walker M, Bethell D, Schiffrin D J and Whyman R J 1994 *Chem. Soc. Chem. Commun.* 801–2
[49] Templeton A C, Wuelfing M P and Murray R W 2000 *Acc. Chem. Res.* **33** 27–36
[50] de la Fuente J M and Penedés S 2006 *Biochim. Biophys. Acta* **1760** 636–51
[51] Aslan Pérez-Luna V H 2002 *Langmuir* **18** 6059–65

B.2 A ceramic microreactor for the synthesis of water soluble CdS and CdS/ZnS nanocrystals with on-line optical characterization.

Sara Gómez de Pedro, Mar Puyol, David Izquierdo, Íñigo Salinas, Jesús Martínez de la Fuente and Julián Alonso Chamarro. Nanoscale, 4(4), 1328-1335 (2012).

Nanoscale

Dynamic Article Links

Cite this: *Nanoscale*, 2012, **4**, 1328

www.rsc.org/nanoscale

PAPER

A ceramic microreactor for the synthesis of water soluble CdS and CdS/ZnS nanocrystals with on-line optical characterization

Sara Gómez-de Pedro,[a] Mar Puyol,[a] David Izquierdo,[b] Iñigo Salinas,[b] J. M. de la Fuente[c] and Julián Alonso-Chamarro*[a]

Received 17th October 2011, Accepted 1st December 2011
DOI: 10.1039/c2nr11525e

In this paper, a computer controlled microreactor to synthesize water soluble CdS and CdS/ZnS nanocrystals with *in situ* monitoring of the reaction progress is developed. It is based on ceramic tapes and the Low-Temperature Co-fired Ceramics technology (LTCC). As well the microsystem set-up, the microreactor fluidic design has also been thoroughly optimized. The final device is based on a hydrodynamic focusing of the reagents followed by a three-dimensional micromixer. This generates monodispersed and stable CdS and core–shell CdS/ZnS nanocrystals of 4.5 and 4.2 nm, respectively, with reproducible optical properties in terms of fluorescence emission wavelengths, bandwidth, and quantum yields, which is a key requirement for their future analytical applications. The synthetic process is also controlled in real time with the integration of an optical detection system for absorbance and fluorescence measurements based on commercial miniaturized optical components. This makes possible the efficient managing of the hydrodynamic variables to obtain the desired colloidal suspension. As a result, a simple, economic, robust and portable microsystem for the well controlled synthesis of CdS and CdS/ZnS nanocrystals is presented. Moreover, the reaction takes place in aqueous medium, thus allowing the direct modular integration of this microreactor in specific analytical microsystems, which require the use of such quantum dots as labels.

Introduction

Inorganic nanocrystalline semiconductors (quantum dots) are one of the most interesting nanomaterials due to their different emission colors caused by their size-dependent properties.[1–4] These uncommon properties owing to the quantum size effects make them very suitable for use in multiple applications which include their use in light-emitting devices,[5–8] solar cells,[9,10] as well as in computing and biological fields.[11–15] Their use as luminescent labels in analytical systems is one of their most engaging applications.[16–22] In this way, semiconductor nanocrystals can replace the commonly used dyes in a more efficient way, as nanocrystals are not limited by the photobleaching problems that are usually present for organic colorants.[23–25]

Optical properties of quantum dots depend strongly on their shape and size, which is on the one hand very attractive. However, this can sometimes cause reproducibility problems if their synthesis is not strictly controlled. Thus, closely controlling the synthetic stages of the nanocrystals plays an important role in order to achieve homogeneous particles with the same optical properties.[26–29]

Automated and miniaturized continuous-flow synthetic methods offer a great advantage over conventional chemical processes,[30] and also for the synthesis of nanoparticles.[31–35] They take the advantages of miniaturization, reducing significantly the waste of reagents and allowing to better define the reagents addition, the grade of mixture and its concentration. As the whole process can be easily automated, it is possible to control the different parameters of the reaction, and then, to obtain more homogeneous colloidal suspensions. Automation also gives the possibility of synthesizing the required volumes of nanocrystal suspensions, by continuously working and refilling of the reagents.

This paper reports a microreactor based on a ceramic material for the easy and controlled synthesis of water soluble CdS and CdS/ZnS quantum dots with *in situ* optical characterization. The proposed procedure combines the advantages of the use of a microfluidic system, with the ones derived from the fact that the reaction takes place in aqueous medium. Then, it would be possible to directly attach the microreactor to other analytical microsystems, which require the use of quantum dots as labels (such as in analytical or bioanalytical applications) without intermediate stages of solubilization.[36–39] Few other microfluidic

[a]*Grup de Sensors i Biosensors, Departament de Química, Univ. Autonoma Barcelona, Edifici Cn, 08193, Bellaterra, Catalonia, Spain. E-mail: julian.alonso@uab.es; Fax: +34 9358 12477; Tel: +34 9358 12149*
[b]*Grupo de Tecnologías Fotónicas, Instituto de Investigación en Ingeniería de Aragón, Universidad de Zaragoza, Campus Río Ebro - Edificio I + D + i, Mariano Esquillor, s/n, 50018 Zaragoza, Spain. E-mail: isalinas@unizar.es*
[c]*Instituto de Nanociencia de Aragón (INA), Universidad de Zaragoza, Campus Río Ebro, Edificio I + D, Mariano Esquillor, s/n, 50018 Zaragoza, Spain. E-mail: jmfuente@unizar.es*

systems have been proposed for the synthesis of nanocrystals, which are based on the most common synthetic batch methods. Some of them are based on silicon technology[40,41] and consist of patterned microchannels etched or molded in a substrate and sealed by additional substrates. These require special facilities for their prototyping and also a post fabrication process, thus being as a result a slow and expensive prototyping process. Other are based on polymers, which are cheap and easy to manufacture but sometimes present sealing problems and poor chemical and thermal stability.[42,43]

Since a few years ago, our research group is committed to the use of other materials such as ceramic tapes based on the LTCC technology[44–46] with the same philosophy.

This technology enables the construction of multilayered systems, which can also integrate other mechanic, electronic and fluidic components in a single device.[47,48] For instance, complex three-dimensional structures such as 3D serpentine passive mixers have been integrated without the need of sophisticated facilities, such as clean rooms. These mixers force convection and, diffusion profiles can be easily obtained. Pre-treatment components, like filters of different diameters, have been also successfully developed. In this sense, other elements such as ion-exchange resins can be integrated in order to eliminate interfering compounds or just to concentrate samples. Moreover, due to the compatibility of the ceramic material with conductive pastes, resistor/thermistor couples can be integrated in those cases requiring a controlled moderate or high temperature to carry out specific reactions such as in bioassays. Regarding detection systems, not only can transparent windows be easily developed to define optical flow cells, but also electrochemical detectors, as screen-printed tracks and electrodes, have also been embedded. All this can be obtained without post-fabrication treatments or procedures, allowing fast prototyping at low cost.[49,50]

On the other hand, the ceramic material is chemically resistant to a wide range of reagents (aqueous or even organic solvents), thus is suitable to perform the syntheses of different types of nanomaterials.

Taking advantage of the fast and easy fabrication of three-dimensional structures, which enable the integration of reactors and detection systems in the same monolithic prototype, a miniaturized optical detection system has been developed and adapted to the microreactor for the real-time absorbance and fluorescence monitoring of the products of the synthesis, obtaining a high performance and portable system for the controlled synthesis of CdS/ZnS nanocrystals.[51,52]

Experimental

Ceramic device construction

Designs of the different layers were drawn in a CAD program, taking into account that ceramic layers shrink *ca.* 15% in each axis during the sintering process. Patterns were transferred on ceramic layers (low-temperature co-fired ceramics 951 AX tapes with a thickness of 254 μm supplied by DuPont) with a laser micromachining tool (Protolaser 200).[49] Then, the different layers were overlapped and laminated by means of a thermo-compression process, which consists in the application of 3000 psi for 40 s at 90 °C. Finally, they were sintered in an air atmosphere in a programmable box furnace (Carbolite CBCWF11/23P16, Afora, Spain) by applying a temperature profile consisting of 5 stages. A first ramp, where the temperature was increased from room temperature until 350 °C at 2 °C min^{-1}, was applied. Then, 30 min of stabilization at 350 °C were required followed by a second heating ramp until 850 °C at 2 °C min^{-1}. After 30 min more of stabilization, cooling to 25 °C was performed.

Microsystem set-up

Reagents were propelled to the microreactor by syringe pumps (540060 TSE systems) incorporating 1–10 mL glass syringes (Hamilton series GASTIGHT 1000 TLL). The connection between the syringe pumps and the microfluidic system was made using PTFE (polytetrafluoroethylene) tubes (i.d. 0.9 mm). Three-way isolation valves (NResearch incorporates®) were connected to syringes, which allowed the possibility of refilling. The whole system was computer controlled, therefore reagents dispensing to the microreactor could be easily well defined, by providing the desired flow pattern. To secure the sealing of fluidic connections, o-rings and conic PTFE cones were joined between the PTFE tubes and the microreactor using a homemade connection aluminum piece.[53]

Reagents and apparatus

All solutions were prepared in double distilled water. Cadmium nitrate tetrahydrate, sodium sulfide, N-(2-mercaptopropionyl) glycine (tiopronin), zinc nitrate hexahydrate and rhodamine 6G were provided by Sigma-Aldrich with a minimal purity of 99.0%. pH was adjusted with a pH meter GL22 (Crison).

A Shimadzu UV-310PC UV-Vis-NIR double-beam scanning spectrophotometer (Kyoto, Japan) was used to record spectra between 800 and 200 nm.

The shape and dimensions of the core of the particles were measured by a high resolution transmission electron microscope (HRTEM), JEOL 2011 (Tokyo, Japan). The samples were prepared by dipping a copper grid, which was coated with a thin carbon film, in the nanocrystal suspension.

The purification of the colloidal obtained, in order to perform HRTEM measurements, was carried out by centrifugal filtration in 4 ml centrifugal filter devices (CENTRIPLUS YM30, MICROCON, MWCO 30000) at 3000 rpm for 30 min.

Optical system

The components of the measurement absorbance and fluorescence PCBs (Printed Circuit Boards) are shown in Fig. 1a, where both systems are drown together but they are actually separated in two modules (Fig. 1b). To ensure the simultaneous measurement of the nanocrystals absorbance and fluorescence, two modulated Light Emitting Diodes (LEDs) mounted in two separated PCBs, where two photodetectors are integrated, were used. LEDs from Roithner Lasertechnik XSL-365-5E (Vienna, Austria) had their emission peak at 365 nm, matching with the SPR band of the particles absorbance spectrum and excitation wavelength. They were modulated and controlled by a Data Acquisition Card (DAQ), which generates the two modulating signal for each LED and captures the detected signal to transfer

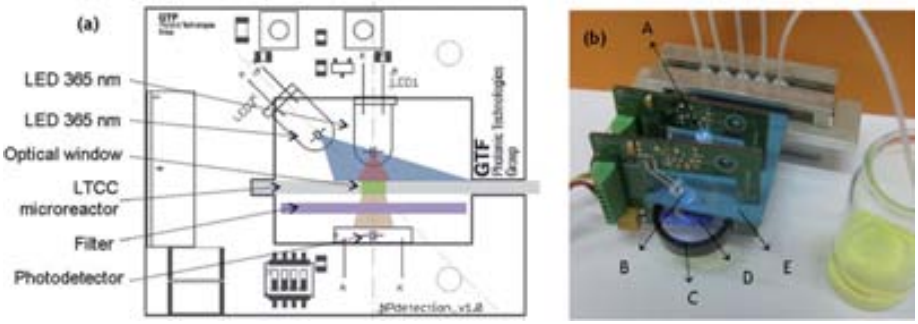

Fig. 1 a) Scheme of the absorbance and fluorescent measurement set-up. b) Optical system and microreactor coupling. A: Absorbance LED, B: Fluorescence LED, C: high pass filter, D: PIN photodetector, E: ceramic microreactor.

them to a control PC, which process them. The whole system, DAQ and boards, were powered by the computer through the USB connector, simplifying the system.

The DAQ (NI USB-6211 from National Instruments) generates two sine waves at different frequency ($f1$ and $f2$) and sends them to the PCBs. The sampling frequency used to generate these waves inside the DAQ was dynamically adjusted to 128 times the highest modulation frequency to avoid problems in the synchronization of the signals inside the DAQ. The sampling frequency of the analog to digital conversion of the signals was fixed to 10 kS s^{-1} (1 kS s^{-1} = 1000 samples per second). These raw data are sent to the PC, where they are processed using lock-in amplification to increase the signal to noise ratio and the dynamic range of the measurement. This amplification also allows the use of the detection system in ambient light without interferences.

The light transmitted through the optical windows of the LTCC microreactor was detected by a PIN Hamamatsu S1337-66BR large active area photodiode soldered in front of the absorbance LED. Light absorption generates a fluorescent emission at 540 nm. To measure this fluorescence, another optical window was designed. The excitation LED was tilted 45 degrees from the normal to the microreactor surface to reduce interferences of the light source to the detector, and the rest is avoided by a high pass optical filter with a cut-off wavelength at 500 nm (FEL500 from Thorlabs). An image of the absorbance and fluorescence optical detection systems coupled to the microreactor is showed in Fig. 1b.

Results and discussion

For the synthesis of quantum dots two main routes exist.[54] One requires the use of organic solvents and high temperatures in order to decompose organometallic reagents to achieve their rearrangement and forming nanocrystals.[55–58] The other, involves the use of greener reagents in aqueous medium using polyphosphates[59] or thiols[60–62] as stabilizing agents. The first approach requires a later modification procedure in order to solubilize the obtained quantum dots in water for their use in biological and analytical applications, which at the end results in a decrease of their quantum yields.[63] The second route is simplest and avoids subsequent modifications, being possible to use the synthesized nanocrystals immediately.

Few syntheses of quantum dots in water have been proposed to date. Most of them involve the use of NaHTe or NaHSe reagents, which have to be formed *in situ* by the reaction of aluminum or tellurium precursors and H_2SO_4 under an inert atmosphere, and generate gases, which are undesirable in microfluidic applications. Moreover, refluxes are required at about 100 °C in order to obtain adequate photoluminescent emissions.[64–66] Herein, a direct aqueous synthesis, which does not require the *in situ* formation of the precursor reagents and that does not produce gases, is employed. The method consists of the reaction of cadmium nitrate with sodium sulfide, using tiopronin (TP) as stabilizing agent at room temperature.[59,67] Tiopronin, a non-natural amino acid, has not only been widely used as a capping agent in the stabilization of such type of nanocrystals, but also in silver and gold colloidal suspensions obtaining well dispersed, uniform metal nanoparticles which are stable for months.[68,69] Moreover, it procures solubility in water medium and provides active groups for subsequent on-line reactions, when the nanocrystals are going to be used as labels in analysis systems.[70–73]

However, the reaction requires a very strict control of kinetics in order to achieve uniform and well dispersed nanocrystals. A key point in the reaction is the first contact of reagents, in order to obtain a supersaturated concentration of reagents in a short time. In this way, seeds of particles are rapidly formed and they grow up slowly by diffusion.[74]

Microreactors permit an exhaustive kinetic control, enabling fast controllable mass and temperature transfer and thus, are ideal systems for the synthesis of nanocrystals. However, their configuration must be adapted to each synthetic procedure.

The proposed microreactor consists in 3 inlet channels joined in a unique point, where the three reagents meet and are initially mixed. A mixture of cadmium nitrate and tiopronin solutions (previously adjusted to pH 10.0) is inserted in the central inlet channel. At both sides sodium sulfide is flowed in. This configuration allows hydrodynamic focusing, which entails a controllable laminar flow, and therefore, the first contact of reagents can be well defined.[75,76] After the confluence point, a three-dimensional serpentine mixer is built to force a chaotic flow, which generates a more efficient mixture.[77,78] In this way, diffusion is forced inside the channels and the growth of the crystals is more homogeneous.[49]

Reagents concentration and hydrodynamic parameters also have an important role in nanocrystals synthesis, as the molar relationship of reagents strongly affects the properties of the obtained nanoparticles. In this case, a mixed solution of 5 mM $Cd(NO_3)_2$ and 10 mM of TP was prepared and adjusted to pH

10.0 with NaOH, and a 10 mM solution of Na_2S was employed. Syringes were filled with these reagents and after an exhaustive study of the hydrodynamic conditions (continuous/discontinuous and simultaneous/sequential patterns of reagents dosing, volume and flow rate ratios of reagents, among others), the best quantum dots in terms of quantum yield, fluorescence bandwidth, and stability were obtained by mixing at the same flow rate of 0.5 μL s^{-1} all the reagents with a hydrodynamic focusing configuration. In these conditions, the molar relationship of reagents is 1 : 2 : 4 (Cd^{2+}/TP/S^{2-}). The obtained nanocrystals were stable in water and the colloidal solution had a yellow color, which under ultraviolet illumination emitted in the green.

Absorption spectra revealed a maximum absorption band centered at 368 nm (Fig. 2a). Excitation at this wavelength gave a wide emission band centered at 583 nm (Fig. 2b) with a full-width at half-maximum (FWHM) of 180 nm. Fluorescence quantum yields (Φ_f) were calculated relative to rhodamine 6G in water (95%, $\lambda_{exc} = 488$ nm),[79] turning out to be very low (5%).

The shape and dimensions of the core were determined by high resolution transmission electron microscopy (HRTEM), after the colloidal was purified by centrifugation. Images show almost spherical nanocrystals of approximately 4.5 nm (Fig. 2c) after counting an amount of 200 nanoparticles. The electron diffraction (SAED) pattern of the selected area (Fig. 2d) shows bright rings at distances of 0.340, 0.251 and 0.193 corresponding to 002, 102 and 103 lattice planes of the hexagonal (wurtzite) crystal structure of CdS (JCPDS no. 01-0780).

In order to improve the fluorescence efficiency, core–shell CdS/ZnS nanoparticles were synthesized.[80,81] For this purpose, the configuration of the microreactor was modified to incorporate an additional auxiliary channel for the addition of a zinc nitrate solution. The main channel was also elongated to ensure the reaction of zinc with the previously synthesized CdS nanocrystals. At this point, the introduction of a three-dimentional micromixer could cause the formation of ZnS instead of the desired shell over the CdS quantum dots. In order to achieve slower mass transferences, the elongation consisted in a simple longitudinal channel, where reagents were mixed by diffusion. A schematic of the microreactor is depicted in Fig. 3.

The reagents concentration and hydrodynamic parameters of the modified microfluidic reactor were as well optimized in order to also improve the size dispersion of the obtained nanocrystals.

In this case, the best results in terms of quantum yields, FWHM and stability, were obtained using an optimized dosing and mixing protocol with the hydrodynamic focusing configuration in the first confluence point. It consists of a sequential dosage of 0.5 μL of a mixture of 5 mM cadmium nitrate and 10 mM tiopronin solution (adjusted at pH 10.0) every 1 s at 2.5 μL s^{-1} flow rate in a continuous flow of a 10 mM sodium sulfide solution at 1.25 μL s^{-1} flow rate, and a continuous flow of a 5 mM zinc nitrate solution at 0.67 μL s^{-1}. In these conditions, a more efficient mixture of the reagents in the initial confluence point is achieved due to the different flow rate of the reagents and the sequential dosing of the cadmium salt. The molar relationship of reagents was approximately 1 : 2 : 1.6 : 10 (Cd^{2+}/TP/Zn^{2+}/S^{2-}). An example of the synthesis optimization is shown in Fig. 4. The dosage volumes and flow rates of cadmium nitrate and sodium sulfide reagents were firstly optimized in order to achieve the higher concentration of nanocrystals and the minimal FWHM.

As expected, an increase of the dosage volume of cadmium nitrate or of the flow rate of sodium sulfide solution entailed a displacement of the emission wavelength to higher values (Fig. 4a and b). This is because the concentration of seeds was higher and there were more reagents available to grow. Therefore, bigger nanocrystals were formed. However, for the highest flow rates, wider emission bands were observed, indicating a higher size dispersion of the nanocrystals. This is probably due to the residence time in the microfluidic device, since at the highest flow rates nanocrystals have not enough time to grow inside and part of the reaction takes place outside the microfluidic system, obtaining, as a result, an uncontrolled growth of

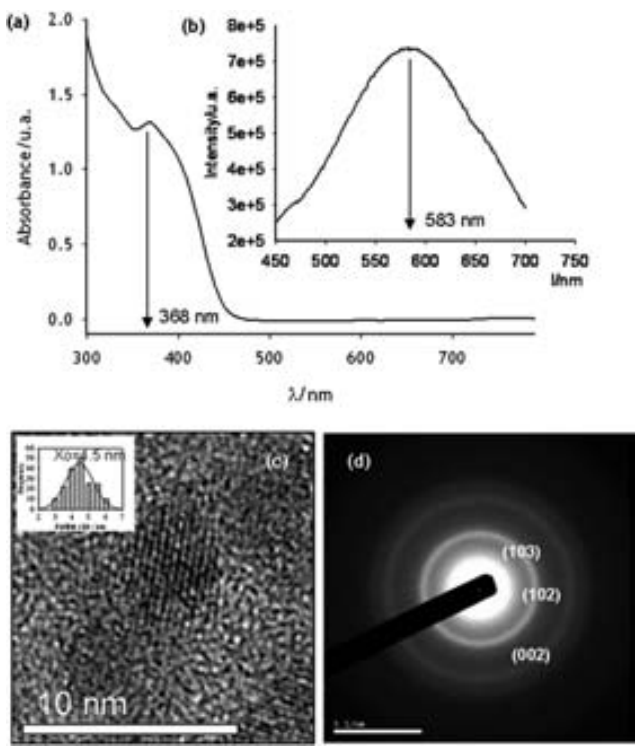

Fig. 2 (a) UV-vis and (b) fluorescence emission spectra, (c) a HRTEM image and (d) a SAED pattern of CdS nanocrystals synthesized in the microreactor.

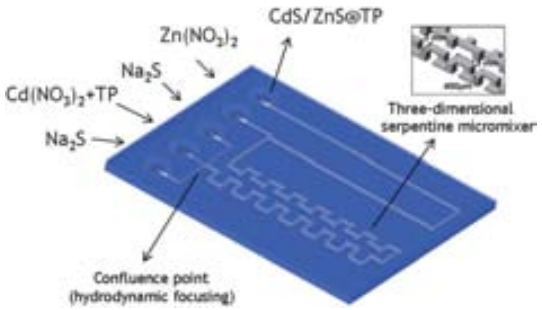

Fig. 3 The ceramic microreactor design for the synthesis of core–shell nanocrystals, incorporating the concept of hydrodynamic focusing, a three-dimensional serpentine micromixer for the formation of the core quantum dots and a longitudinal channel for the shell formation.

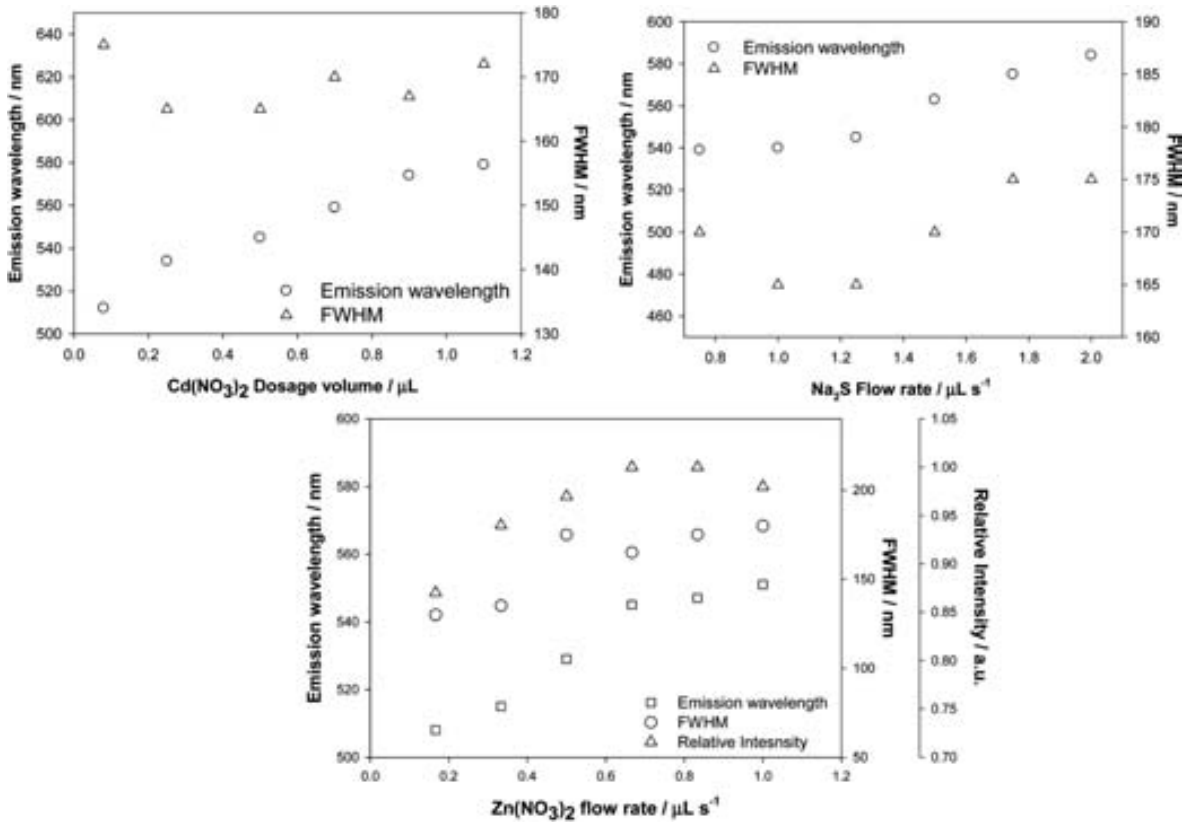

Fig. 4 Optimization of the hydrodynamic parameters: influence of the flow rates in the emission wavelength, the FWHM and the intensity of fluorescence. Reagent concentrations and flow rates were of 0.5 μL of a 5 mM cadmium nitrate and 10 mM tiopronin solution (adjusted at pH 10.0) every 1 s at 2.5 μL s^{-1} flow rate, 10 mM of sodium sulfide solution at 1.25 μL s^{-1} flow rate, and a 5 mM zinc nitrate solution at 0.67 μL s^{-1}; except for the reagent of study in each case. (a) Influence of cadmium nitrate dosage volume. The tested volumes were 0.08, 0.25, 0.50, 0.70, 0.90 and 1.10 μL. (b) Influence of the sodium sulfide solution flow rate. The tested flow rates were 0.75, 1.00, 1.25, 1.50, 1.75 and 2.00 μL s^{-1}; (c) Influence of zinc nitrate solution flow rate. The tested flow rates were 0.17, 0.33, 0.50, 0.67, 0.83 and 1.00 μL s^{-1}.

the nanocrystals. A 0.5 μL of $Cd(NO_3)_2$ dosage volume and 1.25 μL s^{-1} flow rate of Na_2S solution provided the minimal FWHM, which means a more uniform colloidal suspension.

The flow rate of the zinc nitrate solution was optimized in order to achieve the highest fluorescence intensity (quantum yield), which is related to the number of layers that cover the core of the nanoparticles. As it can be observed in Fig. 4c, an increase of the zinc nitrate solution flow rate entailed the displacement of the emission wavelength to higher values and the intensity enhance. As has been previously reported,[82–84] the fluorescence intensity rises by increasing the number of shell layers, until no improvement is observed. However, too many layers covering the core of the nanocrystal involve a decrease of the quantum yield. A flow rate of 0.67 μL s^{-1} showed the highest fluorescence intensity with a moderate band width.

Absorption spectra of the synthesized core–shell nanocrystals with the optimized conditions were recorded with the spectrophotometer, revealing a maximum absorption band centered in 363 nm (Fig. 5a). The emission fluorescence spectrum exhibits a band centered at 545 nm of a 165 nm FWHM (Fig. 5b). As can be seen, the discontinuous dispensing of the cadmium salt in the continuous flow of sodium sulfide improves the homogeneity of the synthesized nanoparticles, as is also noticeable in the obtained histogram from HRTEM images.

When CdS and CdS/ZnS emission spectra are compared, it is possible to notice the displacement of the emission band to lower wavelengths. This shift is probably due to the slightly different mean size of the nanocrystals, which is confirmed by microscopy measurements.

HRTEM images show homogeneous nanocrystals with an average size of 4.2 nm (Fig. 5c). The lattice fringes from the HRTEM image (Fig. 5d) indicate crystalline nanoparticles. Quantum yields of the obtained nanocrystals were increased as expected to 27%.

The repeatability of the synthesis was evaluated by comparing the maximum emission fluorescence wavelength and FWHM from ten identical syntheses (Fig. 6). From these results, it can be stated that the media emission wavelength of the synthesis is 540 ± 8 nm and the FWHM is of 170 ± 10 nm.

The last challenge in order to achieve an automated and controlled system for the nanocrystals synthesis was the integration of the absorbance and fluorescence monitoring system. In this way, any possible variation of the synthetic procedure owing to, for instance, channel obstruction or incorrect dosage of the reagents could be immediately detected and solved.

The microreactor design was again modified to incorporate two optical windows, embedded at the end of the main channel. For this purpose, the main channel carrying the formed

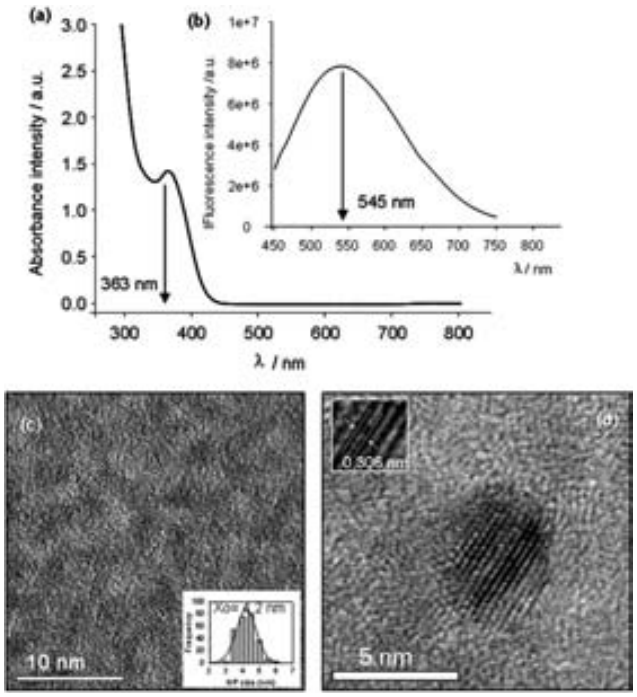

Fig. 5 (a) UV-vis and (b) fluorescence emission spectra of the obtained CdS/ZnS nanocrystals, (c) a TEM image of the obtained quantum dots using the ceramic microreactor and (d) a HRTEM image with the lattice fringes highlighted.

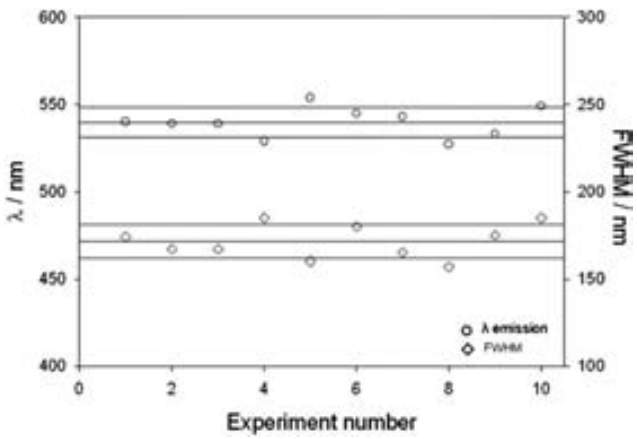

Fig. 6 Characterization of the CdS/ZnS synthesis repeatability by the emission fluorescence wavelength and the FWHM.

nanocrystals was enlarged, widened and brought to the surface of the microfluidic platform, where a 2 mm-diameter round hollow was drilled in all the layers to define an optical flow cell with enlarged optical path. Two transparent glass layers were attached in the top and bottom layers using polydimethylsiloxane (PDMS), also ensuring the sealing of the detection chamber. This flow cell configuration allowed the real-time monitoring of the chemical reaction process, using as well absorbance as fluorescence signals.

Optical windows were aligned to the LEDs and detectors of the optical system for absorbance and fluorescence measurements. The high pass optical filter was placed behind the window for fluorescence measurements, just before the photodetector.

Fig. 7 shows an example of the recorded absorption and fluorescence measurements at 365 nm during a synthesis, where the dosage of cadmium nitrate was intentionally on-line modified. The three different employed volumes, corresponding to 0.5 μL (the optimized one) (1), 0.25 μL (2) and 0.08 μL (3) can be perfectly distinguished. Both signals (absorbance and fluorescence) have the same tendency, as a decrease in absorbance intensity entails a reduction in its fluorescence. These emission intensity values are different for each of the three employed cadmium dosages; the maximum value corresponding to the higher dispensed volume, the middle with 0.25 μL, and the minimal value with the lower dosage. Likewise, the intensity values are constant when the same dosing conditions are used, demonstrating the repeatability of the obtained colloidal suspension, and there are no drifts in the recording line, showing that there is no dead volume in the optical chamber.

As the optimized dosage volume gives the higher signal, a decrease in the recording line implies the malfunction of the synthetic procedure, making it feasible to take appropriate actions to solve any problem in the shortest time.

Conclusions

To summarize, an automatic system for the synthesis of CdS/ZnS nanocrystals based on a ceramic microreactor and an on-line optical detection module has been reported in this paper. Since the whole process is automated, the reagents addition and the grade of mixture can be well defined, making it possible to better control the obtained nanocrystals, when compared to batch processes. The approach not only takes the advantages from the automatization, but also from microfluidics. One can control the grade of mixture and diffusion of reagents depending on the size and conformation of the channels, the type of mixers, the confluence point of the reagents and the hydrodynamics. In this sense, by a hydrodynamic focusing of reagents and the introduction of three-dimensional micromixers or simple channels, the different kinetic requirements of the reaction of nanocrystals can be achieved, obtaining in this way reproducible nanoparticles.

The present approach also takes advantages from the LTCC technology, which permits a fast prototyping without the requirement of special facilities or postfabrication steps; resulting in a low cost, rapid and easy fabrication technology. Moreover, the developed integrated absorbance and fluorescence monitoring system provides robustness and autonomy to the device. The system can immediately detect any possible error during the synthetic process, due to for instance, incorrect dosage of reagents, leaks at the joins of the syringes or channel obstructions, and then lead to the possibility of solving them in real time.

In this work, homogeneous, stable and highly reproducible nanocrystals of 4.5 and 4.2 nm (CdS and CdS/ZnS, respectively) have been obtained. The coverage of CdS with ZnS to form the core–shell quantum dots by the modification of the initial microfluidic platform has improved their quantum yield and particle size dispersion. The obtained quantum dots are excellent candidates to be applied in analytical applications as labels because their optical properties are controlled and well defined.

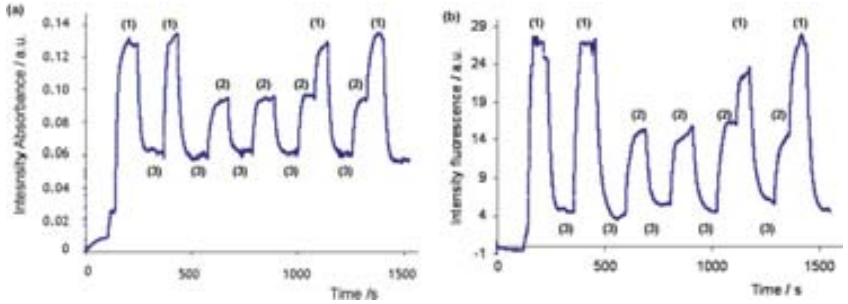

Fig. 7 Absorbance (a) and fluorescence emission (b) graphics recorded using the miniaturized optical system at different flow rates; 0.5 μL (cadmium dosage volume 1), 0. 25 μL (dosage volume 2) and 0.08 μL (dosage volume 3).

In this sense, this system can be directly integrated in subsequent LTCC microfluidic platforms to develop a lab-on-a-chip with on-line synthesis of the labels.

Acknowledgements

This work has been supported by the Spanish "Comisión Interministerial de Ciencia y Tecnología" through projects CICYT-CTQ2009-12128 and the Consolider Ingenio 2010 project CSD2006 -12. JMF thanks ARAID for financial support.

Notes and references

1 X. Peng, L. Manna, W. Yang, J. Wickham, E. Scher, A. Kadavanich and A. P. Alivisatos, *Nature*, 2000, **404**, 59–61.
2 J. Young-wook, C. Jin-sil and J. Cheon, *Angew. Chem., Int. Ed.*, 2006, **45**, 3414–3439.
3 C. B. Murray, D. J. Noms and M. G. Bawendi, *J. Am. Chem. Soc.*, 1993, **115**, 8706–8715.
4 C. Burda, X. Chen, R. Narayanan and M. A. El-Sayed, *Chem. Rev.*, 2005, **105**, 1025–1102.
5 A. Aharoni, T. Mokari, I. Popov and U. Banin, *J. Am. Chem. Soc.*, 2006, **128**, 257–264.
6 X. Duan, Y. Huang, Y. Cui, J. Wang and C. M. Lieber, *Nature*, 2001, **409**, 66–69.
7 S. A. McDonald, G. Konstantatos, S. Zhang, P. W. Cyr, E. J. D. Klem, L. Levina and E. Sargent, *Nat. Mater.*, 2005, **4**, 138–142.
8 Q. Sun, Y. A. Wang, L. S. Li, D. Wang, T. Zhu, J. Xu, C. Yang and Y. Li, *Nat. Photonics*, 2007, **1**, 717–722.
9 A. J. Nozik, *Phys. E.*, 2002, **14**, 115–120.
10 K. S. Leschkies, R. Divakar, J. Basu, E. Enache-Pommer, J. E. Boercker, C. B. Carter, U. R. Kortshagen, D. J. Norris and E. S. Aydil, *Nano Lett.*, 2007, **7**, 1793–1798.
11 J. Shen, L. D. Sun and C. H. Yan, *Dalton Trans.*, 2008, 5687–5697.
12 L. Yang and Y. Li, *Analyst*, 2006, **131**, 394–401; T. Asefa, C. T. Duncanc and K. K. Sharmac, *Analyst*, 2009, **134**, 1980–1990.
13 X. Zhang, S. Li, X. Jin and S. Zhang, *Chem. Commun.*, 2011, **47**, 4929–4931.
14 R. Gill, M. Zayats and I. Willner, *Angew. Chem., Int. Ed.*, 2008, **47**, 7602–7625.
15 P. Alivisatos, *Nat. Biotechnol.*, 2004, **22**, 47–52.
16 P. L. Lee, a Y. C. Suna and Y. C. Ling, *J. Anal. At. Spectrom.*, 2009, **24**, 320–327.
17 K. M. Gattás-Asfura and R. M. Leblanc, *Chem. Commun.*, 2003, 2684–2685.
18 Y. Kim, R. C. Johnson and J. T. Hupp, *Nano Lett.*, 2001, **1**, 165–167.
19 S. Roy, J. H. Soh and Z. Gao, *Lab chip*, 2011, **11**, 1886–1894.
20 B. R. Schudel, M. Tanyeri., A. Mukherjee, C. M. Schroeder and P. J. A. Kenis, *Lab chip*, 2011, **11**, 1916–1923.
21 A. Burns, H. Owb and U. Wiesner, *Chem. Soc. Rev.*, 2006, **35**, 1028–1042.
22 S. M. Borisov and I. Klimant, *Analyst*, 2008, **133**, 1302–1307.
23 U. Resch-Genger, M. Grabolle, S. Cavaliere-Jaricot, R. Nitschke and T. Nann, *Nat. Methods*, 2008, **5**, 763–775.
24 W. J. Parak, T. Pellegrino and C. Plank, *Nanotechnology*, 2005, **16**, R9.
25 X. Michalet, F. F. Pinaud, L. A. Bentolila, J. M. Tsay, S. Doose, J. J. Li, G. Sundaresan, A. M. Wu, S. S. Gambhir and S. Weiss, *Science*, 2005, **28**, 538–544.
26 P. D. Cozzoli, T. Pellegrino and L. Manna, *Chem. Soc. Rev.*, 2006, **35**, 1195–1208.
27 X. Wang, J. Zhuang, Q. Peng and Y. Li, *Nature*, 2005, **1**, 437–439.
28 J. Park, J. Joo, S. G. Kwon, Y. Jang and T. Hyeon, *Angew. Chem., Int. Ed.*, 2007, **46**, 4630–4660.
29 M. Green and P. O'Brien, *Chem. Commun.*, 1999, 2235–2241.
30 M. Brivio, W. Verboom and D. N. Reinhoudt, *Lab Chip*, 2006, **6**, 329–344.
31 R. L. Hartman and K. F. Jensen, *Lab Chip*, 2009, **9**, 2495–2507.
32 T. H. Yoon, S. H. Park, K. I. Min, X. Zhang, S. J. Haswell and D. P. Kim, *Lab Chip*, 2008, **8**, 1454–1459.
33 W. Luan, H. Yang, S. Tu and Z. Wang, *Nanotechnology*, 2007, **18**, 175603.
34 S. J. Haswell, R. J. Middleton, B. O'Sullivan, V. Skelton, P. Watts and P. Styring, *Chem. Commun.*, 2001, 391–398.
35 A. M. Nightingale and J. C. de Mello, *J. Mater. Chem.*, 2010, **20**, 8454–8463.
36 C. C. Huang and H. T. Chang, *Anal. Chem.*, 2006, **78**, 8332–8338.
37 E. M. Ali, Y. Zheng, H. Yu and J. Y. Ying, *Anal. Chem.*, 2007, **79**, 9452–9458.
38 G. K. Darbha, A. K. Singh, U. S. Rai, E. Yu, H. Yu and P. C. Ray, *J. Am. Chem. Soc.*, 2008, **130**, 8038–8043.
39 L. Basabe-Desmonts, D. N. Reinhoudt and M. Crego-Calama, *Chem. Soc. Rev.*, 2007, **36**, 993–1017.
40 S. Marrea and K. F. Jensenb, *Chem. Soc. Rev.*, 2010, **39**, 1183–1202.
41 R. Kikkeri, P. Laurino, A. Odedra and P. H. Seeberger, *Angew. Chem., Int. Ed.*, 2010, **49**, 2054–2057.
42 A. M. Nightingale, S. H. Krishnadasan, D. Berhanu, X. Niu, C. Drury, R. McIntyre, E. Valsami-Jonesb and J. C. deMello, *Lab Chip*, 2011, **11**, 1221–1227.
43 H. Wang, X. Li, M. Uehara, Y. Yamaguchi, H. Nakamura, M. Miyazaki, H. Shimizu and H. Maeda, *Chem. Commun.*, 2004, 48–49.
44 M. R. Gongora-Rubio, P. Espinoza-Vallejos, L. Sola-Laguna and J. J. Santiago-Avilés, *Sens. Actuators, A*, 2001, **89**, 222–241.
45 G. A. Groß, T. Thelemann, S. Schneider, D. Boskovic and J. M. Köhler, *Chem. Eng. Sci.*, 2008, **63**, 2773–2784.
46 S. Achmann, M. Hämmerle, J. Kita and R. Moos, *Sens. Actuators, B*, 2008, **135**, 89–95.
47 H. Teterycz, J. Kita, R. Bauer, L. J. Golonka, B. W. Licznerski, K. Nitsch and K. Wisniewski, *Sens. Actuators, B*, 1998, **47**, 100–103.
48 L. J. Golonka, H. Roguszczak, T. Zawada, J. Radojewski, I. Grabowska, M. Chudy, A. Dybko, Z. Brzozka and D. Stadnik, *Sens. Actuators, B*, 2005, **111**, 396–402.
49 N. Ibañez-García, C. S. Martínez-Cisneros, F. Valdés and J. Alonso, *TrAC, Trends Anal. Chem.*, 2008, **27**, 24–33.
50 M. R. Gongora-Rubio, P. Espinoza-Vallejos, L. Sola-Laguna and J. Santiago-Aviles, *Sens. Actuators, A*, 2001, **89**, 222–41.
51 L. Rivera, D. Izquierdo, I. Garcés, I. Salinas, J. Alonso and Mar Puyol, *Sens. Actuators, B*, 2009, **137**, 420–425.

52 L. Rivera, M. Puyol, F. Villuendas and J. Alonso, *Sens. Actuators, B*, 2008, **134**, 863–868.
53 S. Gómez-de Pedro, M. Puyol and J. Alonso-Chamarro, *Nanotechnology*, 2010, **21**, 415603.
54 N. Gaponik, D. V. Talapin, A. L. Rogach, K. Hoppe, E. V. Shevchenko, A. Kornowski, A. Eychmüller and H. Weller, *J. Phys. Chem. B*, 2002, **106**, 7177–7185.
55 J. E. B. Katari, V. Colvin and A. P. Alivisatos, *J. Phys. Chem.*, 1994, **98**, 4109–4117.
56 Z. A. Peng and X. Peng, *J. Am. Chem. Soc.*, 2001, **123**, 183–184.
57 D. V. Talapin, A. L. Rogach, A. Kornowski, M. Haase and H. Weller, *Nano Lett.*, 2001, **1**, 207–211.
58 L. Qu and X. Peng, *J. Am. Chem. Soc.*, 2002, **124**(9), 2049–2055.
59 L. Spanhel, M. Haase, H. Weller and A. Henglein, *J. Am. Chem. Soc.*, 1987, **109**, 5649–5655.
60 H. Li, W. Y. Shih and W. H. Shih, *Ind. Eng. Chem. Res.*, 2007, **46**(7), 2013–2019.
61 T. Vossmeyer, L. Katsikas, M. Giersig, I. G. Popovic, K. Diesner, A. Chemseddine, A. Eychmüller and H. Weller, *J. Phys. Chem.*, 1994, **98**, 7665–7673.
62 M. T. Harrison, S. V. Kershaw, M. G. Burt, A. Eychmüller, H. Weller and A. L. Rogach, *Mater. Sci. Eng., B*, 2000, **69**, 355–360.
63 R. Wargnier, A. V. Baranov, V. G. Maslov, V. Stsiapura, M. Artemyev, M. Pluot, A. Sukhanova and I. Nabiev, *Nano Lett.*, 2004, **4**, 451–457.
64 L. Qi, H. Co1lfen and M. Antonietti, *Nano Lett.*, 2001, **1**(2), 61–65.
65 D. W. Deng, J. S. Yu and Y. Pan, *J. Colloid Interface Sci.*, 2006, **299**, 225–232.
66 H. Peng, L. Zhang, C. Soeller and J. Travas-Sejdic, *J. Lumin.*, 2007, **127**, 721–726.
67 J. M. de la Fuente, M. Fandel, C. C. Berry, M. Riehle, L. Cronin, G. Aitchison and A. S. G. Curtis, *ChemBioChem*, 2005, **6**, 989–991.
68 M. J. Hostetler, J. E. Wingate, C.-J. Zhong, J. E. Harris, R. W. Vachet, M. R. Clark, J. D. Londono, S. J. Green, J. J. Stokes, G. D. Wignall, G. L. Glish, M. D. Porter, N. D. Evans and R. W. Murray, *Langmuir*, 1998, **14**, 17–30.
69 T. Huang and R. W. Murray, *J. Phys. Chem. B*, 2003, **107**, 7434–7440.
70 C.-K. Chiang, C.-C. Huang, C.-W. Liu and H.-T. Chang, *Anal. Chem.*, 2008, **80**, 3716–3721.
71 W. J. Jin, M. T. Fernández-Argüelles, J. M. Costa-Fernández, R. Pereiro and A. Sanz-Medel, *Chem. Commun.*, 2005, 883–885.
72 Y. Xia and C. Zhu, *Analyst*, 2008, **133**, 928–932.
73 B. Tang, J. Niu, C. Yu, L. Zhuo and J. Ge, *Chem. Commun.*, 2005, 4184–4186.
74 V. K. LaMer and R. Dinegar, *J. Am. Chem. Soc.*, 1950, **11**, 4847–54.
75 J. B. Knight, A. Vishwanath, J. P. Brody and R. H. Austin, *Phys. Rev. Lett.*, 1998, **80**, 3863–3866.
76 G. M. Walker, M. S. Ozers and D. J. Beebe, *Sens. Actuators, B*, 2004, **98**, 347–355.
77 R. H. Liu, M. A. Stremler, K. V. Sharp, M. G. Olsen, J. G. Santiago, R. J. Adrian, H. Aref and D. J. Beebe, *J. Microelectromech. Syst.*, 2000, **9**, 190–197.
78 R. A. Vijayendran, K. M. Motsegood, D. J. Beebe and D. E. Leckband, *Langmuir*, 2003, **19**, 1824–1828.
79 H. V. Drushel, A. L. Sommers and R. C. Cox, *Anal. Chem.*, 1963, **35**, 2166–2172.
80 P. Reiss, M. Protière and L. Li, *Small*, 2009, **5**, 154–168.
81 H. Z. Wang, H. Nakamura, M. Uehara, Y. Yamaguchi, M. Miyazaki and H. Maeda, *Adv. Funct. Mater.*, 2005, **15**, 603–608.
82 B. O. Dabbousi, J. Rodriguez-Viejo, F. V. Mikulec, J. R. Heine, H. Mattoussi, R. Ober, K. F. Jensen and M. G. Bawendi, *J. Phys. Chem. B*, 1997, **101**, 9463–9475.
83 D. V. Talapin, A. L. Rogach, A. Kornowski, M. Haase and H. Weller, *Nano Lett.*, 2001, **1**, 207–211.
84 A. V. Baranov, Yu. P. Rakovih, J. F. Donegan, T. S. Perova, R. A. Moore, D. V. Talapin, A. L. Rogach, Y. Masumoto and I. Nabiev, *Phys. Rev. B: Condens. Matter*, 2003, **68**, 165306.

B.3 Microreactor with integrated temperature control for the synthesis of CdSe nanocrystals.

Sara Gómez de Pedro, Cynthia S. Martínez Cisneros, Mar Puyol and Julián Alonso Chamarro. Lab on a Chip, 12 (11), 1979-1986 (2012).

View Online / Journal Homepage
Dynamic Article Links

Lab on a Chip

Cite this: DOI: 10.1039/c2lc00011c

www.rsc.org/loc

PAPER

Microreactor with integrated temperature control for the synthesis of CdSe nanocrystals†‡

Sara Gómez-de Pedro, Cynthia S. Martínez-Cisneros, Mar Puyol and Julián Alonso-Chamarro*

Received 4th January 2012, Accepted 13th April 2012
DOI: 10.1039/c2lc00011c

The recent needs in the nanosciences field have promoted the interest towards the development of miniaturized and highly integrated devices able to improve and automate the current processes associated with efficient nanomaterials production. Herein, a green tape based microfluidic system to perform high temperature controlled synthetic reactions of nanocrystals is presented. The device, which integrates both the microfluidics and a thermally controlled platform, was applied to the automated and continuous synthesis of CdSe quantum dots. Since temperature can be accurately regulated as required, size-controlled and reproducible quantum dots could be obtained by regulating this parameter and the molar ratio of precursors. The obtained nanocrystals were characterized by UV-vis and fluorescence spectrophotometry. The band width of the emission peaks obtained indicates a narrow size distribution of the nanocrystals, which confirms the uniform temperature profile applied for each synthetic process, being the optimum temperature at 270 °C (full width at half maximum = 40 nm). This approach allows a temperature controlled, easy, low cost and automated method to produce quantum dots in organic media, enhancing its application from laboratory-scale to pilot-line scale processes.

Introduction

The development of microfluidic devices based on different microfabrication technologies and materials has received increasing attention in recent years, becoming one of the most promising research areas in the microsystems field. The advantages provided by microfluidic devices has promoted their application to environmental monitoring,[1] biomedical analysis,[2] biological studies,[3] industrial and pharmaceutical control, among others.

Regarding current microfluidic applications, microreactors have emerged as an attractive approach for nanoparticles synthesis in nanoscale science and technology. This responds to their capability to provide high control levels, when compared with conventional macroscale reactions and the possibility they offer to automate the synthetic process.[4–6] In this sense, the synthesis of semiconductor nanocrystals has become one of the most interesting areas of research due to their wide application in multiple fields such as catalysis, electronics, biomedical and optical devices.[7–10] The interest in the use of these nanomaterials comes from their quantum-size effects, which provide them with unique electronic, magnetic and optical properties not exhibited by their respective bulk material.[11–12] Cadmium selenide (CdSe) quantum dots display one of the most valued optical quantum-size effect: its tunable size-dependent photoluminescence across the visible spectrum.[13,14] This property confers CdSe nanocrystals the possibility of replacing fluorophores in tag applications since they are photostable, show sharp emission spectra along the whole visible region and present larger lifetimes.[15] Nevertheless, properties exhibited by nanocrystals are closely linked to the synthesis process applied.[7,14,16,17] Therefore, it should be ideally performed under extremely controlled conditions.

The most usual synthetic procedure for the synthesis of quantum dots requires high temperatures and for cadmium and selenium precursors, solvents and organic surfactants that coat the nanocrystals during their growth, preventing their aggregation.

In this approach, the selection and control of temperature during the synthesis of nanocrystals is crucial in order to obtain well-defined and stable colloidal suspensions. The importance of this physical parameter during the synthesis process relies not only on its influence to achieve uniform nanocrystals, but also on determining quantum dots size, making feasible the attainment of different fluorescent emitting nanocrystals as a function of temperature.[18–20] The synthesis of reproducible nanocrystals is also conditioned by other important reaction parameters such as the molar relation of reagents, addition of precursors, stirring ratio, mass transference and fluctuations of temperature and concentrations.[14,21–23] Most of these parameters are difficult to control when the process is performed in batch conditions. This issue can be overcome when microreactors associated with

Sensors & Biosensors Group, Department of Chemistry, Autonomous University of Barcelona, Edifici Cn, 08193 Bellaterra, Catalonia, Spain. E-mail: julian.alonso@uab.es; Fax: 34 9358 12477; Tel: 34 9358 12533

† Published as part of a themed issue in collaboration with the III International Workshop on Analytical Miniaturization and NANOtechnologies, Barcelona, 2012

‡ Electronic supplementary information (ESI) available. See DOI: 10.1039/c2lc00011c/

microfluidic devices are applied, since most of these parameters can be automatically controlled by means of computer assisted systems. The use of microfluidic devices allows the preparation of high quality nanoparticles with key advantages such as fast thermal- and mass-transfer rates and continuous materials production. As a matter of fact, the microfluidic approach has been successfully applied to the synthesis of numerous metal, metal-oxide and semiconductor nanoparticles, including CdSe.[24–37]

Microfluidic devices for nanoparticles synthesis are usually based on silicon and glass technologies. This responds to the well established microfabrication processes which allow the synthesis of highly precise structures with dimensions in the order of a few micrometers.[38] Nevertheless, the integration of the different technological platforms associated with these kind of systems implies high costs and long-term fabrication procedures. Polymers present an alternative to silicon and glass, providing some advantages including lower manufacturing time (once the master is fabricated), multilayer approach (three-dimensional structures), transparency (for optical detection systems) and lower fabrication costs. Nevertheless, most of these materials cannot be used at the high temperatures required for CdSe nanocrystal synthesis, and usually present bonding and sealing problems between layers, which is an undesirable condition for microfluidic systems. The use of ceramic materials for microfluidic systems applied to high temperature reactions has considerably grown in recent years due to their high thermal and chemical stability. In this sense, the green tape or LTCC (low temperature cofired ceramics) technology, originally conceived for electronic purposes, emerges as an excellent alternative for this application.[39] This technology is well established for both low-volume, high-performance (military, spatial) and high-volume, low-cost (portable wireless, automotive) applications.[40] Moreover, its compatibility with screen printing techniques and multilayer approach enables the development of highly integrated devices that can include many of the stages associated with a specific analytical process, leading to real microTAS (micro Total Analysis System); for instance, the integration of conditioning stages such as thermostatization results crucial for many reactions.[41–45] LTCC-based microsystems that integrate thermal conditioning stages more frequently found in the bibliography are focused on PCR (polymerase chain reaction) systems[46] and reactions that involve enzymes.[47] Nevertheless, the development of microfluidic systems applied to high temperature nanocrystal synthesis has not received the same attention, which is reflected by the scarce existence of bibliography on this topic. Continuous microfluidic devices for semiconductor nanoparticles synthesis are usually developed using independent modules, where electronics and fluidics are miniaturized and separately developed from the heating system, which is usually based on macro apparatus to regulate temperature. Most of these systems consist of glass or polytetrafluoroethylene (PTFE) capillaries emerged in external oil-baths where reagents are warmed up.[24–31] Other approaches consist of placing entire glass, silicon or plastic microfluidic platforms over hot plates at high temperatures.[32,33] Scarce literature related to the miniaturization and integration of microfluidic and heating systems can be found in the bibliography due to the complexity associated with conventional methodologies.[34] In this sense, a multilayer technology able to be applied in the development of both kinds of platforms would be desirable. The LTCC technology provides a way to develop miniaturized monolithic or modular devices that integrate microfluidics, electronics, sensors and actuators (heaters).[43,47]

In this work, a LTCC-based microfluidic system for high temperature reactions is presented. The device integrates the microfluidics and a miniaturized thermally controlled platform, both developed using the same fabrication technology, and was applied to the continuous size-controlled synthesis of CdSe quantum dots. Even though the LTCC technology allows the development of monolithic devices, in this case a modular configuration was preferred due to the advantages provided by this approach: exchangeability/replacement of the microfluidic platform in case of malfunction or the analytical process needs. Since temperature can be regulated as required, using a specifically designed electronic system, CdSe quantum dots emitting/absorbing at different wavelengths were easily obtained. Moreover, to increase the system reliability, its operation was automated by means of a set of solenoid valves and syringe pumps that allows its operation under unattended conditions.

Experimental

Chemicals

Cadmium oxide (CdO, 99.99%, Aldrich), trioctylphosphine (TOP, 90%, Aldrich), tryoctylphosphine oxide (TOPO, 99%, Aldrich), oleic acid (OA) (Ph Eur, Fluka), Oleylamine (OLA, 70%, Aldrich), 1-octadecene (ODE, 90%, Aldrich), selenium powder (Se, 99.5%, Aldrich) and rhodamine 6 G (Sigma) were purchased from Sigma-Aldrich. Analytical grade chloroform and methanol were used for further processing.

Stock solutions

Stock solutions were newly prepared for each synthesis. Three cadmium precursor solutions were prepared to evaluate different Cd : Se molar ratios (1 : 10, 1 : 1 and 2 : 1, respectively). The first Cd stock solution consisted of 32.1 mg of CdO (0.25 mmol), 317 μL of OA (1 mmol), 2.5 g of TOPO (6.45 mmol) and 5 mL of OLA (15.2 mmol). The mixture was warmed up in a round-bottom flask at 190 °C until a pale yellow solution was observed (around 40 min). The mixture obtained was diluted with 7.5 mL of ODE. The other two Cd precursors were similarly prepared. The 1 : 1 molar ratio consisted of 321.25 mg of CdO (2.5 mmol), 4 mL of OA (12.6 mmol), 3 g of TOPO (7.8 mmol), 5 mL of OLA (15.2 mmol) and 3 mL of ODE. The 2 : 1 molar ratio consisted of 802.5 mg of CdO (6.25 mmol), 10 mL of OA (32 mmol), 3.3 g of TOPO (8.5 mmol) and 5 mL of OLA (15.2 mmol).

The selenium precursor was prepared mixing 197.4 g (2.5 mmol) of selenium powder with 5 mL of TOP (10.1 mmol) and 10 mL of OLA (21.25 mmol) in another round-bottom flask at room temperature.

Materials and methods

DuPont 951 green tape was used as the substrate for the fabrication of the microfluidic and thermal platforms. The embedded heater was screen printed using a gold cofirable conductor paste DuPont 5742. Via filling was performed using

DuPont 6141. As a temperature sensor, a commercial class A PT100 (Innovative Sensor Technology, Switzerland) was placed under the thermal platform by means of epoxy (EPO-TEK® H20E).

A PIC18F4431 microcontroller (Microchip Inc., USA) was used to implement a digital PID (proportional-integral-derivative) control system to maintain temperature at the desired value. All the electronic components used to implement the digital PID control were carefully selected to improve the system response and reduce noise effects in the signal. The user interface for temperature monitoring in the microanalyzer was developed on a personal computer through a virtual instrument specifically designed for this application.

The continuous flow system set-up consisted of a set of two syringe pumps (540 060 TSE systems) coupled to 10 ml syringes (Hamilton series GASTIGHT 1000 TLL) connected to the ceramic microfluidic platform with PTFE tubes (i.d. 0.9 mm). Additionally, a set of three-way solenoid valves (161T031, NResearch, NJ, USA) was used for the automatic filling of the syringes by means of specially developed software. O-rings and conic PTFE cones were connected between the microfluific platform and the PTFE tubes to secure the sealing of the system. The use of this experimental set-up enabled the automation of the continuous synthesis of quantum dots with the minimum user interaction, increasing the repeatability of the process and the production ratio.

Prior to characterization of the obtained nanocrystals from the ceramic microreactor, a reversible flocculation was performed with anhydrous methanol. The flocculate obtained was separated from the supernatant by centrifugation and redispersed again in chloroform.

Quantum dots (QDs) were characterized using a double-beam scanning spectrophotometer that recorded the UV-vis spectra (Shimadzu UV-310PC UV-Vis-NIR, Kyoto, Japan). The excitation/emission spectra were obtained by means of a spectrofluorometer (Fluorolog® Modular Spectrofluorometer, Horiba Jobin Yvon). Emission spectra were obtained from the excitation of quantum dots using the first absorption peak, being checked by the excitation spectra of the nanocrystals. Quantum yields (QY) were calculated by comparing the integrated emission from QDs diluted in chloroform regarding rhodamine 6G.[48]

Results and discussion

Microsystem fabrication

The general fabrication process of a LTCC-based miniaturized device has been described in detail elsewhere.[39] A three-dimensional view of the platforms that integrate the microsystem developed in this work for the continuous and automated synthesis of quantum dots is depicted in Fig. 1. It was developed in a modular configuration (microfluidic and thermal platforms were separately fabricated) to increase its reliability. In this way, if a thermal unit or a microfluidic platform with different characteristics is required, it can be replaced without requiring the rebuilding of the complete device. Moreover, if any of the platforms presents operational problems it can be replaced without affecting the other elements. Using this modular approach, once both platforms were fabricated, they were mechanically attached taking care to obtain the highest surface

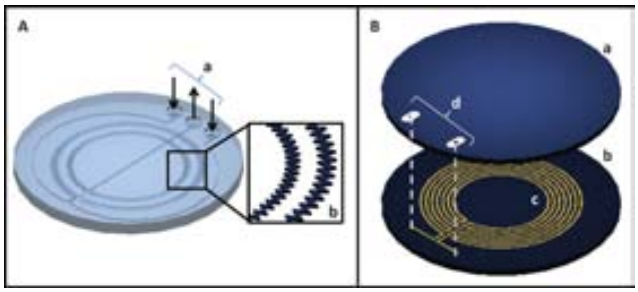

Fig. 1 LTCC-based microsystem for CdSe quantum dots synthesis (6 mm diameter and 2 mm depth). A: microfluidic platform; a: inlets/outlet; b: amplification of a microreactor region. B: thermal platform showing the embedded heater; a: cover of the heater; b: base where heater was screen-printed; c: embedded gold-based heater; d: pads for external electronic control.

contact for optimum heat transfer between them. Heat transfer between platforms was favored by the high thermal conductivity presented by LTCC materials (3 W/mK) when compared with other microfabrication materials such as polymers or glass.

As seen in Fig. 1A, the microfluidic platform includes two inlets for reagents and one outlet through which the produced quantum dots are collected. The two inlets send reagents through two simple channels around the microreactor before they meet each other downstream. This process acts as a pretreatment step for preheating reagents before mixing. Channels converged in a Y-shape point downstream before getting into the microreactor (Z-shape mixer). A bi-dimensional micromixer (200 μm width, 200 μm height) was preferred for this application, since it introduces the chaotic mixing required for an improved mass transference between reagents. This approach avoids thermal fluctuations on the liquid caused by its flow in different levels when three dimensional mixers are introduced. The micromixer configuration was designed in a circular shape and considering the heater position inside the thermal platform to achieve the best alignment between both platforms, when mechanically attached. In this way, an optimum and uniform heat transfer between the microreactor and the heater embedded in the thermal platform was obtained. Using this approach, during their flow through the microreactor, reagents are exposed to specific, uniform and controlled temperature levels provided by the thermal platform. The complete microfluidic platform consisted of eight stacked layers where the microreactor was embedded.

The thermal platform consists of a nine-layer block where the heater was embedded. The heater was screen-printed over the fifth layer (in the middle of the block), as shown in Fig. 1B, to promote a more uniform heat distribution through the *z*-axis. External pads were defined on the top layer to connect the embedded heater to the external electronic control circuit by means of electrical vias. The heater design was developed on the basis of a radial and uniform distribution of temperature and trying to avoid a highly elevated heat point in the center of the platform. The nine layers that constitute the thermal platform make it robust, avoiding its break up during the high temperature cycles at which the evaluated reactions occur. For temperature sensing and establishing the PID control feedback, a class A PT100 sensor was placed over the thermal platform trying to obtain the optimum alignment

with the microreactor embedded in the microfluidic platform. For temperature optimization inside the microreactor, a characterization process regarding heat distribution on the thermal platform was performed using an EMC Scanner with an IR Probe (RS321EH, Detectus AB) (ESI‡). During these studies, a uniform radial distribution of temperature was observed in the xy plane (Fig. S.1, ESI‡). Regarding the *z*-axis thermal distribution, measurements at the top and the bottom of the device were carried out to extrapolate temperature inside the microreactor, considering the material thermal transfer coefficient and the number of layers used for its fabrication (Fig. S.2, ESI‡).

Electronics for temperature control

Since temperature level and distribution are crucial parameters to be considered for proper QDs synthesis, a dedicated temperature controller with a digital PID topology was designed and implemented on a PIC18F4431 microcontroller. A personal computer was applied as a user interface for monitoring purposes. As previously mentioned, the PCB for temperature control was separately fabricated to avoid any damage due to the high temperatures at which the microreactor operates. A block diagram of the electronics involving the digital PID control is shown in Fig. 2A. Temperature was measured with the PT100, whose signal was conditioned through a signal conditioning circuit (SCC) that kept current at a constant value in accordance to the PT100 datasheet. In this way, interference with temperature measurements due to self-heating could be avoided. The SCC provided a potential directly related to resistive changes produced in the PT100 as a consequence of temperature. The signal provided by the SCC was applied to the analog to digital converter integrated in the PIC microcontroller as a feedback to the digital PID control system. This signal was traduced to temperature according to the equation corresponding to class A PT100 sensors: $t \geqslant 0$ °C, $R(t) = R_0\,(1 + A{\cdot}t + B{\cdot}t^2)$, where: $A = 3.9083 \times 10^{-3}$ °C^{-1}, $B = -5.775 \times 10^{-7}$ °C^{-1}, $R_0 = 100\ \Omega$.

This equation was included in the microcontroller software. The feedback signal was used to estimate the error and to correct it using the differential equations programmed in the digital PID control. The control signal produced by the PID (a pulse width modulated signal, PWM) was amplified and applied to the gold-based heater embedded into the thermal platform through a MOSFET (metal oxide semiconductor field effect transistor).

The thermal platform was configured to work at different temperature levels (180 °C–280 °C) according to the needs associated with the quantum dots produced. Fig. 2B presents the obtained temperature response, once the PID control parameters were carefully optimized, for different experiments performed using 270 C as a set point. As seen in this figure, a highly stable temperature profile was always obtained. The system took about ten minutes to stabilize before reaching a steady state at the desired temperature. Slow temperature transitions during stabilization were preferred in order to avoid abrupt thermal changes that could stress/brake the thermal platform. Small peak overshoots of about 8 °C were observed at the beginning for each of the temperature levels evaluated in this study. Signal variations in the order of ± 0.5 °C were observed on the steady state of the system response.

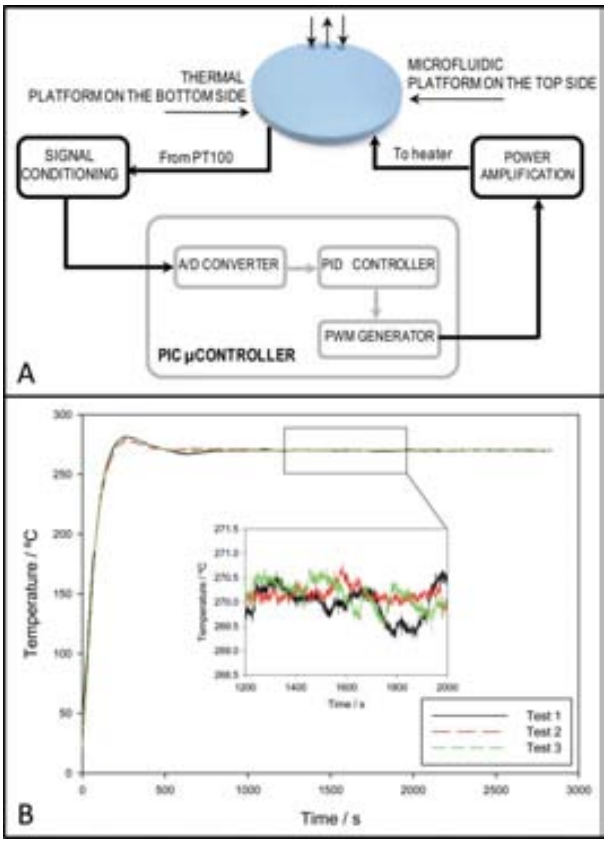

Fig. 2 Electronics for thermal control. A: block diagram of the electronics developed for a precise digital PID temperature control. B: system responses obtained during three experiments performed at a set-point of 270 °C once the PID parameters were optimized. Small variations in the order of ± 0.5 °C were observed.

Synthesis of nanocrystals

As explained previously, three basic elements are required for the synthesis of CdSe nanocrystals: metallic compounds, organic surfactants and solvents. It is well known that choosing suitable organic surfactants is one of the most important issues in order to obtain well dispersed nanocrystals. Surfactants not only form complexes with the reactive monomer generated while heating, but also prevent further growth and aggregation by their coordination on the nanoparticle surface.[49] Moreover, they play an important role in limiting the dissolution of smaller crystals and permitting the formation of larger ones (Ostwald ripening).

In this work, the reaction selected to carry out the synthesis of CdSe nanocrystals into the described microreactor was a modification of the Peng's procedure, which is based on CdO, Se powder and the triple ligand of TOPO, OA and OLA.[27,30] This reaction does not require an inert environment, as it employs stable and less hazardous reagents, which makes it easier to scale down the reaction.

The procedure is based on the trioctylphosphine–selenium (TOPSe)/trioctylphosphine oxide–cadmium (TOPOCd) system[31,34,35] and the use of oleic acid and oleylamine. This method exhibits some benefits regarding such reactions. Previous studies have demonstrated the efficiency of TOPO in reducing the

reaction time of the synthesis when performed in microfluidic systems without involving the poor reproducibility shown by devices where only TOP is used.[27,50] Moreover, TOPO passivates the surface of the nanocrystal in the most reactive sites, being feasible to achieve not only better size distributions, but also increased photoluminiscence efficiencies.[51] It has also been demonstrated that OA contributes to the reduction of the colloidal dispersion due to its efficiency for surface capping nanocrystals.[30] Finally, the low reactivity of OLA in air, its low melting point and strong packing density have promoted its application as a ligand of CdSe nanocrystals in microreactor systems, making the synthesis of high-quality quantum dots easier.[34,35,52,53] Moreover, the use of OLA enables bigger nanocrystals to be obtained and the temperature required by the reaction can be reduced due to its high-surface bonding ability.[53–55] In this study, ODE was selected as the noncoordinating solvent due to its high boiling point (320 °C), its low toxicity, low reactivity with precursors and its high capabilities as a solvent, making the reaction more feasible. Additionally, ODE allows the reaction to take place without the need of an inert atmosphere.[30,56]

By adjusting the molar ratio of the reagents, QDs of different sizes can be obtained. To achieve an extended range of nanocrystals with different optical properties, three different molar ratios were tested at different temperatures. The first synthesis were carried out with a 1 : 10 Cd : Se molar ratio. In this case, due to the large excess of selenium, the cadmium precursor was rapidly consumed, leading to the formation of small sized nanocrystals. Therefore, nanocrystals produced at this molar ratio involve absorption and emission peaks at lower wavelengths.[35,57] Later syntheses were performed using 1 : 1 and 2 : 1 molar ratios, respectively.

Many studies regarding the optimization of hydrodynamic parameters in microfluidic reactors have been presented.[28,30] They were considered for the followed evaluation of the effect of molar ratios and temperatures on the obtained QDs optical properties and only a basic study regarding flow rates and residence time was performed. Both parameters are closely related, the lower the flow rate, the larger the residence time of reagents inside a specific microfluidic system. As Bawendi and co-workers concluded, large residence times entail an uncontrolled growth of nanocrystals, producing a wider size distribution of quantum dots.[35] On the other hand, shorter residence times produce the uncompleted reaction of the colloidal suspension. Once optimized, a 60 μL min^{-1} flow rate with a microreactor volume of 55 μL were finally selected to carry out the assays presented in this work.

As previously explained, temperature plays a crucial role during the nanocrystals synthesis procedure. At low temperatures the formation of monomers needed for the nucleation and growth of QDs cannot be formed, due to the high energy barrier. On the other hand, the use of high temperatures normally produces an uncontrolled growth of nanocrystals, obtaining wider size distributions.[19,28,49]

In this work, the effect of temperature was varied in the range from 180 °C to 280 °C. This range provided enough heat to allow the rearrangement and annealing of atoms within the nanocrystal growing during the synthesis process.[19] As can be observed in Fig. 3A, a displacement of 48 nm in the fluorescence emission peak occurred when the temperature was increased from 180 to 280 °C. Sharp emission peaks for all the synthesized CdSe nanocrystals were obtained. According to these results, FWHM (full width at half maximum) values of the band luminescence around 50 nm were observed. The sharpness of the peaks indicates a narrow size distribution of the nanocrystals which confirms the uniform temperature profile applied for each synthesis process. Images of the QDs obtained at the whole temperature range under evaluation are presented in Fig. 3. They are highly diluted with chloroform (approximately 1 : 50) in order to avoid fluorescence autoquenching.

The optimum temperature, intrinsic on each reaction, [19,28] at which the narrowest fluorescence absorption/emission peak and the higher emission intensity were obtained, was found to be 270 °C (Fig. 4A). At this temperature, the FWHM was minimal at *ca.* 40 nm. Fig. 4B shows the shape, dimension and size distribution of the nanocrystals synthesized at the optimum temperature, obtained by transmission electron microscopy (TEM). The average size of the QDs was found to be 3.3 ± 0.4 nm, obtained by counting an amount of approximately 500 nanoparticles. Fig. 4C display a high resolution TEM (HRTEM) image which shows a lattice fringe distance of 0.215 nm of the CdSe QDs, revealing a preferential hexagonal growth of CdSe

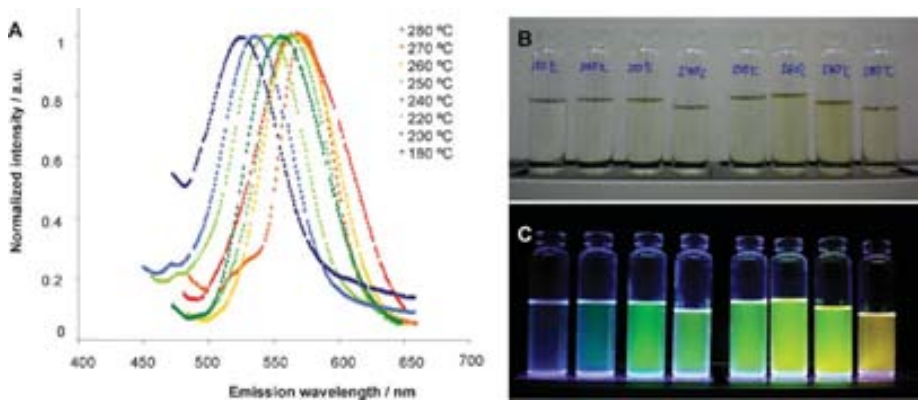

Fig. 3 A: fluorescence emission spectra of the nanocrystals synthesized in the microreactor from 180 to 280 °C with a molar ratio of Cd : Se 1 : 10. B: images of the obtained QDs colloidal solutions, highly diluted with chloroform, from the different tested range of temperatures under room and UV (C) light.

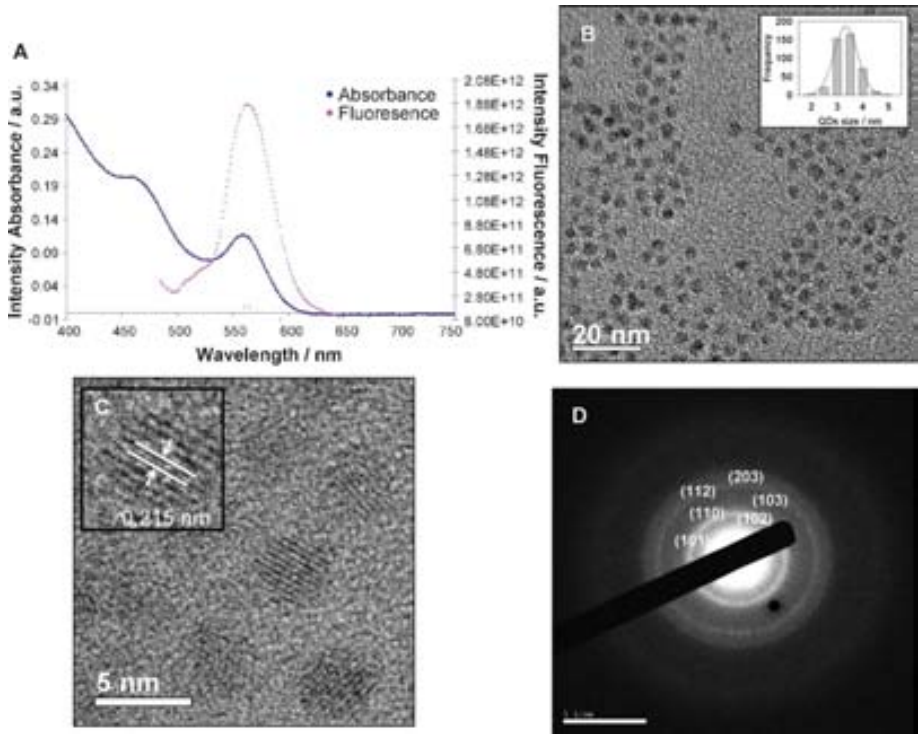

Fig. 4 A: absorption (in blue) and fluorescence emission (in pink) spectra of the CdSe quantum dots synthesized in the microreactor at 270 °C. TEM image (B), HRTEM image (C) with the lattice fringes highlighted, and SAED pattern image (D) of the obtained CdSe quantum dots.

NPs on the (110) plane (JCPDS card No:08-0459). The clear ring structure of the selected area electron diffraction (SAED) pattern image of the nanocrystals (Fig. 4D) indicates its crystalline structure. The bright rings observed can be attributed to (101), (102), (110), (103) (112) and (203) lattice planes of the hexagonal (wurtzite) crystal structure of CdSe.

Fig. 5 shows a three-dimensional graphic of the dependence of fluorescence emission and excitation wavelength from the reaction temperature when a molar ratio of Cd : Se 1 : 10 was used. Both parameters increase with increasing temperature. As the temperature was increased, the maximum fluorescence peak shifted to higher wavelengths, following a well-defined straight line. Regarding the relationship between excitation wavelength and temperature, the same linear tendency was perceived. The excitation peaks were selected according to the first absorption maximum of the UV-visible spectra. When higher temperatures were used, a bathochromic shift effect on the absorption peaks was also observed. Excitation peaks (absorption maxima) were correlated with the emission maxima obtained for nanocrystals, being in agreement with other work.[27,58]

The obtained nanocrystals exhibit larger Stokes shift values than common dyes, which sometimes show overlapped excitation and emission spectra. This makes their application to multiple research fields more feasible. Fig. S.4 (ESI‡) displays the calculated Stokes shifts for the ten studied temperatures. A mean value of 103 ± 3.2 nm is obtained and the graphic shows a negligible variation of this parameter.

Quantum yields were also determined providing values from 25 to 55%.[48] Higher QYs values were obtained as temperature increased,[58] with the exception of the synthesis occurring at 280 °C, where a slightly lower yield was observed.

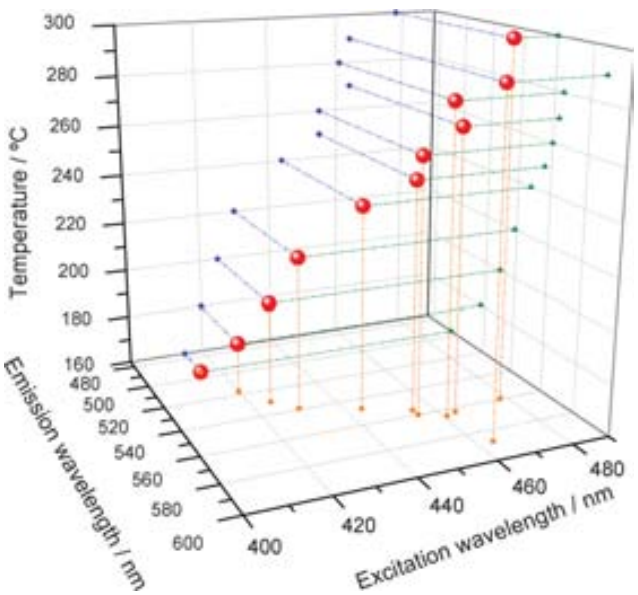

Fig. 5 Correlation between fluorescence emission peaks, excitation wavelengths and temperatures during the synthesis of nanocrystals with a Cd : Se molar ration of 1 : 10.

With the aim of obtaining larger nanocrystals to cover the whole visible absorption spectrum, two more molar ratios were tested, 1 : 1 and 2 : 1 (Cd : Se) (Fig. 6). The tested range of temperatures was the same for all experiments.

The second set of experiments corresponded to a 1 : 1 molar ratio. Until 240 °C, the behavior of the synthesis process was comparable to that obtained for a 1 : 10 molar ratio in terms of

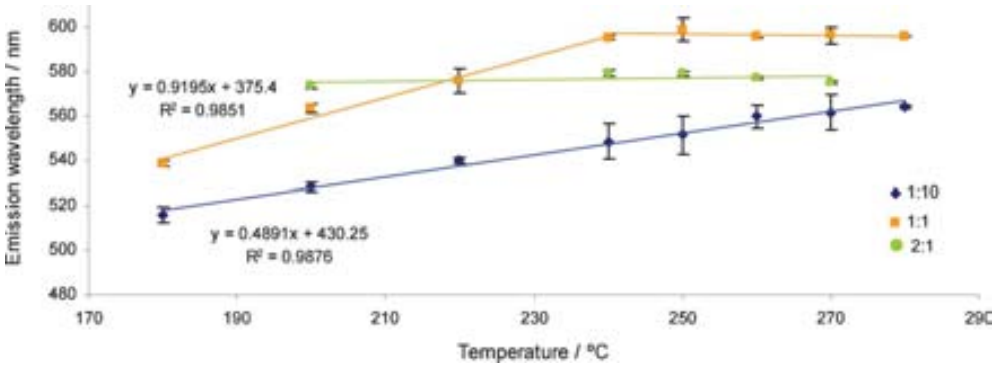

Fig. 6 Maximum intensity of fluorescence emission peaks obtained for the three different tested Cd : Se molar ratios 1 : 10, 1 : 1 and 2 : 1 with the error bars.

the increasing emission peak and quantum yields, and the constant Stokes shifts. Nevertheless, in this case, both the absorption (498–555 nm) and fluorescence (532–572 nm) emission peaks shifted to larger wavelengths. On the other hand, over 240 °C, the absorption (585 nm) and fluorescence (595 nm) emission peaks remained constant for the different tested temperatures. This effect is associated with the molar ratio used since although higher quantities of Cd monomers are formed, the lack of Se prevents their growth, hindering the formation of higher nanocrystals. FWHM were still calculated on 50 nm, demonstrating the narrow size distribution.

When performing the temperature experiments with a 2 : 1 molar ratio, almost the same QDs were obtained. The absorption and emission peaks, Stokes shifts and quantum yields were practically invariable with the increasing temperature from 200 to 270 °C. At 200 °C larger QDs can be obtained than with lower Cd : Se ratios, however, at this ratio, this is the temperature threshold at which QDs size depends on temperature.

Therefore, it seems that for each molar ratio, a temperature threshold exists above which no larger particles can be formed, because there is a lack of selenium. On the other hand, on increasing the molar ratio of Cd : Se, larger nanocrystals can be obtained at the same temperature.

The ESI includes graphics that show the correlation observed between temperature and emission/absorption fluorescence for the three molar rations tested during the nanoparticles synthesis.‡

Conclusions

A ceramic microsystem, based on the modular integration of microfluidic and thermal platforms, is proposed for its application to the automatic and controlled synthesis of CdSe nanocrystals at high temperatures. The microfluidic module with an embedded bi-dimensional micromixer was attached to a thermal platform where a gold-based heater was embedded. The microreactor design enabled the generation of a turbulent flow inside the system that improved the reaction performance without affecting the temperature distribution on reagents. The heating module was developed considering a radial and uniform temperature distribution in accordance to the microreactor design. The configuration of the thermal platform in order to work at different controlled temperatures (180 °C–280 °C) during the synthesis processes allowed semiconductor nanoparticles absorbing/emitting at almost the whole visible spectrum to be obtained, since their optical properties depend on their quantum-size effects. The quantum yields obtained here were found to be between 25 and 55% and the Stokes shifts remained constant. The thermal conductivity provided by LTCC materials favored heat transfer between platforms, allowing the establishment of uniform and confident temperatures through the microfluidic platform. This was demonstrated with the narrow band widths observed with each synthesis, characteristic of narrow size distributions in the colloidal suspension.

This microreactor allows a temperature controlled, easy, low cost and automated method of synthesizing quantum dots in organic media, thus becoming a great approach from laboratory-scale to pilot-line scale processes. It also demonstrates the versatility provided by the ceramic materials, when applied to high temperature reactions in terms of thermal stability and fast prototyping. For instance, if further applications require higher quantum yields, an additional channel could be easily introduced in the microreactor for the coverage of CdSe nanocrystals with a ZnSe shell, establishing a lower temperature area in the microfluidic platform.

Additionally, a monolithic device for a dedicated application could be easily developed by the integration of the microfluidic and the thermal platform in the same substrate.

Acknowledgements

This work has been supported by the Spanish Ministry of Science and Innovation (MICINN) through projects CTQ2009-12128 and the Consolider Ingenio 2010 project CSD2006 -12 and Catalonia Government through SGR 2009 -0323.

References

1 A. González-Crevillén, M. Hervás, M. A. López, M. C. González and A. Escarpa, *Talanta*, 2007, **74**, 342–357.
2 K. M. Ainslie and T. A. Desai, *Lab Chip*, 2008, **8**, 1864–1878.
3 J. Rajagopalan and M. T. A. Saif, *J. Micromech. Microeng.*, 2011, **21**, 054002.
4 J. B. Edel, R. Fortt, J. C. deMello and A. J. deMello, *Chem. Commun.*, 2002, 1136–1137.
5 . I. Shestopalov, J. D. Tice and R. F. Ismagilov, *Lab Chip*, 2004, **4**, 316–321.
6 B. F. Cottam, S. Krishnadasan, A. J. deMello, J. C. deMello and M. S. P. Shaffer, *Lab Chip*, 2007, **7**, 167–169.

7 M. Green and P. O'Brien, *Chem. Commun.*, **1999**, 2235–2241.
8 A. Aharoni, T. Mokari, I. Popov and U. Banin, *J. Am. Chem. Soc.*, 2006, **128**, 257–264.
9 X. Zhang, S. Li, X. Jin and S. Zhang, *Chem. Commun.*, 2011, **47**, 4929–4931.
10 R. C. Somers, M. G. Bawendi and D. G. Nocera, *Chem. Soc. Rev.*, 2007, **36**, 579–591.
11 A. P. Alivisatos, *Science*, 1996, **271**, 933–937.
12 C. Burda, X. Chen, R. Narayanan and M. A. El-Sayed, *Chem. Rev.*, 2005, **105**, 1025–1102.
13 B. O. Dabbousi, J. Rodriguez-Viejo, F. V. Mikulec, J. R. Heine, H. Mattoussi, R. Ober, K. F. Jensen and M. G. Bawendi, *J. Phys. Chem. B*, 1997, **101**, 9463–9475.
14 L. Qu and X. Peng, *J. Am. Chem. Soc.*, 2002, **124**, 2049–2055.
15 U. Resch-Genger, M. Grabolle, S. Cavaliere-Jaricot, R. Nitschke and T. Nann, *Nat. Methods*, 2008, **5**, 763–775.
16 A. M. Smith and S. Nie, *Analyst*, 2004, **129**, 672–677.
17 S. Kumar and T. Nann, *Small*, 2006, **2**, 316–329.
18 J. Park, J. Joo, S. G. Kwon, Y. Jang and T. Hyeon, *Angew. Chem., Int. Ed.*, 2007, **46**, 4630–4660.
19 Y. Yin and A. P. Alivisatos, *Nature*, 2005, **437**, 664–670.
20 A. L. Rogach, D. V. Talapin, E. V. Shevchenko, A. Kornowski, M. Haase and H. Weller, *Adv. Funct. Mater.*, 2002, **12**, 653–664.
21 L. Qu, A. Peng and X. Peng, *Nano Lett.*, 2001, **1**, 333–337.
22 W. W. Yu and X. G. Peng, *Angew. Chem., Int. Ed.*, 2002, **41**, 2368–2371.
23 C. B. Murray, C. R. Kagan and M. G. Bawendi, *Annu. Rev. Mater. Sci.*, 2000, **30**, 545–610.
24 A. M. Nightingale and J. C. deMello, *J. Mater. Chem.*, 2010, **20**, 8454–8463.
25 A. M. Nightingale, S. H. Krishnadasan, D. Berhanu, X. Niu, C. Drury, R. McIntyre, E. Valsami-Jones and J. C. deMello, *Lab Chip*, 2011, **11**, 1221–1227.
26 H. Wang, X. Li, M. Uehara, Y. Yamaguchi, H. Nakamura, M. Miyazaki, H. Shimizu and H. Maeda, *Chem. Commun.*, 2004, 48–49.
27 H. Yang, W. Luan, S. Tu and Z. M. Wang, *Cryst. Growth Des.*, 2009, **9**, 1569–1574.
28 H. Nakamura, A. Tashiro, Y. Yamaguchi, M. Miyazaki, T. Watari, H. Shimizu and H. Maeda, *Lab Chip*, 2004, **4**(3), 237–240.
29 A. J. deMello, *ChemPhysChem*, 2009, **10**, 2612–2614.
30 W. Luan, H. Yang, S. Tu and Z. Wang, *Nanotechnology*, 2007, **18**, 175603.
31 H. Nakamura, Y. Yamaguchi, M. Mikazaki, H. Maeda, M. Uehara and P. Mulvaney, *Chem. Commun.*, 2002, **23**, 2844–2845.
32 R. M. Tiggelaar, P. van Male, J. W. Berenschot, J. G. E. Gardeniers, R. E. Oosterbroek, M. de Croon, J. C. Schouten, A. van den Berg and M. C. Elwenspoek, *Sens. Actuators, A*, 2005, **119**(1), 196–205.
33 B. K. H. Yen, A. Gunther, M. A. Schmidt, K. F. Jensen and M. G. Bawendi, *Angew. Chem.*, 2005, **117**, 5583–5587.
34 E. M. Chan, A. P. Alivisatos and R. A. Mathies, *J. Am. Chem. Soc.*, 2005, **127**, 13854–13861.
35 B. K. H. Yen, N. E. Stott, K. F. Jensen and M. G. Bawendi, *Adv. Mater.*, 2003, **15**(21), 1858–1862.
36 E. M. Chan, R. A. Mathies and A. P. Alivisatos, *Nano Lett.*, 2003, **3**(2), 199–201.
37 S. Krishnadasan, J. Tovilla, R. Vilar, A. J. deMello and J. C. deMello, *J. Mater. Chem.*, 2004, **14**(17), 2655–2660.
38 C. A. Zorman and R. J. Parro, *Phys. Status Solidi B*, 2008, **245**(7), 1404–1424.
39 N. Ibáñez-García, C. S. Martínez-Cisneros, F. Valdés and J. Alonso, *TrAC, Trends Anal. Chem.*, 2008, **27**(1), 24–33.
40 L. J. Golonka, T. Zawada, J. Radojewski, H. Roguszczak and M. Stefanow, *Int. J. Appl. Ceram. Technol.*, 2006, **3**(2), 150–156.
41 M. Baeza, C. López, J. Alonso, J. López-Santin and G. Alvaro, *Anal. Chem.*, 2010, **82**(3), 1006–1011.
42 C. S. Martinez-Cisneros, Z. daRocha, M. Ferreira, F. Valdes, A. Seabra, M. Gongora-Rubio and J. Alonso-Chamarro, *Anal. Chem.*, 2009, **81**, 7448–7453.
43 C. S. Martinez-Cisneros, N. Ibanez-Garcia, F. Valdes and J. Alonso, *Sens. Actuators, A*, 2007, **138**, 63–70.
44 G. Fercher, A. Haller, W. Smetana and M. J. Vellekoop, *Analyst*, 2010, **135**, 965–970.
45 S. Gómez-de Pedro, M. Puyol and J. Alonso, *Nanotechnology*, 2010, **21**, 415603.
46 P. Bembnowicz, M. Malodobra, W. Kubicki, P. Szczepanska, A. Gorecka-Drzazga, J. Dziuban, A. Jonkisz, A. Karpiewska, T. Dobosz and L. Golonka, *Sens. Actuators, B*, 2010, **150**, 715–721.
47 K. Malecha, D. G. Pijanowska, L. J. Golonka and W. Torbicz, *Sens. Actuators, B*, 2009, **141**, 301–308.
48 H. V. Drushel, A. L. Sommers and R. C. Cox, *Anal. Chem.*, 1963, **35**, 2166–2172.
49 C. de Mello Doneg, P. Liljeroth and D. Vanmaekelbergh, *Small*, 2005, **1**, 1152–1162.
50 Q. Dai, D. Li, H. Chen, S. Kan, H. Li, S. Gao, Y. Hou, B. Liu and G. Zou, *J. Phys. Chem. B*, 2006, **110**, 16508–16513.
51 D. Wu, M. E. Kordesch and P. G. V. Patten, *Chem. Mater.*, 2005, **17**, 6436–6441.
52 L. Cademartiri, E. Montanari, G. Calestani, A. Migliori, A. Guagliardi and G. A. Ozin, *J. Am. Chem. Soc.*, 2006, **128**, 10337–10346.
53 X. Zhong, Y. Feng and Y. Zhang, *J. Phys. Chem. C*, 2007, **111**, 526–531.
54 D. Wu, M. E. Kordesch and P. G. V. Patten, *Chem. Mater.*, 2005, **17**, 6436–6441.
55 C. Landes, M. Braun, C. Burda and M. A. El-Sayed, *Nano Lett.*, 2001, **1**, 667–670.
56 N. Pradhan, D. Goorskey, J. Thessing and X. Peng, *J. Am. Chem. Soc.*, 2005, **127**, 17586–17587.
57 Q. Lianhua and X. Peng, *J. Am. Chem. Soc.*, 2002, **124**, 2049–2055.
58 A. Toyota, H. Nakamura, H. Ozoco, K. Yamashita, M. Uehara and H. Maeda, *J. Phys. Chem. C*, 2010, **114**, 7527–7534.

Microreactor with integrated temperature control for the synthesis of CdSe nanocrystals

Sara Gómez-de Pedro, Cynthia S. Martínez-Cisneros, Mar Puyol and Julián Alonso*

***Corresponding author**: Fax: 34 9358 12477 Tel: 34 9358 12533; E-mail: julian.alonso@uab.es. Sensors & Biosensors Group, Department of Chemistry, Autonomous University of Barcelona, Edifici Cn, 08193 Bellaterra, Catalonia, Spain.

Electronic Supplementary Information (ESI)

Table of contents

Temperature characterization of the microsystem

The microsystem was thermally evaluated using an EMC scanner with an IR Probe (RS321EH, Detectus AB) in order to estimate the temperature distribution.

The isothermal maps of the thermal and fluidic platforms in the xy-axis were recorded, obtaining a uniform radial distribution in all cases. Since the maps were highly similar, only one of them is presented in figure S1, corresponding to the distribution of temperature on the top of the microfluidic platform. The presented isothermal map was obtained by coupling mechanically the microfluidic platform over the heating module, as in the synthesis of nanocrystals, and maintaining temperature in the sensor zone at 270 ºC.

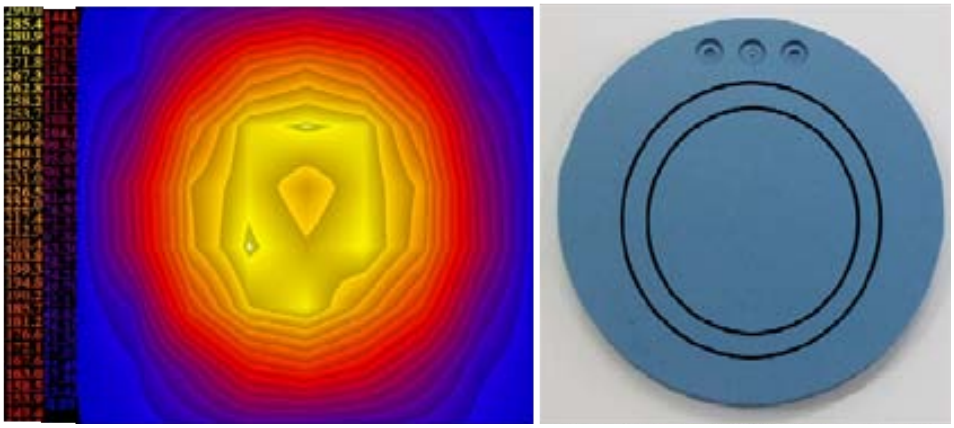

Fig. S.1 (A) Isothermal map obtained for the microfluidic platform coupled to the thermal one; (B) image of the corresponding microfluidic module. The two black circles represents where the microfluidic channels are placed.

To determine the thermal gradient in the z-axis, punctual measurements on the area of the PT100 sensor were performed on both sides of the microsystem (thermal and microfluidic). Temperature was found to be 270ºC and 255ºC on the bottom of the thermal and on the top of the microfluidic platforms, respectively.
Considering the number of layers used for its fabrication and the placement regarding both, the microchannel and the resistor in the microsystem (Figure S.2), a temperature of 268.2ºC can be assumed in the microfluidic channel.

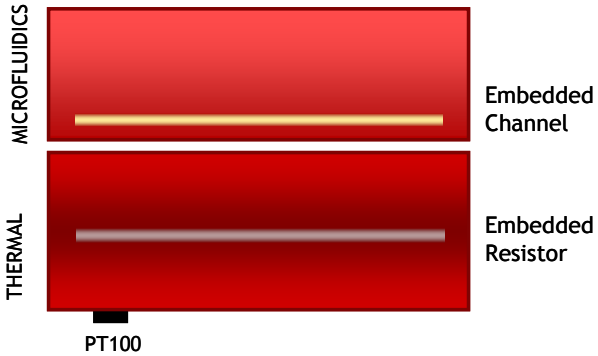

Fig. S.2 Schematic diagram of the temperature analysis developed to estimate temperature in the microfluidic channel.

Supplementary figures

Fig S3: Correlation peaks with temperature

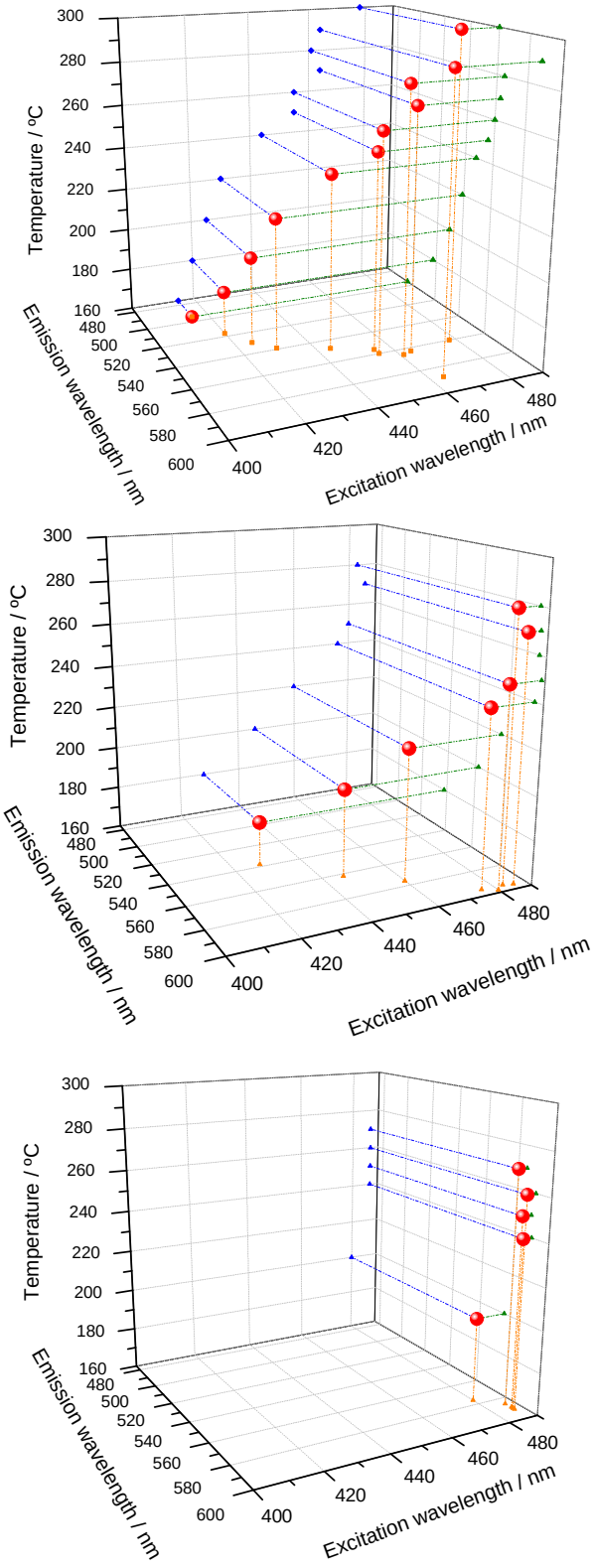

Fig. S.3 Correlation between fluorescence emission peaks, excitation wavelengths and temperatures during the synthesis of nanocrystals with a Cd/Se molar ration of 1:10, 1:1 and 1:2 (from top to bottom).

Fig S4: Stokes shifts

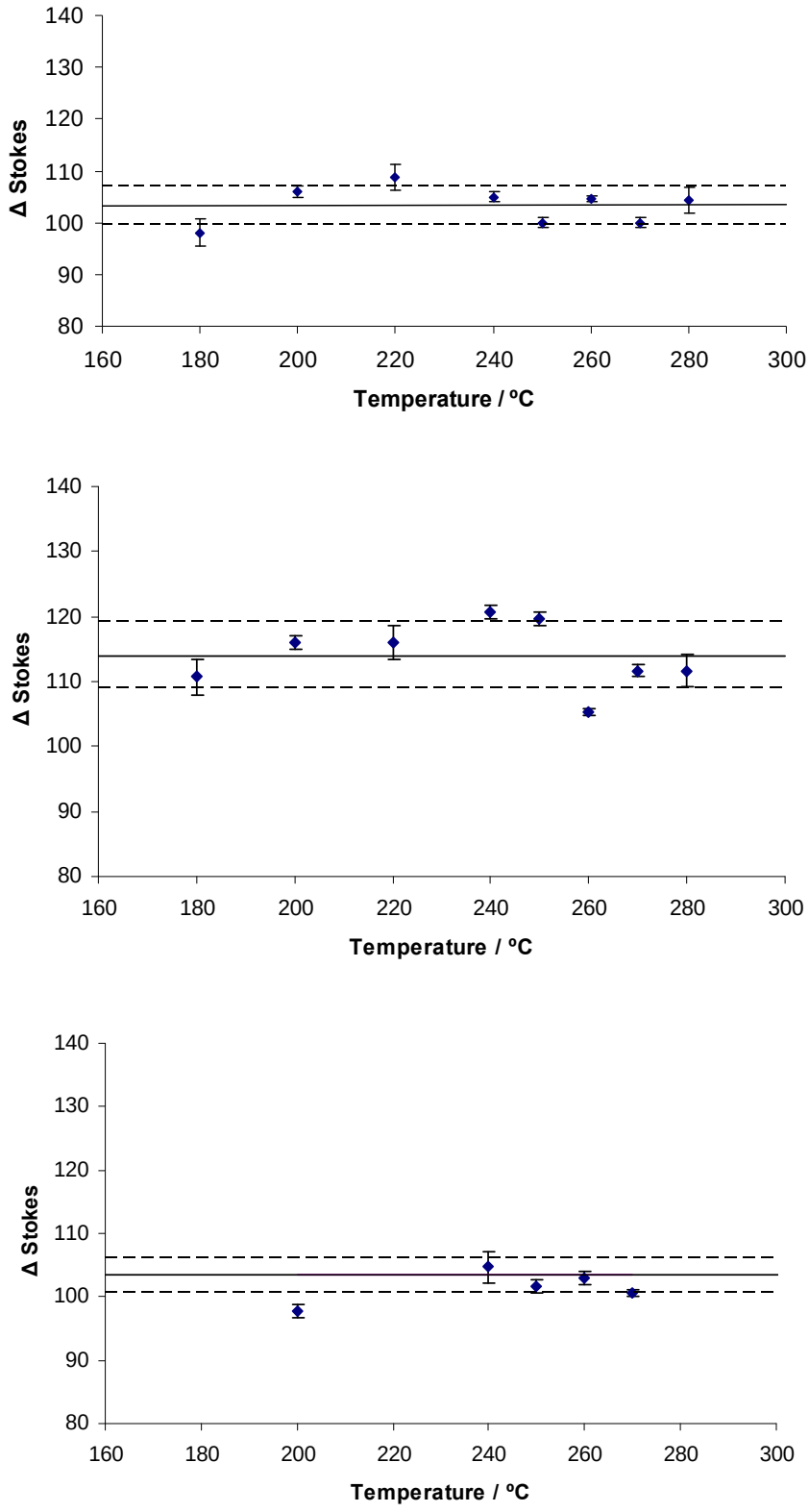

Fig. S.4 Stokes shifts for the synthesized quantum dots at different temperatures and molar relationship of reagents (from top to bottom 1:10, 1:1 and 1:2). The mean value, the standard deviation and the error bars are represented.

B.4 Design, fabrication and characterization of microreactors for high temperature syntheses.

Cynthia S. Martínez Cisneros, Sara Gómez de Pedro, Joan García García, Mar Puyol and Julián Alonso Chamarro. Chemical Engineering Journal, 211-212, 432-441 (2012).

Chemical Engineering Journal 211-212 (2012) 432–441

Contents lists available at SciVerse ScienceDirect

Chemical Engineering Journal

journal homepage: www.elsevier.com/locate/cej

Design, fabrication and characterization of microreactors for high temperature syntheses

Cynthia S. Martínez-Cisneros [a], Sara Gómez-de Pedro [a], Mar Puyol [a], Joan García-García [b], Julián Alonso-Chamarro [a,*]

[a] Sensors & Biosensors Group, Department of Chemistry, Autonomous University of Barcelona, Edifici Cn, 08193 Bellaterra, Catalonia, Spain
[b] Department of Electronic Engineering, Autonomous University of Barcelona, 08193 Bellaterra, Catalonia, Spain

HIGHLIGHTS

- A new technological approach for microreactors fabrication is proposed.
- The microreactors integrate microfluidics and high temperature actuators.
- Their thermal and hydrodynamic performance was exhaustively characterized.
- Devices can be applied to the intensification of processes, e.g. quantum dots synthesis.

ARTICLE INFO

Article history:
Received 25 June 2012
Received in revised form 18 September 2012
Accepted 22 September 2012
Available online 4 October 2012

Keywords:
Process intensification
Microreactor
High temperature synthetic processes
Quantum dots
On-line syntheses
Thermal/microfluidic characterization

ABSTRACT

Microfluidic reactors offer many potential advantages in several research and industrial fields such as processes intensification, which includes a better reaction control (kinetics and thermodynamics), a high throughput and a safer operational environment (reduced manipulation of dangerous reagents and low sub-products generation). Nevertheless, scaling-down limitations appear concerning the materials used in the fabrication of microreactors for most of the liquid-phase reactions, since they usually require high temperatures (up to 300 °C), solvents and organic reagents. In this work, the development of a set of modular and monolithic microreactors based on the integration of microfluidics and a thermal platform (sensor/high-temperature heater) is proposed to perform high temperature reactions. The reliability and performance of both configurations were evaluated through an exhaustive characterization process regarding their thermal and microfluidic performance. Obtained results make the devices viable for their application in controlled and reproducible synthetic processes occurring at high temperatures such as the synthesis of quantum dots. The proposed microfluidic approach emerge as an engaging tool for processes intensification, since it provides better mass and temperature transfer than conventional methods with a reduction not only of the size and energy consumption, but also of by-products and reagents consumption.

1. Introduction

Conventional chemical syntheses commonly require the use of round-bottomed flasks, beakers, test tubes or even more complex equipments. Additionally, they are usually performed under moderate or high temperatures in organic media, involving the use of oil/sand baths or hot plates. In concrete, the temperature at which a reaction takes place is one of the most important parameters to be considered, since all reactions require a minimal energy to reach the activation threshold that enables to transform the reagents into a desired product. Increasing the temperature in a reaction, not only provides the necessary energy for the reaction to take place, but also favors kinetics [1]. Elimination reactions [2], nucleophilic substitutions [3], thermal cycloadditions [4], intramolecular rearrangements [5] and palladium catalyzed reactions [6] are some of the reactions that demand moderate temperatures. Other reactions involving thermal decompositions require higher temperatures, since in these processes it is necessary to break chemical bonds of reagents [7]. In fact, some nanomaterials syntheses, which nowadays are extensively studied due to their wide range of applications, require temperatures that might reach values up to 300 °C, for example quantum dots synthesis [8–10].

Chemical research is focused on the synthesis of new compounds, their application, and on process intensification. Hence, it is important to develop new equipment or techniques, which

* Corresponding author. Tel.: +34 9358 12533; fax: +34 9358 12477.
E-mail address: julian.alonso@uab.es (J. Alonso-Chamarro).

1385-8947/$ - see front matter © 2012 Elsevier B.V. All rights reserved.
http://dx.doi.org/10.1016/j.cej.2012.09.101

drastically improve the whole synthetic process by minimizing energy consumption, size, amount of reagents and by-products and, obviously, the total costs of the process [1,11–13]. Optimization studies regarding the improvement of reaction yields as well as the minimization of undesired sub-products constitute crucial parameters to take into account. In this sense, the miniaturization concept appears as a promising approach to better control certain reaction parameters. The miniaturization and integration of all the stages associated to such procedures would increase the system robustness and would enable its automation, promoting an improved control over some parameters during reactions such as temperature and reaction time. Miniaturized systems offer additional advantages such as the significant reduction of reagents consumption, which is becoming of major importance due to environmental concerns, and safer conditions when reactions involve the manipulation of hazardous reagents.

In recent years, microfluidic systems have been increasingly used for synthetic purposes due to the advantages that they confer and the evolution that they have suffered from simple basic devices to more complex systems [11,14–21]. These systems not only can be directly attached to pre-treatment steps or analytical instruments (such as chromatographs or spectrophotometers) but also can integrate some of them, even monolithically [22,23]. Some studies reveal that the high surface area to volume ratio of microreactors improves mass and heat transfer, giving nearly gradientless conditions, which are desirable for the determination of reaction kinetics [24,25]. This allows carrying out reactions under more precisely controlled conditions than those provided by conventional macroscale reactors [11,26], leading to improved purity and yield of the desired products and minimizing the need of performing collateral reactions and the formation of undesirable by-products [27–31]. Moreover, microfluidics represents a better option than conventional methodologies for the synthesis of compounds that require an inert atmosphere, since the environment can be completely controlled in a simple way inside the microfluidic channels. Indeed, the degradation of certain sensitive products can be better avoided inside microreactors [14]. Another relevant advantage is the possibility to automate the whole process through the use of pumps, valves and computer-controlled elements, which increases reproducibility and autonomy, reduces possible risks associated to hazardous reagents and provides real-time information regarding the reaction evolution. As a matter of fact, microfluidic approaches have been successfully applied to the synthesis of numerous metal, metal–oxide and semiconductor nanoparticles [32–34].

Miniaturized systems applied as high temperature microreactors are usually implemented using independent modules, where different technological platforms such as microfluidics, thermal modules, detection systems and electronics are integrated. Most of these systems consist on glass, silicon or plastic microfluidic platforms immerged in external oil-baths [35,36] or placed over hot plates at high temperatures [37,38]. These modular approaches provide certain advantages that include easy exchangeability/replacement of the platforms in case of malfunction, versatility in case of changing experimental needs and simple design and fabrication. Nevertheless, automatic and more robust devices (monolithic or more compact modular systems) are required for specific applications. Most microreactors found in the bibliography are based on silicon/glass, since these materials provide physical and chemical stability and a well-established fabrication procedure that permits the integration of electronic components such as heaters and sensors (thin-film technology). However, scarce literature related to the development of monolithic microreactors that integrate microfluidics and heating systems can be found in the literature [39,40]. This may respond to the complexity associated to conventional methodologies used for their fabrication. Tiggelaar et al. proposed a high temperature microreactor that included an integrated sensor/actuator system based on the microelectronics technology [37]. The high integration level offered by this microreactor is remarkable but the fabrication process involves high costs, highly skilled staff, special conditions (clean room) and lasting procedures. In order to overcome these issues, alternative technologies based on a simple multilayer approach compatible with the high temperatures associated to most synthetic processes would be desirable. In this sense, the LTCC (Low Temperature Cofired Ceramics) technology provides a way to develop miniaturized monolithic or modular devices that integrate microfluidics, electronics, sensors and actuators (heaters) [41,42]. Their chemical resistivity, once fired in a furnace, makes LTCC devices feasible for chemical applications where organic reagents or corrosive solvents are needed. Moreover, due to the high fusion temperature of materials involved in LTCC technology, up to 850 °C, they are preferable for high temperature applications over other multilayer technologies, such as those based on polymers. Several microreactors based on LTCC materials regarding nanoparticles synthesis [43–45], polymerase chain reaction systems [44,46], enzyme-based determinations [45] and biochemical diagnoses [47], among other applications, can be found in the bibliography.

Herein, we propose the development of highly efficient ceramic microreactors to perform moderate or high temperature reactions. The reliability and performance of modular and monolithic approaches has been evaluated, taking advantage of the properties offered by the LTCC technology, through a detailed hydrodynamic and thermal characterization. To demonstrate the feasibility of the proposed approaches, the modular configuration was applied for the continuous and controlled synthesis of quantum dots, since its synthetic procedure involves temperatures around 300 °C. Nevertheless, since temperature can be precisely controlled as desired, several reactions involving temperature can be carried out in order to obtain nanomaterials or compounds of different nature.

2. Materials and methods

DuPont 951 green tapes (thickness at green stage: 254 μm) were used as substrate for the fabrication of modular and monolithic configurations of a set of microreactors involving microfluidic and thermal platforms. The thermal platform consists on an embedded heater screen-printed using gold cofirable conductor paste DuPont 5742 (fired resistivity <5 mΩ/sq). This paste was selected on the basis of its suitability to provide high conductive paths where high power dissipation is a must. Via filling was performed using DuPont 6141 (fired resistivity <3 mΩ/sq). Both conductive pastes are perfectively compatible with the whole LTCC fabrication process. As temperature sensor, a commercial class A PT100 (Innovative Sensor Technology, Switzerland) was glued over the device surface by means of epoxy (EPO-TEK® H20E). A PIC18F4431 microcontroller (Microchip Inc., USA) was used to implement a digital PID (proportional-integral-derivative) control system that maintains temperature at a prefixed value. All the analog/digital electronic components used to implement the control system were carefully selected on the basis of improving the system precision and increasing the signal to noise ratio. The user interface for temperature monitoring during the tests was developed on a personal computer through a virtual instrument specifically designed for this application.

To perform the thermal characterization of the microreactor, an EMC Scanner with an integrated IR Probe (RS321EH, Detectus AB) was used. The mixing efficiency of the microfluidic structure embedded in the microreactor was evaluated by means of a qualitative visual characterization performed through a stereo microscope Leica S6D equipped with a DFC290 digital camera (Leica

Microsystems S.L.U., Spain). For this purpose, two syringe pumps (540060 TSE systems) coupled to 10 mL syringes (Hamilton series GASTIGHT 1000 TLL) connected to the ceramic microfluidic platform with PTFE tubes (i.d. 0.9 mm) were applied.

3. Microsystems fabrication

The general fabrication process of the LTCC-based microsystems starts with their design using computer assisted design (CAD) software. Since it is a multilayer approach, the design has to be decomposed in layers on the xy-plane, which once overlapped create a desired three-dimensional structure. These CAD designs are transferred to green ceramic tapes by an etching machine (in this case, a laser machine). Then, the screen printing step is performed on those patterned layers that require integrating conductive tracks (such as heaters) or vias to connect conducting tracks at different layers. Once the conductive screen-printing paste is dried, all layers are aligned and laminated by a thermo-compression procedure consisting on applying 3000 psi for 60 s at 100 °C. Finally, the laminated block is sinterized in a programmable furnace, where different temperature profiles are applied. The whole process, which takes place in less than 1 day, is depicted in Fig. 1 and described in detail elsewhere [48].

As previously mentioned in this work, microreactors for synthetic processes based on modular and monolithic configurations were evaluated and compared. In order to characterize the hydrodynamic and thermal performance of both approaches, four devices were designed and fabricated: a modular thermal platform, a modular microfluidic platform, a modular microfluidic platform with exposed channel and a monolithic system with both platforms integrated in the same unit.

Fig. 2A presents the layers that once overlapped constitute the modular thermal platform. It consists of a nine-layer block with a screen-printed gold-based heater. It is embedded in the middle of the block (fifth layer) to promote a more uniform heat distribution through the *z*-axis. The nine layers that constitute the thermal platform provide it robustness. The heater design was developed on the basis of a radial and uniform distribution of temperature and trying to avoid a highly elevated heat point in the center of the platform. By defining seven laps of a gold-based screen-printed conductor (0.7 mm width, 8 μm height), a 13 Ω heater was obtained. External pads were defined on the top layer of the thermal platform to connect the embedded heater to an external electronic control set-up, since the high working temperatures associated to the microreactor avoids the surface integration of electronic devices involved by the control system. For temperature sensing and establishing the PID control feedback, a class A PT100 sensor was placed over the thermal platform trying to obtain the optimum xy-alignment with the microreactor zone, which was embedded in the modular microfluidic platform later attached.

The layers that once overlapped constitute the modular microfluidic platform are shown in Fig. 2B. The microfluidic structure includes two inlets for reagents and one outlet through which the product of the reaction is collected. The complete microfluidic platform consists of eight stacked layers, where the microreactor is embedded. The two inlets allow introducing the reagents into the system through two simple channels around the microreactor before they meet each other downstream. This structure acts as a pretreatment step for preheating reagents before mixing. Channels converge in a Y-shape point downstream before getting into the microreactor (Z-shape mixer). A bi-dimensional micromixer (200 μm width, 200 μm height) was preferred for this application. It introduces the chaotic mixing profile required for faster and more homogeneous mixing, avoiding thermal fluctuations on the liquid, which could be produced if three dimensional mixers were used. The circular configuration of the micromixer was selected in accordance to the expected radial thermal distribution regarding the heater embedded in the thermal platform. Therefore, a proper alignment between both platforms, when mechanically attached, would provide a more uniform heat distribution on the xy plane of the microchannel. Using this approach, reagents are exposed to specific, uniform and controlled temperature levels provided by the thermal platform during their flow through.

To perform a qualitative visual characterization of the fluidics/hydrodynamics of the microreactor, a new modular microfluidic platform, identically to that previously presented, was constructed; but leaving half of the microfluidic structure open to

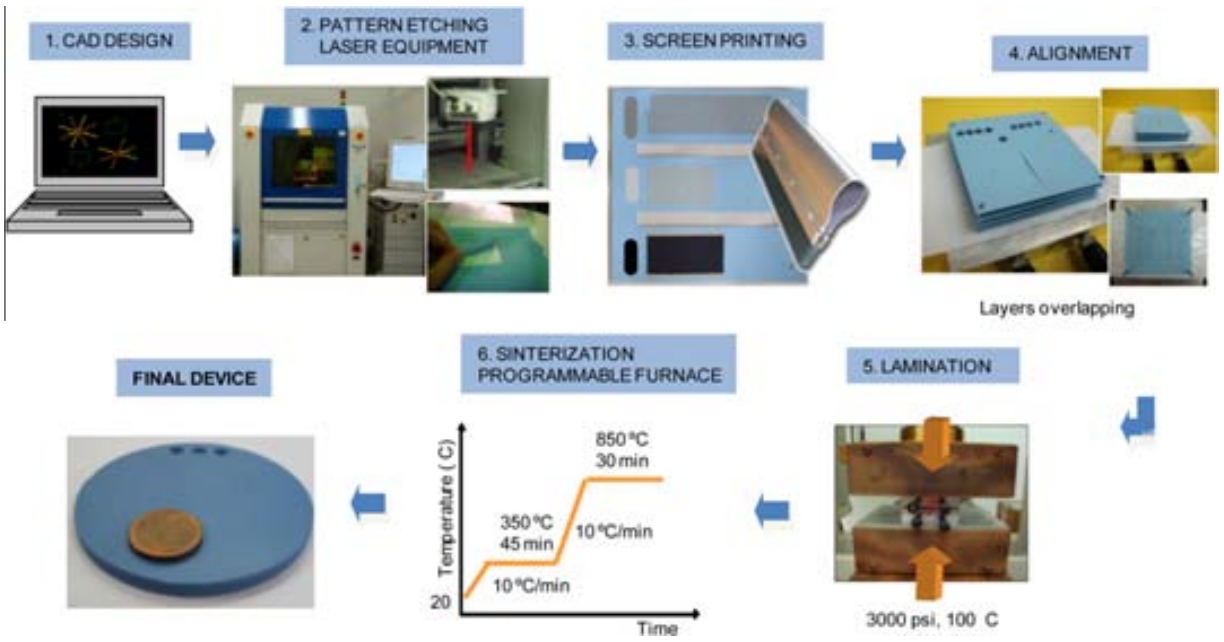

Fig. 1. Fabrication procedure of the LTCC microsystems.

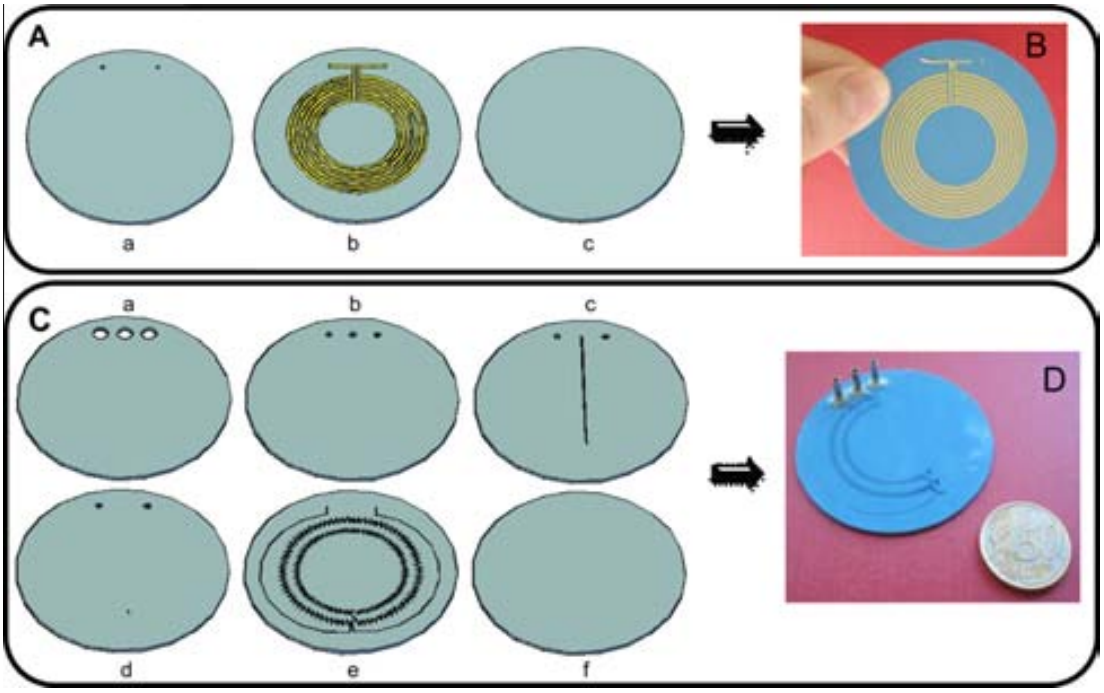

Fig. 2. Layer by layer design of both platforms integrating the LTCC microreactor. (A) Thermal platform; (a) top layer (4×); (b) screen-printed heater (1×); (c) bottom layer (4×). (B) Picture of the thermal platform fabricated. (C) Microfluidic platform; layers (a and f) were fabricated by duplicate; the microfluidic structure was embedded at layer (e). (D) Picture of the microfluidic platform, which includes an exposed section regarding the micromixer.

air. In this case, once sinterized, the exposed section of the device was covered with a polymeric foil, permitting its inner visualization but ensuring its hermetic sealing (see Fig. 1C).

Finally, to estimate the advantages provided by a monolithic device in terms of heat distribution, taking advantage of the properties provided by the LTCC technology, a microsystem including the microfluidic and thermal platforms in the same device was fabricated. The monolithic design was based on those previously exposed for modular platforms.

4. Electronic set-up for temperature control

Since temperature level and distribution are crucial parameters to be considered for several reactions to properly take place, a dedicated temperature controller with a digital PID topology was designed and implemented on a PIC18F4431 microcontroller, using a personal computer for monitoring purposes. The electronic circuit for temperature control was separately fabricated to avoid that the high temperatures at which the microreactor operates would produce any damage to it. A block diagram of the electronics implemented in this work is shown in Fig. 3.

The analog stage of the electronic circuit was designed for conditioning the signal provided by the PT100 sensor, keeping intensity constant through it for avoiding its self heating, and amplifying the control signal generated by the PID controller (a pulse width modulated signal, PWM) before being applied to the embedded heater (actuator). The feedback signal obtained from the PT100 sensor was used to estimate the error and to correct it using specific differential equations programmed in the digital PID control system implemented in the microcontroller code. The control signal produced by the PID was amplified and applied to the gold-based heater embedded into the thermal platform. The thermal platform was configured to work at a wide temperature range (180–300 °C) in order to fulfill needs associated to specific synthetic process under evaluation. Nevertheless, such ceramic microreactors could be applied for any reaction performed at higher temperatures, where other materials cannot operate, since its fusion temperature is up to 850 °C.

5. Results and discussion

To demonstrate the microreactor performance when applied to synthetic processes, it was thermally and hydraulically characterized. In this sense, its mixing capabilities and thermal distribution were characterized.

5.1. Fluidic characterization

To demonstrate that the microfluidic structure designed and embedded into the microsystem was able to provide an efficient mixture of reagents, a qualitative visual characterization of its fluidics/hydrodynamics was performed. For this study, the modular microfluidic device with half of its structure exposed was used. Using this approach, it was possible to examine its interior by means of a stereo microscope. To probe the reagents mixture inside the Z-shape bi-dimensional channel proposed as mixer, different tests using dyes (phenol red and methylene blue, both 1 mM and propelled by syringe pumps at 60 μL/min) at room temperature were performed inside the microreactor. For this purpose, four different points of the microchannel were selected the visual exploration (see frames 1, 2, 3 and 4 presented in Fig. 4).

Sequence depicted by frames 1, 2, 3 and 4 in Fig. 4C allows visualizing the mixing process while reagents flow through the microreactor. When dyes go through the region enclosed by frame 1, both dyes can be clearly differentiated, showing a near ideal laminar flow profile. On the contrary, by the time that reagents reach the zone enclosed by frame 3, an almost homogeneous coloration can be observed, which results complete when the liquid reaches the zone framed in 4. Thus, it can be stated that a good mixture of both dyes is achieved before the end of the first circular turn, which makes clear the efficiency provided by the micromixer embedded into the LTCC microreactor.

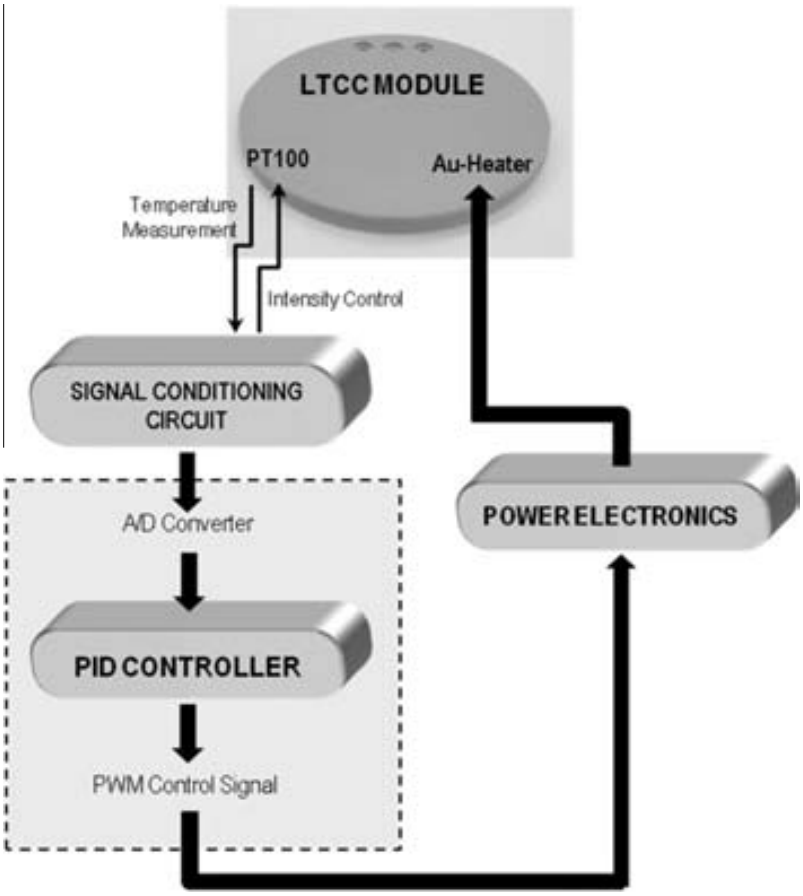

Fig. 3. Block diagram of the digital/analog electronics for an accurate control of temperature inside the microreactor.

5.2. Thermal characterization

Once the PID control parameters were optimized, a highly stable temperature profile was obtained during all the studies performed in this work. The system was predefined to take about ten minutes to stabilize before reaching the steady state at the desired temperature. A slow response with soft temperature transitions was preferred in order to avoid abrupt thermal changes that could stress/brake the thermal platform. A small peak overshoot of about 8 °C was observed at the beginning of the control system operation. Signal variations in the order of ±0.5 °C were observed on the steady state of the system response.

As previously mentioned in this work, modular and monolithic configurations were developed and tested in order to obtain microreactors with an efficient configuration. A modular approach (microfluidic and thermal platforms separately fabricated and later attached) increases the system reliability. If a thermal unit or a microfluidic platform with different characteristics is required, it can be replaced without requiring rebuilding the complete device. Moreover, if any of the platforms presents operational problems it can be replaced without affecting the other elements. On the other hand, a monolithic configuration may be preferred for those applications that require dedicated devices with a higher integration level, robustness and the minimum of movable elements. All the evaluation procedures regarding modular and monolithic configurations were performed at 270 °C and using the EMC scanner with an IR Probe for obtaining the corresponding isothermal maps.

5.2.1. Modular system

As a first approach, the isothermal map regarding both sides of the modular thermal platform was obtained. Since maps at both sides were highly similar, only one of them is presented in Fig. 5A and B shows the isothermal map coupled to a picture of the experimental set-up used during this experiment. As seen in this figure, a radial and uniform heat distribution in the xy plane is obtained over the thermal platform. Small deformations at the limits of the device are assumed to be caused by the presence of the metallic connectors used to energize the embedded heater. Regarding the *z*-axis thermal distribution, punctual measurements at the top and the bottom of the device were carried out at the zone where the temperature sensor was placed. As expected, both measurements corresponded to the predefined set point: 270 °C. This concordance can be associated to an efficient thermal distribution over the *z*-axis.

Once the modular thermal platform was evaluated, the modular microfluidic platform was mechanically coupled taking care on obtaining the highest surface contact regarding an optimum heat transfer between them. Heat transfer between platforms was favored by the thermal conductivity presented by LTCC materials (3 W/mK). Fig. 5C presents a picture of the experimental set-up that includes the isothermal map obtained on the microfluidic platform once coupled to the thermal one. As seen in this figure, a radial distribution over the region corresponding to the placement of the microchannels (see red lines in Fig. 5C) inside the microfluidic platform was obtained, assuring a xy uniform thermal distribution. To determine the thermal gradient in the *z*-axis, punctual measurements were performed on both sides of the microsystem (thermal and microfluidics). Temperature was found to be 270 °C and 255 °C on the thermal and microfluidic platform, respectively. The difference observed might be caused not only by the thermal transfer among the different number of ceramic layers that compose both platforms, but also by the presence of

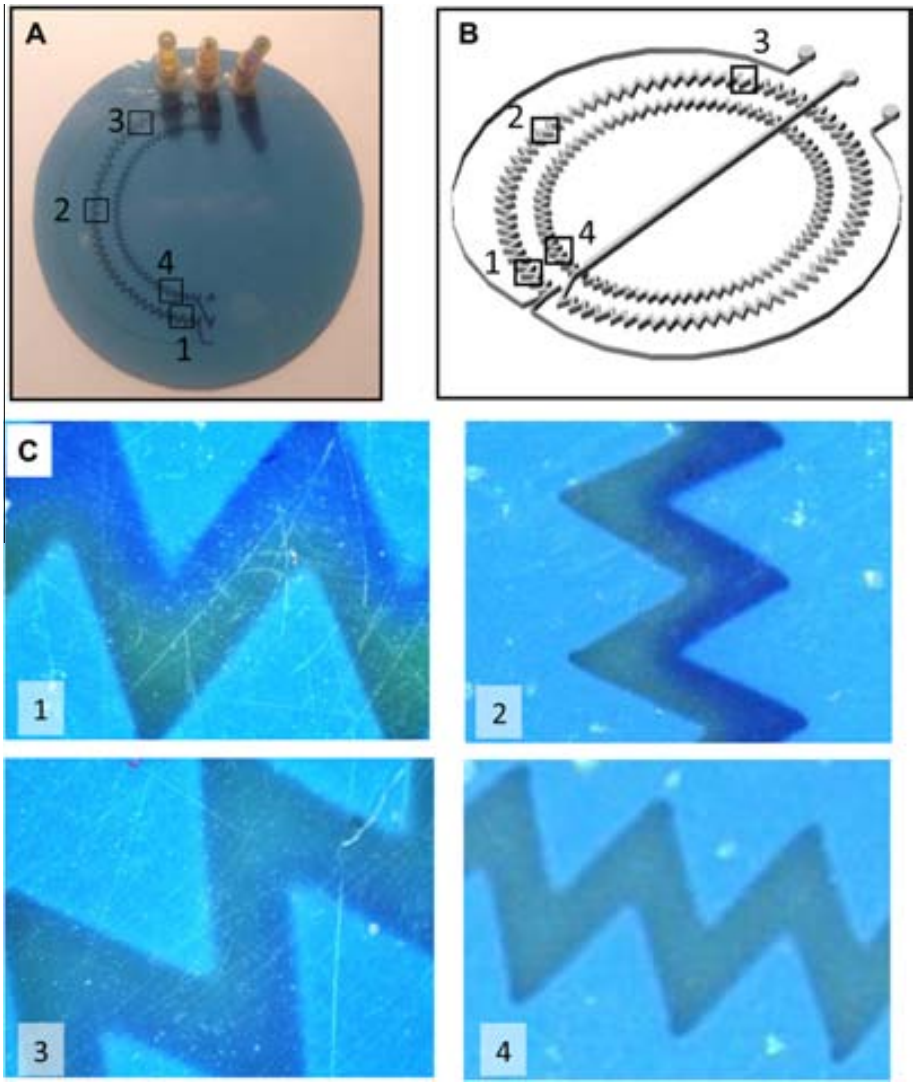

Fig. 4. Fluidic/hydrodynamic qualitative visual characterization of the microfluidic system. (A) Picture of the open to air microfluidic platform covered with a polymeric foil. (B) Three-dimensional inner view of the microfluidic platform. (C) Photographs corresponding to frames at different points of the micromixer.

the air gap at the coupling region. The effect of the air gap can be minimized by the use of a thermal conductive paste that favors heat transfer among the surfaces in contact. To estimate the temperature inside the embedded microfluidic channel, a scheme regarding layers distribution and temperature measurements was performed (see Fig. 5D). According to this diagram and considering the material thermal transfer coefficient, a temperature of 268.2 °C can be assumed inside the microfluidic channel, which is pretty close to the desired temperature predefined as set point (270 °C). In this sense, a temperature gradient of about 1.8 °C/layer was estimated.

5.2.2. Monolithic system

To evaluate the advantages provided by a monolithic device in terms of heat distribution, a microsystem with a monolithic configuration including the microfluidic and thermal platform in the same device was developed and characterized in a similar way than the modular approach was.

Fig. 6 shows the isothermal map obtained on both sides of the monolithic microsystem (top and bottom). As seen in this figure, a radial and uniform distribution pretty similar to that obtained using the modular approach was obtained on both sides of the monolithic microsystem. In this case, punctual temperature measurements were also performed in the regions corresponding to the sensor position. Temperature values of 270 °C and 260 °C were obtained at the bottom and the top of the microsystem, respectively. Following the same procedure as previously with the modular configuration, the *z*-axis gradient was estimated. In this case, a temperature gradient of 1.2 °C per layer was obtained. This improvement regarding results obtained with the modular configuration may respond to the elimination of the air gap between platforms. This favors heat transfer among platforms since no additional interface is introduced. In this case, the temperature inside the microchannel might be estimated to be 268.8 °C.

5.3. Proof of concept: microreactor application in the synthesis of quantum dots

To validate the performance of the proposed microreactors in high temperature synthetic processes, the synthesis of CdSe quantum dots was performed, since its formation depends strongly on the temperature applied and its fluctuation [49,8]. The reaction consisted on mixing two precursor solutions, one containing selenium and other with cadmium in a 1:1 molar ratio. The solution mixtures consisted of other chemical reagents for conferring stabilization to the nanocrystals formed [50,51]. The selenium pre-

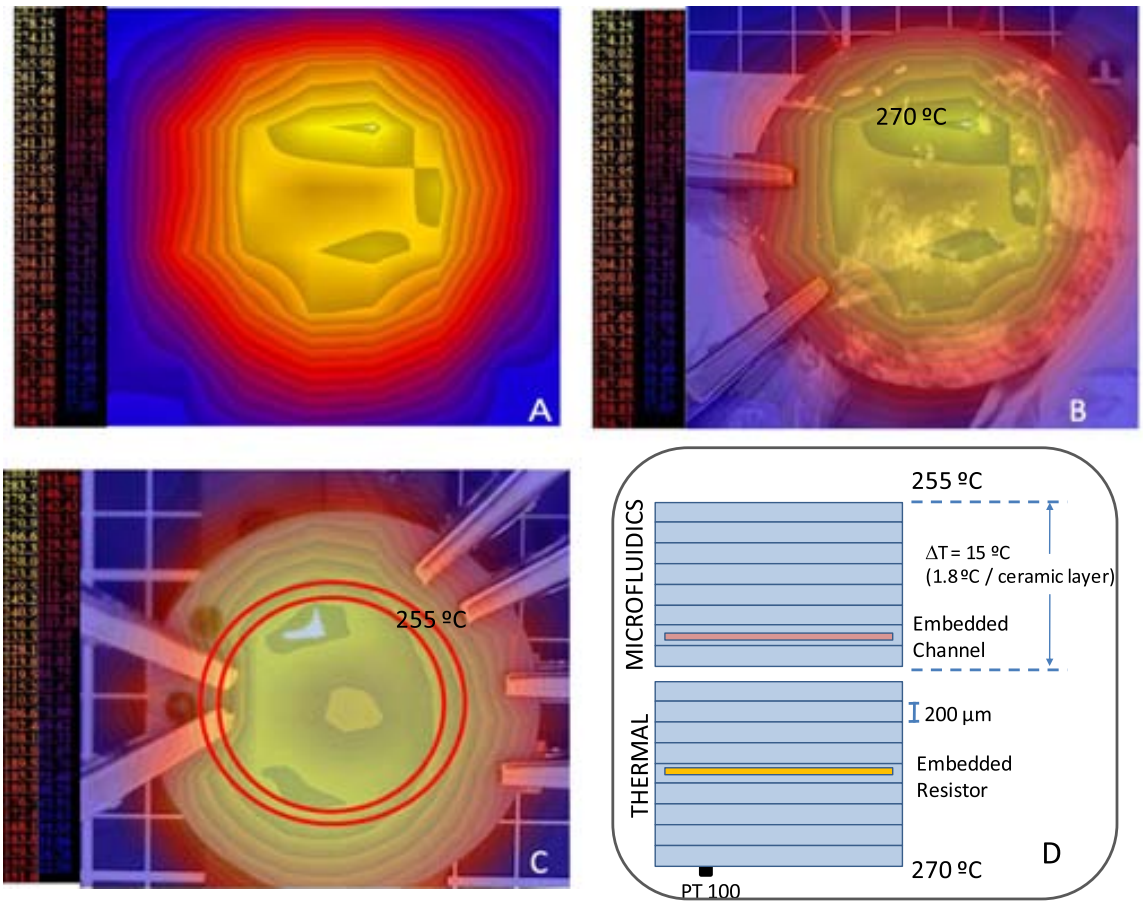

Fig. 5. Thermal characterization of the microreactor based in a modular configuration. (A) Isothermal map obtained on the surface of the modular thermal platform. (B) Isothermal map of the modular thermal platform overlapped to a picture of the experimental set-up. (C) Isothermal map obtained on the surface of the modular microfluidic platform coupled to the thermal one. (D) Schematic diagram of the temperature analysis developed to estimate temperature inside the microfluidic channel. In (B and C), punctual temperature measurements in the zone of the sensor are indicated. (For interpretation of the references to colour in this figure legend, the reader is referred to the web version of this article.)

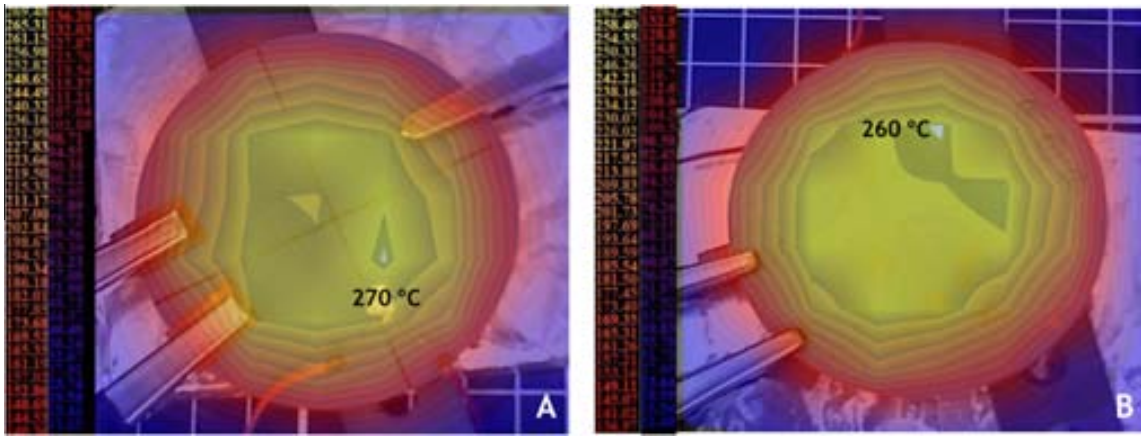

Fig. 6. Isothermal maps obtained on the bottom (A) and the top (B) of the monolithic microsystem. Punctual temperature measurements in the zone of the sensor are indicated (set point of the control system: 270 °C).

cursor was prepared by mixing 197.4 g (2.5 mmols) of selenium powder (99.5%, Aldrich) with 5 mL of trioctylphosphine (TOP, 10.1 mmols, 90%, Aldrich) and 10 mL of oleylamine (OLA, 21.25 mmols, 70%, Aldrich) at room temperature. The cadmium solution consisted of 321.25 mg of cadmium oxide (CdO, 2.5 mmols, 99.99%, Aldrich), 4 mL of oleic acid (OA, 12.6 mmols, Ph Eur, Fluka), 3 g of tryoctylphosphine oxide (TOPO, 7.8 mmols, 99%, Aldrich), 5 mL of OLA (15.2 mmols) and 3 mL of 1-octadecene (ODE, 90%, Aldrich). Once precursors were freshly prepared, they were introduced in two syringe pumps, which propelled the solutions to the microreactor at a continuous flow rate of 60 µL/min. As commented before, the temperature of the heating platform was

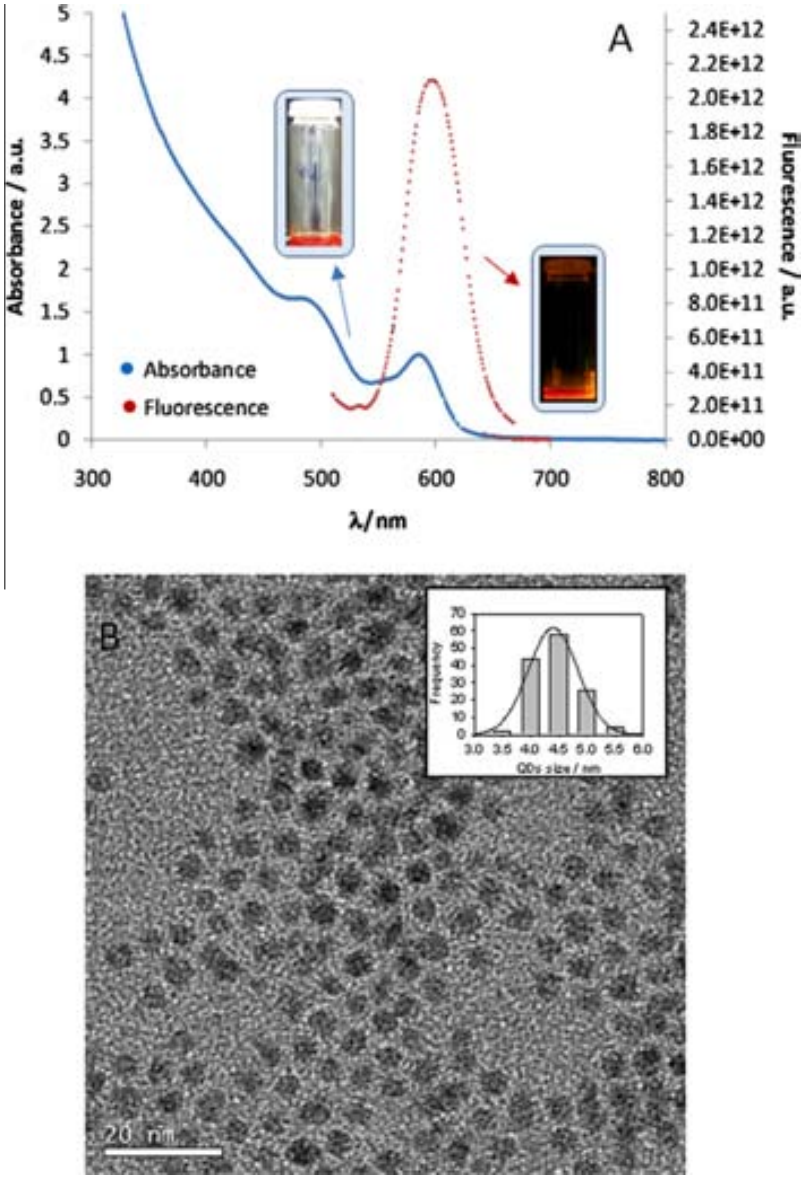

Fig. 7. (A) Absorbance (584 nm) and emission fluorescence (596 nm) spectra of the CdSe quantum dots synthesized in the modular microreactor. Images of the solutions of the obtained nanoparticles under visible and UV light can be also observed. (B) TEM image from the quantum dots synthesized.

fixed at 270 °C. Since CdSe nanocrystals present colored solutions and fluorescent properties, the absorbance and fluorescence properties of the nanoparticles obtained were characterized. Fig. 7 shows the absorbance (Shimadzu UV-310PC UV–Vis-NIR, Kyoto, Japan) and fluorescence (Fluorolog_Modular Spectrofluorometer, Horiba Jobin Yvon) spectra recorded and an image of the solution obtained under visible and UV light.

As can be noticed, the spectra are well defined, indicating the formation of uniform nanocrystals [49], whose properties correspond to those expected according to the working temperature predefined in the microreactor configuration. The shape and size of the nanocrystals were also characterized by transmission electron microscopy (TEM) (JEOL 2011, Tokyo, Japan), obtaining, as expected, uniform quantum dots with an average size of 4.4 ± 0.4 nm (Fig. 7B). Moreover, no incompatibility between the material and the organic solvents used was observed, which makes clear the proper selection of the ceramic material for reactions involving organic solvents at moderate or high temperatures. According to these results, the correct function of the LTCC-based microreactor can be assumed and extrapolated to the synthesis of other nanoparticles/nanomaterials or other reactions where high and accurate temperatures are required.

6. Conclusions

To summarize, ceramic microreactors have been proposed for their application in reactions involving solvents and organic reagents at moderate or high temperatures. The approaches proposed take advantage of microfluidics, since when compared with conventional methods the waste of reagents and the generation of residues is drastically reduced. Moreover, the possible automation of the whole process not only confers a safer operational environment, but also introduces a stricter control over the whole chemical process (higher reproducibility, repeatability, etc.). The ceramic substrate material confers physical and chemical resistivity to the microreactor, being feasible to carry out reactions involving organic solvents. Additionally, the high working temperatures

affordable with these materials make possible to perform synthesis at high temperatures, where other microfabrication materials such as polymers cannot operate. On the other hand, the fabrication technology of the ceramic microsystems is rapid and does not require special facilities such as clean rooms or specialized staff, which leads to low cost devices.

Two different approaches have been presented, one based on a modular configuration and other on a monolithic approach. The modular proposal confers the possibility of exchanging/replacing one of the modules in case of malfunction or different experimental requirements. On the other hand, it has been observed that the monolithic approach confers more confident results, since the absence of an air gap between platforms enables a better thermal transfer and, therefore, a more uniform temperature distribution along the z-axis (lower temperature gradient). This approach should be used in those cases where the synthetic procedure is well established (dedicated devices) and the temperature plays a crucial parameter. After a hydrodynamic and a thermal characterization, both approaches were defined as a good option for being applied to the chemical syntheses with specific temperature requirements. Hydrodynamic characterization with dyes has showed up the good grade of mixture obtained by the bidimensional micromixer introduced. Likewise, the thermal characterization applied to both approaches (modular and monolithic) demonstrated a radial and uniform distribution not only over its surface but also in its inner. As a proof of concept, the modular configuration was applied to the synthesis of nanocrystals, since its formation requires a strict control of several conditions, including temperature, obtaining comparable results to those obtained in the literature, which entails the perfect operation of the microsystem.

Acknowledgements

This work has been supported by the Spanish Ministry of Science and Innovation (MICINN) through project CTQ2009-12128 and the Consolider Ingenio 2010 project CSD2006 -12 and Catalonia Government through SGR 2009-0323. Authors would like to acknowledge Emma Rossinyol for performing HRTEM measurements.

References

[1] M. Smith, J. March, March's Advanced Organic Chemistry, Reactions, Mechanisms, and Structure, 6th ed., Wiley-Interscience, Hoboken, 2007.
[2] D.M. Crumpton, K.I. Goldberg, Five-coordinate intermediates in carbon−carbon reductive elimination reactions from Pt(IV), J. Am. Chem. Soc. 122 (5) (2000) 962–963.
[3] I. Roth, S. Spange, Kinetic studies on the nucleophilic aromatic substitution of fluoronitrobenzene derivatives with polyvinylamine in water mediated by 2,6-O-dimethyl-β-cyclodextrin, Macromolecules 38 (2005) 10034–10041.
[4] S. Abele, S. Höck, G. Schmidt, J.-A. Funel, R. Marti, High-temperature Diels–Alder reactions: Transfer from batch to continuous mode, Org. Process Res. Dev. doi: 10.1021/op200320w.
[5] J.A. Rincón, M. Barberis, M. González-Esguevillas, M.D. Johnson, J.K. Niemeier, W.M. Sun, Safe, convenient ortho-Claisen thermal rearrangement using a flow reactor, Org. Process Res. Dev. 15 (6) (2011) 1428–1432.
[6] T. Laird, Book review of catalysis of organic reactions, Org. Process Res. Dev. 13 (6) (2009) 1432.
[7] M. Damm, T.N. Glasnov, C.O. Kappe, Translating high-temperature microwave chemistry to scalable continuous flow processes, Org. Process Res. Dev. 14 (1) (2010) 215–224.
[8] J. Park, J. Joo, S.G. Kwon, Y. Jang, T. Hyeon, Synthesis of monodisperse spherical nanocrystals, Angew. Chem. Int. Ed. 46 (2007) 4630–4660.
[9] M. Salavati-Niasari, F. Davar, Z. Fereshteh, Synthesis and characterization of ZnO nanocrystals from thermolysis of new precursor, Chem. Eng. J. 146 (3) (2009) 498–502.
[10] V. Cocheteau, P. Mur, T. Billon, E. Scheid, B. Caussat, Development of an original model for the synthesis of silicon nanodots by low pressure chemical vapor deposition, Chem. Eng. J. 140 (1–3) (2008) 600–608.
[11] W.-Y. Lin, Y. Wang, S. Wang, H.-R. Tseng, Integrated microfluidic reactors, Nano Today 4 (2009) 470–481.
[12] D. Webb, F. Jamison, Continuous flow multi-step organic synthesis, Chem. Sci. 1 (2010) 675–680.
[13] C. Wiles, P. Watts, Continuous flow reactors a tool for the modern synthetic chemist, Eur. J. Org. Chem. (2008) 1655–1671.
[14] C. Wiles, P. Watts, Continuous flow reactors: a perspective, Green Chem. 14 (2012) 38–54.
[15] R.L. Hartman, K.F. Jensen, Microchemical systems for continuous-flow synthesis, Lab Chip 9 (2009) 2495–2507.
[16] M. Luty-Błocho, K. Fitzner, V. Hessel, P. Löb, M. Maskos, D.D. Metzke, K. Pacławski, M. Wojnicki, Synthesis of gold nanoparticles in an interdigital micromixer using ascorbic acid and sodium borohydride as reducers, Chem. Eng. J. 171 (1) (2011) 279–290.
[17] Clemens.B. Minnich, Lasse. Greiner, Christian. Reimers, Marc. Uerdingen, Marcel.A. Liauw, Bridging the gap: anested-pipereactor for slow reactions in continuous flow chemical synthesis, Chem. Eng. J. 168 (2) (2011) 759–764.
[18] Tobias Illg, Volker Hessel, Patrick Löb, Jaap C. Schouten, Novel Process Window for the safe and continuous synthesis of tert.-butyl peroxy pivalate in a microreactor, Chem. Eng. J. 167 (2) (2011) SI504–SI509.
[19] Lahbib Abahmane, Andrea Knauer, J. Michael Köhler, G. Alexander Groß, Synthesis of polypyridine derivatives using alumina supported gold nanoparticles under micro continuous flow conditions, Chem. Eng. J. 167 (2–3) (2011) 519–526.
[20] S.-T. Tu, X. Yu, W. Luan, H. Löwe, Development of microchemical, biological and thermal systems in China: a review, Chem. Eng. J. 163 (3) (2010) 165–179.
[21] H. Löwe, R.D. Axinte, D. Breuch, C. Hofmann, J.H. Petersen, R. Pommersheim, A. Wang, Flow chemistry: Imidazole-based ionic liquid syntheses in micro-scale, Chem. Eng. J. 163 (3) (2010) 429–437.
[22] E.M. Chan, A.P. Alivisatos, R.A. Mathies, High-temperature microfluidic synthesis of CdSe nanocrystals in nanoliter droplets, J. Am. Chem. Soc. 127 (2005) 13854.
[23] J. Kobayashi, Y. Mori, K. Okamoto, R. Akiyama, M. Ueno, T. Kitamori, et al., A microfluidic device for conducting gas-liquid-solid hydrogenation reactions, Science 304 (2004) 1305.
[24] K. Wang, Y.C. Lu, Y. Xia, H.W. Shao, G.S. Luo, Kinetics research on fast exothermic reaction between cyclohexanecarboxylic acid and oleum in microreactor, Chem. Eng. J. 169 (1–3) (2011) 290–298.
[25] G. Arzamendi, I. Uriz, P.M. Diéguez, O.H. Laguna, W.Y. Hernández, A. Álvarez, M.A. Centeno, J.A. Odriozola, M. Montes, L.M. Gandía, Selective CO removal over Au/CeFe and CeCu catalysts in microreactors studied through kinetic analysis and CFD simulations, Chem. Eng. J. 167 (2–3) (2011) 588–596.
[26] J.-I. Yoshida, A. Nagaki, T. Yamada, Flash chemistry: fast chemical synthesis by using microreactors, Chem. Eur. J. 14 (2008) 7450–7459.
[27] H. Song, D.L. Chen, R.F. Ismagilov, Reactions in droplets in microfluidic channels, Angew. Chem. Int. Ed. 45 (2006) 7336–7356.
[28] X. Zhang, E.S.M. Lai, R. Martin-Aranda, K.L. Yeung, An investigation of Knoevenagel condensation reaction in microreactors using a new zeolite catalyst, Appl. Catal. A 261 (1) (2004) 109–118.
[29] J. Ma, M. Zhang, L. Lu, X. Yin, J. Chen, Z. Jiang, Intensifying esterification reaction between lactic acid and ethanol by pervaporation dehydration using chitosan–TEOS hybrid membranes, Chem. Eng. J. 155 (3) (2009) 800–809.
[30] W. Ferstl, M. Schwarzer, S. Loebbecke, E. Fritz-Langhals, J. Stohrer, Process optimization of a catalyzed bleach oxidation for the production of functionalized aldehydes using microreaction technology, Chem. Eng. J. 135 (S1) (2008) S292–S297.
[31] Y.S.S. Wan, K.L. Yeung, A. Gavriilidis, TS-1oxidation of aniline to azoxybenzene in amicrostructuredreactor, Appl. Catal. A 281 (1–2) (2005) 285–293.
[32] Y. Song, J. Hormes, C.S.S.R. Kumar, Microfluidic synthesis of nanomaterials, Small 4 (2008) 698–711.
[33] J. Kim, Z. Li, I. Park, Direct synthesis and integration of functional nanostructures in microfluidic devices, Lab on a Chip 11 (2011) 1946–1951.
[34] S. Gómez-de Pedro, C.S. Martínez-Cisneros, M. Puyol, J. Alonso-Chamarro, Microreactor with integrated temperature control for the synthesis of CdSe nanocrystals, Lab Chip 12 (2012) 1979–1986.
[35] A.M. Nightingale, S.H. Krishnadasan, D. Berhanu, X. Niu, C. Drury, R. McIntyre, E. Valsami-Jones, J.C. deMello, A stable droplet reactor for high temperature nanocrystal synthesis, Lab Chip 11 (2011) 1221–1227.
[36] H. Yang, W. Luan, S. Tu, Z.M. Wang, High temperature synthesis of CdSe nanocrystals in a serpentine microchannel: wide size tenability achieved under a short residence time, Cryst. Growth Des. 9 (2009) 1569–1574.
[37] R.M. Tiggelaar, P. van Male, J.W. Berenschot, J.G.E. Gardeniers, R.E. Oosterbroek, M. de Croon, J.C. Schouten, A. van den Berg, M.C. Elwenspoek, Fabrication of a high-temperature microreactor with integrated heater and sensor patterns on an ultrathin silicon membrane, Sens. Actuators A 119 (2005) 196–205.
[38] B.K.H. Yen, A. Gunther, M.A. Schmidt, K.F. Jensen, M.G. Bawendi, A microfabricated gas-liquid segmented flow reactor for high-temperature synthesis: the case of CdSe quantum dots, Angew. Chem Int. Ed. 117 (2005) 5583–5587.
[39] E.M. Chan, A.P. Alivisatos, R.A. Mathies, High-temperature microfluidic synthesis of CdSe nanocrystals in nanoliter droplets, J. Am. Chem. Soc. 127 (2005) 13854–13861.
[40] S.-T. Tu, X. Yu, W. Luan, H. Löwe, Development of micro chemical, biological and thermal systems in China: a review, Chem. Eng. J. 163 (3) (2010) 165–179.
[41] C.S. Martinez-Cisneros, N. Ibanez-Garcia, F. Valdes, J. Alonso, LTCC microflow analyzers with monolithic integration of thermal control, Sens. Actuator A-Phys. 138 (2007) 63–70.

[42] K. Malecha, D.G. Pijanowska, L.J. Golonka, W. Torbicz, LTCC microreactor for urea determination in biological fluids, Sens. Actuator B – Chem. 141 (2009) 301–308.
[43] S. Gomez-dePedro, M. Puyol, D. Izquierdo, I. Salinas, J.M. delaFuente, J. Alonso-Chamrro, A ceramic microreactor for the synthesis of water soluble CdS and CdS/ZnS nanocrystals with on-line optical characterization, Nanoscale 4 (2012) 1328–1335.
[44] P. Bembnowicz, M. Malodobra, W. Kubicki, P. Szczepanska, A. Gorecka-Drzazga, J. Dziuban, A. Jonkisz, A. Karpiewska, T. Dobosz, L. Golonka, Preliminary studies on LTCC based PCR microreactor, Sens. Actuators B 150 (2010) 715–721.
[45] S. Gómez-de Pedro, M. Puyol, J. Alonso-Chamarro, Continuous flow synthesis of nanoparticles using ceramic microfluidic devices, Nanotechnology 21 (2010) 415603.
[46] D.J. Sadler, R. Changrani, P. Roberts, C.F. Chou, F. Zenhausern, Thermal management of BioMEMS: temperature control ceramic-based PCR and DNA detection devices, IEEE Trans. Comp. Pack. Technol. 26 (2003) 309–316.
[47] M. Baeza, C. Lopez, J. Alonso, J. Lopez-Santin, G. Alvaro, Ceramic microsystem incorporating a microreactor with immobilized biocatalyst for enzymatic spectrophotometric assays, Anal. Chem. 82 (2010) 1006–1011.
[48] N. Ibanez-Garcia, C.S. Martinez-Cisneros, F. Valdes, J. Alonso, Green-tape ceramics. New technological approach for integrating electronics and fluidics in microsystems,, TRAC-TRENDS in Anal. Chem. 27 (2008) 24–33.
[49] L. Qu, X. Peng, Control of photoluminescence properties of CdSe nanocrystals in growth, J. Am. Chem. Soc. 124 (2002) 2049–2055.
[50] H. Yang, W. Luan, S. Tu, Z.M. Wang, High-temperature synthesis of cdse nanocrystals in a serpentine microchannel: wide size tunability achieved under a short residence time, Cryst. Growth Des. 9 (2009) 1569–1574.
[51] W. Luan, H. Yang, S. Tu, Z. Wang, Open-to-air synthesis of monodisperse CdSe nanocrystals via microfluidic reaction and its kinetics, Nanotechnology 18 (2007) 175603.

B.5 Optical microfluidic system based on ionophore modified gold nanoparticles for the continuous monitoring of mercuric ion.

Sara Gómez de Pedro, Daniela Lopes, Sergey Miltsov, David Izquierdo, Julián Alonso Chamarro and Mar Puyol. Sensors and Actuators B, 194, 19-26 (2014).

Sensors and Actuators B 194 (2014) 19–26

Contents lists available at ScienceDirect

Sensors and Actuators B: Chemical

journal homepage: www.elsevier.com/locate/snb

Optical microfluidic system based on ionophore modified gold nanoparticles for the continuous monitoring of mercuric ion

Sara Gómez-de Pedro[a], Daniela Lopes[a], Sergey Miltsov[b], David Izquierdo[c], Julián Alonso-Chamarro[a], Mar Puyol[a,*]

[a] Sensors & Biosensors Group, Department of Chemistry, Autonomous University of Barcelona, Edifici Cn, 08193 Bellaterra, Catalonia, Spain
[b] Department of Chemistry, St. Petersburg State University, Universitetskii pr. 26, St. Petersburg 198504, Petrodvorets, Russian Federation
[c] Grupo de Tecnologías Fotónicas, Instituto de Investigación en Ingeniería de Aragón, Universidad de Zaragoza, Campus Río Ebro – Edificio I+D+i, Mariano Esquillor, s/n, 50018 Zaragoza, Spain

ARTICLE INFO

Article history:
Received 11 October 2013
Received in revised form
17 December 2013
Accepted 19 December 2013
Available online 27 December 2013

Keywords:
Mercury monitoring
Microfluidics
Thiourea modified gold nanoparticles
Optical detection

ABSTRACT

An optical microfluidic system based on the use of modified gold nanoparticles for monitoring Hg(II) is presented. The system is based on the specific recognition of the heavy metal by a new synthesized ionophore based on a modified thiourea, which is attached to the gold nanoparticles. This interaction generates a change on the gold Surface Plasmon Resonance (SPR) band. The sensitivity and selectivity of the procedure is firstly studied in batch. The obtained results demonstrate the mercury selective response over the different tested ions that can be found in environmental water samples. Due to the remarkable unusual rapid signal change observed during the interaction of the metal and the modified gold nanoparticles, the reaction can be easily performed in a microfluidic system. Results obtained by using the microfluidic system revealed improved analytical features compared to batch experiments such as a lower detection limit (11 ppb), higher sensitivity and faster analysis time, all this with an easy and automated procedure. Therefore, the approach has shown great potential for designing low cost instrumentation for automatic in-field discrete or continuous measurements of Hg(II).

1. Introduction

The growth of industrialization, urbanization and human population increases pollution problems. Industrial wastes, even in very small concentrations, are often extremely toxic. Among other heavy metals, mercury is one of the greatest concerns due to its bioaccumulation [1] and because it can be easily released in water, soil or air by some different industrial and anthropogenic sources [2,3], it produces toxic effects in living organisms [4]. Because of its importance for human health, there is a strong need to develop new methods for its determination and on-site monitoring.

Current analytical methods for Hg(II) detection are based on electrochemical methods [5], inductively coupled plasma mass spectrometry [6], cold vapor atomic absorbance [7] or fluorescence [8] spectrometry and high performance liquid chromatography [9]. All they are time consuming analytical approaches that frequently require qualified personnel and cannot perform in-field measurements. To overcome these limitations, other simpler methods based on the use of different (bio)sensors incorporating selective or specific recognition elements and optical detection have been proposed, which also show low detection limits [10,11]. Some of them are based on the use of DNAzymes, oligonucleotides or cells [12,13], which considerably increase the cost of the whole procedure, and usually cannot be reused. On the other hand, methods such as optodes, which are based on the use of fluoro/chromophores and iononophores, have also been widely used due to the high selectivity accomplished by the ionophores and their relative simple preparation [14,15]. However, the stability and life time of membranes is still a challenge, since dye leaching and/or photobleaching is a frequent problem.

The use of nanoparticles as signal transduction elements seems to offer great advantages. In concrete, metallic nanoparticles, such as gold colloidal, exhibit a strong SPR (Surface Plasmon Resonance) band of high molar absorption coefficient, which is highly sensitive to changes on the nanoparticles surface and the surrounding media [12]. Some analytical approaches based on the use of gold nanoparticles for heavy metals detection take advantage of the absorption wavelength shift, from red to blue, derived from the interaction of the capping ligand/modifier of the nanoparticles with the analyte, which produces the particle aggregation [16,17]. In this sense, there are several proposed optical sensors based on gold nanoparticles showing very low detection limits, which demonstrate the simplicity of the approach [18,19]. Despite this fact, the sensors have not been designed for the in situ monitoring.

* Corresponding author. Tel.: +34 9358 12533; fax: +34 9358 12477.
E-mail address: mariadelmar.puyol@uab.cat (M. Puyol).

0925-4005/$ – see front matter © 2013 Elsevier B.V. All rights reserved.
http://dx.doi.org/10.1016/j.snb.2013.12.076

Miniaturization of analytical processes and microfluidics can provide several advantages over conventional methods. By reducing size of the developed analytical systems, it is possible to minimize the energy consumption, making feasible the development of low cost portable devices to perform in field measurements [20]. Moreover, microfluidics for continuous monitoring minimizes the amount of the required reagents and therefore the wastes generation, thus reaching a greener chemistry. Microfluidics offers also better control, in a very reproducible way, over certain mixture/reaction parameters than conventional methods, such as mass and heat transfer, thanks to the possibility of computer-controlled elements [21,22]. Furthermore, microfluidic platforms can integrate all the necessary steps of the analytical procedure, such as the sample collection, sample pretreatment, the required analytical separations, reactions and detection.

Very few papers have been presented until the date related to the monitoring of heavy metals in microfluidic systems based on nanomaterials, and they are based on the use of expensive reagents and costly and bulky instrumentation, as well as complicated pretreatment steps [23–25]. Herein, we purpose a simple, economic and miniaturized microfluidic system based on the use of modified gold nanoparticles for a rapid continuous monitoring of Hg(II).

Due to the optical properties of the thiourea-modified gold colloidal, it is possible to follow absorbance changes produced from the interaction of the ionophore with the heavy metal. On the other hand, analysis performed in the microfluidic system allows the easy and automatic manipulation of fluidics meanwhile changes on the absorption maximum of the nanoparticles is continuously monitored.

2. Materials and methods

2.1. Chemicals, materials and instruments

For the synthesis of gold nanoparticles, hydrogen tetrachloroaurate (III) hydrate was provided by Fluka (p.a. ACS, ≥49% Au); sodium borohydride by Panreac with 98% purity and tiopronin (N-(2-Mercaptopropionyl)glycine) (TP) was obtained from Sigma–Aldrich with 99% purity. All solutions were prepared in double distilled water. For the synthesis of the ionophore the following reagents were also purchased from Sigma–Aldrich: p-hydroxyacetanilide; potassium carbonate; 1,4-dibromobutane; carbon tetrachloride; thiourea; *n*-butanol; ethanol; NaOH; HCl; CH_2Cl_2; Na_2SO_4; sulfanilic acid; thiophosgene; THF and ether. Boron trifluoride dimethanol complex 50% was supplied from Acros.

Mercuric ion stock solution is prepared with mercury (II) nitrate monohydrate 99% and sodium acetate and acetic acid. All purchased from Sigma–Aldrich.

The purification of the obtained colloidal was performed by centrifugal filtration in 4 mL centrifugal filter devices (CENTRIPLUS YM30, MICROCON, MWCO 30000) at 3000 rpm for 30 min. For UV–visible spectra, a Shimadzu UV-310PC UV–vis–NIR double-beam scanning spectrophotometer (Kyoto, Japan) was used between 800 and 200 nm. The shape and dimensions of the core of the particles were measured by a transmission electron microscope (TEM), JEOL 1400, and a high resolution electron microscope (HRTEM), JEOL 2011 (Tokyo, Japan). Samples were prepared by dipping a copper grid, coated with a thin carbon film, in the gold nanoparticles suspension at room temperature. A Malvern Instruments Ltd., Zetasizer Nano ZS (Worcestershire, UK) was used for Dynamic Light Scattering (DLS) and ζ potential measurements. For RMN measurements, a Bruker 250 MHz equipment (Karlsruhe, Germany) was used. Elemental analysis was performed by an Optima 4300DV, Perkin-Elmer Inductively Coupled Plasma Optical Emission Spectrometry (ICP-OES) (Massachusetts, USA).

For the microfluidic platform construction a micromilling Computer Numerically Controlled (CNC) machine (Protomat C100/HF, LPKF Laser & Electronics, Garbsen, Germany) and a specially fabricated uniaxial hydraulic press (Talleres Francisco Camp S.A., Granollers, Spain) were used.

Different grades of COC Topas (Topas Advanced Polymers, Florence, KY, USA) were chosen as polymeric substrate: Topas 6013 layers (from 500 to 1000 μm) and Topas 8007 foils (25 μm).

2.2. Preparation of the selective recognition optical element

The first step was the synthesis of the gold colloidal suspension and, in order to make selective the response of the measurement system to Hg(II), a new ionophore based on a thiourea derivative was synthesized. This was later attached to the surface of the gold nanoparticles, the whole acting as the recognition and transducing element.

2.2.1. Synthesis and characterization of AuNPs@Tiopronin

The synthesis of gold nanoparticles (AuNPs) was performed in a ceramic microfluidic platform, thoroughly described elsewhere [26]. Tiopronin was chosen as the colloidal stabilizer to prevent aggregation and to make feasible the manipulation of AuNPs. Briefly, aqueous solutions of 1 mM $HAuCl_4$, 1.5 mM $NaBH_4$ and 1 mM tiopronin placed in Hamilton syringes (Hamilton series GASTIGHT 1000 TLL, Bonaduz, GR, Switzerland) were propelled by means of syringe pumps (540060 TSE systems, Bad Homburg Germany) to the ceramic microfluidic platform, which consisted of four reagent inlets and a three-dimensional serpentine micromixer. Once the chemical and hydrodynamic parameters of the reaction were optimized, the dispensing protocol consisted in the continuous pumping of the $NaBH_4$ solution at a 1 μl s^{-1} flow rate, where 0.7 μl of the $HAuCl_4$ solution was sequentially dispensed every 2 s at a 2.5 μl s^{-1} flow rate. These solutions were mixed in the serpentine and after that, the tiopronin solution was continuously pumped at 0.5 μl s^{-1}. The obtained particles were purified by centrifugation. The final solution was adjusted to pH 8.5, since it ensures the ionization of the tiopronin functional group, which confers an extra stabilization to the colloidal for the electrostatic repulsions generated. In this way, the colloidal can be stored for a long time. UV–vis spectroscopy characterization showed a stable SPR band centered at 518 nm. Transmission electron microscopy (TEM) and electron diffraction (SAED) pattern of the selected area revealed crystalline homogeneous particles of a mean core size of 3.4 nm. Meanwhile, dynamic light scattering (DLS) and ζ potential results gave particles of 10.1 nm hydrodynamic diameter and −36.1 mV. NPs characterization is shown in the Supporting Information (Fig. S1).

2.2.2. Synthesis and characterization of the ionophore

Since thiourea and its derivatives usually present chelating capability toward heavy metals, the goal was to synthesize a derivative, which could also be easily attached to the gold surface. For this purpose, different strategies can be selected, such as coupling by physical interactions (hydrophobic, electrostatic) or by using the specific recognition of biomolecules, one of them attached to the AuNPs (such as the avidin–biotin interaction). In this case, a simple covalent coupling has been preferred, since it confers higher stability to nanoparticles. Thus, a N-(4-sulfonatophenyl)-N′-[4-(4-mercaptobutoxy)-phenyl]thiourea was synthesized. Its structure has a short C_4 hydrocarbon chain with a -SH terminal group (a mercaptobutoxy group) to be linked to the gold surface and a sulfonate group to assure its solubility in water. A scheme from the synthetic route is depicted in Fig. 1 and consisted of five simple reactions.

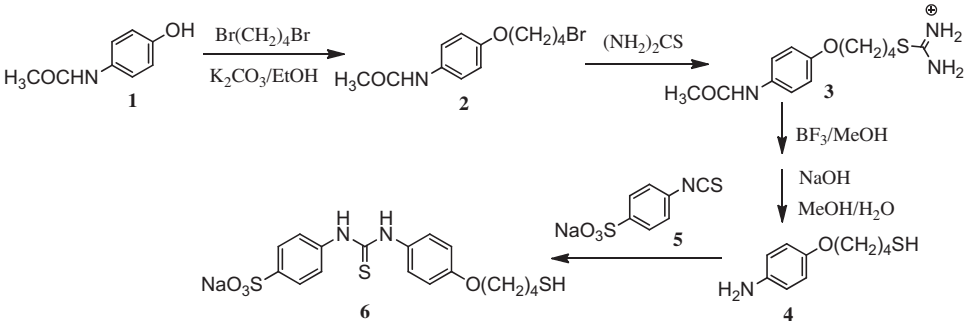

Fig. 1. Scheme from the synthetic route of the ionophore N-(4-sulfonatophenyl)-N'-[4-(4-mercaptobutoxy)-phenyl]thiourea sodium salt (**6**).

^{1}H RMN and mass spectroscopy data are given next (also shown in Supporting Information, Fig. S2). The total yield of the reaction was 9.3%.

Synthesis of 4-(4-bromobutoxy)-acetanilide (2) [27]: A mixture of p-hydroxyacetanilide (**1**) (7.57 g, 50 mmol), potassium carbonate (6.90 g, 50 mmol) and 1,4-dibromobutane (16.2 g, 75 mmol) in ethanol (250 mL) was heated at reflux. When the reaction was completed (about 8 h) the mixture was poured into crushed ice and crystallized from carbon tetrachloride. Yield 6.72 g, 47%. m.p. 100–102 °C (lit.[24] m.p. 101–102 °C).

^{1}H NMR (DMSO-d6): 1.74–1.88 (m, 2H), 1.89–2.03 (m, 2H), 2.00 (s, 3H), 3.59 (t, *J* = 7 Hz, 2H), 3.94 (t, *J* = 7 Hz, 2H), 6.85(d, *J* = 9 Hz, 2H), 7.46(d, *J* = 9 Hz, 2H), 9.76 (s, 1H).

*Synthesis of 4-(4-acetamidophenoxy)-butylisothiuronium bromide (**3**)*: A mixture of (**2**) (5.72 g, 50 mmol) and thiourea (1.52 g, 50 mmol) was heated at reflux for 5 h in *n*-butanol (50 mL). After cooling, the precipitate was filtered out and washed with cold ethanol and ether. After drying on air, it yielded 6.00 g, 83%. ^{1}H NMR (DMSO-d6): 1.77 (br.s, 4H), 2.00 (s, 3H), 3.22 (t, *J* = 6 Hz, 2H), 3.94 (t, *J* = 6 Hz, 2H), 6.85 (d, *J* = 10 Hz, 2H), 7.48 (d, *J* = 10 Hz, 2H), 8.97 (br.s, 2H), 9.10 (br.s, 2H), 9.84 (s, 1H).

*Synthesis of 4-(4-aminophenoxy)-butanethiol (**4**)*: 5.43 g (15 mmol) of (**3**) and 10.0 mL (95 mmol) of boron trifluoride dimethanol complex 50% in 60 mL of methanol were heated at refluxed for 10 h (NMR of the probe showed absence of NH-protons). The mixture was transferred to a screw-capped Shott 100 mL bottle, and argon was bubbled while a solution of 5.0 g (125 mmol) NaOH in 20 mL of water was added on cooling in ice water. The bottle was closed and heated in a boiling water bath for 4 h. Then the solution was neutralized with HCl up to pH 5 (under argon), the solvents were evaporated in vacuo and the residue was taken up with CH_2Cl_2. The extract was dried with Na_2SO_4. The solvent evaporated in vacuo and the residue was stirred with hot hexane, filtered and after evaporation of hexane in vacuo, it yielded 1.27 g (43%) of yellowish oil. ^{1}H NMR ($CDCl_3$): 1.39 (*t*, J = 7 Hz, 1H), 1.70–2.00 (m, 4H), 2.60 (q, *J* = 7 Hz, 2H), 3.91(t, *J* = 6 Hz, 2H), 6,40 (d, *J* = 9 Hz, 2H), 6.75 (d, *J* = 9 Hz, 2H).

*Synthesis of 4-isothiacyanatobenzoic acid sodium salt (**5**) (Modified procedure from* [28]*)*: Sulfanilic acid (1.73 g, 10 mmol) was dissolved in 15 mL of water, containing 2.46 g (30 mmol) of sodium acetate. Thiophosgene (1.15 g, 10 mmol) in 1.5 mL of THF was added. After stirring at room temperature for 2 h the precipitate was filtered, washed with cold ethyl acetate and dried in vacuo. Yield 1.47 g (62%). ^{1}H NMR (D_2O): 7.34 (d, *J* = 8 Hz, 2H), 7.72 (d, *J* = 8 Hz, 2H).

Synthesis of N-(4-sulfonatophenyl)-N′-[4-(4-mercaptobutoxy)-phenyl]thiourea sodium salt (**6**): 4-Isothiacyanatobenzoic acid sodium salt (**5**) (173 mg, 1 mmol) was dissolved in 2 mL of dry dimethylacetamide under stirring at room temperature. 4-(4-Aminophenoxy)-butanethiol (**4**) (197 mg, 1 mmol) was added, and stirring was continued for 24 h. The resulting solution was poured into 30 mL of dry ether. The precipitate was washed for several times with ether and dried in vacuo. Yield 386 mg, 89%. m.p. > 300 °C ^{1}H NMR (DMSO-d6): 1.60–1.90 (m, 5H), 2.54 (q overlapped with DMSO, 2H), 3.90–4.05 (m, 2H), 6.89 (d, *J* = 9 Hz, 2H), 7.31 (d, *J* = 9 Hz, 2H), 7.42 (d, *J* = 9 Hz, 2H), 7.54 (d, *J* = 9 Hz, 2H), 9.71 (s, 1H), 9.77 (s, 1H). NMR H1 (D_2O): 1.64 (br.s, 2H), 1.75 (br.s, 2H), 2.47 (br.s, 2H), 3.98 (br.s, 2H), 6.92 (br.s, 2H), 7.13 (br.s, 2H), 7.35 (br.s, 2H), 7.69 (br.s, 2H).

ES-MS(-): 411.0347 (calc 411.0507).

2.2.3. Synthesis and characterization of AuNPs@Ionophore

The final step was the ligand exchange on the AuNPs surface, which was accomplished by just mixing a solution of purified AuNPs@TP with an aqueous solution of the ionophore, taking into account that an excess of ionophore (1:10 of AuNPs:Ionophore) is necessary in order to obtain the desired exchange. The complete reaction took place in 12 h. Then, the solution was filtered repeated times in order to eliminate the excess of ionophore and the tiopronin present in the solution. Since the ionophore absorbs at 260 nm, the purification process could be followed by UV–vis spectroscopy of the filtered solution. The spectra of the modified gold colloidal show the characteristic SPR band at around 525 nm and a new band at 260 nm appears demonstrating the surface modification (Fig. 2). The obtained ionophore-activated AuNPs (AuNPs@Ionophore) were characterized by DLS and ζ potential at slightly basic pH values (7.5) to ensure its stability for a long time, which revealed stable (−31.4 mV) and larger particles (17.8 nm) (Supporting Information, Fig. S3). Results concerning TEM analysis revealed a mean size of 3.7 nm AuNPs@Ionophore (Fig. 2b). Inductively coupled plasma optical emission spectrometry (ICP-OES) results gave the calculated ratio of S:Au before and after the ligand exchange, which were 0.1 and 0.3 respectively (Supporting Information, Fig. S3). This also ensured that the ligand exchange was done.

2.3. Microfluidic system and set-up

2.3.1. Design and construction of the microfluidic platform

The microfluidic platform was fabricated with Cyclic Olefin Copolymer (COC), an amorphous polymer, which permits the construction and integration of bi and three-dimensional structures using a multilayer approach [29]. Polymers offer some advantages over other materials [30] as simple, cheap and rapid prototyping and the possibility of developing disposable devices due to their low cost. Furthermore, they are compatible with further integration of other components by means of UV curing adhesives. In concrete, COC, as a thermoplastic polymer, is in addition found at different polymerization grades, which entails that it is possible to use the ones with lower glass transition temperatures (Tg) as sealing layers. Thus, a simple lamination process permits obtaining specific 3D structures by a simple multilayer approach.

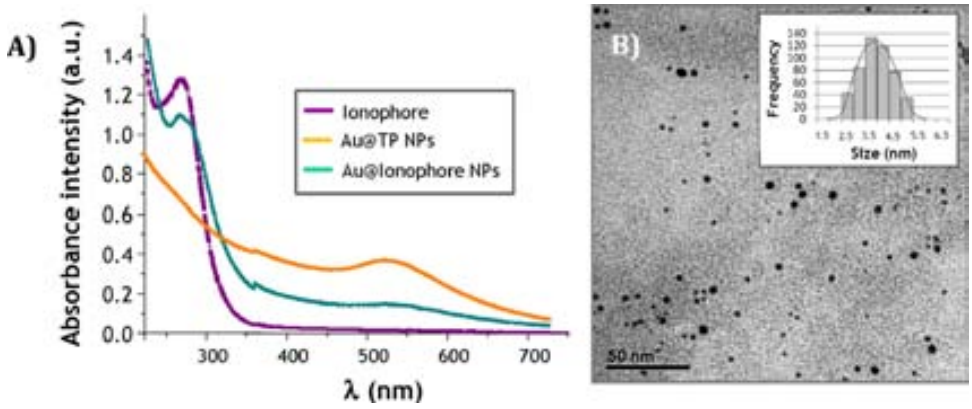

Fig. 2. (A) UV–vis spectra of the ionophore, the gold nanoparticles stabilized with tiopronin (Au@TP NPs) and with the ionophore (Au@Ionophore NPs) in solution (not at the same concentration). (B) TEM image from 3.7 nm Au@Ionophore NPs.

The constructed microfluidic platform consisted of three layers of the polymeric substrate. Once the design was created by means of Computer-Aided Design (CAD) software, it was transferred to a micromilling CNC machine in order to mechanize the polymeric substrate. Different grades of COC Topas were used. Topas 6013 layers (from 500 to 1000 μm) were used to mechanize the microfluidic structures, while Topas 8007 foils (25 μm) were used as adhesive layers. Once the pattern was mechanized by means of different End Mill and Spiral Drill Tools, the different layers were aligned, using fiducial holes, and laminated through a thermo compression process to completely seal the microfluidic platform. This lamination consisted in the following temperature profile at 4–6 bar pressure: a first drop temperature ramp from room temperature to 108 °C, a 10–15 min of temperature stabilization and a temperature decrease until room conditions.

The constructed microfluidic device consists of two initial inlets for reagents, a bidimensional micromixer of 400 μm width (total micromixer volume of 95 μL), a 2 cm × 1 mm × 1 mm (20 μL) optical detection chamber and a collection channel to the outlet. The total volume of the microfluidic platform is of 130 μL. Optical fibers are directly connected to the optical chamber by means of their insertion and gluing into two mechanized guides (1 cm × 1 mm × 1 mm) at both sides. A picture of the microfluidic device is shown in Fig. 3.

2.3.2. *Microsystem set-up and optical system*

The whole set-up was also composed of a flow injection analysis (FIA) system, which includes a peristaltic pump (Gilson Minipuls® 3, Middleton, USA) and an injection valve (Hamilton MVP, Bonaduz, GR, Switzerland). PTFE tubes (i.d. 0.9 mm) were used to connect the microsystem to chemical solutions.

On the other hand, a low Numerical Aperture Polymer Optical Fiber (NA POF) (Toray PMU-CD 1002–22-E, Tokyo, Japan) is used for light injection and a high NA POF (Mitsubishi ESKA Premier GH4001, Tempe, USA) for light collection from the optical window (Fig. 3). These fibers were directly glued (using a UV-Curing Norland Optical Adhesive: NOA61, Cranbury, NJ, USA) to the microsystem.

The optical detection system consists of the following components: a 525 nm Light Emitting Diode (LED) (Roithner Lasertechnik B5B-433-B525, Vienna, Austria), which is mounted in a Printed Circuit Board (PCB) and matches the absorption maximum of the AuNPs SPR band; a photomultiplier (H6780-03, Hamamatsu, Japan) and a Data Acquisition Card (National Instruments NI USB-6211, Austin, USA), which is connected to a PC that controls the system and modulates the LED signal. Details from the optical system are described elsewhere [31].

3. Results and discussion

In order to demonstrate the general features of the proposed microsystem, in terms of enhanced sensitivity, adequate selectivity toward Hg(II), easy handling of low volumes of reagents, adequate analysis time, automation and portability for in situ monitoring, and for comparison purposes, modified AuNPs were initially characterized with a conventional spectrophotometer in a batch mode. Sensitivity and selectivity were determined by mixing different aliquots of the colloidal solution AuNPs@Ionophore with increasing concentrations of mercuric ion, which were prepared in a 0.01 M acetic acid/sodium acetate buffer adjusted to pH 5.5. The modification of the absorption signal of the resulting SPR band was followed.

With the aim of achieving the maximum sensitivity and detection limit, different concentrations of the colloidal, obtained by dilution of the purified AuNPs@Ionophore, were tested. Solutions of about 1.5×10^{-3}% $HAuCl_4$ (4.7×10^{-8} M), 2.3×10^{-3}% (7.5×10^{-8} M) and 3.0×10^{-3}% (9.6×10^{-8} M), (calculated by a calibration curve using a commercial gold colloid of a 5 nm mean size (Aldrich), with an extinction coefficient of 2.3×10^{6} M^{-1} cm^{-1}) were prepared. The intermediate concentration gave the best results in terms of sensitivity and was chosen as the optimized to perform the following studies. Response to mercury (II) at low concentration range (0, 20, 40, 60, 80, and 100 ppb) and at high concentration range (0, 20, 40, 60, 80, and 100 ppm) was tested by performing three different calibration experiments with each concentration range, demonstrating the interaction of the metal with the ionophore. As it is already reported, this change is probably due to a change in the refractive index on the surface of the AuNPs generated from the interaction metal-ionophore [32,33]. Linear least squares fitting of the calibration curves gave a mean sensitivity (as the mean of the three slopes) of $4.03 \times 10^{-4} \pm 0.06 \times 10^{-4}$ a.u. ppm^{-1} Hg^{2+} and $6.3 \times 10^{-5} \pm 0.6 \times 10^{-5}$ a.u. ppb^{-1} Hg^{2+} for high and low concentration ranges respectively (Fig. 4) [34]. A detection limit, calculated as three times the standard deviation of the blank signal (AuNPs@Ionophore), of 67 ± 3 ppb can be achieved in batch conditions.

The interaction time of the metal-ionophore to achieve a stationary signal appears to be of few seconds. This signal could not be reversed despite the addition of chelating compounds, such as ethylenediaminetetraacetic acid (EDTA) or thiourea into the reaction cuvette.

Selectivity of the method was also determined by comparison of the response of the AuNPs@Ionophore to mercury with the one obtained with different potential interfering ions such as Ni^{2+}, Pb^{2+}, Cd^{2+}, Fe^{2+}, Mg^{2+}, K^{+}, Ba^{2+}, Cu^{2+} and Al^{3+} all at 100 ppm

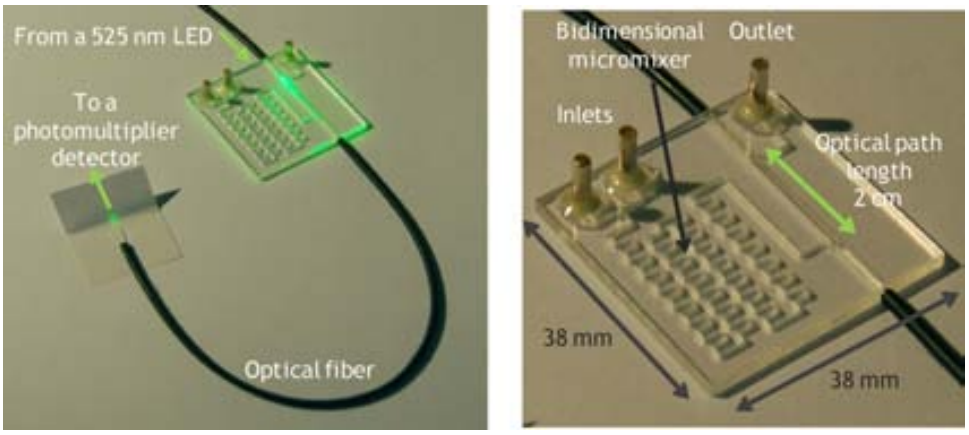

Fig. 3. Pictures from the constructed microfluidic platform for the continuous monitoring of Hg(II).

concentration. As Fig. 5A shows, only mercuric ion gave a significant change in the absorption signal of the SPR band. Furthermore, a simplification of the Fixed Interference Method (FIM) was performed since it reproduced the final situation of the analytical measurement more closely. The signal of a solution containing 1 ppm of Hg^{2+} was compared with the signal of the same solution containing a higher concentration of an interfering ion as a background. 10 ppm Ni^{2+} and Cu^{2+} were selected, while 1 ppm of Pb^{2+} and Cd^{2+} were used, since a lower concentration of these ions is expected to be found in water samples. Again, the presence of the tested metal ions does not result in a significant increase in the absorption signal (Fig. 5B).

3.1. Microfluidic system for the monitoring of Hg(II)

One of the aims of the work was to develop an optical microfluidic system, which exploited and improved the physicochemical properties of the AuNPs@Ionophore as a selective recognition optical element and provided a simple and portable method for the in situ monitoring of Hg(II). The use of a microfluidic system to perform an analytical measurement can avoid some of the problems related with the lack of reproducibility of the analytical methods when using nanomaterials, while allows controlling and managing small volumes of fluids. As it is well known, some quality parameters as sensitivity and response time of AuNPs are highly dependent on the size and concentration of the colloidal. This has been proved to be overcome by the use of microreactors [26]. As these quality parameters are also highly affected by kinetics, microfluidics is an excellent tool for the optimization of mass-transfer rates and other mixture parameters, which also affect sensitivity and improve the analysis time. In this sense, the hydrodynamic parameters of the system must be first optimized.

A continuous flow injection analysis (FIA) system was employed as the analytical method for the microfluidic platform operation. A certain plug of sample was injected by means of an external injection valve into a continuous flowing carrier solution of 0.01 M acetic/acetate buffer at pH = 5.5, as a conditioning solution, and this flow was mixed inside the microfluidic platform with a continuously flowing solution of AuNPs@Ionophore before reaching the detection area. A T-shape confluence point is preferred to assure an efficient mixture of both solutions, which are also mixed throughout a bidimensional meander micromixer before reaching the detection chamber, where the absorbance signal of the SPR band maximum is continuously recorded. The blank signal is taken when

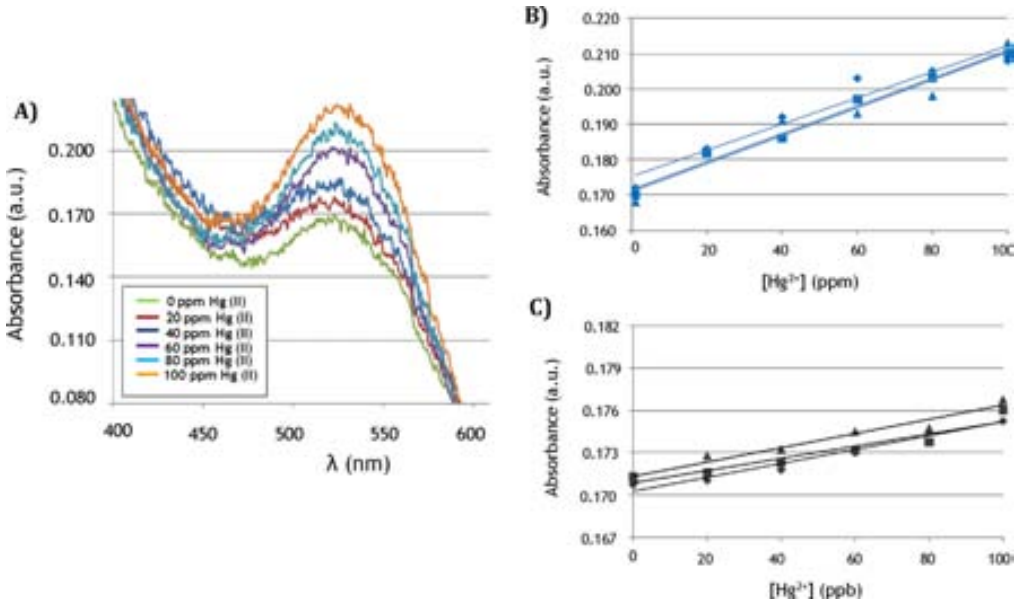

Fig. 4. Response from AuNPs@Ionophore to Hg(II) (A) Example of the absorbance spectra. (B) Response at high concentration range (0, 20, 40, 60, 80, and 100 ppm). (C) Response at low concentration range (0, 20, 40, 60, 80, and 100 ppb). Plotted calibration curves from B and C graphics correspond to three different calibration experiments.

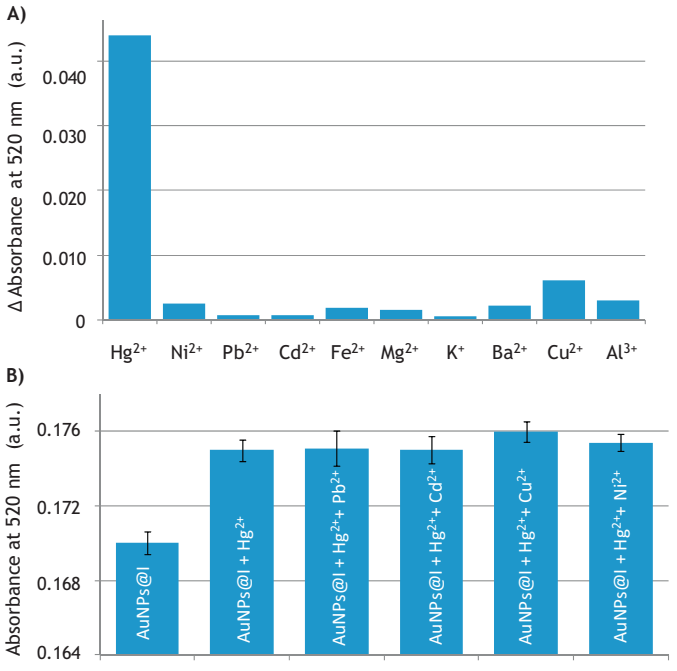

Fig. 5. Absorbance signals at 525 nm from the selectivity tests performed with the AuNPs@Ionophore. (A) Absorbance signal variation at 100 ppm concentration level of all the metals. (B) Signal (each one per triplicate) from blank and 1 ppm Hg^{2+} solutions containing 1 ppm Pb^{2+}, 10 ppm Ni^{2+}, 10 ppm Cu^{2+}, 1 ppm Cd^{2+}.

AuNPs@Ionophore, mixed with the conditioner solution, reach the detection chamber. Therefore, a transitory signal is obtained due to the sample crossing, which corresponds to the absorption signal increase of the SPR band due to the metal-AuNPs@Ionophore interaction. With the purpose of optimizing the injection volume and flow rate, an intermediate concentration of mercuric ion (100 ppb) was selected to ensure a significant response of the system. 100, 300 and 500 μL of sample volumes were injected into the pumped carrier at 0.8 mL min^{-1}. The flow rate of AuNPs@Ionophore was also 0.8 mL min^{-1}. For the optimization of flow rate, 0.8, 1.6 and 3.2 mL min^{-1} flows, measured at the outlet, were tested. As it can be seen in Fig. 6A and B, a 300 μL injection volume and a total flow rate of 1.6 mL min^{-1} were the optimum values as a compromise between sampling rate and analytical sensitivity.

Sensitivity and detection limit were evaluated from calibration curves at low mercuric ion concentrations. Thus, solutions of 20, 40, 60, 80 and 100 ppb of Hg^{2+} were injected into the microsystem at the optimized hydrodynamic conditions. Fig. 7A shows an example of the obtained recorded results. As it can be observed, peaks showed a very high signal to noise ratio and are totally recovered, which demonstrated the complete renewal of the volumes on the detection chamber. Fig. 7B shows the comparison of three calibration experiments performed in bath with three other ones performed with the microsystem. The sensitivity (mean slope of the three calibration curves) was of $2.07 \times 10^{-4} \pm 0.06 \times 10^{-4}$ a.u. ppb^{-1} Hg^{2+} and the detection limit, calculated as three times the standard deviation of the blank signal, was of 11.0 ± 0.6 ppb.

As it can be observed, a clear sensitivity improvement in terms of slope and detection limit is achieved when using the proposed microfluidic system. The later should be further improved to reach the regulations from the Environmental Protection Agency (EPA) (2 ppb) [35]. In this sense, the microfluidic platform allows increasing the optical path length and thus, sensitivity can be enhanced. Other systems already described in the literature based on the use of modified gold nanoparticles show better sensitivity in terms of limit of detection but on the other hand, they require costly bioreagents [36–38] or a large reaction time [39–42], or are not fully described for comparison purposes. Selectivity of the present approach is comparable or even better to other methods [17,40]. On the other hand, a working range of 11–100 ppb was achieved,

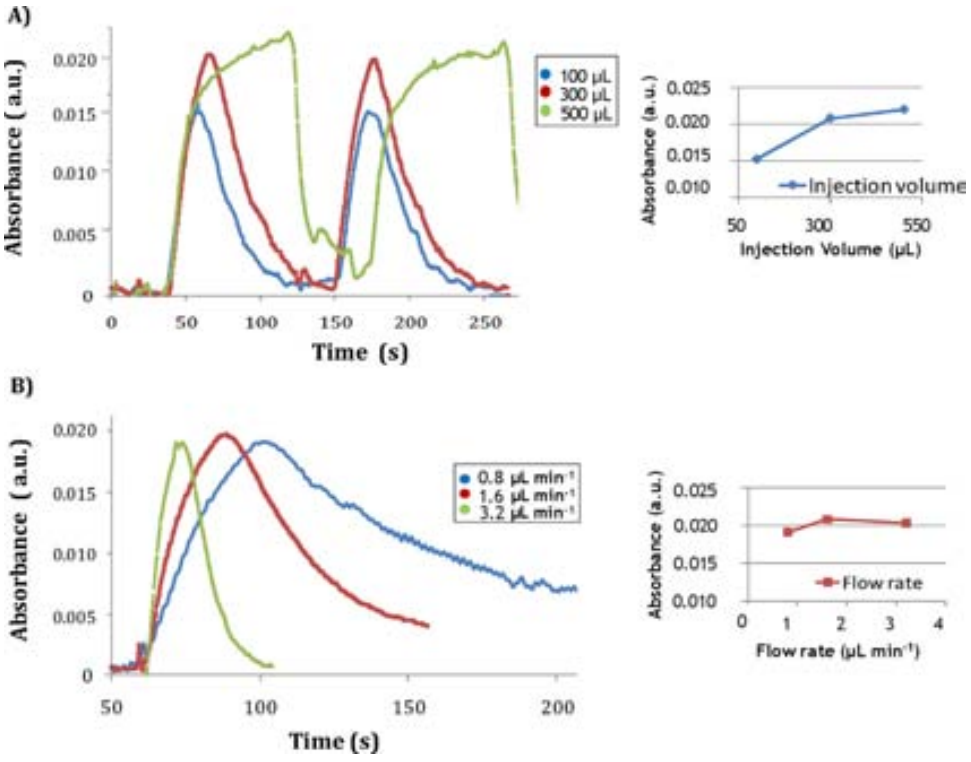

Fig. 6. Hydrodynamic parameters optimization of the microfluidic system for 100 ppb mercuric ion. (A) Injection volume optimization at a total flow rate (measured at the outlet) of 1.6 mL min^{-1}. (B) Flow rate optimization for 300 μL sample injection volume.

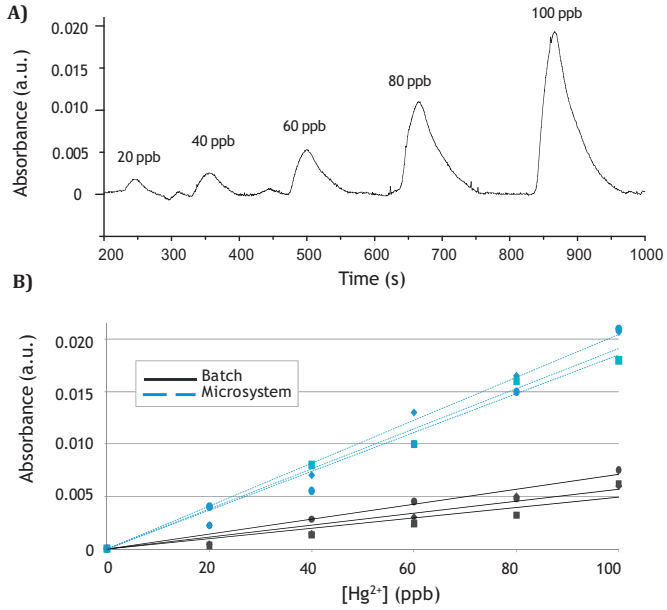

Fig. 7. (A) Example of the obtained signal from a mercury (II) calibration. (B) Comparison of the calibration curves obtained with the batch procedure and using the microfluidic system at the low concentration range.

which is shorter than other reported values [36,38,40,43] but may be enlarged because no signal saturation is observed till the highest concentration tested. Furthermore, the experiments performed with the proposed modified AuNPs in a batch mode analysis showed that it would be possible to detect mercury also in the range of ppm. Therefore, the calibration procedure of the microsystem should be optimized depending on the level of mercury to be determined. The remarkable advantage of the microsystem approach is the possibility of performing in situ monitoring. Actually, a sample throughput of 18 samples h^{-1} has been calculated, which can also be increased by reducing the stabilization time to the baseline signal between standards/sample injections.

4. Conclusions

A simple optical microfluidic system for continuously monitoring Hg(II) is presented. The detection method is based on the selective recognition of mercury by a thiourea derivative, which was specifically designed and synthesized for this purpose and which was attached onto gold nanoparticles surface. The synthetic process of the ionophore is simple and based on low cost reagents, and AuNPs are proposed as optical transducer due to their excellent properties; their SPR band is highly sensitive to changes derived from the metal–ionophore interaction. Moreover, they do not present photostability problems as commonly used organic dyes. This represents a long life-term reagent, which can be stored once synthesized. Results on the characterization of the optical recognition element revealed a high sensitivity and selectivity to mercury over Ni^{2+}, Pb^{2+}, Cd^{2+}, Fe^{2+}, Mg^{2+}, Ba^{2+}, Cu^{2+} and Al^{3+}, which demonstrate the suitability of the recognition element to the proposed Hg(II) detection. In order to exploit and improve the properties of the AuNPs@Ionophore and to develop a simple and portable method for the in situ monitoring of Hg(II), a polymeric microfluidic system was designed, constructed and tested. After the optimization of the hydrodynamic parameters, it was possible to improve sensitivity and detection limit, while taking advantage from microfluidics. Miniaturization enables the possibility of performing in-field measurements at lower cost and at lower reagents consumption. Thus, the proposal emerges as an appropriate approach for in situ unattended Hg(II) monitoring with a high sample throughput. It is of easy operation and the analytical process is automated.

Acknowledgements

This work has been supported by the Spanish Ministry of Science and Innovation (MICINN) through projects CTQ2009-12128 and CTQ2012-36165, co-funded by FEDER, and Catalonia Government through SGR 2009-0323. Thanks to Ignasi Villarroya for ICP-OES measurements.

Appendix A. Supplementary data

Supplementary data associated with this article can be found, in the online version, at http://dx.doi.org/10.1016/j.snb.2013.12.076.

References

[1] T.W. Clarkson, L. Magos, G.J.N. Myers, The toxicology of mercury – current exposures and clinical manifestations, Engl. J. Med. 349 (2003) 1731–1737.
[2] J. Loredo, M.D. Petit-Domínguez, A. Ordóñez, M.P. Galán, R. Fernández-Martínez, R. Alvarez, M.I. Rucandio, Surface water monitoring in the mercury mining district of Asturias (Spain), J. Hazard. Mater. 176 (2010) 323–332.
[3] F. Di Natale, A. Lancia, A. Molino, M. Di Natale, D. Karatza, D. Musmarra, Capture of mercury ions by natural and industrial materials, J. Hazard. Mater. 132 (2006) 220.
[4] L.M. Campbell, D.G. Dixon, R.E. Hecky, A review of mercury in Lake Victoria, East Africa: implications for human and ecosystem health, J. Toxicol. Environ. Health B 6 (4) (2003) 325–356.
[5] H. Khani, M.K. Rofouei, P. Arab, V.K. Gupta, Z. Vafaei, Multi-walled carbon nanotubes-ionic liquid-carbon paste electrode as a super selectivity sensor: application to potentiometric monitoring of mercury ion(II), J. Hazard. Mater. 183 (2010) 402–409.
[6] M.N. Rashed, Monitoring of contaminated toxic and heavy metals, from mine tailings through age accumulation, in soil and some wild plants at Southeast Egypt, J. Hazard. Mater. 178 (2010) 739–746.
[7] N. Ferrúa, S. Ceruttia, J.A. Salonia, R.A. Olsina, L.D. Martinez, Preconcentration and determination of mercury in biological and environmental samples by cold vapor-atomic absorption spectrometry, J. Hazard. Mater. 141 (3) (2007) 693–699.
[8] L.P. Yu, X.P. Yan, Flow injection online sorption preconcentration coupled with cold vapor atomic fluorescence spectrometry with online oxidative elution for determination of trace mercury in water samples, At. Spectrosc. 25 (3) (2004) 145–153.
[9] M.V.B. Krishna, J. Castro, T.M. Brewer, R.K. Marcus, Online mercury speciation through liquid chromatography with particle beam/electron ionization mass spectrometry detection, J. Anal. At. Spectrom. 22 (2007) 283–291.
[10] J. Zhang, Y. Zhou, W. Hu, L. Zhang, Q. Huang, T. Ma, Highly selective fluorescence enhancement chemosensor for Hg^{2+} based on rhodamine and its application in living cells and aqueous media, Sens. Actuators B: Chem. 183 (2013) 290–296.
[11] F. Ma, W. Shi, H. Mi, J. Luo, Y. Lei, Y. Tian, Triphenylamine-based conjugated polymer/I-complex as turn-on optical probe for mercury(II) ion, Sens. Actuators B: Chem. 182 (2013) 782–788.
[12] X. Xue, F. Wang, X. Liu, One-step, room temperature, colorimetric detection of mercury (Hg^{2+}) using DNA/nanoparticle conjugates, J. Am. Chem. Soc. 130 (11) (2008) 3244–3245.
[13] H.Y. Lee, K.M.K. Swamy, J.Y. Jung, G. Kim, J. Yoon, Sens. Actuators B: Chem. 182 (2013) 530–537.
[14] A.R. Firooz, A.A. Ensafi, Z. Hajyani, A highly sensitive and selective bulk optode based on dithiacyclooctadecane derivative incorporating chromoionophore V for determination of ultra trace amount of Hg(II), Sens. Actuators B: Chem. 177 (2013) 710–716.
[15] A.R. Firooz, M. Movahedi, A.A. Ensafi, Selective and sensitive optical chemical sensor for the determination of Hg(II) ions based on tetrathia-12-crown-4 and chromoionophore I, Sens. Actuators B: Chem. 171–172 (2012) 492–498.
[16] C.Y. Lin, C.J. Yu, Y.H. Lin, W.L. Tseng, Colorimetric sensing of silver(I) and mercury(II) ions based on an assembly of Tween 20-stabilized gold nanoparticles, Anal. Chem. 82 (2010) 6830–6837.
[17] G.K. Darbha, A.K. Singh, U.S. Rai, E. Yu, H.T. Yu, P.C. Ray, Selective detection of mercury(II) ion using nonlinear optical properties of gold nanoparticles, J. Am. Chem. Soc. 130 (2008) 8038–8043.
[18] B. Leng, L. Zou, J. Jiang, H. Tian, Colorimetric detection of mercuric ion (Hg^{2+}) in aqueous media using chemodosimeter-functionalized gold nanoparticles, Sens. Actuators B: Chem. 140 (2009) 162–169.
[19] N. Zhang, G. Li, Z. Cheng, X. Zuo, Rhodamine B immobilized on hollow Au–HMS material for naked-eye detection of Hg^{2+} in aqueous media, J. Hazard. Mater. 229–230 (2012) 404–410.
[20] M. Smith, J. March, March's Advanced Organic Chemistry, Reactions, Mechanisms, and Structure, 6th ed., Wiley-Interscience, Hoboken, 2007.

[21] A.J.L. Morgan, J. Naylon, S. Gooding, C. John, O. Squires, J. Lees, D.A. Barrow, A. Porch, Efficient microwave heating of microfluidic systems, Sens. Actuators B: Chem. 181 (2013) 904–909.
[22] K. Wang, Y.C. Lu, Y. Xia, H.W. Shao, G.S. Luo, Kinetics research on fast exothermic reaction between cyclohexanecarboxylic acid and oleum in microreactor, Chem. Eng. J. 169 (1–3) (2011) 290–298.
[23] M. Li, H. Gou, I. Al-Ogaidi, N. Wu, Nanostructured sensors for detection of heavy metals: a review, ACS Sustain. Chem. Eng. 1 (2013) 713–723.
[24] Y. Date, S. Terakado, K. Sasaki, A. Aota, N. Matsumoto, H. Shiku, K. Ino, Y. Watanabe, T. Matsue, N. Ohmura, Microfluidic heavy metal immunoassay based on absorbance measurement, Biosens. Bioelectron. 33 (2012) 106–112.
[25] J.P. Lafleur, S. Senkbeil, T.G. Jensen, J.P. Kütter, Gold nanoparticle-based optical microfluidic sensors for analysis of environmental pollutants, Lab. Chip. 12 (2012) 4651–4656.
[26] S. Gómez-de Pedro, M. Puyol, J. Alonso-Chamarro, Continuous flow synthesis of nanoparticles using ceramic microfluidic devices, Nanotechnology 21 (2010) 415603.
[27] J. Parrick, L.K. Mehta, R.J. Hodgkiss, The synthesis of a potential anti-cancer agent containing the caffeine and 1,2,4-benzotriazine moieties, J. Heterocycl. Chem. 30 (2) (1993) 323–327.
[28] E. Guillaume, A. Panchaud, M. Affolter, V. Desvergnes, M. Kussmann, Differentially isotope-coded N-terminal protein sulphonation: combining protein identification and quantification, Proteomics 6 (8) (2006) 2338–2349.
[29] J. Do, C.H. Ahn, A polymer lab-on-a-chip for magnetic immunoassay with on-chip sampling and detection capabilities, Lab. Chip. 8 (2008) 542–549.
[30] J.S. Kuo, D.T. Chiu, Disposable microfluidic substrates: transitioning from the research laboratory into the clinic, Lab. Chip. 11 (2011) 2656–2665.
[31] S. Gomez-de Pedro, M. Puyol, D. Izquierdo, I. Salinas, J.M. de la Fuente, J. Alonso-Chamarro, A ceramic microreactor for the synthesis of water soluble CdS and CdS/ZnS nanocrystals with on-line optical characterization, Nanoscale 4 (2012) 1328–1335.
[32] Y. Dang, H.W. Li, B. Wang, Y. Wu, Selective detection of trace Cr^{3+} in aqueous solution by using 5,5-dithiobis (2-nitrobenzoic acid)-modified gold nanoparticles, ACS Appl. Mater. Interfaces 1 (2009) 1533–1538.
[33] G. Aragay, J. Pons, J. Ros, A. Merkoçi, Aminopyrazole-based ligand induces gold nanoparticle formation and remains available for heavy metal ions sensing. A simple "mix and detect" approach, Langmuir 26 (12) (2010) 10165–10170.
[34] J.M. Slocik, J.S. Zabinski, D.M. Phillips, R.R. Naik, Colorimetric response of peptide-functionalized gold nanoparticles to metal ions, Small 5 (2008) 548–551.
[35] EPA, U.S. (2001) EPA-823-F-01-01.
[36] C.W. Liu, Y.T. Hsieh, C.C. Huang, Z.H. Lin, H.T. Chang, Detection of mercury(II) based on Hg^{2+}–DNA complexes inducing the aggregation of gold nanoparticles, Chem. Commun. 19 (2008) 2242–2244.
[37] J.-S. Lee, C.A. Mirkin, Chip-based scanometric detection of mercuric ion (Hg^{2+}) using DNA-functionalized gold nanoparticles, Anal. Chem. 80 (2008) 6805–6808.
[38] L. Li, B.X. Li, Y.Y. Qi, Y. Jin, Label-free aptamer-based colorimetric detection of mercury ions in aqueous media using unmodified gold nanoparticles as colorimetric probe, Anal. Bioanal. Chem. 393 (2009) 2051–2057.
[39] C.-C. Huang, H.-T. Chang, Parameters for selective colorimetric sensing of mercury (II) in aqueous solutions using mercaptopropionic acid-modified gold nanoparticles, Chem. Commun. (12) (2007) 1215–1217.
[40] Y.L. Hung, T.M. Hsiung, Y.Y. Chen, Y.F. Huang, C.C. Huang, Colorimetric detection of heavy metal ions using label-free gold nanoparticles and alkanethiols, J. Phys. Chem. C 114 (39) (2010) 16329–16334.
[41] X. Chen, Y. Zu, H. Xie, A.M. Kemas, Z. Gao, Coordination of mercury(II) to gold nanoparticle associated nitrotriazole towards sensitive colorimetric detection of mercuric ion with a tunable dynamic range, Analyst 136 (2011) 1690–1696.
[42] Y. Li, P. Wu, H. Xu, Z. Zhang, X. Zhong, Highly selective and sensitive visualizable detection of Hg^{2+} based on anti-aggregation of gold nanoparticles, Talanta 84 (2011) 508–512.
[43] G.K. Darbha, A.K. Singh, U.S. Rai, E. Yu, H.T. Yu, P.C. Ray, Selective detection of mercury (II) ion using nonlinear optical properties of gold nanoparticles, J. Am. Chem. Soc. 130 (2008) 8038–8043.

Biographies

Sara Gómez-de Pedro received her M.Sc. at the Sensors and Biosensors Group of the Autonomous University of Barcelona in 2007. She is currently finishing her Ph.D. in analytical chemistry at the same university. Her research interests include the development of microfluidic systems for the synthesis of metallic and semiconductor nanoparticles and their use in (bio)analytical applications. She is also concerned about the characterization of new chromo(fluoro)ionophores for their use in optochemical sensors.

Daniela Lopes finished her M.Sc. in Pharmaceutical Sciences at the Faculty of Pharmacy of Oporto University in 2012. Currently she is starting her Ph.D. under the Doctoral Program on Cellular and Molecular Biotechnology Applied to Health Sciences (Oporto University). The focus of her work is drug-membrane interaction.

Sergey Miltsov received his Ph.D. in Organic Chemistry in 1987 at the Leningrad State University. He was a Senior Researcher in the Chemistry Institute of Saint Petersburg State University and he is currently Full Professor at the same university. His research interests include the synthesis of cyanine dyes and other chromoionophores, selective ionophores as well as the chemistry of organohalogen compounds.

David Izquierdo received his Ph.D. degree in 2011 at the Photonic Technologies Group (GTF) from the University of Zaragoza. His research interests include integrated optics, optochemical sensors, optical characterization instrumentation and broadband communications systems.

Julián Alonso-Chamarro received his Ph.D. in analytical chemistry in 1987 at the Autonomous University of Barcelona. He is a professor of analytical chemistry at the same University. He has co-authored more than 110 research papers on (Bio)Chemical Sensors and Automated Flow Systems and is the author of different patents about Sensor and Analytical Instrumentation for environmental monitoring. His research interests include microsystems for chemical analysis, μTAS, optical and electrochemical microsensors, synthesis of ionophores and dyes for chemical sensing, and the development of automatic analyzers for environmental and industrial control.

Mar Puyol obtained her Ph.D. in analytical chemistry about integrated waveguide absorbance optochemical sensors in 2002 at the Autonomous University of Barcelona (UAB). She is actually lecturing and working as a researcher at the same university. Her research interests include the study and characterization of new chromo(fluoro)ionophores to develop optochemical sensors for environmental applications. She is concerned about the development of microfluidic systems for the synthesis of nanoparticles and their integration in flow systems for (bio)analytical applications.

Optical microfluidic system based on ionophore modified gold nanoparticles for the continuous monitoring of mercuric ion

Sara Gómez-de Pedro [a], Daniela Lopes [a], Sergey Miltsov [b], David Izquierdo [c], Julián Alonso-Chamarro [a] and Mar Puyol [a,*]

***Corresponding author**: Sensors & Biosensors Group, Spain; E-mail: mariadelmar.puyol@uab.cat

Supporting Information (SI)

Figure S1: Characterization of gold nanoparticles stabilized with tiopronin

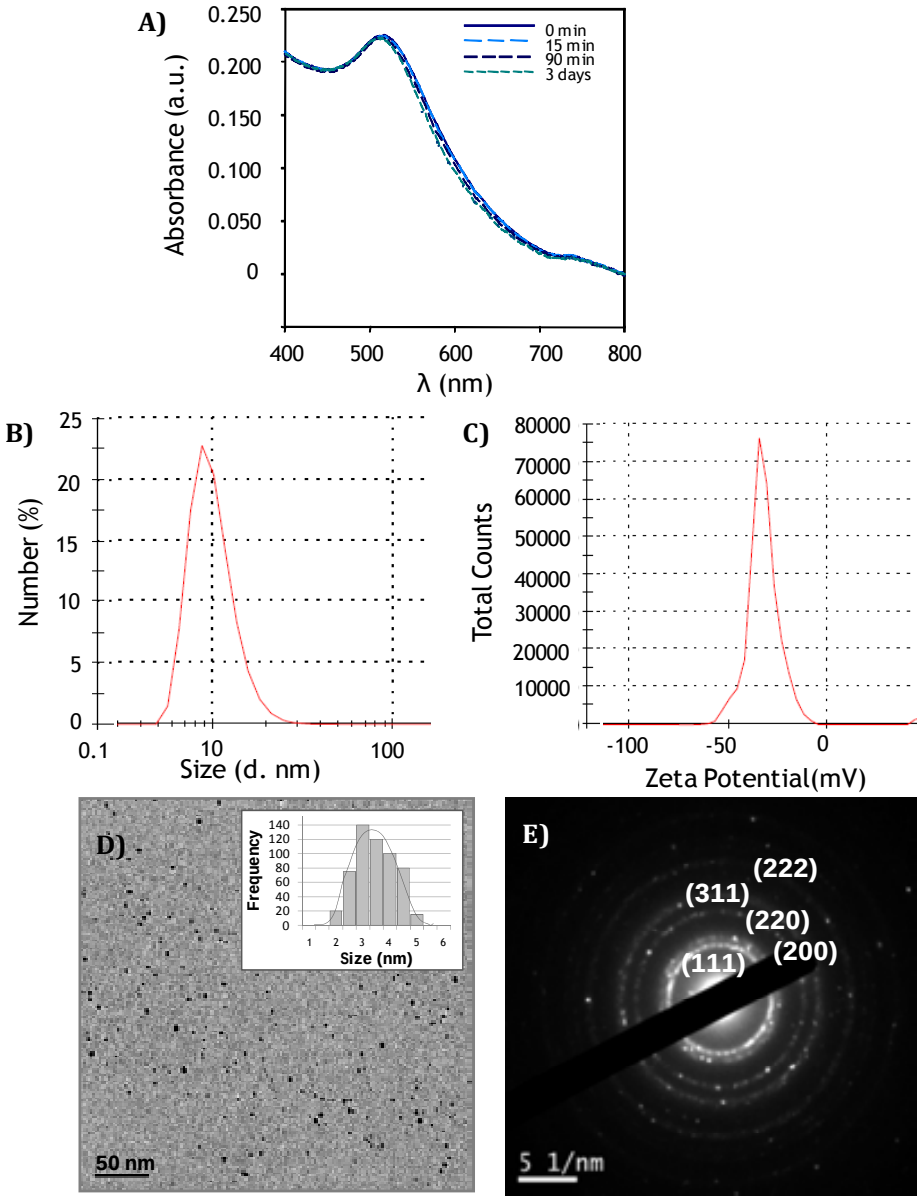

Fig. S1. UV-Vis spectra of gold nanoparticles stabilized with tiopronin (absorbance maximum located at 518 nm). **B)** Size Distribution by Number graphic (10.10 nm) **C)** ζ Potential Distribution graphic (-36.1 mV) at pH 8.5. **D)** Transmission Electron Microscopy (TEM) and **(E)** electron diffraction (SAED) pattern of the selected area images from 3.4 nm gold NPs tiopronin stabilized obtained with the ceramic microreactor.

Figure S2: Characterization of the ionophore

A)

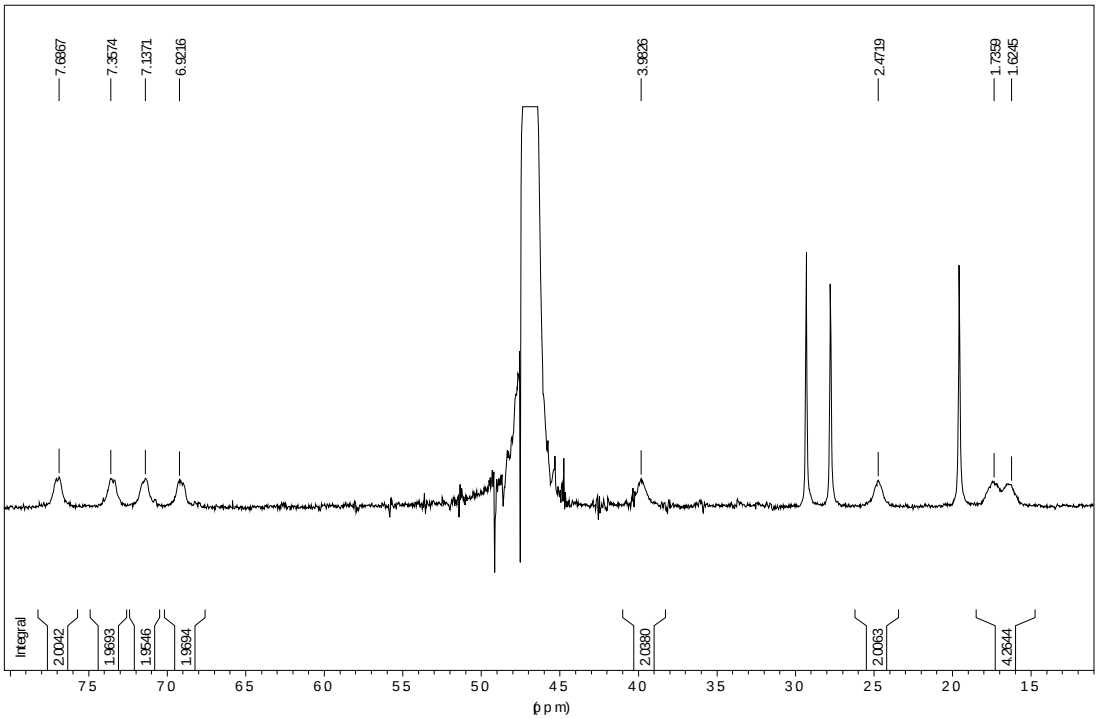

B)

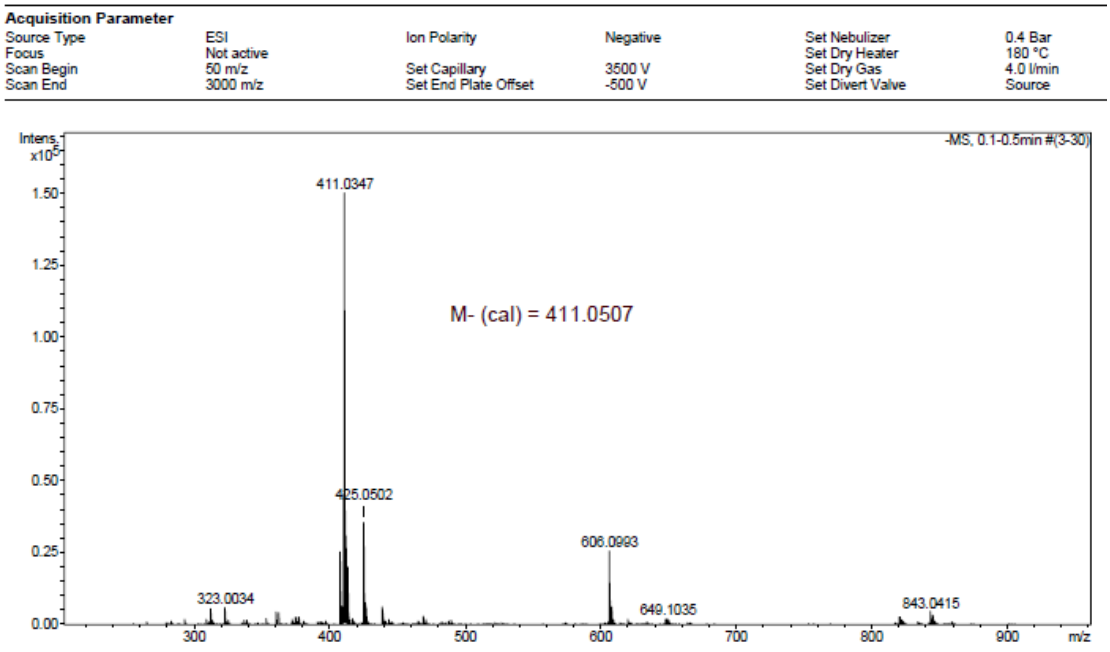

Fig. S2. A) ^{1}H RMN spectrum of the ionophore in D_2O. SH and NH are not visible in D_2O. Three sharp signals are the residue of $(CH_3)_2NCOCH_3$. **B)** Mass spectrum ionophore report.

Figure S3: Characterization of gold nanoparticles modified with the new ionophore

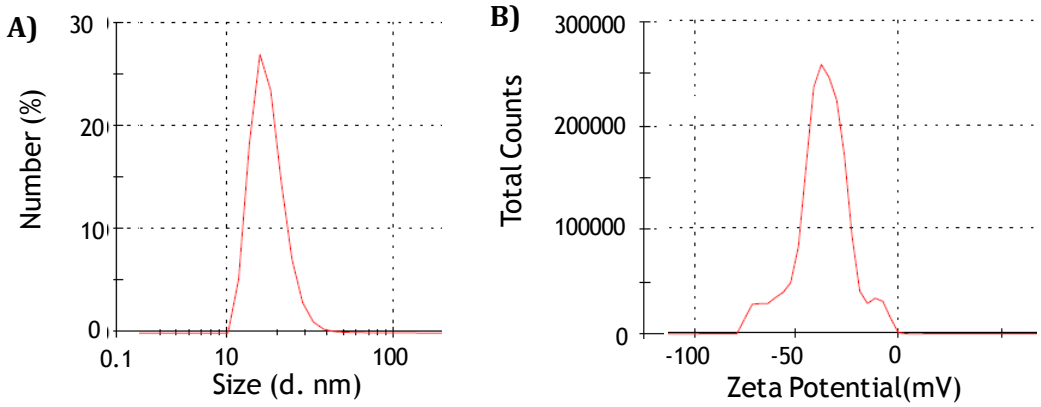

C)

Sample	Au (mg/L)	S (mg/L)	S:Au
Au@TP NPs	29.2	2.1	0.1
Au@Ion NPs	26.4	7.1	0.3

Fig. S3. A) Size Distribution by Number graphic (17.80 nm) **B)** ζ Potential Distribution graphic (-31.4 mV) at pH 7.5. **C)** Inductively coupled plasma optical emission spectrometry (ICP-OES) results and calculated ratio of S:Au.

B.5 Optical microfluidic system based on ionophore modified gold nanoparticles for the continuous monitoring of mercuric ion.

Sara Gómez de Pedro, Daniela Lopes, Sergey Miltsov, David Izquierdo, Julián Alonso Chamarro and Mar Puyol. Sensors and Actuators B, 194, 19-26 (2014).

Nanoscale

PAPER

View Article Online
View Journal | View Issue

Cite this: *Nanoscale*, 2014, **6**, 6018

Microsystem-assisted synthesis of carbon dots with fluorescent and colorimetric properties for pH detection

S. Gómez-de Pedro,[a] A. Salinas-Castillo,*[b] M. Ariza-Avidad,[b] A. Lapresta-Fernández,[b] C. Sánchez-González,[c] C. S. Martínez-Cisneros,[a] M. Puyol,[a] L. F. Capitan-Vallvey[b] and J. Alonso-Chamarro[a]

Received 29th January 2014
Accepted 7th March 2014

DOI: 10.1039/c4nr00573b

www.rsc.org/nanoscale

The present paper describes the use of a microfluidic system to synthesize carbon dots (Cdots) and their use as optical pH sensors. The synthesis is based on the thermal decomposition of ascorbic acid in dimethyl sulfoxide. The proposed microsystem is composed of a fluidic and a thermal platform, which enable proper control of synthesis variables. Uniform and monodispersed 3.3 nm-sized Cdots have been synthesized, the optical characterization of which showed their down/upconversion luminescence and colorimetric properties. The obtained Cdots have been used for pH detection with down and upconverison fluorescent properties as excitation sources. The naked eye or a photographic digital camera has also been implemented as detection systems with the hue parameter showing a linear pH range from 3.5 to 10.2. On the other hand, experiments on the cytotoxicity and permeability of the Cdots on human embryonic kidney cells revealed their adsorption on cells without causing any impact on the cellular morphology.

1. Introduction

The recent application of fluorescent nanoparticles (NPs) such as quantum dots, dye-doped NPs and rare earth-based NPs in biomedical sensing and imaging has become a major subject of research over the last few years. Although a wide range of diverse photoluminescent NPs have been developed from new materials, an increased concern about their potential environmental and human health toxicity exists.[1] Moreover, there are some NP-associated drawbacks such as modification of their surface for a particular function which involves highly time-consuming processes.

At the moment, one of the most attractive NPs are carbon dots (Cdots), which have recently had a major relevance in analytical and bioanalytical chemistry mainly due to their excellent luminescent properties and high biocompatibility as well as their low cost synthesis.[2] However, although these Cdots are very promising NPs in nanotechnology and nano-biomedicine, much research needs to be done either to investigate their potential in sensor development or to identify novel synthesis approaches. In addition, Cdots show size dependent photoluminescence and upconversion luminescence properties leading to anti-Stokes type emissions.[3]

Many different approaches have been presented to date to synthesize Cdots. They are based on two routes, top-down and bottom-up methods. The top-down methods synthesize Cdots from larger carbon materials (graphite, carbon nanotubes, carbon soots, activated carbon), using arc discharge, laser ablation or electrochemical oxidation.[4] The bottom-up routes synthesize Cdots from molecular precursors by combustion, thermal decomposition, acid dehydration, ultrasonic or microwave pyrolysis.[5] However, most of these synthetic approaches present poor reproducibility, which leads to the formation of Cdots with different optical and electronic properties in the different batches produced.

In this sense, microfluidic systems can offer some advantages when synthesizing nanoparticles. They permit proper control of some critical synthesis variables such as the mass and temperature transference due to the small dimensions of the fluidic channels, which are, in contrast, difficult to manage in conventional methods. Moreover, the addition of reagents can be computer-controlled, which permits varying as desired flow rates or injection volumes to obtain products of reactions of different characteristics as well as conferring safety to the operator. On the other hand, the easy and fast modification of the hydrodynamic parameters permits performing many different reactions in a short time, which considerably simplifies the optimization process for the synthesis of

[a]*Sensors & Biosensors Group, Departament of Chemistry, Auntonomus University, Edifici Cn., 08193 Bellatera, Catalonia, Spain*

[b]*ECsens, Department of Analytical Chemistry, Faculty of Sciences, University of Granada, E-18071 Granada, Spain. E-mail: alfonsos@ugr.es; Fax: +34 958 243 328; Tel: +34 958 248 436*

[c]*Department of Physiology, School of Pharmacy, University of Granada, Granada 18071, Spain*

nanomaterials. All this leads to the production of uniform and well dispersed colloids in a reproducible way, namely with the same electronic, optical and chemical properties, which is of great importance for the application of nanomaterials in the (bio)analytical field. Proof of all the advantages enumerated is the large number of papers devoted to that in the literature.[6]

Ceramic microfluidic systems have shown great potential in the synthesis of nanoparticles.[7] This material and its associated technology (Low-Temperature Co-fired Ceramics technology (LTCC)) allow the integration of diverse electronic or fluidic components in a simple, low cost and rapid way. Its multilayer approach enables easy construction of three-dimensional structures, and its compatibility with screen-printing techniques permits integration of many electronic components, such as detection or heating systems.[8,9]

Herein, we synthesize Cdots in a microfluidic system composed of two modules, one for microfluidics and another for heating and temperature control. A proper optimization of the chemical and hydrodynamic parameters has been performed in order to obtain stable and well-dispersed Cdots. As far as we are aware, no microfluidic approach has yet been reported for synthesizing Cdots.

The optical properties of the obtained Cdots have been used for the development of a fluorescent sensor for pH detection using UV and NIR excitation sources. Additionally, due to color changes of Cdots, the visual detection of pH was possible by using digital camera photography and the hue (H) parameter.

Finally, the cytotoxicity and permeability of the NPs in human embryonic kidney cells have also been studied to demonstrate their suitability as sensors or labels in biomedical applications by bioimaging.

2. Experimental

Microsystem materials and components

DuPont 951 green tape (DupontTM, Germany) was used to fabricate both the microfluidic and the heating modules. DuPont 5742 gold cofirable conductor paste was required in order to perform the screen-printing step for the construction of the heating platform, since the gold paste acts as the resistor. DuPont 6141 paste was used to fill the vials of the heating platform. For temperature control, a class A PT100 temperature sensor was preferred (Innovative Sensor Technology, Switzerland). The sensor was glued to the bottom of the heating module by means of epoxy (EPO-TEK® H20E, Billerica, MA, USA), and a PIC18F4431 microcontroller (Microchip Inc., Arizona, USA) was used for the digital PID control system, which controls the temperature as desired.

In the flow system, a 10 mL syringe (Hamilton series GASTIGHT 1000 TLL, Bonaduz, GR, Switzerland) was required, where reagents were placed for their injection into the microfluidic system by means of a syringe pump (540 060 TSE systems, Bad Homburg, Germany). To complete the fluidic system, PTFE tubes (i.d. 0.9 mm) were used between the syringe and the microfluidic platform, and o-rings and conic PTFE cones were used for their connection.

Instrumentation

Optical properties of the nanoparticles were obtained by means of Varian Cary Eclipse (Varian Ibérica, Madrid, Spain) and Fluorolog1 Modular (Horiba Jobin Yvon, France) spectrofluorometers. Zeta-potential measurement was carried out on a Zetasizer Nano ZS90 (Malvern, Worcestershire, U.K.). XRD was performed at the Centre of Scientific Instrumentation (University of Granada, Spain) on a Fisons-Carlo Erba analyser model EA 1108. The FTIR spectra of the powdered samples were recorded with a ThermoNicolet IR200FTIR (Thermo Fisher Scientific Inc., Madrid, Spain) by using KBr pellets.

The shape and dimensions of the core of the particles were measured using a high resolution electron microscope (HRTEM), JEOL 2011 (Tokyo, Japan). The samples were prepared by dipping a copper grid, which was coated with a thin carbon film, into the carbon dot suspension.

A Crison pH meter (Crison Instruments, Barcelona, Spain, model Basic 20) was used for pH measurements.

pH measurement procedure

The pH of 2 mL of Cdot solutions was regulated by adding different volumes of required concentrations of HCl or NaOH and measuring it with a pH meter. The fluorescence spectra and the image capture with a digital camera were recorded at different pH values.

Image acquisition and treatment for colorimetric pH determination

For image acquisition and digitization, a Canon PowerShot G12 (Madrid, Spain) was used. To keep all the image-gathering under the same conditions a Cube Light Box was developed. The vials with 2 mL of Cdots were located inside the box, so they were not exposed to external light. The only light source was an LED (Light-Emitting Diode) system with direct current. All parameters of the camera were set and optimized. The vial position was fixed for all experiments.

The obtained images were stored in the TIFF (True Image File Format) file format to prevent any loss of information since it does not compress the image. To extract the hue parameter from each sensing element in the scanned image, software developed by the research group in Matlab was used. The H coordinate was calculated from the R, G and B coordinates of each pixel using eqn (1). The H value, determined for each sensing element, was the mode of the hues calculated for all the pixels in the solution, since this parameter provides low error during image processing.

$$H = \begin{cases} \left(\dfrac{G-B}{\max_{\text{channel}} - \min_{\text{channel}}} + 0\right) \Big/ 6; & \text{if } \max = R^* \\ \left(\dfrac{B-R}{\max_{\text{channel}} - \min_{channel}} + 2\right) \Big/ 6; & \text{if } \max = G \\ \left(\dfrac{R-G}{\max_{\text{channel}} - \min_{\text{channel}}} + 4\right) \Big/ 6; & \text{if } \max = B \end{cases} \quad (1)$$

* if H is less than 0 then add 1 to H.

Cell culture

Human embryonic kidney HEK293 cells were cultured in Dulbecco's modified Eagle's medium (DMEM) supplemented with 10% fetal bovine serum, 2 mM L-glutamine and 1% penicillin–streptomycin solution at 37 °C with 5% humidified CO_2. Cells were plated at 20 000 cells per well onto glass bottom Petri dishes previously coated with 10 g mL^{-1} poly-L-lysine. After 24 h in culture, the cells were incubated for 24 or 48 h at 37 °C with different concentrations of Cdots (0.1, 0.2, 0.4, 0.6, 0.8, 1 mg mL^{-1}) dispersed in complete culture medium.

Cytotoxicity assay

In vitro proliferation assay compared the growth rate of HEK293 cells using 3-(4,5-dimethyl-1,3-thiazol-2-yl)-2,5-diphenyl-2*H*-tetrazol-3-ium bromide (MTT) after plating 2×10^4 cells per well on a 96-well flat-bottom plate for 24 and 48 h at 37 °C in 5% CO_2. MTT (5 mg mL^{-1}) reagent was added to each well and incubated for 4 h at 37 °C. Thereafter, 150 mL per well of 100% DMSO were added, mixed thoroughly to dissolve the dark blue crystals and the plates were subsequently read on an ELISA reader at a wavelength of 570 nm.

Fluorescence microscopy

Fluorescence measurements were performed with a Zeiss (Oberkochen, Germany) Axiovert 200 inverted microscope fitted with an ORCA-ER CCD camera (Hamamatsu, Bridgewater, NJ) through a 20× air objective. Nanoparticles were excited at 360/380 nm using a computer-controlled Lambda10-2 filter wheel (Sutter Instruments, Novato, CA), and emitted fluorescence was filtered with a 440/535 nm long-pass filter. Images were processed with Image J software.

3. Results and discussion

3.1 Design and fabrication of the microsystem

The microsystem for the synthesis of Cdots was based on two separate modules: a microfluidic platform and a heating module with temperature control. The general fabrication procedure of ceramic microsystems is detailed elsewhere.[10] Since the LTCC technology is a multilayer approach, the final design of the device has to be divided into different layers in order to create the partial design by means of computer-assisted design (CAD) software. In this step, it has to be taken into account the ~15% shrinkage on each axis of DuPont 951 green tape during the sintering process. Once the design is done, a laser machine (LPKF Protolaser 200, Garbsen, Germany) transfers the diverse patterns to different layers. The next step in the construction of the device involves screen-printing of those layers that require conductive paste. In this case, this step was necessary in the layers which formed the heating platform (resistor and vias to connect the tracks). The heater was constructed in the base of a gold paste screen-printed resistor, which was deposited in a radial configuration. Then, the slabs were aligned in aluminium plates using fiducial holes and laminated by a thermo-compression process at 100 °C and 3000 psi. The LTCC layers were finally sintered in a programmable box furnace (Carbolite CBCWF11/23P16, Afora, Barcelona, Spain) by applying a temperature profile.

As explained before, two different modules were preferred to carry out the synthesis of carbon dots, which were mechanically attached to obtain the best contact between them. In this way, if one of the modules has to be modified, it can be replaced without changing the other one. Both modules were designed and constructed based on a previous microsystem.[9]

The fluidic platform had one inlet for the entrance of reagents followed by a simple Z shape channel to increase the residence time of reagents inside the microsystem and allow their thermal conditioning, and one outlet from which the formed Cdots leave the system. The Z-shape fluidic structure was constructed in a circular configuration in order to make it coincide with the resistance of the heating module. Moreover, the channel for reagents was constructed in only one layer of the ceramic substrate, since deeper channels could generate no uniform thermal patterns through the solution. All this contributes to obtaining well controlled heat transfer from the thermal platform to the liquid flowing in the microfluidic platform, which ensures the optimal and uniform formation of carbon dots through the microsystem.[11] As can be observed in Fig. 1, the whole module consisted of 7 ceramic layers, which once sintered formed a block of 6.0 mm diameter and 1.4 mm thickness. An image of the different layers that compose both the fluidic and the heating platforms is depicted in Fig. 1.

To make proper control of the temperature feasible, a class A PT100 sensor was attached by means of epoxy on the reverse of the bottom layer, taking care of the position of the sensor in the central zone of the resistor. Electronics for temperature control is detailed elsewhere.[9] Briefly, a temperature controller with a digital PID topology was implemented on a computer controlled PIC18F4431 microcontroller. An electronic circuit maintained a constant intensity in order to avoid interference with temperature measurements due to self-heating, and amplified the control signal generated by the PID controller. The system estimated the error from the PT100 sensor through the obtained feedback signal and corrected it by specific differential equations programmed in the digital PID control system implemented in the microcontroller code. Then, the signal was amplified and applied to the gold resistor. The system was programmed to work from 150 to 250 °C.

Heat transfer in the thermal platform exhibited a radial distribution, and it was found to provide the temperature desired in the fluidic system, since the sensor is located trying to obtain the optimum *xy*-alignment with the microreactor zone.[11]

3.2 Synthesis of Cdots

For the synthesis of Cdots, ascorbic acid (Panreac, 99%) was chosen as a simple and low cost source of carbon, and dimethyl sulfoxide (DMSO) (Baker Chemical, 0.3% water) was preferred as solvent due to the high temperatures that this compound can bear.

In order to obtain controllable and reproducible carbon dots, optimization of certain parameters of the microsystem is

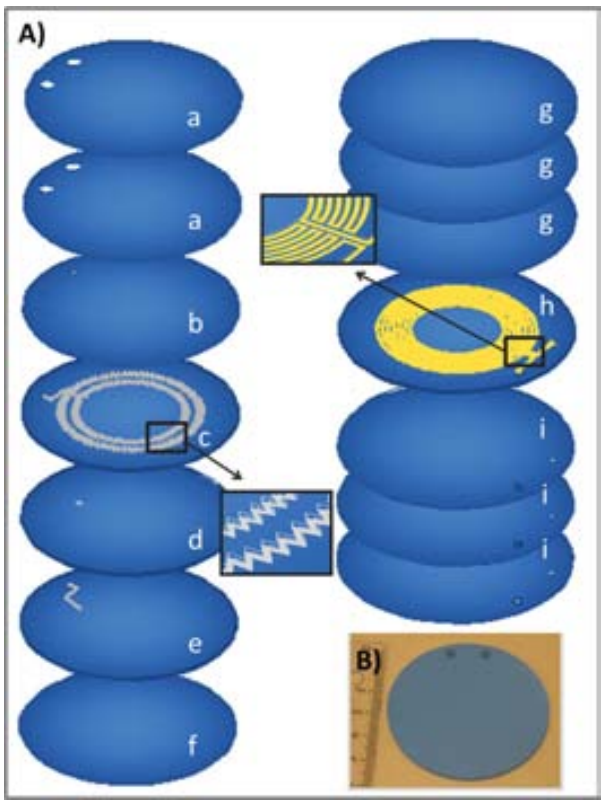

Fig. 1 (A) Scheme of the different layers that compose the microfluidic system for the synthesis of carbon dots. Layers (a–f) correspond to the microfluidic platform: (a) top layers, where o-rings are placed; (b) entrance and exit for reagents and the product; (c) inlet for reagents and the bidimensional micromixer; (d) intermediate layer for the connexion of the fluidic structure; (e) outlet for the synthesized carbon dots; (f) bottom layer. Layers (g–i) compose the thermal platform: (g) top layers; (h) embedded screen-printed heater; (i) bottom layers with vias to connect the tracks of the resistance. (B) Picture of both the microfluidic and the heating platforms mechanically attached.

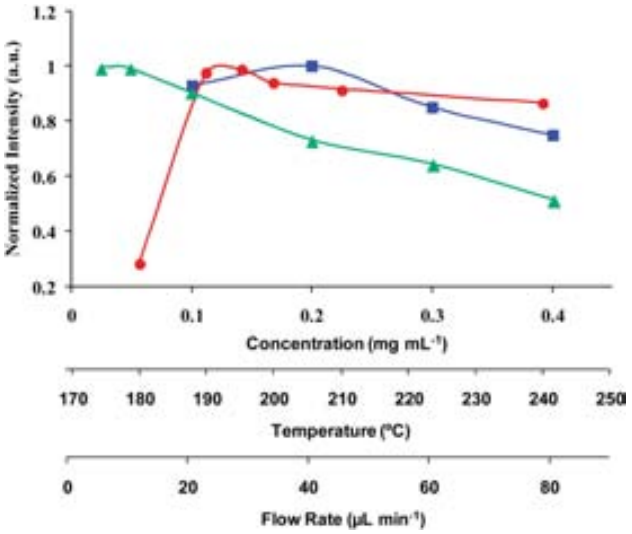

Fig. 2 Optimization of the chemical and hydrodynamic parameters for the synthesis of Cdots in the ceramic microfluidic system (λ_{exc} = 325 nm, λ_{em} = 420 nm). Red circles: temperature (°C), blue squares: concentration (µg mL^{-1}), green triangles: flow rate (µL min^{-1}).

required. The optimized values were determined as a function of the maximum fluorescence intensity recorded with a spectrofluorometer, since the synthesized Cdots are designed to use for sensing and bioimaging applications.

As in many other nanoparticle syntheses that involve the decomposition of reagents, temperature plays an important role. Thus, the first parameter to study was the reaction temperature. Since ascorbic acid has a melting point of 188 °C, six different temperatures around this value (180, 190, 195, 200, 210 and 240 °C) were chosen. The concentration of ascorbic acid and the flow rate were fixed to 0.1 mg mL^{-1} and 20 µL min^{-1}, respectively. As can be observed in Fig. 2, only a weak fluorescence intensity was observed from the Cdots synthesized at 180 °C, which indicates the poor formation of the nanoparticles at temperatures below the ascorbic acid melting point. A clear improvement is observed when performing the reaction under the same conditions but by increasing the temperature over this threshold. On the other hand, from 190 °C up to 240 °C the fluorescence intensity remained practically constant. The small decrease observed is probably due to the decomposition of the solvent (boiling point of 189 °C), which generates gaseous species such as SO_2.[12] Thus, 190 °C was preferred as the optimized value for temperature to perform the synthesis. All the fluorescence emission spectra of the Cdots synthesized exhibit the same maximum peak, located over 420 nm.

The effect of varying the concentration of ascorbic acid was also studied. Four different concentrations were evaluated (0.1, 0.2, 0.3 and 0.4 mg mL^{-1}), while temperature was fixed at 190 °C and flow rate at 20 µL min^{-1}. As shown in Fig. 2, the concentration at which higher intensity of fluorescence was observed under these conditions was 0.2 mg mL^{-1}, and thus, this value was selected for further optimization.

Finally, the variation in the flow rate of reagents in the microfluidic system was evaluated, while the remaining parameters were fixed at the optimized conditions (a temperature of 190 °C and an ascorbic acid concentration of 0.2 mg mL^{-1}). The tested values included 5, 10, 20, 40, 60 and 80 µL min^{-1}. As presented in Fig. 2, the more slowly the liquid flowed in the system, the higher fluorescence was achieved. This was in concordance with the fact that the time that reagents spend in the microfluidic system determines the reaction time for the formation of colloids. This is a critical variable,[13] and, in this work, 10 µL min^{-1} (instead of 5 µL min^{-1}) was selected as a compromise between the intensity of fluorescence and the final amount of the colloid obtained in a reasonable synthesis time.

3.3 Characterization of Cdots

Cdots synthesized in the microsystem were dialyzed against Milli-Q water using spectra/pro-dialysis membrane with a cut-off of 1 kDa for their purification and characterized by several techniques.

The core and shape of the nanoparticles were determined by Transmission Electron Microscopy (TEM). Fig. 3A shows a TEM image, where monodispersed spherical carbon dots can be

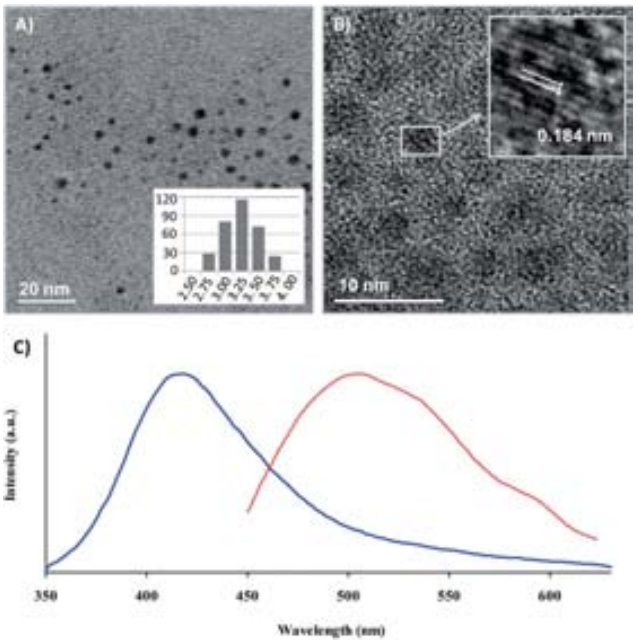

Fig. 3 Characterization of the synthesized Cdots in the microfluidic system. (A) TEM image with the size-histogram and the calculated average size. (B) HRTEM image and an amplification with the lattice fringes highlighted. (C) Fluorescence emission spectrum by UV excitation at 325 nm (in blue) and by NIR excitation at 850 nm (in red).

observed. The average size found was 3.3 ± 0.3 nm from the counting of more than 250 particles, which demonstrates the synthesis reproducibility of the microsystem. HRTEM (High-Resolution Transmission Electron Microscopy) images (Fig. 3B) revealed crystalline nanoparticles, as was also proved by the clear ring structure of the selected area electron diffraction (SAED) pattern image. Lattice planes with 0.18 nm spacing were found in the crystalline images from the colloid, which is consistent with the (102) diffraction planes of sp^2 graphitic carbon.[14] The bright rings observed in the SAED pattern can be attributed to (100) and (102) lattice planes of graphite (inset of Fig. 3B).

The FTIR spectrum of Cdots showed the typical bands of stretching vibrations of O–H at 3400 cm^{-1}, the ester group at 1780 cm^{-1} and C=O at 1622 cm^{-1}. The X-ray diffraction (XRD) pattern displayed a broad diffraction peak at $2\Phi = 20.5°$. Different zeta potential values were obtained for the synthesized Cdots, varying from acid pH (8 mV) to basic pH (−14 mV), which confirms the presence of carboxyl groups on the surface of the nanoparticles.

Cdots exhibited excellent water solubility and blue luminescence under UV excitation light (365 nm). Using quinine sulphate as standard, the fluorescence quantum yield was found to be 2.6%, which is comparable to previous reports.

To further explore the optical properties of Cdots, a detailed fluorescence study was performed using different excitation wavelengths (Fig. 3C). It is remarkable that these Cdots also exhibit good upconversion fluorescent properties besides their strong luminescence in the visible region under NIR excitation sources. Fig. 3C shows the fluorescent spectra of Cdots excited at 325 nm with emission in the range of 360–500 nm (see Fig. 3C blue), and excited by longer wavelength light (maximum intensity with 850 nm excitation, see Fig. 3C red) with the up-conversion emissions located in the range of 450–600 nm. Therefore, these results suggest that Cdots may be used as a powerful component in biological applications as well as an appropriate sensor design for environmental applications.

3.4 Sensing applications

It is already known that Cdots are pH sensitive. Indeed, diverse studies can be found in the literature which describe the sensitivity of Cdots to pH depending on their external composition (carbonyls, amines, hydroxyls, esters, *etc.*). In particular, a previous study showed that Cdots synthesized from ascorbic acid pyrolysis were capable of detecting small pH changes by colorimetry or fluorimetry.[5c] That is, the intensity of fluorescence change with protonation and deprotonation of the carboxyl groups of the surface Cdots cause electrostatic doping/charging of the Cdots and shift the Fermi level. Similarly, the

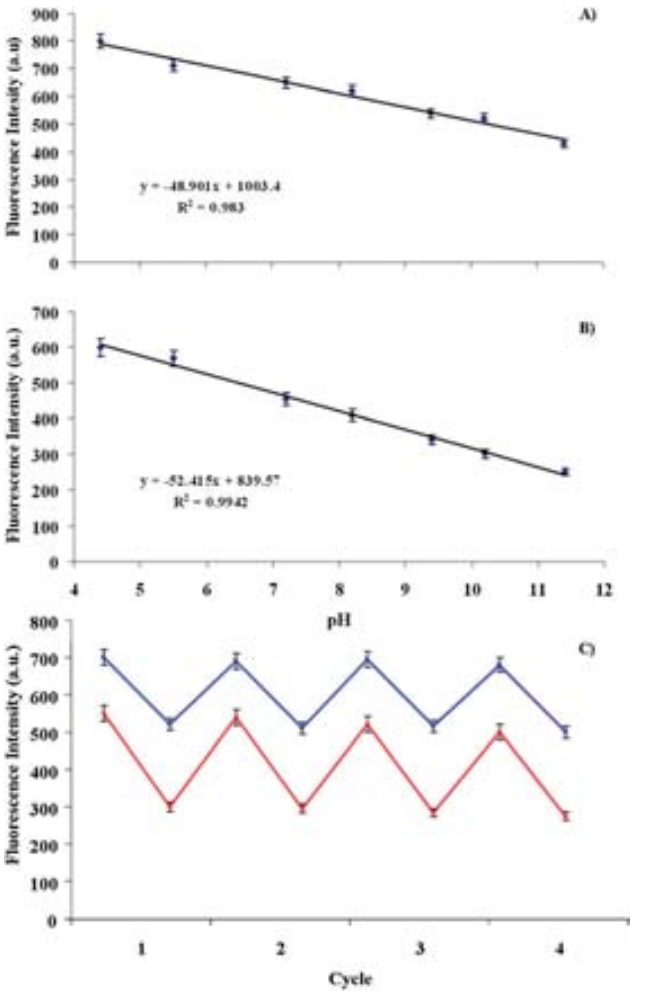

Fig. 4 Linear calibration plots for pH detection are shown in (A) for fluorescence (λ_{exc} = 325 nm, λ_{ems} = 420 nm) and (B) for up-conversion fluorescence (λ_{exc} = 850 nm, λ_{ems} = 505 nm). (C) Plots of the fluorescence intensity as a function of pH cycles ($\lambda_{exc/ems}$ = 325/420 nm blue), ($\lambda_{exc/ems}$ = 850/505 nm red).

color of the Cdot solution change with pH causes electronic changes of π–π* and n–π* by refilling or depleting their valence bands.[15]

Since the obtained Cdots have the same matrix, it is expected that they have the same behavior and therefore, one can take advantage of this fact to advance their application as pH sensors.

Fluorescent sensor for pH. The influence of pH on the synthesized Cdots in the pH range of 2–11 was studied. The results showed that the maximum fluorescence emission (420 nm) of the Cdots at 325 nm excitation decreased linearly as the pH increased from 4.5–11.5 (Fig. 4A), and the same results were obtained by excitation at 850 nm and emission at 505 nm (Fig. 4B).

The good emission fluorescence presented at 400 or 505 nm by the Cdots over a wide range of pH (4.5–11.5) makes them valuable for future use in biological applications.

In order to test the reversibility of the proposed nanosensor, the pH of Cdots was changed from 5 to 10 and back to 5 four times, and the fluorescence was measured by down and upconverting excitation emission values in all cases. The results confirmed the good reversibility of the nanosensor (see Fig. 4C). The relative standard deviations were less than 5% for the five measurements.

Colorimetric sensor for pH. Once the change in the color intensity of Cdots with pH was observed, it is reasonable to use these properties to determine pH by measurement of color from images captured using a camera. By far, the most commonly used color space is RGB, the coordinates of which are used for processing with multivariate techniques. However, we used the HSV color space in this work, whose main characteristic is that it represents useful information about the color in one single parameter, the *H* coordinate. Previous studies from our research group have shown that the use of *H* value is stable, simple to calculate, and easily obtained from commercial devices, maintaining superior precision with variations in reagents' colorimetric concentration, detector spectral response and illumination.[16]

As seen in Fig. 5A, the effect of pH on the color of Cdots is reflected by a shift from grey colors corresponding to acid pH values to yellow-orange color associated with medium pH values, and to brown color related to more basic pH values, which can also be easily observed by the naked eye. The relationship between the analytical parameter *H* and the pH was adjusted to a sigmoidal fit using a Boltzmann type equation, giving an apparent pK_a value of 6.7, which is in concordance with the acidic groups present on the surface of the Cdots.[17] As can be seen from both approaches, a wide linear range can be obtained from pH 3.5 to 10.2 (Fig. 5B).

Bioimaging and cytotoxicity. Fluorescence microscopy allowed us to examine the cellular localization of Cdots in HEK293 cells. Interestingly, we found that fluorescent Cdots were adsorbed on the cell membrane of HEK293 cells after a short incubation time (24 h) (right panel in Fig. 6A). Cells showed dot shaped localization of Cdots (red arrow, Fig. 6A) throughout cell bodies and did not reveal any impact of the Cdots on the cellular morphology. No evidence of fluorescence was observed in the control sample of untreated cells (data not

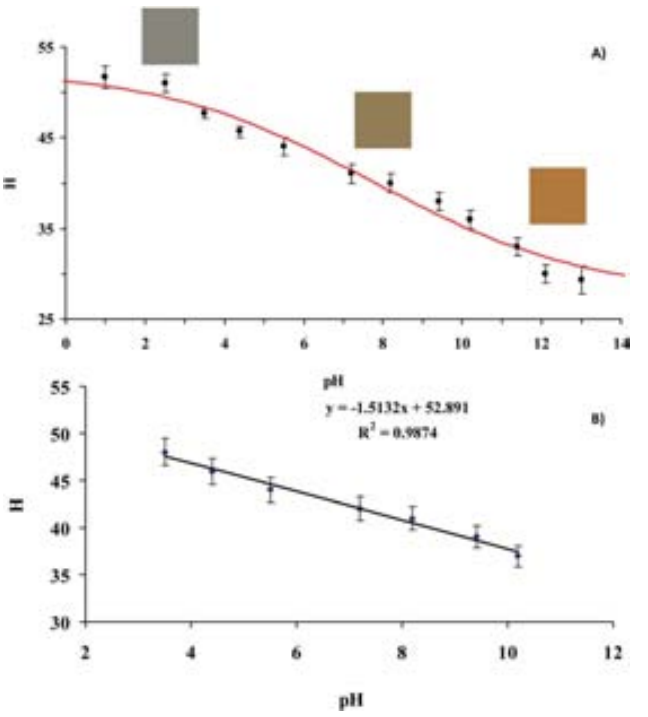

Fig. 5 (A) Colorimetric response of Cdots in the pH range 1.5–13. (B) Linear range for pH colorimetric detection.

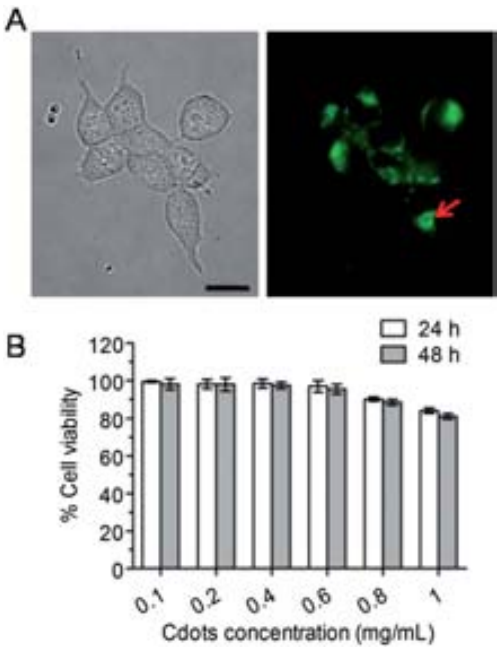

Fig. 6 Biological characterization of Cdots in HEK293 cells. (A) Transmitted light brightfield image of HEK293 cells (left panel) and fluorescence image showing in green the Cdots in the membrane edges and localized in small dots (red arrow). Scale bar = 10 μM. (B) MTT assay revealed no change in cell viability of HEK293 cells following a treatment with increasing concentrations of Cdots for 24 and 48 h at 37 °C.

shown). As shown in Fig. 6B, cell viability was not affected in the presence of these concentrations of Cdots, demonstrating that these non-toxic nanoparticles can act as suitable biosensors or bioimaging devices in living organisms.

4. Conclusions

A microfluidic system has been proposed for the automatic synthesis of carbon dots. The system is composed of two separate platforms to increase its versatility, one for heating and control of the temperature and the other for microfluidics. The radial configuration of the heater as well as of the microfluidic pattern, which perfectly matches with the screen-printed resistor, permits a controlled mass and temperature transference. Once the hydrodynamic parameters of the microsystem were optimized, Cdots with suitable optical properties were obtained. The narrow size distribution observed in the characterization of the synthesized Cdots demonstrates the reproducibility of the microsystem. Further characterization of the synthesized Cdots showed the pH dependence of their optical properties which were used for the development of a pH fluorescent sensor using both UV and NIR excitation sources. The naked eye and a photographic digital camera were used as detection systems for the colorimetric pH measurement and were implemented using the *H* parameter, obtaining a linear response over a wide range of pH values. Cytotoxicity and permeability studies on cells did not reveal any impact on the cellular morphology. Viability of cells was not affected in the presence of different concentrations of Cdots, demonstrating their suitability for biosensing or bioimaging applications in the biomedical field.

Acknowledgements

This work was supported by Projects CTQ2009-14428-C02-01, CTQ2009-12128 and CTQ2012-36165 from the Ministerio de Economia y Competitividad (Spain), SGR 2009 -0323 from Catalonia Government and P10-FQM-5974 from the Junta de Andalucía (Spain). These projects were partially supported by European Regional Development Funds (ERDF). Our thanks to "Reincorporacion de Doctores UGR" programs and Greib start-up projects for young researchers.

Notes and references

1 (*a*) D. Mhamma, W. Ramadan, A. Rana, C. Rode, B. Hannuyer and S. Orgale, *Green Chem.*, 2011, **13**, 1990; (*b*) J. Ming, R. Liu, G. Liang, Y. Yu and F. Zhao, *J. Mater. Chem.*, 2011, **21**, 10929.

2 (*a*) K. Qu, J. Wang, J. Ren and Xi. Qu, *Chem.–Eur. J.*, 2013, **19**(22), 7243; (*b*) L. Zhou, Y. Lin, Z. Huang, J. Ren and X. Qu, *Chem. Commun.*, 2012, **48**(8), 1147.

3 (*a*) S. N. Baker and G. A. Baker, *Angew. Chem., Int. Ed.*, 2010, **49**, 2; (*b*) J. C. G. Estevez da Silva and H. M. R. Gonçalves, *Trends Anal. Chem.*, 2011, **30**, 1327; (*c*) S. K. Bhunia, A. Saha, A. R. Maity, S. C. Ray and N. R. Jana, *Sci. Rep.*, 2013, **3**, 1473; (*d*) H. Li, Z. Kang, Y. Liu and S. T. Lee, *J. Mater. Chem.*, 2012, **22**, 24230.

4 (*a*) H. Ming, Z. Ma, Y. Liu, K. Pan, H. Yu, F. Wang and Z. Kang, *Dalton Trans.*, 2012, **41**, 9526; (*b*) L. Zheng, Y. Chi, Y. Dong, J. Lin and B. Wang, *J. Am. Chem. Soc.*, 2009, **131**, 4564.

5 (*a*) X. Zhai, P. Zhang, C. Liu, J. Bai, W. Li, L. Dai and W. Liu, *Chem. Commun.*, 2012, **48**, 7955; (*b*) A. Salinas-Castillo, M. Ariza-Avidad, C. Pritz, M. Camprubí-Robles, B. Fernández, M. J. Ruedas-Rama, A. Megía-Fernández, A. Lapresta-Fernández, F. Santoyo-Gonzalez, A. Schrott-Fischer and L. F. Capitan-Vallvey, *Chem. Commun.*, 2013, **49**, 1103; (*c*) X. Jia, J. Li and E. Wang, *Nanoscale*, 2012, **4**, 5572.

6 (*a*) A. M. Nightingale, S. H. Krishnadasan, D. Berhanu, X. Niu, C. Drury, R. McIntyre, E. Valsami-Jones and J. C. deMello, *Lab Chip*, 2011, **11**, 1221; (*b*) H. Wang, X. Li, M. Uehara, Y. Yamaguchi, H. Nakamura, M. Miyazaki, H. Shimizu and H. Maeda, *Chem. Commun.*, 2004, 48; (*c*) E. M. Chan, A. P. Alivisatos and R. A. Mathies, *J. Am. Chem. Soc.*, 2005, **127**, 13854.

7 (*a*) S. Gomez-de Pedro, M. Puyol, D. Izquierdo, I. Salinas, J. M. de la Fuente and J. Alonso-Chamarro, *Nanoscale*, 2012, **4**(4), 1328; (*b*) S. Gomez de Pedro, M. Puyol and J. Alonso, *Nanotechnol.*, 2010, **21**(41), 415603.

8 (*a*) C. S. Martinez-Cisneros, Z. daRocha, M. Ferreira, F. Valdes, A. Seabra, M. Gongora-Rubio and J. Alonso-Chamarro, *Anal. Chem.*, 2009, **81**, 7448; (*b*) G. Fercher, A. Haller, W. Smetana and M. J. Vellekoop, *Analyst*, 2010, **135**, 965.

9 S. Gómez-de Pedro, C. S. Martínez-Cisneros, M. Puyol and J. Alonso-Chamarro, *Lab Chip*, 2012, **12**, 1979.

10 N. Ibáñez-García, C. S. Martínez-Cisneros, F. Valdés and J. Alonso, *TrAC, Trends Anal. Chem.*, 2008, **27**, 24.

11 C. S. Martínez-Cisneros, S. Gómez-de Pedro, J. García-García, M. Puyol and J. Alonso-Chamarro, *Chem. Eng. J.*, 2012, **211–212**, 432.

12 F. C. Thyrion and G. Debecker, *Int. J. Chem. Kinet.*, 1973, **5**, 583.

13 B. K. H. Yen, N. E. Stott, K. F. Jensen and M. G. Bawendi, *Adv. Mater.*, 2003, **15**, 1858.

14 L. Tian, D. Ghosh, W. Chen, S. Pradhan, X. Chang and S. Chen, *Chem. Mater.*, 2009, **21**, 2803.

15 (*a*) J. L. Chen and X. P. Yan, *Chem. Commun.*, 2011, **47**, 3135; (*b*) W. Kong, H. Wu, Z. Ye, R. Li, T. Xu and B. Zhang, *J. Lumin.*, 2014, **148**, 238.

16 (*a*) K. Cantrell, M. M. Erenas, I. De Orbe-Payá and L. F. Capitán-Vallvey, *Anal. Chem.*, 2010, **82**, 531; (*b*) M. Ariza-Avidad, M. P. Cuellar, A. Salinas-Castillo, M. C. Pegalajar, J. Vukovic and L. F. Capitán-Vallvey, *Anal. Chim. Acta*, 2013, **783**, 56.

17 A. Lapresta-Fernández and L. F. Capitán-Vallvey, *Anal. Chim. Acta*, 2011, **706**, 328.

